frontiers | Research Topics

The impact of the space environment on microbial growth and behavior

Edited by
Camilla Urbaniak, Donatella Tesei and Rob Van Houdt

Published in
Frontiers in Microbiology

ISSN 1664-8714
ISBN 978-2-8325-4714-4
DOI 10.3389/978-2-8325-4714-4

About Frontiers

Frontiers is more than just an open access publisher of scholarly articles: it is a pioneering approach to the world of academia, radically improving the way scholarly research is managed. The grand vision of Frontiers is a world where all people have an equal opportunity to seek, share and generate knowledge. Frontiers provides immediate and permanent online open access to all its publications, but this alone is not enough to realize our grand goals.

Frontiers journal series

The Frontiers journal series is a multi-tier and interdisciplinary set of open-access, online journals, promising a paradigm shift from the current review, selection and dissemination processes in academic publishing. All Frontiers journals are driven by researchers for researchers; therefore, they constitute a service to the scholarly community. At the same time, the *Frontiers journal series* operates on a revolutionary invention, the tiered publishing system, initially addressing specific communities of scholars, and gradually climbing up to broader public understanding, thus serving the interests of the lay society, too.

Dedication to quality

Each Frontiers article is a landmark of the highest quality, thanks to genuinely collaborative interactions between authors and review editors, who include some of the world's best academicians. Research must be certified by peers before entering a stream of knowledge that may eventually reach the public - and shape society; therefore, Frontiers only applies the most rigorous and unbiased reviews. Frontiers revolutionizes research publishing by freely delivering the most outstanding research, evaluated with no bias from both the academic and social point of view. By applying the most advanced information technologies, Frontiers is catapulting scholarly publishing into a new generation.

What are Frontiers Research Topics?

Frontiers Research Topics are very popular trademarks of the *Frontiers journals series*: they are collections of at least ten articles, all centered on a particular subject. With their unique mix of varied contributions from Original Research to Review Articles, Frontiers Research Topics unify the most influential researchers, the latest key findings and historical advances in a hot research area.

Find out more on how to host your own Frontiers Research Topic or contribute to one as an author by contacting the Frontiers editorial office: frontiersin.org/about/contact

The impact of the space environment on microbial growth and behavior

Topic editors

Camilla Urbaniak — Planetary Protection Center of Excellence, NASA Jet Propulsion Laboratory, United States

Donatella Tesei — University of Natural Resources and Life Sciences Vienna, Austria

Rob Van Houdt — Belgian Nuclear Research Centre (SCK CEN), Belgium

Citation

Urbaniak, C., Tesei, D., Van Houdt, R., eds. (2024). *The impact of the space environment on microbial growth and behavior*. Lausanne: Frontiers Media SA. doi: 10.3389/978-2-8325-4714-4

Table of contents

frontiers | Frontiers in Microbiology

TYPE Editorial
PUBLISHED 22 March 2024
DOI 10.3389/fmicb.2024.1390100

OPEN ACCESS

EDITED AND REVIEWED BY
Andreas Teske,
University of North Carolina at Chapel Hill, United States

*CORRESPONDENCE
Camilla Urbaniak
camilla.urbaniak@jpl.nasa.gov

†These authors have contributed equally to this work

RECEIVED 22 February 2024
ACCEPTED 08 March 2024
PUBLISHED 22 March 2024

CITATION
Urbaniak C, Tesei D and Van Houdt R (2024) Editorial: The impact of the space environment on microbial growth and behavior. *Front. Microbiol.* 15:1390100. doi: 10.3389/fmicb.2024.1390100

Editorial: The impact of the space environment on microbial growth and behavior

Camilla Urbaniak[1,2*†], Donatella Tesei[3†] and Rob Van Houdt[4†]

[1]NASA Jet Propulsion Laboratory, California Institute of Technology, Pasadena, CA, United States, [2]ZIN Technologies-powered by Voyager Space, Middleburg Heights, OH, United States, [3]University of Natural Resources and Life Sciences, Vienna, Austria, [4]Microbiology Unit, Nuclear Medical Applications, Belgian Nuclear Research Centre (SCK CEN), Mol, Belgium

KEYWORDS

space microbiology, planetary protection, microbial behavior, habitability and astrobiology, spaceflight, space environment adaptation, microorganisms

Editorial on the Research Topic
The impact of the space environment on microbial growth and behavior

Microorganisms play an important role in life and can adapt to and survive in harsh and changing environments. Their ability to thrive in hostile conditions is reflected not only by their survival and activity in Earth's most extreme environments but also in low Earth orbit (LEO) and outer space (Olsson-Francis et al., 2018; Thombre et al., 2022). Spaceflight and the space environment present unique stressors compared to Earth (microgravity, galactic cosmic radiation, solar UV radiation, space vacuum, thermal extremes) to which microbes are exposed, but how they adapt and respond, especially in the context of deep-space exploratory missions, is still poorly understood (Tesei et al., 2022). Studies to date, though, have shown that these responses can range from being beneficial for human exploration—such as potential applications in biological life support systems (BLSS), *in situ* resource utilization (ISRU) and astronaut therapeutics (Koehle et al., 2023)—to negatively impact long duration missions (e.g., biofilm formation, increased virulence, and reduced susceptibility to antimicrobial agents), which pose risks to astronaut's health and spacecraft integrity (Wilson et al., 2007; Kim et al., 2013; Urbaniak et al., 2018). Hence, investigating the reaction of microorganisms to space conditions and the alterations in their physiology, not only helps to shed light on the molecular basis of tolerance, but also holds implications for both space exploration and astrobiology missions. This Research Topic features published articles pertaining to microbial adaption under spaceflight or simulated Mars conditions (Puig et al., Averesch et al., Blachowicz et al., Fagliarone et al., Gesztesi et al., Muñoz-Hisado et al.), life in extreme environments on Earth (Moors et al.) and planetary protection (Stott et al., Dean et al., Seto et al., Mogul et al., Kimura et al.).

The Research Topic starts off with a primary research article by Puig et al., testing the survival of genetically engineered *Escherichia coli* to simulated low earth orbit conditions. Enhanced survival to radiation, extreme temperature and low pressure was achieved through the insertion of the *Dsup* radiation resistance gene and the DNA damage repair genes, *recA* and *uvrD*

(Puig et al.). DNA repair mechanisms were also shown by Fagliarone et al. to be essential for the survival of the cyanobacterium *Chroococcidiopsis* sp. CCMEE 029 in Mars cryosphere conditions, specifically the key genes *ftsZ* and *sulA*. The studies by Blachowicz et al. and Averesch et al. conducted aboard the International Space Station (ISS) provide valuable insights into the adaptability of filamentous fungi. Blachowicz et al. examined the response of *Aspergillus niger* during a 12-day growth period on the ISS, unveiling genomic, proteomic and metabolomic changes indicative of adaptive strategies (Blachowicz et al.). Averesch et al. investigated the growth of *Cladosporium sphaerospermum* on the ISS for 26 days, revealing accelerated growth and better radiation absorption compared to ground controls. Using a proteomics approach, Muñoz-Hisado et al. studied the adaptation of *Bacillus subtilis* and *Curtobacterium flacumfaciens* to growth under Martian conditions and showed that *B. subtilis* had an elevated stress response, increased catabolism and increased mobility and biofilm formation, while *C. flacumfaciens* strengthened its cell envelope to help protect the cell from the extracellular environment. The reasons for the differences observed between Mars-like conditions, LEO and Earth could be due to the diffusion limited environment of space where the change in gravity experienced by microbes is due to changes in fluid mixing responses (Gesztesi et al.). Gesztesi et al.'s calculations provide researchers with an inside look at suspension culture behavior in the diffusion-limited environment of microgravity at the scale of individual cells.

To explore factors that could influence the habitability of planetary bodies, Moors et al. conducted a study in the Dallol complex in Ethiopia. Their research revealed that specific physio-chemical parameters, such as water activity and kosmochaotropicity, play a crucial role in determining whether microbial life could thrive in a particular environment (Moors et al.).

As we explore the possibility of present or extant life beyond LEO, planetary protection (forward and backward contamination) becomes a key concern. As such, there is a need for appropriate sterilization and bioburden reduction methods, and for creating and testing (biological) indicators to validate sterilization. Kimura et al. compared various bioburden reduction techniques, such as dry heat, UV light, isopropyl alcohol (IPA), hydrogen peroxide (H_2O_2), vaporized hydrogen peroxide (VHP), and oxygen/argon plasma, and showed that dry heat is better for heat-resistant components, while VHP or plasma is recommended for non-heat-resistant components (Kimura et al.). Dean et al. investigated the use of infrared heaters to examine the survivability of heat-resistant spores, challenged the current recommended heat microbial reduction exposure of 500°C for 0.5 s and suggested a re-evaluation based on spore survival data. Stott et al. explored membrane filtration as a valid alternative to pour-plate processing as it can process larger sample volumes and reduce data variance in estimating spore bioburden on spacecraft hardware. Finally, Seto et al. explored biological indicators, specifically yeast prions, that could be used to develop, test and ultimately validate sample return mission sterilization systems, over the traditional spore-based biological indicators that are currently insufficient.

In conclusion, the research presented in this Research Topic underscores the significance of understanding fungal and bacterial biology in space environments, revealing promising pathways for leveraging their adaptability to support sustainable space exploration. However, it also emphasizes the imperative of careful consideration of planetary protection, paving the way for future experiments to advance our understanding of microbial behavior in extra-terrestrial settings.

Author contributions

CU: Writing – original draft, Writing – review & editing. DT: Writing – original draft, Writing – review & editing. RV: Writing – original draft, Writing – review & editing.

Funding

The author(s) declare that no financial support was received for the research, authorship, and/or publication of this article.

Acknowledgments

We would like to thank all contributing authors for their submissions to this Research Topic and express our appreciation to the reviewers for their valuable comments and inputs.

Conflict of interest

CU was employed by ZIN Technologies-powered by Voyager Space.

The remaining authors declare that the research was conducted in the absence of any commercial or financial relationships that could be construed as a potential conflict of interest.

Publisher's note

References

Kim, W., Tengra, F. K., Young, Z., Shong, J., Marchand, N., Chan, H. K., et al. (2013). Spaceflight promotes biofilm formation by pseudomonas aeruginosa. *PLoS ONE* 8, e62437. doi: 10.1371/journal.pone.0062437

Koehle, A. P., Brumwell, S. L., Seto, E. P., Lynch, A. M., and Urbaniak, C. (2023). Microbial applications for sustainable space exploration beyond low earth orbit. *Npj Micrograv.* 9, 47. doi: 10.1038/s41526-023-00285-0

Olsson-Francis, K., Ramkissoon, N. K., Price, A. B., Slade, D. J., Macey, M. C., and Pearson, V. K. (2018). "Chapter 2 - the study of microbial survival in extraterrestrial environments using low earth orbit and ground-based experiments," in *Methods in Microbiology*, eds. V. Gurtler, and J. T. Trevors (Cambridge, MA: Academic Press). doi: 10.1016/bs.mim.2018.07.003

Tesei, D., Jewczynko, A., Lynch, A. M., and Urbaniak, C. (2022). Understanding the complexities and changes of the astronaut microbiome for successful long-duration space missions. *Life* (Basel. Switzerland) 12, 495. doi: 10.3390/life12040495

Thombre, R. S., Kaur, K., Jagtap, S. S., Dixit, J., and Vaishampayan, P. V. (2022). "Chapter 6 - microbial life in space," in *New Frontiers in Astrobiology*, eds. R. Thombre, and P. Vaishampayan (Amsterdam: Elsevier). doi: 10.1016/B978-0-12-824162-2.00013-0

Urbaniak, C., Sielaff, A. C., Frey, K. G., Allen, J. E., Singh, N., Jaing, C., et al. (2018). Detection of antimicrobial resistance genes associated with the international space station environmental surfaces. *Sci. Rep*. 8, 814. doi: 10.1038/s41598-017-18506-4

Wilson, J. W., Ott, C. M., Honer zu Bentrup, K., Ramamurthy, R., Quick, L., Porwollik, S., et al. (2007). Space flight alters bacterial gene expression and virulence and reveals a role for global regulator Hfq. *Proc. Natl. Acad. Sci. U S A*. 104, 16299–16304. doi: 10.1073/pnas.0707155104

frontiers in Microbiology

ORIGINAL RESEARCH
published: 14 December 2021
doi: 10.3389/fmicb.2021.789668

DNA Damage Protection for Enhanced Bacterial Survival Under Simulated Low Earth Orbit Environmental Conditions in *Escherichia coli*

Jaume Puig[1,2], *Nastassia Knödlseder*[1,2], *Jaume Quera*[2,3,4], *Manuel Algara*[2,3,4] and *Marc Güell*[1,2]*

[1] Translational Synthetic Biology Laboratory, Experimental and Health Sciences Department, Universitat Pompeu Fabra, Barcelona, Spain, [2] Experimental and Health Sciences Department, Universitat Pompeu Fabra, Barcelona, Spain, [3] Radiation Oncology Department, Hospital del Mar, Parc de Salut Mar, Barcelona, Spain, [4] IMIM Hospital del Mar Medical Research Institute, Barcelona, Spain

Some organisms have shown the ability to naturally survive in extreme environments, even outer space. Some of these have natural mechanisms to resist severe DNA damage from conditions such as ionizing and non-ionizing radiation, extreme temperatures, and low pressures or vacuum. A good example can be found in *Deinococcus radiodurans*, which was exposed to severe conditions such as those listed in the Exposure Facility of the International Space Station (ISS) for up to three years. Another example are tardigrades (*Ramazzottius varieornatus*) which are some of the most resilient animals known. In this study, the survival under simulated Low earth Orbit (LEO) environmental conditions was tested in *Escherichia coli*. The radiation resistance of this bacteria was enhanced using the Dsup gene from *R. varieornatus*, and two more genes from *D. radiodurans* involved in DNA damage repair, RecA and uvrD. The enhanced survival to wide ranges of temperatures and low pressures was then tested in the new strains. This research constitutes a first step in the creation of new bacterial strains engineered to survive severe conditions and adapting existing species for their survival in remote environments, including extra-terrestrial habitats. These strains could be key for the development of environments hospitable to life and could be of use for ecological restoration and space exploration. In addition, studying the efficacy and the functioning of the DNA repair mechanisms used in this study could be beneficial for medical and life sciences engineering.

Keywords: astrobiology, DNA repair, directed molecular evolution, UV survival, radiation resistance, low pressure, outer space

OPEN ACCESS

Edited by:
Virginia Helena Albarracín, CONICET Center for Electron Microscopy (CIME), Argentina

Reviewed by:
Ivan Glaucio Paulino-Lima, Blue Marble Space Institute of Science (BMSIS), United States
Elin Moe, Universidade Nova de Lisboa, Portugal

***Correspondence:**
Marc Güell
marc.guell@upf.edu

Specialty section:
This article was submitted to Extreme Microbiology, a section of the journal Frontiers in Microbiology

Received: *05 October 2021*
Accepted: *23 November 2021*
Published: *14 December 2021*

Citation:
Puig J, Knödlseder N, Quera J, Algara M and Güell M (2021) DNA Damage Protection for Enhanced Bacterial Survival Under Simulated Low Earth Orbit Environmental Conditions in Escherichia coli. Front. Microbiol. 12:789668. doi: 10.3389/fmicb.2021.789668

1. INTRODUCTION

Microorganisms and bacteria are essential for the biosphere, persevering in a wide variety of environmental conditions, some of which could be considered "extreme." However, this definition has a strong anthropocentric criterion, since the conditions we may perceive as "extreme" are nominal and/or optimal for the growth of several species (Rothschild and Mancinelli, 2001). Furthermore, extremophilic life has constituted a large part of the evolutionary history of life, as our

understanding of the environment is based on the current planetary surface conditions on Earth, which have only occurred for a short period of time compared to the existence of life (Knoll, 2015).

Some of these resilient organisms have been isolated or tested inside and outside the International Space Station (ISS), orbiting in the Low Earth Orbit (LEO), ∼360 km above Earth's surface (Bijlani et al., 2021). This is the case of some species of tardigrades, such as *Ramazzottius varieornatus* (Jönsson et al., 2008), and bacteria such as *Deinococcus radiodurans* (Kawaguchi et al., 2020). In addition to these experiments, space agencies have stated that microbes are key to developing extra-terrestrial habitats. Microbes could be used for oxygen production (Leigh Mascarelli, 2010), fixing carbon dioxide (Callaway, 2019), etc., using the present conditions and atmosphere as a launch pad for an environment hospitable to life. This study focused on studying the possibilities behind the development of environments hospitable to life in conditions like those on the ISS or Mars by exploring the limits of life and the genetic mechanisms needed to expand those limits. This could not only have an impact on developing extra-terrestrial habitats and ecological restoration, but could also help study the potential of panspermia and microbe transfer, and the exploration of extinct and extant life.

The key to bacterial survival under harsh environments resides, among other aspects, in the cellular mechanisms of DNA protection and repair (Laval, 1996). With this aim, bacteria have developed several genetic and molecular mechanisms. Understanding and being able to enhance these existent mechanisms or introducing new genetic systems from resilient species is crucial not only for the development of bacteria capable to persevere under extreme conditions but could also benefit medical and life sciences engineering addressing treatments or diseases related to severe environments or conditions.

The conditions studied during this research included high doses of ionizing radiation in the form of X-rays, non-ionizing radiation in the form of UV fluence, high and low temperatures, low pressures, and vacuum. The base parameters used for this study were extracted from the *D. radiodurans* exposure at the Exposure Facility of the Japanese Experimental Module (JEM) of the ISS (Kawaguchi et al., 2016, 2020; Yamagishi et al., 2018) during the space mission "Tanpopo." These values were compared to those measured at the equator of Mars and on Earth's surface (**Table 1**).

Radiation in space mainly consists of two types: Solar Cosmic Radiation (SCR) and Galactic Cosmic Radiation (GCR) (Hellweg and Baumstark-Khan, 2007). The first one consists of low energy solar wind particles that constantly flow out of the Sun, and highly energetic solar particle events which originate from the magnetically disturbed regions of the Sun, which sporadically emit bursts of energetic charged particles (Wilson et al., 1999). This type of radiation varies depending on the distance from the emitter, in this case, the Sun. On the other hand, the Galactic Cosmic Radiation originates in Space beyond our Solar System. These ionizing radiation types can cause different kinds of DNA damage, including double and single strand breaks (DSBs and SSBs, respectively) (Kobayashi et al., 1995; Moeller et al., 2012) and base and sugar modifications (Shuryak and Brenner, 2010). Additionally, ultraviolet radiation exposure can also induce DSBs and SSBs, as well as other effects like pyrimidine dimerization (Horneck et al., 1984). In the last decades there has been a notable interest in understanding the mechanisms by which some bacteria, like *D. radiodurans*, can decrease the effects of long-term exposure to ionizing or UV radiation (Munteanu et al., 2015). Furthermore, many ionizing radiation-based treatments, common for example to treat some kinds of cancer, harm not only the targeted tissue, but also the surrounding area, limiting the effectiveness of these treatments and increasing their adverse effects. These issues highlight the urgent need for a better comprehension of the radiation protective mechanisms.

TABLE 1 | Measured values for the different environmental factors studied on the Exposure Facility aboard the ISS (Kawaguchi et al., 2020), the equator of Mars (Kminek and Bada, 2006; Cortesão et al., 2021), and Earth's surface (Shahbazi-Gahrouei et al., 2013; Merino et al., 2019).

Environmental factor	Exposure facility ISS *(LEO)*	Mars *(at equator)*	Earth's surface[a]
UV Fluence	124 – 177 MJ/m^2/year	∼ 50 J/m^2	-
Ionizing Radiation	232 ± 5 mGy/year	∼ 200 mGy/year	∼ 200 mGy/year
Temperature Range	29 ± 5 ∼ −42 ± 5°C	20 ∼ −73°C	495 ∼ −98.6°C [b]
Pressure Range	10^{-4} ∼ 10^{-7} Pa	500 ∼ 1000 Pa	0.1 ∼ 112 MPa

[a] *These parameters apply for all the planet, but are not specific to a certain region.*
[b] *In absence of geothermal influence, the highest surface temperature reported on Earth is ∼71°C (Mildrexler et al., 2011).*

To study the effects of ionizing radiation on cellular survival, this project follows the guidelines established by Harris et al. (2009). In this article, the authors used evolved strains of *Escherichia coli* to perform a directed evolution process that led to the increase of the surviving fraction of the different strains. The dose range of the study was replicated, with levels from 0 to 3,000 Grays (Gy), much higher than the natural environmental values on Earth, which varies depending on the specific location, being in the order of ∼200 milligrays per year (Shahbazi-Gahrouei et al., 2013). The 3,000 Gy exposure would equate to >12500 years of exposure at the Exposure Facility of the ISS and ∼15000 years on the surface of Mars. However, different aspects must be considered. On one hand, the rate at which radiation affects the cells will have a direct impact on the effectiveness of their DNA repair mechanisms. On the other hand, both the ISS and Mars are shielded from the cosmic radiation mentioned earlier, the first one by the Earth's upper layers of the atmosphere and geomagnetic field, and the second one by its own thin atmosphere, which offers a minimal protection against cosmic radiation (Berger et al., 2020). Analyzing the survival of the cells to higher radiation levels can be beneficial to understand the DNA repair mechanisms needed for space exploration, but also to study the possibility of facing harsher environments. To expose the cells to such levels of ionizing radiation, the Radiotherapy Department of Hospital del Mar allowed the use of a *Varian*

True-Beam STX® accelerator, capable of generating high-energy X-rays to reach up to 3,000 Gy. The *E. coli* cells first underwent a UV fluence and an ionizing radiation exposure, after which the surviving fractions and growth rates were studied. The exposed cells were then transformed with plasmids containing genes encoding for two proteins from *D. radiodurans*: RecA and uvrD; and one from the tardigrade *R. varieornatus*: Dsup. These genes have been studied for their roles in enhancing radiation resistance and reducing DNA damage (Kim et al., 2002; Munteanu et al., 2015; Kirke et al., 2020). RecA and uvrD, from *D. radiodurans*, both have an orthologous gene in *E. coli* with a similarity of ∼53.5 and ∼28% at an amino acid level, respectively. RecA has been studied and demonstrated to be relevant for the *D. radiodurans*'s cellular damage repair and natural radiation resistance (Kim et al., 2002; Munteanu et al., 2015). This protein has a critical role in biological processes requiring homologous DNA pairing and recombination (Roca and Cox, 1997). UvrD is also suspected of having a big impact on this radiation resistance. However, the role of this protein to the DNA repair for *D. radiodurans*'s radiation resistance is still not clear (Munteanu et al., 2015). Dsup, from the tardigrades spp. *Ramazzottius varieornatus*, has been previously studied for its DNA repair capabilities in human and plant cells (Hashimoto et al., 2016; Kirke et al., 2020), and its effect on *E. coli*'s radiation resistance was characterized during this study. Dsup is a highly charged nuclear protein which can bind to DNA and protect chromatin from hydroxyl radicals (Chavez et al., 2019), which are commonly generated by ionizing radiation. Once the bacteria were transformed with the plasmids containing the genes encoding for the mentioned proteins, a directed evolution process was performed, studying the effect of these genes on the surviving fraction of the different strains when exposed to both ionizing and UV radiation. After this process, single colonies were selected, and their individual surviving fractions were tested once more.

The temperature of a body in Space, which is determined by the absorption and emission of energy, depends on multiple factors, including the position of the body with respect to the Sun or other orbiting bodies, size, surface, etc. (Kawaguchi et al., 2013). Consequently, the temperature range varies significantly depending on the environment the cells are in. For instance, the temperature at the Exposure Facility of the ISS varies between 29 ± 5 and -42 ± 5°C (Kawaguchi et al., 2020), but at the equator of Mars, the range can go from 20 to −73°C (Cortesão et al., 2021). Moreover, high, and low temperatures can lead to molecular damage, but also to desiccation, which can induce DSBs or SSBs (Dose et al., 1992; Yang et al., 2009), ultimately causing severe DNA damage. To induce and test the temperature resistance of the exposed *E. coli* cells, the guidelines described by Takahashi et al. (2011) were followed. In this study, they described a temperature cycles experiment designed to simulate the temperature changes outside the ISS, with 90-min cycles, which is the approximate duration of a "day" aboard the ISS, in which the temperature varies from 80 to −80°C. To analyze the cellular response to continuous exposure, multiple consecutive cycles can be performed. During this study, a similar approach was performed to test the resistance of the selected strains from the ionizing and UV radiation exposure experiments.

Low pressures and vacuum have negative effects in gene expression and cellular growth (Gasset et al., 1994). Moreover, vacuum can cause cell dehydration and desiccation, which can lead to severe damage to the DNA, but also on other cell components, such as the lipid membranes, proteins, and nucleic acids (Dose et al., 1991; Cox, 1993). Due to the wide range of DNA damage that vacuum and low pressures can cause; it has been suggested that the radiation resistance of the *Deinococcus* spp. might be partially related to or a consequence of an adaptation to prolonged desiccation (Mattimore and Battista, 1996). However, this is yet to be proven. For this study, the pressure values used during the *D. radiodurans* test before its approval for the Tanpopo mission (Kawaguchi et al., 2013, 2020) and the values estimated for Mars' equator (Cortesão et al., 2021) were considered. Ultimately, due to technical limitations, the values used in this study were a little bit higher, around 7 kPa. However, these values correspond to a ∼93% vacuum and proved to have an important impact on cellular survival.

Although they are not known to cause several damages to the DNA, salinity and pH can affect the availability of water, therefore limiting the survival of microorganisms. Saline environments include a large fraction of Earth, with a range that goes from a ∼3–4% salinity in marine environments, to up to 49.7% salinity in salt inclusions (Scambelluri et al., 1997), highly influencing water activities and availability, which at its turn affects microorganism proliferation and survival. The salinity range deemed optimum for isolated microorganisms ranges between 0 and 35% (Merino et al., 2019). On the other hand, the most severe pH values in which microorganisms have been isolated are at pH 0 and pH 12.5, with an optimal pH between 0.7 and 11 for most species (Merino et al., 2019). pH has a big impact on microorganisms, affecting the ability of the cells to keep a steady neutral pH to enable cellular functions and metabolism (Krulwich et al., 2011; Jin and Kirk, 2018). In this study, the survival of the selected strains was tested for several values of salinity and pH, by means of carrying out a growth analysis. This information could help understand how microorganisms can adjust to other extra-terrestrial environments with salinity or pH values different from the ones found on the ISS facilities, such as Mars or Enceladus, which can have wide ranges of both parameters (Merino et al., 2019).

2. MATERIALS AND METHODS

2.1. Strains and Cell Culture

E. coli strain K-12 MG1655 was cultured overnight in LB medium (0.5% yeast extract, 1% peptone from casein, 1% sodium chloride) at 37°C in an incubator with shaking at 200 rpm until it reached the desired optical density (OD). When desired, cultures were supplemented with 50 μg/mL chloramphenicol. *D. radiodurans* strain R1 (ATCC 13939) was purchased from DSMZ-German Collection of Microorganisms and Cell Cultures GmbH. *D. radiodurans* was cultured overnight in medium 53 (1% peptone from casein, 0.5% yeast extract, 0.5% glucose, 0.5% sodium chloride) at 30°C in an incubator with shaking at 200 rpm until it reached the desired OD.

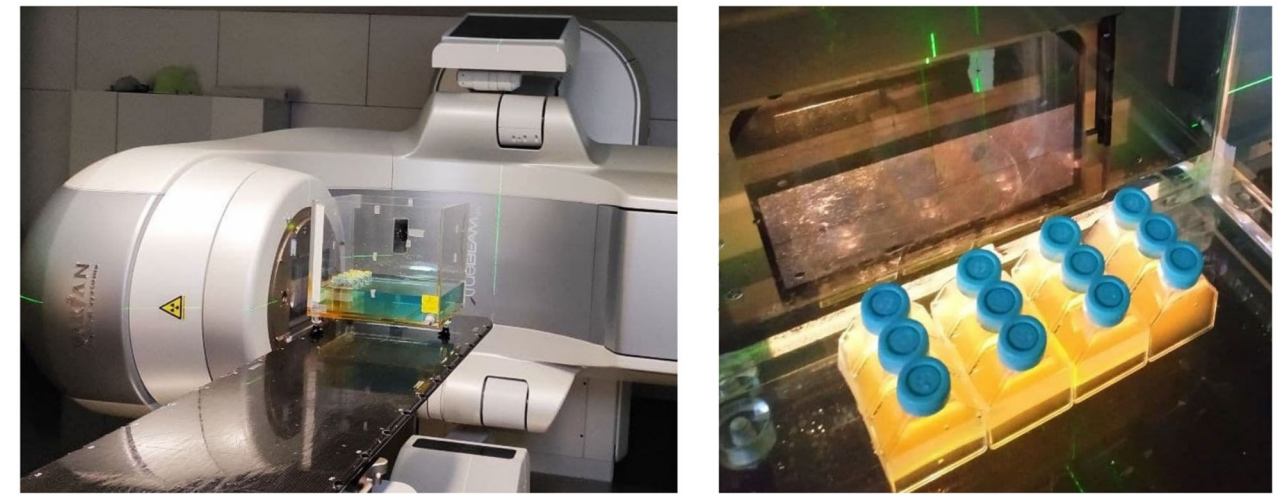

FIGURE 1 | First Ionizing Radiation exposure experiment setup, featuring the *Varian True-Beam STX*® accelerator used **(A)**, and the positioning of the flasks inside the water model at a Source-Skin Distance of 65 cm **(B)**.

2.2. Ionizing and UV Radiation Exposures

2.2.1. UV Fluence Exposure

UV Fluence exposures were performed using a *GS GENE LINKER*^{TM} *UV Chamber* (Bio-Rad). A dose of 400 mJ (∼ 5 mJ/cm^2) was used to generate mutagenesis without drastically reducing the survival rate (Shibai et al., 2017), thus increasing the efficiency of the experiment. A saturated wild-type *E. coli* culture was diluted to an Optical Density at 600 nm (OD_{600nm}) of 0.0625 and grown in a 37°C shaker for ∼1 h until it reached an exponential phase of OD_{600nm} 0.5 (Sezonov et al., 2007). The cell culture at exponential phase was then distributed to sterile Petri dishes (15 ml each) to amplify the exposed surface and avoid UV shielding during the UV Fluence exposure. The Petri dishes were exposed to 400 mJ of UV Fluence in triplicates. The cultures were then diluted up to 200 ml of fresh LB medium and grown overnight in a 37°C shaker until culture saturation.

2.2.2. Ionizing Radiation Exposure

After 18–20 h, the 200 ml saturated culture was again diluted to an OD_{600nm} of 0.0625 and incubated in a 37°C shaker for an additional hour until it reached an exponential growth phase with an OD_{600nm} of 0.5. The culture was then distributed in 13 cell culture flasks (65 ml each), one per intended IR dose. A *Varian True-Beam STX*® accelerator was then used to expose the cells to a continuous spectrum of X-ray photons produced by a potential accelerator of 6 MeV (**Figure 1**). The studied doses were set between 0 and 3,000 Gy in steps of 250 Gy, at a dose rate of 12.6 Gy per minute and with an overall estimated error of the absorbed dose of 3.6%. During the exposure, a flask was extracted per each dose, substituting it by a flask filled with water to maintain the dose homogeneity. The survival rates were then studied following the guidelines described in the Data Acquisition Analysis section. The surviving cultures were stored at –80°C.

2.2.3. Inducible Plasmid Construction and Transformation

To amplify RecA and UvrR genes of *D. radiodurans*, genomic DNA was extracted by using *Bacterial Genomic DNA Isolation Kit* (Norgen Biotek Corp.) from the wild-type strain following manufacturer's instructions. Genes were amplified using *KAPA HiFi HotStart ReadyMix* (Roche) and primer pair *RecA_SpeI_fwd* and *RecA_PstI_rev*, and *uvrD_SpeI_fwd* and *uvrD_PstI_rev* (**Supplementary Table S1**) from *D. radiodurans* genomic DNA to add SpeI and PstI restriction sites. The Dsup gene was amplified with primer pair *Dsup_XbaI_fwd* and *Dsup_SpeI_rev* from plasmid pCXN2KS-Dsup (Addgene), (Hashimoto et al., 2016) to add XbaI and SpeI restriction sites. In summary, the PCR mix was prepared by mixing 50 ng template DNA, 0.3 μM of each primer, 12.5 μl of *KAPA HiFi HotStart ReadyMix* and H_2O to a final volume of 25 μl. The cycling protocol was run as followed: Initial denaturation for 3 min at 95°C followed by 25 cycles of 98°C for 20 s, 61°C for 15 s, and 72°C for 2 min; and a final elongation for 2 min at 72°C. PCR products were column purified using the *QIAQuick PCR purification kit* (Qiagen). One microgram of purified DNA coding for uvrD, RecA or Dsup were subsequently digested for 1 h with either PstI, XbaI or SpeI (NEB) as required. Plasmid pSB1AC3 was digested first with EcoRI and XbaI to insert the arabinose inducible promoter pBAD/araC (iGEM Registry of Biological Parts code BBa_I0500), which was previously amplified to add EcoRI and XbaI restriction sites using the primer pair *pAra_EcorI_fwd* and *pAra_XbaI_rev* (**Supplementary Table S1**). Digested pSB1AC3 and digested pBAD/araC were ligated using T4 DNA Ligase (NEB). The cloning was checked using colony PCR and sequencing. In a second step, the newly acquired plasmid pSB1AC3-pBAD/araC was digested with XbaI (Dsup), SpeI (RecA, UvrD) and PstI (Dsup, RecA, UvrD) restriction enzymes depending on the gene to be inserted. Then, the previously digested genes RecA, UvrD,

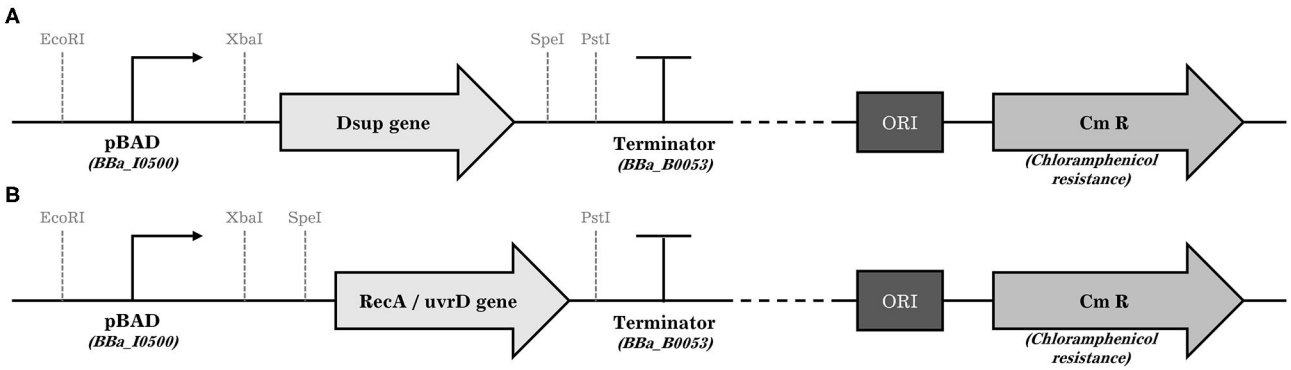

FIGURE 2 | General schemes of the plasmids introduced to the surviving cells. The position of the restriction sites in the case of the Dsup gene **(A)** and the RecA and uvrD genes **(B)**, promoter, gene of interest, terminator, the origin of replication, and the chloramphenicol resistance gene is shown.

and Dsup were cloned downstream of the arabinose inducible promoter resulting in the final plasmids pSB1AC3-pBAD/araC-RecA, pSB1AC3-pBAD/araC- UvrD, and pSB1AC3-pBAD/araC-Dsup (**Figure 2**). The complete plasmids were then verified using colony PCR and sequencing.

Five milliliters of surviving cells from the first IR exposure were grown overnight in a 37°C shaker until culture saturation and grown to an OD_{600nm} of ∼0.4. Competent cells were prepared by washing the cells three times with ice-cold sterile distilled water, and finally resuspended in ice-cold sterile 10% glycerol. The electrocompetent cells were transformed with the plasmids containing one of the three genes through a 2.5 kV pulse using a *Gene Pulser Xcell*^{TM} (Bio-Rad) and plated on LB plates supplemented with 50 μg/mL chloramphenicol and incubated overnight at 37°C. All colonies were picked for the following experiments minimizing the loss of population variability. The cells were inoculated in 50 ml of fresh LB medium supplemented with 50 μg/mL chloramphenicol and grown in a 37°C shaker until culture saturation.

2.2.4. RNA Extraction and qPCR Analysis

Bacterial o/n cultures of *E. coli* RecA, uvrD, Dsup, and a wild-type control were diluted to a starting OD_{600nm} of 0.0625 in duplicates per sample and induced by adding 1.32 μl/ml of arabinose. After reaching an exponential phase culture, bacteria were pelleted, resuspended in 1 mL LB medium and 2 mL *RNAprotect Bacteria Reagent* (Qiagen) was added to each sample. RNA was extracted using *miRNeasy mini kit* (Qiagen) following manufacturer's instructions with some modifications. Bacterial pellet was resuspended with Trizol reagent (Qiagen), and then subjected to 45 s of bead lysis using *FastPrep FP120* at speed 6.5. Additionally, an on-column DNase digest was performed. RNA was eluted in 30 ul nuclease free H_20. RNA concentration was quantified using a *Nanodrop One* spectrometer and 2 μg of RNA was used from each sample to synthesize cDNA by reverse transcription using a *High-Capacity cDNA Reverse Transcription Kit* (Applied Biosystems) following manufacturer's instructions. The obtained cDNA was diluted 20 times whereof 4 μl were used per reaction. Each reaction was supplemented with 6 ul of Mix containing 5 μl *PowerUp SYBR green MasterMix* (Applied Biosystems) complemented with 0.5 μl (500 nM) of each primer fwd and rev. qPCR was performed in three technical replicates using dedicated primers against each gene and an endogenous control targeting the *E. coli* RecA gene. All primers can be found in the **Supplementary Table S2**.

2.2.5. Directed Evolution Process

The saturated 50 ml cultures from the *E. coli* strains wild-type K-12, an exposed control, RecA, uvrD, and Dsup producing strains were exposed to Ionizing Radiation up to 3,000 Gy by following the same guidelines as in the previous exposure, diluting the cultures up to 300 ml each and incubating them until they reached an exponential growth phase. When diluted, the cultures were induced with 1.32 μl/ml of arabinose to activate the expression of the genes encoding RecA, UvrD and Dsup (Gonzalez-Flo et al., 2020). However, due to space restrictions and to maintain dose homogeneity, the studied doses were reduced to 0, 500, 1,500 and 3,000 Gy, at a dose rate of 12.6 Gy per minute. Besides, due to technical constraints, between the 500 and the 1,500 doses, a pause of 20–30 min was done. The cells were exposed up to two times, studying the impact and efficacy of the gene products, as well as the response of the cell strains to a continuous exposure to high levels of Ionizing Radiation. During the second exposure, a wild-type *D. radiodurans* culture in an exponential growth phase was also exposed. In each exposure, the surviving fraction was obtained following the guidelines described in the Data Acquisition Analysis section.

2.2.6. Colony Selection

Following the last Ionizing Radiation exposure, the growth of a total of 138 colonies was analyzed, both with and without a previous exposure to 400 mJ of UV Fluence. This exposure was performed following the guidelines established in the previous UV exposure, without inducing the genes. The analyzed colonies were 12 from the wild-type *E. coli* strain, 6 from the UV-exposed *E. coli*, 12 from the control strain, 26 from the RecA strain, 30 from the uvrD strain and 52 from the Dsup strain. The growth rate analysis was studied using an *Infinite M NANO+*

Plate-Reader (TECAN) to measure the OD at 600 nm, starting with an $OD_{600nm} < 0.1$. From the data obtained, the best performing colonies of the RecA (1), uvrD (1), and Dsup (3) strains were selected.

2.2.7. Final Ionizing and UV Radiation Survival Tests

The three selected colonies of the Dsup strain, which had the biggest survival rates in the previous radiation exposures, were exposed a fourth time to study the final Ionizing Radiation resistance of these strains. The exposure was done following the guidelines of the previous exposures, but only exposing to 0 and 500 Gy. The exposed samples included the three colonies, strains C15, C16, and C17, and the surviving population from the last IR exposure.

To test the UV Fluence survival of the new *E. coli* strains, a culture of each strain including the selected colonies, the populations and the wild-types *E. coli* K-12 and *D. radiodurans* were inoculated and grown overnight at 37 or 30°C, respectively. The cultures were then diluted to an OD_{600nm} of 0.0625, induced with 1.32 μl/ml of arabinose, and grown until an exponential growth phase. The cultures were transferred to sterile Petri dishes and exposed to different doses of UV Fluence using a *GS GENE LINKER™ UV Chamber* (Bio-Rad), exposing the cells to up to 785 mJ ($\sim$ 10 mJ/cm^2), which corresponds to a $\sim$ 30% of the UV Fluence on the ISS Exposure Facility per minute. This value was selected according to the technical limitations and was considered when analyzing the survival results. The surviving fraction was then obtained following the guidelines described in the Data Acquisition Analysis section.

2.2.8. Whole Genome Sequencing and Analysis

From the selected colonies for the RecA, uvrD and Dsup strains, a gDNA extraction was performed using the *Bacterial Genomic DNA Isolation Kit* (Norgen Biotek Corp.). Whole Genome Sequencing (WGS) of the colonies was then conducted by the *Microbial Genome Sequencing Center* (Pittsburgh, PA) and the sequences were compared with the wild-type genome of *E. coli* K-12 MG1655. The analysis was done using the *breseq* software from Barrick Lab (The University of Texas at Austin, 2014) (Deatherage and Barrick, 2014).

2.3. Low Pressure and Temperature Exposure

2.3.1. Low Pressure and Vacuum Simulation

The low-pressure conditions were achieved by using a desiccator coupled to a vacuum pump applying a negative pressure of –700 mmHg, exposing the cells to a pressure around 7 kPa. The cells were grown overnight in a 37 or 30°C shaker according to their optimal growth temperature. The RecA, uvrD, and Dsup strains were grown with and without inducing the genes. After 18–20 h of growth, the OD_{600nm} was measured to be around 1, and the cultures were distributed in 1 ml tubes. Two tubes were prepared by strain, one was left as a liquid culture, and the other was centrifuged at 10,000 ×g and pelleted, removing the supernatant and drying the pellet. After the sample preparation, the tubes spent 0, 3 or 7 days in the desiccator at a pressure $\sim$7 kPa, after which they were prepared for the temperature cycles experiment.

2.3.2. Temperature Cycles Simulation

Following the guidelines established by Takahashi et al. (2011), the temperature cycles experiment was designed to reach from 50 to –80°C in 90 min cycles, simulating each temperature using a thermal bath and a freezer respectively. Each cycle consisted of cooling the cells at –80°C for 20 min, leaving them at room temperature for 25 min, heating up to 50°C for 20 min and finally leaving them at room temperature for an additional 25 min. For each low-pressure sample, 0, 1, and 3 temperature cycles were performed, performing up to 5 temperature cycles in the case of the 7 days low pressure exposure. After the completion of their respective low pressure and temperature cycles exposures, the surviving fraction was obtained following the guidelines described in the Data Acquisition Analysis section.

To study the temperature variation of the samples during each cycle, Newton's law of cooling was used, calculating the proportionality constant k experimentally. The resulting plot in **Figure 3** shows how the temperature varied over time during each cycle.

2.4. Salinity and pH Cultures

The growth of the selected colonies from the RecA, uvrD, and Dsup strains, as well as wild-type *E. coli* were tested when different salinity and pH conditions were present on the media. An *Infinite M NANO+* Plate-Reader (TECAN) was used to measure the OD_{600nm} of the liquid cultures during >20 h, studying their growth rates. The cultures were grown overnight in a 37 or 30°C shaker according to their optimal growth temperature and were then used to inoculate 200 μl of fresh LB media with the different pH or salinity conditions in a 96-well plate, which was then used for the OD_{600nm} measurements. The Plate-Reader was set at 37°C with shaking, and the OD_{600nm} was measured every 10 min for >20 h.

The LB media was prepared with different concentrations of salt, ranging from 0 to a 57% of NaCl with respect to the rest of the media ingredients, or pH, with values between 3 and 11, using HCl and NaOH to compensate the acidity and alkalinity until the desired pH values were reached.

2.5. Data Acquisition and Analysis

The surviving fraction of the exposed cultures for the different conditions studied was calculated by the Colony-Forming Units (CFU) of each exposed culture. The cultures were first serially diluted up to 10^{-6} and nine drops of 5 μl per each dilution were placed in three separate LB agar plates to have triplicates. The surviving fraction of each strain was calculated from the titer of the surviving population, which was calculated from the CFU of the culture one day after the exposure, divided by the titer of the non-exposed culture, the control dose. The errors were also calculated from this data, dividing the standard deviation by the square root of the number of drops counted per sample.

In the Ionizing Radiation exposures, the linear-quadratic model was used to study the surviving fractions (Brenner et al., 1998). The model, seen in Equation (1), was fitted to the experimental data using Python programming language and the Lethal Doses for the 90% of the population (LD10) were calculated.

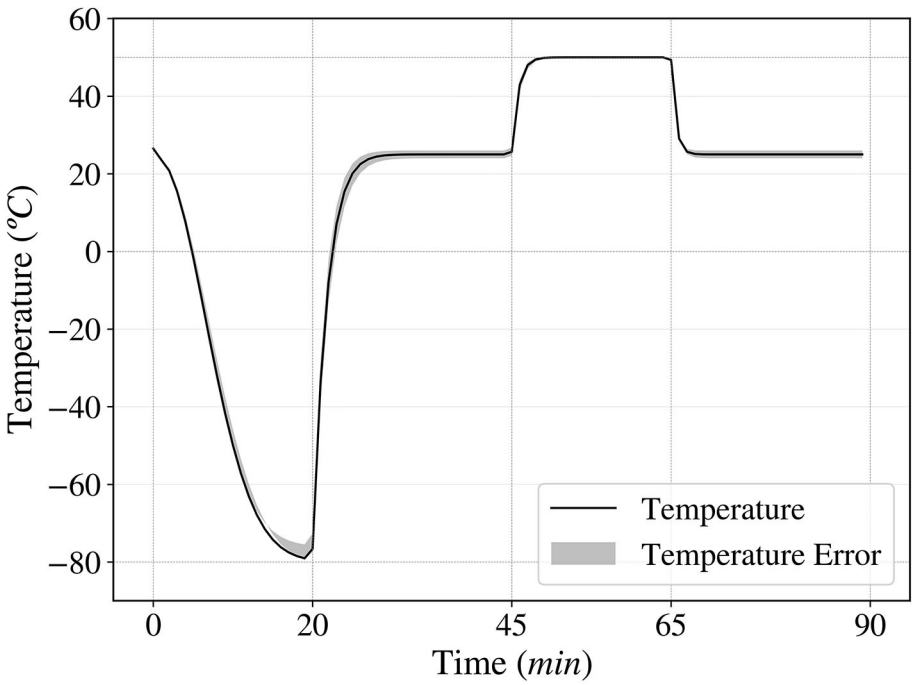

FIGURE 3 | Temperature fluctuation over time in one cycle, ranging from –80 to 50°C. A complete cycle consists of 20 min at –80°C, 25 min at room temperature, 20 min at 50°C and 25 min at room temperature.

$$S(D) = e^{-\alpha D - \beta D^2} \quad (1)$$

3. RESULTS

3.1. Enhancing Ionizing Radiation Resistance

Ionizing Radiation can cause different kinds of DNA damage, including DSBs and SSBs (Kobayashi et al., 1995; Moeller et al., 2012), base and sugar modifications (Shuryak and Brenner, 2010), etc. In addition, non-ionizing radiation such as ultraviolet can also induce such effects, like pyrimidine dimerization (Horneck et al., 1984). Protecting the DNA against this damage and repairing it is the key to enhancing the resistance to radiation exposures. To determine the survival of wild-type *Escherichia coli* to ionizing radiation, random mutagenesis was induced, and the cells were exposed to X-rays. These exposures showed an increase in survival in more than one and a half orders of magnitude when previously exposed to UV fluence compared to the wild-type control (**Figure 4**). The data obtained was fitted to a linear-quadratic model, used to simulate cellular survival when exposed to radiation (Brenner et al., 1998). The fitted data showed a good correlation between the experimental points and the mathematical model (**Figure 4**).

After being transformed with the genes encoding for RecA, uvrD, and Dsup, the cells were then exposed twice to Ionizing Radiation, studying the surviving fraction after each exposure and analyzing the progress obtained with the different genes. In **Figure 5**, the surviving fractions of the different strains for the second (A) and third (B) X-ray exposure are shown. While the control and the RecA strain decreased their survival, uvrD had a similar survival as the wild-type. The Dsup strain increased the survival in more than 2 orders of magnitude with respect to the wild-type in the 3,000 Gy dose, increasing progressively throughout the exposures. *D. radiodurans* obtained a very high survival rate at 3,000 Gy.

This data was fitted using the linear-quadratic model, and the Lethal Dose that would kill 90% of the population (LD10) was calculated for the three evolved strains and the wild-type control. The Dsup strain had a LD10 around 1.68 kGy, while the wild-type and the uvrD strains were both around 1.09 kGy. The RecA strain obtained the worst results, with a LD10 of $\sim$ 0.98 kGy.

After selecting single colonies from the RecA, uvrD, and Dsup strains, the colonies selected from the Dsup strain were exposed to Ionizing Radiation up to 500 Gy, analyzing the survival of the colonies and the population. After this exposure (**Figure 6**), some colonies showed better results, but all significantly increased the survival with respect to the wild-type *E. coli*. Dsup C16 strain had the best performance, with almost a total cellular survival after the 500 Gy exposure.

The *E. coli* and *D. radiodurans* wild-types, together with the RecA, uvrD, and Dsup strain populations and single colonies were finally exposed to UV Fluence up to 785 mJ ($\sim$ 10 mJ/cm^2, **Figure 7**). The results showed a similar survival between the *E. coli* and *D. radiodurans* wild-types. The rest of the *E. coli* strains also showed similar survivals, with no relevant increase or decrease in any case.

The Whole Genome Sequencing (WGS) and analysis performed for a total of 5 colonies from the *E. coli* strains RecA (1), uvrD (1), and Dsup (3), which can be seen in the **Supplementary Table S2**, revealed more differences in the DNA

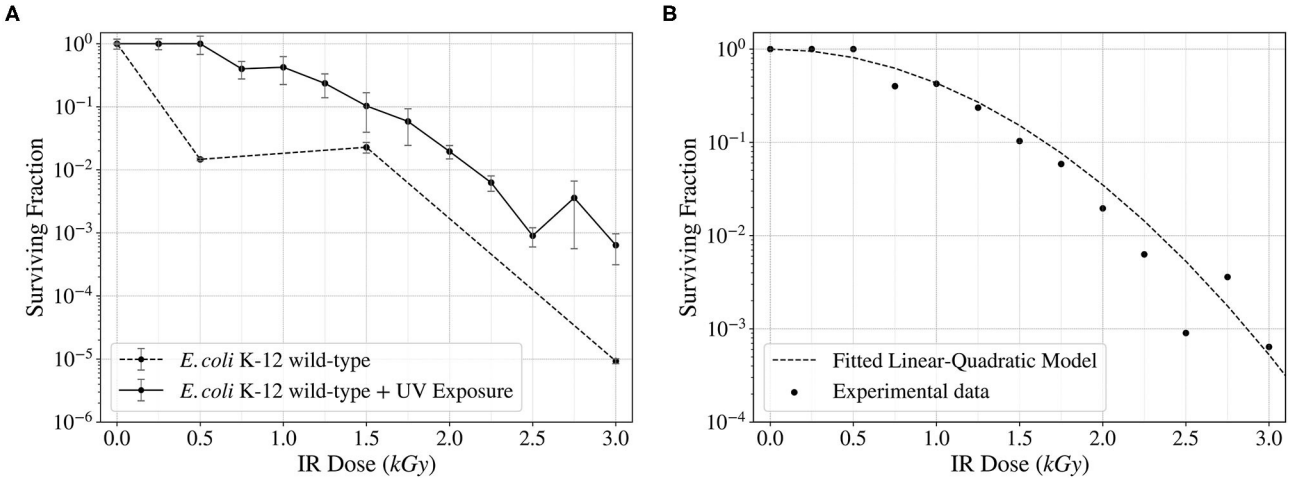

FIGURE 4 | Surviving fraction of wild-type *E. coli* K-12 cells after being exposed to a continuous spectrum of X-rays (Ionizing Radiation) up to 3,000 Gy (12.6 Gy/min). Comparison of the surviving fraction with and without a previous UV Fluence exposure **(A)** and fitted linear-quadratic model showing the trend of the surviving frequency **(B)**.

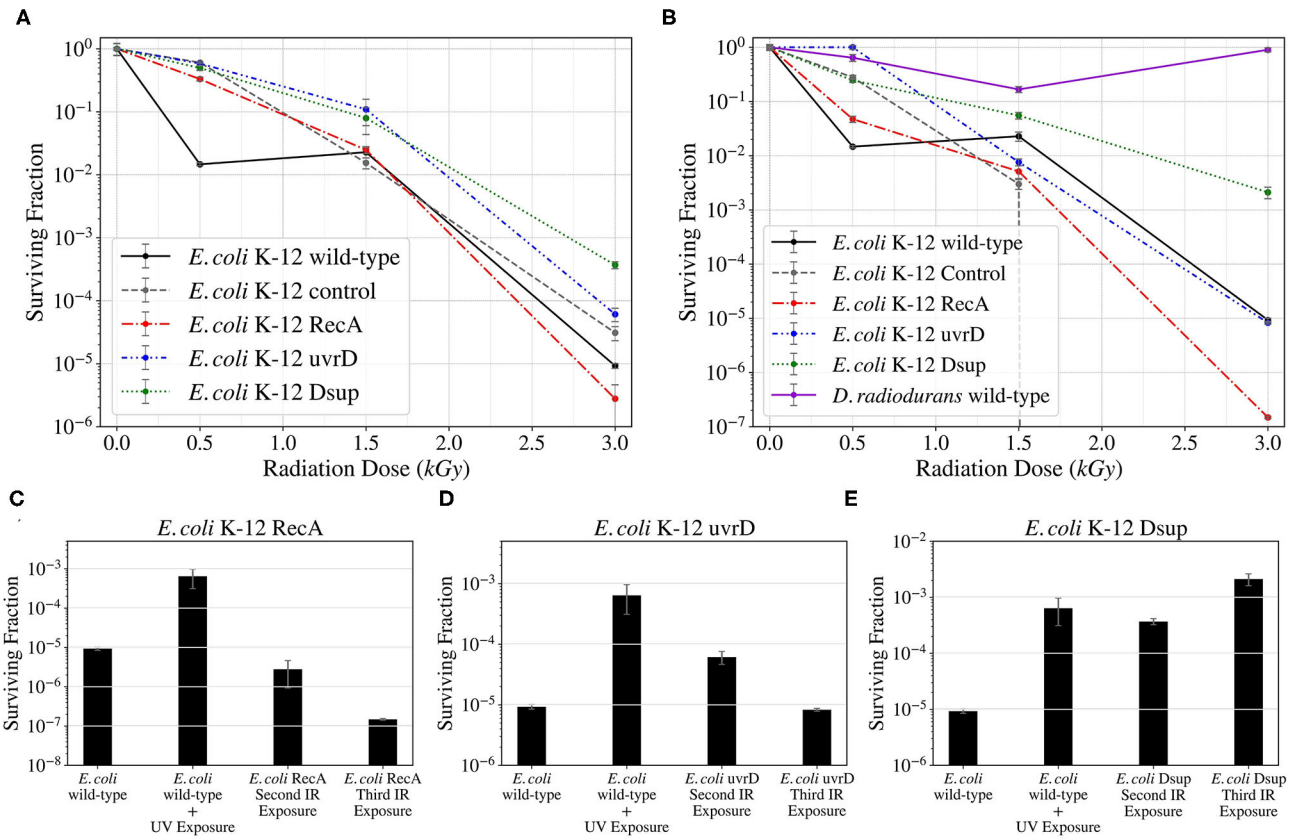

FIGURE 5 | Survival curves for the different *E. coli* strains and *D. radiodurans* for the second **(A)** and third **(B)** Ionizing Radiation exposures as part of the directed evolution process; and progress bars of the survival of the RecA **(C)**, uvrD **(D)**, and Dsup **(E)** strains through the different Ionizing Radiation exposures.

repair efficiency of the three genes, with Dsup showing a very high efficacy and the C15 strain having no relevant genetic mutations with respect to the wild-type control. uvrD showed the lowest impact on preventing DNA damage, with a higher number of mutations than the other strains. From the sequencing results obtained, no relevant mutations can be seen that could

unequivocally explain an increase in survival under high levels of radiation.

3.2. Vacuum and Temperature Testing

Vacuum and high and low temperatures can lead to desiccation, causing severe damage to the DNA, such as DSBs and SSBs (Dose et al., 1992; Yang et al., 2009), but also to other cell components (Dose et al., 1991). Before exposing the cells to a series of temperature cycles from –80 to 50°C in 90 min, the cells were either exposed to 0, 3, or 7 days to low pressures in the order of 7 kPa. In this study, the effect of cellular aggregation to enhance survival was tested, exposing the cultures both pelleted and non-pelleted. As shown in **Figure 8**, in the case of *D. radiodurans* (B), cell aggregation had a big impact on survival, with an increase of the surviving fraction when the culture was pelleted. However, in the case of *E. coli* (A), cell aggregation did not have a significant impact on the surviving fraction, with a little increase of survival in the case of the pelleted culture.

When studying the survival of the wild-type *E. coli* and the selected colonies from the RecA, uvrD, and Dsup strains to the different low-pressure exposures and temperature cycles (**Figure 9**); the wild-type had the highest survival in the three cases. However, for the RecA, uvrD, and Dsup strains the overall survival depended on the low-pressure exposure times, with better survival after the 3-day exposure than the 0 or the 7 days. The three strains had similar surviving fractions, with no relevant improvement in cellular survival for the tested conditions.

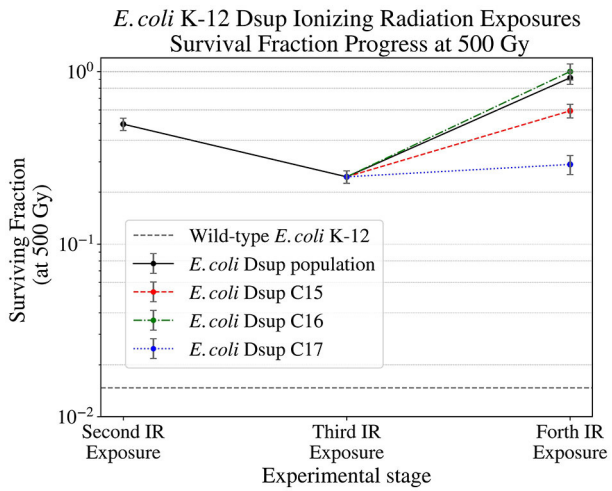

FIGURE 6 | Surviving fraction of the *E. coli* Dsup strain at 500 Gy (12.6 Gy/min) during the second, third, and final Ionizing Radiation exposures, showing the progress on the survival of this strain and its selected colonies.

3.3. Salinity and pH Testing

Salinity and pH can have a big impact on the growth and survival of cells, mainly affecting the availability of water, and therefore cellular metabolism. The strains obtained during the previous experiments were tested in different salt concentrations and pH values to study their growth in these conditions.

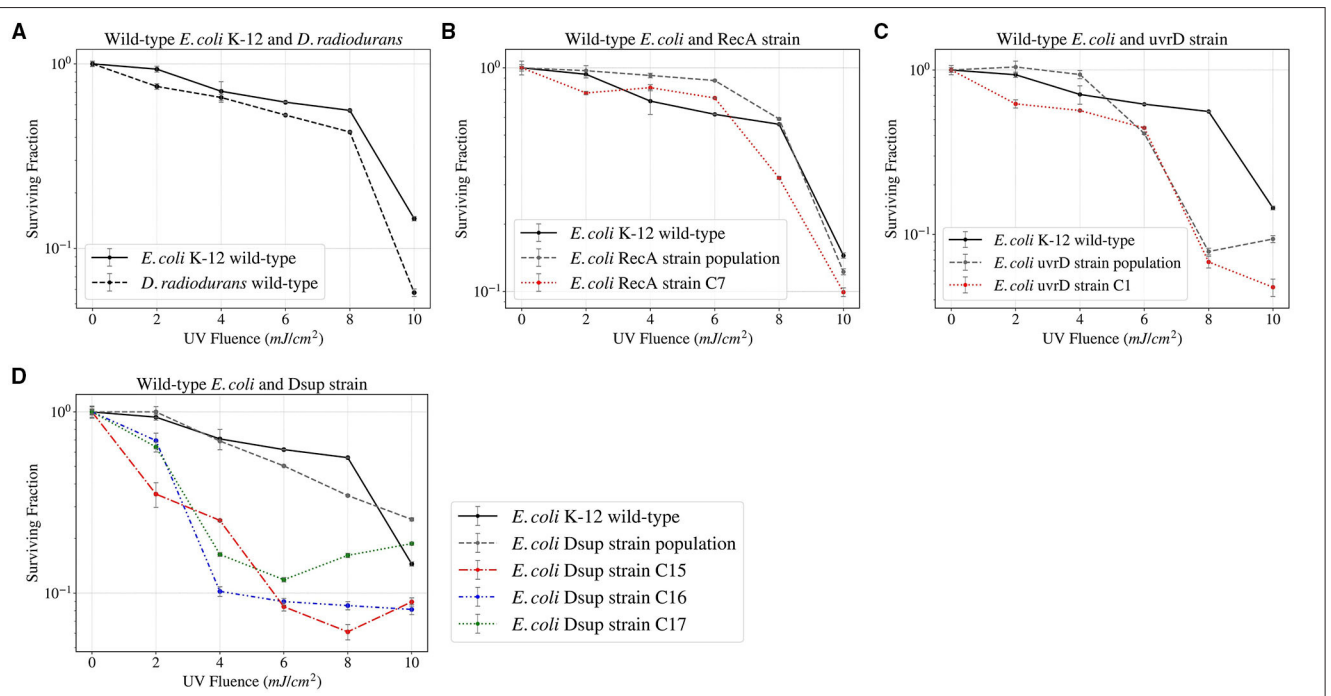

FIGURE 7 | Survival curves of the different *E. coli* and *D. radiodurans* strains after UV Fluence exposure up to 785 mJ.

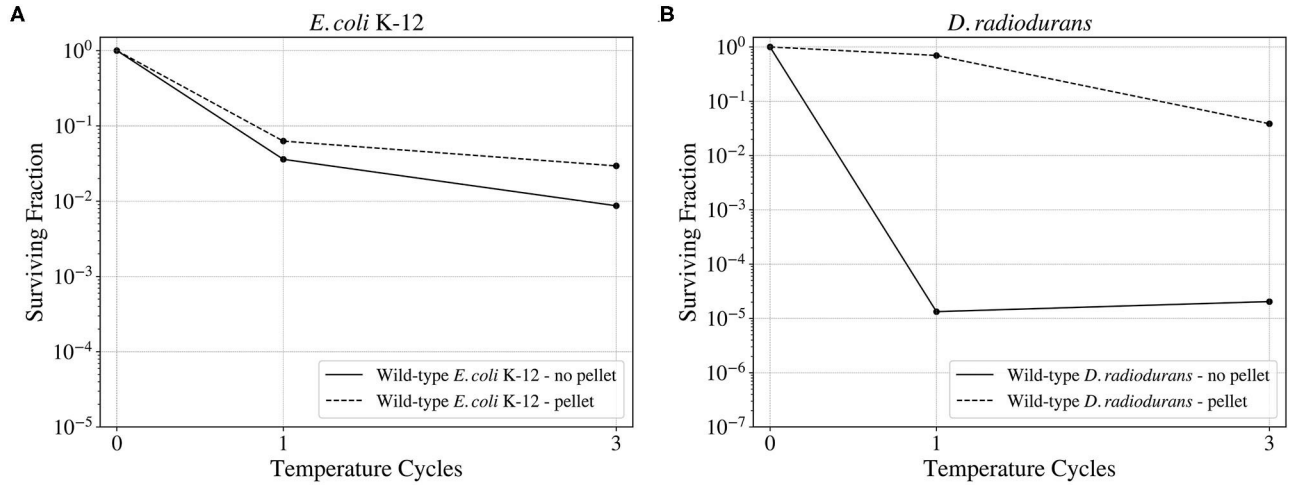

FIGURE 8 | Surviving fraction of the wild-type *E. coli* K-12 cells **(A)** and *D. radiodurans* **(B)** after a 3-day exposure to a ∼93% vacuum and 3 temperature cycles from –80 to 50°C. Comparison between the survival of the aggregated and the non-aggregated cultures.

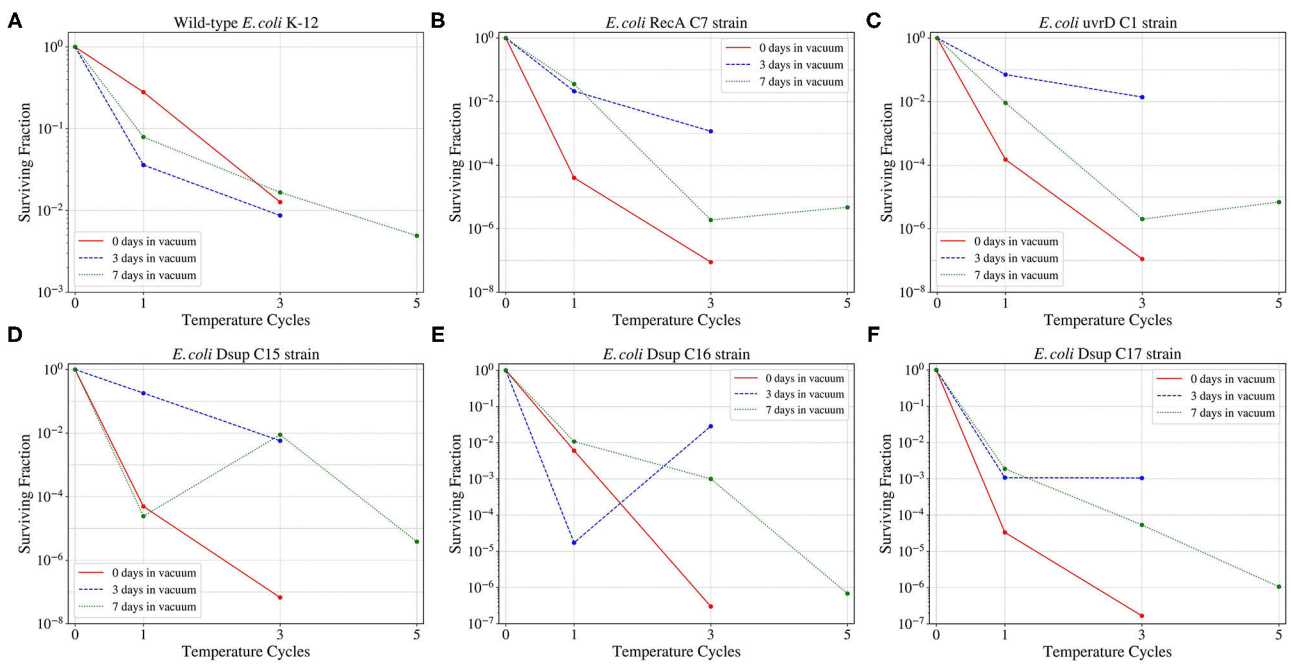

FIGURE 9 | Survival of the wild-type *E. coli* K-12 strain **(A)** and the different RecA **(B)**, uvrD **(C)**, and Dsup **(D–F)** selected colonies to the temperature cycles from –80 to 50°C after 0, 3, 7 days exposures to a ∼93% vacuum.

The salinity growth rate analysis (**Figure 10**) revealed that all the different strains tested could persevere and survive for all the conditions, therefore the known limits for these strains would be from 0 to 20 g per liter of LB media. The results were very similar between the different strains, with a faster growth for salinity around 5 g/l and slight variations for the rest of concentrations. In general, the Dsup strains showed a faster growth in most of the salinity conditions, with a small difference with respect to the rest of the tested strains.

The pH growth analysis (**Figure 11**) revealed the importance of a neutral pH for cellular growth, with no growth for the pH values 3 or 11 for any of the tested strains. For pH values between 5 and 9, all the strains were able to grow, with a slower growth in the case of the RecA strain. The rest of the strains showed similar results, with a faster growth at pH 7. In all the cases, growth with

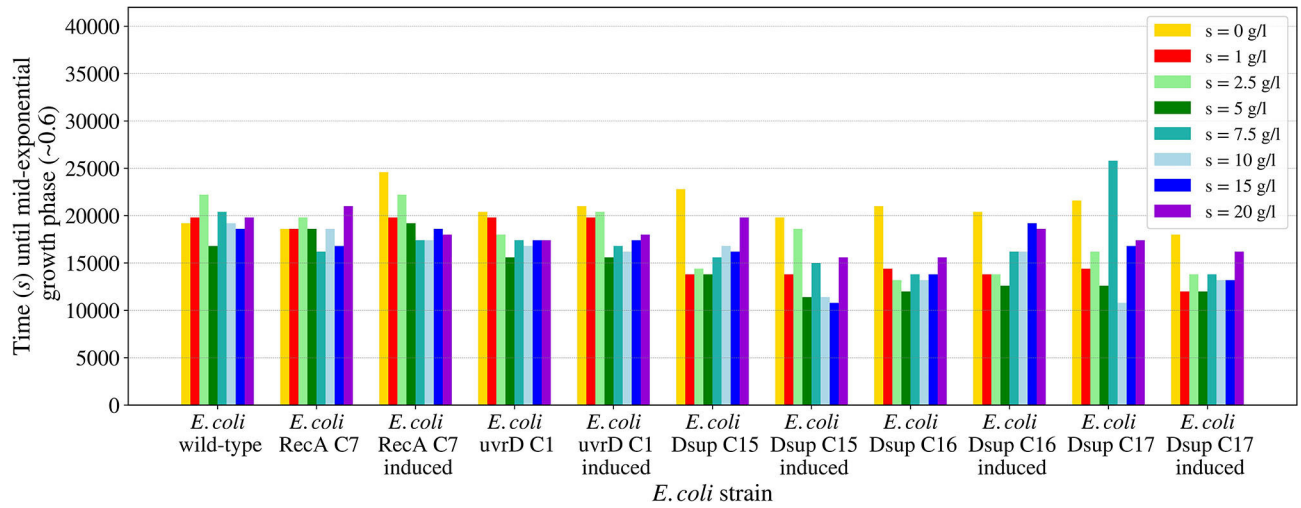

FIGURE 10 | Time needed for the *E. coli* wild-type and the selected colonies of the RecA, uvrD, and Dsup strains to reach mid-exponential growth phase (OD_{600nm} ~0.6) when inoculated in LB media with different salinities. The effects of the gene products were tested with and without induction to detect any possible effects on cellular growth.

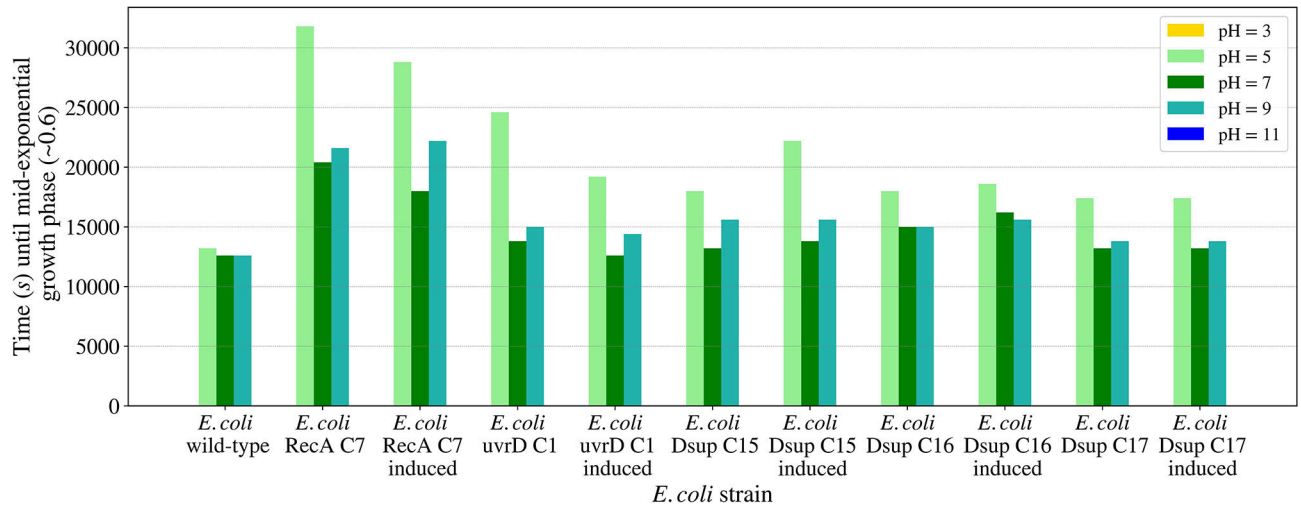

FIGURE 11 | Time needed for the *E. coli* wild-type and the selected colonies of the RecA, uvrD, and Dsup strains to reach mid-exponential growth phase (OD_{600nm} ~0.6) when inoculated in LB media with different pH values. The effects of the gene products were tested with and without induction to detect any possible effects on cellular growth.

pH 5 was slower than pH 9, showing a bigger effect of acid pH values to cellular growth.

4. DISCUSSION

The initial ionizing and non-ionizing radiation exposures showed an increased survival when a first exposure to UV fluence was performed compared to a lack of the non-ionizing radiation exposure. This increase, which was of about 1.5 orders of magnitude with respect to the non-irradiated wild-type control, may be attributed to the mutagenesis and phenotypic adaptation generated by this exposure, but also to the filtering of the most vulnerable cells. The survival curve was fitted using a linear-quadratic model, and the experimental data followed the model as expected. Despite that, this increase was not maintained after selecting the surviving fraction, as can be seen in the control samples in **Figure 5**.

The different *E. coli* strains transformed with a plasmid containing one of the *D. radiodurans* or *R. varieornatus* genes revealed a big difference in the efficacies of the gene products in *E. coli*, as well as a big variation in the surviving fraction. This variability can be seen in **Figure 5**. The strain containing the RecA gene, from *D. radiodurans*, showed a progressive

decrease in the surviving fraction. The strain containing the uvrD gene, from *D. radiodurans*, showed similar survival values to those obtained with the wild-type *E. coli* K-12. These lack or detrimental effects could be due to the interference with the orthologous gene of *E. coli*, with which they have a 53.5 and a 28% of similarity in an aminoacid level respectively. RecA is a central enzyme of DNA repair, and has been transplanted from pseudomonas to *E. coli* affecting DNA repair capacity (Baitin et al., 2006). However, the case of *D. radiodurans*, a more phylogenetically distant species, may be more complex. Indeed, it has been shown recently that in order to transfer effectively recombinogenic properties further modifications are required. For instance, compatible pairs of recombinases (phage origin in this case) and single stranded binding proteins (SSB) were required (Filsinger et al., 2021). RecA has a very close and dynamic relationship with SSB, displacement of the latter is modulated by RecA C-terminal (Eggler et al., 2003). *D. radiodurans* has a very unusual SSB which is twice the size and acts as a dimer instead of the classical tetramer (Ngo et al., 2013). Future plans of this project will include co-transformation with *D. radiodurans* RecA together with SSB. Unlike in *E. coli*, uvrD has a key role in *D. radiodurans*. Again, uvrD activity is strongly modulated by SSB (Stelter et al., 2013). Future work, will also include co-transformation with this protein. The Dsup gene, from *R. varieornatus*, showed an increase in more than two orders of magnitude in the surviving fraction, effectively enhancing *E. coli*'s resistance to radiation exposure after 3 X-rays exposures. The experimental data was fitted to a linear-quadratic model, allowing the full characterization of the survival throughout the dose span tested, but also the calculation of the Lethal Doses, after which 90% of the cells died (LD10). The LD10 of the wild-type *E. coli* was $\sim$ 1.09 kGy, while for the Dsup strain, the LD10 after the three X-rays exposures was $\sim$ 1.68 kGy, increasing in almost 600 Gy. In the case of the RecA strain, the LD10 was $\sim$ 0.98 kGy, lower than the one for the wild-type. The uvrD strain had a LD10 similar to the one for the wild-type *E. coli*. These values confirm the significant enhancement of the survival for the Dsup strain with respect to the wild-type, proving the capacity of the Dsup protein to protect the DNA from the hydroxyl radicals that can be caused by the exposure to X-rays and the corresponding effect on cellular survival.

A final test of the surviving fraction of three selected colonies and the population of the Dsup strain when exposed to X-rays up to 500 Gy showed an almost total survival for this dose in one of the colonies and a generalized increase in the survival throughout the different ionizing radiation exposures (**Figure 6**). The 500 Gy exposure would equate to $\sim$ 2500 years of exposure on the Exposure Facility of the ISS. Furthermore, increasing the time span until the same dosage is reached could have a direct positive impact on cell survival, allowing the DNA repair mechanisms to act with higher effectiveness. The Whole Genome Sequencing (WGS) results showed a higher efficiency of the Dsup gene in DNA protection, with similar results for the RecA colony, whereas the uvrD gene showed the lowest efficiency. The UV exposure survival analysis revealed similar results for all the different strains and a higher surviving fraction in the case of wild-type *E. coli* when compared to *D. radiodurans*. This UV fluence exposure reached $\sim$ 30% of the UV fluence observed on the Exposure Facility of the ISS per minute, so further exposures to higher doses could be done in order to analyze the limitations of the new strains.

A further prolongation of the directed evolution process by adding additional cycles and even exposing the cells to higher doses of ionizing radiation or changing the dose rate could lead to an improvement of the surviving fraction of the *E. coli* Dsup strain. In addition, X-rays were chosen due to their high energy and penetration capacities, but exposing the cells to ionizing radiation types such as gamma or neutron radiation could be important to test the survival of the cells under LEO environmental conditions. Higher UV doses could also be tested to further examine the limits of the strains developed during the study.

The vacuum and pressure tests revealed the insignificance of cell aggregation for *E. coli*'s survival. While *D. radiodurans* showed an increase in the surviving fraction after being aggregated of approximately 3 orders of magnitude with respect to the non-aggregated sample, *E. coli*'s survival showed no significant variation with or without aggregation after spending 3 days at 7 kPa and being exposed to three temperature cycles. These results are consistent with the rest of the temperature and pressure conditions tested for *E. coli* and *D.radiodurans* wild-types.

With respect to the effects of the cells transformed with the genes encoding for RecA, uvrD, and Dsup, the surviving fraction decreased for all the selected colonies of the different *E. coli* transformed strains in comparison with the wild-type *E. coli*, with similar values and responses. The exposure of the cells to 3 days under 7 kPa showed the best survival results, with lower surviving fractions for cells exposed to the temperature cycles after 0 or 7 days under 7 kPa of pressure. These results could be due to the activation of the DNA repair mechanisms during the vacuum exposure and being already active during the beginning of the temperature cycles. However, after a longer period of vacuum exposure, the DNA repair mechanisms start to lose their effectiveness.

To further study the limitations of the studied strains, as well as other bacteria, directed evolution processes could be applied to enhance the survival of the cells to vacuum or high/low temperatures. Moreover, some genes from extremophile species have been identified and related to thermal resistance (Gonzalez-Blasco et al., 2000; Zhang and Griffiths, 2003; Ritter et al., 2014), which could be introduced to the cells and characterized. However, thermal and vacuum resistance is not only a matter of genetics, but also of cell components and protein melting and degradation. Therefore, selecting a bacteria already capable of surviving in similar conditions could be the best option to develop extra-terrestrial habitats.

The studied salinity values showed no major impairments for the growth of the tested *E. coli* strains, with similar growths in all the cases from 0 to 20 g/l of sodium chloride. In the case of pH, the viability range for all the strains showed to be between 5 and 9, with no growth for either pH 3 or 11. These results are consistent with previous studies on *E. coli*'s growth in media with different pH concentrations (Ross et al., 2003). The *E. coli*

RecA strain needed more time to reach the mid-exponential phase at pH 5. However, this difference is not considered significant.

This study has evidenced that an enhancement of cellular resistance to harsh environments is possible but is also limited by the current knowledge on the natural genetic and molecular mechanisms of protection and DNA repair existing in extremophiles. Consequently, increasing the knowledge on these mechanisms is still key to develop resistant bacterial strains able to survive under extreme conditions and develop extra-terrestrial habitats. In this study, the cellular resistance of *E. coli* was enhanced to the point that it should allow the survival of some of the selected strains in environments like the equator of Mars, but also outside of the International Space Station in the Low Earth Orbit. New tests and procedures should be performed to further study and characterize the surviving possibilities and limitations of the evolved strains. For instance, the biological shielding properties of cell aggregation could increase the survival to UV radiation, but also to corpuscular Ionizing Radiation, such as beta or gamma rays. Shielding bacteria from radiation, especially UV, has proven to be very effective for the survival of *B. subtilis* spores in space (Horneck et al., 1994). As for charged particles radiation, shielding could also be beneficial, as proved in previous studies with *D. radiodurans* (Paulino-Lima et al., 2011). Also, a combination between vacuum and continuous wide temperature cycles exposure should be done to further characterize and potentially expand the limits of the selected strains.

The development of environments hospitable to life and the possibilities of building extra-terrestrial habitats are tied to the knowledge and capacity of enhancing bacterial, fungi, and cellular resistance to the existent conditions. For this, many environmental factors must be considered, but also some ethical and moral concerns. The selection of the most adequate species for the development of the desired ecosystem has a major role, and the capacity of controlling the survival of the introduced species is key for the preservation of the natural conditions. The preservation of environments and the avoidance of microbe transfer has led to many serviceable spacecrafts and satellites being terminated to minimize the risks of microbe transfer, as was the case of NASA's orbiter Cassini (Yam et al., 2009), which was burned in Saturn's atmosphere before an eventual crash into Enceladus, which has been studied as an eminently habitable environment. These procedures comply with the planetary protection protocols, established to minimize the risks of depositing Earth microbes into possibly habitable environments. However, it has been proven impossible to construct a microbe-free spacecraft, and experiments such as the ones done with *D. radiodurans* prove that some species can remain viable in outer space. These studies have led to very strict policies on space exploration, but still, the risks are not eliminated. In addition, the idea of human exploration adds more concerns to this field, and any human mission in space would almost certainly have to break those policies to survive. On the other hand, space exploration is not the only source of microbe transfer, as debris caused by asteroid impacts could also carry potentially viable microbes. All this leads to the conclusion that eventual microbe transfer is inevitable unless space exploration is abandoned, and no exchange between other planets or organic matter is happening.

Space exploration is essential for survival, expanding not only our knowledge and resources, but also opening the door to many new possibilities. However, as this study has revealed, there is still plenty of knowledge and resources to be gained on Earth that could help in the exploration and development of extra-terrestrial habitats. Additionally, many life science engineering strategies could be potentially used in this field, and the search of Earth's life limits and their expansion could provide some insight into the generation of habitable environments. Space is believed to be the last frontier, but the truth is, we are still a frontier to ourselves.

DATA AVAILABILITY STATEMENT

The datasets presented in this study can be found in online repositories. The names of the repository/repositories and accession number(s) can be found at: https://www.ebi.ac.uk/ena, PRJEB47882.

AUTHOR CONTRIBUTIONS

JP performed the experiments with help of NK and supervision of MG. The study was designed by JP, NK, and MG. MA and JQ helped and supervised the ionizing radiation exposures. JP, NK, JQ, MA, and MG wrote the manuscript. All authors contributed to the article and approved the submitted version.

FUNDING

This study has received funds from Captació Talent - Fundació La Caixa, the Office of Naval Research (Award N62909-18-1-2155), Ramón y Cajal program (Grant agreement RYC-2015-17734). NK is funded by the Sociedad Española de Quimicos Cosmeticos (SEQC) and thanks the SEQC for the participation at the 33rd IFSCC Congress.

ACKNOWLEDGMENTS

The authors want to thank the current members of the Translational Synthetic Biology Laboratory and the Department of Experimental and Health Sciences (DCEXS) of Universitat Pompeu Fabra at the Barcelona Biomedical Research Park (PRBB) and the Radiation Oncology Department of Hospital del Mar for their valuable comments and assistance. We also want to specially thank the former members of the iGEM 2020 UPF_Barcelona team, Júlia Mir, Sira Mogas, and Dr. Amal Rahmeh for their comments and encouragement.

SUPPLEMENTARY MATERIAL

The Supplementary Material for this article can be found online at: https://www.frontiersin.org/articles/10.3389/fmicb.2021.789668/full#supplementary-material

REFERENCES

Baitin, D. M., Bakhlanova, I. V., Kil, Y. V., Cox, M. M., and Lanzov, V. A. (2006). Distinguishing characteristics of hyperrecombinogenic RecA protein from pseudomonas aeruginosa acting in *Escherichia coli*. *J. Bacteriol.* 188, 5812–5820. doi: 10.1128/JB.00358-06

Berger, T., Matthiä, D., Burmeister, S., Zeitlin, C., Rios, R., Stoffle, N., et al. (2020). Long term variations of galactic cosmic radiation on board the international space station, on the moon and on the surface of mars. *J. Space Weather Space Clim.* 10:34. doi: 10.1051/swsc/2020028

Bijlani, S., Singh, N. K., Eedara, V. V. R., Podile, A. R., Mason, C. E., Wang, C. C. C., et al. (2021). *Methylobacterium ajmalii* sp. nov., isolated from the international space station. *Front. Microbiol.* 12:639396. doi: 10.3389/fmicb.2021.639396

Brenner, D. J., Hlatky, L. R., Hahnfeldt, P. J., Huang, Y., and Sachs, R. K. (1998). The linear-quadratic model and most other common radiobiological models result in similar predictions of time-dose relationships. *Radiat. Res.* 150, 83–91. doi: 10.2307/3579648

Callaway, E. (2019). *E. coli* bacteria engineered to eat carbon dioxide. *Nature* 576, 19–20. doi: 10.1038/d41586-019-03679-x

Chavez, C., Cruz-Becerra, G., Fei, J., Kassavetis, G. A., and Kadonaga, J. T. (2019). The tardigrade damage suppressor protein binds to nucleosomes and protects DNA from hydroxyl radicals. *Elife* 8:e47682. doi: 10.7554/eLife.47682.014

Cortesão, M., Siems, K., Koch, S., Beblo-Vranesevic, K., Rabbow, E., Berger, T., et al. (2021). MARSBOx: fungal and bacterial endurance from a Balloon-Flown analog mission in the stratosphere. *Front. Microbiol.* 12:601713. doi: 10.3389/fmicb.2021.601713

Cox, C. S. (1993). Roles of water molecules in bacteria and viruses. *Orig. Life Evol. Biosph.* 23, 29–36. doi: 10.1007/BF01581988

Deatherage, D. E., and Barrick, J. E. (2014). Identification of mutations in laboratory-evolved microbes from next-generation sequencing data using breseq. *Methods Mol. Biol.* 1151, 165–188. doi: 10.1007/978-1-4939-0554-6_12

Dose, K., Bieger-Dose, A., Kerz, O., and Gill, M. (1991). DNA-strand breaks limit survival in extreme dryness. *Orig. Life Evol. Biosph.* 21, 177–187. doi: 10.1007/BF01809446

Dose, K., Bieger-Dose, A., Labusch, M., and Gill, M. (1992). Survival in extreme dryness and DNA-single-strand breaks. *Adv. Space Res.* 12, 221–229. doi: 10.1016/0273-1177(92)90176-X

Eggler, A. L., Lusetti, S. L., and Cox, M. M. (2003). The C terminus of the *Escherichia coli* RecA protein modulates the DNA binding competition with single-stranded DNA-binding protein. *J. Biol. Chem.* 278, 16389–16396. doi: 10.1074/jbc.M212920200

Filsinger, G. T., Wannier, T. M., Pedersen, F. B., Lutz, I. D., Zhang, J., Stork, D. A., et al. (2021). Characterizing the portability of phage-encoded homologous recombination proteins. *Nat. Chem. Biol.* 17, 394–402. doi: 10.1038/s41589-020-00710-5

Gasset, G., Tixador, R., Eche, B., Lapchine, L., Moatti, N., Toorop, P., et al. (1994). Growth and division of *Escherichia coli* under microgravity conditions. *Res. Microbiol.* 145, 111–120. doi: 10.1016/0923-2508(94)90004-3

Gonzalez-Blasco, G., Sanz-Aparicio, J., Gonzalez, B., Hermoso, J. A., and Polaina, J. (2000). Directed evolution of beta -glucosidase a from paenibacillus polymyxa to thermal resistance. *J. Biol. Chem.* 275, 13708–13712. doi: 10.1074/jbc.275.18.13708

Gonzalez-Flo, E., Alaball, M. E., and Macia, J. (2020). Two-component biosensors: unveiling the mechanisms of predictable tunability. *ACS Synth. Biol.* 9, 1328–1335. doi: 10.1021/acssynbio.0c00010

Harris, D. R., Pollock, S. V., Wood, E. A., Goiffon, R. J., Klingele, A. J., Cabot, E. L., et al. (2009). Directed evolution of ionizing radiation resistance in *Escherichia coli*. *J. Bacteriol.* 191, 5240–5252. doi: 10.1128/JB.00502-09

Hashimoto, T., Horikawa, D. D., Saito, Y., Kuwahara, H., Kozuka-Hata, H., Shin-I, T.,et al. (2016). Extremotolerant tardigrade genome and improved radiotolerance of human cultured cells by tardigrade-unique protein. *Nat. Commun.* 7:12808. doi: 10.1038/ncomms12808

Hellweg, C. E., and Baumstark-Khan, C. (2007). Getting ready for the manned mission to mars: the astronauts' risk from space radiation. *Naturwissenschaften* 94, 517–526. doi: 10.1007/s00114-006-0204-0

Horneck, G., Bucker, H., Dose, K., Martens, K. D., Bieger, A., Mennigmann, H. D., et al. (1984). Microorganisms and biomolecules in space environment experiment ES 029 on spacelab-1. *Adv. Space Res.* 4, 19–27. doi: 10.1016/0273-1177(84)90220-5

Horneck, G., Bucker, H., and Reitz, G. (1994). Long-term survival of bacterial spores in space. *Adv. Space Res.* 14, 41–45. doi: 10.1016/0273-1177(94)90448-0

Jin, Q., and Kirk, M. F. (2018). pH as a primary control in environmental microbiology: 1. Thermodynamic perspective. *Front. Environ. Sci.* 6:21. doi: 10.3389/fenvs.2018.00021

Jönsson, K. I., Rabbow, E., Schill, R. O., Harms-Ringdahl, M., and Rettberg, P. (2008). Tardigrades survive exposure to space in low earth orbit. *Curr. Biol.* 18, R729–R731. doi: 10.1016/j.cub.2008.06.048

Kawaguchi, Y., Shibuya, M., Kinoshita, I., Yatabe, J., Narumi, I., Shibata, H., et al. (2020). DNA damage and survival time course of deinococcal cell pellets during 3 years of exposure to outer space. *Front. Microbiol.* 11:2050. doi: 10.3389/fmicb.2020.02050

Kawaguchi, Y., Yang, Y., Kawashiri, N., Shiraishi, K., Takasu, M., Narumi, I., et al. (2013). The possible interplanetary transfer of microbes: assessing the viability of deinococcus spp. under the ISS environmental conditions for performing exposure experiments of microbes in the tanpopo mission. *Orig. Life Evol. Biosph.* 43, 411–428. doi: 10.1007/s11084-013-9346-1

Kawaguchi, Y., Yokobori, S.-I., Hashimoto, H., Yano, H., Tabata, M., Kawai, H., et al. (2016). Investigation of the interplanetary transfer of microbes in the tanpopo mission at the exposed facility of the international space station. *Astrobiology* 16, 363–376. doi: 10.1089/ast.2015.1415

Kim, J.-I., Sharma, A. K., Abbott, S. N., Wood, E. A., Dwyer, D. W., Jambura, A., et al. (2002). RecA protein from the extremely radioresistant bacterium deinococcus radiodurans: expression, purification, and characterization. *J. Bacteriol.* 184, 1649–1660. doi: 10.1128/JB.184.6.1649-1660.2002

Kirke, J., Jin, X.-L., and Zhang, X.-H. (2020). Expression of a tardigrade dsup gene enhances genome protection in plants. *Mol. Biotechnol.* 62, 563–571. doi: 10.1007/s12033-020-00273-9

Kminek, G., and Bada, J. L. (2006). The effect of ionizing radiation on the preservation of amino acids on mars. *Earth Planet. Sci. Lett.* 245, 1–5. doi: 10.1016/j.epsl.2006.03.008

Knoll, A. H. (2015). *Life on a Young Planet: The First Three Billion Years of Evolution on Earth – Updated Edition*. Princeton University Press.

Kobayashi, Y., Shimizu, T., Tanaka, A., Taucher-Scholz, G., Watanabe, H., Kikuchi, M., et al. (1995). 2● 8 RBE/LET effects of heavy ions on inactivation in dry cells of deinococcus radiodurans. *JAERI Rev.* 95:50.

Krulwich, T. A., Sachs, G., and Padan, E. (2011). Molecular aspects of bacterial pH sensing and homeostasis. *Nat. Rev. Microbiol.* 9, 330–343. doi: 10.1038/nrmicro2549

Laval, J. (1996). Role of DNA repair enzymes in the cellular resistance to oxidative stress. *Pathol. Biol.* 44, 14–24.

Leigh Mascarelli, A. (2010). Methane-eating microbes make their own oxygen. *Nature*. doi: 10.1038/news.2010.146

Mattimore, V., and Battista, J. R. (1996). Radioresistance of deinococcus radiodurans: functions necessary to survive ionizing radiation are also necessary to survive prolonged desiccation. *J. Bacteriol.* 178, 633–637. doi: 10.1128/jb.178.3.633-637.1996

Merino, N., Aronson, H. S., Bojanova, D. P., Feyhl-Buska, J., Wong, M. L., Zhang, S., et al. (2019). Living at the extremes: extremophiles and the limits of life in a planetary context. *Front. Microbiol.* 10:780. doi: 10.3389/fmicb.2019.00780

Mildrexler, D. J., Zhao, M., and Running, S. W. (2011). Satellite finds highest land skin temperatures on earth. *Bull. Am. Meteorol. Soc.* 92, 855–860. doi: 10.1175/2011BAMS3067.1

Moeller, R., Reitz, G., Li, Z., Klein, S., and Nicholson, W. L. (2012). Multifactorial resistance of *Bacillus subtilis* spores to high-energy proton radiation: role of spore structural components and the homologous recombination and non-homologous end joining DNA repair pathways. *Astrobiology* 12, 1069–1077. doi: 10.1089/ast.2012.0890

Munteanu, A.-C., Uivarosi, V., and Andries, A. (2015). Recent progress in understanding the molecular mechanisms of radioresistance in deinococcus bacteria. *Extremophiles* 19, 707–719. doi: 10.1007/s00792-015-0759-9

Ngo, K. V., Molzberger, E. T., Chitteni-Pattu, S., and Cox, M. M. (2013). Regulation of deinococcus radiodurans RecA protein function via modulation of active and inactive nucleoprotein filament states. *J. Biol. Chem.* 288, 21351–21366. doi: 10.1074/jbc.M113.459230

Paulino-Lima, I. G., Janot-Pacheco, E., Galante, D., Cockell, C., Olsson-Francis, K., Brucato, J. R., et al. (2011). Survival of *Deinococcus radiodurans* against laboratory-simulated solar wind charged particles. *Astrobiology* 11, 875–882. doi: 10.1089/ast.2011.0649

Ritter, A. C., Bacciu, D., Santi, L., Rubino, S., Uzzau, S., and Tondo, E. C. (2014). Expression of ompr gene in the acid adaptation and thermal resistance of salmonella enteritidis SE86. *J. Infect. Dev. Ctries* 8, 474–479. doi: 10.3855/jidc.3584

Roca, A. I., and Cox, M. M. (1997). "RecA protein: Structure, function, and role in recombinational DNA repair," in *Progress in Nucleic Acid Research and Molecular Biology*, Vol. 56, eds W. E. Cohn and K. Moldave (Academic Press), 129–223.

Ross, T., Ratkowsky, D. A., Mellefont, L. A., and McMeekin, T. A. (2003). Modelling the effects of temperature, water activity, pH and lactic acid concentration on the growth rate of *Escherichia coli*. *Int. J. Food Microbiol.* 82, 33–43. doi: 10.1016/S0168-1605(02)00252-0

Rothschild, L. J., and Mancinelli, R. L. (2001). Life in extreme environments. *Nature* 409, 1092–1101. doi: 10.1038/35059215

Scambelluri, M., Piccardo, G. B., Philippot, P., Robbiano, A., and Negretti, L. (1997). High salinity fluid inclusions formed from recycled seawater in deeply subducted alpine serpentinite. *Earth Planet. Sci. Lett.* 148, 485–499. doi: 10.1016/S0012-821X(97)00043-5

Sezonov, G., Joseleau-Petit, D., and D'Ari, R. (2007). *Escherichia coli* physiology in Luria-Bertani broth. *J. Bacteriol.* 189, 8746–8749. doi: 10.1128/JB.01368-07

Shahbazi-Gahrouei, D., Gholami, M., and Setayandeh, S. (2013). A review on natural background radiation. *Adv. Biomed. Res.* 2:65. doi: 10.4103/2277-9175.115821

Shibai, A., Takahashi, Y., Ishizawa, Y., Motooka, D., Nakamura, S., Ying, B.-W., and Tsuru, S. (2017). Mutation accumulation under UV radiation in *Escherichia coli*. *Sci. Rep.* 7:14531. doi: 10.1038/s41598-017-15008-1

Shuryak, I., and Brenner, D. J. (2010). Effects of radiation quality on interactions between oxidative stress, protein and DNA damage in *Deinococcus radiodurans*. *Radiat. Environ. Biophys.* 49, 693–703. doi: 10.1007/s00411-010-0305-1

Stelter, M., Acajjaoui, S., McSweeney, S., and Timmins, J. (2013). Structural and mechanistic insight into DNA unwinding by *Deinococcus radiodurans* UvrD. *PLoS ONE* 8:e77364. doi: 10.1371/journal.pone.0077364

Takahashi, Y., Hashimoto, H., Nakagawa, T., and Shibata, S. (2011). Survivability of moss and fungal spores in tests simulating conditions of the ISS outer wall. *Biol. Sci. Space* 25, 83–92. doi: 10.2187/bss.25.83

Wilson, J. W., Cucinotta, F. A., Shinn, J. L., Simonsen, L. C., Dubey, R. R., Jordan, W. R., Jones, T. D., Chang, C. K., and Kim, M. Y. (1999). Shielding from solar particle event exposures in deep space. *Radiat. Meas.* 30, 361–382. doi: 10.1016/S1350-4487(99)00063-3

Yam, C. H., Davis, D. C., Longuski, J. M., Howell, K. C., and Buffington, B. (2009). Saturn impact trajectories for cassini End-of-Mission. *J. Spacecr. Rockets* 46, 353–364. doi: 10.2514/1.38760

Yamagishi, A., Kawaguchi, Y., Hashimoto, H., Yano, H., Imai, E., Kodaira, S., et al. (2018). Environmental data and survival data of *Deinococcus aetherius* from the exposure facility of the Japan experimental module of the international space station obtained by the tanpopo mission. *Astrobiology* 18, 1369–1374. doi: 10.1089/ast.2017.1751

Yang, Y., Yokobori, S.-I., and Yamagishi, A. (2009). Bacterial survival in response to desiccation and high humidity at above zero and subzero temperatures. *Adv. Space Res.* 43, 1285–1290. doi: 10.1016/j.asr.2009.01.018

Zhang, Y., and Griffiths, M. W. (2003). Induced expression of the heat shock protein genes uspa and grpe during starvation at low temperatures and their influence on thermal resistance of *Escherichia coli* O157:H7. *J. Food Prot.* 66, 2045–2050. doi: 10.4315/0362-028X-66.11.2045

Conflict of Interest: The authors declare that the research was conducted in the absence of any commercial or financial relationships that could be construed as a potential conflict of interest.

frontiers | Frontiers in Microbiology

ORIGINAL RESEARCH
published: 29 April 2022
doi: 10.3389/fmicb.2022.871110

Qualification of Membrane Filtration for Planetary Protection Flight Implementation

*Kristina Vaikovna Stott[1], Lyssa Morgan[1], Caitlin Shearer[2], Morgan Byrd Steadham[2], Mihaela Ballarotto[2] and Ryan Hendrickson[1]**

[1] Jet Propulsion Laboratory, California Institute of Technology, Pasadena, CA, United States, [2] Johns Hopkins University Applied Physics Laboratory, Laurel, MD, United States

OPEN ACCESS

Edited by:
Rob Van Houdt,
Belgian Nuclear Research Centre, Belgium

Reviewed by:
Nancy Merino,
Physical and Life Sciences Directorate, Lawrence Livermore National Laboratory (DOE), United States
Peter Leslie Croot,
National University of Ireland, Galway, Ireland

***Correspondence:**
Ryan Hendrickson
Ryan.C.Hendrickson@jpl.nasa.gov

Specialty section:
This article was submitted to Extreme Microbiology, a section of the journal Frontiers in Microbiology

Received: 07 February 2022
Accepted: 12 April 2022
Published: 29 April 2022

Citation:
Stott KV, Morgan L, Shearer C, Steadham MB, Ballarotto M and Hendrickson R (2022) Qualification of Membrane Filtration for Planetary Protection Flight Implementation. Front. Microbiol. 13:871110. doi: 10.3389/fmicb.2022.871110

Planetary protection is the practice of preventing forward and backward contamination of solar system bodies. Spacecraft and associated surfaces are sampled to ensure compliance with bioburden requirements. Current planetary protection sampling and processing methodologies consist of extracting microbial cells from wipe or swab samples through a procedure (NASA Standard Assay) that includes sonication, heat shock, and pour-plate steps. The pour-plate steps are laborious and prolonged. Moreover, results can be imprecise because only a fraction of the sample fluid is plated for CFU enumeration (80% for swabs and 25% for wipes). Thus, analysis requires that a pour fraction extrapolation factor be applied to CFU counts to account for bioburden in the remaining sample volume that is not plated. This extrapolation results in large variances for data, decreasing the accuracy of spore bioburden estimation of spacecraft hardware. In this study, we investigated the use of membrane filtration as an alternative method to pour-plate processing. Membrane filtration is an appealing methodology for planetary protection because it can process greater sample volumes and reduces the data variance for bioburden enumeration. A pour fraction extrapolation factor is still applied for both swabs and wipes (92%), however, it is a greater pour fraction than the pour-plate method. Here we present data collected by the Jet Propulsion Laboratory and the Applied Physics Laboratory to experimentally determine the equivalency of membrane filtration to pour-plate methodology for implementation during the NASA Standard Assay. Additionally, we outline the planned procedures for two membrane filtration systems: Pall® Laboratory Manifold system and Milliflex® Plus Vacuum Pump System. Both systems demonstrated equivalence of the membrane filtration method to the pour-plate method.

Keywords: planetary protection, membrane filtration (MF), NASA Standard Assay, spores, *Bacillus atrophaeus*

Abbreviations: APL, Applied Physics Laboratory; CFU, colony forming units; JPL, Jet Propulsion Laboratory; MF, membrane filtration; NASA, National Aeronautics and Space Administration; NSA, NASA Standard Assay (as a method); TSA, trypticase soy agar.

INTRODUCTION

Planetary protection is a field concerned with the responsible exploration of space (Meltzer, 2012). Extraterrestrial life detection has been a key goal in the field of astrobiology. Per a white paper report from the Biosignatures Standards of Evidence Community Workshop, it is critical for the astrobiology community to develop a universal scientific framework for life detection claims to ensure clear and consistent communication with the scientific community and the public. If organisms were found on a celestial body, it would be necessary to determine the origin of that life – is it native to that extraterrestrial environment, or is it spacecraft-borne from Earth? In 1967, the United Nations Outer Space Treaty put forth guidelines to preserve the scientific integrity of future explorations (United Nations, 1967), namely in Article IX of the treaty. Since then, the Committee on Space Research has updated the guidelines that national space agencies can adopt as part of their mission planning (COSPAR, 2008). In compliance with the Committee on Space Research policies, the National Aeronautics and Space Administration (NASA) monitors spacecraft bioburden to minimize the inadvertent contamination of solar system planets or moons (forward contamination) (Committee on Preventing the Forward Contamination of Mars, National Research Council, 2006). Although spacecraft and their components are assembled in cleanroom facilities (Moissl et al., 2007), spore-forming microbes are likely to persist (Venkateswaran et al., 2003; La Duc et al., 2004a,b; Crawford, 2005; Osman et al., 2006; Satomi et al., 2006). For this reason, the NASA standard spore assay was developed to estimate the aerobic spore-forming organisms on spacecraft hardware surfaces, using a cultivation-dependent method, as described by NASA procedures and guidelines (NPG: 5340.1D).

The compilation of procedures for assessing the microbial burden on spacecraft hardware, including the NASA Standard Assay procedure, is found in NASA-HDBK-6022, Handbook for the Microbial Examination of Space Hardware (2010). Briefly, the NASA Standard Assay is a culture method designed to enumerate microbial burden from spacecraft that has been sampled *via* a sterile cotton swab or polyester wipe suitable for small and large hardware surfaces, respectively. Microbes present on these sampling devices are extracted during a sonication step. Samples are then heated to $80 \pm 2°C$, to target heat-shock resistant spores. Next, 2.0- or 4.0-mL portions of the sample fluid are aseptically pipetted into Petri dishes (also referred to as plates), and sterile molten trypticase soy agar (TSA) is added to each plate. Once the mixture is solidified, plates are incubated (32°C, 3 days), and Colony Forming Units (CFU) are counted at 24, 48, and 72 h.

Planetary Protection Engineers at the Jet Propulsion Laboratory (JPL) have extensively used the NASA Standard Assay (NSA) for flight missions, including the InSight and Mars Science Laboratory missions (Benardini et al., 2014; Hendrickson et al., 2020) as well as the recent Mars 2020 mission. While the method is effective, it is inefficient in terms of labor, since 2–4 plates must be generated per swab and 13–25 plates per wipe. Moreover, results can be imprecise because only a fraction of the sample fluid is plated for enumeration (80% for swabs and 25% for wipes). This requires that a pour fraction extrapolation factor be applied to CFU results to account for the remaining sample that is not plated.

Thus, for the current Europa Clipper mission, we investigated a more sustainable method, membrane filtration, as an alternative to the pour-plate method for processing samples. Membrane filtration (MF) has been extensively studied (Grinnell, 1929; Bowman et al., 1967; Blosse et al., 1998; Wang et al., 2008; Onyango et al., 2010), used in the healthcare, food, and water industries (Bordner et al., 1978; Solomon et al., 1978; Sharpe et al., 1979; Smith et al., 1993; Lee et al., 2007; Crittenden et al., 2012), and approved for use on European Space Agency missions (ECSS-Q-ST-70-55 Working Group, 2008). For planetary protection applications, MF is an attractive alternative because the entire sample volume can be processed, increasing the accuracy of spore burden estimation of spacecraft hardware. Moreover, compared with the pour-plate method, MF has an overall cost savings due to a reduction in labor and or materials.

Although the Office of Planetary Protection has approved MF for use, NASA-HDBK-6022 does not include a specific procedure. Here we describe the equipment, materials, processes, and analyses used to develop a membrane filtration protocol to effectively enumerate bioburden from spacecraft surfaces, comparable to the pour-plate method. Specifically, results in this paper describe two independent studies: Jet Propulsion Laboratory Biotechnology and Planetary Protection Group (using Pall® Laboratory Manifold and Filter Funnels, Whatman® 0.2 μm cellulose acetate filter, and standard Petri dish with TSA) and Johns Hopkins University Applied Physics Laboratory – Materials Engineering and Planetary Protection Section (using Milliflex® Plus Vacuum Pump, Milliflex-100, 0.22 μm white gridded funnel and filter unit, and Prefilled Milliflex® Culture Media Cassettes).

MATERIALS AND METHODS

NASA Standard Assay

Per NASA-HDBK-6022 (2010) samples are acquired using cotton swabs or 9″ × 9″ polyester wipes and processed *via* the associated NSA procedure. Both swab and wipe samples are premoistened with sterile DI water since they come in direct contact with flight hardware during sampling. As per NASA-HDBK-6022 (2010), swab samples are suspended in 10 mL 18.2 MΩ deionized water and wipes are suspended in 200 mL of planetary protection (PP) rinse solution for processing. PP rinse (buffered solution + Tween 80) was prepared in accordance with NASA-HDBK-6022 (2010). Samples then are processed *via* sonication for 2 min in an aqueous bath of 0.02% v/v Tween 80, at 19–27 kHz (**Figures 1**, **2**). Samples then undergo "heat shock" at 80°C for 15 min to enable the detection of aerobic, mesophilic, and cultivable spores. Samples are then quickly cooled to 30–35°C. Portions (2 or 4 mL) of each sample are poured into sterile Petri dishes followed by a standard growth medium required by NASA-HDBK-6022 (2010), trypticase soy agar (TSA). The plates are incubated at 32°C for a period of

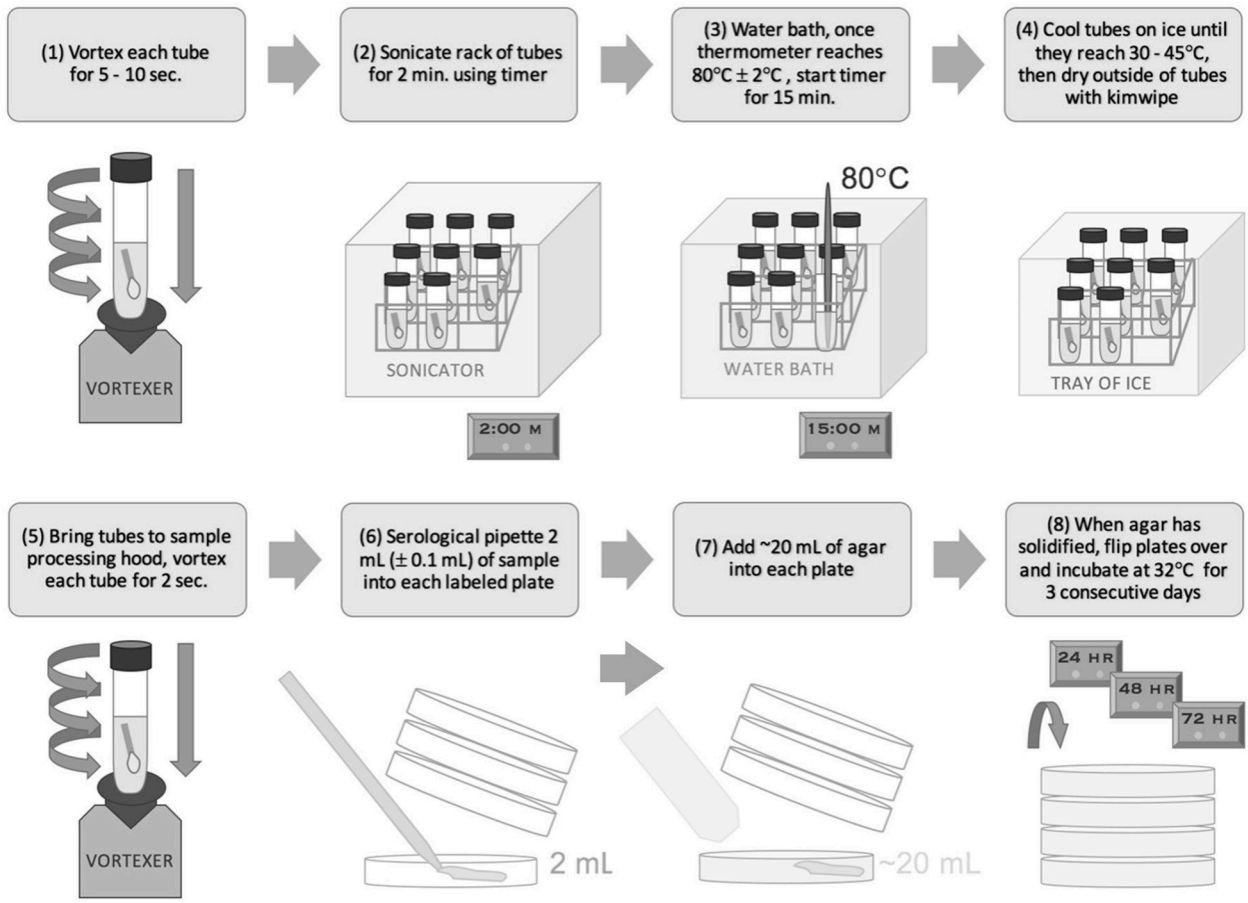

FIGURE 1 | NASA Standard Assay for swab samples.

72 h, during which planetary protection engineers count colony forming units (CFUs) every 24 h.

Preparation of Samples (Axenic Cultures; Jet Propulsion Laboratory)

Bacillus atrophaeus spores (∼1 μm) were obtained from Mesa Laboratories (#9372, Bozeman, MT, United States). A working spore stock solution was prepared containing 100 spores/mL. Following vortexing, 50 μL of the spore stock solution was transferred each into the three sample types: wipes, swabs, and control. Wipe samples refer to glass bottles containing only 200 mL of planetary protection (PP) rinse solution. PP rinse (buffered solution) was prepared in accordance with NASA-HDBK-6022 (2010). Swab samples refer to glass test tubes containing only 10 mL 18.2 MΩ deionized water. The wipe and swab sampling devices themselves (Polyester wipes, TX3211, Texwipe, Kernersville, NC, United States; Cotton Tipped Applicators, 806WC, Puritan, Guilford, ME, United States) were excluded during testing to minimize the potential variability of CFU recovery efficiency; the devices were previously validated by the Planetary Protection Office, thus we focused on comparing the methodologies only. The control samples refer to 50 μL of the working spore stock solution that was directly plated onto TSA plates.

Preparation of Samples (Soil and *B. atrophaeus* Solutions; Applied Physics Laboratory)

Bacillus atrophaeus spores (∼1 μm) were obtained from Mesa Laboratories (#9372, Bozeman, MT, United States). *B. atrophaeus* has long been used as a model planetary protection organism as it grows well in the NSA incubation conditions (Aerobic, 32C, grows on TSA) and has a clear red pigmentation that can help distinguish it from potential contamination. Soil from APL's campus was selected for its diverse, undefined, and abundant spore population instead of cleanroom samples that have a lower overall spore abundance and much higher variability in spore populations. Two types of solutions were made to directly compare NSA and MF: soil in DI water and *B. atrophaeus* in DI water. The soil solutions consisted of three trials (low, medium, and high concentrations, denoted as Soil concentration 1, 2, and 3, respectively) and the *B. atrophaeus* solutions consisted of one trial. Each trial consisted of one set of pour-plate samples, and two sets of membrane filtration samples for redundancy, denoted

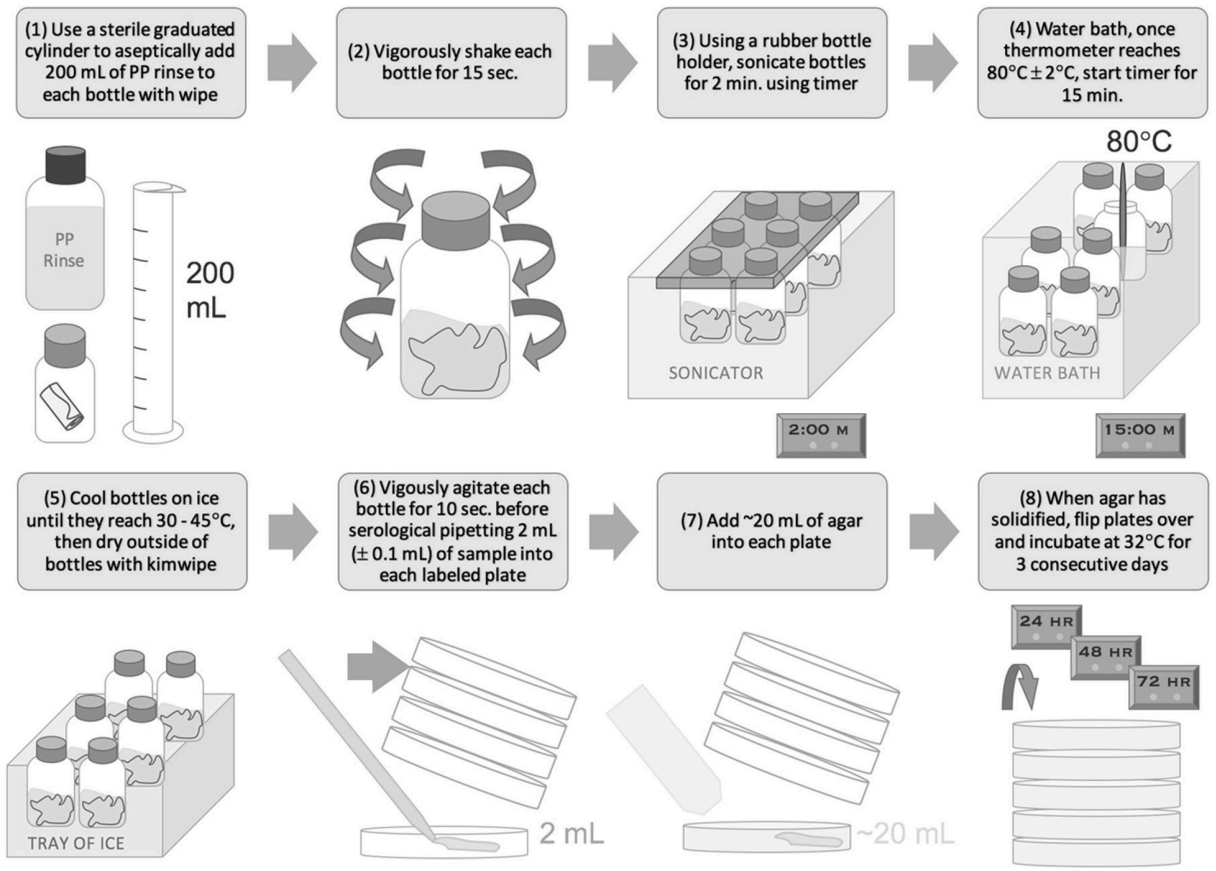

FIGURE 2 | NASA Standard Assay for wipe samples.

as "MF-APL 1" and "MF-APL 2," each with 20 replicates. For the soil solutions, 1 g of dried soil was dried in open indoor air over the course of 1 week. It was then suspended in DI water and passed through a 20 μm filter to remove large solids. Spores were selected for by heat shocking the DI soil solution for 15 min at 80°C per NASA-HDBK-6022 (2010), thus assuming only spores remained in the soil samples after the heat shock. This starting solution was then serially diluted to a dilution factor of 1:10,000. For *B. atrophaeus* solutions, the *B. atrophaeus* spore stock was diluted to achieve approximately 1.25 spores/mL. Each sample consisted of 8 mL DI water to imitate a swab sample. A wipe-equivalent sample was not tested.

Pour Plating

In accordance with the NASA Standard Assay, swab and wipe samples, as prepared in section "Preparation of Samples (Axenic Cultures; Jet Propulsion Laboratory)" or "Preparation of Samples (Soil and *B. atrophaeus* Solutions; Applied Physics Laboratory)," were sonicated, heat shocked, cooled, and processed *via* pour plating (NSA) (**Figures 1**, **2**). For wipe samples, 4 mL was dispensed each into 12 Petri dishes and 2 mL was dispensed into 1 Petri dish, to total 50 mL of processed volume (PN 351029, Corning, Tewksbury, MA, United States) and filled with 1.5% TSA (Difco™ Tryptic Soy Agar PN 236920, BD Biosciences, Franklin Lakes, NJ, United States, or equivalent) using a peristaltic pump (Delta Scientific Medical Fill Master, or equivalent). For swab samples, 4 mL was dispended each into 2 Petri dishes and filled with TSA (alternatively 2 mL each into 4 Petri dishes). Plates were then incubated at 32°C and enumerated at 24, 48, and 72 h. Since only a fraction (50 mL for wipes and 8 mL for swabs) of the total sample volume (200 mL for wipes and 10 mL for swabs) is plated, the CFU enumerated at 72 h was multiplied by the pour fraction to extrapolate the final CFU. For wipe samples a pour fraction of 4× was applied to CFU results since 25% of the sample was processed (50/200 mL). For swab samples a pour fraction of 1.25× was applied to CFU results since 80% of the sample was processed (8/10 mL). A negative control consisting of a petri dish consisting of only poured TSA was included in each sample set to ensure no contamination occurred during the processing.

Membrane Filtration (Pall Laboratory Manifold System; Jet Propulsion Laboratory)

The membrane filtration equipment includes a 3-place laboratory manifold with hose barb cap, end cap, and manifold valves (PN 4889, Pall, Port Washington, NY, United States). The equipment

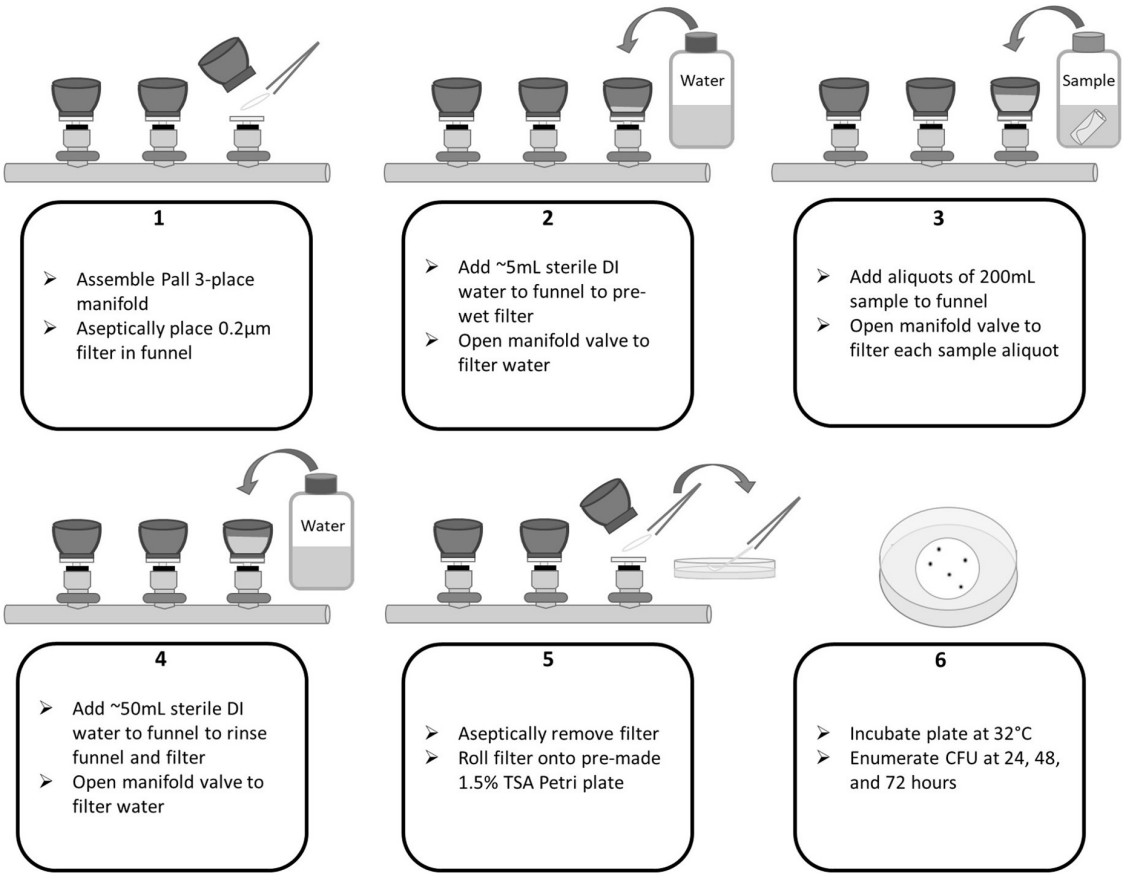

FIGURE 3 | Pall Laboratory Manifold flow diagram for membrane filtration of wipe samples.

also includes manifold standard adapters (PN 4891, Pall, Port Washington, NY, United States), 150 mL magnetic filter funnels (PN 424, Pall, Port Washington, NY, United States), Whatman 0.2 µm cellulose acetate membrane filters (PN 10404112, Cytiva, Marlborough, MA, United States), forceps, 1/4″ inner diameter Tygon E-3603 laboratory tubing (Saint-Gobain, Malvern, PA, United States), and a 1 L glass filter flask.

The membrane filtration setup was assembled in a laminar flow environment or Class II, Type A2 biological cabinet and consisted of the following: The Pall laboratory manifold was first connected to a filter flask using Tygon tubing and a rubber stopper. The barbed end of the filter flask was attached to a vacuum source *via* Tygon tubing. The 150 mL magnetic filter funnels were placed into each of the three manifold openings *via* the manifold standard adapters, and subsequently, the 0.2 µm Whatman filters were placed inside the magnetic filter funnels using sterile forceps.

In accordance with the NASA Standard Assay, swab and wipe samples were sonicated, heat shocked, and cooled. To begin membrane filtration (MF), 5 mL of sterile 18.2 MΩ deionized water was filtered through each funnel to wet the filters. Next, the entire volume of each sample (10 mL for swabs or 200 mL for wipes) was poured into a filter funnel. For swabs, an additional 40 mL DI water was added to ensure a minimum of 50 mL is filtered through the funnel. The volumes were filtered *via* vacuum and the sample allowed to drain completely. A negative control consisting of only sterile 18.2 MΩ deionized water was included in each sample set to ensure no contamination occurred during the processing. The funnels and filters were rinsed of potentially inhibitory residues with an additional ∼50 mL of sterile water followed by filtration. Using sterile forceps, the membrane filters were removed from the funnels and placed into sterile Petri dishes prepared with TSA by slowly rolling the filter onto the solidified agar to avoid trapped air bubbles underneath the filter. Plates were then incubated at 32°C and enumerated at 24, 48, and 72 h. See **Figures 3**, **4** for process flow diagram. Since the entire sample volume is filtered for both wipe and swab samples (in the absence of sampling devices), the CFU enumerated at 72 h represents the final CFU (i.e., the pour fraction is 100%).

Membrane Filtration (Millipore Milliflex PLUS System; Applied Physics Laboratory)

The membrane filtration equipment includes a Milliflex Plus Pump Single Head Kit (PN MXPPLUS01, MilliporeSigma, Burlington, MA, United States), Milliflex-100, 100 mL, 0.22 µm white gridded funnel and filter in one (PN MXGSWG124,

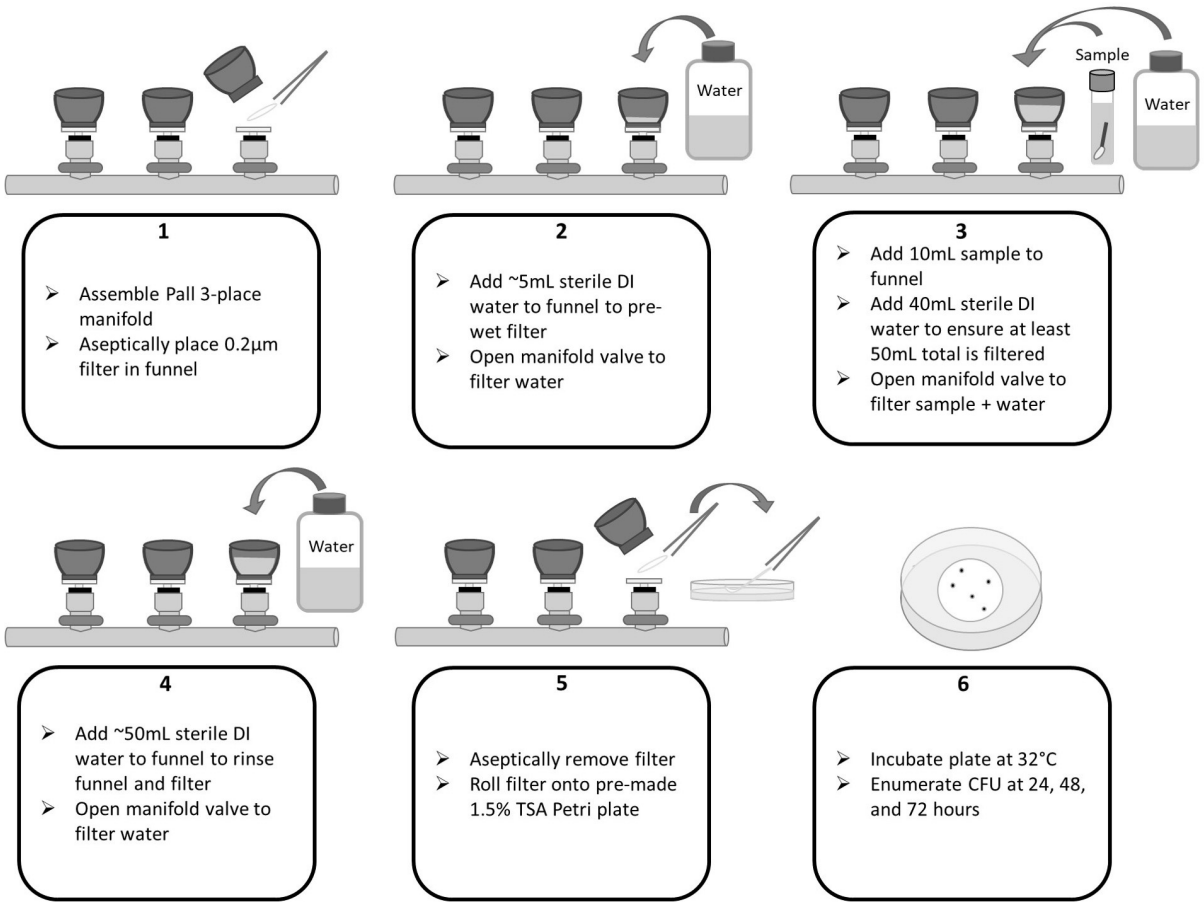

FIGURE 4 | Pall Laboratory Manifold flow diagram for membrane filtration of swab samples.

MilliporeSigma, Burlington, MA, United States), Milliflex Cassette prefilled with Tryptic Soy Agar (PN MXSMCTS48, MilliporeSigma, Burlington, MA, United States), and forceps.

The membrane filtration setup was assembled in a laminar flow environment and consisted of the following: the sterilized pump head is seated onto the pump and wiped down with 70% isopropyl alcohol (IPA). The system is turned on and "manual" filtration mode is selected. Using sterile forceps, the mesh spacer from a funnel is moved to the pump head. Next the funnel is pushed down over the mesh spacer and pump head. The clear cover is removed from the funnel and temporarily set aside.

In accordance with the NASA Standard Assay, swab and wipe samples were sonicated, heat shocked, and cooled. To begin membrane filtration (MF), 8 mL of each sample was added to the funnel. For experiments conducted in this study, APL added 8 mL of sample instead of 10 mL. To ensure a minimum of 50 mL is filtered through the funnel, DI water was added. The "Start" button is pressed on the pump to initiate filtration. A negative control consisting of only sterile DI was included in each sample set to ensure no contamination occurred during the processing. The funnels and filters were rinsed of potentially inhibitory residues with an additional ∼50 mL of sterile water followed by filtration. The "Start" button was pressed again to initiate the automated drying process to remove excess moisture from the filter. Following filtration, the clear cover is returned to the funnel. The entire funnel assembly is removed from the pump head (mesh spacer is left behind) and fitted onto a TSA cassette by pushing down on the funnel assembly until a "click" is heard. The funnel is removed and the clear cover is moved to the cassette. Plates were then incubated at 32°C and enumerated at 24, 48, and 72 h. See **Figures 5**, **6** for process flow diagram. The entire sample volume (8 mL) was filtered (in the absence of sampling devices). Thus, the CFU enumerated at 72 h represents the final CFU (i.e., the pour fraction is 100%).

RESULTS

Pall Laboratory Manifold System (Jet Propulsion Laboratory)

Colony forming units (CFU) recovery was compared between the two methods, NSA and MF, for wipe samples, using a known concentration of *B. atrophaeus* spores (**Figure 7A** and **Table 1**). Each method tested, and a control, consisted of thirty replicates. Non-parametric Mann–Whitney *U* analysis (significance level of 0.05) was conducted comparing the median CFU counts

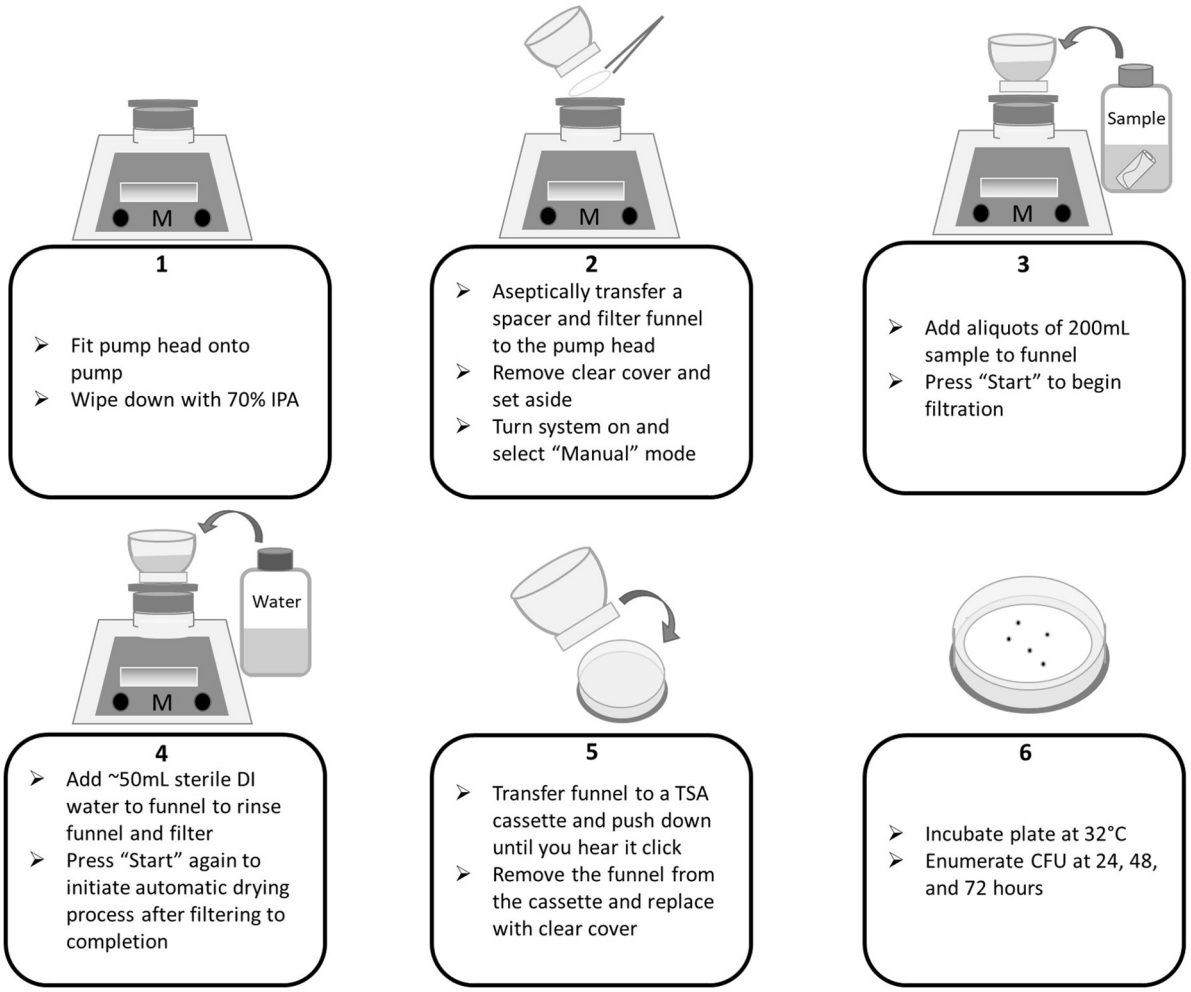

FIGURE 5 | Milliflex flow diagram for membrane filtration of wipe samples.

between methods. Mann–Whitney *U* test was utilized as data resulted in non-normal distribution indicating the need for a non-parametric test, as there is no assumption of normality or equal variances. The sample medians were statistically equivalent between each method, including the control (**Table 2**; *z* value for all method comparisons > critical value of −1.96 and <+1.96). The NSA method resulted in a considerably larger CFU recovery data range than the MF method or control, among which eight out of thirty replicates resulted in zero CFU after 72 h of incubation. These results are not surprising since, with the NSA method, only 50 out of 200 mL is plated; applying a pour fraction extrapolation factor (0.25) leads to greater variance, decreasing the accuracy of spore bioburden estimation. These results demonstrate that the NSA and MF methods are comparable in CFU recovery, but NSA has a higher variance. Moreover, MF allows for greater resolution of bioburden *via* processing of total volume compared with the NSA method.

CFU recovery was compared between the two methods, NSA and MF, for swab samples, using a known concentration of *B. atrophaeus* spores (**Figure 7B** and **Table 1**). Each method tested, and a control, consisted of thirty replicates. A non-parametric Mann Whitney U analysis (significance level of 0.05) was also used to compare the median CFU counts between methods, because data resulted in non-normal distribution. The sample medians were statistically equivalent between the NSA and MF methods (**Table 2**; *z* value of −1.693 > critical value of −1.96 and <+1.96). However, the control median was not statistically equivalent to either the NSA (**Table 2**; *z* value of −3.813 < critical value of −1.96) or MF (**Table 2**; *z* value of −3.013 < critical value of −1.96) methods. This recovery loss in the NSA and MF methods could be due to the lack of surfactant since swab samples are submerged in water and not PP rinse like the wipes; the recovery efficiency may be reduced due to spores adhering to the side of the glass during processing, as no surfactant is present to decrease surface tension. The NSA method resulted in a larger CFU recovery data range than the MF method, among which three out of thirty replicates resulted in zero CFU after 72 h of incubation. These results are not surprising since, with the NSA method, only 8 out of 10 mL is plated; applying a pour fraction extrapolation

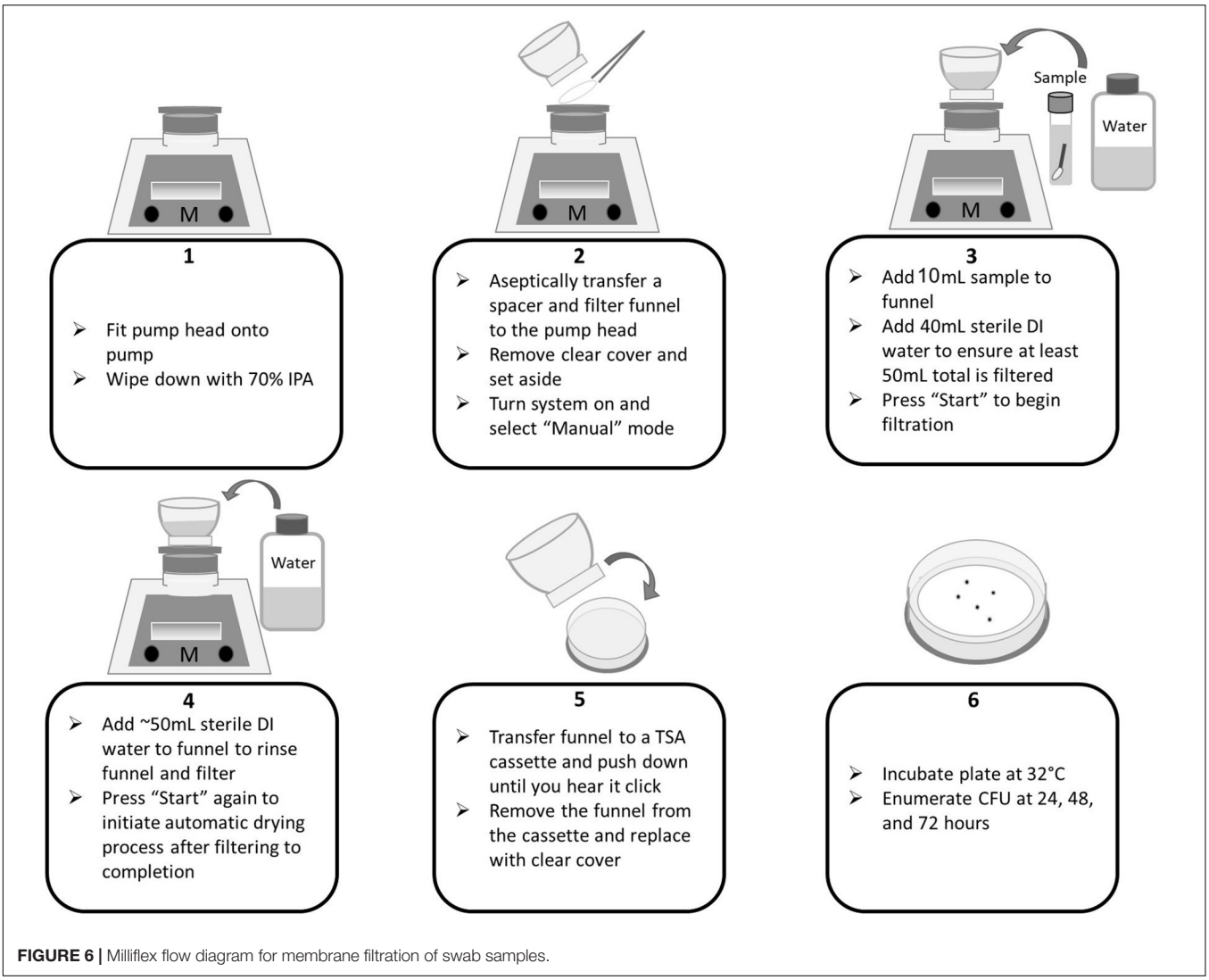

FIGURE 6 | Milliflex flow diagram for membrane filtration of swab samples.

factor (0.8) leads to greater variance (albeit less so than wipe samples), decreasing the accuracy of spore bioburden estimation. These results demonstrate that the NSA and MF methods are comparable in CFU recovery. Moreover, MF allows for greater resolution of bioburden *via* processing of total volume compared with the NSA method.

Millipore Milliflex PLUS System (Applied Physics Laboratory)

CFU recovery was compared between the two methods, NSA and MF, for soil solutions using three different spore concentrations (low, medium, and high, denoted as soil concentration 1, 2, and 3, respectively). Results show that the MF method had higher mean CFUs than the NSA method (**Figures 8A–C** and **Table 3**). In two out of the three sample sets tested, the mean CFUs captured for the methods differed by less than one. *T*-Test was performed after evaluating the distribution of the differences between paired values, where the distribution of the differences should be approximately normally distributed for the *T*-Test to be implemented. For these sample sets, MF and NSA were found to be statistically equivalent (p-value > 0.05, **Table 4**). For one of the sample sets (concentration 1), the methods were found to not be statistically equivalent (p-value < 0.05) with MF collecting more CFUs. Altogether, the MF method is able to recover the same CFU number or more compared to the NSA method. MF and NSA perform similarly even at different concentrations. Moreover, the MF data generally had smaller standard deviation suggesting improved precision compared to NSA.

CFU recovery was compared between the two methods, NSA and MF, for *B. atrophaeus* solutions. There was less than 10% difference in the mean CFUs counted for each method (**Figure 8D** and **Table 3**). MF and NSA methods were shown to be statistically equivalent (p-value > 0.05, **Table 4**).

Membrane Filtration Pour Fraction Extrapolation Factor

In the method comparison studies performed by JPL and APL, we excluded the wipe and swab sampling devices themselves during

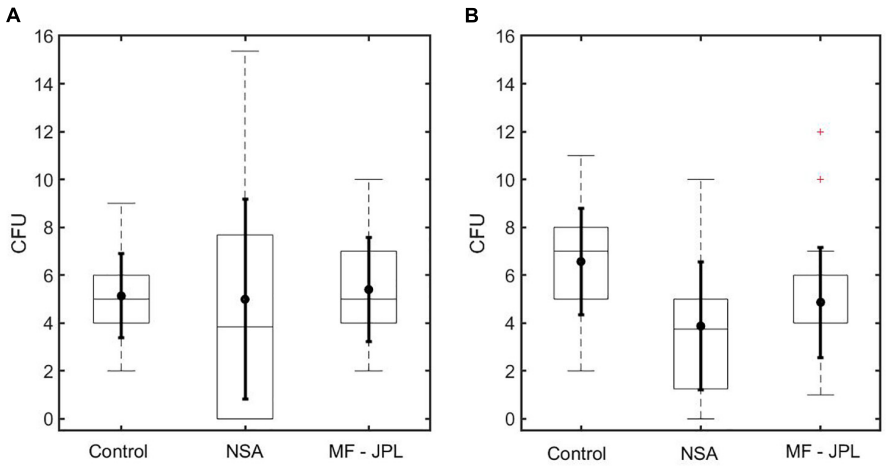

FIGURE 7 | JPL CFU recovery results. Box plot marks the 25th and 75th percentiles. Solid dot in box plot marks the mean. Solid horizontal line in box plot marks the median. Dotted vertical line in box plot marks extreme points. Solid vertical line in box plot marks the standard deviation. Plus sign in box plot denotes outlier. **(A)** CFU recovery comparing NSA and MF-JPL for wipe samples. Results demonstrate similar median between control, NSA, and MF-JPL. Larger data range can be observed with NSA method due to pour fraction extrapolation. **(B)** CFU recovery comparing NSA and MF-JPL for swab samples. Results demonstrate similar median between NSA and MF-JPL. The control median was not similar to either the NSA or MF-JPL methods, likely due to the lack of surfactant since swab samples are submerged in water. Larger data range can be observed with NSA method due to pour fraction extrapolation. MF-JPL median is 4 (overlaps with bottom of box in box plot).

TABLE 1 | CFU recovery comparing NSA and MF (JPL).

Method	Mean (CFU)	Standard deviation (CFU)
Wipe with PP rinse		
Control	5.13	1.76
NSA	4.99	4.18
MF	5.40	2.16
Swab with water		
Control	6.57	2.21
NSA	3.88	2.67
MF	4.87	2.30

TABLE 2 | Statistical equivalence comparing NSA and MF (JPL).

Sample condition	Mann–Whitney *U*: Value, Z crit = ±1.959 (alpha = 0.05)	Statistically equivalent?
Wipe with PP rinse		
Control vs. NSA	−0.798	Yes
Control vs. MF	−0.444	Yes
NSA vs. MF	−1.183	Yes
Swab with water		
Control vs. NSA	−3.813	No
Control vs. MF	−3.013	No
NSA vs. MF	−1.693	Yes

testing to minimize the potential variability of CFU recovery efficiency. Thus, for MF experiments, the pour fraction was 100%. To determine the pour fraction of MF with the sampling devices included, we measured the final volume poured out from each vessel (glass test tubes containing swabs and glass media bottles containing wipes) compared with the initial volume (10 mL for swabs and 200 mL for wipes). From 36 replicates, the average final volume was 9.55 mL for swabs (standard deviation = 0.07) and 185.11 mL for wipes (standard deviation = 1.94). The remaining volume was contained in the sampling devices (∼0.45 mL for swabs and ∼14.89 mL for wipes) and was unable to be extracted during processing. Subtracting the standard deviation values from the average final volumes, we calculated a 95% pour fraction for swabs and a 92% pour fraction for wipes. Thus, for implementation of MF as part of the NASA Standard Assay, we recommend using a 92% pour fraction overall for simplicity for both swabs and wipes.

DISCUSSION

In both the JPL and APL data, we observed a lower mean in the NSA method compared to the MF method. This result may be explained by the fact that with the NSA method, a fraction of the sample volume is plated. When planetary protection engineers sample flight hardware, it is common to expect CFU in the lower ranges (0–5) given that flight hardware is routinely cleaned. With the NSA method, these lower CFU values can skew the mean. While an extrapolation factor is applied, this mathematically derived number may not represent an experimentally derived number. In other words, when only 25% of the sample volume for wipes, or 80% of the sample volume for swabs, is processed with the NSA, there is always the possibility that there may be ≥1 CFU in the un-plated suspension. The only way to obtain a true experimentally derived number is to process the entire sample volume; with MF, 0 CFU is more likely a "true" 0 than with the NSA method since the entire volume is plated with MF. Another possible explanation for the reduction in CFUs is

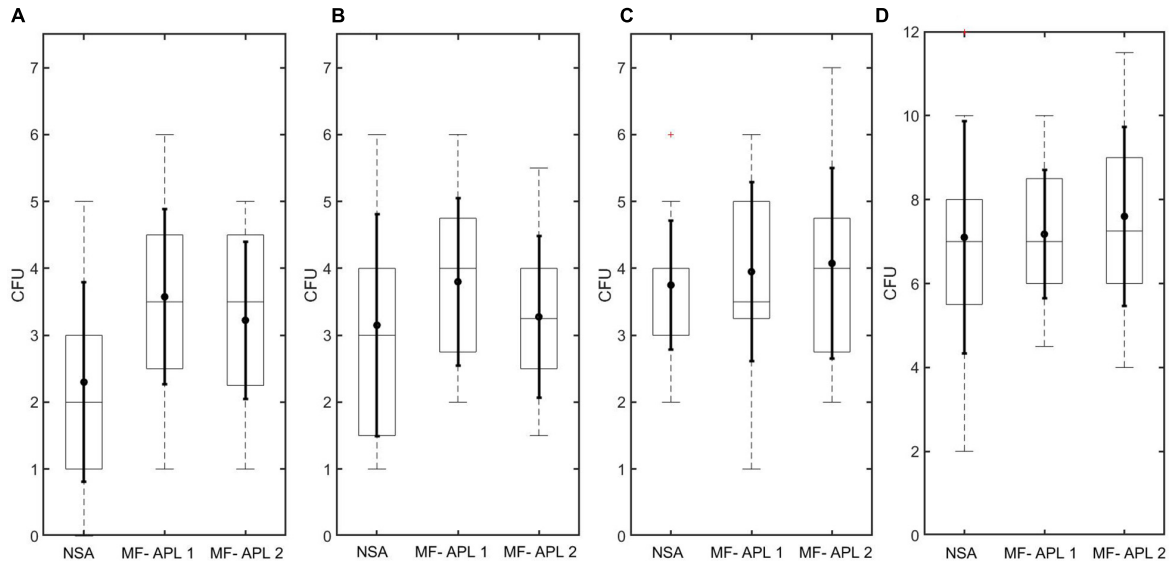

FIGURE 8 | APL CFU recovery results. Box plot marks the 25th and 75th percentiles. Solid dot in box plot marks the mean. Solid horizontal line in box plot marks the median. Dotted vertical line in box plot marks extreme points. Solid vertical line in box plot marks the standard deviation. Plus sign in box plot denotes outlier. **(A–C)** CFU recovery comparing NSA and MF-APL for soil samples in 8 mL DI water for three different spore concentrations. **(D)** CFU recovery comparing NSA and MF-APL for *Bacillus atrophaeus* samples in 8 mL DI water.

TABLE 3 | CFU recovery comparing NSA and MF (APL).

Method	Spore source	Mean (CFU)	Standard deviation (CFU)
NSA	Soil concentration 1	2.300	1.4903
MF 1	Soil concentration 1	3.575	1.3106
MF 2	Soil concentration 1	3.225	1.1751
NSA	Soil concentration 2	3.150	1.6631
MF 1	Soil concentration 2	3.800	1.2503
MF 2	Soil concentration 2	3.275	1.2083
NSA	Soil concentration 3	3.750	0.9665
MF 1	Soil concentration 3	3.950	1.3367
MF 2	Soil concentration 3	4.075	1.426
NSA	*B. atrophaeus*	7.100	2.7701
MF 1	*B. atrophaeus*	7.175	1.5241
MF 2	*B. atrophaeus*	7.600	2.1312

TABLE 4 | Statistical equivalence comparing NSA and MF (APL).

Sample condition	Spore source	*T*-test *P*-value	Statistically equivalent?
NSA vs. MF 1	Soil concentration 1	0.006	No
NSA vs. MF 2	Soil concentration 1	0.039	No
MF 1 vs. MF 2	Soil concentration 1	0.4407	Yes
NSA vs. MF 1	Soil concentration 2	0.141	Yes
NSA vs. MF 2	Soil concentration 2	0.809	Yes
MF 1 vs. MF 2	Soil concentration 2	0.212	Yes
NSA vs. MF 1	Soil concentration 3	0.6211	Yes
NSA vs. MF 2	Soil concentration 3	0.4021	Yes
MF 1 vs. MF 2	Soil concentration 3	0.7868	Yes
NSA vs. MF 1	*B. atrophaeus*	0.9028	Yes
NSA vs. MF 2	*B. atrophaeus*	0.4511	Yes
MF 1 vs. MF 2	*B. atrophaeus*	0.4214	Yes

the less-than-ideal oxygen availability in agar with pour-plate methods (Van der Meeren et al., 2001; Somerville and Proctor, 2013). Even though the agar layer is relatively thin, and some have reported the quick recovery of oxygen in agar medium at <1 cm post-autoclaving (Van der Meeren et al., 2001), the oxygen availability to microbes embedded in agar is far less than what is available to surface-grown microbes. As previously described, the growth conditions of the NSA result in an underestimation of overall microbes recovered (La Duc et al., 2007; Ghosh et al., 2010; Moissl-Eichinger et al., 2015; Hendrickson et al., 2021), however, this did not impact the results of this study as only equivalency was investigated.

Should planetary protection engineers elect to use MF as part of the NASA Standard Assay, they may need to vary the number of filters required for each sample based on the expected cleanliness of the sampled surfaces. For example, facility samples from surfaces that may be less rigorously cleaned than flight hardware (e.g., floors, benches, ground support equipment, etc.) may require two or more filters be used on a single wipe sample to prevent filter saturation or coalescing of colonies, for accurate CFU enumeration.

In our results, we reported the recovery loss in the swab samples when comparing NSA and MF with the control. This could be due to the lack of surfactant since swab samples are submerged in water and not PP rinse like the wipes. Future studies may focus on experimenting with swabs submerged in PP rinse and potentially changing the NASA Standard Assay to suspend swabs in PP Rinse instead of water, to optimize the recovery efficiency by reducing the possibility of spores

adhering to the side of the glass walls of the sampling tubes during processing.

In our study, we elected to use a sterilizing grade filter (pore size of 0.2 μm). The industry standard for testing bacterial retention in any sterilizing grade filter is a recovery challenge of 1×10^7 cfu/cm^2 *Brevundimonas diminuta* bacteria (ASTM International, 2020) given Dr. Frances Bowman's observation that this bacterium could repeatedly penetrate a 0.45 μm rated filter but not a 0.2 μm filter (Bowman et al., 1967; Duda et al., 2012; Ghuneim et al., 2018). However, the planetary protection engineer could elect to use a 0.45 μm filter (used in many applications for the microbiological examination of water, pharmaceuticals, and food) provided they perform testing similar to this study demonstrating equivalence with the NASA Standard Assay pour-plate method. In addition to considering a different pour size for the membrane filtration filter, future studies could also experiment with different filter materials (e.g., polyvinylidene fluoride or mixed cellulose esters).

The results from our study demonstrate that samples processed with MF result in equivalent bioburden detection capabilities with far less bioburden estimation variance than the NSA method. This was true for samples tested by JPL and APL, using both Pall® Laboratory Manifold and Milliflex® Plus Vacuum Pump Systems, respectively. MF is capable of processing a larger sample volume with less data variance, leading to a higher resolution of spore bioburden compared with the NSA method. Moreover, the MF method is a more sustainable option given the ability to process larger sample volumes; fewer plates means reduced TSA, cost, waste, and energy consumption.

DATA AVAILABILITY STATEMENT

The original contributions presented in the study are included in the article/supplementary material, further inquiries can be directed to the corresponding author/s.

AUTHOR CONTRIBUTIONS

KS contributed to JPL data interpretation, coordination with APL, and drafted the manuscript. LM contributed to JPL experimental design and laboratory experiments, statistical analysis, and initial chart development. RH contributed to JPL experimental design, coordination with APL, and data analysis and interpretation. CS and MS contributed to APL laboratory experiments. MB contributed to APL experimental design, coordination with JPL, and data analysis and interpretation. All authors contributed to reading and editing the manuscript, and approved the final manuscript.

FUNDING

This research was carried out at the Jet Propulsion Laboratory, California Institute of Technology, under a contract with the National Aeronautics and Space Administration (80NM0018D0004), supported by the Europa Clipper Project. This research was also carried out at Johns Hopkins University Applied Physics Laboratory, supported by the Europa Clipper Project. The funders had no role in study design, data collection and interpretation, writing of the manuscript, or decision to submit this work for publication.

ACKNOWLEDGMENTS

We would like to acknowledge Hyung Park for initial project oversight. We would also like to acknowledge Emily Klonicki and Sarah Yearicks for compiling initial information related to results and materials and methods.

REFERENCES

ASTM International (2020). *Standard Test Method for Determining Bacterial Retention of Membrane Filters Utilized for Liquid Filtration*. West Conshohocken: ASTM, F838–F820.

Benardini, J. N. III, La Duc, M. T., Beaudet, R. A., and Koukol, R. (2014). Implementing planetary protection measures on the Mars Science Laboratory. *Astrobiology* 14, 27–32. doi: 10.1089/ast.2013.0989

Blosse, P. T., Boulter, E. M., and Sundaram, S. (1998). Diminutive bacteria: implications for sterile filtration. *Am. Biotechnol. Lab.* 16, 38–40.

Bordner, R., Winter, J. A., Scarpino, P., and (Eds.). (1978). *Microbiological Methods for Monitoring the Environment: Water and Wastes. Cincinnati, OH: Environmental Protection Agency, Office of Research and Development, Environmental Monitoring and Support Laboratory*. Washington, D.C: United States Environmental Protection Agency.

Bowman, F. W., Calhoun, M. P., and White, M. (1967). Microbiological methods for quality control of membrane filters. *J. Pharm. Sci.* 56, 222–225. doi: 10.1002/jps.2600560214

Committee on Preventing the Forward Contamination of Mars, National Research Council (2006). *Preventing the Forward Contamination of Mars*. Washington, DC: National Academies Press.

COSPAR (2008). *COSPAR Planetary Protection Policy, 20 October 2002, Amended March 2008*. Houston, TX: COSPAR.

Crawford, R. L. (2005). Microbial diversity and its relationship to planetary protection. *Appl. Environ. Microbiol.* 71, 4163–4168. doi: 10.1128/AEM.71.8.4163-4168.2005

Crittenden, J. C., Trussell, R. R., Hand, D. W., Howe, K. J., and Tchobanoglous, G. (2012). *MWH's Water Treatment: Principles and Design*. Hoboken, NJ: John Wiley & Sons.

Duda, V. I., Suzina, N. E., Polivtseva, V. N., and Boronin, A. M. (2012). Ultramicrobacteria: formation of the concept and contribution of ultramicrobacteria to biology. *Microbiology* 81, 379–390. doi: 10.1134/S0026261712040054

ECSS-Q-ST-70-55 Working Group (2008). *Microbial Examination of Flight Hardware and Clean rooms. ECSS-Q-ST-70-55C, European Cooperation for Space Standardization, ESA Requirements and Standards Division, European Space Agency*. Noordwijk: European Space Research and Technology Centre ESTEC.

Ghosh, S., Osman, S., Vaishampayan, P., and Venkateswaran, K. (2010). Recurrent isolation of extremotolerant bacteria from the clean room where phoenix spacecraft 1092 components were assembled. *Astrobiology.* 10, 325–335. doi: 10.1089/ast.2009.0396

Ghuneim, L. J., Jones, D. L., Golyshin, P. N., and Golyshina, O. V. (2018). Nano-Sized and filterable bacteria and archaea: biodiversity and function. *Front. Microbiol.* 9:1971. doi: 10.3389/fmicb.2018.01971

Grinnell, F. B. (1929). Observations on some of the factors involved in filtration experiments. *J. Bacteriol.* 18, 175–180. doi: 10.1128/jb.18.3.175-180.1929

Handbook for the Microbial Examination of Space Hardware (2010). *NASA Technical Handbook (NASA-HDBK-6022)*. Washington, DC: NASA Headquarters.

Hendrickson, R., Kazarians, G., and Benardini, J. N. III (2020). Planetary protection implementation on the interior exploration using seismic investigations, geodesy and heat transport mission. *Astrobiology* 20, 1151–1157. doi: 10.1089/ast.2019.2098

Hendrickson, R., Urbaniak, C., Minich, J. J., Aronson, H. S., Martino, C., Stepanauskas, R., et al. (2021). Clean room microbiome complexity impacts planetary protection bioburden. *Microbiome* 9:238. doi: 10.1186/s40168-021-01159-x

La Duc, M. T., Dekas, A., Osman, S., Moissl, C., Newcombe, D., and Venkateswaran, K. (2007). Isolation and characterization of bacteria capable of tolerating the extreme conditions of clean room environments. *Appl. Environ. Microbiol.* 73, 2600–2611. doi: 10.1128/AEM.03007-06

La Duc, M. T., Kern, R., and Venkateswaran, K. (2004a). Microbial monitoring of spacecraft and associated environments. *Microbial. Ecol.* 47, 150–158. doi: 10.1007/s00248-003-1012-0

La Duc, M. T., Satomi, M., and Venkateswaran, K. (2004b). *Bacillus odysseyi* sp. nov., a round-spore-forming bacillus isolated from the Mars Odyssey spacecraft. *Int. J. Syst. Evol. Microbiol.* 54, 195–201. doi: 10.1099/ijs.0.02747-0

Lee, S. Y., Chang, S. S., Shin, J. H., and Kang, D. H. (2007). Membrane filtration method for enumeration and isolation of *Alicyclobacillus* spp. from apple juice. *Lett. Appl. Microbiol.* 45, 540–546. doi: 10.1111/j.1472-765X.2007.02229.x

Meltzer, M. (2012). *When Biospheres Collide: A History of NASA's Planetary protection programs*, 4234. Washington, DC: NASA Aeronautics and Space Administration.

Moissl, C., Osman, S., La Duc, M. T., Dekas, A., Brodie, E., DeSantis, T., et al. (2007). Molecular bacterial community analysis of clean rooms where spacecraft are assembled. *FEMS Microbiol. Ecol.* 61, 509–521. doi: 10.1111/j.1574-6941.2007.00360.x

Moissl-Eichinger, C., Auerbach, A. K., Probst, A. J., Mahnert, A., Tom, L., Piceno, Y., et al. (2015). Quo vadis? Microbial profiling revealed strong effects of cleanroom maintenance and routes of contamination in indoor environments. *Sci. Rep.* 5:9156. doi: 10.1038/srep09156

Onyango, L. A., Dunstan, R. H., and Roberts, T. K. (2010). Filterability of staphylococcal species through membrane filters following application of stressors. *BMC Res. Notes* 3:152. doi: 10.1186/1756-0500-3-152

Osman, S., Satomi, M., and Venkateswaran, K. (2006). *Paenibacillus pasadenensis* sp. nov. and *Paenibacillus barengoltzii* sp. nov., isolated from a spacecraft assembly facility. *Int. J. Syst. Evol. Microbiol.* 56, 1509–1514. doi: 10.1099/ijs.0.64085-0

Satomi, M., La Duc, M. T., and Venkateswaran, K. (2006). *Bacillus safensis* sp. nov., isolated from spacecraft and assembly-facility surfaces. *Int. J. Syst. Evol. Microbiol.* 56, 1735–1740. doi: 10.1099/ijs.0.64189-0

Sharpe, A. N., Peterkin, P. I., and Dudas, I. S. T. V. A. N. (1979). Membrane filtration of food suspensions. *Appl. Environ. Microbiol.* 37, 21–35. doi: 10.1128/aem.37.1.21-35.1979

Smith, L. O. R. I., Carroll, K., and Mottice, S. (1993). Comparison of membrane filters for recovery of legionellae from water samples. *Appl. Environ. Microbiol.* 59, 344–346. doi: 10.1128/aem.59.1.344-346.1993

Solomon, B. A., Castino, F., Lysaght, M. J., Colton, C. K., and Friedman, L. I. (1978). Continuous flow membrane filtration of plasma from whole blood. *ASAIO J.* 24, 21–26.

Somerville, G. A., and Proctor, R. A. (2013). Cultivation conditions and the diffusion of oxygen into culture media: the rationale for the flask-to-medium ratio in microbiology. *BMC Microbiol.* 13:9. doi: 10.1186/1471-2180-13-9

United Nations (1967). *Treaty on Principles Governing the Activities of States in the Exploration and use of Outer Space, Including the Moon and Other Celestial Bodies*. Washington, D.C: Outer Space Treaty.

Van der Meeren, P., De Vleeschauwer, D., and Debergh, P. (2001). Determination of oxygen profiles in agar-based gelled in vitro plant tissue culture media. *Plant cell Tissue Organ Cult.* 65, 239–245. doi: 10.1023/A:1010698225362

Venkateswaran, K., Kempf, M., Chen, F., Satomi, M., Nicholson, W., and Kern, R. (2003). *Bacillus nealsonii* sp. nov., isolated from a spacecraft-assembly facility, whose spores are γ-radiation resistant. *Int. J. Syst. Evol. Microbiol.* 53, 165–172. doi: 10.1099/ijs.0.02311-0

Wang, Y., Hammes, F., Düggelin, M., and Egli, T. (2008). Influence of size, shape, and flexibility on bacterial passage through micropore membrane filters. *Environ. Sci Technol.* 42, 6749–6754. doi: 10.1021/es800720n

Conflict of Interest: The authors declare that the research was conducted in the absence of any commercial or financial relationships that could be construed as a potential conflict of interest.

frontiers | Frontiers in Microbiology

ORIGINAL RESEARCH
published: 30 June 2022
doi: 10.3389/fmicb.2022.893071

The International Space Station Environment Triggers Molecular Responses in *Aspergillus niger*

*Adriana Blachowicz[1,2], Jillian Romsdahl[1], Abby J. Chiang[3], Sawyer Masonjones[4], Markus Kalkum[3], Jason E. Stajich[4], Tamas Torok[5], Clay C. C. Wang[1,6] and Kasthuri Venkateswaran[2]**

[1]Department of Pharmacology and Pharmaceutical Sciences, School of Pharmacy, University of Southern California, Los Angeles, CA, United States, [2]Biotechnology and Planetary Protection Group, Jet Propulsion Laboratory, California Institute of Technology, Pasadena, CA, United States, [3]Department of Immunology and Theranostics, Beckman Research Institute of City of Hope, Duarte, CA, United States, [4]Department of Microbiology and Plant Pathology, Institute for Integrative Genome Biology, University of California, Riverside, Riverside, CA, United States, [5]Ecology Department, Lawrence Berkeley National Laboratory, Berkeley, CA, United States, [6]Department of Chemistry, Dornsife College of Letters, Arts, and Sciences, University of Southern California, Los Angeles, CA, United States

OPEN ACCESS

Edited by:
Donatella Tesei, University of Natural Resources and Life Sciences Vienna, Austria

Reviewed by:
Ekaterina Dadachova, University of Saskatchewan, Canada
Corrado Nai, FEMS Federation of European Microbiological Societies, Netherlands

***Correspondence:**
Kasthuri Venkateswaran
kjvenkat@jpl.nasa.gov

Specialty section:
This article was submitted to Extreme Microbiology, a section of the journal Frontiers in Microbiology

Received: *09 March 2022*
Accepted: *30 May 2022*
Published: *30 June 2022*

Citation:
Blachowicz A, Romsdahl J, Chiang AJ, Masonjones S, Kalkum M, Stajich JE, Torok T, Wang CCC and Venkateswaran K (2022) The International Space Station Environment Triggers Molecular Responses in Aspergillus niger. Front. Microbiol. 13:893071. doi: 10.3389/fmicb.2022.893071

Due to immense phenotypic plasticity and adaptability, *Aspergillus niger* is a cosmopolitan fungus that thrives in versatile environments, including the International Space Station (ISS). This is the first report of genomic, proteomic, and metabolomic alterations observed in *A. niger* strain JSC-093350089 grown in a controlled experiment aboard the ISS. Whole-genome sequencing (WGS) revealed that ISS conditions, including microgravity and enhanced irradiation, triggered non-synonymous point mutations in specific regions, chromosomes VIII and XII of the JSC-093350089 genome when compared to the ground-grown control. Proteome analysis showed altered abundance of proteins involved in carbohydrate metabolism, stress response, and cellular amino acid and protein catabolic processes following growth aboard the ISS. Metabolome analysis further confirmed that space conditions altered molecular suite of ISS-grown *A. niger* JSC-093350089. After regrowing both strains on Earth, production of antioxidant—Pyranonigrin A was significantly induced in the ISS-flown, but not the ground control strain. In summary, the microgravity and enhanced irradiation triggered unique molecular responses in the *A. niger* JSC-093350089 suggesting adaptive responses.

Keywords: *Aspergillus niger*, International Space Station, metabolome, proteome, genome

INTRODUCTION

The International Space Station (ISS) is a research facility orbiting at an approximate altitude of 250 miles that is utilized to study physiological, psychological, and immunological responses of humans living in isolation (Mehta et al., 2004; Crucian et al., 2013; Cucinotta, 2014; Benjamin et al., 2016; Ombergen et al., 2017). However, the distinct ISS environment, which includes microgravity and enhanced irradiation, affects the metabolism of all living organisms aboard the ISS including humans. There is a growing body of research that focuses on molecular characterization of animal (Ijiri, 2003; Tavella et al., 2012), plant (Link et al., 2003; Driss-Ecole

et al., 2008; Kittang et al., 2014), and microbial (Rabbow et al., 2003; Benoit et al., 2006) responses to the conditions encountered in the ISS. Among the most studied microorganisms are various species of bacteria (Klaus et al., 1997; Weng et al., 1998; Nickerson et al., 2000; Vaishampayan et al., 2012), yeast (Takahashi et al., 2001; Purevdorj-Gage et al., 2006; Altenburg et al., 2008; Liu et al., 2008; Crabbé et al., 2013), and black fungi (Onofri et al., 2008, 2012, 2015). However, there are few reported studies that characterize the molecular responses of filamentous fungi (Romsdahl et al., 2018, 2019, 2020; Blachowicz et al., 2019b).

Filamentous fungi are producers of a myriad of bioactive compounds or secondary metabolites (SMs). These SMs often confer environmental advantage, which facilitate survival in hostile niches despite not being directly essential for survival (Keller et al., 2005; Fox and Howlett, 2008; Brakhage and Schroeckh, 2011; Rohlfs and Churchill, 2011; Brakhage, 2013). SMs span from potent bioactive molecules used in the drug discovery processes (Borel et al., 1995; Elander, 2003; Mulder et al., 2015) or other branches of the industry (Vandenberghe et al., 2000; Rodríguez Couto and Toca Herrera, 2006; Piscitelli et al., 2010; Dhillon et al., 2011) to health hazardous toxins (Barnes, 1970; Shephard, 2008; Hof and Kupfahl, 2009; Eaton and Groopman, 2013). Altered production of various SMs is one potential mechanism of fungal adaptation to extreme environments. For example, increased production of melanin, a pigment with UV protective properties, was observed in fungi isolated from Chernobyl nuclear power plant (Dadachova et al., 2008) and "Evolution Canyon" (Singaravelan et al., 2008). One such highly melanized fungal species is *Aspergillus niger*.

Industrially important *A. niger* (Schuster et al., 2002) has been isolated from various ecological niches, including decaying leaves (Nikolcheva et al., 2003), common households (Adams et al., 2013; Barberán et al., 2015), and the ISS (Checinska et al., 2015). The *A. niger* strain JSC-093350089 isolated from the surface of the US compartment of the ISS was previously characterized using multi-omics techniques. Performed analyses revealed genetic variance typical for the *A. niger* clade, increased abundance of proteins involved in starvation response, oxidative stress, and cell wall modulation (Romsdahl et al., 2018), and alteration in SM production levels when compared to well-studied *A. niger* ATCC 1015 strain (Romsdahl et al., 2019). However, definite ascribing of observed molecular alterations to the ISS environment was not possible, since the strains were not grown in microgravity using a controlled experiment with ground counterparts. Nevertheless, in-depth characterization of ISS-isolated JSC-093350089 *A. niger* provided insight into potential space-induced molecular phenotypes.

This study is the first report of the multi-omics characterization of *A. niger* JSC-093350089 grown aboard the ISS and compared to ground controls. To study the impact of the enhanced irradiation and microgravity on JSC-093350089, the strain was transported to and grown aboard the ISS. Upon return to Earth, ISS-grown samples, along with ground controls, were immediately processed for metabolomic, proteomic, and genomic analyses with the aim of obtaining important insights into the adaptive responses of *A. niger* to space conditions. In addition, ISS-grown samples were regrown on Earth to identify any conserved molecular alterations.

MATERIALS AND METHODS

Isolation and Identification of *Aspergillus niger*

Procedures to isolate and identify *A. niger* collected from the ISS were described previously (Romsdahl et al., 2018). In brief, sterile swabs soaked in saline solution were used to sample the ISS surface and transported to Earth. Particles retrieved from the swab were spread into potato dextrose agar (PDA) plates and any growing colonies were purified, collected, and further analyzed. One of the collected isolates was identified as *A. niger via* ITS region sequencing, which was subsequently confirmed *via* whole-genome sequencing (WGS).

Growth Conditions

JSC-093350089 was cultivated on glucose minimal medium (GMM) agar plates (6 g/l $NaNO_3$, 0.52 g/l KCl, 0.52 g/l $MgSO_4{\cdot}7H_2O$, 1.52 g/l KH_2PO_4, 10 g/l D-glucose, and 15 g/l agar supplemented with 1 ml/l of Hutner's trace elements) covered with a cellophane membrane. Each of 10 prepared Petri plates (D = 10 cm) was inoculated with 1×10^7 conidia/plate. Subsequently, plates were sealed with 3 M™ Micropore™ Surgical Tape (VWR International, Radnor, PA, United States) and placed in four Biological Research in Canister (BRIC) systems (three and two plates/BRIC). BRICs were divided into two groups, which were exact mimics, and transferred to 4°C. The exact timeline of the experiment is presented in **Supplementary Figure 1**. The whole experiment lasted 42 days from preparing the payload by a science team prior to launch till the handout of the ISS-grown samples back to the science team after the flight. The first group of BRICs was sent to the ISS and continuously kept at 4°C (1–20 days) prior to being transferred to ambient temperature for the active growth phase ~22°C for 12 days (21–32 days). After that time BRICs were stored at 4°C before returning to Earth (33–42 days). Upon arrival to Earth, BRICs were turned over to the science team for the downstream analyses, which commenced immediately. The second group of BRICs, treated as controls, was kept on Earth at Kennedy Space Center (KSC) and mimicked the ISS experiment timeline with roughly 2 h of delay. BRICs containing control samples were shipped from KSC to research team along with the ISS-grown samples. Lastly, for an additional secondary metabolite analysis, 1×10^7 conidia/plate of the ISS- and ground-grown JSC-093350089 were grown on GMM medium at 28°C for 5 days.

Genomic DNA Extraction and Whole-Genome Sequencing

Mycelia and conidia were collected from ground-and ISS-grown JSC-09335008 GMM agar plates. DNA was extracted using the Power Soil DNA Isolation Kit (Mo Bio Laboratories, Carlsbad, California, United States) following the manufacturers protocol. Extracted DNA was checked for quality using Qubit 2.0

Fluorometer and used for paired-end library preparation with TruSeq Nano DNA Library Preparation Kit (Illumina, San Diego, California, United States) followed by WGS at the Duke Center for Genomic and Computational Biology. Samples were sequenced using a HiSeq 4,000 Illumina Sequencer generating 101 base long reads.

Genetic Variation Identification

Illumina sequence reads were trimmed using Trimmomatic v 0.36 (Bolger et al., 2014) and checked for quality using FastQC v 0.11.5 (Andrews, 2010). The genome and annotation files for *A. niger* CBS 513.88, (Pel et al., 2007) were downloaded from the FungiDB web portal (Stajich et al., 2012). Reads were mapped to CBS 513.88 the reference genome using the Burrows-Wheeler Aligner (BWA) software package v 0.7.12 (Li and Durbin, 2009) and further processed with SAMtools v 1.6 to generate sorted BAM files (Li et al., 2009). SNPs and INDELs were identified using GATK v 3.7 (DePristo et al., 2011). Duplicates were marked using Picard-tools MarkDuplicates[1] to remove PCR artifacts. Sequence reads containing putative INDELs were realigned using GATK's IndelRealigner to generate an updated BAM file. Variants within each sample were called using GATK's Haplotype Caller. GATK's VariantFiltration was used to filter each VCF file based on stringent cutoffs for quality and coverage {SNPs: QD < 2.0, MQ < 40.0, QUAL < 100, FS > 60.0, MQRankSum < −12.5, SOR > 4.0, ReadPosRankSum < −8.0; Indels: QD < 2.0, FS > 200.0, MQRankSum < −12.5, SOR > 4, InbreedingCoeff < −0.8, ReadPosRankSum < −20.0}, so that only high-quality variants remained.

Protein Extraction

Mycelia and conidia from GMM agar plates were collected and stored at −80°C prior to protein extraction. Proteins were extracted with the lysis buffer consisting of 100 mm triethylammonium bicarbonate (TEAB) with 1:100 Halt Protease Inhibitor Cocktail (Thermo Scientific, Rockford, IL) and 200 µg/ml phenylmethylsulfonyl fluoride (Sigma-Aldrich, St. Louis, MO, United States). Mycelia and conidia were homogenized by bead beating using Precellys 24 homogenizer (Bertin, Rockville, MD). The lysed fungal material was centrifuged at 17,000 g for 15 min and the protein concentration in the supernatants was measured by the Bradford assay (Bio-Rad Laboratories, Inc. Hercules, CA, United States).

Tandem Mass Tag (TMT) Labeling

A 100 µg proteins from each sample were precipitated in 20% trichloroacetic acid (TCA) at 4°C. Protein pellets were washed with ice-cold acetone and re-suspended in 25 µl TEAB (100 mM) and 25 µl 2,2,2-trifluoroethanol (TFE). Proteins were reduced with 1 µl of tris(2-carboxyethyl)phosphine (TCEP, 500 mM), alkylated with iodoacetamide (IAA, 30 mM), and digested with 2.5 µg/sample of trypsin/lysC (Promega, Madison, WI, United States) overnight at 37°C. The digested peptides were quantified using the Pierce Quantitative Colorimetric Peptide Assay (Thermo Scientific, Waltham, MA, United States). 40 µg of peptides from each specific sample was labeled with the Thermo Scientific TMTsixplex Isobaric Mass Tagging Kit (JSC-E1 (ground 1) with TMT^6-128, JSC-E2 (ground 2) with TMT^6-130, JSC-S1 (ISS 1) with TMT^6-129, JSC-S2 (ISS 2) with TMT^6-131) according to the manufacturer's protocol. All labeled-peptide mixtures were combined into a single tube, mixed, and fractionated using the Thermo Scientific Pierce High pH Reversed-Phase Peptide Fractionation Kit. While this kit usually uses eight fractions with step elution of up to 50% acetonitrile, ninth fraction was added eluting at 100% acetonitrile. Nine fractionated samples were dried using a SpeedVac concentrator and re-suspended in 1% (v/v) formic acid prior to liquid chromatography with tandem mass spectrometry (LC-MS/MS) analysis.

LC–MS/MS Analysis

The samples were analyzed on an Orbitrap Fusion Tribrid mass spectrometer with an EASY-nLC 1,000 Liquid Chromatograph, a 75 µm × 2 cm Acclaim PepMap100 C18 trapping column, and a 75 µm × 25 cm PepMap RSLC C18 analytical column, and an Easy-Spray ion source (Thermo Scientific, Waltham, MA, United States). The peptides were eluted at 45°C with a flow rate of 300 nl/min over a 110 min gradient, from 3 to 30% solvent B (100 min), 30–50% solvent B (3 min), 50–90% solvent B (2 min), and 90% solvent B (2 min). The solvent A was 0.1% formic acid in water and the solvent B was 0.1% formic acid in acetonitrile.

The full MS survey scan (m/z 400–1,500) was acquired at a resolution of 120,000 and an automatic gain control (AGC) target of 2×10^5 in the Orbitrap with the 50 ms maximum injection time for MS scans. Monoisotopic precursor ions were selected with charge states 2–7, a ± 10 ppm mass window, and 70 s dynamic exclusion. The MS^2 scan (m/z 400–2000) was performed using the linear ion trap with the 35% collision-induced dissociation (CID) energy. The ion trap scan rate was set to "rapid," with an AGC target of 4×10^3, and a 150 ms maximum injection time. Ten fragment ions from each MS^2 experiment were subsequently selected for an MS^3 experiment. The MS^3 scan (m/z 100–500) was performed to generate the TMT reporter ions in the linear ion trap using higher-energy collisional dissociation (HCD) at a 55% collision energy, a rapid scan rate and an AGC target of 5×10^3, and a maximum injection time of 250 ms.

Proteome Data Analysis

All MS data (MS^1, MS^2, and MS^3) were searched using the Proteome Discoverer (version 2.2.0.388, Thermo Scientific) with the Sequest-HT searching engines against an *Aspergillus niger* CBS 513.88 database containing 10,549 sequences (NCBI). The searches were performed with the following parameters: 2 maximum missed cleavage sites, 6 minimum peptide length, 5 ppm tolerance for precursor ion masses, and 0.6 Dalton tolerance for fragment ion masses. The static modification settings included carbamidomethyl of cysteine residues, and

[1]https://broadinstitute.github.io/picard/

dynamic modifications included oxidation of methionine, TMT6plex modification of lysine ε-amino groups and peptide N-termini, and acetyl modification of protein N-terminus. A false discovery rate (FDR) of 1% was set using a target-decoy database search. The reporter ions integration tolerance was 0.5 Da and the co-isolation threshold was 75%. The average signal-to-noise threshold of all reporter peaks was bigger than 10. The total intensity of a reporter ion for a protein was calculated based on the sum of all detected reporter ions of associated peptides from that protein. The ratios between an abundance of a reporter and the average abundance of all reporters were used to estimate the abundance ratio of each protein.

For statistical analysis, the sum of reporter ion intensities for each protein was Log2 transformed and the biological duplicate and technical triplicate measurement for each protein was averaged. Only the proteins that were identified and quantified in both biological and technical replicates were used for the analysis. Student t-test was performed to identify proteins with changed abundance. Proteins with value of $p < 0.05$ were further evaluated for increased and decreased abundance using a cut-off value of $\geq \pm 1$ fold (Log2) change.

Secondary Metabolite Extraction and Analysis

Upon return to Earth single plates from both ground- and ISS-kept BRICs were used to collect agar plugs in triplicate for secondary metabolite (SM) extraction. Plugs were extracted with 3 ml of methanol and 1:1 methanol/dichloromethane each followed by 1 h sonication. Crude extract was evaporated *in vacuo* to yield a residue that was then suspended in 1 ml of 20% dimethyl sulfoxide/methanol and 10 µl was examined by high-performance liquid chromatography-photodiode array detection-mass spectrometry (HPLC-DAD-MS) analysis. HPLC–MS was carried out using ThermoFinnigan LCQ Advantage ion trap mass spectrometer with an RP C18 column (Alltech Prevail C18 3 mm 2.1 × 100 mm) at a flow rate 125 µl/min. The solvent gradient for LC–MS was 95% acetonitrile/H2O (solvent B) in 5% acetonitrile/H2O (solvent A) both containing 0.05% formic acid, as follows: 0% solvent B from 0 min to 5 min, 0 to 100% solvent B from 5 min to 35 min, 100% solvent B from 35 min to 40 min, 100 to 0% solvent B from 40 min to 45 min, and re-equilibration with 0% solvent B from 45 min to 50 min. The SM profiles of ISS- and ground-grown JSC-093350089, which were regrown at 28°C were obtained following the procedure described above.

SM Statistical Analysis

To compare the yields of produced SMs in ISS-grown, ground-grown, and regrown samples, the area under the electrospray ionization curve (ESI) was integrated for each compound. SM data collected from three independent biological replicates of ISS- and ground-grown, and regrown JSC-093350089 were used for testing statistical significance of production yields of identified SMs by Welch's corrected t-test. The data are presented as column charts with corresponding error bars. Data analysis was conducted using GraphPad Prism version 7.

RESULTS

Genome Variation in the ISS-Grown JSC-093350089 *Aspergillus niger*

The genomes of ISS-flown and ground-grown JSC-093350089 were compared to identify occurring genetic variations. Obtained reads were aligned to the CBS 513.88 reference genome and single-nucleotide polymorphisms (SNPs) present in the ground control were filtered. This revealed presence of 375 SNPs and 620 INDELs that occurred because of the exposure to conditions aboard the ISS (**Table 1**). All identified genetic variations are summarized in **Supplementary Tables 1** and **2**, presenting SNPs and INDELs, respectively. Distribution of non-synonymous point mutations among genes is presented in **Table 2**. Interestingly, about 80% of these mutations occurred in chromosome VIII and 13% occurred in chromosome XII, while the remaining 7% were distributed among other chromosomes (**Supplementary Figure 2A**). The majority of missense point mutations (75%) were observed within genes of unknown function. However, several characterized genes containing missense SNPs have DNA-binding activity (An06g01180, An08g11890, and An12g00840), DNA polymerase activity (An08g11520), protein kinase and transferase activity (An08g12110), phospholipase activity (An08g12250), and chromosome anchoring RacA protein binding activity (An12g06420; **Table 2**). Additional, mutations like one stop lost, one start gained and one 5 prime untranslated region (UTR) mutation were observed. Most of the observed SNPs (~55%) and INDELs (71%) were located in intergenic regions (**Table 1**). Interestingly, unlike SNPs, INDELs were distributed throughout all chromosomes. However, similarly to SNPs, the highest number of INDELS was found in chromosomes VIII and XII. Among observed INDELS 109 caused frameshift, 14 lead to disruptive inframe deletion, and a few caused start lost and stop gained (**Supplementary Table 2**; **Supplementary Figure 2B**).

TABLE 1 | Summary of genetic variations observed in ISS-grown JSC-093350089 when compared to ground control.

	Type of mutation	Occurrence number
SNPs	Intergenic	205
	Missense	79
	Splice region	4
	Start gained	1
	Stop lost	1
	5 prime UTR	1
	Synonymous	84
Total no. of SNPs		375
INDELs	Intergenic	444
	5 prime UTR	10
	Conservative inframe deletion	8
	Disruptive inframe deletion	14
	Frameshift	109
	3 prime UTR	15
	Splice region	11
	Start lost	1
	Stop gained	8
Total no. of INDELs		620

Proteomic Characterization of ISS-Grown JSC-093350089 *Aspergillus niger*

Differentially expressed proteins in ISS-grown JSC-093350089 strain were investigated following the extraction of total protein from two biological replicates of ISS-grown and ground control counterpart strains. Due to the low yields of extracted proteins, biological replicates were combined and divided into two parts that were then TMT labeled and subtracted to analysis *via* LC–MS/MS followed by spectrum/sequence matching using *A. niger* CBS 513.88 protein database (NCBI). Protein abundance ratios in ISS-grown JSC-093350089 were normalized to Earth-grown counterparts, which enabled identification of 70 up- and 142 downregulated proteins (fold change (FC) > |2|, $p < 0.05$) in response to space conditions (**Supplementary Tables 3** and **4**, respectively). AspGD Gene Ontology (GO) Slim terms (Cerqueira et al., 2014) were used to study the distribution of differentially expressed proteins in ISS-grown JSC-093350089 when compared to ground controls (**Figure 1**). Among differentially expressed proteins, 29 were involved in carbohydrate metabolism, 18 in stress responses, 21 in amino acid metabolism, and 15 in protein catabolic processes (**Figure 1**). Protein GO term enrichment analysis was conducted using FungiDB (Stajich et al., 2012), which revealed that significantly over-represented upregulated biological processes included carbohydrate metabolic processes (28% of all upregulated proteins) and stress response (10%), whereas significantly over-represented downregulated processes included cellular amino acid metabolic processes (13%), proteasomal ubiquitin-independent (10%) and dependent processes (10%), and proteasomal protein catabolic processes (10%; **Supplementary Table 5**).

The majority of differentially expressed proteins in ISS-grown JSC-093350089 *A. niger* were involved in carbohydrate metabolism (**Table 3**). Interestingly, eight of these genes, including cellobiohydrolases A and B (An07g09330 and An01g11660), XlnA 1,4-β-xylanase (An03g00940), and D-xylose reductases XyrA and XdhA (An01g03740 and An12g00030) were regulated by XlnR. XlnR is a transcriptional regulator involved in degradation of polysaccharides, xylan, cellulose, and D-xylose (Hasper et al., 2000). β-glucanases An11g01540 and An02g00850, which are involved in carbon starvation response in *A. niger* (Nitsche et al., 2012), were at minimum 3-fold upregulated in ISS-grown strain. α-1,2-mannosidases An08g08370, An13g01260 were at least 3.5-fold upregulated, whereas pyruvate decarboxylase PdcA (An02g06820) was nearly 3-fold upregulated. Pyruvate kinase PkiA (An07g08990), pyruvate dehydrogenase Pda1 (An07g09530), and isocitrate lyase AcuD (An01g09270) were at least 2-fold less abundant in ISS-grown samples. Several proteins involved in the stress response were differentially expressed in ISS-grown JSC-093350089 (**Table 4**). Proteins exhibiting at least 2-fold upregulation included cell wall organization protein EcmA (An04g01230) and An16g07920, whose orthologs play a role in salt stress response. Downregulated stress response proteins included heat shock protein An06g01610, DNA-binding protein HttA (An11g11300), and quinone reductase An12g06300. Lastly, a variety of proteins involved in cellular amino acid processes (**Table 5**), and protein catabolic processes (**Table 6**) were downregulated.

TABLE 2 | Single-nucleotide polymorphisms (SNPs) in ISS-grown JSC-093350089 when compared to ground control.

Function	Gene	Base mutation when compared to ground control	Type of mutation
RNA polymerase II transcription factor activity, sequence-specific DNA binding	An06g01180	An06_G279214A	5 prime UTR
RNA-directed DNA polymerase activity and role in RNA-dependent DNA replication	An08g11520	An08_G2725926T An08_T2726169G An08_C2726328A An08_T2726340C An08_A2726541G An08_A2726556G An08_C2726566A An08_G2726574T An08_G2726997A An08_C2727012T An08_G2728798A An08_C2729323T An08_G2726128T	Missense Stop lost
DNA-binding activity	An08g11890	An08_A2824556C An08_C2824566G	Missense
Protein kinase and transferase activity	An08g12110	An08_G2869126A An08_T2869564C	Missense
Phospholipase	An08g12250	An08_C2920251G An08_A2920254C An08_C2920298T An08_A2920340G	Missense
DNA binding, RNA polymerase II transcription factor activity	An12g00840	An12_T222942C An12_G222974T An12_G222982A An12_G223213A An12_G223422C An12_G223434A An12_A223471G An12_G222400A	Missense Splice region
RacA binding protein, polarized cell growth	An12g06420	An12_A1548559G An12_G1548931A An12_A1548987G An12_A1549053C	Missense
Unknown function	An08g08380	An08_C1997243T	Missense
Unknown function	An08g11220	An08_A2664300G An08_C2664502A	Missense
Unknown function	An08g11230	An08_G2666099A An08_T2666106C	Splice region
Unknown function	An08g11540	An08_A2731686T An08_T2731695C An08_T2733283C An08_C2733499T	Missense
Unknown function	An08g11550	An08_G2734928C	Missense
Unknown function	An08g11570	An08_C2737667T	Missense
Unknown function	An08g11650	An08_G2765994T An08_G2766002T	Missense
Unknown function	An08g11670	An08_G2768423A	Missense
Unknown function	An08g11830	An08_T2814800G	Missense
Unknown function	An08g11840	An08_T2817189C An08_A2817202G	Missense
Unknown function	An08g11860	An08_G2818780C An08_G2819091A An08_T2819644G	Missense

(Continued)

TABLE 2 | Continued

Function	Gene	Base mutation when compared to ground control	Type of mutation
Unknown function	An08g11870	An08_G2820964A An08_C2821036T An08_C2821061T An08_T2821094C An08_A2821104C An08_C2821119A An08_T2821648G An08_C2821664T An08_T2821693A An08_G2821697A An08_A2821958T An08_G2821978A An08_T2822640C An08_G2821995A	Missense
Unknown function	An08g11880	An08_G2824016C	Missense
Unknown function	An08g11910	An08_C2827842A An08_C2828992G	Missense
Unknown function	An08g11940	An08_A2835378G	Missense
Unknown function	An08g11950	An08_T2836585A An08_T2836586C An08_A2837163G	Missense
Unknown function	An08g11960	An08_A2839341G An08_G2839738A	Missense
Unknown function	An08g12230	An08_C2911588T An08_T2911676C An08_G2912446C An08_T2912451G An08_A2913614T An08_T2911894A	Missense Splice region
Unknown function	An08g12230	An08_G2913874C	Start gained
Unknown function	An08g12240	An08_A2916240C	Missense
Unknown function	An12g05800	An12_T1429831C	Missense

Metabolomic Characterization of ISS-Grown JSC-093350089 *Aspergillus niger*

Alterations in SM production in response to ISS conditions were assessed by extracting organic compounds from three biological replicates of ISS- and ground-grown JSC-093350089. The extracts were analyzed using HPLC-DAD-MS. Compounds were identified based on mass, UV absorption, and retention time, which were in agreement with literature (Chiang et al., 2011; **Figure 2**). Assessment of SM production yields revealed slight decrease in production of bicoumanigrin A, fonsecinones B and C, aurasperones C and B, and kotanin in ISS-grown isolate. Production levels of pestalamide B, nigerazine B, and nigragillin exhibited a reduction of approximately 50% when compared to control strains.

Both ISS- and ground-grown JSC-093350089 were regrown at 28°C and SMs production was evaluated. Due to the difference in growth temperature, obtained SM profiles of regrown isolates differed from those grown on the ISS (~22°C; **Figure 3**), as the trend in the production of SMs was the opposite of the one observed immediately after growth on the ISS. The majority of identified compounds showed slight increase in the production levels. Further, statistically significant increase in the production of the antioxidant pyranonigrin A (Miyake et al., 2007) and kotanin was observed when compared to ground controls.

DISCUSSION

It is critical to study molecular changes occurring in living organisms to understand the adaptation mechanisms allowing for surviving in extreme environments. One of such scientifically intriguing environments is the ISS, which is characterized by the presence of enhanced irradiation and microgravity. Due to its uniqueness, the ISS is under constant microbial monitoring, which allows for the isolation of wide array of microorganisms that often-become subjects of scientific investigations (Checinska et al., 2015; Knox et al., 2016; Checinska Sielaff et al., 2017; Venkateswaran et al., 2017; Bijlani et al., 2021). However, like in the case of the *A. niger* strain JSC-093350089 (Romsdahl et al., 2018, 2020), these investigations are more of a descriptive nature as definitive ascribing of observed molecular changes requires precisely controlled experiments. Therefore, to further investigate the differences in JSC-093350089 that were observed when compared to a "terrestrial" strain, the isolate was sent to the ISS in a planned experiment. Genomic, proteomic, and metabolomic alterations occurring in ISS-grown samples were analyzed following sample return and compared to ground-grown counterparts.

Genome analysis of ISS-grown JSC-093350089 revealed the introduction of SNPs and INDELs in response to space conditions. Interestingly, the majority of observed non-synonymous SNPs and INDELS were located within chromosomes VIII and XII, which suggests that only selected regions of the genome undergo positive selection to confer selective advantage while adapting to the space environment. This is in agreement with previous reports of space-induced genetic variations, as ISS-grown *Aspergillus nidulans* (Romsdahl et al., 2019) and spaceflight-grown *Staphylococcus aureus* (Guo et al., 2015) both exhibited genetic mutations that occurred in specific clustered regions of the genome. Although the functions of many genes containing non-synonymous SNPs were unknown, several of these genes possessed transposable element and DNA-binding activity. One such gene, An08g11520, was an analogue of transposon I factor and has RNA-directed DNA polymerase activity, which is consistent with genetic changes observed in transposable element genes in both *A. nidulans* (Romsdahl et al., 2019) and *S. aureus* (Guo et al., 2015). Alterations in transposable element genes likely influence their activity and lead to the introduction of variations within the genome in response to environmental stress (Capy et al., 2000; Muszewska et al., 2017). The results from this study further underscore the significant role of transposable elements in adaptation to the spacecraft environment. Future studies should investigate the functions of uncharacterized genes containing non-synonymous SNPs, as such knowledge may provide key information on how fungi adapt to space conditions. Noteworthy, when radioadapted strain of *Exophiala dermatitidis* and the non-radioadapted control strain were exposed to Polonium-210, a mostly transcriptomic rather than genomic response to radiation was observed in radioadapted strain. This suggests that strains previously exposed to irradiation respond to subsequent exposures in a unique way (Malo et al., 2021). Based on the observations reported for *E. dermatitidis*, it is plausible that *A. niger*

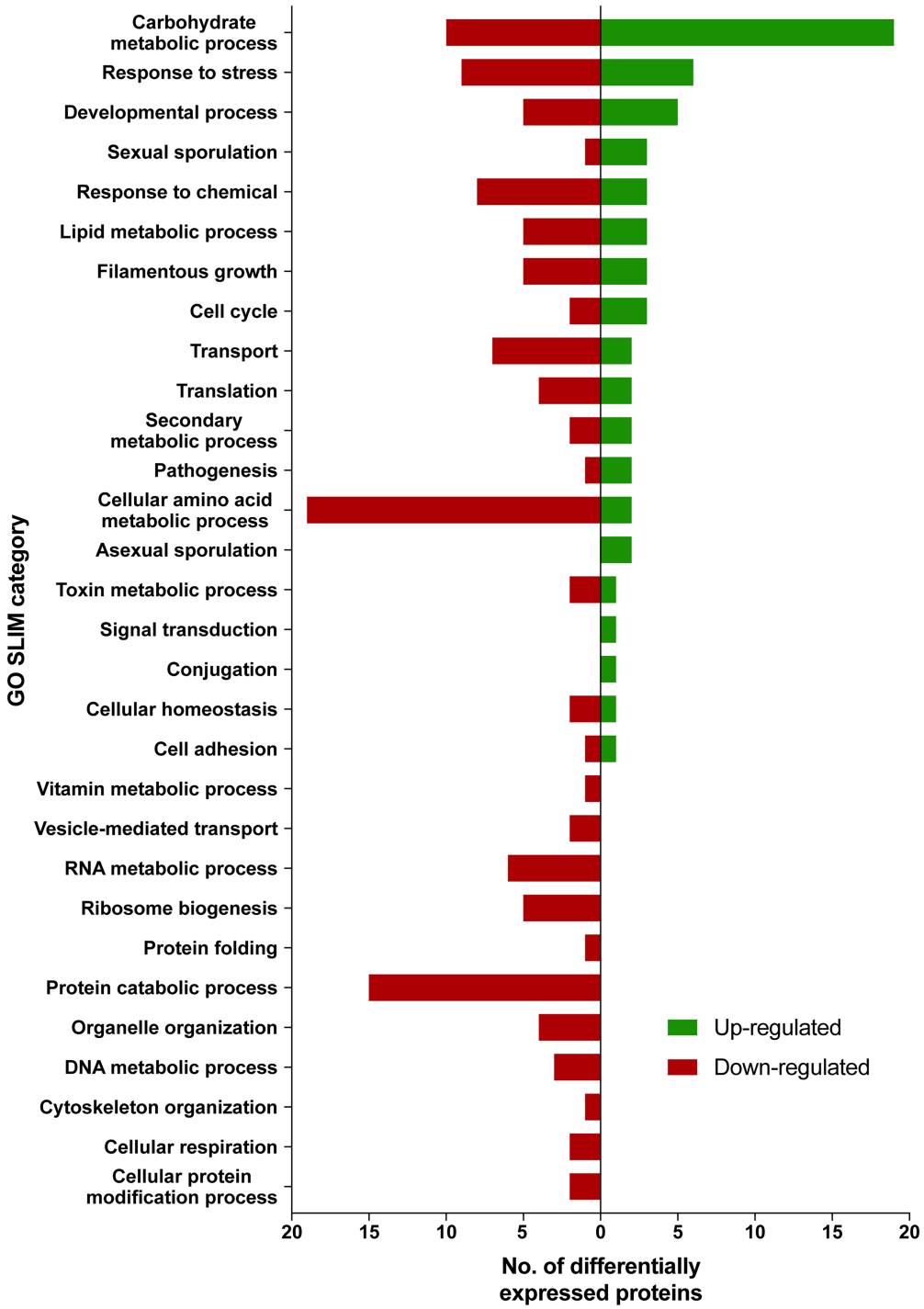

FIGURE 1 | AspGD GO Slim terms of differentially expressed proteins in ISS-grown JSC-093350089. Differentially expressed proteins in FC > |2|, $p < 0.05$ were mapped to terms representing various biological processes using AspGD Gene Ontology (GO) Slim Mapper.

JSC-093350089 strain response to the ISS environment was also unique, as it was previously isolated from the ISS and likely radioadapted itself. However, such assumption may not be confirmed in the current study, as there is no available not-radioadapted control for the *A. niger* JSC-093350089 strain. Future studies should be warranted to investigate whether *A. niger* JSC-093350089 strain's response to the ISS environment changes with consecutive exposures to the ISS environment when compared to the *original* ISS isolate. Finally, it has been previously reported that in *Aspergillus* genome intragenic regions

TABLE 3 | Differentially expressed proteins involved in carbohydrate metabolism.

ORF	Protein	CAZy Family	Function / Activity	Relative protein abundance*	*p*-value
An03g00940	XlnA/XynA	GH10	1,4-β-xylanase	2.22	2.66E-03
An01g11660	CbhB	GH7, CBM1	Cellobiohydrolase B	2.00	2.49E-03
An03g00500		GH30	1,6-β-glucosidase	1.97	6.91E-03
An11g01540		GH16	β-glucanase	1.93	4.20E-03
An08g08370		GH92	α-1,2-mannosidase	1.93	5.22E-03
An13g01260		GH92	α-1,2-mannosidase	1.83	4.16E-03
An15g04900		AA9, CBM1	β-1,4-glucanase D	1.77	2.18E-02
An11g03340	AamA	GH13	acid α-amylase	1.71	8.95E-04
An02g00850		GH16	β-glucanase	1.70	4.28E-02
An11g01120	Alr	–	Erythrose reductase	1.65	7.94E-04
An15g07800	AgtC	GH13	4-α-glucanotransferase	1.61	2.64E-03
An03g00960	AxhA	GH62	α-L-arabinofuranosidase	1.60	9.66E-03
An02g06820	PdcA	–	Pyruvate decarboxylase	1.57	5.76E-03
An02g11150	AglB	GH27	α-galactosidase II	1.37	2.89E-03
An08g01710	AbfC	GH51	Arabinofuranosidase	1.36	4.94E-04
An14g02760	EglA	GH12	β-1,4-glucanase	1.27	6.70E-05
An14g02070		CEnc	Acetylxylan esterase	1.27	8.67E-03
An05g02410		GH2	Glycoside hydrolase	1.10	1.77E-02
An07g09330	CbhA	GH7	Cellobiohydrolase A	1.07	1.44E-03
An01g03740	XyrA	–	D-xylose reductase	−1.08	2.59E-02
An12g00030	XdhA	–	D-xylulose reductase	−1.10	1.72E-02
An07g08990	PkiA	–	Pyruvate kinase	−1.12	2.92E-03
An18g06500		–	Phosphomannomutase	−1.14	6.84E-03
An12g03070	GlaB	GH15	Glucoamylase	−1.38	7.87E-03
An11g02550		–	Phosphoenolpyruvate carboxykinase	−1.51	3.44E-03
An15g01920	McsA	–	2-Methylcitrate synthase	−1.55	2.18E-02
An01g09270	AcuD	–	Isocitrate lyase	−1.59	9.83E-03
An15g03550		GH43	Hydrolase	−1.60	9.18E-04
An07g09530	Pda1	–	Pyruvate dehydrogenase	−2.19	2.00E-03

**Log2 fold change of ISS-grown JSC-093350089 compared to Earth-grown counterpart ($p < 0.05$).*

contain high-level developmental and metabolic transcriptional regulators (Noble and Andrianopoulos, 2013; Lim et al., 2021). Therefore, the high occurrence of SNPs and INDELS in the intergenic regions may contribute to developing the space environment-induced phenotype in *A. niger* JSC-093350089.

Investigation into the proteome of ISS- and ground-grown JSC-093350089 revealed that space conditions induce changes in protein expression when compared to ground controls. Observed, alterations in proteins involved in carbohydrate metabolism upon exposure to space conditions stay in agreement with previous studies of *A. niger* JSC-093350089 (Romsdahl et al., 2018), and other filamentous fungi, including *Aspergillus fumigatus* (Blachowicz et al., 2019a,b) and *A. nidulans* (Romsdahl et al., 2019). Similarly, a black fungus *Knufia chersonesos* exposed to low-shear simulated microgravity (LSSMG) also exhibited differential expression of proteins involved in carbohydrate metabolism (Tesei et al., 2021). On the other hand, a yeast, *Candida albicans,* exposed to spaceflight environment on the "SJ-10" satellite for 12 days showed decreased abundance of proteins involved in carbon metabolism, suggesting that yeast and filamentous fungi differ in adaptive responses to space environment (Wang et al., 2020). Additionally, ISS-grown JSC-093350089 exhibited upregulation of starvation-induced glycoside hydrolases, including AamA, and CbhB. This further confirms that changes in carbohydrate metabolism, may be a result of adaptation to scarce nutrient availability on ISS surfaces, due to the maintained cleaning regimen. Further, differential expression of XlnR-regulated proteins appears to be a key adaptive response to microgravity and enhanced irradiation, as both this and the previous study characterizing the space-induced molecular phenotype of JSC-093350089 (Romsdahl et al., 2018) revealed differential expression of various XlnR-regulated proteins. Activation of XlnR-regulated metabolic pathways leads to use of versatile carbon sources (Hasper et al., 2000), which may facilitate survival in hostile space environments. A few proteins upregulated in ISS-grown JSC-093350089 were involved in stress response, including the cell wall organization protein EcmA and flavohemoglobin, whose analogue in *Aspergillus flavus* has been reported to have a function correlated with hyphal growth phenotype (te Biesebeke et al., 2010). These observations further suggest that modulation of fungal growth and cell organization is an essential response to space conditions.

Metabolomic analysis of ISS-grown JSC-09335008 showed alterations in secondary metabolite production in response to the space environment. This observation was not surprising, as fungi often respond to versatile environmental conditions by altering the type and yield of produced SMs (Brakhage, 2013). Interestingly, ISS-grown JSC-09335008 showed decreased

TABLE 4 | Differentially expressed proteins involved in stress response.

ORF	Protein	Function / Activity	Relative protein abundance*	*p*-value
An01g14960		Asparaginase	2.21	6.46E-04
An14g02460	FhbA	Flavohemoglobin	1.56	1.45E-03
An01g02320	RasA	Ras GTPase	1.21	8.76E-03
An07g04620		Hypothetical protein	1.11	5.81E-03
An16g07920		Hypothetical protein	1.08	2.87E-02
An04g01230	EcmA	Cell wall organization protein	1.02	8.38E-04
An04g04130		Ornithine transaminase	−1.03	1.31E-02
An16g07110	Ach1	Acetyl-CoA hydrolase	−1.06	2.25E-02
An04g04870		Superoxide dismutase	−1.08	4.71E-03
An01g03740	XyrA	D-xylose reductase	−1.08	2.59E-02
An07g08990	PkiA	Pyruvate kinase	−1.12	2.92E-03
An08g00970	Rps28	Ribosomal protein of the small subunit	−1.16	4.09E-03
An02g07210	PepE	Acid aspartic protease	−1.21	1.27E-04
An12g06300		Quinone reductase	−1.25	3.28E-02
An11g11300	HttA	DNA-binding activity and role in DNA repair	−1.30	2.81E-03
An09g05870	Ndk1	Nucleoside-diphosphate kinase	−1.53	5.79E-04
An02g06560		Glutathione peroxidase / transferase activity	−1.69	9.56E-03
An06g01610		Heat shock protein	−2.08	5.35E-03

**Log2 fold change of ISS-grown JSC-093350089 compared to Earth-grown counterpart ($p < 0.05$).*

TABLE 5 | Differentially expressed proteins involved in cellular amino acid metabolic process.

ORF	Protein	Function / Activity	Relative protein abundance*	*p*-value
An01g14960		Asparaginase	2.21	6.46E-04
An12g00160		Malate dehydrogenase	1.27	2.72E-03
An14g06010		Chorismate mutase	−1.01	1.50E-02
An04g04130		Ornithine transaminase	−1.03	1.31E-02
An16g02970		Glycine / Serine hydroxymethyltransferase	−1.05	2.74E-04
An11g09510		Aspartate semialdehyde dehydrogenase	−1.06	2.35E-03
An01g06530		Branched-chain-amino acid transaminase activity	−1.18	2.49E-02
An15g05770		Hydrogen sulfide / sulfur amino acid biosynthetic process	−1.19	1.43E-03
An15g00610		Imidazoleglycerol-phosphate dehydratase	−1.19	1.40E-03
An05g00410		Glycine/Serine hydroxymethyltransferase	−1.22	8.63E-03
An13g00550		3-Deoxy-7-phosphoheptulonate synthase	−1.36	6.77E-03
An09g03940	Ilv2	Ketol-acid reductoisomerase	−1.40	1.08E-03
An02g10750		Cysteine synthase	−1.45	3.84E-03
An11g02170		Fumarylacetoacetate hydrolase	−1.47	1.64E-03
An15g02490		Homoisocitrate dehydrogenase activity, role in lysine biosynthesis	−1.48	8.47E-03
An02g07250	AgaA	Arginase	−1.54	2.86E-03
An02g12430	IcdA	Isocitrate dehydrogenase	−1.59	1.38E-03
An08g01960		Adenosylhomocysteinase	−1.62	4.43E-03
An17g00910		Gamma-aminobutyrate transaminase	−1.72	5.69E-03
An11g02160		Maleylacetoacetate isomerase	−1.83	4.49E-03
An03g04280		Protein with similarity to pyridoxine synthesis component pyroA of *Aspergillus nidulans*	−1.88	9.72E-03

**Log2 fold change of ISS-grown JSC-093350089 compared to Earth-grown counterpart ($p < 0.05$).*

production of all SMs, which is the opposite production pattern observed during the initial characterization of the metabolome of JSC-09335008 when compared to a "terrestrial" strain (Romsdahl et al., 2020). This discrepancy may be related to the fact that metabolomic profile of ISS-isolated JSC-09335008 was compared to the well-studied ATCC 1015 strain, rather than a "proper" JSC-09335008 ground control. Further investigation of the space environment-induced SM profile of the JSC-09335008 strain should be conducted to confirm whether decreased production of pestalamide B, nigerazine B (alkaloid), and nigragillin (alkaloid) are important biological adaptations. Given that sending experiments to the ISS is not readily available, it will be critical to use more easily accessible microgravity simulators, like High Aspect Ratio Vessels—HARV, or random positioning machines—RPMs to gain more insights in the space-induced phenotype of *A. niger* JSC-09335008 strain.

Finally, to gain insight into observed differences in acquired SMs profiles between current and previous study (Romsdahl et al., 2020) further experiment was conducted. Both ISS- and ground-grown JSC-09335008 were regrown in the same conditions (28°C for 5 days) as used in the previous study, which resulted in observing similar trends in SM production. After regrowing at 28°C, the ISS-grown JSC-09335008 produced higher yields of all SMs when compared to the regrown ground control, including approximately 60% increased production of the antioxidant pyranonigrin A. Pyranonigrin A was previously proposed to have a radioprotective nature, as pyranonigrin A-deficient JSC-09335008 strain was more sensitive to UVC exposure than the wild type JSC-09335008 strain (Romsdahl et al., 2020). Interestingly, pyranonigrin A production was not detected in the ISS- and ground-grown samples following the

TABLE 6 | Differentially expressed proteins involved in protein catabolic process.

ORF	Protein	Function / Activity	Relative protein abundance*	*p*-value
An02g07210	PepE	Acid aspartic protease	−1.21	1.27E-04
An18g06800	Pre10	20S CP alpha subunit of the proteasome	−1.27	1.08E-03
An04g01800		Hypothetical protein	−1.53	2.50E-03
An02g07040	Scl1	20S CP alpha subunit of the proteasome	−1.84	4.37E-03
An02g03400	Pup2	20S CP alpha subunit of the proteasome	−1.84	5.62E-03
An11g04620		Endopeptidase	−1.95	1.20E-02
An07g02010	Pre8	20S CP alpha subunit of the proteasome	−1.99	2.83E-03
An11g06720	Pre9	20S CP alpha subunit of the proteasome	−1.99	9.48E-03
An18g06680		Role in proteasomal ubiquitin-independent protein catabolic process	−2.03	4.65E-03
An04g01870		Endopeptidase activator activity	−2.05	5.99E-03
An18g06700	Pre7	20S CP beta subunit of the proteasome	−2.08	2.59E-03
An11g01760		Protein similar to proteasome 20S subunit Pre2p	−2.10	9.96E-04
An13g01210		Endopeptidase	−2.12	4.55E-03
An15g00510	Pre5	20S CP alpha subunit of the proteasome	−2.13	3.01E-03
An02g10790	Pre6	20S CP alpha subunit of the proteasome	−2.18	6.04E-03

**Log2 fold change of ISS-grown JSC-093350089 compared to Earth-grown counterpart ($p < 0.05$).*

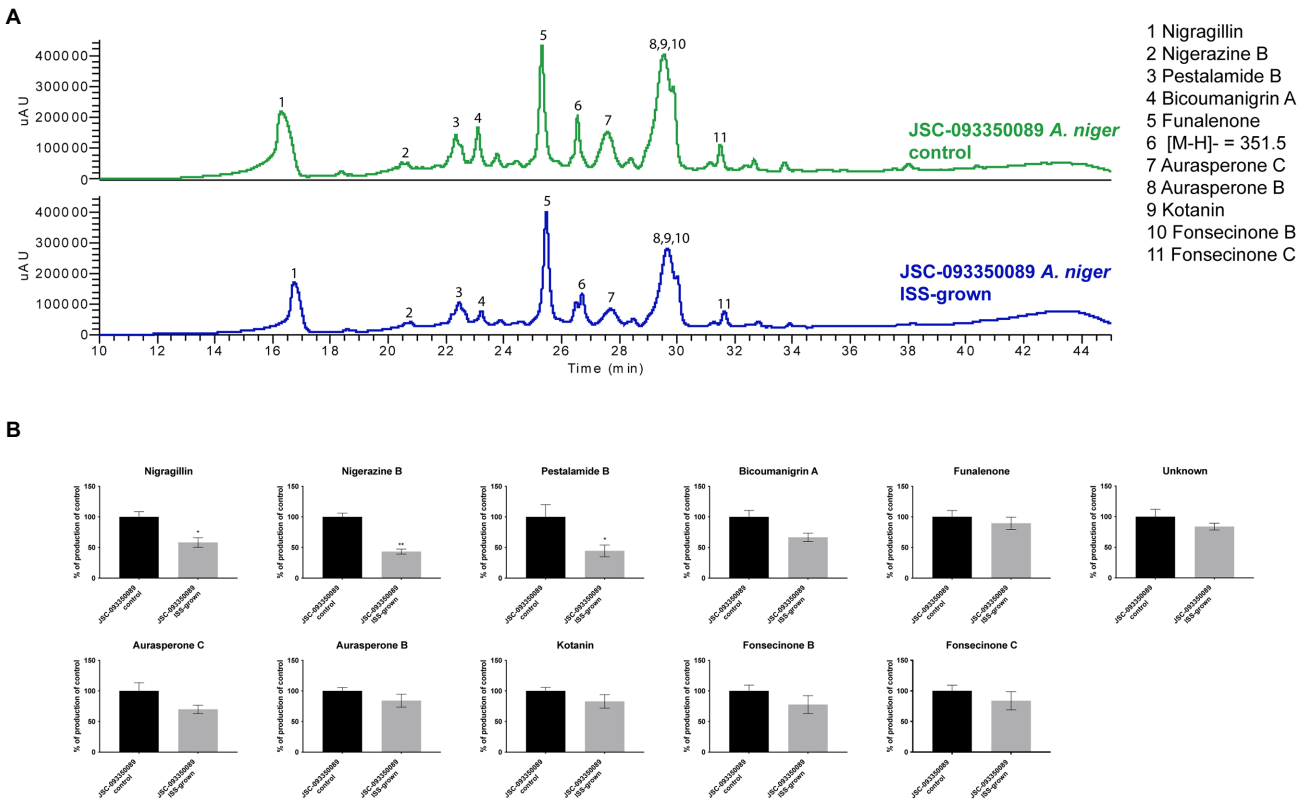

FIGURE 2 | Secondary metabolite production of ISS-grown JSC-093350089 when compared to ground controls. **(A)** Secondary metabolite profiles of ISS- and ground-grown JSC-093350089 when grown on GMM. **(B)** Metabolite quantification showing the percent change for each metabolite in relation to ground-grown JSC-093350089; significance was determined using Welch's t-test. "*" means and indicates statistical significance.

experiment on the ISS where growth temperature was about at 22°C. Due to this temperature-dependent discrepancy in observed SM profiles, the most important question to address is whether pyranonigrin A truly provides *A. niger* protection while in space. Such protection could potentially have various biotechnological applications for use of pyranonigrin A, including within human space programs and cancer therapies. Therefore, studies confirming pyranonigrin A potential as a radioprotective agent should be warranted. Finally, future studies should examine production of pyranonigrin A under various temperatures aboard the ISS, as well as its protective nature within the space environment to definitively answer this question.

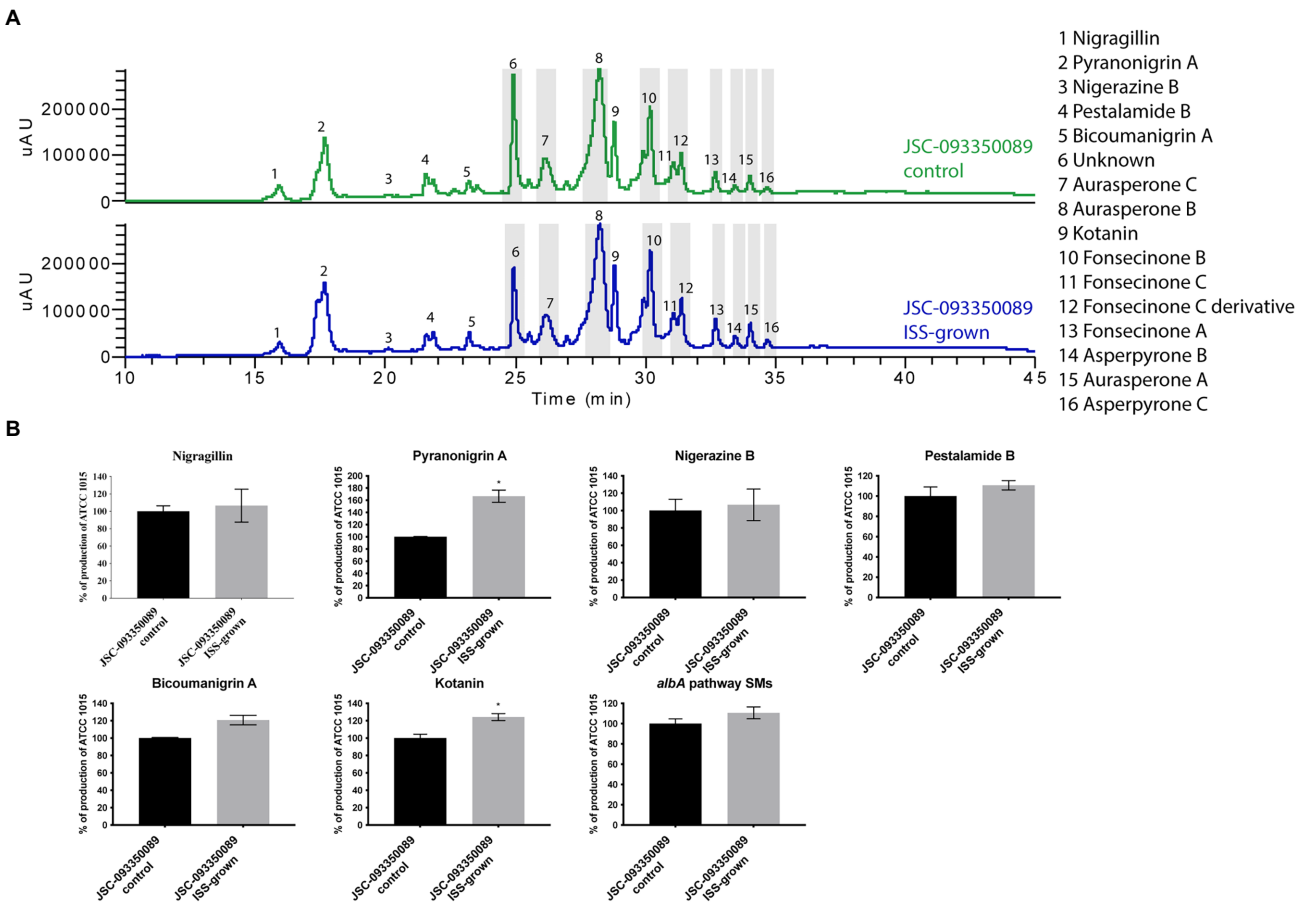

FIGURE 3 | Secondary metabolite production of regrown ISS- and ground-grown JSC-093350089. **(A)** Secondary metabolite profiles of regrown ISS- and ground-grown JSC-093350089 when grown on GMM. **(B)** Metabolite quantification showing the percent change for each metabolite in relation to regrown ground-grown JSC-093350089; significance was determined using Welch's t-test. "*" means and indicates statistical significance.

This study is the first report of the multi-omics response of *A. niger* to space conditions during a controlled experiment, which enhances our understanding of its space-induced phenotype. Such understanding may be translated to development of protective measures for both astronauts and the spacecraft during future manned space explorations, as *A. niger* is ubiquitous fungus present in many human-occupied closed habitats (Checinska et al., 2015; Blachowicz et al., 2017). Lastly, a thorough understanding of the space-induced secondary metabolomic alterations of industrially important *A. niger* may result in creating a potent producer of compounds of interest during space voyages.

DATA AVAILABILITY STATEMENT

Raw WGS reads for JSC-093350089 ISS- and ground-grown are available in the NCBI SRA, under accession numbers SAMN25997338 and SAMN25997339 and BioProject accession number PRJNA807647. Proteomics data is accessible through Massive with the dataset identifier MSV000088986.

AUTHOR CONTRIBUTIONS

AB drafted the manuscript, contributed to sample processing, and conducted data analysis and interpretation. JR contributed to sample processing and data interpretation. AC and MK conducted protein sample processing, LC–MS analyses, and data processing. SM and JS contributed to genome analysis. TT designed the study and drafted the manuscript. KV and CW conceptualized the project, coordinated the flight experiment, designed the study, interpreted the data, and drafted the manuscript. All authors contributed to the article and approved the submitted version.

FUNDING

This research was supported by the Center for the Advancement of Science in Space (CASIS) and sponsored by the International Space Station U.S. National Laboratory under grant/agreement number UA-2015-207 awarded to KV that funded a portion of the fellowship for AB. The funders had no role in study

design, data collection and interpretation, the writing of the manuscript, or the decision to submit the work for publication.

ACKNOWLEDGMENTS

Part of the research described in this publication was carried out at the Jet Propulsion Laboratory, California Institute of Technology, under a contract with NASA. We would like to thank astronaut Jeff Williams for handling the samples aboard the ISS and CASIS Team for coordinating this effort.

SUPPLEMENTARY MATERIAL

The Supplementary Material for this article can be found online at: https://www.frontiersin.org/articles/10.3389/fmicb.2022.893071/full#supplementary-material

REFERENCES

Adams, R. I., Miletto, M., Taylor, J. W., and Bruns, T. D. (2013). Dispersal in microbes: fungi in indoor air are dominated by outdoor air and show dispersal limitation at short distances. *ISME J.* 7:1460. doi: 10.1038/ismej.2013.84

Altenburg, S. D., Nielsen-Preiss, S. M., and Hyman, L. E. (2008). Increased filamentous growth of *Candida albicans* in simulated microgravity. *Genomics Proteomics Bioinformatics* 6, 42–50. doi: 10.1016/S1672-0229(08)60019-4

Andrews, S. (2010). FastQC: a quality control tool for high throughput sequence data. Available at: https://www.scienceopen.com/document?vid=de674375-ab83-4595-afa9-4c8aa9e4e736 (Accessed October 31, 2018).

Barberán, A., Dunn, R. R., Reich, B. J., Pacifici, K., Laber, E. B., Menninger, H. L., et al. (2015). The ecology of microscopic life in household dust. *Proc. R. Soc. B* 282:20151139. doi: 10.1098/rspb.2015.1139

Barnes, J. M. (1970). Aflatoxin as a health Hazard*. *J. Appl. Bacteriol.* 33, 285–298. doi: 10.1111/j.1365-2672.1970.tb02200.x

Benjamin, C. L., Stowe, R. P., St. John, L., Sams, C. F., Mehta, S. K., Crucian, B. E., et al. (2016). Decreases in thymopoiesis of astronauts returning from space flight. *JCI Insight*. 1:e88787. doi: 10.1172/jci.insight.88787

Benoit, M. R., Li, W., Stodieck, L. S., Lam, K. S., Winther, C. L., Roane, T. M., et al. (2006). Microbial antibiotic production aboard the international Space Station. *Appl. Microbiol. Biotechnol.* 70, 403–411. doi: 10.1007/s00253-005-0098-3

Bijlani, S., Singh, N. K., Eedara, V. V. R., Podile, A. R., Mason, C. E., Wang, C. C. C., et al. (2021). Methylobacterium ajmalii sp. nov., isolated From the international Space Station. *Front. Microbiol.* 12:639396. doi: 10.3389/fmicb.2021.639396

Blachowicz, A., Chiang, A. J., Elsaesser, A., Kalkum, M., Ehrenfreund, P., Stajich, J. E., et al. (2019a). Proteomic and Metabolomic characteristics of Extremophilic Fungi Under simulated Mars conditions. *Front. Microbiol.* 10:1013. doi: 10.3389/fmicb.2019.01013

Blachowicz, A., Chiang, A. J., Romsdahl, J., Kalkum, M., Wang, C. C. C., and Venkateswaran, K. (2019b). Proteomic characterization of *Aspergillus fumigatus* isolated from air and surfaces of the international Space Station. *Fungal Genet. Biol.* 124, 39–46. doi: 10.1016/j.fgb.2019.01.001

Blachowicz, A., Mayer, T., Bashir, M., Pieber, T. R., De León, P., and Venkateswaran, K. (2017). Human presence impacts fungal diversity of inflated lunar/Mars analog habitat. *Microbiome* 5:62. doi: 10.1186/s40168-017-0280-8

Bolger, A. M., Lohse, M., and Usadel, B. (2014). Trimmomatic: a flexible trimmer for Illumina sequence data. *Bioinformatics* 30, 2114–2120. doi: 10.1093/bioinformatics/btu170

Borel, J. F., Kis, Z. L., and Beveridge, T. (1995). "The History of the Discovery and Development of Cyclosporine (Sandimmune®)," in *The Search for Anti-Inflammatory Drugs: Case Histories from Concept to Clinic*. eds. V. J. Merluzzi and J. Adams (Boston, MA: Birkhäuser Boston), 27–63.

Brakhage, A. A. (2013). Regulation of fungal secondary metabolism. *Nat. Rev. Microbiol.* 11, 21–32. doi: 10.1038/nrmicro2916

Brakhage, A. A., and Schroeckh, V. (2011). Fungal secondary metabolites – strategies to activate silent gene clusters. *Fungal Genet. Biol.* 48, 15–22. doi: 10.1016/j.fgb.2010.04.004

Capy, P., Gasperi, G., Biémont, C., and Bazin, C. (2000). Stress and transposable elements: co-evolution or useful parasites? *Heredity* 85, 101–106. doi: 10.1046/j.1365-2540.2000.00751.x

Cerqueira, G. C., Arnaud, M. B., Inglis, D. O., Skrzypek, M. S., Binkley, G., Simison, M., et al. (2014). The *Aspergillus* genome database: multispecies curation and incorporation of RNA-Seq data to improve structural gene annotations. *Nucleic Acids Res.* 42, D705–D710. doi: 10.1093/nar/gkt1029

Checinska, A., Probst, A. J., Vaishampayan, P., White, J. R., Kumar, D., Stepanov, V. G., et al. (2015). Microbiomes of the dust particles collected from the international Space Station and spacecraft assembly facilities. *Microbiome* 3:50. doi: 10.1186/s40168-015-0116-3

Checinska Sielaff, A., Kumar, R. M., Pal, D., Mayilraj, S., and Venkateswaran, K. (2017). Solibacillus kalamii sp. nov., isolated from a high-efficiency particulate arrestance filter system used in the international Space Station. *Int. J. Syst. Evol. Microbiol.* 67, 896–901. doi: 10.1099/ijsem.0.001706

Chiang, Y.-M., Meyer, K. M., Praseuth, M., Baker, S. E., Bruno, K. S., and Wang, C. C. C. (2011). Characterization of a polyketide synthase in *Aspergillus* Niger whose product is a precursor for both dihydroxynaphthalene (DHN) melanin and naphtho-γ-pyrone. *Fungal Genet. Biol.* 48, 430–437. doi: 10.1016/j.fgb.2010.12.001

Crabbé, A., Nielsen-Preiss, S. M., Woolley, C. M., Barrila, J., Buchanan, K., McCracken, J., et al. (2013). Spaceflight enhances cell aggregation and random budding in *Candida albicans*. *PLoS One* 8:e80677. doi: 10.1371/journal.pone.0080677

Crucian, B., Stowe, R., Mehta, S., Uchakin, P., Quiriarte, H., Pierson, D., et al. (2013). Immune system dysregulation occurs during short duration spaceflight on board the space shuttle. *J. Clin. Immunol.* 33, 456–465. doi: 10.1007/s10875-012-9824-7

Cucinotta, F. A. (2014). Space radiation risks for astronauts on multiple international Space Station missions. *PLoS One* 9:e96099. doi: 10.1371/journal.pone.0096099

Dadachova, E., Bryan, R. A., Howell, R. C., Schweitzer, A. D., Aisen, P., Nosanchuk, J. D., et al. (2008). The radioprotective properties of fungal melanin are a function of its chemical composition, stable radical presence and spatial arrangement. *Pigment Cell Melanoma Res.* 21, 192–199. doi: 10.1111/j.1755-148X.2007.00430.x

DePristo, M. A., Banks, E., Poplin, R. E., Garimella, K. V., Maguire, J. R., Hartl, C., et al. (2011). A framework for variation discovery and genotyping using next-generation DNA sequencing data. *Nat. Genet.* 43, 491–498. doi: 10.1038/ng.806

Dhillon, G. S., Brar, S. K., Verma, M., and Tyagi, R. D. (2011). Utilization of different agro-industrial wastes for sustainable bioproduction of citric acid by *Aspergillus niger*. *Biochem. Eng. J.* 54, 83–92. doi: 10.1016/j.bej.2011.02.002

Driss-Ecole, D., Legué, V., Carnero-Diaz, E., and Perbal, G. (2008). Gravisensitivity and automorphogenesis of lentil seedling roots grown on board the international Space Station. *Physiol. Plant.* 134, 191–201. doi: 10.1111/j.1399-3054.2008.01121.x

Eaton, D. L., and Groopman, J. D. (2013). *The Toxicology of Aflatoxins: Human Health, Veterinary, and Agricultural Significance*. United States: Elsevier.

Elander, R. P. (2003). Industrial production of β-lactam antibiotics. *Appl. Microbiol. Biotechnol.* 61, 385–392. doi: 10.1007/s00253-003-1274-y

Fox, E. M., and Howlett, B. J. (2008). Secondary metabolism: regulation and role in fungal biology. *Curr. Opin. Microbiol.* 11, 481–487. doi: 10.1016/j.mib.2008.10.007

Guo, J., Han, N., Zhang, Y., Wang, H., Zhang, X., Su, L., et al. (2015). Use of genome sequencing to assess nucleotide structure variation of *Staphylococcus aureus* strains cultured in spaceflight on Shenzhou-X, under simulated microgravity and on the ground. *Microbiol. Res.* 170, 61–68. doi: 10.1016/j.micres.2014.09.001

Hasper, A. A., Visser, J., and Graaff, L. H. D. (2000). The *Aspergillus niger* transcriptional activator XlnR, which is involved in the degradation of the polysaccharides xylan and cellulose, also regulates d-xylose reductase gene expression. *Mol. Microbiol.* 36, 193–200. doi: 10.1046/j.1365-2958.2000.01843.x

Hof, H., and Kupfahl, C. (2009). Gliotoxin in *Aspergillus fumigatus*: an example that mycotoxins are potential virulence factors. *Mycotoxin Res.* 25, 123–131. doi: 10.1007/s12550-009-0020-4

Ijiri, K. (2003). Life-cycle experiments of medaka fish aboard the international space station. *Adv. Space Biol. Med.* 9, 201–216. doi: 10.1016/S1569-2574(03)09008-7

Keller, N. P., Turner, G., and Bennett, J. W. (2005). Fungal secondary metabolism — from biochemistry to genomics. *Nat. Rev. Microbiol.* 3, 937–947. doi: 10.1038/nrmicro1286

Kittang, A.-I., Iversen, T.-H., Fossum, K. R., Mazars, C., Carnero-Diaz, E., Boucheron-Dubuisson, E., et al. (2014). Exploration of plant growth and development using the European modular cultivation system facility on the international Space Station. *Plant Biol.* 16, 528–538. doi: 10.1111/plb.12132

Klaus, D., Simske, S., Todd, P., and Stodieck, L. (1997). Investigation of space flight effects on Escherichia coli and a proposed model of underlying physical mechanisms. *Microbiology* 143, 449–455. doi: 10.1099/00221287-143-2-449

Knox, B. P., Blachowicz, A., Palmer, J. M., Romsdahl, J., Huttenlocher, A., Wang, C. C. C., et al. (2016). Characterization of *Aspergillus fumigatus* isolates from air and surfaces of the international Space Station. *Clin. Vacc. Immun.* 1, e00227–e00216. doi: 10.1128/mSphere.00227-16

Li, H., and Durbin, R. (2009). Fast and accurate short read alignment with burrows-wheeler transform. *Bioinformatics* 25, 1754–1760. doi: 10.1093/bioinformatics/btp324

Li, H., Handsaker, B., Wysoker, A., Fennell, T., Ruan, J., Homer, N., et al. (2009). The sequence alignment/map format and SAMtools. *Bioinforma. Oxf. Engl.* 25, 2078–2079. doi: 10.1093/bioinformatics/btp352

Lim, C. S., Weinstein, B. N., Roy, S. W., and Brown, C. M. (2021). Analysis of fungal genomes reveals commonalities of intron gain or loss and functions in intron-poor species. *Mol. Biol. Evol.* 38, 4166–4186. doi: 10.1093/molbev/msab094

Link, B. M., Durst, S. J., Zhou, W., and Stankovic, B. (2003). Seed-to-seed growth of *Arabidopsis Thaliana* on the international space station. *Adv. Space Res.* 31, 2237–2243. doi: 10.1016/S0273-1177(03)00250-3

Liu, H.-Z., Wang, Q., Liu, X.-Y., and Tan, S.-S. (2008). Effects of spaceflight on polysaccharides of *Saccharomyces cerevisiae* cell wall. *Appl. Microbiol. Biotechnol.* 81, 543–550. doi: 10.1007/s00253-008-1692-y

Malo, M. E., Schultzhaus, Z., Frank, C., Romsdahl, J., Wang, Z., and Dadachova, E. (2021). Transcriptomic and genomic changes associated with radioadaptation in Exophiala dermatitidis. *Comput. Struct. Biotechnol. J.* 19, 196–205. doi: 10.1016/j.csbj.2020.12.013

Mehta, S. K., Cohrs, R. J., Forghani, B., Zerbe, G., Gilden, D. H., and Pierson, D. L. (2004). Stress-induced subclinical reactivation of varicella zoster virus in astronauts. *J. Med. Virol.* 72, 174–179. doi: 10.1002/jmv.10555

Miyake, Y., Ito, C., Itoigawa, M., and Osawa, T. (2007). Isolation of the antioxidant pyranonigrin-A from rice mold starters used in the manufacturing process of fermented foods. *Biosci. Biotechnol. Biochem.* 71, 2515–2521. doi: 10.1271/bbb.70310

Mulder, K. C. L., Mulinari, F., Franco, O. L., Soares, M. S. F., Magalhães, B. S., and Parachin, N. S. (2015). Lovastatin production: From molecular basis to industrial process optimization. *Biotechnol. Adv.* 33, 648–665. doi: 10.1016/j.biotechadv.2015.04.001

Muszewska, A., Steczkiewicz, K., Stepniewska-Dziubinska, M., and Ginalski, K. (2017). Cut-and-paste transposons in Fungi with diverse lifestyles. *Genome Biol. Evol.* 9, 3463–3477. doi: 10.1093/gbe/evx261

Nickerson, C. A., Ott, C. M., Mister, S. J., Morrow, B. J., Burns-Keliher, L., and Pierson, D. L. (2000). Microgravity as a novel environmental signal affecting *Salmonella enterica* Serovar Typhimurium virulence. *Infect. Immun.* 68, 3147–3152. doi: 10.1128/IAI.68.6.3147-3152.2000

Nikolcheva, L. G., Cockshutt, A. M., and Bärlocher, F. (2003). Determining diversity of freshwater Fungi on decaying leaves: comparison of traditional and molecular approaches. *Appl Env. Microbiol* 69, 2548–2554. doi: 10.1128/AEM.69.5.2548-2554.2003

Nitsche, B. M., Jørgensen, T. R., Akeroyd, M., Meyer, V., and Ram, A. F. (2012). The carbon starvation response of *Aspergillus niger* during submerged cultivation: insights from the transcriptome and secretome. *BMC Genomics* 13:380. doi: 10.1186/1471-2164-13-380

Noble, L. M., and Andrianopoulos, A. (2013). Fungal genes in context: genome architecture reflects regulatory complexity and function. *Genome Biol. Evol.* 5, 1336–1352. doi: 10.1093/gbe/evt077

Ombergen, A. V., Demertzi, A., Tomilovskaya, E., Jeurissen, B., Sijbers, J., Kozlovskaya, I. B., et al. (2017). The effect of spaceflight and microgravity on the human brain. *J. Neurol.* 264, 18–22. doi: 10.1007/s00415-017-8427-x

Onofri, S., Barreca, D., Selbmann, L., Isola, D., Rabbow, E., Horneck, G., et al. (2008). Resistance of Antarctic black fungi and cryptoendolithic communities to simulated space and Martian conditions. *Stud. Mycol.* 61, 99–109. doi: 10.3114/sim.2008.61.10

Onofri, S., de la Torre, R., de Vera, J.-P., Ott, S., Zucconi, L., Selbmann, L., et al. (2012). Survival of rock-colonizing organisms after 1.5 years in outer space. *Astrobiology* 12, 508–516. doi: 10.1089/ast.2011.0736

Onofri, S., de Vera, J.-P., Zucconi, L., Selbmann, L., Scalzi, G., Venkateswaran, K. J., et al. (2015). Survival of Antarctic Cryptoendolithic Fungi in simulated Martian conditions On board the international Space Station. *Astrobiology* 15, 1052–1059. doi: 10.1089/ast.2015.1324

Pel, H. J., de Winde, J. H., Archer, D. B., Dyer, P. S., Hofmann, G., Schaap, P. J., et al. (2007). Genome sequencing and analysis of the versatile cell factory *Aspergillus niger* CBS 513.88. *Nat. Biotechnol.* 25, 221–231. doi: 10.1038/nbt1282

Piscitelli, A., Pezzella, C., Giardina, P., Faraco, V., and Sannia, G. (2010). Heterologous laccase production and its role in industrial applications. *Bioeng. Bugs* 1, 254–264. doi: 10.4161/bbug.1.4.11438

Purevdorj-Gage, B., Sheehan, K. B., and Hyman, L. E. (2006). Effects of low-shear modeled microgravity on cell function, gene expression, and phenotype in *Saccharomyces cerevisiae*. *Appl Env. Microbiol* 72, 4569–4575. doi: 10.1128/AEM.03050-05

Rabbow, E., Rettberg, P., Baumstark-Khan, C., and Horneck, G. (2003). The SOS-LUX-LAC-FLUORO-toxicity-test on the international Space Station (ISS). *Adv. Space Res.* 31, 1513–1524. doi: 10.1016/S0273-1177(03)00086-3

Rodríguez Couto, S., and Toca Herrera, J. L. (2006). Industrial and biotechnological applications of laccases: a review. *Biotechnol. Adv.* 24, 500–513. doi: 10.1016/j.biotechadv.2006.04.003

Rohlfs, M., and Churchill, A. C. L. (2011). Fungal secondary metabolites as modulators of interactions with insects and other arthropods. *Fungal Genet. Biol.* 48, 23–34. doi: 10.1016/j.fgb.2010.08.008

Romsdahl, J., Blachowicz, A., Chiang, A. J., Chiang, Y.-M., Masonjones, S., Yaegashi, J., et al. (2019). International Space Station conditions alter genomics, proteomics, and metabolomics in *Aspergillus nidulans*. *Appl. Microbiol. Biotechnol.* 103, 1363–1377. doi: 10.1007/s00253-018-9525-0

Romsdahl, J., Blachowicz, A., Chiang, A. J., Singh, N., Stajich, J. E., Kalkum, M., et al. (2018). Characterization of *Aspergillus niger* isolated from the international Space Station. *Microbial systems* 3, e00112–e00118. doi: 10.1128/mSystems.00112-18

Romsdahl, J., Blachowicz, A., Chiang, Y.-M., Venkateswaran, K., and Wang, C. C. C. (2020). Metabolomic analysis of *Aspergillus niger* isolated From the international Space Station reveals enhanced production levels of the antioxidant Pyranonigrin A. *Front. Microbiol.* 11:931. doi: 10.3389/fmicb.2020.00931

Schuster, E., Dunn-Coleman, N., Frisvad, J., and van Dijck, P. (2002). On the safety of *Aspergillus niger* – a review. *Appl. Microbiol. Biotechnol.* 59, 426–435. doi: 10.1007/s00253-002-1032-6

Shephard, G. S. (2008). Impact of mycotoxins on human health in developing countries. *Food Addit. Contam. Part A* 25, 146–151. doi: 10.1080/02652030701567442

Singaravelan, N., Grishkan, I., Beharav, A., Wakamatsu, K., Ito, S., and Nevo, E. (2008). Adaptive melanin response of the soil fungus *Aspergillus niger* to UV radiation stress at "evolution canyon", Mount Carmel Israel. *PLoS ONE* 3:2993. doi: 10.1371/journal.pone.0002993

Stajich, J. E., Harris, T., Brunk, B. P., Brestelli, J., Fischer, S., Harb, O. S., et al. (2012). FungiDB: an integrated functional genomics database for fungi. *Nucleic Acids Res.* 40, D675–D681. doi: 10.1093/nar/gkr918

Takahashi, A., Ohnishi, K., Takahashi, S., Masukawa, M., Sekikawa, K., Amano, T., et al. (2001). The effects of microgravity on induced mutation in Escherichia coli and *Saccharomyces cerevisiae*. *Adv. Space Res.* 28, 555–561. doi: 10.1016/S0273-1177(01)00391-X

Tavella, S., Ruggiu, A., Giuliani, A., Brun, F., Canciani, B., Manescu, A., et al. (2012). Bone turnover in wild type and Pleiotrophin-transgenic mice housed for three months in the international Space Station (ISS). *PLoS One* 7:e33179. doi: 10.1371/journal.pone.0033179

te Biesebeke, R., Levasseur, A., Boussier, A., Record, E., van den Hondel, C. A. M. J. J., and Punt, P. J. (2010). Phylogeny of fungal hemoglobins and expression analysis of the *Aspergillus oryzae* flavohemoglobin gene fhbA during hyphal growth. *Fungal Biol.* 114, 135–143. doi: 10.1016/j.mycres.2009.08.007

Tesei, D., Chiang, A. J., Kalkum, M., Stajich, J. E., Mohan, G. B. M., Sterflinger, K., et al. (2021). Effects of simulated microgravity on the proteome and Secretome of the Polyextremotolerant black fungus Knufia chersonesos. *Front. Genet.* 12:638708. doi: 10.3389/fgene.2021.638708

Vaishampayan, P. A., Rabbow, E., Horneck, G., and Venkateswaran, K. J. (2012). Survival of *Bacillus pumilus* spores for a prolonged period of time in real space conditions. *Astrobiology* 12, 487–497. doi: 10.1089/ast.2011.0738

Vandenberghe, L. P. S., Soccol, C. R., Pandey, A., and Lebeault, J.-M. (2000). Solid-state fermentation for the synthesis of citric acid by *Aspergillus niger*. *Bioresour. Technol.* 74, 175–178. doi: 10.1016/S0960-8524(99)00107-8

Venkateswaran, K., Singh, N. K., Sielaff, A. C., Pope, R. K., Bergman, N. H., Tongeren, S. P., et al. (2017). Non-toxin-producing *Bacillus cereus* strains belonging to the *B. anthracis* Clade Isolated from the International Space Station. *mSystems* 2:17. doi: 10.1128/mSystems.00021-17

Wang, J., Liu, Y., Zhao, G., Gao, J., Liu, J., Wu, X., et al. (2020). Integrated proteomic and metabolomic analysis to study the effects of spaceflight on *Candida albicans*. *BMC Genomics* 21:57. doi: 10.1186/s12864-020-6476-5

Weng, M., Li, J., Gao, H., Li, M., Wang, P., and Jiang, X. (1998). Mutation induced by space conditions in *Escherichia coli* strains. *Space Med. Med. Eng.* 11, 245–248.

Conflict of Interest: The authors declare that the research was conducted in the absence of any commercial or financial relationships that could be construed as a potential conflict of interest.

The handling editor DT declared a past co-authorship with the authors AC, MK, JS, and KV.

Publisher's Note: All claims expressed in this article are solely those of the authors and do not necessarily represent those of their affiliated organizations, or those of the publisher, the editors and the reviewers. Any product that may be evaluated in this article, or claim that may be made by its manufacturer, is not guaranteed or endorsed by the publisher.

frontiers | Frontiers in Microbiology

ORIGINAL RESEARCH
published: 05 July 2022
doi: 10.3389/fmicb.2022.877625

Cultivation of the Dematiaceous Fungus *Cladosporium sphaerospermum* Aboard the International Space Station and Effects of Ionizing Radiation

Nils J. H. Averesch[1,2]*, *Graham K. Shunk*[3,4] *and Christoph Kern*[5,6]

[1] Department of Civil and Environmental Engineering, Stanford University, Stanford, CA, United States, [2] Center for the Utilization of Biological Engineering in Space, Berkeley, CA, United States, [3] Physics Department, North Carolina School of Science and Mathematics, Durham, NC, United States, [4] Higher Orbits "Go for Launch!" Program, Leesburg, VA, United States, [5] Department of Statistics, Ludwig Maximilian University of Munich, Munich, Germany, [6] School of Social Sciences, University of Mannheim, Mannheim, Germany

OPEN ACCESS

Edited by:
Camilla Urbaniak, NASA Jet Propulsion Laboratory, United States

Reviewed by:
Tamas Torok, Berkeley Lab (DOE), United States
Adriana Blachowicz, NASA Jet Propulsion Laboratory, United States

***Correspondence:**
Nils J. H. Averesch
nils.averesch@uq.net.au

Specialty section:
This article was submitted to Extreme Microbiology, a section of the journal Frontiers in Microbiology

Received: *16 February 2022*
Accepted: *17 May 2022*
Published: *05 July 2022*

Citation:
Averesch NJH, Shunk GK and Kern C (2022) Cultivation of the Dematiaceous Fungus Cladosporium sphaerospermum Aboard the International Space Station and Effects of Ionizing Radiation. Front. Microbiol. 13:877625. doi: 10.3389/fmicb.2022.877625

In Space, cosmic radiation is a strong, ubiquitous form of energy with constant flux, and the ability to harness it could greatly enhance the energy-autonomy of expeditions across the solar system. At the same time, radiation is the greatest permanent health risk for humans venturing into deep space. To protect astronauts beyond Earth's magnetosphere, advanced shielding against ionizing as well as non-ionizing radiation is highly sought after. In search of innovative solutions to these challenges, biotechnology appeals with suitability for *in situ* resource utilization (ISRU), self-regeneration, and adaptability. Where other organisms fail, certain microscopic fungi thrive in high-radiation environments on Earth, showing high radioresistance. The adaptation of some of these molds to areas, such as the Chernobyl Exclusion Zone has coined the terms positive "radiotropism" and "radiotrophy", reflecting the affinity to and stimulation by radiation, and sometimes even enhanced growth under ionizing conditions. These abilities may be mediated by the pigment melanin, many forms of which also have radioprotective properties. The expectation is that these capabilities are extendable to radiation in space. To study its growth in space, an experiment cultivating *Cladosporium sphaerospermum* Penzig ATCC® 11289™ aboard the International Space Station (ISS) was conducted while monitoring radiation beneath the formed biomass in comparison to a no-growth negative control. A qualitative growth advantage in space was observable. Quantitatively, a 1.21 ± 0.37-times higher growth rate than in the ground control was determined, which might indicate a radioadaptive response to space radiation. In addition, a reduction in radiation compared to the negative control was discernable, which is potentially attributable to the fungal biomass.

Keywords: space radiation, micro-fungi, *Cladosporium sphaerospermum*, radiotrophy, biotechnology, *in situ* resource utilization

INTRODUCTION

Background

With concrete efforts to send humans to the Moon by 2024 under the Artemis program and establish a permanent presence on the next rock from Earth by 2028, humankind looks to Mars as the next big leap in space exploration (NASA, 2020). In preparation for prolonged human exploration missions venturing beyond Earth-orbit and deeper into space, the required capabilities increase significantly (Loff, 2018). While advanced transportation solutions led by the public and private sectors alike (e.g., SLS/Orion, Starship, New Glenn) are pivotal and have already reached high technological readiness, resource-management and life-support systems, as well as crew health and performance, are equally essential. Therefore, any mission scenario [cf. "Design Reference Architecture 5.0" (Drake and Watts, 2014) or "Mars Base Camp" Cichan et al., 2017)] must include innovative solutions that can meet the needs and address the hazards of prolonged residence on celestial surfaces. In particular, meeting energy demands is critical to extending the duration of mission scenarios; proposed solutions have included nuclear power or photovoltaics (Abel et al., 2021). However, both are significant with respect to the up-mass requirements of the hardware. The storage of energy in the form of electricity is further limited by the weight of batteries. Therefore, chemical energy carriers that are based on *in situ* resources would be pivotal.

In situ resource utilization (ISRU) is being seen as an essential concept to extend capabilities without penalizing or sacrificing redundancy, as well as to break the supply chain from Earth, which is pivotal to sustaining human exploration of deep space (Hall, 2017). For ISRU, biotechnology holds some of the most promising approaches (Menezes et al., 2015; Rothschild, 2016; Verseux et al., 2016; Nangle et al., 2020; Berliner et al., 2021a). Fundamentally, the ability of biology to fix inorganic carbon can generate carriers of energy and substrates for biotechnology in the form of biomass, which can be converted into more reduced carbon feedstocks, e.g., methane (Averesch, 2021).

Earth's global carbon cycle relies on sunlight—non-ionizing electromagnetic (wave) radiation of the visible spectrum—to fix inorganic carbon. Ionizing radiation, a much more energetic form of radiation, mostly originates from nuclear decay (on Earth's surface and below) and is comparatively rare. In space, ionizing radiation is ubiquitous and consists mostly of energetic particles, two types of which are primarily encountered on celestial bodies like Earth's Moon or Mars: Solar Energetic Particles (SEPs) and Galactic Cosmic Rays (GCRs). These high-energy particles in the range of hundreds of MeV/nuc to GeV/nuc can penetrate deep into the regolith, where they produce secondary particles, including neutrons and γ-rays (Hassler et al., 2014). This radiation environment presents a significant and constant energy flux independent of most environmental factors (unlike sunlight, which can be intermittent due to dust storms on Mars)—being able to harness (parts of) this energy would provide a steady source of energy.

Nevertheless, radiation is also the greatest threat to the short- and long-term health of astronauts on long-duration deep-space missions (Cucinotta et al., 2012; Chancellor et al., 2014; Afshinnekoo et al., 2020). Over the time of one year the average person on Earth is dosed with about 6.2 mSv (ANS, 2020; NRC, 2021), while the average astronaut on the International Space Station (ISS) is exposed to an equivalent of ∼144 mSv (Cucinotta et al., 2008); one year into a 3-year mission to Mars, an astronaut would already have accumulated some 400 mSv, primarily from Galactic Cosmic Radiation (GCR) (Letaw et al., 1988). While the particular health effects of radiation exposure on interplanetary travel have not been fully assessed (Chancellor et al., 2018), it is clear that adequate protection against cosmic radiation is crucial for missions beyond Earth orbit; however, solutions are more restricted by up-mass limitations than any other factor of space travel (Ambroglini et al., 2016).

Among all domains of life, there exist extremophiles that live and persist in highly radioactive environments, including bacteria, fungi, and higher organisms, such as insects (Krisko and Radman, 2013; Kalawate and Mehetre, 2015). Further, certain microscopic fungi that populate the Chernobyl Exclusion Zone and Nuclear Power Plant, where radiation levels are 3–5 orders of magnitude above normal background levels, show a phenomenon called "positive radiotropism" as ionizing radiation becomes an orienting factor for these molds (Zhdanova et al., 2004; Karpenko et al., 2006; Belozerskaya et al., 2010). Additionally, some of these dematiaceous fungi have also been found to populate the interiors of spacecraft in low Earth orbit (LEO), where exposure to ionizing radiation is also intensified (Dadachova and Casadevall, 2008). Black molds and their conidia have been found to remain viable even after exposure to an equivalent radiation dose of several months' worth of space radiation (Cortesão et al., 2020); radiation even appears to stimulate their germination (Tugay et al., 2006). How these organisms protect themselves from radiation damage has been the subject of intense study, and specifically, melanin has been explored as a biotechnological means for radioprotection (Pacelli et al., 2017; Malo et al., 2018). As an antioxidant, melanin appears to play a major role in the "radioadaptation" of these molds (Tugay et al., 2011; Eisenman and Casadevall, 2012; Pacelli et al., 2017; Malo et al., 2018). The pigment has also been the subject of investigation as a potential mediator in the transfer of energy from radiation onto metabolism (Dadachova et al., 2007; Dadachova and Casadevall, 2008; Turick et al., 2011). Based on the observed "radiostimulation" of melanogenesis as well as the growth advantage that putatively results from the exposure of these molds to high radiation, the concept of "radiosynthesis" has been developed. If found veritable, melanin could be perceived as loosely analogous to chlorophyll in photosynthesis.

Concept

Here, the dematiaceous melanotic micro-fungus *Cladosporium sphaerospermum* Penzig ATCC® 11289™ (cf. **Supplementary Information 1, Section A**) was cultivated in LEO on the ISS. The preference of certain *C. sphaerospermum*

Abbreviations: CPM, counts per minute; GCR, Galactic Cosmic Radiation; GCRs, Galactic Cosmic Rays; HZE, high atomic number and energy; ISRU, *in situ* resource utilization; ISS, International Space Station; LEO, low Earth orbit; PDA, potato dextrose agar; RT, room temperature.

isolates for environments with extreme radiation levels on Earth is well documented (Zhdanova et al., 2004; Ledford, 2007; Dadachova and Casadevall, 2008). Consequently, it has been hypothesized that similar proliferation occurs in response to the high radiation environment off-Earth and that such melanized fungi can be utilized for radioprotection in space (Cordero, 2017; Pacelli et al., 2017). The objective of this experiment was to conduct a proof-of-principle study on a single payload, utilizing basic flight hardware for an autonomous experiment in the unique radiation environment of the ISS. This offered the opportunity to test the mold's (growth) response in space while monitoring radiation levels against a no-growth negative control to assess its potential to serve as a bioregenerative means for radioprotection.

MATERIALS AND METHODS

Experimental Setup

Space Tango (Space Tango, Inc., Lexington, KY, US) was contracted for experimental design and construction (terrestrial logistics and on-orbit operations) (CASIS, 2020). The initial concept for the experimental design was adapted by Space Tango for assembly of the flight hardware and implementation aboard the ISS within TangoLab™ facilities. The flight hardware was housed in a $4'' \times 4'' \times 8''$ double unit standard-size CubeLab™ hardware module and consisted of the following main components: two Raspberry Pi 3 Model B+ (Raspberry Pi Foundation, Caldecote, Cambs., UK) single-board computers, EP-0104 DockerPi PowerBoard (Adafruit Industries, New York, NY, US), PocketGeiger Type5 (Radiation Watch, Miyagi, JP) with the PIN photodiode X100-7 SMD (First Sensor AG, Berlin, DE), Raspberry Pi Camera v2 (Raspberry Pi Foundation, Caldecote, Cambridgeshire, UK) light source (0.8 W LED-strip) for imaging, DHT22 integrated environmental sensor suite (Aosong Electronics Co. Ltd, Huangpu District, Guangzhou, CN) for temperature and humidity readings, a real-time WatchDog™ timer (Brentek International Inc., York, PA, US), and D6F-P0010A1 (Omron Electronics LLC, Hoffman Estates, IL, US) electronic flow-measurement system. One Raspberry Pi ("auxiliary-computer") running Raspbian v10.18 was dedicated to photography, lighting, temperature, humidity, and electronic flow measurement (EFM) readings, while the second Raspberry Pi ("flight-computer") controlled radiation measurements, stored in a probed Logger Memobox (Fluke Corporation, Everett, WA, US). The assembled flight hardware was calibrated and vetted before flight; in particular, the consistency of the two radiation sensors was confirmed so that no apparent deviation in recorded ionizing events existed between them.

Cladosporium sphaerospermum (ATCC® 11289™, strain designation CBS 2 [CBS 193.54, IMI 49637]) was obtained from Microbiologics® (St. Cloud, Minnesota, US), catalog no. 01254P (supplied as KWIK-STIK™). The growth medium was potato dextrose agar "PDA" (Carolina Biological, Burlington, NC, US) obtained as a "Prepared Media Bottle" (approx. composed of 15 g/L agar, 20 g/L glucose, and 4 g/L starch). A total of 20 ml of PDA (dyed with orange 1) was used to fill the two compartments of a split Petri dish (100 × 15 mm). The agar plate was sealed with "Parafilm M" post-inoculation. With a total height of the Petri dish of 15 mm and a 75 cm^2 surface area, the thickness of the PDA was ∼13.33 mm, leaving an ∼1.67 mm gap for the fungal growth layer and/or gaseous headspace. To minimize latent growth while in transit, the setup was fully assembled before inoculation of the medium according to manufacturer directions for the KWIK-STIK™ product. A block chart of the experimental flight-hardware setup is given in **Figure 1**; further details are provided in **Supplementary Information 1, Section B**.

Vetting for Cold-Stow

The response of *C. sphaerospermum* CBS 2 to cold storage was determined in a preliminary experiment. A total of six Petri dishes containing PDA were inoculated with the fungus; five were stored at 4°C, with one kept at room temperature (RT) as a control. Plates were removed sequentially after 1, 5, 10, 15, and 20 days. Fungal growth on each plate was monitored at RT and compared to the control.

On-Orbit Implementation

The equipment was packaged with the inoculated Petri dish before the flight and accommodated in a sealed 2U CubeLab™ (SpaceTango, 2021) between December 2018 and January 2019. Lead-time before the launch was 2 days in cold-stow. Transition time to LEO was 3 days (∼1 week to "power-on" after inoculation)[1], transported to the ISS (U.S. Destiny Laboratory) in cold storage (4°C) on SpaceX mission CRS-16.

In orbit, the experiment was oriented such that the Petri dish (and radiation sensors) faced away from Earth. Pictures of the Petri dish were taken in 30-m intervals for 576 h, resulting in 1,139 images (13 gaps scattered throughout the runtime). Temperature and humidity were measured on average every ∼81 s throughout the 622.5-h run-time of the experiment (the three temperature sensors recorded 27,764 readings each). Radiation was measured incrementally, i.e., counts of ionizing events per recording interval, on average every ∼95 s, as well as cumulatively (total counts); 23,607 radiation and noise counts were recorded by each radiation sensor. The stand-alone lab was active aboard the ISS for ∼26 days, with data downlinked on average every 2–3 days (10 data packages in total) before data collection stopped. The experiment awaited its return to Earth in June 2019. All the collected data can be found in **Supplementary Information 2**, where the temperature profiles are rendered under "temp" and the recorded radiation data are compiled under "rad" ("g_cont" and "g_exp" are the incremental data, whereas "g_cont_t" and "g_exp_t" are the cumulative data; columns with the suffix "n" in the nametag are noise-counts); growth-data from the on-orbit experiment was merged with the ground control growth-data and can be found under "growth."

Ground Controls

In addition to the preflight growth test and integrated on-orbit negative control, Earth-based growth experiments

[1]launch: 5/12/2018, 18:16 UTC; berthing: 8/12/2018, 15:36 UTC; power on: 9/12/2018 12:54 UTC.

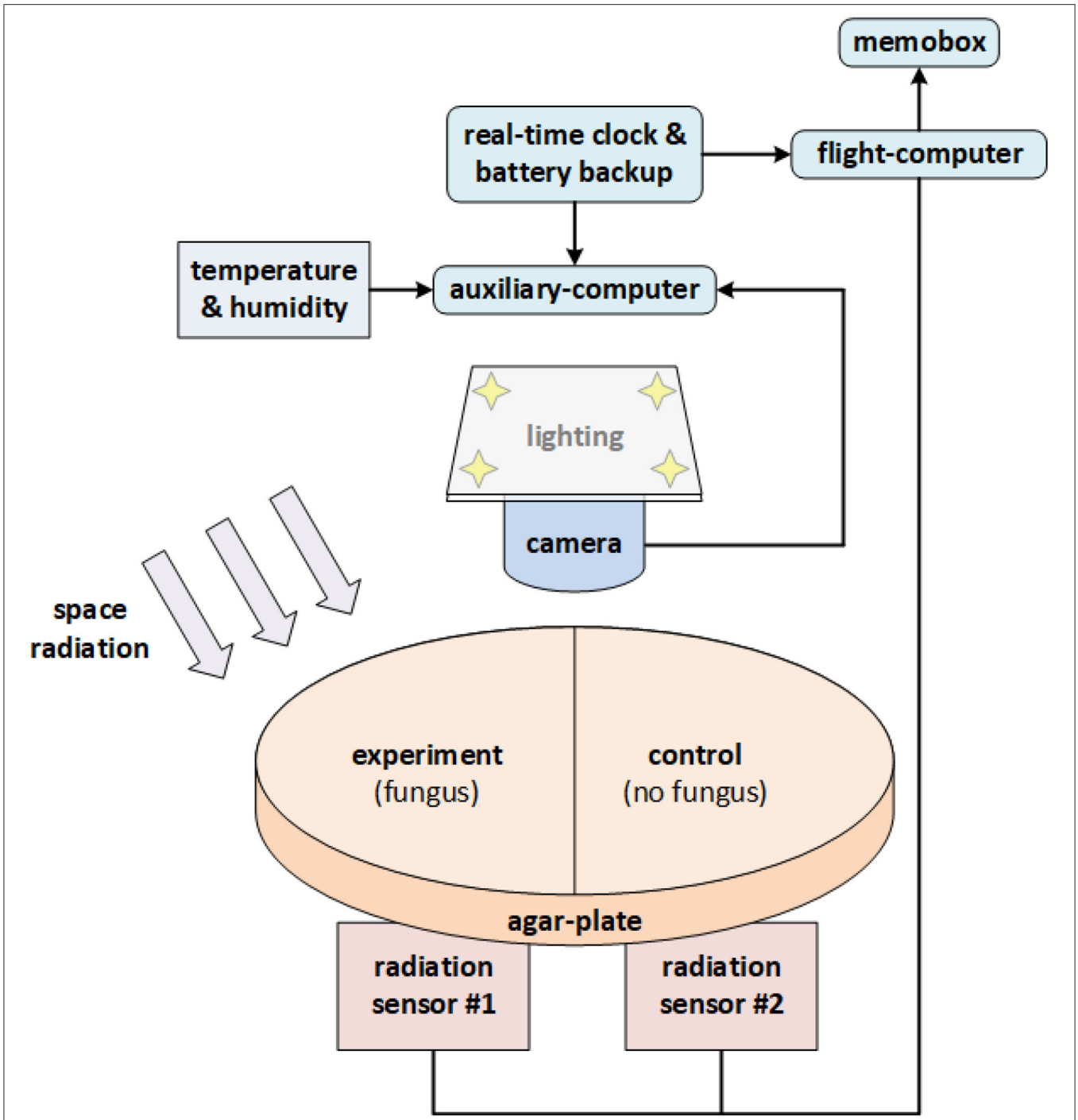

FIGURE 1 | Block chart of the experimental flight-hardware setup. The single (split) Petri dish accommodated both the experiment (agar + fungus), as well as the negative control (agar only). The two (square) radiation sensors were situated in parallel directly beneath the Petri dish (one for each side). Note that "shielding" is one-sided only (for simplicity of experimental setup and to reduce mass).

were performed post-flight, replicating the conditions of the flight experiment without radiation. The same methods and techniques were applied when preparing the cultures on a solid medium. As a means of ground control, a time-dependent temperature profile analogous to the on-orbit experiment was replicated, and graphical data were collected at the same intervals to record the growth behavior.

Evaluation of Growth

Photographs of the cultures were processed with MATLAB (The MathWorks Inc., Natick, MA, US) (MATLAB, 2020) to derive the average brightness values for congruent subsections of each image (cf. **Supplementary Information 1, Section C**) as a proxy for biomass formation. The average brightness values were normalized to render the relative optical density (OD) ranging from zero to one (cf. **Supplementary Information 2**, "growth" for raw and processed data) over time. Exponential regression models (implemented in R, cf. **Supplementary Information 1, Section D**) allowed specific growth rates "k" to be determined. Based on these, a relative difference between k_{exp} for the on-orbit experiment and the ground control, k_{ctrl}, was estimated.

Evaluation of On-Orbit Radiation

The average difference of radiation counts from the incremental data recorded by the radiation sensors of the control- and fungus-side were plotted over the runtime of the on-orbit experiment by means of locally estimated scatterplot smoothing (Cleveland et al., 1992). Based on the growth data (relative OD), different phases were defined. Phase 1, the initial phase, was defined as relative OD measures below 50% of the maximum, corresponding to the first 19 h. Phase 2, the growth phase, was defined for relative OD measures between 5 and 95% of the maximum, correspondingly starting 5 h after $t_0 = 0$ h and ending 46 h after i_0. Phase 3, the stationary phase, comprised data from 200 to 622 h after t_0, corresponding to relative OD measures >99% of the total maximum.

Validation of Statistical Robustness

Logistic growth curve models were fitted to the relative OD measures from the ground controls and on-orbit experiments to test for differences in the slopes of the curves and hence growth behavior. Differences in radiation counts over time between the experiment and the negative control of the on-orbit experiment were modeled with a set of robust regressions. Data preparation and model specification are outlined in **Supplementary Information 1, Section D**.

RESULTS AND DISCUSSION

Pre-flight—Cold-Stow Growth-Test

The "Cold-Stow" experiment showed that for all refrigerated sample plates of *C. sphaerospermum* inoculated on PDA, there was nominal fungal growth immediately upon removal from incubation at 4°C (i.e., no fungal growth prior to t_0) for all trialed timeframes. Furthermore, all samples exhibited similar growth once at ambient temperature, regardless of the time spent in cold storage (data not shown).

Microbial Growth Advantage On-Orbit

From the point the hardware was powered on aboard the ISS, the temperature rose sharply, starting at 22°C and reaching 30°C within the first day, stabilizing after ∼1 week around 31.5 ± 2.4°C for the remaining time of the experiment (cf. **Supplementary Information 2**, "temperature" for temperature profiles as well as humidity data).

Many molds are characterized by slow growth and require up to 2 weeks for significant biomass formation to occur at an optimum temperature of around 25°C (Bosshard, 2011) (only 27 of 50 *Cladosporium* spp. reached growth after 1 week). In the on-orbit lab, *C. sphaerospermum* reached maximum growth and full coverage of the PDA already after 2 days, as discernible from the photographic data (cf. **Supplementary Information 1, Section B**), as well as the derived growth curve, shown in **Figure 2**. Comparison with the ground controls indicates that the fungus may have experienced faster-than-normal growth aboard the ISS, as modeled in **Supplementary Information 1, Section D**. Specifically, the growth rate in the on-orbit experiment was on average 1.21 ± 0.37-times higher (based on $k_{ground\_1} = 0.241\ h^{-1}$, $k_{ground\_2} = 0.231\ h^{-1}$, $k_{ground\_3} = 0.196\ h^{-1}$ and $k_{flight} = 0.299\ h^{-1}$, for the ground controls and on-orbit experiment, respectively, cf. **Supplementary Information 1, Section D**).

While not immediately numerically tangible, it is worth mentioning that in preliminary ground control experiments, often poor growth was observed at 30°C, as compared to RT (data not shown, not used to establish the growth curves), with only sporadic coverage of the PDA with fungal colonies (cf. **Supplementary Information 1, Section B**). Only experiments where full coverage of the agar with *C. sphaerospermum* was achieved were selected as representative ground controls; even then a large deviation existed between the three replicates (error bars depicted in **Figure 2**, cf. also **Supplementary Information 2**, "growth" for raw-data and additional plots). The observation that higher-than-optimum incubation temperatures on Earth rapidly hindered growth is in accordance with the literature (Zalar et al., 2007). It strengthens the conclusion that space benefited the fungi's overall physiology, where observed growth was strong and homogenous throughout the agar.

The growth advantage in space may be attributable to the stimulating effect of ionizing radiation of the space environment on the fungus, analogous to Earth-based scenarios: when subjected to high levels of γ-radiation (500-times stronger than usual), the metabolism of melanized fungi appears to be significantly increased, with an indication of enhanced growth (Dadachova et al., 2007). Measured by the dose equivalent [144 mSv/a for the ISS and 2.4–6.2 mSv/a for Earth (Cucinotta et al., 2008; ANS, 2020; NRC, 2021)], the radiation on the ISS is about 20- to 60-times stronger than the average background on Earth, however, about 80% of this is attributable to energized particles derived from GCRs and SEPs. Therefore, if radiotrophy was present, the fraction of electromagnetic (γ-) rays utilizable by the fungus may not have been equivalently significant. In addition, particle radiation is vastly more damaging (Cucinotta et al., 2017), which would at least partially negate the beneficial effect. It is plausible that the free-radical scavenging properties of the antioxidant melanin protected the cells against

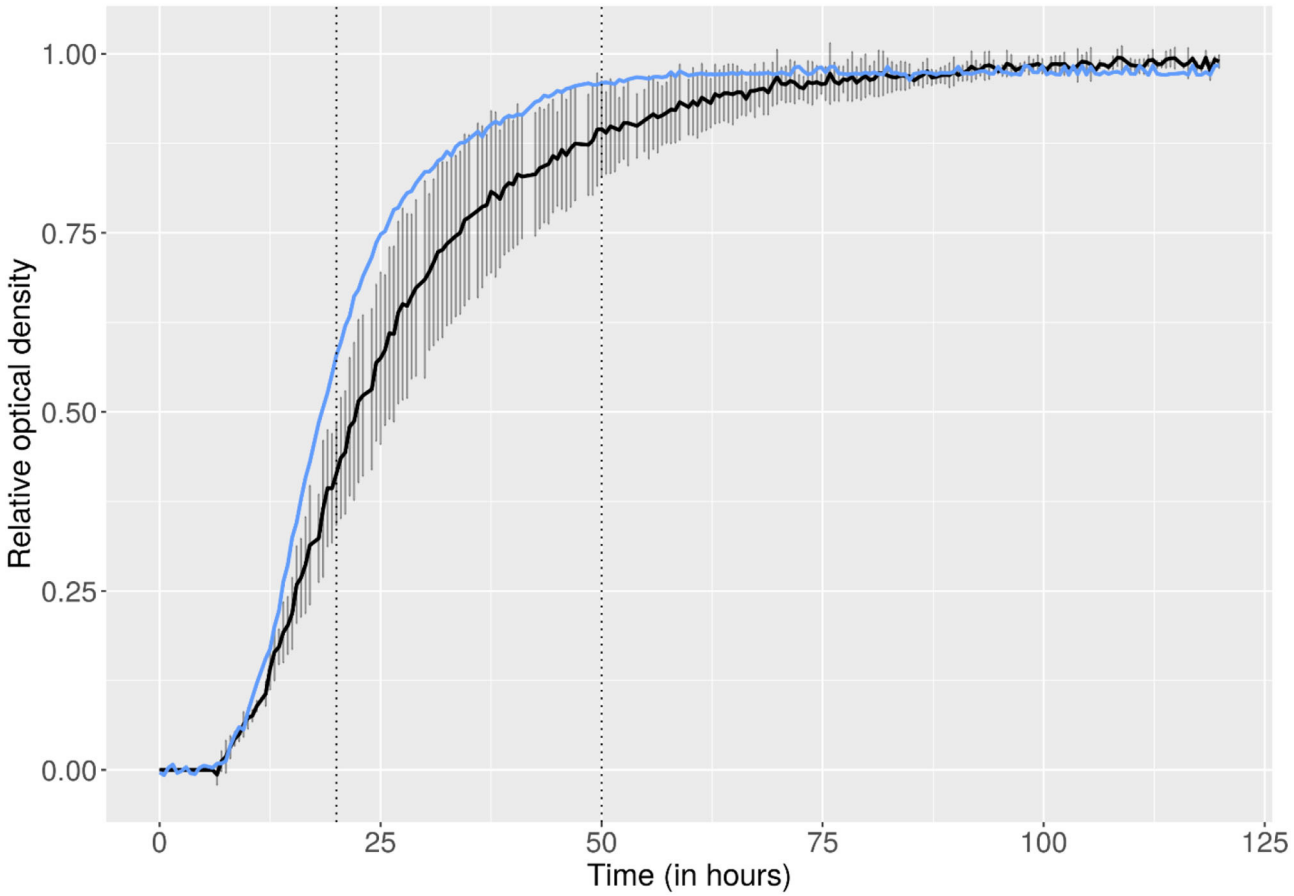

FIGURE 2 | Growth curves (initial 120 h shown) for *C. sphaerospermum* cultivated on solid medium (PDA), depicted by means of connected data points of relative optical densities. While the on-orbit experiment (blue) was a single run, the ground control growth experiment (black) was conducted three times (two replicates in each of the three runs; t_0 was normalized based on the onset of exponential growth of the flight experiment). Error bars show the standard deviation between the three separate runs of the ground control.

radiation damage, minimizing the detrimental effects inherent to the radiation of the space environment (Cordero et al., 2017; Sharma et al., 2021). The occurrence of radiotrophy, radiotropism, or a radioadaptive response can, however, not be unambiguously proven, as the potential role of microgravity and its impact on fungal growth, whether beneficial or detrimental, cannot be assessed and/or gauged with the employed experimental setup.

While melanization likely confers some degree of radioresistance to many strains of *C. sphaerospermum*, radiotropism or even radiotrophy of all the subspecies of this cosmopolitan fungus is not given, as it may only have evolved in a local subset during radiation exposure in the Chernobyl Exclusion Zone. Nevertheless, different isolates of the mold from the Chernobyl Nuclear Power Plant showed a positive response to irradiation, including a control sample obtained from uncontaminated soil (Dadachova and Casadevall, 2008). This is particularly striking since *C. sphaerospermum* was the only species where this was the case (Zhdanova et al., 2004). Further, enhanced metabolism of *C. sphaerospermum* subjected to ionizing radiation was reported for an unspecified ATCC®-strain[2] of this species (Dadachova et al., 2007). Therefore, it seems plausible that many *C. sphaerospermum* strains could present radioadaptive and radiostimulative characteristics. It is, however, not a given that this is also valid for the high-energy particle radiation in space, and further in-depth studies are needed to substantiate or refute this. It could also prove worthwhile to study other melanotic micro-fungi in a space environment for indications of radiotropism or radiotrophy, e.g., isolates of *Cladosporium cladosporioides*, *Aspergillus versicolor*, *Hormoconis resinae*, or certain *Penicillium* species that have been found to thrive in and around the Chernobyl Nuclear Power Plant (Zhdanova et al., 2004; Dighton et al., 2008), as well as *Wangiella dermatitidis* and *Cryptococcus neoformans*, which have also been investigated for their radioresistance as well as radioadaptation and radiotrophy in related Earth-based studies

[2]ATCC® currently lists 16 strains of the species *Cladosporium sphaerospermum* in their collection, none of which appear to have been obtained from Ukraine or derived from one of the original Chernobyl isolates.

(Dadachova and Casadevall, 2008; Malo et al., 2019). Subsequent studies could and should also aim to differentiate the impact of microgravity on the (growth) phenotype of these micro-fungi in space. First approaches to studying these molds' responses on a systems-level in the space context have already been made (Singh et al., 2017; Blachowicz et al., 2019).

If radiotrophy continues to prove plausible and appears to be extendable to the radiation of space, it would be tantalizing to aim for the storage of this energy in chemical form as a biotechnological method for ISRU. Actual radiosynthesis, however, remains to be shown, let alone the reduction of carbon compounds into forms with higher energy content or fixation of inorganic carbon driven by ionizing radiation. If, however, radiotrophy is extendable to off-Earth scenarios and the plausibility of radiosynthesis is substantiated, the hypothesis may be established that extraterrestrial life could rely upon analogous mechanisms to harness energy where other forms are unavailable. Black fungi have already been suggested as models for exobiology due to their ability to tolerate extreme physicochemical parameters (Tesei, 2022). With discoveries suggesting the presence of subterranean waterbodies on Mars and icy moons like Enceladus (Witze, 2014; Diez, 2018; Piqueux et al., 2019), this raises the question of whether life may exist within.

Radiation Measurements in Space

Due to the nature of the employed radiation sensors (PIN photodiode), dosimetric data was not obtained. Nevertheless, approximations can be made regarding the radiation levels (e.g., absorbed dose) to which the experiment was exposed (cf. **Supplementary Information 1, Section B**). As per the trends of the daily cumulative counts (cf. **Supplementary Information 2**, "dose" for plots and charts), the periodic fluctuations of the recorded radiation events are correlated with dosimetric data from the U.S. Destiny Laboratory, in particular, those attributed to the transition of the spacecraft through the South Atlantic Anomaly [cf. flight path of the ISS (Lodge-Paolini, 2021)]. Natural phenomena, rather than false measurements, being the explanation for spikes in radiation counts is supported by the observation that these coincide for both sensors throughout the entire experiment, i.e., high radiation events were picked up by both sensors alike. Consequently, this underscores the consistency of the measurements.

Attenuation of Radiation in the Orbit

Independent of the absolute radiation levels, only the relative difference in ionizing events recorded beneath each side of the Petri dish was significant for the experiment. Compared to the negative control, fewer radiation counts were recorded directly beneath the side of the PDA populated with *C. sphaerospermum*, total as well as per minute (147 vs. 151 CPM, cf. **Supplementary Information 2**, "rad," columns "g_cont_t" and "g_exp_t"), over the runtime of the experiment. To rule out that this apparent difference was only an effect of, e.g., the radiation sensors' base-deviation, a change in the relative difference between the CPM of the experiment and negative control throughout the experiment that correlates with biomass formation is necessary. As per **Figure 3**, which displays the average difference of incremental radiation counts using locally estimated scatterplot smoothing, a more significant difference in radiation counts was observable in the late stage of the experiment with full fungal growth compared to the initial hours when minimal biomass existed.[3] This apparent relationship between the amount of fungal biomass (and putatively the melanin content) and the change in recorded radiation events could indicate attenuation of ionizing radiation. Since only one side of the radiation sensors was protected by the fungus, it is postulated that also only half of the radiation was blocked. Considering the comparatively thin layer of biomass, this may indicate a profound ability of *C. sphaerospermum* to absorb space radiation in the measured spectrum. Another plausible explanation is that conversion of the nutrients contained in the medium into biomass and metabolic end-products and exchange of those with the environment (e.g., consumption of oxygen and production of carbon dioxide) altered the elemental composition of the combined substances in the Petri dish, which resulted in a change in the radiation-blocking properties. However, this theory bears limited potential since the Petri dish and the hardware assembly were sealed.

Statistical Significance and Robustness

Statistical robustness tests were performed with (A) fungal growth data and (B) radiation attenuation data (as provided in **Supplementary Information 2**, "growth" and "rad") with the goal of validating the significance of the drawn conclusions. Specifically, for (A), it was validated that the slope of the growth curve based on the flight-experiment data is steeper than the slope of the growth curves based on the ground control data and that this difference is statistically significant. For (B), it was validated that there is an insignificant difference in the average level of radiation measured beneath the negative control and the fungus/experimental condition in the initial stage of the on-orbit experiment (minimal growth), and the average level of radiation measured beneath the negative control is higher than beneath the fungus/experimental condition in the late stage of the on-orbit experiment (full growth). This supports the hypothesis that the difference in radiation levels beneath the negative control and the fungus/experimental could be attributable to the presence of fungal biomass. A detailed description of the methods, as well as specific results and interpretation of these, can be found in **Supplementary Information 1, Section D**.

The Potential of Melanin as a Radioprotector in Space

In radiotrophic fungi, melanin has been proposed as the primary compound that provides radioprotection through dissipation of radiation energy and its absorption through antioxidant activity, as well as direct interaction with the radiation, limiting the generation of free radicals and/or trapping and neutralizing ionized molecules (Cordero, 2017; Pacelli et al.,

[3] Although no further gain in optical density was observable later than two days into the experiment, an additional week of maturation was allowed before fungal growth was considered complete and metabolism stationary.

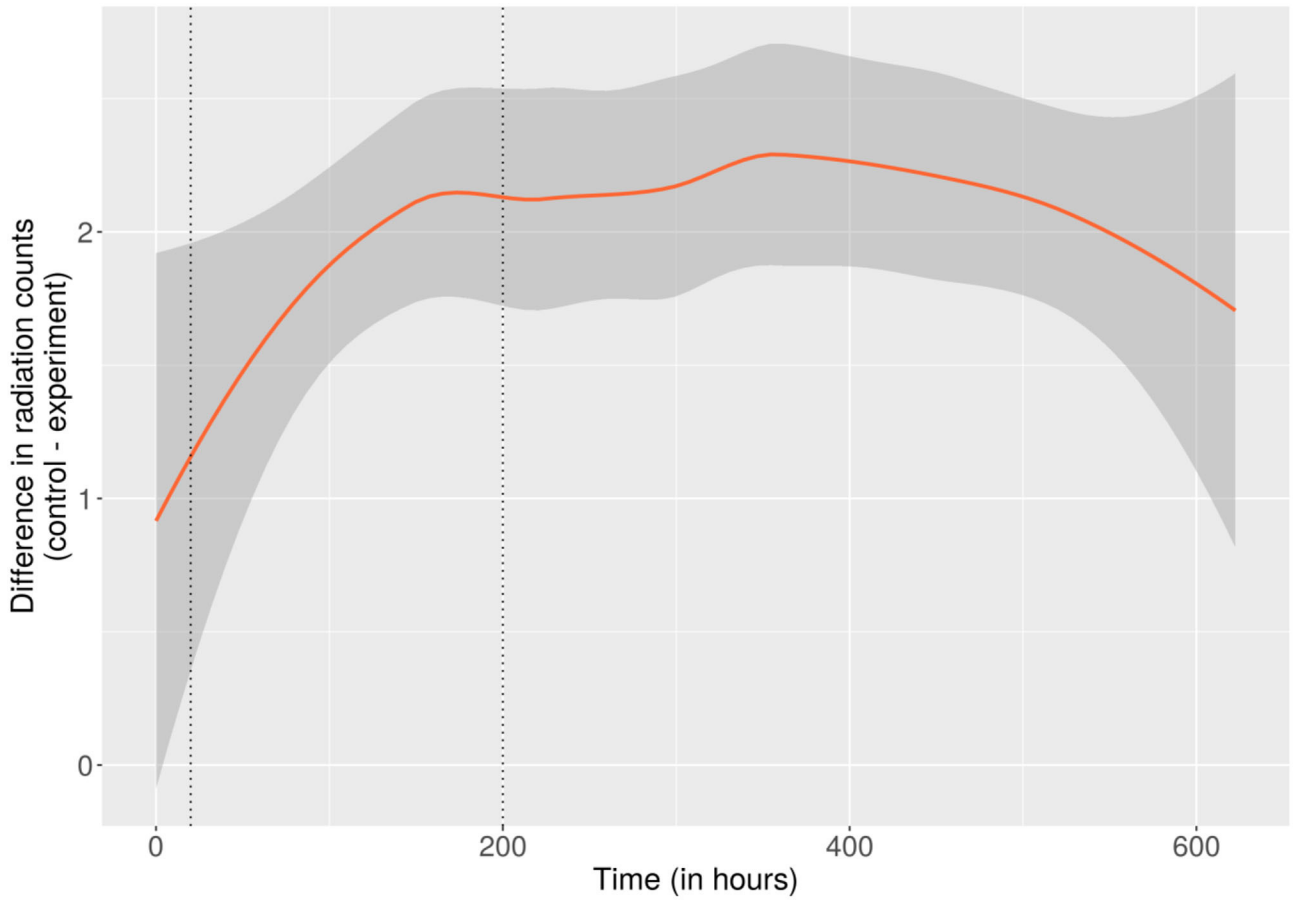

FIGURE 3 | Difference between the incremental radiation counts of the control- and the fungus-side of the on-orbit experiment over the runtime of the experiment. As such, the trendline displays the average difference between the radiation counts measured at intervals of ~1.5 m of locally estimated scatterplot smoothing. The area shaded gray around the trendline corresponds to a 95% confidence band around the smoothed values. Dotted vertical lines were placed for orientation at the time points where growth reached 50% (of the maximum relative OD) and where the formation of biomass and melanin was considered complete (200 h). A more significant difference is apparent toward the later 2/3 of the experiment (200–622 h), where biomass and melanin content were presumably constant, potentially caused by attenuation of the transmitted radiation. The full dataset and additional plots (incremental and cumulative) of the complete radiation data over the whole course of the experiment can be found in **Supplementary Information 2**, under "rad".

2017; Malo et al., 2018, 2019). Various natural and (semi-) synthetic melanin-based compounds and composites have been investigated for their ability to block ionizing and non-ionizing radiation and were found to possess significant attenuation capacity (Schweitzer et al., 2009; Cordero et al., 2017; Pombeiro-Sponchiado et al., 2017; El-Bialy et al., 2019; Cao et al., 2020, 2021). For radiation mostly composed of energetic protons or neutrons, substances that are high in hydrogen have the greatest stopping power (Lloyd and Townsend, 2018). As live biomass commonly has a high water content [~60%, (BioNumbers, 2010)], melanized microbes may present an excellent passive shield, particularly for GCR. However, this will require extensive further theoretical and experimental studies (cf. **Supplementary Information 1, Section B**).

Nevertheless, regardless of how effective a radiation attenuator may be, passive shielding against GCR is ultimately limited by mass density (Dartnell et al., 2007; Chancellor et al., 2018). As a biological compound, natural melanin may be readily available through ISRU and producible by means of biotechnology (Martínez et al., 2019). To increase density, as well as for structural purposes, fungal biomass or melanin itself could be integrated with *in situ* resources that are abundant at the destination, such as regolith (Simonsen et al., 1991), analogous to the concept of Martian "biolith" (Shiwei et al., 2020). In a different application, layers of melanin could be applied to components, such as EVA-suites or inflatable spacecraft and infrastructure, as a constituent of fibrous composites (Blachowicz and Ehrmann, 2021), e.g., in textiles or as resin, to protect them from the surface damage caused by ultraviolet light.

The Potential of Fungi for ISRU in Space

Leveraging existing resources at outposts on moons and other planets to increase the availability and durability of structural components reduces the required haul of construction material

and/or prefabricated elements from Earth. Besides cost savings by reducing up-mass, independence from a supply chain also improves redundancy and robustness of mission-design scenarios. To that end, a multitude of different approaches exists, many of which are still inhibited by the extent of their initially required critical hardware (Gruenwald, 2014; Cichan et al., 2017). Autonomous 3D printing of infrastructure from composites of regolith, for example, has been proposed and demonstrated (MIS, 2020). However, this approach still requires major auxiliary equipment and raw materials for the binding resin. If all materials could be derived or produced on-site, additive manufacturing may become immediately more applicable.

Due to the saprotrophic nature of many fungi, these microorganisms are able to utilize a breadth of carbon compounds and biomass for growth; on Mars, this could be cyanobacterial lysate and/or organic waste, both of which have previously been proposed as substrates for biotechnology (Verseux et al., 2016; Billi et al., 2021). While proven to help produce raw materials (Cockell et al., 2020; Santomartino et al., 2022) and feedstocks for consumables and durable goods (Averesch and Rothschild, 2019), biomanufacturing and bioprocess engineering for space applications are still in the early stages of development (Berliner et al., 2021a,b). Nevertheless, fungi have already been investigated by NASA as a potentially enabling technology to obtain structural components through the application of mycotecture (Rothschild et al., 2019). Expanding the range of organisms being tested for growth on regolith would validate the feasibility of employing melanotic fungi to form composites with *in situ* resources. 3D-bioprinting has already been shown to be feasible with fungal mycelium (Krassenstein, 2014) – advanced additive manufacturing technologies may ultimately allow the creation of smart "living composite" materials that are adaptive, self-healing, and largely autonomous (Nguyen et al., 2018). These "Engineered Living Materials" may provide a game-changing solution to obtain and recover resources and energy and allow the tailored autonomous construction of structural and supporting components in remote locations (Rothschild, 2016).

CONCLUSION

With a basic experimental setup implemented as a single small payload on the ISS, it could be shown that the dematiaceous fungus *C. sphaerospermum* can be cultivated in space while being subjected to the unique microgravity and radiation environment of LEO. Growth characteristics indicated an advantage of cultivation on-orbit compared to the ground control. This could be associated with increased radiation in space, potentially causing a radioadaptive response of the microbe, as has been suggested in analogous Earth-based studies. Further, monitoring radiation throughout the experiment indicated that the melanized fungal biomass may have radioprotective properties in space.

Harnessing cosmic radiation and storage of the energy in chemical bound form (biomass) offers the unique opportunity to supplement (biobased) ISRU, reducing the risk of intermittency. Being living organisms, micro-fungi self-replicate from microscopic amounts, which could allow significant savings in up-mass. Biotechnology would thus prove to be an invaluable asset to life support and resource management for explorers on future missions to the Moon, Mars, and beyond.

DATA AVAILABILITY STATEMENT

The original contributions presented in the study are included in the article/**Supplementary Material**, and further inquiries can be directed to the corresponding author/s.

AUTHOR CONTRIBUTIONS

GS and colleagues of Team Orion conceived of the idea for the study in 2018 and composed the funding proposal. Based on the initial results, GS and colleagues compiled a draft report that served as the basis for the manuscript. NA joined the team in early 2020, comprehensively analyzed the existing data, conducted supporting experiments, researched additional data, and composed the manuscript with support from GS, which was published as a preprint (Shunk et al., 2020). CK subsequently amended the study with regression models and statistical robustness analyses for Journal submission. All authors have read and approved the final version of the manuscript. Correspondence and requests for materials should be addressed to NA.

FUNDING

The Higher Orbits Foundation provided funding for the implementation of this project through the Go For Launch! program. NA was partially supported under NASA grant or cooperative agreement award number NNX17AJ31G.

ACKNOWLEDGMENTS

As members of Team Orion, Xavier R. Gomez, Srikar P. Kaligotla, Finn H. Poulin, and Jamison R. Fuller were instrumental in the conception and planning of the experiment. We extend our thanks to the Higher Orbits Foundation for providing funding for this project through the Go For Launch! program and space Tango for the technical solution, logistics, and implementation of the experiment. Specifically, our gratitude goes out to Michelle Lucas of Higher Orbits and Gentry Barnett of Space Tango. Additional acknowledgments go to Kerry Lee of the NASA SRAG for help with obtaining dosimetric data for the timeframe of the experiment.

SUPPLEMENTARY MATERIAL

The Supplementary Material for this article can be found online at: https://www.frontiersin.org/articles/10.3389/fmicb.2022.877625/full#supplementary-material

REFERENCES

Abel, A. J., Berliner, A. J., Mirkovic, M., Collins, W. D., Arkin, A. P., and Clark, D. S. (2021). Photovoltaics-driven power production can support human exploration on Mars. *arXiv* 2110.14757. doi: 10.3389/fspas.2022.868519

Afshinnekoo, E., Scott, R. T., Mackay, M. J., Pariset, E., Cekanaviciute, E., Barker, R., et al. (2020). Fundamental biological features of spaceflight: advancing the field to enable deep-space exploration. *Cell* 183, 1162–1184. doi: 10.1016/j.cell.2020.10.050

Ambroglini, F., Battiston, R., and Burger, W. J. (2016). Evaluation of superconducting magnet shield configurations for long duration manned space missions. *Front. Oncol.* 6. 97. doi: 10.3389/fonc.2016.00097

ANS (2020). *Radiation Dose Calculator*. American Nuclear Society. Available online at: https://ans.org/pi/resources/dosechart/msv.php (accessed November 23, 2021).

Averesch, N. J. H. (2021). Choice of microbial system for *in-situ* resource utilization on Mars. *Front. Astron. Space Sci*. 8, 700370. doi: 10.3389/fspas.2021.700370

Averesch, N. J. H., and Rothschild, L. J. (2019). Metabolic engineering of *Bacillus subtilis* for production of *para*-aminobenzoic acid – unexpected importance of carbon source is an advantage for space application. *Microb. Biotechnol.* 12, 703–714. doi: 10.1111/1751-7915.13403

Belozerskaya, T., Aslandi, K., Ivanova, A., Gessler, N., Egorova, A., Karpenko, A., et al. (2010). "Characteristics of extremophylic fungi from chernobyl nuclear power plant," in *Current Research, Technology and Education Topics in Applied Microbiology and Microbial Biotechnology, Vol. 2*, ed A. Mendez-Vilas (Badajoz), 88–94. Available online at: https://docplayer.net/21778708-Current-research-technology-and-education-topics-in-applied-microbiology-and-microbial-biotechnology.html

Berliner, A., Hilzinger, J. M., Abel, A. J., McNulty, M., Makrygiorgos, G., Averesch, N. J. H., et al. (2021a). Towards a biomanufactory on Mars. *Front. Astron. Space Sci. [Preprint].* doi: 10.20944/preprints202012.0714.v1

Berliner, A. J., Lipsky, I., Ho, D., Hilzinger, J. M., Vengerova, G., Makrygiorgos, G., et al. (2021b). Space bioprocess engineering on the horizon. *Preprints* 2021120401. doi: 10.20944/preprints202112.0401.v2

Billi, D., Fernandez, B. G., Fagliarone, C., Chiavarini, S., and Rothschild, L. J. (2021). Exploiting a perchlorate-tolerant desert cyanobacterium to support bacterial growth for *in situ* resource utilization on Mars. *Int. J. Astrobiology* 20, 29–35. doi: 10.1017/S1473550420000300

BioNumbers (2010). "BNID 103689", in: *The Database of Useful Biological Numbers*. Harvard University. Available online at: https://bionumbers.hms.harvard.edu/bionumber.aspx?id=103689

Blachowicz, A., Chiang, A. J., Elsaesser, A., Kalkum, M., Ehrenfreund, P., Stajich, J. E., et al. (2019). Proteomic and metabolomic characteristics of extremophilic fungi under simulated Mars conditions. *Front. Microbiol.* 10, 1013. doi: 10.3389/fmicb.2019.01013

Blachowicz, T., and Ehrmann, A. (2021). Shielding of cosmic radiation by fibrous materials. *Fibers* 9, 60. doi: 10.3390/fib9100060

Bosshard, P. P. (2011). Incubation of fungal cultures: how long is long enough? *Mycoses* 54, e539–e545. doi: 10.1111/j.1439-0507.2010.01977.x

Cao, W., McCallum, N. C., Ni, Q. Z., Li, W., Boyce, H., Mao, H., et al. (2020). Selenomelanin: an abiotic selenium analogue of pheomelanin. *J. Am. Chem. Soc.* 142, 178–179. doi: 10.1021/jacs.0c05573

Cao, W., Zhou, X., McCallum, N. C., Hu, Z., Ni, Q. Z., Kapoor, U., et al. (2021). Unraveling the structure and function of melanin through synthesis. *J. Am. Chem. Soc.* 143, 2622–2637. doi: 10.1021/jacs.0c12322

CASIS (2020). *ISS National Lab Commercial Service Providers: Space Tango, Inc*. ISS National Laboratory. Available online at: https://www.issnationallab.org/implementation-partners/space-tango-inc/ (accessed November 23, 2021).

Chancellor, J. C., Blue, R. S., Cengel, K. A., Auñón-Chancellor, S. M., Rubins, K. H., Katzgraber, H. G., et al. (2018). Limitations in predicting the space radiation health risk for exploration astronauts. *NPJ Microgravity* 4, 1–11. doi: 10.1038/s41526-018-0043-2

Chancellor, J. C., Scott, G. B. I., and Sutton, J. P. (2014). Space radiation: the number one risk to astronaut health beyond low Earth orbit. *Life* 4, 491–510. doi: 10.3390/life4030491

Cichan, T., Bailey, S. A., Antonelli, T., Jolly, S. D., Chambers, R. P., Clark, B., et al. (2017). Mars base camp: an architecture for sending humans to Mars. *New Space* 5, 203–218. doi: 10.1089/space.2017.0037

Cleveland, W. S., Grosse, E., and Shyu, W. M. (1992). "Local regression models," in *Statistical Models in S, 1st Edn,* eds. J. M. Chambers and T. J. Hastie (New York, NY: Wadsworth and Brooks/Cole) 624.

Cockell, C. S., Santomartino, R., Finster, K., Waajen, A. C., Eades, L. J., Moeller, R., et al. (2020). Space station biomining experiment demonstrates rare earth element extraction in microgravity and Mars gravity. *Nat. Commun.* 11, 5523. doi: 10.1038/s41467-020-19276-w

Cordero, R. J. B. (2017). Melanin for space travel radioprotection. *Environ. Microbiol.* 19, 2529–2532. doi: 10.1111/1462-2920.13753

Cordero, R. J. B., Vij, R., and Casadevall, A. (2017). Microbial melanins for radioprotection and bioremediation. *Microb. Biotech.* 10, 1186–1190. doi: 10.1111/1751-7915.12807

Cortesão, M., De Haas, A., Unterbusch, R., Fujimori, A., Schütze, T., Meyer, V., et al. (2020). *Aspergillus niger* spores are highly resistant to space radiation. *Front. Microbiol.* 11, 560. doi: 10.3389/fmicb.2020.00560

Cucinotta, F. A., Kim, M.-H. Y., and Chappell, L. J. (2012). *Space Radiation Cancer Risk Projections and Uncertainties*. Hanover, MD: NASA.

Cucinotta, F. A., Kim, M.-H. Y., Willingham, V., and George, K. A. (2008). Physical and biological organ dosimetry analysis for international space station astronauts. *Radiat. Res.* 170, 127–138. doi: 10.1667/RR1330.1

Cucinotta, F. A., To, K., and Cacao, E. (2017). Predictions of space radiation fatality risk for exploration missions. *Life Sci. Space. Res.* 13, 1–11. doi: 10.1016/j.lssr.2017.01.005

Dadachova, E., Bryan, R. A., Huang, X., Moadel, T., Schweitzer, A. D., Aisen, P., et al. (2007). Ionizing radiation changes the electronic properties of melanin and enhances the growth of melanized fungi. *PLoS One* 2, e457. doi: 10.1371/journal.pone.0000457

Dadachova, E., and Casadevall, A. (2008). Ionizing radiation: how fungi cope, adapt, and exploit with the help of melanin. *Curr. Opin. Microbiol.* 11, 525–531. doi: 10.1016/j.mib.2008.09.013

Dartnell, L. R., Desorgher, L., Ward, J. M., and Coates, A. J. (2007). Modelling the surface and subsurface Martian radiation environment: implications for astrobiology. *Geophys. Res. Lett.* 34:L02207. doi: 10.1029/2006GL027494

Diez, A. (2018). Liquid water on Mars. *Science* 361, 448–449. doi: 10.1126/science.aau1829

Dighton, J., Tugay, T., and Zhdanova, N. (2008). Fungi and ionizing radiation from radionuclides. *FEMS Microbiol.* 281, 109–120. doi: 10.1111/j.1574-6968.2008.01076.x

Drake, B. G., and Watts, K. D. (2014). *Human Exploration of Mars Design Reference Architecture 5.0, Addendum #2*. Hanover, MD: NASA.

Eisenman, H. C., and Casadevall, A. (2012). Synthesis and assembly of fungal melanin. *Appl. Microbiol. Biotechnol.* 93, 931–940. doi: 10.1007/s00253-011-3777-2

El-Bialy, H. A., El-Gamal, M. S., Elsayed, M. A., Saudi, H. A., and Khalifa, M. A. (2019). Microbial melanin physiology under stress conditions and gamma radiation protection studies. *Radiat. Phys. Chem.* 162, 178–186. doi: 10.1016/j.radphyschem.2019.05.002

Gruenwald, J. (2014). Human outposts on Mars: engineering and scientific lessons learned from history. *CEAS Space J.* 6, 73–77. doi: 10.1007/s12567-014-0059-8

Hall, L. (2017). *In-Situ Resource Utilization*. NASA. Available online at: http://www.nasa.gov/isru (accessed November 23, 2021).

Hassler, D. M., Zeitlin, C., Wimmer-Schweingruber, R. F., Ehresmann, B., Rafkin, S., Eigenbrode, J. L., et al. (2014). Mars' surface radiation environment measured with the Mars Science Laboratory's Curiosity Rover. *Science* 343, 1244797. doi: 10.1126/science.1244797

Kalawate, A., and Mehetre, S. (2015). Isolation and characterization of mold fungi and insects infecting sawmill wood, and their inhibition by gamma radiation. *Radiat. Phys. Chem.* 117, 191–197. doi: 10.1016/j.radphyschem.2015.08.016

Karpenko, Y. V., Redchitz, T. I., Zheltonozhsky, V. A., Dighton, J., and Zhdanova, N. N. (2006). Comparative responses of microscopic fungi to ionizing radiation and light. *Folia Microbiol.* 51, 45. doi: 10.1007/BF02931449

Krassenstein, B. (2014). *3D Printing With Fungus - Artist Creates Chairs and Other Objects Out of Mushrooms*. 3DPrint.com. Available online at: https://3dprint.com/7279/3d-print-fungus-mycelium/ (accessed November 23, 2021).

Krisko, A., and Radman, M. (2013). Biology of extreme radiation resistance: the way of deinococcus radiodurans. *Cold Spring Harb. Perspect. Biol.* 5. a012765. doi: 10.1101/cshperspect.a012765

Ledford, H. (2007). Hungry fungi chomp on radiation. *Nature*. doi: 10.1038/news070521-5

Letaw, J. R., Silberberg, R., and Tsao, C. H. (1988). "Galactic Cosmic Radiation Doses to Astronauts Outside the Magnetosphere," in *Terrestrial Space Radiation and Its Biological Effects, Nato ASI Series Edn*, eds. P. D. McCormack, C. E. Swenberg and H. Bücker (Boston, MA: Springer US), 663–673. doi: 10.1007/978-1-4613-1567-4_46

Lloyd, C. W., and Townsend, S. (2018). "Space radiation", ed. K. K. Reeves. NASA. Available online at: https://www.nasa.gov/sites/default/files/atoms/files/space_radiation_ebook.pdf

Lodge-Paolini, M. (2021). *ISSTracker*. Scarborough, ME: Myflipside Media, LLC. Available online at: http://www.isstracker.com/historical (accessed November 23, 2021).

Loff, S. (2018). *Moon to Mars*. NASA. Available online at: http://www.nasa.gov/topics/moon-to-mars (accessed November 23, 2021).

Malo, M. E., Bryan, R. A., Shuryak, I., and Dadachova, E. (2018). Morphological changes in melanized and non-melanized *Cryptococcus neoformans* cells post exposure to sparsely and densely ionizing radiation demonstrate protective effect of melanin. *Fungal Biol.* 122, 449–456. doi: 10.1016/j.funbio.2017.08.010

Malo, M. E., Frank, C., and Dadachova, E. (2019). Assessing melanin capabilities in radiation shielding and radioadaptation. *J. Med. Imaging Radiat. Sci.* 50, S2. doi: 10.1016/j.jmir.2019.11.011

Martínez, L. M., Martinez, A., and Gosset, G. (2019). Production of melanins with recombinant microorganisms. *Front. Bioeng. Biotechnol.* 7, 285. doi: 10.3389/fbioe.2019.00285

MATLAB (2020). *Read and Analyze Image Files - MATLAB and Simulink*. MathWorks. Available online at: https://www.mathworks.com/help/matlab/import_export/read-and-analyze-image-files.html (accessed November 23, 2020).

Menezes, A. A., Cumbers, J., Hogan, J. A., and Arkin, A. P. (2015). Towards synthetic biological approaches to resource utilization on space missions. *J. R. Soc. Interface* 12, 20140715. doi: 10.1098/rsif.2014.0715

MIS (2020). *Made In Space*. Made In Space, Inc. Available online at: https://madeinspace.us/ (accessed November 23, 2021).

Nangle, S. N., Wolfson, M. Y., Hartsough, L., Ma, N. J., Mason, C. E., Merighi, M., et al. (2020). The case for biotech on Mars. *Nat. Biotechnol.* 38, 401–407. doi: 10.1038/s41587-020-0485-4

NASA (2020). *Artemis Plan*. NASA. Available online at: https://www.nasa.gov/sites/default/files/atoms/files/artemis_plan-20200921.pdf (accessed November 23, 2021).

Nguyen, P. Q., Courchesne, N.-M. D., Duraj-Thatte, A., Praveschotinunt, P., and Joshi, N. S. (2018). Engineered living materials: prospects and challenges for using biological systems to direct the assembly of smart materials. *Adv. Mater.* 30, 1704847. doi: 10.1002/adma.201704847

NRC (2021). *Personal Annual Radiation Dose Calculator*. Nuclear Regulatory Commission. Available online at: https://www.nrc.gov/about-nrc/radiation/around-us/calculator.html (accessed November 23, 2021).

Pacelli, C., Bryan, R. A., Onofri, S., Selbmann, L., Shuryak, I., and Dadachova, E. (2017). Melanin is effective in protecting fast and slow growing fungi from various types of ionizing radiation. *Environ. Microbiol.* 19, 1612–1624. doi: 10.1111/1462-2920.13681

Piqueux, S., Buz, J., Edwards, C. S., Bandfield, J. L., Kleinböhl, A., Kass, D. M., et al. (2019). Widespread shallow water ice on Mars at high latitudesand midlatitudes. *Geophys. Res. Lett.* 46, 14290–14298. doi: 10.1029/2019GL083947

Pombeiro-Sponchiado, S. R., Andrade, G. S.S. C. R., Lisboa, H. F., and Gonçalves, R. C. R. (2017). "Production of melanin pigment by fungi and its biotechnological applications," in *Melanin,* ed. M. Blumenberg (New York, NY: University Langone Medical Center, IntechOpen). doi: 10.5772/67375

Rothschild, L. J. (2016). Synthetic biology meets bioprinting: enabling technologies for humans on Mars (and Earth). *Biochem. Soc. Trans.* 44, 1158–1164. doi: 10.1042/BST20160067

Rothschild, L. J., Maurer, C., Paulino Lima, I. G., Senesky, D., Wipat, A., and Head, J. I. (2019). *Myco-Architecture off Planet: Growing Surface Structures at Destination*. NASA.

Santomartino, R., Zea, L., and Cockell, C. S. (2022). The smallest space miners: principles of space biomining. *Extremophiles* 26, 7. doi: 10.1007/s00792-021-01253-w

Schweitzer, A. D., Howell, R. C., Jiang, Z., Bryan, R. A., Gerfen, G., Chen, C.-C., et al. (2009). Physico-chemical evaluation of rationally designed melanins as novel nature-inspired radioprotectors. *PLoS One* 4, e7229. doi: 10.1371/journal.pone.0007229

Sharma, S., Smith, R. S. H., Lee, N. A., Wilson, S. L., Smith, M. M., and Oxman, N. (2021). "Exogenous pigments shield microorganisms from spaceflight-induced changes", in: *bioRxiv [Preprint]*. (*bioRxiv.org*). doi: 10.1101/2021.07.29.454367

Shiwei, N., Dritsas, S., and Fernandez, J. G. (2020). Martian biolith: A bioinspired regolith composite for closed-loop extraterrestrial manufacturing. *PLoS One* 15, e0238606. doi: 10.1371/journal.pone.0238606

Shunk, G. K., Gomez, X. R., Kern, C., and Averesch, N. J. H. (2020). Growth of the radiotrophic fungus *Cladosporium sphaerospermum* aboard the international space station and effects of ionizing Radiation. *bioRxiv [Preprint]*. doi: 10.1101/2020.07.16.205534

Simonsen, L. C., Nealy, J. E., Townsend, L. W., and Wilson, J. W. (1991). Martian regolith as space radiation shielding. *J. Spacecr. Rockets* 28, 7–8. doi: 10.2514/3.26201

Singh, N. K., Blachowicz, A., Romsdahl, J., Wang, C., Torok, T., and Venkateswaran, K. (2017). Draft genome sequences of several fungal strains selected for exposure to microgravity at the international space station. *Genome Announc.* 5, e01602–01616. doi: 10.1128/genomeA.01602-16

SpaceTango (2021). *Space Tango | TangoLab*. Space Tango, Inc. Available online at: https://spacetango.com/tangolab/ (accessed November 23, 2021).

Tesei, D. (2022). Black fungi research: out-of-this-world implications. *Encyclopedia* 2, 212–229. doi: 10.3390/encyclopedia2010013

Tugay, T., Zhdanova, N. N., Zheltonozhsky, V., Sadovnikov, L., and Dighton, J. (2006). The influence of ionizing radiation on spore germination and emergent hyphal growth response reactions of microfungi. *Mycologia* 98, 521–527. doi: 10.1080/15572536.2006.11832654

Tugay, T. I., Zheltonozhskaya, M. V., Sadovnikov, L. V., Tugay, A. V., and Farfán, E. B. (2011). Effects of ionizing radiation on the antioxidant system of microscopic fungi with radioadaptive properties found in the chernobyl exclusion zone. *Health Phys.* 101, 375–382. doi: 10.1097/HP.0b013e3181f56bf8

Turick, C. E., Ekechukwu, A. A., Milliken, C. E., Casadevall, A., and Dadachova, E. (2011). Gamma radiation interacts with melanin to alter its oxidation–reduction potential and results in electric current production. *Bioelectrochem.* 82, 69–73. doi: 10.1016/j.bioelechem.2011.04.009

Verseux, C., Baqu,é, M., Lehto, K., Vera, J.-P. P. D., Rothschild, L. J., and Billi, D. (2016). Sustainable life support on Mars – the potential roles of cyanobacteria. *Int. J. Astrobiol.* 15, 65–92. doi: 10.1017/S147355041500021X

Witze, A. (2014). Icy Enceladus hides a watery ocean. *Nature*. doi: 10.1038/nature.2014.14985. Available online at: https://www.nature.com/articles/nature.2014.14985

Zalar, P., De Hoog, G. S., Schroers, H. J., Crous, P. W., Groenewald, J. Z., and Gunde-Cimerman, N. (2007). Phylogeny and ecology of the ubiquitous saprobe *Cladosporium sphaerospermum*, with descriptions of seven new species from hypersaline environments. *Stud. Mycol.* 58, 157–183. doi: 10.3114/sim.2007.58.06

Zhdanova, N. N., Tugay, T., Dighton, J., Zheltonozhsky, V., and McDermott, P. (2004). Ionizing radiation attracts soil fungi. *Mycol. Res.* 108, 1089–1096. doi: 10.1017/S0953756204000966

Conflict of Interest: The authors declare that the research was conducted in the absence of any commercial or financial relationships that could be construed as a potential conflict of interest.

frontiers | Frontiers in Microbiology

ORIGINAL RESEARCH
published: 11 July 2022
doi: 10.3389/fmicb.2022.909997

Establishing Sterility Assurance for *Bacillus canaveralius* 29669 Spores Under High Heat Exposure

Zachary Steven Dean[1*†], *Michael DiNicola*[2†], *Emily Klonicki*[1], *Scott Roberts*[3], *Brian Gregory Clement*[1] *and Lisa Guan*[1*]

[1] *Jet Propulsion Laboratory, California Institute of Technology, Biotechnology and Planetary Protection, Pasadena, CA, United States,* [2] *Jet Propulsion Laboratory, California Institute of Technology, Systems Modeling, Analysis, and Architectures Group, Pasadena, CA, United States,* [3] *Jet Propulsion Laboratory, California Institute of Technology, Materials Development and Manufacturing Technology Group, Pasadena, CA, United States*

The ever-increasing complexity in critical spacecraft hardware and materials has led to the development of new microbial reduction procedures as well as to changes in established processes such as heat microbial reduction (HMR). In the space biology field of Planetary Protection, 500°C for 0.5 s is the current HMR recommendation to reduce microorganisms from flight hardware. However, more studies are needed to effectively determine the microbial reduction capability of high-temperature (more than 200°C), short-duration (under 30 s) heat exposures. One of the many recent microbial reduction bioengineering research avenues harnesses electromagnetic energy for microbial reduction, with previous investigations demonstrating that infrared heaters are capable of the short temperature ramp time required for rapid heating investigations above 200°C. Therefore, this study employed a 6 kW infrared heater to determine the survivability of heat resistant *Bacillus canaveralius* 29669 to high-temperature, short-duration infrared temperatures. While *B. canaveralius* 29669 spores can survive microbial heat reduction processes above 200°C, we found evidence suggesting that the 500°C for 0.5 s temperature sterilization specification for Planetary Protection should be updated. This research presents spore survival data and a corresponding model pointing to a re-evaluation of the recommended HMR exposure of 500°C for 0.5 s, while simultaneously meeting requirements on the forward biological contamination of solar system bodies and opening up design possibilities for future spacecraft hardware.

Keywords: Planetary Protection, heat microbial reduction, endospores, spacecraft bioburden, infrared heating, survival modeling, heat-resistant microorganisms

OPEN ACCESS

Edited by:
Rob Van Houdt,
Belgian Nuclear Research Centre, Belgium

Reviewed by:
Graham Christie,
University of Cambridge, United Kingdom
Peter Setlow,
UCONN Health, United States
Lei Rao,
China Agricultural University, China

***Correspondence:**
Zachary Steven Dean
zachary.s.dean@jpl.nasa.gov
Lisa Guan
lisa.guan@jpl.nasa.gov

†These authors share first authorship

Specialty section:
This article was submitted to Extreme Microbiology, a section of the journal Frontiers in Microbiology

Received: *31 March 2022*
Accepted: *23 May 2022*
Published: *11 July 2022*

Citation:
Dean ZS, DiNicola M, Klonicki E, Roberts S, Clement BG and Guan L (2022) Establishing Sterility Assurance for Bacillus canaveralius 29669 Spores Under High Heat Exposure. Front. Microbiol. 13:909997. doi: 10.3389/fmicb.2022.909997

1. INTRODUCTION

Space exploration and interplanetary travel has revealed that terrestrial microbial life might be capable of survival in extraterrestrial environments (Chyba and Phillips, 2002; Saffary et al., 2002; McLean et al., 2006). As outer solar system missions continue to explore potentially habitable environments such as Mars and ocean worlds, planetary protection practices will be critical to prevent the deposition of terrestrial microorganisms, or forward contamination, and preserve data collected in future life-detection missions (Bruckner et al., 2009). The current era of Mars exploration has already motivated a number of recent advances in Planetary Protection as

upcoming landed ocean worlds exploration requires heightened Planetary Protection sterilization protocols to ensure stringent cleanliness and reduce biocontamination (Pratt and Smith, 2020).

Bioburden, the microbial load on a product, consists of microorganisms that are capable of establishing a viable colony forming unit (International Organization for Standardization, 2010). These microorganisms can come from diverse sources such as human contact, air flow systems, material processing during spacecraft assembly, raw materials, and other environmental vectors that the material is exposed to (Whyte and Eaton, 2015). Microbial communities on spacecraft surfaces can range from fungi, bacterial spores, and dormant microorganisms, depending on the environmental conditions. These organisms vary widely in their ability to survive in extreme conditions. For example, researchers have studied the extremophile *Bacillus canaveralius* 29669, the current model organism for Planetary Protection heat sterilization studies, which was isolated from microbial fallout in clean rooms during the assembly of the Viking missions to Mars. Spores from this bacterial species are thirty times more resistant to dry heat than *Bacillus atrophaeus*, the universally-accepted heat microbial reduction indicator organism (Schubert and Beaudet, 2011). The exact reasoning for *B. canaveralius* 29669's heat resistance is unknown, but its genome contains a gene coding for a glycogen branching enzyme from hyperthermophile *Thermococcus kodakaraensis* which may contribute to its heat tolerance (Seuylemezian et al., 2018).

The Planetary Protection group at the NASA Jet Propulsion Laboratory is responsible for mitigating the bioburden of spacecraft destined for other moons or planets, such as Europa. Forms of Planetary Protection microbial reduction techniques used in missions include vaporized hydrogen peroxide, heat microbial reduction (HMR), and alcohol disinfection. These methods are implemented in cleanrooms and used on spacecraft in order to reduce the biological matter that may contaminate the hardware (Pillinger et al., 2006). In addition to bioburden reduction capabilities, Planetary Protection must also take into account hardware compatibility to microbial reduction techniques when determining the optimal disinfection techniques and standards.

HMR is a microbial reduction technique where spacecraft and mechanical components are kept at high temperatures under controlled humidity for a predetermined exposure time. HMR is the most commonly used approach for reducing bioburden on spacecraft hardware. NASA recently revised HMR specifications to provide D-values, which are the defined times and temperatures required to reduce viable bacteria by 90%, for temperatures up to 200°C (NASA Science Mission Directorate, 2008). *D*-values for higher temperatures are derived by Viking-era (1970s) findings, which are not appropriate for predicting lethality above a 3-log reduction (Shirey et al., 2017). The NASA HMR specifications for absolute sterility, defined as a 12-log reduction, requires hardware to undergo HMR at 500°C for 0.5 s (NASA Science Mission Directorate, 2008).

Previous investigations evaluating heat sterilization techniques have demonstrated that electromagnetic radiation is capable of high temperature sterilization (e.g., 500°C in 30 s), and that the heating, not the infrared wavelength photochemical effects, cause significant microbial killing (Kempf et al., 2005). Despite significant research on heat microbial reduction, there is still a lack of data for the high-temperature, short-duration heat exposures that will assist in determining the minimal temperature and exposure time necessary for the efficient sterilization. In this study, an infrared (IR) halogen lamp system was designed, built, and employed to test survival of *B. canaveralius* 29669 spores exposed to temperatures above 200°C for <30 s. *B. canaveralius* 29669 spores are used as the model microorganism for this study due to its high heat resistance and its role in informing current NASA requirements (NASA Science Mission Directorate, 2017). The objective is to use experimental results and mathematical modeling to bound the time-temperature at which the Sterility Assurance Level (SAL), or probability that one or more microorganisms survive, reaches 10^{-6} (Swenson, 2012). As part of this analysis, we will also investigate the probability that an individual microorganism survives, *s*, as well as *D*-values and *z*-values associated with these experiments.

2. MATERIALS AND METHODS

2.1. Preliminary Spore Evaluation and Spore Strain Selection

The *B. canaveralius* 29669 organisms used in this study were obtained from the American Type Culture Collection (Manassas, VA) with spore production carried out following previously described methods (Schubert and Beaudet, 2011). Six sub-cultures derived from the original *B. canaveralius* 29669 parent culture were characterized in this study's investigation. The six sub-cultures were tested to identify the batch most closely matching the *D*-value from the *B. canaveralius* 29669 culture used to determine the 2008 NPR Planetary Protection heat sterilization parameters, 39.7 min at 150°C (Kempf et al., 2008; NASA Science Mission Directorate, 2017). Five microliters of 1.5×10^6 *B. canaveralius* 29669 spores per μL suspended in deionized water were spotted onto the bottom of thin-walled, flat-bottom stainless steel thermal spore exposure vessels, or TSEVs, that are 1.27 cm internal diameter, 10.16 cm long, and a wall thickness of 0.025 cm (**Supplementary Figure 1A**; Kempf et al., 2008). After spotting with spores, the TSEVs were then dried in a biological safety hood overnight (8 h minimum). Following overnight drying, the TSEVs were then placed in a lyophilizer (Millrock Technology, Inc., Kingston, NY) for an hour. The spore heat survival experiments were then executed in a high-temperature thermometer calibration oil bath (Model 6330, Hart Scientific, American Fork, UT, **Supplementary Figure 1B**) filled with a silicone oil (Hart bath fluid #5017, Dow Corning silicone oil type 710, Hart Scientific, American Fork, UT). The bath temperature was preheated to 150°C for 30 min and held to within ±0.05° of the target temperature during the exposures with continuous oil stirring to facilitate equal temperature distribution to all TSEVs. Thermocouples were calibrated through immersion in the thermometer calibration bath prior to use. The inoculated TSEVs were placed under 1.5 Torr vacuum conditions using

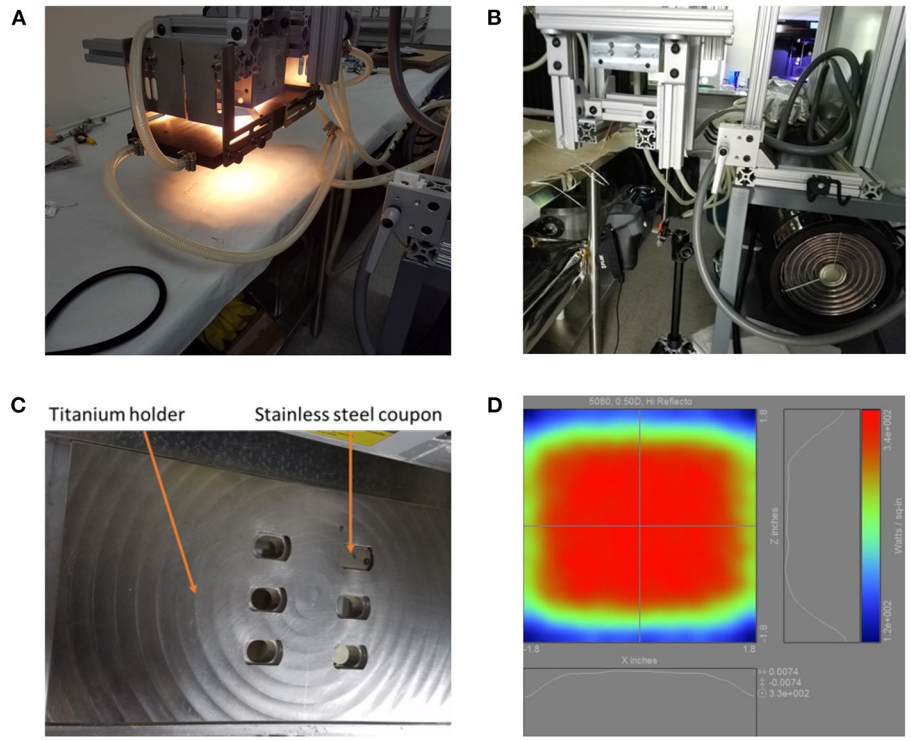

FIGURE 1 | The 5080 high temp infrared heater lamp setup. **(A)** The lamp is shown turned on. White light appears in the photo, but the majority of the light originating out of the bulbs is infrared. **(B)** The IR heat exposure setup including the FLIR T650sc camera, 5080 high temp IR heater lamp, and the titanium holder support structure consisting of 80/20 aluminum. **(C)** The titanium coupon holder with one stainless steel coupon inserted. **(D)** Projected heating profile for objects under the lamp.

a silicone rubber septum (ST-495, Specialty Silicone Products, Inc., Ballston Spa, NY) and an aluminum crimp-seal (20 mm, Wheaton Science Products, Millville, NJ); this allowed for exposure of the spores in a controlled humidity environment. The septum was penetrated with a needle (22-gauge, side-hole, Hamilton Company, Reno, NV) and evacuated with a vacuum pump (TriScroll 300, Varian Vacuum Technologies, Lexington, MA). Temperature from the TSEV thermocouples was recorded using an Agilent 34970 data logger (Agilent Technologies, Inc., Santa Clara, CA) and a custom LabView program (version 6.0, National Instruments, Austin, TX). After completing the heat exposure, the TSEVs were removed and immediately placed in an ice bath until cooled to room temperature.

Following cooling and after removing the crimp seal and septum, 1 mL of sterile deionized water was added to each TSEV to acquire spores. The TSEVs were then resealed and vortexed for 10 s before sonicating at 25 kHz for 2 min. The TSEVs were then vortexed again for 10 s. The samples were then serially diluted from 10^{-1} to 10^{-5} with 100 uL of the original TSEV spore sample into 900 uL of sterile water and 1 mL of each subsequent dilution (into 9 mL of DI water) was plated in tryptic soy agar (Difco Tryptic Soy Agar, BD Biosciences, Franklin Lakes, NJ). The colonies were counted after four days of incubation at 37°C. Unheated samples were processed as positive controls with TSEVs lacking organisms serving as negative controls.

2.2. High Heat Infrared Lamp Experimental Design and Setup

The 5080-06-02-6kW-24 High Temp IR Heater (Precision Control Systems, Inc., Eden Prairie, MN) used in this experiment includes six 1,000 W T3 short wavelength halogen lamps (**Figure 1**). The IR heater's ability to transfer infrared energy to the coupons was characterized prior to exposing coupons and spores to heat by using K-type thermocouples spot welded to stainless steel coupons in each position within the titanium coupon holder (**Supplementary Figure 2**). In addition, the ability of the IR heater to warm a single location on the holder for 5–8 s was also measured (**Supplementary Figure 3**).

2.2.1. *Bacillus canaveralius* 29669 Spore Emissivity on Kapton Stainless Steel Coupons

While polyimide tape (Kapton) emissivity is 0.95 and stainless steel type 301 emissivity is 0.54–0.63 at a temperature of 300 K (Emissivity Coefficients Materials, 2003) the emissivity of *B. canaveralius* 29669 spores is not known. The emissivity of carbon at 300 K is 0.81, and because spores are made largely of carbon this is a reasonable rough estimate. However, to gather more accurate information on *B. canaveralius* 29669 spore emissivity, dried *B. canaveralius* 29669 spores at a known temperature were measured with the T650sc camera (**Figure 2**). An accurate emissivity leads to a more precise infrared record of the *B.*

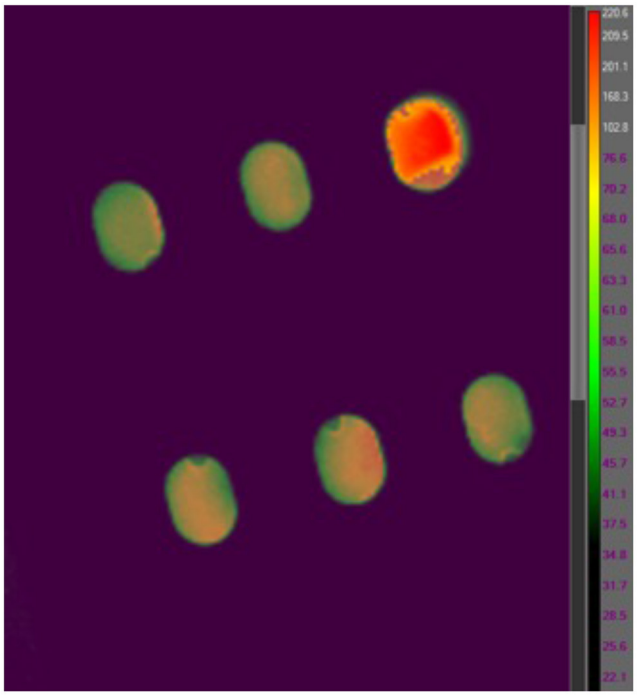

FIGURE 2 | An example coupon IR heating image from the FLIR T650sc IR camera viewed in FLIR ResearchIR 14. The coupon measured is located in the upper-right corner of the image. The other five coupon slots are out of focus, and the temperatures are not representative.

canaveralius 29669 spore temperature during heating. First, a 5 μL droplet of *B. canaveralius* 29669 spores was spotted on polyimide-taped stainless steel coupons. Then, the coupons were placed in a dry block heater that was heated to 150°C. After the coupon temperature reached steady state, the temperature of the spore spots was measured with the IR camera, and the emissivity was adjusted until the temperature shown on ResearchIR for the spore spots reached the estimated 150°C temperature (**Figure 2**). The experiment showed that the spore spot on Kapton-taped stainless steel coupons produces an emissivity of 0.914, which falls within expected values.

2.2.2. Coupon Preparation and Inoculation for IR Heating

For each exposure, custom (8 mm wide by 13 mm long by 0.5 mm thick) stainless steel coupons (**Supplementary Figure 4A**) were flattened and high temperature polyimide tape (1/4" wide) was placed on the coupons. The taped coupons were autoclaved at 121°C for 15 min in a sealed glass petri dish prior to inoculating with spores. Inoculation of spores was performed in a biosafety hood by first diluting the spores to 8×10^5 spores/μL using deionized water, then vortexing the spores for 5 s. Diluting spores is done to prevent spore overlap and allow for a monolayer to form during the drying and heating process. A 5 μL spore spot was then pipetted onto the center of the polyimide tape and the spores were dried overnight (at least 8 h) in a biosafety hood.

2.2.3. High Heat Infrared Exposure and Imaging

Inoculated coupons were placed in the titanium holder (**Figure 1**) with the spores facing away from the 5080 IR lamp. A T650sc IR camera (FLIR Systems, Inc., Wilsonville, OR) was placed directly under the titanium holder to image the temperature change of the spores throughout the exposure at 30 Hz (one image per 0.033 s). The 5080 High Temp IR Heater was used as the IR source (**Figure 1**). The titanium coupon holder with coupons was placed 0.2 inches from the IR heater quartz window and heating elements during the spore exposure experiments. To irradiate the samples, the IR lamp was used at 6 kW. Once the desired heating time was reached, the lamp was turned off as well as physically displaced from the coupon holder to prevent further heating. For survivor ratio estimates, coupons were immediately placed in sterile 10 mL glass screw-cap test tubes; for fraction negative (binary, growth/no-growth test) measurements (Harris and Skopek, 1985), coupons were placed into a 10 mL glass screw-cap test tube with 10mL pre-sterilized (autoclaved at 121°C for 15 min) trypticase soy broth (Bacto Tryptic Soy Broth, BD Biosciences, Franklin Lakes, NJ). All IR images were analyzed using FLIR ResearchIR 14. To measure coupon spot temperatures the emissivity was set to 0.914, and 16 pixels were averaged across the center of each coupon with the coupon distance from the camera fixed during exposures to maintain coupon size and image resolution throughout the experiment.

2.2.4. Post-exposure Spore Processing and Culture

After each IR heat exposure, coupons were processed in a biosafety hood. For survivor ratio analysis, 1 mL of sterile, deionized water was added to each tube, submerging each coupon. The tubes were vortexed for 10 s, then sonicated for 2 min and vortexed a second time for 10 s to remove the spores from the surface of the coupons. The samples were then diluted from 10-1 to 10-5 of the original concentration with 1 mL of the initial sample diluted into 9 mL of sterile water. One microliter of each dilution was then plated in tryptic soy agar (Difco Tryptic Soy Agar, BD Biosciences, Franklin Lakes, NJ). The colonies were counted after 24, 48, and 72 h of incubation at 37°C. Unexposed (unheated) samples were processed as positive controls, and coupons without spores were processed as negative controls.

For fraction negative (binary, growth/no-growth test) analysis, the same procedure was followed as with survivor ratio tests; however, coupons were transferred to 10 mL screw-cap test tubes containing tryptic soy broth immediately following exposure. Fraction negative turbidity compared to positive control (unexposed) samples and negative control (coupon blank) samples distinguished complete sterilization from surviving populations after incubation at 37°C for 72 h with shaking at 100 RPM.

2.3. Mathematical Method

The mathematical model developed for this study aims to estimate the probability of sterilization under various heat

exposure conditions.[1] It does so by defining a model, within a probabilistic framework, of the processes involved with generating the data observed from the HMR experiments. Rather than assuming fixed experimental parameters such as the starting population and protocol recovery efficiency, the model takes these parameters as distributions based on data collected from control experiments. Direct observation (CFU counts, growth/no growth) from the heat exposure experiments were then used to further calibrate the distributions of these parameters, particularly the D-value and z-value for *Bacillus canaveralis* 29669. The D-value is the time required at a specified temperature to reduce the number of viable organisms by 90%, and the z-value is the number of degrees required to decrease the D-value by 90%. The model performs this calibration using Bayes' Theorem, which essentially informs the model of the data generating process with the observed data to evaluate which D-values and z-values are more or less likely, relative to our knowledge prior to experimental observation. This information, together with a key assumption that the survival process is memoryless (to be discussed further in Section 2.3.4), allows the model to calculate the probability of individual microorganism survival and SALs for products with a given bioburden for a wide range of heat treatments of different time durations and temperatures.

The model has two main submodels to capture the experimental parameters: (1) a seeding model, developed in Section 2.3.1, that considers how many spores are on the coupon prior to heat treatment; and (2) a survival and recovery model that considers the exposure of the inoculated coupon to heat treatment and the survival and recovery of microorganisms from the coupon after heat treatment, first for survival ratio experiments in Section 2.3.2 and then for fraction-negative experiments in Section 2.3.3.

2.3.1. Seeding Model

The experimental process described in Section 2.2.2 begins with the seeding of a coupon with a targeted number of $\sim 10^6$ colony forming units (CFU). This involves taking a spore stock solution of volume V containing a *B. canaveralius* 29669 and applying sonication and vortexing to give the solution a uniform titer, τ. A volume $x \ll V$ of spore stock is then extracted *via* pipette from the stock solution and transferred onto a coupon. Given that the titer of the spore stock used for this study is on the order of 10^8 CFU/mL and the volume extracted is 5 μL, the number of CFU in the solution, $\eta = \tau V$, is very large compared to how many CFU are being extracted into the pipette, τx. Losses due to CFU transfer to the coupon may result in a slightly lower but still uniform titer, τ', of the solution transferred to the coupon than in the original solution.

All materials and reagents are tested for sterility according to manufacturer recommendations to avoid outside contamination that could introduce non-uniformities or heterogeneity of species into this process. Given the uniformity of the spore stock solution that is sampled, the probability, ρ, that an individual CFU is transferred from the solution to the coupon is the same for all CFU present in the solution, and $\rho = \frac{x\tau}{\eta} \times \frac{x\tau'}{x\tau} = \frac{x\tau'}{\eta} \ll 1$. Since sonication and vortexing obstruct microbial dependencies being formed between microorganisms, such as clumping or biofilm formation, it is reasonable to assume the transfer of individual CFUs from the spore stock to the coupon are independent; that is, the event that a given CFU is transferred from the stock solution to the coupon does not affect the chances of this event occurring for another CFU. Combining these independence and uniformity properties gives us that the number of CFU transferred from the spore stock to the coupon follows a binomial distribution with parameters η and ρ, where η is large and ρ is small. Note that the expected number of CFU transferred from the spore stock to the coupon is $\eta\rho = x\tau'$, which is constant for a given inoculation level, and is approximately equal to the variance of CFU transferred from the spore stock to the coupon $\eta\rho(1-\rho)$, since $1 - \rho \approx 1$. It follows that the probability that n CFU are transferred from the original spore stock solution to a given coupon approximately follows a Poisson distribution with mean parameter $\lambda \approx x\tau'$:

$$p(n \mid \lambda) = e^{-\lambda}\frac{\lambda^n}{n!}. \tag{1}$$

This study will treat λ as a parameter with a corresponding probability distribution. This distribution is initially estimated using control experiments and further calibrated simultaneously with other model parameters with observations from HMR experiments. Further discussion can be found in **Supplementary Material** (Section 1.2).

2.3.2. Survival and Recovery Model: Survival Ratio Experiments

Let $S(T)$, Φ and Θ_d, $d = 1, \ldots, 5$, be random variables taking values on the unit interval. $S(T)$ will represent the probability that an individual microorganism survives heat treatment T, and is referred to as the survival function. This function is parameterized by the D-value at the reference temperature $T_0 = 150°$C and z-value. The D-value and z-value are parameters that are treated as random variables that take values $\delta(T_0)$ and z. **Supplementary Material** (Section 1.1) contains the derivation of the survival function. The term, T, is a time-temperature profile described as a continuous real-valued function of time, t. We note that the model described in this study does not capture uncertainty in the time-temperature profile stemming from the emissivity factor calibration in discussed in Section 2.2.1. The variable Φ will represent the probability that an individual microorganism that survived heat treatment is extracted from the coupon and survives extraction into a water solution. Finally, Θ_d will represent the probability that an individual microorganism is transferred from the solution of extracted survivors into the sample taken from dilution of magnitude d, is plated and

[1] *A word on notation used in this document*: The notation $p(x \mid y)$ will be used to denote the conditional probability function of a random variable (or random vector) X taking the value x given another random variable (vector) Y takes the value y. When X is discrete, $p(x \mid y)$ will be understood to be a probability mass function; when X is continuous, $p(x \mid y)$ will be understood to be a probability density function. When we are interested in evaluating this probability function at a specific value x_0, then we will write $p(x = x_0 \mid y)$. Finally, the unconditional probability function of a random variable (vector) X will be denoted as $p(x)$.

produces a CFU in growth medium, respectively. The dilution magnitude is an integer i in the set $\{1, 2, 3, 4, 5\}$; for example, a 10^{-3} dilution has a dilution magnitude of 3. Suppose for the time-being that we know the values of each of these random variables, denoted by $s(T)$, ϕ, and θ_d.

The original experiment described in Section 2.2.4 mostly performed one dilution series (i.e., a single replicate) for each coupon m exposed to heat treatment. The CFU observation from the first denumerable dilution of this series was then reported in the data. For computational reasons, we develop the model to incorporate data from the first replicate and a single dilution only, as prior studies have shown that incorporating more than one dilution does not improve estimates of starting value (Christen and Parker, 2020).

Suppose we observe r_m CFU from the dilution obtained from the mth coupon exposed to heat treatment T_m after plating. In what follows, we will let the function d map the mth coupon to the magnitude of its corresponding dilution magnitude, $d(m)$. For each individual microorganism on coupon m, there are two mutually exclusive outcomes relevant to this study:

1. The microorganism survives heat treatment, is extracted from the coupon and survives extraction, is transferred *via* the dilution of magnitude $d(m)$, plated and grows a CFU. This outcome occurs with probability $s(T_m) \times \phi \times \theta_{d(m)}$.
2. The microorganism either does not survive heat treatment, is not extracted from the coupon or does not survive extraction, or is not transferred *via* the dilution of magnitude $d(m)$, plated and grown into a CFU; that is, the negation of (1). This outcome occurs with probability $1 - s(T_m) \times \phi \times \theta_{d(m)}$.

Under outcome (1), we will say that the microorganism has survived and has been recovered. The model assumes that a surviving microorganism that has been plated will be counted as a single CFU in the data with probability equal to one, and that there is no error in counting. Moreover, if a microorganism ceases to survive at an earlier stage it will not become viable again at a later stage. For example, if a microorganism does not survive heat treatment or extraction, then there is zero probability that it will become viable during dilution or when placed in growth medium for culturing.

As with the seeding process, the design of the HMR experiments takes several measures to ensure uniformity of the materials and processes involved and to avoid outside contamination. These measures help ensure that all CFU follow the same survival function and have the same probability of recovery after exposure to heat treatment. Moreover, sonication and vortexing during extraction obstruct phenomena such as microorganism clumping, allowing us to model CFUs as being recovered independently of one another. Therefore, for modeling purposes we treat all microorganisms as independent of one another and identically distributed in terms of survival (during heat treatment and extraction) and transfer to dilutions for plating.

Now, assume there are n microorganisms seeded onto the coupon prior to heat treatment T_m. The probability that a specific r_m microorganisms survive and are recovered (and $n - r_m$ microorganisms do not survive or are not recovered) is

$$\left[s(T_m)\,\phi\,\theta_{d(m)}\right]^{r_m} \times \left[1 - s(T_m)\,\phi\,\theta_{d(m)}\right]^{n-r_m},$$

where $r_m \leq n$. A specific set of r_m microorganisms can be chosen from the n microorganisms initially on the coupon in $\binom{n}{r_m}$ mutually exclusive ways. Hence, the probability that some set of r_m microorganisms survive and are recovered given that there were n microorganisms initially on the coupon prior to heat treatment is equal to

$$\begin{aligned} &p(r_m \mid n, s(T_m), \phi, \theta_{d(m)}, T_m) \\ &= \binom{n}{r_m} \left[s(T_m)\,\phi\,\theta_{d(m)}\right]^{r_m} \times \left[1 - s(T_m)\,\phi\,\theta_{d(m)}\right]^{n-r_m}, \end{aligned} \quad (2)$$

which is recognized as a binomial distribution with parameters $\left[n, s(T_m)\,\phi\,\theta_{d(m)}\right]$.

In order to capture the uncertainty present in the number of microorganisms seeded onto the coupon prior to heat treatment, we sum over all possible values of n using the model developed in Section 2.3.1. Hence, the probability of observing r_m CFU in the mth survival ratio experiment is

$$\begin{aligned} &p(r_m \mid \lambda, \delta(T_0), z, \phi, \theta_{d(m)}, T_m) \\ &= \sum_{n=r_m}^{\infty} p(n \mid \lambda)\, p(r_m \mid n, s(T_m), \phi, \theta_{d(m)}, T_m) \\ &= e^{-\lambda\, s(T_m)\,\phi\,\theta_{d(m)}} \frac{\left(\lambda\, s(T_m)\,\phi\,\theta_{d(m)}\right)^{r_m}}{r_m!}, \end{aligned} \quad (3)$$

where the second row follows from algebra. This is recognized as a Poisson distribution with mean parameter $\lambda \times s(T_m) \times \phi \times \theta_{d(m)}$. Note that $s(T_m)$ is the survival function evaluated over time temperature profile T_m. This function is parameterized by $\delta(T_0)$ and z; these parameters are suppressed in the notation of $s(T_m)$ for readability.

Since experimental outcomes can be assumed to be independent of one another, the probability of observing the data $\mathbf{r} = (r_1, \ldots, r_M)$ from all survival ratio experiments performed is

$$\begin{aligned} &p(\mathbf{r} \mid \lambda, \delta(T_0), z, \phi, \boldsymbol{\theta}, \mathbf{T}) \\ &\quad = \prod_{m=1}^{M} p(r_m \mid \lambda, \delta(T_0), z, \phi, \theta_{d(m)}, T_m), \end{aligned} \quad (4)$$

where $\boldsymbol{\theta} = (\theta_1, \ldots, \theta_5)$ and $\mathbf{T} = (T_1, \ldots, T_M)$ that associate with each observation r_m the probability $\theta_{d(m)}$ and time-temperature profile T_m. Here, coupon m was exposed to time-temperature profile T_m that resulted in r_m CFU being observed from a dilution of magnitude $d(m)$, for $m = 1, \ldots, M$.

Studies performed prior to performing high temperature HMR experiments allowed the development of distributions characterizing the parameters of the model, referred to as

prior distributions. Independence was assumed among all parameters prior to making observations from the high heat experiments. While this assumption is not realistic, there exists enough data to uncover any correlations during fitting of the model and thereby avoid unnecessary computational time and further assumptions involved with including covariance matrices and positing associated prior distributions. Hence, the joint distribution prior to making observations from high heat experiments is $p[\lambda, \delta(T_0), z, \phi, \boldsymbol{\theta}] = p(\lambda) \times p[\delta(T_0)] \times p(z) \times p(\phi) \times \prod_{i=1}^{5} p(\theta_i)$. The prior distributions for each parameter are further discussed in **Supplementary Material** (Section 1.2). Once prior distributions are defined and observations are made from survival ratio experiments, we employ Bayes' Theorem to calculate the posterior distribution of the parameters $(\lambda, \delta(T_0), z, \phi, \boldsymbol{\theta})$ using Equation (4):

$$p_{SR}(\lambda, \delta(T_0), z, \phi, \boldsymbol{\theta} \mid \mathbf{r}, \mathbf{T}) \propto \; p(\mathbf{r} \mid \lambda, \delta(T_0), z, \phi, \boldsymbol{\theta}, \mathbf{T}) \times p(\lambda, \delta(T_0), z, \phi, \boldsymbol{\theta}) \,. \tag{5}$$

Integrating p_{SR} from Equation (5) over λ, ϕ and $\boldsymbol{\theta}$ gives the joint posterior distribution of $\delta(T_0)$ and z from the survival ratio experiments:

$$= \int_{\boldsymbol{\theta} \in [0,1]^5} \int_{\phi=0}^{1} \int_{\lambda=0}^{\infty} p_{SR}(\lambda, \delta(T_0), z, \phi, \boldsymbol{\theta} \mid \mathbf{r}, \mathbf{T}) \, \mathrm{d}\lambda \, \mathrm{d}\phi \, \mathrm{d}\boldsymbol{\theta} \,. \tag{6}$$

Finally, we can use Equations (3) and (5) to predict the number of microorganisms recovered from a similar survival ratio experiment (either an experiment already performed, or a new experiment) if provided a time-temperature profile, $\widetilde{T}$, dilution magnitude, $\widetilde{d}$, and similar coupon inoculation level. The probability that $r \in \mathbb{N}$ microorganisms on a coupon survive after being exposed to heat treatment $\widetilde{T}$ and are recovered through a dilution of magnitude $\widetilde{d}$ is

$$\begin{aligned} & p_{SR}(r \mid \widetilde{T}, \widetilde{d}, \mathbf{r}, \mathbf{T}) \\ & = \int p(r \mid \lambda, \delta(T_0), z, \phi, \theta_{\widetilde{d}}, \widetilde{T}) \\ & \times p_{SR}(\lambda, \delta(T_0), z, \phi, \boldsymbol{\theta} \mid \mathbf{r}, \mathbf{T}) \, \mathrm{d}\theta_{\widetilde{d}} \, \mathrm{d}\phi \, \mathrm{d}z \, \mathrm{d}\delta(T_0) \mathrm{d}\lambda \,, \end{aligned} \tag{7}$$

where the limits of integration are suppressed in the expression above, but range from 0 to ∞ for $\lambda, \delta(T_0)$ and z, and range from 0 to 1 for ϕ and $\theta_{\widetilde{d}}$. We will use Equation (7) primarily for validation of the model.

2.3.3. Survival and Recovery Model: Fraction-Negative Experiments

A simplification to Equation (4) can be made in order to consider fraction-negative experiments. First, suppose there are M' fraction-negative experiments performed. After being exposed to time-temperature profile T'_m, the observed outcome, r'_m is either 0 (no growth) or 1 (growth). Here, no growth occurs with probability $\left[1 - s(T'_m)\right]^n$, which is the probability that no microorganism survives; and the probability that growth occurs—that one or more microorganisms survive—is equal to one minus the probability of no growth. No extraction or dilution is performed, as CFU are cultured by directly transferring the heat treated coupon into a test tube of tryptic soy broth. Given that the mean number of CFU seeded onto the coupon is equal to λ, the probability of observing growth or no growth from fraction-negative experiment m is

$$\begin{aligned} & p_{FN}(r'_m \mid \lambda, \delta(T_0), z, T'_m) \\ & = \sum_{n=r'_m}^{\infty} p(n \mid \lambda) \left[1 - (1 - s(T'_m))^n\right]^{r'_m} \left[1 - s(T'_m)\right]^{n(1-r'_m)} \\ & = \begin{cases} e^{-\lambda s(T'_m)} & \text{if } r'_m = 0 \\ 1 - e^{-\lambda s(T'_m)} & \text{if } r'_m = 1 \end{cases}, \end{aligned} \tag{8}$$

which is recognized as a Bernoulli random variable with parameter $1 - e^{-\lambda s(T'_m)}$.

While it is reasonable, given the experimental design, to treat the outcomes of fraction-negative experiments as independent of one another, they are not, as a group, independent of survival ratio experiments. Survival ratio experiments were performed first to understand the mortality of *B. canaveralius* 29669 when exposed to heat treatment and hypothesize a narrower interval of temperatures that would sterilize the coupons. This hypothesis was then tested and validated by performing a set of fraction-negative experiments. We model this dependency, first, by incorporating knowledge gained from survival ratio experiments for the *D*-value and *z*-value survival parameters by using the joint *posterior* distribution of $\delta(T_0)$ and z from the survival ratio experiments given by Equation (6) to inform a joint *prior* distribution on $\delta(T_0)$ and z when bringing the fraction-negative experiments into the analysis. Secondly, we recognize that the design of experiments bias fraction-negative experiments to test at temperatures more likely to induce sterilization. Since λ, the only other parameter in the fraction-negative model, is uncorrelated with *D*-value and *z*-value parameters, further informing it with the fraction-negative observations of this study could artificially reduce its value, as we will be more likely to observe no growth the fewer spores there are on the coupon. To avoid this behavior, we let the distribution of λ be given by the posterior distribution $p_{SR}(\lambda \mid \mathbf{r}, \mathbf{T})$ from survival ratio experiments (calculated by integrating Equation (5) over all parameters except λ) and do not allow it to be further informed by the fraction-negative experiments.

Hence, using Equation (8), the probability of observing the data $\mathbf{r}' = \left(r'_1, \ldots, r'_{M'}\right)$ from all fraction-negative experiments performed is

$$p_{FN}(\mathbf{r}' \mid \delta(T_0), z, \mathbf{r}, \mathbf{T}, \mathbf{T}') = \prod_{m=1}^{M'} \int_{\lambda=0}^{\infty} p_{SR}(\lambda \mid \mathbf{r}, \mathbf{T}) \times p_{FN}(r'_m \mid \lambda, \delta(T_0), z, T'_m) \, \mathrm{d}\lambda \,, \tag{9}$$

where $r'_m \in \{0,1\}$ and $\mathbf{T}' = \left(T'_1, \ldots, T'_{M'}\right)$ are the associated time-temperature profiles for each observation. Note the integration over possible values of λ is within the product to capture the uncertainty in the mean number of spores seeded onto each individual coupon.

Finally, using Equations (6) and (9) and applying Bayes' Theorem again, the joint posterior distribution of $\delta(T_0)$ and z after performing the fraction-negative experiments is

$$p_{FN}(\delta(T_0), z \mid \mathbf{r}, \mathbf{r}', \mathbf{T}, \mathbf{T}') \propto p_{FN}(\mathbf{r}' \mid \delta(T_0), z, \mathbf{r}, \mathbf{T}, \mathbf{T}') \times p_{SR}(\delta(T_0), z \mid \mathbf{r}, \mathbf{T}). \quad (10)$$

2.3.4. Predicting the Number of Microorganisms That Survive Heat Treatment and Comparison With the Sterility Assurance Level (SAL)

With the joint posterior distribution of $\delta(T_0)$ and z in-hand, we can calculate the posterior predictive distribution of the number of microorganisms that survive a new heat treatment $\widetilde{T}$ for a given bioburden. That is, if there are n microorganisms on a new coupon prior to heat treatment, then the probability that $\widetilde{n}_s$ survive the heat treatment following time-temperature profile $\widetilde{T}$ is given by

$$p\left(\widetilde{n}_s \mid n, \widetilde{T}, \mathbf{r}, \mathbf{r}', \mathbf{T}, \mathbf{T}'\right) = \int_{\delta(T_0)=0}^{\infty} \int_{z=0}^{\infty} \binom{n}{\widetilde{n}_s} s(\widetilde{T})^{\widetilde{n}_s} \left[1 - s(\widetilde{T})\right]^{n-\widetilde{n}_s} \times p_{FN}(\delta(T_0), z \mid \mathbf{r}, \mathbf{r}', \mathbf{T}, \mathbf{T}') \, \mathrm{d}z \, \mathrm{d}\delta(T_0). \quad (11)$$

This formulation will be used to evaluate the SAL for time-temperature profiles peaking above 270°C, since both survival ratio and fraction-negative experiments were performed at these temperatures. Since all fraction negative experiments saw peak temperatures greater than 270°C, we only use the survival ratio experiments for time-temperature profiles with peak temperatures between 200 and 270°C. More formally, when the peak temperature of $\widetilde{T}$ is between 200 and 270°C and there are n microorganisms on a new coupon prior to heat treatment, then the probability that $\widetilde{n}_s$ survive the heat treatment following time-temperature profile $\widetilde{T}$ is given by

$$p\left(\widetilde{n}_s \mid n, \widetilde{T}, \mathbf{r}, \mathbf{T}\right) = \int_{\delta(T_0)=0}^{\infty} \int_{z=0}^{\infty} \binom{n}{\widetilde{n}_s} s(\widetilde{T})^{\widetilde{n}_s} \left[1 - s(\widetilde{T})\right]^{n-\widetilde{n}_s} \times p_{SR}(\delta(T_0), z \mid \mathbf{r}, \mathbf{T}) \, \mathrm{d}z \, \mathrm{d}\delta(T_0). \quad (12)$$

Note that there is an element of extrapolation when applying this formulation to diverse time-temperature profiles not used in the experiments, as well as to other metallic surfaces different than the steel coupons used in this study. The extrapolation to differently shaped time-temperature profiles (that are within a similar range of temperatures as those used in this study) is reasonable if the survival probability of an individual microorganism is *memoryless*. What this means is that the model assumes that survival of a microorganism over any time interval on the time-temperature profile depends on the temperature experienced on, and time duration of that time interval, but not on the heat treatment the microorganism has already survived up to that time. This characteristic is implicitly assumed in practice when modeling survival with conventional *D*-values. In this study, we make this explicit in the derivation of the survival function (**Supplementary Material**, Section 1.1) and further claim that the assumption of memorylessness is reasonable because the temperatures to which *B. canaveralius* 29669 spores are exposed to in this study render biological repair mechanisms ineffective.

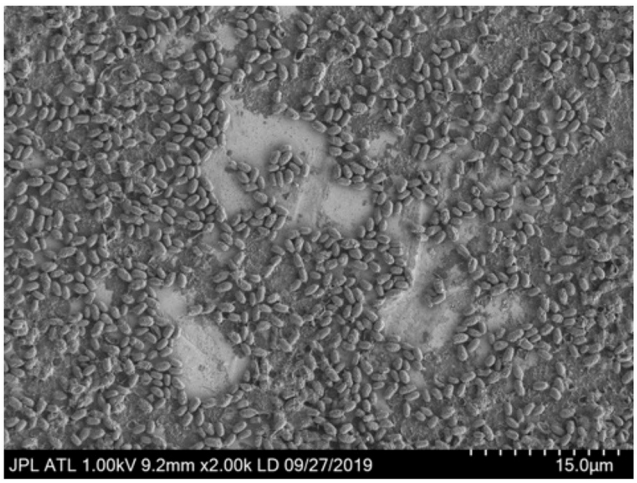

FIGURE 3 | An electron microscope image of *Bacillus canaveralius* 29669 spores used to measure the spore size. 2×10^6 spores per coupon were added before drying and lyophilizing. Based on the overlap in the image as well as a measured 10% coffee ring experience from 4×10^6 spores/coupon dried on Kapton (**Supplementary Figure 6**), a minimal coffee ring effect is expected for the IR exposure experiments. 15 µm is the distance from the farthest left and farthest right hash on the bottom-right side of the image.

We can now respond to the objective of this analysis in the following way:

> Let $\widetilde{T}$ be a constant time-temperature profile taking the temperature T for some amount of time, τ, that is <30 s. Since $\widetilde{T}$ is fully specified by the pair (T, τ), we let $\widetilde{T} = (\mathrm{T}, \tau)$ and we find all (T, τ) such that

$$1 - p\left(\widetilde{n}_s = 0 \mid n, (\mathrm{T}, \tau), \mathbf{r}, \mathbf{r}', \mathbf{T}, \mathbf{T}'\right) = 10^{-6}, \text{if T} \geq 270 \quad (13)$$

$$1 - p\left(\widetilde{n}_s = 0 \mid n, (\mathrm{T}, \tau), \mathbf{r}, \mathbf{T}\right) = 10^{-6}, \text{if T} < 270. \quad (14)$$

To respond to the objective of this study, Equations (13) and (14) will be computed and tabulated for a range of bioburdens, n.

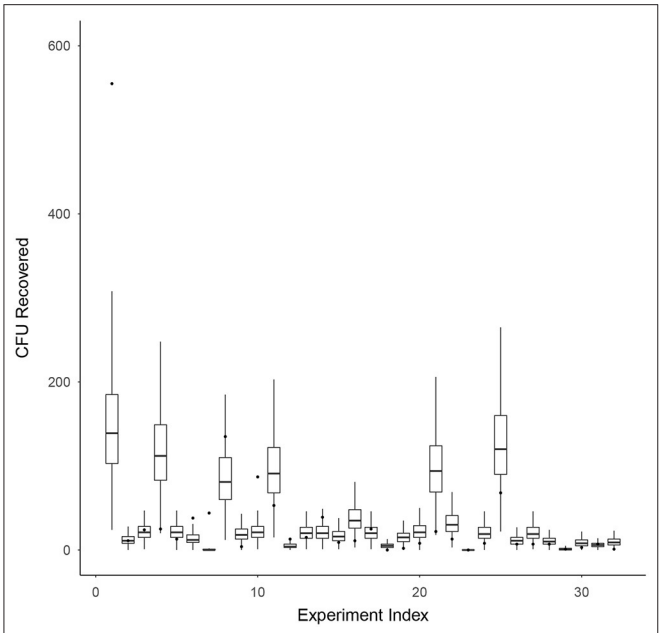

FIGURE 4 | Model validation for survival ratio experiments using Equation (7). This figure compares the model's prediction of the number of CFU recovered (box-whisker plots) against the actual observed number of CFU recovered (black dots) on the vertical axis, for each experiment indexed by the integers 1–32 (horizontal axis). Box and whiskers show 50 and 95% credibility intervals, respectively, for the model's prediction of the number of CFU recovered from each experiment. The mean model prediction is shown with a horizontal line on each box-whisker plot.

3. RESULTS

3.1. Characterizing the *Bacillus canaveralius* 29669 Spore Stock

Seven *B. canaveralius* 29669 spore strains were tested for their ability to survive heat prior to evaluating the microbial reduction effects of IR heat on *B. canaveralius* 29669 spores. The spores were judged based on their heat resistance at 150°C compared to the *B. canaveralius* 29669 spores that the NASA Procedural Requirements are based on Schubert and Beaudet (2011) and NASA Science Mission Directorate (2017). Of the seven isolates tested, M4-6 was the closest match to the survival curve (direct enumeration) from the NASA Procedural Requirements-based strain based on its survival at 150°C (Schubert and Beaudet, 2011). **Supplementary Figure 5** shows the survival curve of M4-6 spores at 150°. The *D*-value of the M4-6 isolate was 46.9 min in controlled humidity conditions, and the target value from the NASA Procedural Requirements strain was 39.7 min, suggesting an 18% increase resistance to dry heat at 150°C.

3.2. Characterization and Design of the High Heat Infrared Lamp Setup

The 5080 High Temp IR Heater's ability to transfer energy to the coupons was characterized prior to spore exposure. K-type thermocouples were spot welded to the stainless steel coupons and the coupons were placed in the custom-machined titanium holder with the thermocouple mounted on the coupon side facing away from the heater. The IR heater's ability to transfer heat to coupons based on the location within the coupon holder was first characterized as shown in **Supplementary Figure 2**. Peak heating was averaged over a 16-pixel area on the coupons for the data shown, and it is reported as resolved by the camera at 30 Hz. The same heating experiment produced 300°C temperatures on the top half (locations 1–3) of the coupon holder and 255°C temperatures on the lower half (locations 4–6) of the holder during 5 s of heating. This finding led to all further experiments, including all microbial reduction experiments, to be run on the top-left corner (position 1) of the titanium plate for increased precision in results as well as the highest heating rate.

The next two characterization runs used the top-left corner (position 1 in **Supplementary Figure 2**) slot of the titanium coupon holder to measure the ability of the IR heater to warm over 5, 6, 7, and 8 s as well as to evaluate the active heating and passive cooling capabilities of the system (**Supplementary Figure 3**). The 5, 6, 7, and 8 s heating times listed are the times from the point where the lamp is turned on until the lamp is turned off; however, the graph shows the coupon cooling rate as well. Five seconds of heating time reached an average of 172°C, 6 s reached an average of 218°C, 7 s reached an average of 263°C, and 8 s reached an average of 295°C; room temperature was held at 21°C for the experiment. Passive cooling from the highest temperature (295°C) to 121.1°C (the reference temperature where food sterilization is measured) took 22 s on average, so the entire heating process from initiating the system to finish was measured to take 30 s total.

3.3. Spore Monolayer on Coupons

Overlapping spores is a concern for microbial reduction studies using heat conducted through a surface given they may insulate other spores from the heat exposure (Deng et al., 2005). To address this concern prior to the heat experiments, the spores were diluted to produce a monolayer of cells. In order to create the monolayer, the scanning electron microscope image (**Figure 3**) was used to measure the size of the *B. canaveralius* 29669 spores. The *B. canaveralius* 29669 spores were measured to be 1.494 μm long by 0.716 μm wide on average.

After determining the spore size and to make sure the spores fit into each spot placed on the stainless steel coupons, the contact angle of the spore-DI water storage solution on the coupon polyimide tape (Kizil et al., 2014) as well as the 5 μL volume of each spot were taken into account to determine the precise area needed to fit the spores: 8.24 mm^2. From the dimensions needed, a maximum of 7.7×10^6 spores were determined to fit within each 5 μL spot while still preventing an overlap. While this calculation does not take into account a coffee ring effect occurring during evaporation of the spore solution, the dried spore spot for the SEM image in **Figure 3** shows 2×10^6 spores/coupon, with minimal overlap occurring. An average of 4×10^6 spores were placed onto the coupons for the IR heating experiments, and a maximum of 10% of the coffee ring effect was measured (**Supplementary Figure 6**); therefore, the coffee ring overlap effect on the spores used in the IR heating experiment was assumed negligible.

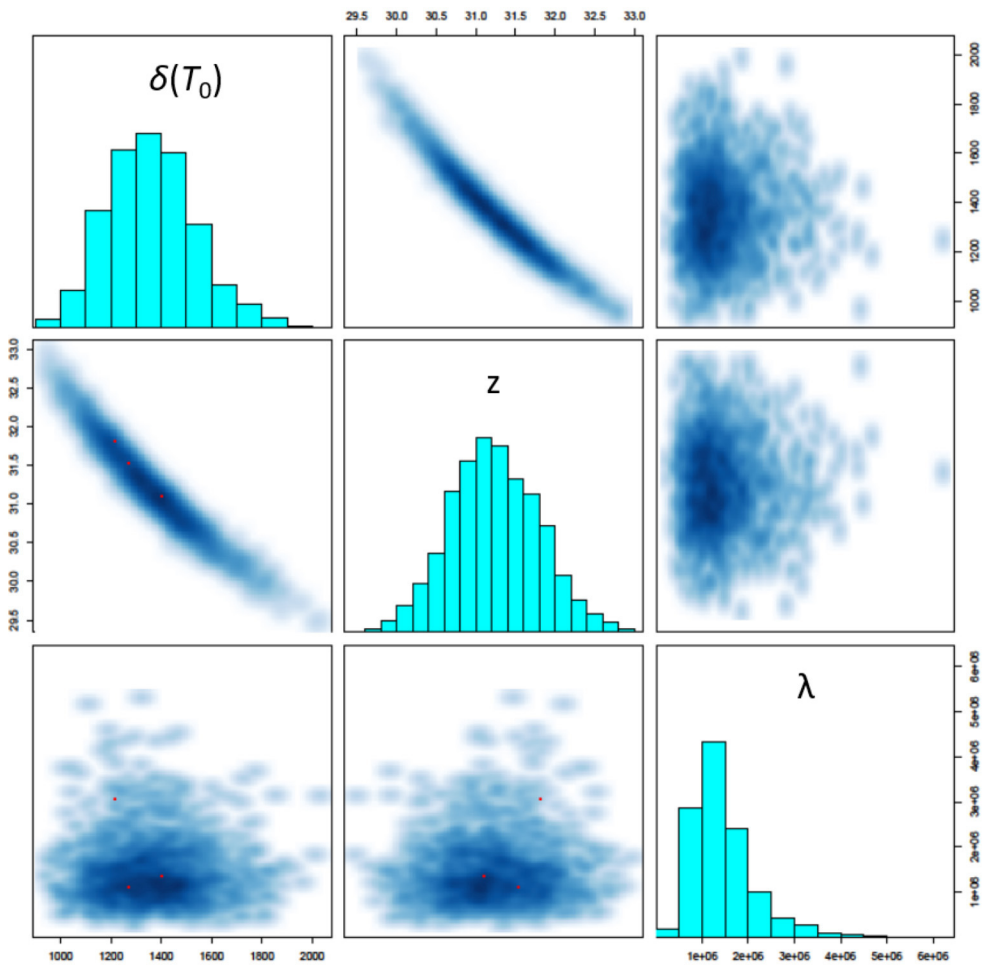

FIGURE 5 | Pairs plot showing simulated posterior marginal distributions of model parameters along the diagonal and pairwise joint distributions off-diagonal. The three most critical parameters to assessing survival in the model are shown here: the *D*-value at 150°C [$\delta(T_0)$], the *z*-value (*z*) and the mean number of microorganisms seeded onto a coupon (λ).

3.4. Infrared Spore Heat Exposure Experiments

B. canaveralius 29669 spores were exposed to short durations of infrared light in an ambient temperature of 21°C and an ambient humidity environment. The coupon temperature was measured with a FLIR T650sc infrared camera pointed directly at the coupons, and the coupon heat was evaluated with FLIR ResearchIR 14 software with the emissivity of the spores on the Kapton taped stainless steel coupons set to 0.914. Only heating above 150°C are used by the model developed in Section 2.3, as this is the temperature at which the *D*-value was studied for spore selection (Section 2.1). This temperature also provided an initial lower bound appropriate for a constant *z*-value survival model. Model results are not sensitive to reasonable changes in this value.

Testing stringent SALs directly (10^{-6}, for example) is not empirically possible due to the logistics needed to effectively evaluate 10^{12} microorganisms on a single coupon at once (as is needed for a direct 10^{-6} SAL test; von Woedtke and Kramer, 2008). Instead, we use a lower density of microorganisms in testing combined with the mathematical model described in Section 2.3 to evaluate high heat exposures that satisfy various sterility assurance levels for a given bioburden.

Due to the low to zero survival numbers expected from the highest temperature experiments (268–334.2°C), fraction negative microbial reduction experiments, were also performed. The method used for the fraction negative experiments, which involved dropping the exposed coupon directly into nutrient broth, provided the sensitivity needed to detect even one surviving organism. Results from the fraction negative experiments can be found in **Supplementary Table 1**. No *B. canaveralius* 29669 extremophiles survived exposures to temperatures ranging from 268 to 334.2°C.

Finally, while evaluating *B. canaveralius* 29669 spore heat survival, the effect of the IR heating system ramp rate as a potential driver for cell death was also investigated. The survival of the *B. canaveralius* 29669 spores was not found to correlate with a temperature ramp rates in a linear model (**Supplementary Figure 7**, $R^2 = 0.081$, p-value = 0.06).

3.5. Mathematical Model

Model validation for survival ratio experiments was conducted using Equation (7). **Figure 4** compares the model's prediction of the number of CFU recovered (box-whisker plots) against the actual observed number of CFU recovered (black dots) on the vertical axis, for each experiment indexed by the integers 1–32 (horizontal axis). Box and whiskers show 50 and 95% credibility intervals, respectively, for the model's prediction of the number of CFU recovered from each experiment. The mean model prediction is shown with a horizontal line on each box-whisker plot. The model appears to be capturing the dispersion in the data well, with only 4 of the 32 experiments (experiment indexes 1, 6, 7, and 10) having actual observations falling outside the 95% credibility intervals of the model.

The three most critical parameters to assessing survival in the model are shown in **Figure 5**: the D-value at 150 °C [$\delta(T_0)$], the z-value (z) and the mean number of microorganisms seeded onto a coupon (λ). The model identifies a D-value with mean 22.7 min and 95% credibility interval (17.5, 29.0), a z-value with mean 31.2°C (30.2, 32.4), and mean number of microorganisms seeded onto a coupon of 1.4×10^6 (5.5×10^5, 3.2×10^6). We also observe strong correlations between the D-value and z-value (as expected), and no significant correlation between these parameters and the mean number of microorganisms seeded onto a coupon (also expected). Note that the D-value at 150°C is significantly lower than that estimated in Section 2.1 prior to performing high temperature HMR experiments. This could be an indicator of a lower z-value at lower temperatures and is an area for further research. The modeled z-values are in-line with expectations prior to performing experiments (which were between 30 and 50°C). Finally, the modeled predictions for the mean number of spores seeded onto a coupon are consistent with the control experiments performed.

The probability of individual microorganism survival, $s(T)$, with respect to the peak temperature of the time-temperature profile T was modeled for each high temperature HMR experiment, based on Equation (10), and is shown in **Figure 6**. The relationship between survival probability and peak temperature is non-linear with a significant drop in probability starting at around 200°C. After 250°C this probability becomes indiscernible from zero on a linear scale, and for peak temperatures $>\sim$290°C becomes vanishingly small ($<10^{-10}$). **Supplementary Figure 8** shows this survival plot in log-space for those wishing to discern the survival probabilities at these higher peak temperatures.

The probability that a product with a bioburden of 1×10^6 is not sterile after being exposed to a given temperature is calculated using Equations (13) and (14), with results shown in **Figures 7A,B** for temperatures above 270°C and below 270°C, respectively. This probability is almost binary with respect to time and temperature, as can be seen by the rapid gradient change from black to yellow. The sterility assurance level (SAL) can be found within the gradient and used to generate a curve to determine time and temperature needed (**Figure 8**).

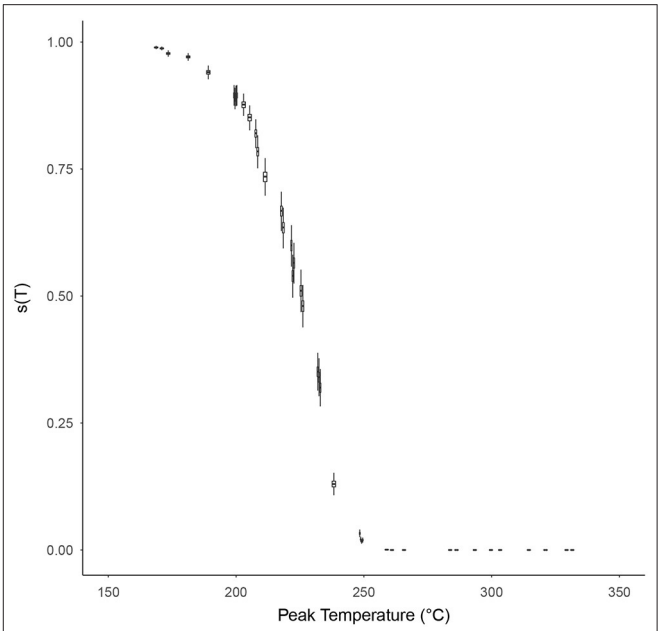

FIGURE 6 | The probability of individual microorganism survival, $s(T)$ (vertical axes), with respect to the peak temperature of the time-temperature profile, T (horizontal axes), for each survival ratio experiment, based on Equation (10). Box and whiskers show 50 and 95% credibility intervals, respectively, while horizontal lines accompanying each box-whisker show the mean value.

4. DISCUSSION

The built-in overly-conservative specifications of the NASA provisions for sterility with HMR carries implications for future Planetary Protection implementation—for both flight missions and on-ground processing. The present study evaluated the survival of *B. canaveralius* 29669 heat-hardy spores at temperatures above 200°C and mathematically modeled the probability of spore survival to identify a refined Planetary Protection sterilization temperature specification. The *B. canaveralius* 29669 spores used in this study served to determine the NASA Procedural Requirements for heat sterilization values (originally NPR8020.12D and proceeded by NID 8020.109A) due to their ability to withstand high temperatures (Schubert and Beaudet, 2011; NASA Science Mission Directorate, 2017). By using the same spores, this experiment demonstrated that the 500°C for 0.5 s time and temperature for sterilization should be revised based on empirical data and modeling. For example, we predict for a bioburden of 1×10^6 *B. canaveralius* 29669 spores, exposure to 292°C for 0.5 s achieves a SAL of 10^{-6}.

The 6 kW high-heat infrared lamp set-up demonstrates the ability to test and record exposures at very high temperatures (>200°C) and millisecond intervals. The IR heating profile using the custom-machined titanium holder was obtained using a 0.914 emissivity found at known temperatures as well as with

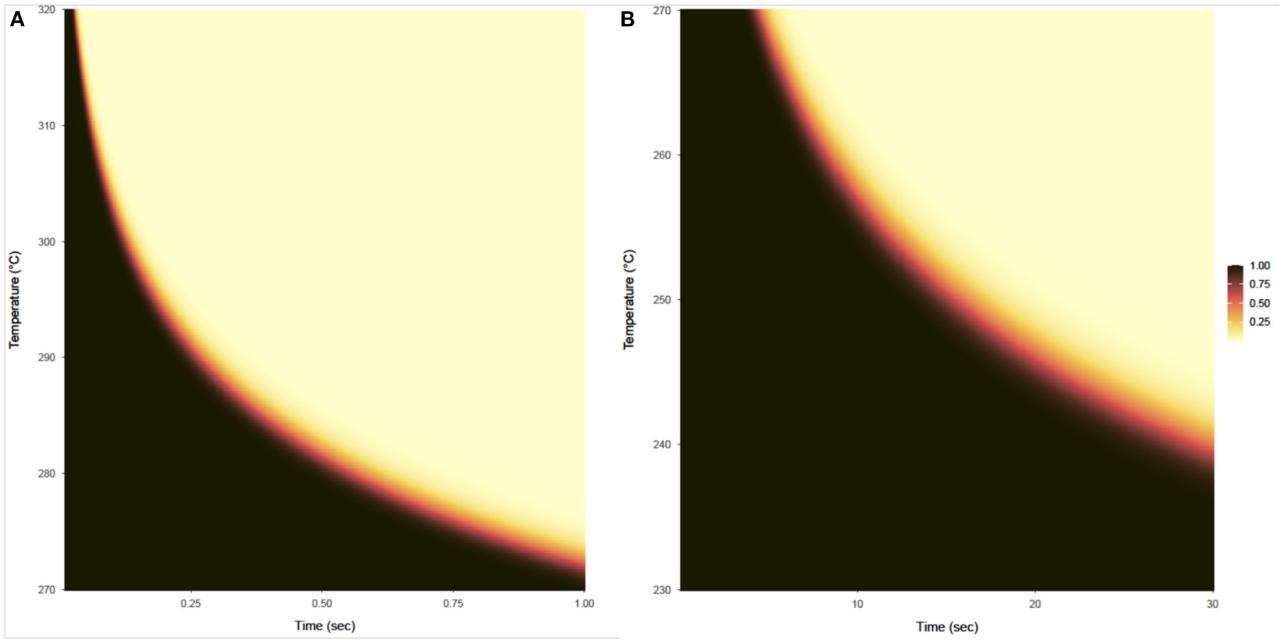

FIGURE 7 | Probability that a product with a bioburden of 1×10^6 is not sterile after being exposed to a given temperature (vertical axis) for a given time (horizontal axis). **(A)** Shows this probability for temperatures from 270 to 320°C and exposure times from 0.01 to 1 s, based on survival ratio and fraction-negative experiments and calculated using the expression on the left side of Equation (13). **(B)** Shows this probability for temperatures from 230 to 270°C for exposure times from 0.1 to 30 s, based on survival ratio experiments only and calculated using the expression on the left side of Equation (14).

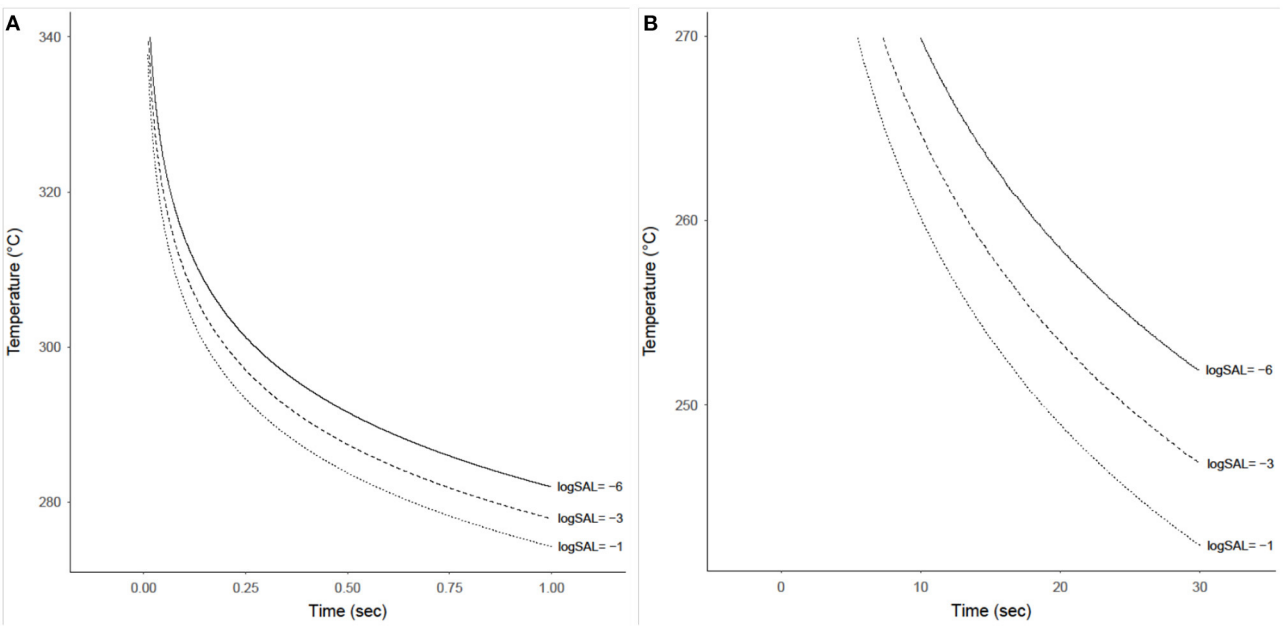

FIGURE 8 | Time-temperature contours achieving sterility assurance levels (SAL) of 10^{-1}, 10^{-3}, and 10^{-6} for a product with an initial bioburden of 1×10^6 prior to heat treatment. **(A)** Shows these contours for temperatures from 275 to 340°C and exposure times from 0.01 to 1 s. **(B)** Shows these contours for temperatures from 240 to 270°C and exposure times from 0.1 to 30 s, although these SAL contours only exist starting at ∼7 s.

thermocouples spot-welded to the stainless steel coupons. The *B. canaveralius* 29669 spores were placed onto Kapton tape at a concentration predicted to produce a monolayer based on spore size and imaging (**Figure 3**), with limited overlap between the spores. Using this setup, a curve of organisms surviving heating versus the peak exposure temperature was

produced as were videos with the infrared heating (and cooling) temperatures over the course of each exposure. In addition, a fraction-negative set of exposures along with their corresponding maximum temperatures and IR heating videos was also produced, with no organisms surviving temperatures above 268°C (**Supplementary Table 1**).

The processes and experimental results generated from the spore exposure experiments are captured, within a probabilistic framework, in the mathematical model developed to assess the probability of sterility. The comprehensive model considers how many spores are on the coupon prior to heat treatment and the survival and recovery efficiency of microorganisms from the coupon after heat treatment. The model was validated using the results from the survival ratio experiments and captured data dispersion well, with only 13% of experiments having actual observations falling outside the 95% credibility intervals of the model. Future analysis will test out-of-sample prediction strength.

The study conservatively demonstrates the likelihood of microorganism survival when exposed to high temperatures at short durations. The first element of conservatism is that this study exclusively used the heat tolerant *B. canaveralius* 29669 as the test organism. In a spacecraft assembly environment the microorganisms present are diverse, with many not being spore-formers and even fewer that have extreme heat tolerance. *B. canaveralius* 29669 was selected as the "worst-case" organism and parameters necessary to render its spores unable to germinate or replicate should apply to all non-heat-tolerant organisms as well. Next, the amount of spores tested on each coupon ($\sim 10^6$) is an over-estimate of the actual amount of spores present on any piece of spacecraft hardware. Smaller populations would need less time to attain the same SAL levels as larger populations. Given these conservative test parameters, the times and temperatures needed to sterilize sparsely distributed non-hardy microbial populations is likely to be even lower than the results presented in **Figure 8**. Therefore, while the results suggest a much less conservative time-temperature profile than the currently approved specification, it still represents an extreme scenario for spacecraft hardware conditions and sufficiently bounds the parameters needed for sterilization. Future work needs to be done to determine any margin that needs to be added in time and temperature to account for thermocouple sensitivity when implementing this for actual flight hardware, particularly at the higher temperatures (over 300°C) where there may be millisecond differences between sterility assurance levels of 10^{-6} and 10^{-1}.

5. CONCLUSION

This study reports experimental evidence supporting a re-evaluation of the current Planetary Protection time and temperature overkill bioburden reduction requirement from 500°C for 0.5 s to a sterility curve where time to sterility can be calculated based on the given high-heat temperature (>200°C). The study demonstrates that results from the *B. canaveralius* 29669 survivor ratio and fraction negative experiments can be used to mathematically model SAL curves.

HMR at high temperatures is often incompatible with spacecraft hardware and poses a limitation to the application of it as a bioburden control method. While in-flight, certain spacecraft zones may also be subject to rapid exposures to high temperature from propellant ignition (e.g., during powered descent), that is currently not accounted for when determining lethality of bioburden. Reassessment of the sterility specifications to a "sterility curve" rather than a point requirement (500°C for 0.5 s) allows for a wider range of time and temperatures that could be compatible with spacecraft materials and support more pre-flight HMR. This result will increase microbial reduction credit that can be taken at lower heat microbial reduction temperatures in Planetary Protection relevant interplanetary missions.

First, seven isolates of *B. canaveralius* 29669 spores, the same extremophile strain used to obtain the NPR 8020.12D (now NID 8020.109A) Planetary Protection heating parameters, were exposed to 150°C heat for 30 min. Of these cultures, the *B. canaveralius* 29669 strain most closely matching the *D*-value (39.7 min at 150°C) from the NPR 8020.12D culture used to set the heating values was used. A 5080 6 kW halogen infrared lamp was then employed and characterized for its ability to precisely increase the temperature of half inch long stainless steel coupons to 350°C in under 10 s. A T650sc infrared camera was also incorporated to accurately and quickly heat spores. The emissivity of the *B. canaveralius* 29669 spores on Kapton-taped stainless steel coupons was determined to be 0.914 using a known temperature, calibrating the T650sc infrared camera. Approximately 4×10^6 *B. canaveralius* 29669 spores were then heated to peak temperatures of 184.7 to 334.2°C on the scale of seconds, using the 5080 halogen lamp, and no organisms survived temperatures above 268°C. Fraction negative (binary, growth/no-growth) tests were performed to confirm the ability of the heat to sterilize the *B. canaveralius* 29669 spores. Finally, the ramp rate for the heater did not correlate to spore death from 35.72 to 50.71°C/s.

DATA AVAILABILITY STATEMENT

The raw data supporting the conclusions of this article will be made available by the authors, without undue reservation.

AUTHOR CONTRIBUTIONS

ZD and MD contributed equally to carrying out the research. ZD performed the heat microbial reduction experiments, the analysis, designed the figures, and drafted the manuscript sections regarding experimental data acquisition, while MD contributed the mathematical modeling analysis, figures, and manuscript sections using Stan software (Stan Development Team, 2021) in RStudio (RStudio Team, 2021). EK contributed to the initial spore characterization research and the initial experiment design. SR supplied the IR camera as well as his IR image acquisition knowledge and assisted in the emissivity measurements. BC wrote and

critically reviewed the manuscript. LG conducted experimental recovery experiments, provided inputs to the modeling, and wrote and critically reviewed the manuscript. All authors contributed to the research design at some point during the project.

FUNDING

The research was carried out at the Jet Propulsion Laboratory, California Institute of Technology, under a contract with the National Aeronautics and Space Administration (80NM0018D0004).

ACKNOWLEDGMENTS

The authors would like to thank the Europa Lander Pre-project for supporting this work. The authors would also like to thank Wayne Schubert for providing the SEM image featured in **Figure 3**.

SUPPLEMENTARY MATERIAL

The Supplementary Material for this article can be found online at: https://www.frontiersin.org/articles/10.3389/fmicb.2022.909997/full#supplementary-material

REFERENCES

Bruckner, J., Osman, S., Conley, C., Venkateswaran, K., and Schaechter, M. (2009). Space microbiology: planetary protection, burden, diversity and significance of spacecraft associated microbes. *Encyclop. Microbiol.* 3, 52–65. doi: 10.1016/B978-012373944-5.00293-5

Christen, J. A., and Parker, A. E. (2020). Systematic statistical analysis of microbial data from dilution series. *J. Agric. Biol. Environ. Stat.* 25, 339–364. doi: 10.1007/s13253-020-00397-0

Chyba, C. F., and Phillips, C. B. (2002). Europa as an abode of life. *Orig. Life Evol. Biosphere* 32, 47–67. doi: 10.1023/A:1013958519734

Deng, X. T., Shi, J., Shama, G., and Kong, M. G. (2005). Effects of microbial loading and sporulation temperature on atmospheric plasma inactivation of bacillus subtilis spores. *Appl. Phys. Lett.* 87:153901. doi: 10.1063/1.2103394

Harris, L., and Skopek, A. (1985). *Sterilization of Medical Products*. North Ryde, NSW: Johnson and Johnson Pvt. Ltd.

International Organization for Standardization (2010). *ISO 8573-1:2010, Compressed Air. Contaminants and Purity Classes*. International Organization for Standardization, 1–7.

Kempf, M., Kirschner, L., and Beaudet, R. A. (2005). "Extended temperature range studies for dry heat microbial reduction," in *47th International Conference on Environmental Systems* (Colorado Springs, CO). doi: 10.4271/2005-01-3096

Kempf, M., Schubert, W., and Beaudet, R. (2008). Determination of lethality rate constants and d-values for *Bacillus atrophaeus* (ATCC 9372) spores exposed to dry heat from 115 c to 170 c. *Astrobiology* 8, 1169–1182. doi: 10.1089/ast.2007.0208

Kizil, H., Pehlivaner, M. O., and Trabzon, L. (2014). "Surface plasma characterization of polyimide films for flexible electronics," in *Advanced Materials Research*, Vol. 970 (Cham: Trans Tech Publications Ltd), 132–135. doi: 10.4028/www.scientific.net/AMR.970.132

McLean, R. J., Welsh, A. K., and Casasanto, V. A. (2006). Microbial survival in space shuttle crash. *Icarus* 181, 323–325. doi: 10.1016/j.icarus.2005.12.002

NASA Science Mission Directorate (2008). *NASA Interim Directive NID 8020.12d*. NASA Science Mission Directorate, 1–49.

NASA Science Mission Directorate (2017). *NASA Interim Directive NID 8020.109a*. NASA Science Mission Directorate, 1–44.

Pillinger, J. M., Pillinger, C., Sancisi-Frey, S., and Spry, J. (2006). The microbiology of spacecraft hardware: lessons learned from the planetary protection activities on the beagle 2 spacecraft. *Res. Microbiol.* 157, 19–24. doi: 10.1016/j.resmic.2005.08.006

Pratt, L. M., and Smith, A. L. (2020). "Expectations for backward planetary protection planning during mars sample return planning," in *2020 IEEE Aerospace Conference* (Big Sky, MT: IEEE), 1–7. doi: 10.1109/AERO47225.2020.9172722

RStudio Team (2021). *RStudio: Integrated Development Environment for R*. Boston, MA: RStudio, PBC.

Saffary, R., Nandakumar, R., Spencer, D., Robb, F. T., Davila, J. M., Swartz, M., et al. (2002). Microbial survival of space vacuum and extreme ultraviolet irradiation: strain isolation and analysis during a rocket flight. *FEMS Microbiol. Lett.* 215, 163–168. doi: 10.1111/j.1574-6968.2002.tb11386.x

Schubert, W. W., and Beaudet, R. A. (2011). Determination of lethality rate constants and d-values for heat-resistant bacillus spores ATCC 29669 exposed to dry heat from 125 c to 200 c. *Astrobiology* 11, 213–223. doi: 10.1089/ast.2010.0502

Seuylemezian, A., Cooper, K., Schubert, W., and Vaishampayan, P. (2018). Draft genome sequences of 12 dry-heat-resistant bacillus strains isolated from the cleanrooms where the viking spacecraft were assembled. *Genome Announce.* 6, 11–13. doi: 10.1128/genomeA.00094-18

Shirey, T. B., Benardini, J. N., and Schubert, W. (2017). "An overview of surface heat microbial reduction as a viable microbial reduction modality for spacecraft surfaces," in *47th International Conference on Environmental Systems* (Charleston, SC).

Stan Development Team (2021). *Stan Modeling Language Users Guide and Reference Manual, 2.29*. Stan Development Team.

Swenson, D. (2012). Factors and principles:the science of sterilization. *AAMI Horizons* Suppl:33–36. doi: 10.2345/0899-8205-12.1.33

von Woedtke, T., and Kramer, A. (2008). The limits of sterility assurance. *GMS Krankenhaushygiene Interdisz.* 3:3.

Whyte, W., and Eaton, T. (2015). Assessment of degree of risk from sources of microbial contamination in cleanrooms. *Airborne. Eur. J. Parent. Pharm. Sci.* 20, 52–62.

process, or service by trade name, trademark, manufacturer, or otherwise, does not constitute or imply its endorsement by the United States Government or the Jet Propulsion Laboratory, California Institute of Technology. Government sponsorship acknowledged.

Conflict of Interest: The authors declare that the research was conducted in the absence of any commercial or financial relationships that could be construed as a potential conflict of interest.

Publisher's Note: All claims expressed in this article are solely those of the authors and do not necessarily represent those of their affiliated organizations, or those of the publisher, the editors and the reviewers. Any product that may be evaluated in this article, or claim that may be made by its manufacturer, is not guaranteed or endorsed by the publisher.

frontiers | Frontiers in Microbiology

TYPE Original Research
PUBLISHED 09 August 2022
DOI 10.3389/fmicb.2022.911091

OPEN ACCESS

EDITED BY
Rob Van Houdt,
Belgian Nuclear Research Centre, Belgium

REVIEWED BY
Tim Sandle,
The University of Manchester,
United Kingdom
Vijayakumar Rajendran,
Majmaah University,
Saudi Arabia

*CORRESPONDENCE
Emily P. Seto
epseto@honeybeerobotics.com

†These authors share first authorship

SPECIALTY SECTION
This article was submitted to Extreme Microbiology, a section of the journal Frontiers in Microbiology

RECEIVED 01 April 2022
ACCEPTED 05 July 2022
PUBLISHED 09 August 2022

CITATION
Seto EP, Hirsch AL, Schubert WW, Chandramowlishwaran P and Chernoff YO (2022) Heat inactivation of stable proteinaceous particles for future sample return mission architecture. *Front. Microbiol.* 13:911091. doi: 10.3389/fmicb.2022.911091

Heat inactivation of stable proteinaceous particles for future sample return mission architecture

Emily P. Seto[1,2*†], Aspen L. Hirsch[3†], Wayne W. Schubert[2], Pavithra Chandramowlishwaran[3] and Yury O. Chernoff[3]

[1]Honeybee Robotics, Altadena, CA, United States, [2]Biotechnology and Planetary Protection Group, Jet Propulsion Laboratory, California Institute of Technology, Pasadena, CA, United States, [3]School of Biological Sciences, Georgia Institute of Technology, Atlanta, GA, United States

The National Aeronautics and Space Administration (NASA) and the European Space Agency (ESA) are studying how to improve the safety of future planetary science sample return missions that would bring back materials to Earth. Backward planetary protection requirements have been identified as a critical technology development focus in order to reduce the possibility of harm to Earth's biosphere from such returned materials. In order to meet these challenges, NASA has identified the need for an appropriate suite of biological indicators (BIs) that would be used to develop, test, and ultimately validate sample return mission sterilization systems. Traditionally, BIs are defined as test systems composed of viable microorganisms that are inactivated when necessary conditions are met during sterilization procedures, providing a level of confidence in the process. BIs used traditionally at NASA have been driven by past mission requirements, mainly focused on spore-formers. However, spore-based BIs are insufficient as the only analog for a nominal case in sample return missions. NASA has directed sample return missions from habitable worlds to manage "potential extraterrestrial life and bioactive molecules" which requires investigation of a range of potential BIs. Thus, it is important to develop a mitigation strategy that addresses various known forms of biology, from complex organisms to biomolecular assemblies (including self-perpetuating non-nucleic acid containing structures). The current effort seeks to establish a BI that would address a stable biomolecule capable of replication. Additional engineering areas that may benefit from this information include applications of brazing, sealing, and impact heating, and atmospheric entry heating. Yeast aggregating proteins exhibit aggregation behavior similar to mammalian prion protein and have been successfully employed by researchers to understand fundamental prion properties such as aggregation and self-propagation. Despite also being termed "prions," yeast proteins are not hazardous to humans and can be used as a cost effective and safer alternative to mammalian prions. We have shown that inactivation by dry heat is feasible for the prion formed by the yeast Sup35NM protein, although at higher temperature than for bacterial spores.

KEYWORDS

backwards planetary protection, planetary protection, mars sample return, prion inactivation, prions, biological indicator, sample return mission

Introduction

As upcoming missions seek to understand life beyond our planetary body, sample return missions will require development of a mitigation strategy to address any potential hazard to Earth's biosphere. As signatories of the 1967 Outer Space Treaty, the United States has agreed to the practice of Planetary Protection (PP) which entails protecting solar system bodies from "forward contamination" by Earth life and protecting Earth from "backward contamination" returned from other solar system bodies (NASA, 2008; NPD 8020.7G). The Committee on Space Research (COSPAR) established by the International Council for Science in 1958 further outlines an international planetary protection policy (Kminek et al., 2017; Committee on Space Research, 2020). This planetary protection policy includes categorization of space missions according to the type of encounter (i.e., flyby, orbiter, lander or sample return) and the target (Kminek et al., 2017; NASA Science Mission Directorate, 2017). Sample return missions are classified as PP Category V, with details that depend on the target planetary body from where samples will be collected. Within this category, missions are classified as the following: "unrestricted" if samples are returned from solar system bodies that have no indication of indigenous life forms or "restricted" if there is scientific evidence to support potential indigenous biological life (NPR 8715.24; NASA, 2021; Committee on Space Research, 2020). As part of the effort to develop strategies for meeting stringent Category V requirements, we investigate backward planetary protection strategies developed to reduce the risk of harmful contamination of Earth with uncontained returned samples. To meet these challenges, the development and implementation of a suitable strategy for the sterilization of returning material is necessary.

The scientific consensus from prior sample return working groups, reviews, and other meetings is that the existing biological indicators typically used to assess sterilization systems are not sufficient to adequately assess the efficacy of a sample return sterilization approach for backward-contamination (Craven et al., 2020). Additional engineering areas that may benefit from this information include applications of brazing, sealing, and impact heating and atmospheric entry heating. Given that heat-resistant spores have been tested for multiple backward PP-related experiments, a combination of the strategies with our approach will be considered to understand and reduce the viability of potentially uncontained returned material through the entire mission architecture.

Traditional self-contained biological indicators (ISO 11138-7, 2019) employ test systems composed of viable microorganisms that are inactivated when necessary conditions are met during sterilization procedures, providing a level of confidence in the process (Sandle, 2019). They are somewhat limited by past mission requirements, which mainly focused on spore-forming bacteria. Unfortunately, it has become clear that spore-based biological indicators are insufficient for a nominal case for both restricted and unrestricted sample return missions (Craven et al., 2020). It was suggested that use of yeast prions could be used as an analog for the bioactive molecules (Craven et al., 2020). Currently, heat resistant biological indicators used by NASA include *Bacillus atrophaeus* ATCC 9372 often used for dry heat microbial reduction (DHMR) processing and an industry standard biological indicator species for dry-heat sterilization (McDonnell, 2017; Bancroft, 2020). For the PP NASA standard assay, *B. atrophaeus* ATCC 9372 has also been used to as a biological indicator for cleanroom-associated surfaces bioburden assessment. *Bacillus* sp. ATCC 29669 is another spore-former associated with NASA flight assembly cleanrooms. The dry heat-resistance of *Bacillus* sp. ATCC 29669 represents the heat-hardy fraction within the NASA heat lethality curves, that is approximately 20 to 35 times more resistant than of *B. atrophaeus*. This resistance is based on D-values which are defined at the decimal reduction time or the time required to reduce a population by 90% at a specified temperature. The inactivation method is known as Dry Heat Microbial Reduction (DHMR). *Bacillus* sp. ATCC 29669 continues to be used as a test organism to validate effects of high heat and DHMR. Many other living systems and their products that exist on Earth should be considered. Developing a mitigation strategy to address all potential life-related forms (based on life as we know it on Earth), including self-perpetuating biomolecules, will be important to address or alleviate concerns about bringing back potentially biologically active material. Prions are biological molecules with the name derived from "proteinaceous infectious particles" (Prusiner, 1982). Prions have proven to be highly resistant to traditional sterilization modalities such as ethylene oxide (EO) and gamma radiation that are usually sufficient for microbial inactivation (Colby and Prusiner, 2011).

At a molecular level, prions are infectious protein isoforms, typically composed of highly ordered fibrous aggregates (amyloids). A prion protein can convert from a soluble form of the same or similar protein into an amyloid form, that is protease-resistant and insoluble (Bruce, 2003; Colby and Prusiner, 2011). Mammalian prion PrP^{Sc} is an infectious agent causing fatal infectious disease such as Creutzfeldt-Jakob disease (CJD) in humans and bovine spongiform encephalopathy (BSE) in cattle (Prusiner, 1998; Colby and Prusiner, 2011). Although prions lack nucleic acid material such as DNA and RNA, they are capable of "Darwinian" evolution and transmission, undergoing "mutations" and "adaptive" changes (Li et al., 2010). High resistance of prions to traditional sterilization methods is due to their unique and stable highly ordered structure (Brown et al., 1990). Many biocidal treatments that are known to be detrimental to microorganisms (for example, DNA damaging treatments) are not effective against prions (McDonnell, 2013). Thus, anti-prion "sterilization" techniques should be based on different principles compared to microorganisms.

The Centers for Disease Control and Prevention (CDC) defines sterilization as a process that destroys or eliminates all forms of microbial life that is carried out by physical or chemical methods (Rutala and Weber, 2001; Rutala et al., 2008). Since this definition emphasizes microorganisms as living forms, the term

"inactivation" would better describe the loss of prion's ability to convert a substrate protein into a prion state (Giles et al., 2017). According to the World Health Organization (WHO), aggressive inactivation strategies such as chemical, physical, and mechanical methods that are usually satisfactory against microbes or viruses, have proven insufficient against PrP^{Sc} (WHO infection control guidelines, 1999). One technique for PrP^{Sc} inactivation that was validated is soaking material in sodium hydroxide (or sodium hypochlorite), removing it and then heat inactivation at 134°C (Rutala and Weber, 2001). However, the use of NaOH and other corrosive chemicals is not applicable for space mission needs due to risks associated during flight. The storage and application of such chemicals during a long duration robotic mission is complex, and was thus ruled out as an option. Therefore, there is a need to address the knowledge gap in prion inactivation.

Dry heat is an accepted process for sterilization not only in pharmaceutical industry but also in the aerospace community and for forward planetary protection efforts. It has been selected as the primary option for backward planetary protection sterilization strategies (Craven et al., 2020). Dry heat is also a NASA-approved technique for microbial reduction for forward planetary protection; therefore, there is extensive experience in reducing the bioburden carried by outward-bound hardware. It is compatible with spacecraft parts and can be applied in vacuum. Heat penetrates below surfaces and encapsulated bioburden and it will be crucial for validating the Mars sample return sterilization system. Heat has been shown to inactivate proteins by increasing kinetic energy of molecules, causing the materials to dissociate.

Studies of prion inactivation are complicated by the biosafety concerns related to prion pathogenicity. This could be overcome by employing prions of yeast *Saccharomyces cerevisiae* as surrogates for sterilization testing. Yeast contains a variety of proteins that can form amyloid-based prions (Liebman and Chernoff, 2012). These proteins are not homologous to mammalian PrP by sequence and are not harmful to humans, however they possess remarkable similarities to PrP^{Sc} and other mammalian amyloids in regard to principles of transmission and structural organization. Yeast prions form fibrous structures enriched in beta-sheets, exhibiting typical characteristics of amyloids, and are capable of converting monomeric protein into a prion form, as in the case of PrP^{Sc} (Chernoff et al., 2020). In yeast cells, prions cause phenotypically detectable changes heritable *via* cytoplasm (Liebman and Chernoff, 2012). Among more than 10 proteins proven to form a prion in yeast cells to date, the Sup35 protein is the most extensively studied (Liebman and Chernoff, 2012). The prion-forming domain of Sup35 is located in the N-proximal region and is distinct from the C-proximal region responsible for the cellular function of Sup35 (termination of translation). The middle (M) region located between N and C modulates solubility. The Sup35NM fragment is typically employed for studying aggregation *in vitro* and is sufficient to transmit all information required for prion proliferation when transformed into the yeast cell (Tanaka et al., 2004).

Yeast prions, and specifically Sup35 (or Sup35NM) protein, provide a tractable experimental tool to investigate the conditions for the heat inactivation of self-perpetuating protein aggregates. In this work, we employed Sup35NM aggregates as a biological indicator for inactivation of prion agents using the potential in-flight sterilization modalities dry heat.

Materials and methods

Expression and purification of Sup35NM-His_6

Escherichia coli strain HMS174 (DE3) pLysS (Novagen) was transformed with pET21b vector containing the NM coding region of Sup35 from *S. cerevisiae* with an attached C-terminal His_6 tag (Allen et al., 2005). Sup35NM-His_6 was expressed and purified as described previously (Yeh et al., 2010). In brief, competent HMS174 (DE3) pLysS cells were transformed with the cloning vector. Sup35NM-His_6 expression was induced using isopropyl β-D-1-thiogalactopyranoside at a final concentration of 1 mM and the cells were harvested following 4 h of induction at 37°C. Cell pellets were stored at-80°C prior to purification. Sup35NM-His_6 was purified *via* Ni-NTA His-tag affinity purification under denaturing conditions. Sup35NM-His_6 was precipitated in ice-cold methanol and the protein pellet was collected *via* centrifugation, washed with ice-cold methanol, and stored at-80°C in 80% methanol until use.

Production of Sup35NM-His_6 aggregates

Sup35NM-His_6 stored in 80% methanol at −80°C was collected by centrifugation. The supernatant was discarded and the pellet was resuspended in 1XPBS. The concentration of protein was measured *via* Bradford's Assay (BIO-RAD) and the solution diluted such that the concentration of Sup35NM-His_6 was 1 mg/ml. The diluted protein solution was transferred to a U-bottom microcentrifuge tube and rotated end-over-end for 48 h at room temperature to form aggregates. Aggregate formation was checked using the "boiled gel" procedure and thioflavin T fluorescence (described below).

Spotting Sup35NM-His_6 aggregates on stainless steel coupons

After confirming aggregation, the concentration of the Sup35NM-His_6 aggregates was adjusted to 1 mg/ml as per data by Bradford's assay. Sterile stainless-steel coupons (Mesa Labs) with a total diameter of 9 mm were then unwrapped from autoclavable pouches and placed in a desiccator, and 50 µl of aggregate solution was pipetted onto each coupon, to cover the flat portion of a coupon with a diameter of 4.9 mm. Coupons were then placed

under vacuum until completely dry. This was repeated twice to ensure a final protein amount of 0.1 mg per coupon.

Exposure to TSEV

The prepared coupons were placed into individual Thermal Spore Exposure Vessels (TSEVs) or stainless-steel tubes and a temperature reference TSEV was exposed on each dry heat run cycle. An additional coupon was prepared (non-heat treated) to serve as a positive control. The TSEVS are placed into a constant high temperature silicone bath and the temperature of the bath was calibrated with a reference thermometer. The TSEVs are held in a modified lid of the bath and the thermocouple junction touched the bottom of the reference coupon to record the actual temperature to which the proteins were being exposed. The TSEV was immersed in the bath simultaneously and the time temperature of the reference TSEV was recorded every second (it takes 30–40 s for the TSEV to reach the set temperature). After heating, the TSEVs were removed from the oil bath and placed into an ice bath to cool. Resulting treated coupons were stored at −80°C and sent on dry ice from JPL where treatment was performed, to Georgia Tech for protein recovery and further analysis.

Protein recovery from coupons

Using sterile forceps, coupons were lightly folded into a "U"-shape so that a coupon could fall into the bottom of a microcentrifuge tube. Once all coupons had been folded and placed into tubes, 200 µl of sterile 1X PBS was added to each coupon-containing tube. Coupons were vortexed for 1 hr then stored at −80°C until use.

Detection of protein and aggregates

SDS-PAGE gel electrophoresis and Western blotting using His_6 antibody (Abcam) were performed as described (Allen et al., 2005). Protein samples were combined in a 1:3 ratio with 4X Loading Buffer (240 mM Tris-Cl, pH 6.8, 8% SDS, 40% glycerol, 12% 2-mercaptoethanol, 0.002% bromophenol blue), either boiled for 10 min (in the case if aggregates would need to be solubilized) or not boiled (if aggregates were to be kept intact) and loaded on a 12% SDS-polyacrylamide gel with a 4% stacking gel. Electrophoresis was performed at approximately 100 V in Tris-glycine-SDS running buffer (25 mM Tris, 192 mM glycine, 0.1% SDS, pH 8.3). In the case of "boiled gel" assay for aggregate detection (Kushnirov et al., 2006), electrophoresis was halted after 1 h and the gel was removed from the running box. The wells were sealed with 4% acrylamide, allowed to polymerize, and the whole gel was wrapped in plastic wrapping and boiled for 10 min. After allowing several minutes for cooling, the gel was placed back in the cassette and electrophoresis continued for about 1.5 h. Proteins were transferred to Hybond-ECL nitrocellulose membrane (Amersham) using a Criterion™ blotter (BIO-RAD), and the membrane was blocked in 5% milk, and then incubated with His_6 primary antibody (Abcam) followed by anti-Rb (HRP) secondary antibody (BioRad). Protein was visualized using ECL detection reagent (Amersham).

Thioflavin T based seeding assay

Thioflavin T based fibrillization assays for detection of the amyloid-seeding activity were conducted as described previously (Sharma et al., 2018). Briefly, Sup35NM-His_6 stored in 80% methanol at −80°C was collected by centrifugation. The supernatant was discarded and the pellet resuspended in 8 M urea buffer (8 M Urea, 100 mM NaH_2PO_4, 10 mM Tris, pH 8.0). Sup35NM-His_6 was concentrated using a 3-kDa filter (EMD Millipore) and diluted 100-fold in 1XPBS. The protein concentration was determined *via* Bradford's Assay (BIO-RAD). The Sup35NM-His_6 monomers were boiled for 10 min prior to starting aggregation experiments to break down any pre-formed aggregates or oligomers.

A stock solution of 1 mM Thioflavin T (ThT) was prepared fresh in 1X PBS. Aggregation experiments were performed in triplicate in a black, clear-bottomed 96 well plate (Greiner CELLSTAR) with a final ThT, Sup35NM-His_6 monomer, and Sup35NM-His_6 aggregate concentration of 10, 5, and 0.025 µM, respectively. ThT assays were carried out in a SpectraMax iD3 microplate reader (Molecular Devices). Fluorescence was recorded every 10 min, with shaking in between readings, using an excitation wavelength of 440 nm and an emission wavelength of 486 nm. Fluorescent readings are interpreted as a measure of the total amount of amyloid aggregates formed.

Results

Recovery of Sup35NM-His_6 aggregates after the dry heat treatment

We sought to develop a series of tests to access the retention and amyloid seeding activity of Sup35NM-His_6 aggregates after exposures to dry heat for using it as a BI for sample return sterilization systems. Dry heat tests were performed at temperatures of 125, 250, and 350°C. To achieve this goal, the recombinant Sup35NM-His_6 protein was purified from *E. coli*, aggregated and immobilized on stainless steel coupons, and subjected to temperature treatment as described in Materials and Methods. Protein recovered from coupons and stored in 1X PBS at −80°C was thawed at room temperature, and protein concentrations were determined using Bradford's assay. Protein solution was then diluted, as appropriate, prior to loading onto the SDS-PAGE gel. Sup35NM-His_6 aggregates produced *in vitro* were used as a loading control. Each protein sample was run on three gels: one gel to be stained with Coomassie Blue, and two gels that were transferred to nitrocellulose membrane and probed using

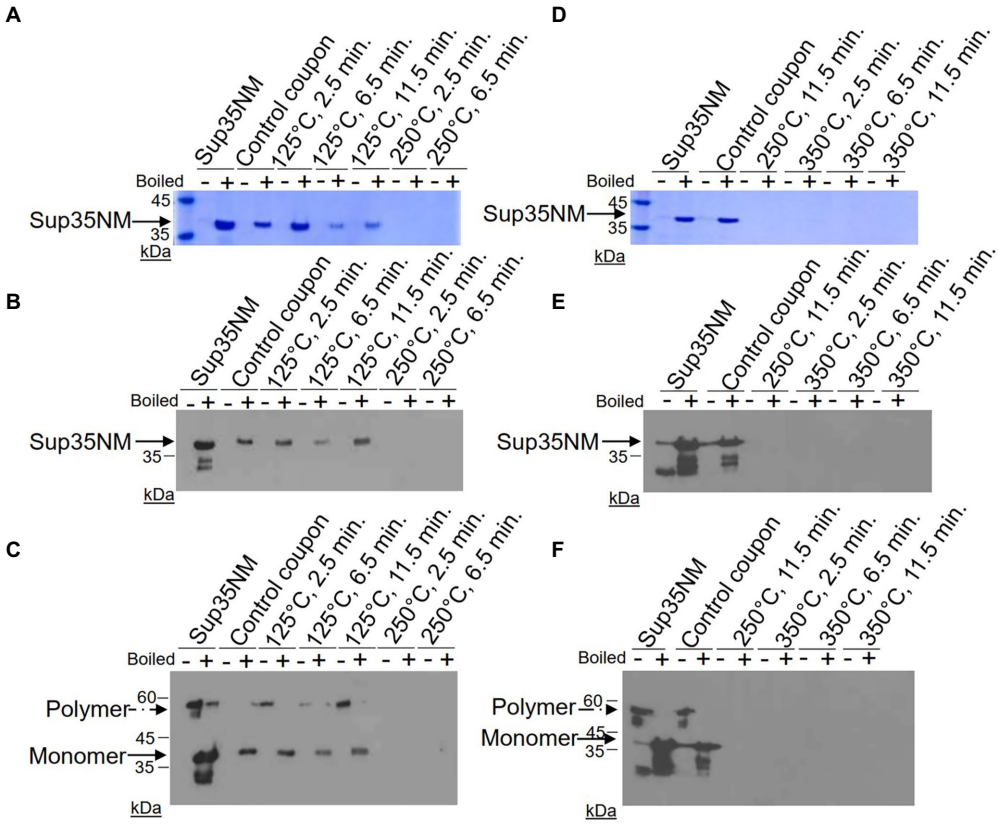

FIGURE 1
Detection of Sup35NM-His_6 aggregates recovered from stainless-steel coupons by SDS-PAGE and Western blotting. Proteins from control coupons, and from coupons treated at 125°C, 250°C and 350°C for various periods of time were analyzed as indicated. *In vitro* aggregated Sup35NM not immobilized on a coupon was used as a control. Amount of proteins loaded was normalized according to Bradford assay. **(A,D)** SDS-PAGE gels stained with Coomassie Blue. Samples were alternated in such a way that not-boiled samples (–) were loaded first, followed by pre-boiled samples (+). Aggregated protein cannot enter the gel without pre-boiling. Left lane contains molecular weight markers. **(B,E)** SDS-PAGE gels analyzed by Western blotting, followed by reaction to anti-His_6 antibodies. Sup35NM-His_{s6} monomer bands are indicated by the solid arrow. Lower bands likely represent proteolytic fragments. **(C,F)** Boiled SDS-PAGE gels analyzed by Western blotting, followed by reaction to anti-His_6 antibodies. Aggregated protein (polymer) in non-boiled samples enters the gel after the gel is boiled. Positions of polymers and monomers are shown by arrows. Lower bands likely represent proteolytic fragments. Gels analyzed by Western were overexposed in order to see even residual amounts of immunoreactive material. Positions of nearest molecular weight markers are indicated on Western gels.

anti-His_6 antibody. Of these two gels, one was prepared using the "boiled gel" procedure, resulting in solubilization of aggregates at 1 h after the start of electrophoresis (see Materials and Methods). While aggregated protein cannot enter the gel, solubilized aggregates are converted into monomers entering the gel, so that in case of "boiled" gel, bands corresponding to initially monomeric protein and initially aggregated protein could be detected at different locations.

Results of these experiments are shown on Figure 1 and summarized in Table 1.* Despite some variability between experiments, protein recovery from control (untreated) coupons was reasonably good (in the range from 23% to 93%, see Table 1), and protein of expected size and aggregated state was always detectable by both Coomassie staining and Westerns (Figure 1; Table 1), indicating both that Sup35NM-His_6 can bind stainless steel, as has been observed with PrP^{Sc} (Flechsig et al., 2001), and that Sup35NM-His_6 aggregates are sufficiently stable to survive desiccation and storage. Protein recovered from coupons treated

TABLE 1 Summary of analysis of Sup35NM-His_6 aggregates recovered from stainless coupons.

Treatment condition	Percent recovery (range)*	Detectability of protein by SDS-PAGE and Western	Seeding ability**
Control (None)	23–93	4 out of 4	4 out of 4
125°C, 2.5 min	47–48	3 out of 3	2 out of 2
125°C, 6.5 min	20–52	3 out of 3	2 out of 2
125°C, 11.5 min	28–70	3 out of 3	2 out of 2
250°C, 2.5 min	7–8	0 out of 3	0 out of 2
250°C, 6.5 min	15–18	0 out of 3	1 out of 2
250°C, 11.5 min	12–39	0 out of 6	0 out of 5
350°C, 2.5 min	10–25	0 out of 3	1 out of 2
350°C, 6.5 min	16–28	0 out of 3	1 out of 2
350°C, 11.5 min	4–23	0 out of 6	0 out of 5

*Determined by Bradford's assay.
**Determined by ThT assay.

at 125°C for any period of time was also detectable by Bradford (Table 1) and SDS-PAGE (Figures 1A–C; Table 1). Amount of the Bradford-detectable material generally decreased (although remained significant, in the range from 7% to 23%) in solutions generated from coupons treated at 250°C or 350°C (Table 1). However, the protein of the expected size was neither seen on the Coomassie gel nor detected by Western (on both regular and "boiled" gels) after these treatments (Figure 1; Table 1). Thus, dry heat at high temperature results in significant degradation of Sup35NM.

Analysis of the amyloid seeding activity of Sup35NM-His$_6$ after heat treatment

Following gel analysis, protein samples recovered from coupons were checked in the ThT based seeding assay (see Materials and Methods) to assess the propensity of recovered protein to seed Sup35NM-His$_6$ aggregation. For this purpose, aggregated protein immobilized from coupons was added to soluble Sup35NM-His$_6$ monomers in a ratio of 1:20, according to Bradford data. Aggregation of Sup35NM-His$_6$ was detected by ThT binding, resulting in fluorescence as described in Materials and Methods. Recovered protein was considered capable of seeding if the aggregation lag time was shortened and the overall curve was shifted upwards compared to spontaneous aggregation of Sup35NM-His$_6$ monomers. Recovered protein was considered inactivated if aggregation in the "seeded" sample occurred at a similar or reduced rate, compared to spontaneous aggregation of monomeric Sup35NM-His$_6$. Results of these experiments are presented on Figures 2–4.

Protein recovered from control (not treated) coupons was always capable of seeding of Sup35NM-His$_6$ monomers (see Control coupon curves on Figures 2–4), though somewhat less efficiently than the *in vitro* aggregated Sup35NM-His$_6$ sample that has not been immobilized on a coupon and then recovered. This generally agreed with protein analysis data described above. Likewise, protein recovered from coupons treated at 125°C for any period of time was able to seed Sup35NM-His$_6$ monomer aggregation, though less efficiently than protein recovered from control coupons or than the control Sup35NM-His$_6$ aggregates (Figure 2; Table 1). In contrast, protein recovered from coupons treated at 250°C for 2.5 (Figure 3A) or 11.5 min (Figure 3C) was unable to seed Sup35NM-His$_6$ monomer aggregation (see also Table 1). Interestingly, protein recovered from one of the two coupons treated at 250°C for 6.5 min was capable of seeding monomer aggregation, despite the lack of Coomassie staining and lack of immunoreactive material detectable by Western blot (Figure 3B; Table 1). Likewise, proteins recovered from one of the two coupons treated at 350°C for 2.5 min (Figure 4A; Table 1) and from one of two coupons treated at 350°C for 6.5 min (Figure 4B; Table 1) was capable of seeding aggregation, despite the lack of immunoreactive material. However, none of the five coupons treated at 350°C for 11.5 min produced any detectable seeding activity (Figure 4C; Table 1), confirming that this treatment consistently eliminates a biologically active prion.

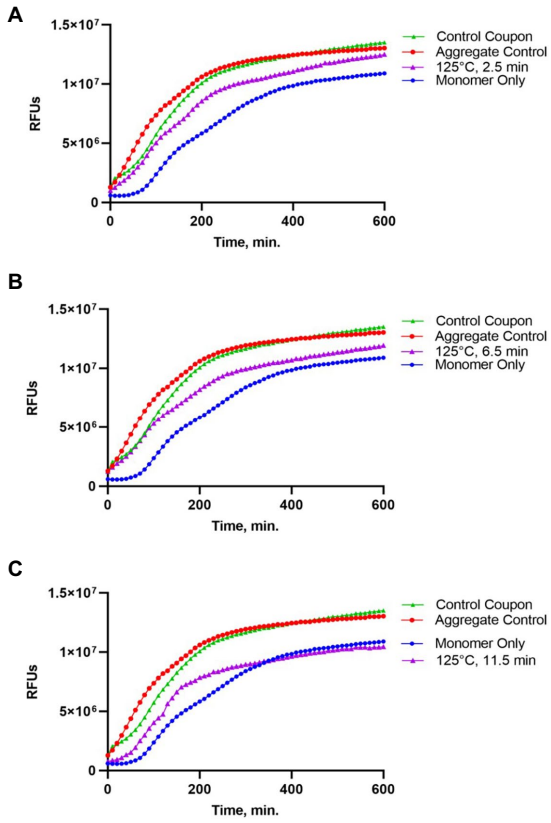

FIGURE 2
Impact of the 125°C treatment on the seeding activity of Sup35NM-His$_6$ aggregates. Sup35NM-His$_6$, recovered from coupons treated at 125°C for 2.5min **(A)**, 6.5min **(B)** and 11.5min **(C)** was analyzed. The protein recovered from coupons (purple, empty triangles) was added to soluble Sup35NM-His$_6$, monomers at 1:20 ratio according to Bradford. Unseeded monomer (blue, filled circles), and monomers seeded by *in vitro* obtained aggregates that were been immobilized on coupons (red, empty circles), or were recovered from untreated control coupons (green, filled triangles) were used for the comparison. Seeding activity is always detected after 125°C treatment, even though it is less efficient than by control aggregates. Typical examples are shown.

Discussion

Dry heat as a tool for prion inactivation

Our data show that Sup35NM aggregates are reproducibly inactivated by the exposures to dry heat at 250°C or 350°C for 11.5 min. Shorter treatments at these temperatures led to inactivation of the seeding activity of Sup35NM in some but not all cases. It remains to be seen if these conditions are applicable to other proteins in prion form. Previous surface

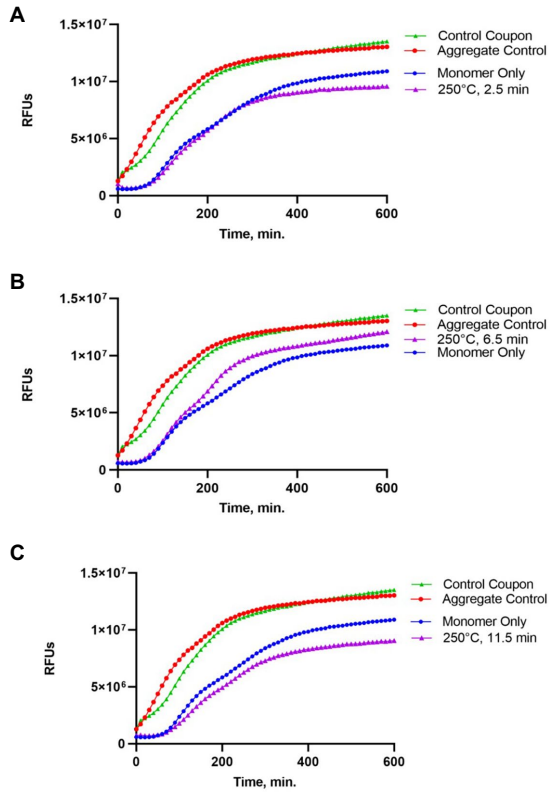

FIGURE 3
Impact of the 250°C treatment on the seeding activity of Sup35NM-His_6 aggregates. Sup35NM-His_6 recovered from coupons treated at 250°C for 2.5min **(A)**, 6.5min **(B)** and 11.5min **(C)** was analyzed. Conditions of the seeding assay and designations are the same as on Figure 2. After 250°C treatment for 2.5min (typical example is shown on **A**) or 11.5min (typical example is shown on **C**), seeding activity was not detected, however it was detected in one of two samples treated for 6.5min (shown on **B**).

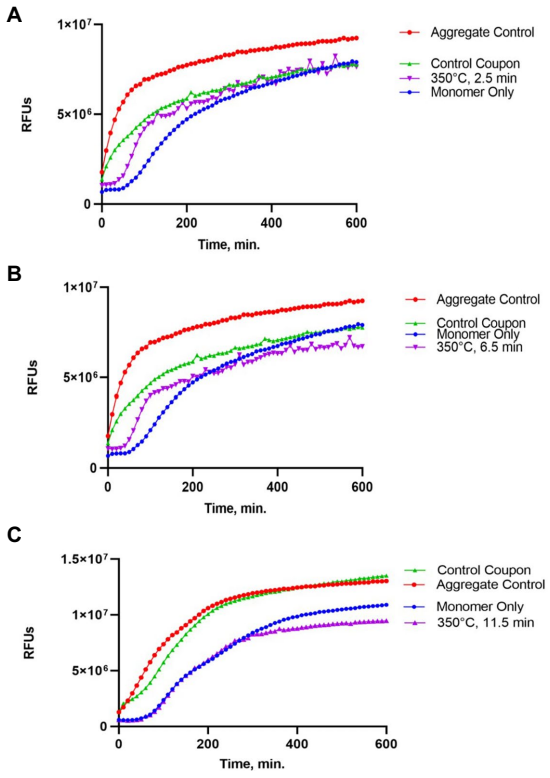

FIGURE 4
Impact of the 350°C treatment on the seeding activity of Sup35NM-His_6 aggregates. Sup35NM-His_6 recovered from coupons treated at 350°C for 2.5min **(A)**, 6.5min **(B)** and 11.5min **(C)** was analyzed. Conditions of the seeding assay and designations are the same as on Figure 2. Weak seeding activity was detected in one out of two samples treated at 350°C for 2.5min (shown on **A**), and in one out of two samples treated at 350°C for 6.5min (shown on **B**), but it was not detected in any of 5 samples treated at 350°C for 11.5min (a typical example is shown on **C**).

decontamination investigations reported that mammalian PrP retained functionality after exposure to 360°C for an hour and even following incineration at 600°C for 15 min (Brown et al., 2000), however another work indicated that dry-heating at temperatures of 600°C and higher (but not 400°C or lower) resulted in inactivation of the PrP-based prion agent of bovine spongiform encephalopathy (Matsuura et al., 2020). However, it is important to highlight that in these experiments, brain material was subjected to heat treatment. Therefore, it is possible that the heat was not evenly distributed throughout the material resulting in prion retention (Rohwer, 1984). Brain tissue is known to be hydrophobic with a high content of lipids and may have contributed to the "protective effect" where the tissue shields the protein from the sterilization source (Rohwer, 1984; Weinstein et al., 2001). For the application of our proposed tests, the surrogate prions were not embedded or prepared in brain homogenate consisted of purified surrogate prion proteins dessicated on a surface. Our approach appears to be more accurate for the development of space mission-related inactivation procedures. However, additional experiments with prion/amyloid proteins other than Sup35 are needed to determine the universality of a heat-based inactivation procedure.

Mechanism of prion inactivation

To completely inactivate prions, they must be either denatured to the point where they are not able to refold into a prion shape, or completely physically destroyed. Prion protein renaturation has not been shown to occur once denaturation has been achieved (Prusiner et al., 1993). It is interesting that in our experiments, Sup35NM retained some seeding (prion) activity even in the conditions where no immunoreactive protein material was detected. One possibility is that while a significant portion of the protein was degraded in these conditions, a portion involved in an amyloid core remained. This assumption is logical as amyloid core is most resistant to

damaging treatments. Indeed, our most sensitive antibodies were to the His_6 tag, which was located at the C-terminus of Sup35NM fragment, that is, outside of the expected location of amyloid core. We also employed the polyclonal Sup35NM antibody (data not shown), but this antibody is much less sensitive, and is likely the least capable of recognizing the Sup35N region due to its poor immunogenicity. It remains to be determined if a complete loss of any detectable seeding activity at 350°C is due to complete destruction of the protein to short non-amyloidogenic peptides and/or to amino acids, or due to dissolution of remaining amyloid aggregates into non-prion monomers.

Biological relevance of prions as indicators

As prions are completely dependent on a substrate protein produced by a host organism/cell for their reproduction, it seems most likely that any hypothetical Martian prion or similar protein assembly (if such an assembly exists and is present in the cached samples) would be incapable of propagating on Earth owing to the lack of available hosts capable of producing a substrate protein of the same or similar amino acid sequence. Also, protein folding and prion propagation depend on temperature and water availability. Since no liquid water has yet been found on Mars' surface in our exploration to date, environmental conditions are not favorable for enabling the propagation of prions.

However, one should note that the recent evidence increasingly points to the ability of some prion and other amyloid proteins to cross-seed non-homologous substrates. Cross-seeding interactions have been described between protein as distant as yeast Sup35 and human tau (Flach et al., 2022) or bacterial curli and human synuclein (Sampson et al., 2020). Even though these cross-seeding interactions are less efficient than homologous seeding, the possibility of the existence of highly promiscuous prions with broad cross-seeding capabilities cannot be excluded. Therefore, further studies on prion inactivation remain relevant to the biosafety aspect of space missions.

Data availability statement

The original contributions presented in the study are included in the article/supplementary material, further inquiries can be directed to the corresponding author.

Author contributions

ES was the Science PI and directed experiments and wrote the manuscript draft. YC senior researcher directed the analytical experimentation and significantly improved this paper. AH carried out all of the laboratory analysis and produced all of the protein. WS PI carried out all of the heat inactivation experiments. All authors contributed to the article and approved the submitted version.

Funding

Supported by the National Aeronautics and Space Administration: NNH18ZDA001N-PPR. The research described in this publication was carried out at the Jet Propulsion Laboratory, California Institute of Technology, under a contract with the National Aeronautics and Space Administration, Honeybee Robotics, and at Georgia Institute of technology under a subcontract from JPL.

Acknowledgments

The decision to implement MSR will not be finalized until NASA's completion of the National Environmental Policy Act (NEPA) process. This document is being made available for information purposes only.

Conflict of interest

ES is employed by the company Honeybee Robotics.

The remaining authors declare that the research was conducted in the absence of any commercial or financial relationships that could be construed as a potential conflict of interest.

Publisher's note

References

Allen, K. D., Wegrzyn, R. D., Chernova, T. A., Müller, S., Newnam, G. P., Winslett, P. A., et al. (2005). Hsp70 chaperones as modulators of prion life cycle: novel effects of Ssa and Ssb on the *S. cerevisiae* prion [PSI+]. *Genetics* 169, 1227–1242. doi: 10.1534/genetics.104.037168

Bancroft, R. (2020). "Biological indicators, chemical indicators, and parametric release," in *Block's Disinfection, Sterilization and Preservation*. eds. G. McDonnell and J. Hansen. *6th* ed (Philadelphia, PA: Wolters Kluwer), 1297–1306.

Brown, P., Liberski, P. P., Wolff, A., and Gajdusek, D. C. (1990). Resistance of scrapie infectivity to steam autoclaving after formaldehyde fixation and limited survival after ashing at 360 degrees C: practical and theoretical implications. *J. Infect. Dis.* 161, 467–472. doi: 10.1093/infdis/161.3.467

Brown, P., Rau, E. H., Johnson, B. K., Bacote, A. E., Gibbs, C. J. Jr., and Gajdusek, D. C. (2000). New studies on the heat resistance of hamster-adapted scrapie agent: threshold survival after ashing at 600 degrees C suggests an inorganic

template of replication. *Proc. Natl. Acad. Sci. U. S. A.* 97, 3418–3421. doi: 10.1073/pnas.050566797

Bruce, M. E. (2003). TSE strain variation. *Br. Med. Bull.* 66, 99–108. doi: 10.1093/bmb/66.1.99

Chernoff, Y. O., Grizel, A. V., Rubel, A. A., Zelinsky, A. A., Chandramowlishwaran, P., and Chernova, T. A. (2020). Application of yeast to studying amyloid and prion diseases. *Adv. Genet.* 105, 293–380. doi: 10.1016/bs.adgen.2020.01.002

Colby, D. W., and Prusiner, S. B. (2011). Prions. *Cold spring Harb. Perspect. Biol.* 3:a006833. doi: 10.1101/cshperspect.a006833

Committee on Space Research (2020). COSPAR Policy on Planetary Protection. COSPAR Bureau (June 17, 2020).

Craven, E., Winters, M., Smith, A. L., Lalime, E., Mancinelli, R., Shirey, B., et al. (2020). Biological safety in the context of planetary protection and Mars Sample Return: a meeting report from the Sterilization Working Group. *Int. J. Astrobiol.* 20, 1–28. doi: 10.1017/S1473550420000397

Flach, M, Leu, C, Martinisi, A, Skachokova, Z, Frank, S, Tolnay, M, et al. (2022). Trans-seeding of Alzheimer-related tau protein by a yeast prion. *Alzheimers Dement.* doi: 10.1002/alz.12581 (Epub ahead of print).

Flechsig, E., Hegyi, I., Enari, M., Schwarz, P., Collinge, J., and Weissmann, C. (2001). Transmission of scrapie by steel-surface-bound prions. *Mol. Med.* 7, 679–684. doi: 10.1007/BF03401958

Giles, K., Woerman, A. L., Berry, D. B., and Prusiner, S. B. (2017). "Bioassays and inactivation of prions," in *Prion Biology*. ed. S. B. Prusiner (New York, NY: Cold Spring Harbor Laboratory Press).

ISO 11138-7 (2019). Sterilization of health care products — Biological indicators.

Kminek, G., Conley, C., Hipkin, V., and Yano, H. (2017). COSPAR Planetary Protection Policy. *Space Research Today*, 200, 12–24.

Kushnirov, V. V., Alexandrov, I. M., Mitkevich, O. V., Shkundina, I. S., and Ter-Avanesyan, M. D. (2006). Purification and analysis of prion and amyloid aggregates. *Methods* 39, 50–55. doi: 10.1016/j.ymeth.2006.04.007

Li, J., Browning, S., Mahal, S. P., Oelschlegel, A. M., and Weissmann, C. (2010). Darwinian evolution of prions in cell culture. *Science* 327, 869–872. doi: 10.1126/science.1183218

Liebman, S. W., and Chernoff, Y. O. (2012). Prions in yeast. *Genetics* 191, 1041–1072. doi: 10.1534/genetics.111.137760

Matsuura, Y., Ishikawa, Y., Murayama, Y., Yokoyama, T., Somerville, R. A., Kitamoto, T., et al. (2020). Eliminating transmissibility of bovine spongiform encephalopathy by dry-heat treatment. *J. Gen. Virol.* 101, 136–142. doi: 10.1099/jgv.0.001335

McDonnell, G. (2013). Decontamination of prions. *Decontamin. Hosp. Healthc.* 346–369. doi: 10.1533/9780857096692.2.346

McDonnell, G. E. (2017). *Antisepsis, Disinfection, and Sterilization: Types, Action, and Resistance*, *2nd Edn.* Washington, DC: ASM Press. 438.

NASA (2008) NPD 8020.7G biological contamination control for outbound and inbound planetary spacecraft (Revalidated 05/17/13 w/change 1).

NASA (2021) NPR 8715.24 planetary protection provisions for robotic extraterrestrial missions

NASA Science Mission Directorate (2017). NASA Interim Directive NID 8020.109a. NASA Science Mission Directorate, 144.

Prusiner, S. B. (1982). Novel proteinaceous infectious particles cause scrapie. *Science* 216, 136–144.

Prusiner, S. B. (1998). Prions. *Proc. Natl. Acad. Sci. U. S. A.*. 95:13363–83. doi: 10.1073/pnas.95.23.13363.

Prusiner, S. B., Groth, D., Serban, A., Stahl, N., and Gabizon, R. (1993). Attempts to restore scrapie prion infectivity after exposure to protein denaturants. *Proc. Natl. Acad. Sci. U. S. A.* 90, 2793, 10.1073/pnas.90.7.2793–2797. PMID: 8464892

Rohwer, R. G. (1984). Virus like sensitivity of the scrapie agent to heat inactivation. *Science* 223, 600–602. doi: 10.1126/science.6420887

Rutala, W. A., and Weber, D. J. (2001). Creutzfeldt-Jakob Disease: recommendations for disinfection and sterilization. *Clin. Infect. Dis.* 32, 1348–1356. doi: 10.1086/319997

Rutala, W. A., and Weber, D. J. (2008). The Healthcare Infection Control Practices Advisory Committee. CDC guideline for disinfection and sterilization in healthcare facilities. Available at: https://www.cdc.gov/infectioncontrol/pdf/guidelines/disinfection-guidelines.pdf (Accessed February 16, 2022).

Sampson, T. R., Challis, C., Jain, N., Moiseyenko, A., Ladinsky, M. S., Shastri, G. G., et al. (2020). A gut bacterial amyloid promotes alpha-synuclein aggregation and motor impairment in mice. *elife* 9:e53111. doi: 10.7554/eLife.53111

Sandle, T. (2019). "Biological indicators," in *Industrial Pharmaceutical Microbiology: Standards and Controls*. ed. T. Sandle. *5th* ed (Passfield: Euromed Communications), 19.1–19.28.

Sharma, A., Behrens, S. H., Chernoff, Y. O., and Bommarius, A. S. (2018). Modulation of the formation of aβ-and sup35nm-based amyloids by complex interplay of specific and nonspecific ion effects. *J. Phys. Chem. B* 122, 4972–4981. doi: 10.1021/acs.jpcb.7b12836

Tanaka, M., Chien, P., Naber, N., Cooke, R., and Weissman, J. S. (2004). Conformational variations in an infectious protein determine prion strain differences. *Nature* 428, 323–328. doi: 10.1038/nature02392

Weinstein, R. A., Rutala, W. A., Weber, D. J., and Disease, C.-J. (2001). Recommendations for disinfection and sterilization. *Clin. Infect. Dis.* 32, 1348–1356. doi: 10.1086/319997

WHO (1999). WHO Infection Control Guidelines for Transmissible Spongiform Encephalopathies: Report of a WHO Consultation, Geneva, Switzerland, 23–26 March 1999.

Yeh, V., Broering, J. M., Romanyuk, A., Chen, B., Chernoff, Y. O., and Bommarius, A. S. (2010). The Hofmeister effect on amyloid formation using yeast prion protein. *Protein Sci.* 19, 47–56. doi: 10.1002/pro.281

frontiers | Frontiers in Microbiology

TYPE Original Research
PUBLISHED 06 March 2023
DOI 10.3389/fmicb.2023.1090740

OPEN ACCESS

EDITED BY
Camilla Urbaniak,
NASA Jet Propulsion Laboratory,
United States

REVIEWED BY
Markus Kalkum,
Beckman Research Institute,
United States
Jason M. Wood,
University of Illinois at Chicago, United States

*CORRESPONDENCE
Rakesh Mogul
✉ rmogul@cpp.edu

SPECIALTY SECTION
This article was submitted to Extreme Microbiology, a section of the journal Frontiers in Microbiology

RECEIVED 05 November 2022
ACCEPTED 20 January 2023
PUBLISHED 06 March 2023

CITATION
Mogul R, Miller DR, Ramos B and Lalla SJ (2023) Metabolomic and cultivation insights into the tolerance of the spacecraft-associated *Acinetobacter* toward Kleenol 30, a cleanroom floor detergent.
Front. Microbiol. 14:1090740.
doi: 10.3389/fmicb.2023.1090740

Metabolomic and cultivation insights into the tolerance of the spacecraft-associated *Acinetobacter* toward Kleenol 30, a cleanroom floor detergent

Rakesh Mogul[1,2]*, Daniel R. Miller[1], Brian Ramos[1] and Sidharth J. Lalla[1]

[1]Chemistry and Biochemistry Department, California State Polytechnic University, Pomona, CA, United States, [2]Blue Marble Institute of Science, Seattle, WA, United States

Introduction: Stringent cleaning procedures during spacecraft assembly are critical to maintaining the integrity of life-detection missions. To ensure cleanliness, NASA spacecraft are assembled in cleanroom facilities, where floors are routinely cleansed with Kleenol 30 (K30), an alkaline detergent.

Methods: Through metabolomic and cultivation approaches, we show that cultures of spacecraft-associated Acinetobacter tolerate up to 1% v/v K30 and are fully inhibited at ≥2%; in comparison, NASA cleanrooms are cleansed with ~0.8-1.6% K30.

Results: For A. johnsonii 2P08AA (isolated from a cleanroom floor), cultivations with 0.1% v/v K30 yield (1) no changes in cell density at late-log phase, (2) modest decreases in growth rate (~17%), (3) negligible lag phase times, (4) limited changes in the intracellular metabolome, and (5) increases in extracellular sugar acids, monosaccharides, organic acids, and fatty acids. For A. radioresistens 50v1 (isolated from a spacecraft surface), cultivations yield (1) ~50% survivals, (2) no changes in growth rate, (3) ~70% decreases in the lag phase time, (4) differential changes in intracellular amino acids, compatible solutes, nucleotide-related metabolites, dicarboxylic acids, and saturated fatty acids, and (5) substantial yet differential impacts to extracellular sugar acids, monosaccharides, and organic acids.

Discussion: These combined results suggest that (1) K30 manifests strain-dependent impacts on the intracellular metabolomes, cultivation kinetics, and survivals, (2) K30 influences extracellular trace element acquisition in both strains, and (3) K30 is better tolerated by the floor-associated strain. Hence, this work lends support towards the hypothesis that repeated cleansing during spacecraft assembly serve as selective pressures that promote tolerances towards the cleaning conditions.

KEYWORDS

***Acinetobacter*, detergent, survival, metabolomics, planetary protection, spacecraft, cleanrooms**

1. Introduction

Maintaining low biological contamination in cleanroom-type facilities are critical components to spacecraft assembly (Rummel, 1992; NASA, 2011; Frick et al., 2014), crewed spacecraft exploration (Spry et al., 2020), delivery of healthcare facilities (Shams et al., 2016; Rutala and Weber, 2019), and the manufacturing of pharmaceuticals (Sandle, 2015). Common to these confined

environments and endeavors are the routine cleansing of non-critical hard surfaces and support equipment with ≥70% v/v ethyl alcohol, 70% v/v isopropyl alcohol, 3% v/v hydrogen peroxide, and/or disposable disinfectant wipes containing quaternary ammonium compounds (Agalloco and Carleton, 2007; Rutala et al., 2008; Wong et al., 2013; Frick et al., 2014; Checinska Sielaff et al., 2019).

For pharmaceutical facilities, and to lesser extent healthcare facilities, the floors are additionally cleansed with disinfectants and/or detergents such as benzalkonium chloride (and other quaternary ammonium compounds), hydrogen peroxide, sodium hypochlorite, and other alternatives (Murtough et al., 2001; Rutala et al., 2008; Sandle, 2012; Eissa et al., 2014; Han et al., 2021; Tembo et al., 2022). While debated in efficacy (Daschner et al., 1982; Meyer and Cookson, 2010; Suleyman et al., 2018), the surface cleaning agents are often rotated in these facilities to minimize potential microbial resistance and/or selection toward the cleaning conditions (Murtough et al., 2001; Sandle, 2012).

For NASA cleanrooms (ISO class 8) where Mars and Europa spacecraft are assembled, the floors are routinely cleansed with ~0.8-1.6% v/v Kleenol 30 (Mogul et al., 2018; Danko et al., 2021), which is an alkaline detergent formulation. Due to the proprietary nature of Kleenol 30, scant information is available regarding the precise chemical composition. Available safety data sheets indicate a composition containing sodium dodecyl benzene sulfonate (1% w/w), polyethylene glycol mono-nonylphenyl ether (1–5% w/w), sodium metasilicate (1–5% w/w), ethylenediaminetetraacetic acid (EDTA; 2% w/w), sodium metasilicate (1–5% w/w), potassium hydroxide (KOH; ~2% v/v; presumably prepared from concentrated KOH), and 2-butoxyethanol (10–15% w/w). When considering the mechanism of cleansing for Kleenol 30, the combined chemical ingredients imply adjustments toward alkalinity (KOH), sequestering of transition and alkaline earth metals through chelation by the metal-binding reagents (EDTA and sodium metasilicate), and sequestering, emulsification, and removal of organics (non-polar, polar, and charged organics) by detergent action (polyethylene glycol mono-nonylphenyl ether, dodecyl benzene sulfonate, and sodium metasilicate).

Yet, despite these robust cleaning practices, spacecraft assembly facilities harbor a persistent yet low abundance microbial bioburden (Danko et al., 2021; Hendrickson et al., 2021). Further, molecular measures reveal the presence of a core microbiome across the spacecraft assembly facilities, International Space Station (Checinska et al., 2015; Checinska Sielaff et al., 2019), and clinical and operating facilities (Shams et al., 2016; Ellingson et al., 2020; Perry-Dow et al., 2022). In spacecraft assembly facilities, the microbiomes are reasonably diverse though generally low in total counts with measures of ~10^3–10^4 16S rRNA m^{-2} (intact cells), ~10^4–10^5 16S rRNA m^{-2} (total cells), 1–40 OTU m^{-2}, ~10^2–10^4 colony forming units m^{-2}, and ~10^1 spores m^{-2} (La Duc et al., 2012; Mahnert et al., 2015; Moissl-Eichinger et al., 2015).

Among the dominant members of the core microbiome across spacecraft and healthcare facilities are the *Acinetobacter* (La Duc et al., 2012; Mora et al., 2016; Hendrickson et al., 2021). The *Acinetobacter* are a Gram-negative bacterial genus associated with desiccation tolerance (McCoy et al., 2012; Farrow et al., 2018), radiation tolerance (La Duc et al., 2003; McCoy et al., 2012), bioemulsification (Pirog et al., 2021), biofilm formation (Yeom et al., 2013; Pompilio et al., 2021), and multi-drug resistance (Peleg et al., 2008).

In Mogul et al. (2018), we showed that *Acinetobacter radioresistens* 50v1, which was isolated from the surface of the pre-flight Mars Odyssey orbiter, could be cultivated in the presence of 1% v/v Kleenol 30, a floor detergent, while utilizing ethanol, a surface cleaner, as a sole carbon source. Additionally, cultivations of *A. radioresistens* 50v1 with Kleenol 30 were shown to yield tri, penta, and octaethylene glycols, which is suggestive of partial biodegradation of polyethylene glycol mono-nonylphenyl ether (a component of the Kleenol 30 formulation) *via* scission of the ether linkage (White, 1993) – to yield the mixed polyethylene glycols (e.g., tri, penta, and octaethylene glycol).

In addition, studies show that clinical strains of *Acinetobacter baumanii* tolerate benzalkonium chloride, which is a biocide and surface cleaner, through biofilm formation (Rajamohan et al., 2009) and increased expression of efflux pump genes (Fernández-Cuenca et al., 2015; Srinivasan et al., 2015). Further, survivability studies on cleanroom-associated *Acinetobacter* reveal extreme tolerances toward aqueous hydrogen peroxide, a surface and floor disinfectant; where the tolerances are perhaps the highest among Gram-negative bacteria (McCoy et al., 2012; Derecho et al., 2014; Mogul et al., 2018). These combined survival characteristics are likely key contributors to the *Acinetobacter* being among the dominant members of the spacecraft and healthcare microbiomes.

Therefore, to obtain molecular and quantitative insights into the tolerances of the cleanroom-associated *Acinetobacter*, we measured the impacts of Kleenol 30 on the survivals, cultivation kinetics, and intracellular and extracellular metabolomes. By design, we profiled *Acinetobacter* strains isolated from differing sub-locations within the NASA cleanrooms for spacecraft assembly (e.g., floor and spacecraft surface) which were subjected to differing cleaning regimes (e.g., Kleenol 30 for the floors vs. isopropyl alcohol and/or ethyl alcohol for spacecraft surfaces). Hence, comparisons across these sub-environments lend support toward the hypothesis that repeated cleansing under the conditions of spacecraft assembly serve as selective pressures that favor or promote biochemical tolerances toward the local cleaning conditions.

2. Materials and methods

2.1. Materials and conditions

Bacterial strains of *A. johnsonii* 2P08AA and *A. radioresistens* 50v1 were obtained through the Planetary Protection Culture Collection at the Jet Propulsion Laboratory. Stocks of ethanol (ENG Scientific) and Kleenol 30 (Mission Laboratories, Los Angeles, CA; Clovis Janitorial) were sterile filtered and stored as 200 µL aliquots at 4°C. Stock solutions of 25 mM Fe^{2+} were prepared using ferrous ammonium sulfate ($Fe(NH_4)_2(SO_4)_2{\cdot}6H_2O$; EM Science) in ultrapure water (18 $M\Omega^{-1}$), followed by sterile filtration (0.2 µm syringe filter, VWR), and storage as 200 µL aliquots at 4°C (with no visible precipitation over long term storage).

Concentrated minimal media (5x MM) were prepared using 30.0 g $Na_2HPO_4{\cdot}7H_2O$ (Sigma), 15.0 g KH_2PO_4 (EM Science), 2.50 g NaCl (Fisher Scientific), 5.00 g NH_4Cl (EM Science) per liter of ultrapure water. Low-osmolarity media (0.2x M9) were prepared by adding 0.4929 g $MgSO_4{\cdot}7H_2O$ (EM Science) and 0.0147 g $CaCl_2{\cdot}2H_2O$ (EM Science) to 200.0 mL 5x MM and dilution to 1.00 L using ultrapure water (to yield 1x M9), followed by an additional 5-fold dilution (200 mL 1x M9 in 1.00 L) to yield 0.2x M9. Final concentrations for ions in 0.2x M9 were 20 µM Ca^{2+}, 400 µM Mg^{2+}, 4.4 mM K^+, 10.7 mM Na^+, and 3.7 mM NH_4^+, along with 5.4 mM Cl^-, 4.5 mM $H_2PO_4^-$, 4.4 mM HPO_4^{2-}, and 0.4 mM SO_4^{2-}.

Lysogeny broth media (LB) were prepared using 10.0 g tryptone (VWR), 5.0 g yeast extract (Amresco), 5.0 g NaCl (Fisher Scientific) and 1 mL of 1 M NaOH (Sigma-Aldrich) per liter of ultrapure water. Agar plates were prepared using 1.0 L LB and 15 g agar (Amresco).

Cultivations were performed in 15 mL screw cap test tubes (Pyrex, borosilicate glass; 13 × 100 mm), which were washed with tap water, rinsed with distilled water, and autoclaved between experiments. All screw cap test tubes were capped tightly and wrapped with parafilm during cultivation to prevent loss of ethanol, which served as a sole supplied carbon source. Cultivations were performed with mild agitation (200 rpm) using a New Brunswick Scientific Innova 4,200 incubator. Cell densities were monitored during cultivation by following agar plate counts and changes in optical density (OD) at 600 nm (Spectronic 20 Genesys). All media were autoclaved at 121°C and 15 psi for 45 min.

2.2. Cultivations with Kleenol 30

Glycerol stocks of *A. radioresistens* 50v1 and *A. johnsonii* 2P08AA were separately streaked onto LB agar plates and incubated at 32°C for ~24 h. Isolated colonies were inoculated into 2.0 mL 0.2x M9 containing 25 μM Fe^{2+} and 0–2.0% *v/v* Kleenol 30 (or 0–40.0 μL). Pre-cultures were initiated by addition of 20.0 μL 90% *v/v* ethanol to yield final concentrations of 150 mM or 1.0% *v/v* ethanol. Pre-cultures were grown to late log phase (OD ~0.6 at ~12 h). Target cultures were prepared using fresh media (2.00 mL) which were inoculated with 20.0 μL (1:100 dilution) of the respective pre-cultures and initiated by addition of 1.0% *v/v* ethanol.

Temporal changes in OD were followed for 0–15 h. Growth kinetics were characterized by regression analysis (Microsoft Excel) using a modified version of the Gompertz equation (Begot et al., 1996), which describes a non-linear bacterial growth model, and yields the parameters of growth rate (k), lag time (L), and an estimate of the maximum change in relative biomass ($\log(N / N_0)$). All regressions were minimized by least squares analysis. Control cultures containing no inoculate showed no growth (OD ≤ 0.002), as did cultures containing inoculate but no ethanol (OD ≤ 0.002), which indicated negligible biological contamination and accumulation of abiotic particles during cultivation.

Survivals of late-log phase cultures (OD ~0.4) were assessed by plating onto LB agar plates. In control experiments, plate counts using 0.2x M9 agar plates supplemented with ethanol (just prior to use) yielded irreproducible results, when compared to LB agar plate, likely due to variances in adsorption of ethanol (under our conditions). For the plate count assays, therefore, aliquots (100 μL) of the cultures (in 0.2x M9/Fe) were transferred to 2.5 mL microcentrifuge tubes, decimally diluted by 10^6-fold using 0.2x M9, and spread (20 μL) onto LB agar plates using sterile plastic cell spreaders. All plates were sealed with parafilm and incubated at 32°C for 24 h. Plates with ≤300 colonies were enumerated and expressed as colony forming using per mL of the parent culture (cfu mL^{-1}).

2.3. Metabolomics of *Acinetobacter* cultivations in Kleenol 30

Cultures of *A. radioresistens* 50v1 and *A. johnsonii* 2P08AA were prepared as described and harvested during early stationary phase (OD ~0.6–0.7, 7–8 h) by centrifugation (3,500 rpm) at 4°C for 15 min (Beckman Coulter Allegra 21R). After centrifugation, the cell pellets and supernatant fractions were separated and, respectively, treated. The supernatants were saved as 500 μL aliquots, dried using a DNA 110 Savant DNA SpeedVac, and stored at −80°C. The pelleted cells were washed twice with 0.2x M9 and stored at −80°C.

Samples were characterized by the West Coast Metabolomics Center using gas chromatography and time-of-flight mass spectrometry (GC-TOF/MS). In brief, dried cells and culture broth were separately resuspended in 2 mL of pre-chilled (−20°C) and degassed extraction solvent (acetonitrile:isopropanol:water, 3:3:2), vortexed for 30 s, shaken for 5 min at 4°C, clarified by centrifugation (~12,000 g), and the resulting supernatant evaporated to dryness. Samples were derivatized by resuspension in 10 μL of 40 mg/mL methoxyamine hydrochloride in pyridine (30°C, 1.5 h) followed by addition of 41 μL N-methyl-N-(trimethylsilyl) trifluoroacetamide (80°C, 30 min); fatty acid methyl esters (e.g., C8-C30) were additionally added to serve as retention index markers (Barupal et al., 2019).

Samples were transferred to crimp top vials and separated on an Agilent 6,890 Gas Chromatograph equipped with a Gerstel automatic liner exchange system (ALEX), multipurpose sample (MPS2) dual rail, Gerstel CIS cold injection system (Gerstel, Muehlheim, Germany), and built-in gas purifier (Airgas, Radnor PA). Chromatographic separation was afforded using a 30 m (0.25 mm i.d.) Rtx-5Sil MS column (0.25 μm 95% dimethyl 5% diphenyl polysiloxane film) with an additional 10 m integrated guard column (Restek, Bellefonte PA). Carrier gas was 99.9999% pure Helium with a constant flow of 1 mL/min.

Sample volumes of 0.5 μL were injected with a 10 μL s^{-1} injection speed on a spitless injector with a purge time of 25 s. Temperature profile included 1 min at 50°C for the oven temperature, an increase of 20°C min^{-1} to 330°C across 14 min, with a final hold for 5 min at 330°C. A temperature of 280°C was used for the transfer line between the gas chromatograph and Leco Pegasus IV time of flight mass spectrometer (single mass analyzer). The measured mass range was 85–500 Da, scan rate was at 17 spectra s^{-1}, electron energy was 70 eV, ion source temperature was 250°C, and detector voltage was 1850 V. Spectra were acquired using the Leco ChromaTOF software vs. 2.32 (St. Joseph, MI) and processed using the BinBase database system (Fiehn et al., 2005, 2010; Trigg et al., 2019), which quantifies (signal-to-noise ratio of 5:1) and matches mass peaks to the Fiehn mass spectral library using retention index (RI) and reference mass spectral information (which are internally compiled by the West Coast Metabolomic Center). Metabolomic data (Study ID ST002380, DatatrackID: 3552) were stored at the NIH Common Fund's National Metabolomics Data Repository (Sud et al., 2016).

2.4. Statistical analyses

Comparisons of the cultivation kinetic parameters were conducted using unpaired Student's t-tests and one- and two-way ANOVA analyses (Microsoft Excel), where statistical relevance was accepted at $p < 0.05$, normal distribution of the data was supported by Shapiro–Wilk tests (Past 4.10; Hammer et al., 2001), and variances were assumed as equal. Metabolomic data were compared using univariate, multivariate, and visual approaches.

Discrete changes in the metabolomes (e.g., trends for a single metabolite) were identified using unpaired Student's *t*-tests (Microsoft Excel) with corrections for multiple testing using a false discovery rate (FDR) of FDR ≤ 0.20 (Benjamini and Hochberg, 1995). For the 700 metabolites in the total study (whole cell and extracellular metabolomes from 2 bacterial strains treated with and without Kleenol 30), normal distributions (Shapiro–Wilk Tests) were indicated for ~92% (646) of the

metabolites. To account for potential underestimations of normality given the sample size ($n = 3$), metabolites exhibiting thresholds for normality of $p > 0.03$ (Shapiro–Wilk Tests) *and* significance of $p < 0.05$ (Student's *t*-tests) were carried forward in the univariate and visual assessments of the data.

Broad structural and metabolic trends were obtained by visualizing the changes in the metabolomes ($p < 0.05$) using MetaMapp[1] and Cytoscape 3.9.1[2] (Barupal et al., 2012), which constitute a statistical organizational approach to yield visual maps of metabolites arranged by known structural patterns and metabolic pathways. Confirmation of broad changes in the metabolomes were obtained using ChemRich[3] (Barupal and Fiehn, 2017), a statistical enrichment tool that compares groups of metabolites based on structural and biochemical classes. For this study, the standard and user-defined classifications in ChemRich included amino acids, monosaccharides, sugar acids, organic acids, fatty acids, lipid-related metabolites, nucleotide-related metabolites, and compatible solutes. Multivariate tests were conducted using canonical correspondence analyses (Past 4.10; Hammer et al., 2001) to correlate the metabolomic trends to differing cultivation growth parameters and conditions.

3. Results

3.1. Cultivation and survival in the presence of Kleenol 30

In Figure 1A we show that the cleanroom-associated *Acinetobacter* tested in this study, *A. johnsonii* 2P08AA and *A. radioresistens* 50v1, readily grow in the presence of ≤1% v/v Kleenol 30 (K30) under low-osmolarity aqueous conditions with ethanol serving as the sole supplied carbon source. Cultivations on 2% v/v K30 did not yield measurable cell densities.

In 0.1% v/v K30, cultures of the floor-associated *A. johnsonii* 2P08AA show no apparent loss in survival, as plate counts (~late log phase) effectively show no difference ($p > 0.05$) in the presence ($2.1 \pm 0.5 \times 10^7$ cfu mL^{-1}) and absence ($2.6 \pm 0.1 \times 10^7$ cfu mL^{-1}) of the detergent. These trends indicate quantitative survival of the 2P08AA strain in the presence of 0.1% v/v K30.

For the spacecraft surface-associated *A. radioresistens* 50v1, in contrast, survivability in 0.1% v/v K30 readily decreases ($p = 0.006$) to 46 ± 6% (propagated error) – as calculated by comparison of cultures cultivated in the presence ($4.0 \pm 0.4 \times 10^7$ cfu mL^{-1}) and absence ($8.8 \pm 0.7 \times 10^7$ cfu mL^{-1}) of 0.1% v/v K30. These trends are indicative of ~50% survival in the presence of 0.1% v/v K30.

In 1.0% v/v K30, survivabilities for the 2P08AA strain (26 ± 12%) and 50v1 strain (22 ± 8%) decrease to similar values – as indicated by comparison of cultures cultivated in the presence (2P08AA, $0.7 \pm 0.3 \times 10^7$ cfu mL^{-1}; 50v1, $1.9 \pm 1.1 \times 10^7$ cfu mL^{-1}) and absence (2P08AA, $2.6 \pm 0.1 \times 10^7$ cfu mL^{-1}; 50v1, $8.8 \pm 0.7 \times 10^7$ cfu mL^{-1}) of 1.0% v/v K30. These trends are indicative of ~70–80% inhibition in the presence of 1.0% v/v K30 across both strains.

3.2. Impacts of Kleenol 30 on the cultivation kinetics

Displayed in Figures 1B–D and Figure 2 are the cultivation kinetic parameters and associated growth curves for *A. johnsonii* 2P08AA and *A. radioresistens* 50v1. Optical measurements (Figure 2, empty blue circles) for cultures were converted to the ratiometric changes in relative biomass (N / N_0) by assuming a direct relationship between optical transmittance and cell density for the initial culture media (N_0) and at the time of measurement (N), as outlined in Begot et al. (1996). Changes in relative biomass (Figure 2, filled red circles, fitted line) were expressed as a log function ($\log(N / N_0)$), plotted over time, and fit to a modified version of the Gompertz equation (Eq. 1), as detailed in Begot et al. (1996) and Mogul et al. (2018). Minimized regressions yielded the parameters of growth rate (k; cell divisions h^{-1}), estimated time in lag phase (L; h), and log of the maximum increase in relative biomass ($\log(N / N_0)_{max}$; unitless dimension).

To account for optical scattering, the maximum increases in relative biomass ($\log(N / N_0)_{max}$) were broadly interpreted as maximum increases in intact cells, cellular aggregation, and/or intra- and extracellular polymeric substances at stationary phase. Reported in this study are the averaged values from the minimized regressions along with standard errors ($n = 3$–5 biological replicates).

$$\log\left(\frac{N}{N_0}\right) = \log\left(\frac{\Delta OD}{\Delta OD_{min}}\right) = A \cdot \exp\left(-\exp\left(\frac{k \cdot e}{A} \cdot (L - t) + 1\right)\right) \quad (1)$$

Comparisons of the growth rates (k) show ~18% decreases for cultivations of the 2P08AA strain in 0.1% v/v K30 ($p = 0.029$) – as calculated by comparison of the difference in growth rates (Figure 1B) between the absence (0.50 ± 0.01 h^{-1}) and presence (0.41 ± 0.02 h^{-1}) of 0.1% v/v K30. The 50v1 strain, in contrast, shows no change in growth rate ($p = 0.05$) in 0.1% v/v K30 – as calculated by comparison of rates (Figure 1B) in the absence (0.39 ± 0.01 h^{-1}) and presence (0.40 ± 0.02 h^{-1}) of 0.1% v/v K30. When cultivated in 1.0% v/v K30, growth rates for the 2P08AA strain (0.22 ± 0.03 h^{-1}) and 50v1 strain (0.35 ± 0.01 h^{-1}) decrease by ~56% ($p = 0.001$) and ~13% ($p = 0.043$), respectively, as calculated by comparison rates (Figure 1B) in the absence (2P08AA, 0.50 ± 0.01 h^{-1}; and 50v1, 0.39 ± 0.01 h^{-1}) of the detergent.

Comparisons by one factor ANOVA analyses confirm that cultivations in the presence of 0.1–1.0% v/v K30 significantly impact the respective growth rates for the 2P08AA ($p = 0.038$, $f = 4.256$) and 50v1 ($p = 0.0002$, $f = 4.459$) strains. Additionally, two factor ANOVA analyses confirm that cultivations in the presence of K30 differentially impact the growth rates of the 2P08AA and 50v1 strains ($p = 0.015$, $f = 5.318$). These combined trends for exponential phase behavior are indicative of higher tolerances toward K30 by the 50v1 strain at 0.1 and 1.0% K30. These trends are opposite to those from plate counts at late-log phase, which indicate a higher tolerance for the 2P08AA strain.

Comparisons of the lag times (L) in 0.1 and 1.0% v/v K30 show decreases for both strains during cultivation (Figure 1C), which is unexpected since the addition of detergents was presumed to inhibit growth and increase the time in lag phase. For the 2P08AA strain, the native lag time of 0.77 ± 0.23 h^{-1} (absence of K30) reduces to negligible values (~0 h) in 0.1 and 1.0% v/v K30. For the 50v1 strain, the native lag time of 2.61 ± 0.24 h^{-1} is ~3-fold longer than 2P08AA strain and decreases by ~70% in 0.1% v/v K30 (0.76 ± 0.15 h^{-1}) and to negligible values in 1.0% v/v K30.

1 http://metamapp.fiehnlab.ucdavis.edu/ocpu/library/MetaMapp2020/www/

2 https://cytoscape.org/

3 https://chemrich.fiehnlab.ucdavis.edu/

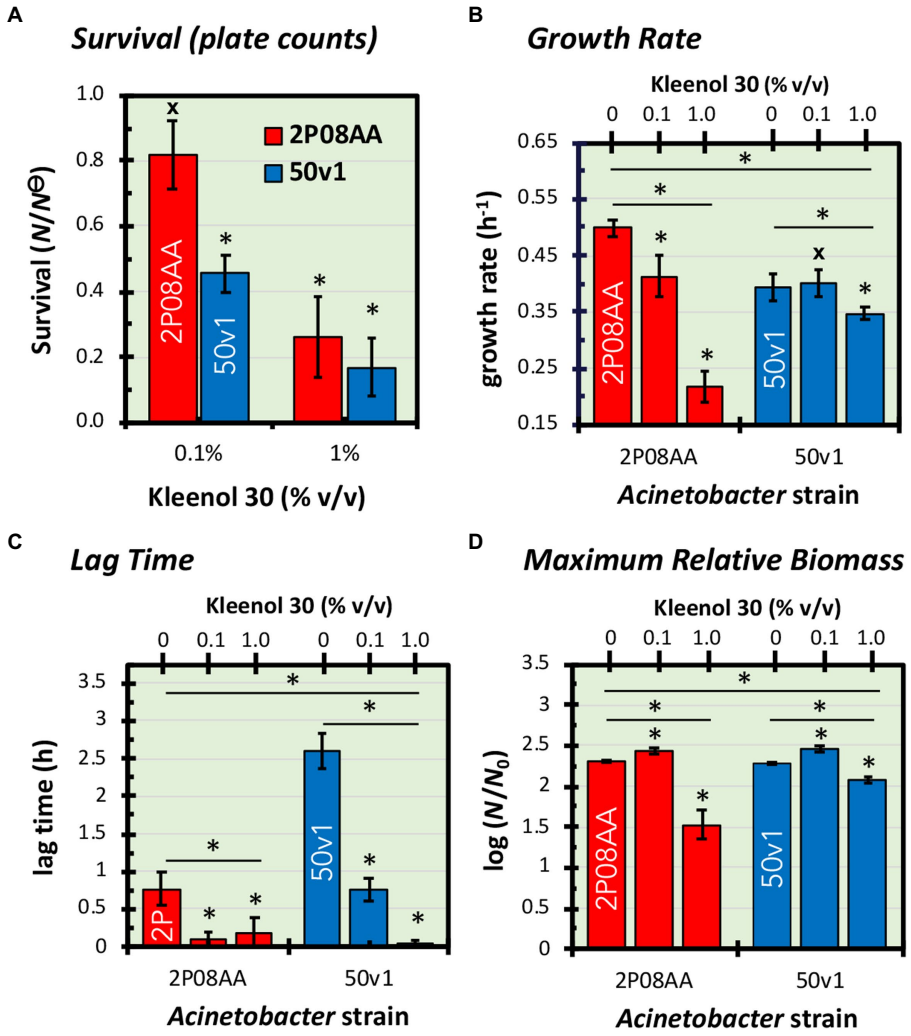

FIGURE 1
Impacts of 0–1.0% v/v Kleenol 30 (K30) on **(A)** the survival and **(B–D)** cultivation kinetics of *Acinetobacter johnsonii* 2P08AA (red) and *Acinetobacter radioresistens* 50v1 (blue). Survival ($N/N^{\ominus}$) is expressed as the ratio of plate counts (cfumL^{-1}) from cultures grown in the absence of K30 ($N^{\ominus}$) and presence of K30 **(N)**. Fitted regressions of growth curves yielded changes in **(B)** growth rates (h^{-1}), **(C)** lag time (h), and **(D)** maximum relative biomass (log (N/N_0)), which is assumed to represent a ratio of the total biomass (N) at stationary phase and the biomass at the start of the culture (N_0). Error bars represent the standard errors (n=4–5, growth curves; n=3–5, plate counts). Univariate tests are represented as asterisks (*) for t-tests with $p < 0.05$, hashtags (#) for t-tests with $p \geq 0.05$, and asterisks (*) with an underlying line for one or two-way ANOVA with $p < 0.05$.

Comparisons by one factor ANOVA analyses confirm that cultivations in the presence of 0.1–1.0% v/v K30 significantly impact the respective lag times for the 2P08AA ($p = 0.00008$, $f = 4.256$) and 50v1 ($p = 0.015$, $f = 4.459$) strains. Additionally, two factor ANOVA analyses confirm that cultivations in the presence of K30 differentially impact the lag times for the 2P08AA and 50v1 strains ($p = 0.006$, $f = 5.318$). These combined trends indicate that K30 induces accelerated entry into the exponential phase in a concentration dependent manner, where the lag phase for the 2P08AA strain is effectively eliminated at ~10-fold lower K30 abundances when compared to the 50v1 strain – under these conditions.

Comparisons of the maximum change in relative biomass ($\log(N/N_0)_{max}$) for cultivations in 0.1% v/v K30 show unexpected increases for both strains (Figure 1D). For the 2P08AA strain, cultivations in 0.1% v/v K30 yield ~40% increases ($p = 0.026$) in maximum apparent biomass when comparing values obtained in absence (2.30 ± 0.02) and presence of (2.44 ± 0.04) of 0.1% v/v K30 and accounting for the log transformation. Similarly, for the 50v1 strain, cultivations in 0.1% v/v K30 yield ~55% increases ($p = 0.048$) in maximum apparent biomass when comparing values obtained in absence (2.28 ± 0.01) and presence of (2.47 ± 0.04) of 0.1% v/v K30 and accounting for the log transformation. When cultivated in 1.0% v/v K30, the 2P08AA strain (1.53 ± 0.18) and 50v1 strain (2.07 ± 0.03) exhibit decreases of ~80% and ~40% in maximum apparent biomass, respectively, which is consistent with the decreased growth rates under these conditions (~56 and ~13%, respectively).

Comparisons by one factor ANOVA analyses confirm that cultivations in the presence of 0.1–1.0% v/v K30 significantly impact the respective maximum changes in relative biomass for the 2P08AA ($p = 0.000003$, $f = 4.256$) and 50v1 strains ($p = 0.000004$, $f = 4.459$). Additionally, two factor ANOVA analyses confirm that cultivations in

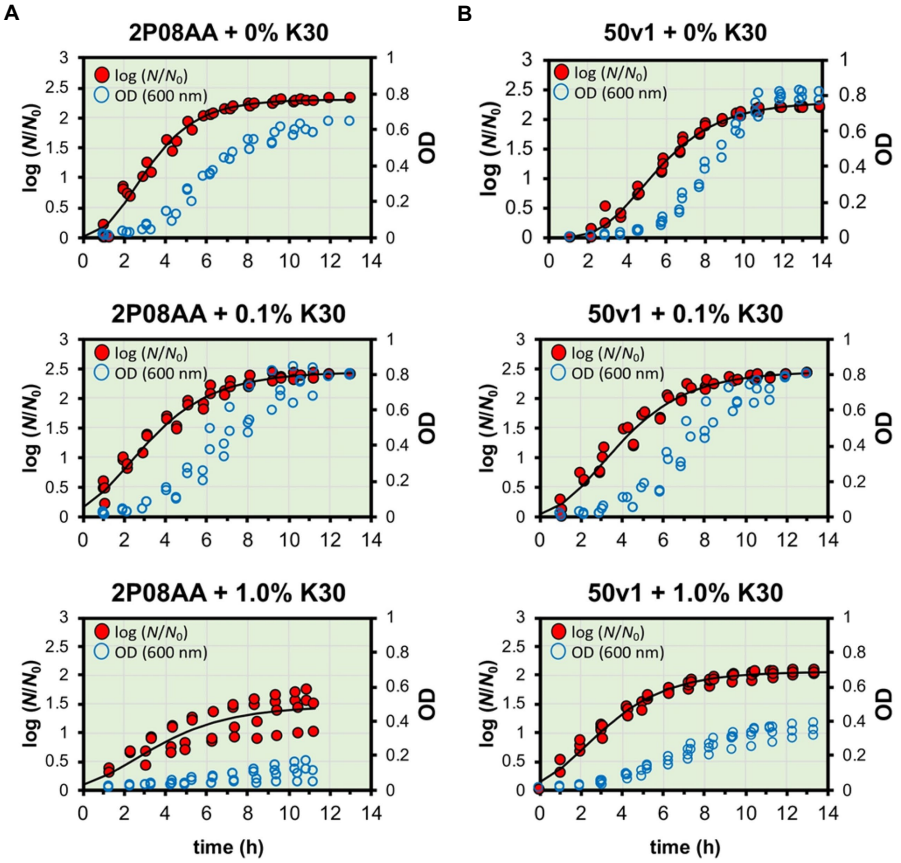

FIGURE 2
Measured and fitted growth curves for *A. johnsonii* 2P08AA (left panel) and *A. radioresistens* 50v1 (right panel) cultured in the presence of 0–1.0% v/v Kleenol 30 at 28°C in 0.2x M9 media containing 25μM Fe^{2+} and 150mM ethanol (the sole supplied carbon source). Optical density measurements (blue empty circles; right-hand y-axis) were converted to log(N/N_0) (red filled circles; left-hand y-axis) as described and fit by non-linear regression to yield the parameters of time in lag phase, growth rates, and maximum ratiometric and logarithmic change in biomass (log (N/N_0)) at stationary phase.

the presence of K30 differentially impact the maximum changes in relative biomass for the 2P08AA and 50v1 strains ($p = 0.007$, $f = 5.318$). Combined, these trends suggest that 0.1% v/v K30 induces changes in apparent biomass in stationary phase.

3.3. Impacts of Kleenol 30 on the intracellular metabolomes

3.3.1. Metabolomic considerations

Metabolomes from whole cells of *A. johnsonii* 2P08AA and *A. radioresistens* 50v1 were compared after cultivation in the absence and presence of 0.1% v/v Kleenol 30 (early stationary phase). Per strain, whole cell extracts yielded a total of 119 intracellular metabolites and free metabolites from the membrane (e.g., free fatty acids and monoacylglycerols). Metabolites from both strains showing important changes ($p < 0.05$) due to cultivation with K30 are listed in Table 1, as are changes (fold-changes) in the respective abundances; changes retaining significance ($p < 0.05$, FDR ≤ 0.20) after correction for multiple testing are underlined.

Displayed in Figure 3 are metabolomic maps for the 2P08AA and 50v1 strains, which readily show the changes resulting from cultivation in K30. The metabolomic maps (MetaMapp graphs) in Figure 3 are organized *via* networks of KEGG reactant pairs (black edges or arrows) and Tanimoto chemical similarity scores (gray edges or arrows). Detected metabolites are presented as nodes (circles). Important changes are highlighted as red nodes (increases in relative abundance), blue nodes (decreases in relative abundance), or yellow nodes (no change). Node sizes signify the relative degree of change (or fold-change).

For the 2P08AA strain (Figure 3A), cultivations in 0.1% v/v K30 yield no statistically discernable impacts to the whole cell metabolome. No changes are observed after accounting for multiple testing (FDR ≤ 0.20, $n = 119$). No changes are observed when parsing the data using ChemRich. While potential increases ($p < 0.05$) are observed in gluconate, analyses in ChemRich provide no support for broad changes in sugar acid content. Despite the potential ($p < 0.05$) decreases in arabinose and increases in sorbitol, analyses in ChemRich show no support for broad changes in monosaccharide composition. Similarly, ChemRich analyses provide no support for broad changes in lipid-related metabolites despite the potential ($p < 0.05$) decreases in phosphoethanolamine and increases in ethanolamine and behenic acid (22:0; long chain saturated fatty acid).

In contrast, the 50v1 strain displays *multiple* changes in the intracellular metabolome due to cultivation in 0.1% v/v K30 (Table 1). After correction for multiple testing (n = 119), significant decreases are observed for lysine, homoserine, ornithine, mannitol, adenosine-5′-monophosphate (5’-AMP), 5′-methylthioadenosine (5′-MTA), and 2,5-dihydroxypyrazine. The whole cell metabolomic maps for the 50v1

10.3389/fmicb.2023.1090740

TABLE 1 Numbered list of metabolites from whole cell extracts of *Acinetobacter johnsonii* 2P08AA and *Acinetobacter radioresistens* 50v1, where the magnitude of decreases (↓) or increases (↑) in the relative abundances after cultivation in 0.1% v/v Kleenol 30 ($p<0.05$) are listed in differing columns and presented in heat-map type coloring to visually represent the magnitude of decreasing (↓: light to dark blue) or increasing (↑: light green to dark red) abundances; the column label of ID# represents the metabolites numbered in Figure 3, CID is the associated PubChem Compound ID, RI is the associated retention index, m/z is the mass to charge ratio for the associated derivatized metabolite, fold-changes represent the ratio of abundances obtained in presence and absence of the K30, asterisks (*) indicate relevance after correction for multiple testing (FDR≤0.20), dashes indicate that the metabolite was not detected, and gray boxes indicate that the option is not applicable.

Whole cell metabolites					2P08AA		50v1	
ID#	Biochemical class	CID	RI	*m/z*	Fold-change			
Amino acids					↓	↑	↓	↑
1	Glycine	750	368,707	248	–	–	1.7	
2	Lysine	5,962	663,483	156	–	–	4.8*	
3	Proline	145,742	364,523	142	–	–	6.0	
4	Serine	951	395,020	218	–	–	1.7	
5	Valine	6,287	313,502	144	–	–	2.2	
6	β-alanine	239	435,564	248	–	–	2.1	
7	Citrulline	750	621,404	157	–	–	2.9	
8	Homoserine	12,647	396,135	146	–	–	2.4*	
9	Ornithine	6,262	594,051	174	–	–	2.9*	
10	Alanine–alanine	5,484,352	636,898	188	–	–	1.7	
Dicarboxylic acids					↓	↑	↓	↑
11	Fumaric acid	444,972	390,016	245	–	–		2.2
12	Malic acid	525	463,180	233	–	–		2.2
13	Tartartic acid	444,305	534,291	292	–	–		1.4
Sugar acids					↓	↑	↓	↑
14	Gluconic acid	6,857,417	693,148	333		5.1	–	–
15	3-phosphoglycerate	724	610,734	227	–	–	4.0	
16	Glyceric acid	439,194	377,495	189	–	–	4.1	
Monosaccharides					↓	↑	↓	↑
17	Arabinose	6,902	550,621	217	1.8		1.9	
18	Mannitol	6,251	663,215	319	–	–	3.7*	
19	Sorbitol	5,780	667,922	217		4.9	–	–
Fatty acids and lipids					↓	↑	↓	↑
20	Behenic acid (22:0)	8,215	920,648	117		15	–	–
21	Ethanolamine	700	344,719	174		2.5	–	–
22	Isopentadecanoic acid	151,014	663,518	117	–	–	2.1	
23	Phosphoethanolamine	1,015	604,335	299	2.9		–	–
24	Stearic acid	5,281	787,622	117	–	–		1.5
Nucleotide-related					↓	↑	↓	↑
25	5'-AMP	6,083	1,038,688	169	–	–	4.5*	
26	5'-CMP	6,131	700,635	243	–	–		1.6
27	5′-MTA	439,176	967,036	236	–	–	4.0*	
28	pyrophosphate	1,023	327,517	110	–	–	2.1	
Pyrimidines					↓	↑	↓	↑
29	Thymidine	5,789	349,402	170	–	–	1.4	
30	Uracil	1,174	385,735	241	–	–	2.1	
Other					↓	↑	↓	↑
31	2,5-dihydroxypyrazine	23,368,901	397,526	241	–	–	4.1*	

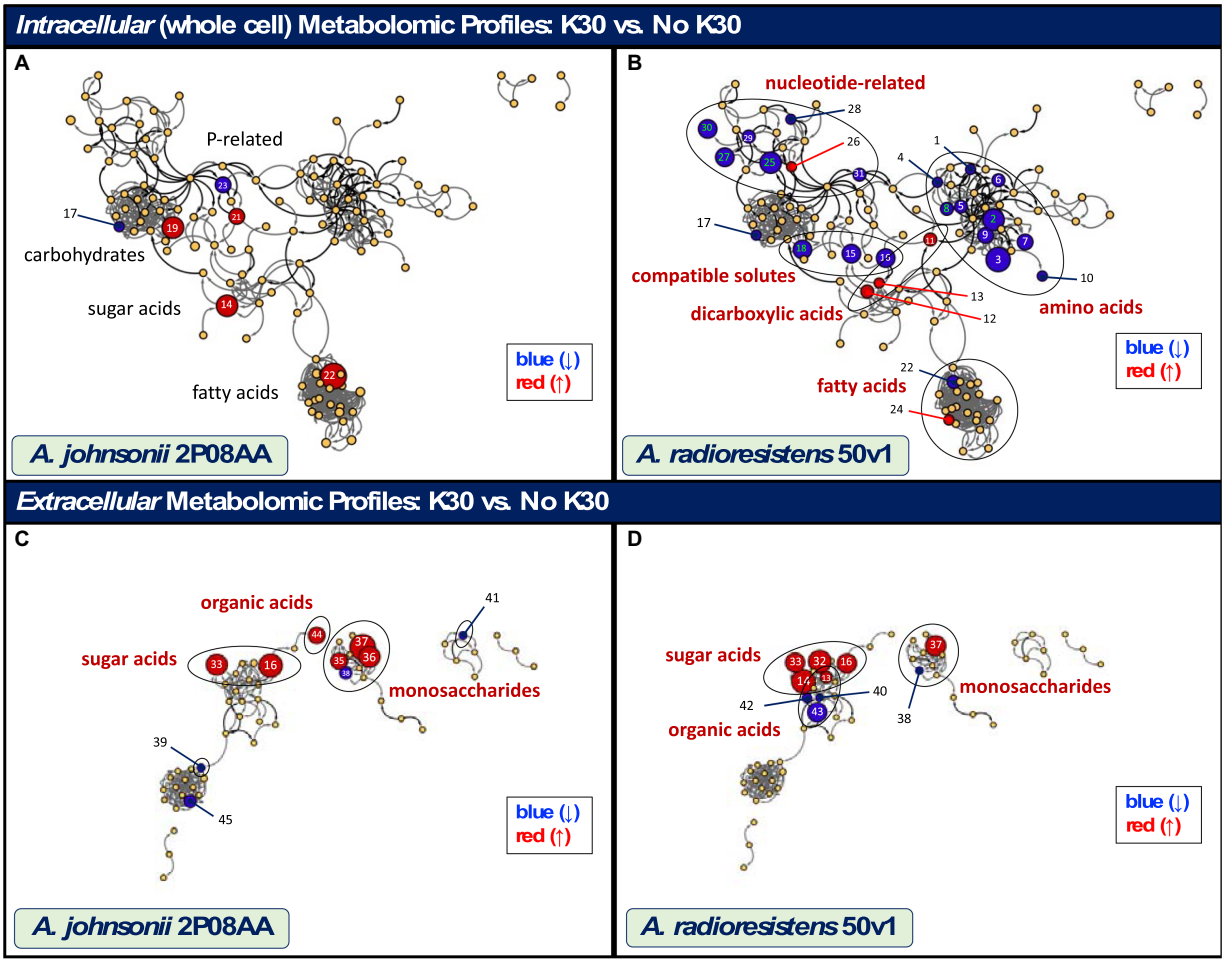

FIGURE 3
Maps showing the impacts of cultivation in 0.1% v/v K30 on the intracellular and extracellular metabolomes of *A. johnsonii* 2P08AA **(A–C)** and *A. radioresistens* 50v1 **(B,D)**. Metabolites are represented as nodes and organized by structural and metabolic connections (MetaMapp and Cytoscape 3.9.1). Important changes in abundance ($p < 0.05$) are represented as red (increases), blue (decreases), and yellow (no change) nodes, where node sizes represent the degree of change. Relevant metabolites that show important (black text; $p < 0.05$) and significant changes (red text; $p < 0.05$; FDR≤0.20), as listed in Tables 1, 2, are displayed using the associated identity numbers (ID#). Shaded circles represent biochemical classes (red text) that show significant changes (ChemRich); biochemical classes showing no change are listed for comparison purposes (black text).

strain in Figure 3B were parsed using MetaMapp and ChemRich and expand on the univariate analyses to reveal differential changes in amino acids, compatible solutes, nucleotide-related metabolites, dicarboxylic acids, sugar acids, and saturated fatty acids.

Impacts to amino acids ($p = 9.1\times10^{-6}$; $Q = 6.7 \times 10^{-5}$; ChemRich) are supported by decreases in the relative abundances of standard amino acids (glycine, lysine, proline, serine, and valine), non-standard amino acids (β-alanine, homoserine, ornithine, and citrulline), and a peptide (alanine–alanine). Dimerization of glycine under the analytical conditions is suggested by detection of 2,5-dihydroxypyrazine (Haffenden and Yaylayan, 2005) with the observed decreases in 2,5-dihydroxypyrazine in cultures with K30 being generally consistent with the decreases in glycine.

Impacts to compatible solutes ($p = 9.6\times10^{-6}$; $Q = 6.7 \times 10^{-5}$; ChemRich) are supported by decreases in mannitol (Empadinhas and da Costa, 2008; Tam et al., 2022), as well as glycerate and 3-phosphoglycerate, which are involved in the biosynthesis of compatible solutes (Franceus et al., 2017). Impacts to nucleotide-related metabolites ($p = 5.2\times10^{-4}$; $Q = 2.4 \times 10^{-3}$; ChemRich) are supported by decreases in 5'-AMP, MTA, pyrophosphate, thymidine, and uracil, along with increases in cytidine-5′-monophosphate (5'-CMP). Impacts to dicarboxylic acids ($p = 4.8\times10^{-3}$; $Q = 1.7 \times 10^{-2}$; ChemRich) are supported by increases in fumarate, malate, and tartrate. No impacts to saturated fatty acids are observed ($p = 0.11$; $Q = 0.31$; ChemRich) despite the decreases in isopentadecanoic acid (branched saturated fatty acid; 13-methyl-14:0, or 15:0 iso) and increases in stearic acid (saturated fatty; 18:0).

3.3.2. Metabolic considerations

Cross referencing of the metabolomic changes to the KEGG database yields probable impacts to several intracellular pathways for the 50v1 strain. Provided in parentheses are the associated KEGG pathway or reaction identifiers.

Inhibition or reduction in Glycine, Serine, and Threonine Metabolism (map00260) is supported by decreases in intracellular glycerate, 3-phosphoglycerate, serine, glycine, and homoserine. Inhibition or reduction in Lysine Biosynthesis (map00300) and Valine, Leucine, and Isoleucine Biosynthesis (map00290) is supported by decreases in lysine and valine; however, no other changes are noted in the respective pathways.

10.3389/fmicb.2023.1090740

TABLE 2 Numbered list of extracellular metabolites from cultures of *A. johnsonii* 2P08AA and *A. radioresistens* 50v1, where the magnitude of decreases (↓) or increases (↑) in the relative abundances after cultivation in 0.1% v/v Kleenol 30 ($p<0.05$) are listed in differing columns and presented in heat-map type coloring to visually represent the magnitude of decreases (↓: light to dark blue) or increases (↑: light green to dark red); the ID# represents the metabolite number from Figure 3 and continues with the numbering order from Table 1, CID is the PubChem Compound ID, RI is the associated retention index, m/z is the mass to charge ratio for the associated derivatized metabolite, fold-changes represent the ratio of abundances obtained in presence and absence of the K30, asterisks (*) indicate relevance after correction for multiple testing (FDR≤0.20), dashes indicate that the metabolite was not detected, gray boxes indicate that the option is not applicable.

Extracellular metabolites					2P08AA		50v1	
ID#	Biochemical class	CID	RI	*m/z*	Fold-change			
Sugar acids					↓	↑	↓	↑
32	Galactonic acid	128,869	690,882	292	–	–		36*
14	Gluconic acid	6,857,417	693,148	333	–	–		46*
33	Gluconolactone	7,027	645,815	220		22		8.8*
16	Glyceric acid	439,194	377,495	189		34		9.3*
34	2-Methylgyceric acid	560,781	372,491	219				1.9
Monosaccharides					↓	↑	↓	↑
35	Fructose	439,709	639,442	307		4.5	–	–
36	Galactose	439,357	647,344	319		22	–	–
37	Mannose	18,950	645,856	205		57		20*
38	Ribose	5,779	553,078	217	2.5		1.9*	
Di and monocarboxylic acids					↓	↑	↓	↑
39	Adipic acid	196	474,435	111	1.9		–	–
13	Tartaric acid	444,305	534,291	292	–	–		2.9*
40	Citramalic acid	1,081	456,203	247	–	–	1.6	
41	3,4-Dihydroxybenzoic acid	72	620,200	193	2.0		–	–
42	4-Hydroxybutanoic acid	10,413	325,027	233	–	–	2.4*	
43	α-ketoglutarate	51	507,392	198	–	–	9.0*	
44	Oxalic acid	971	260,513	190		5	–	–
Fatty acids					↓	↑	↓	↑
45	Pelargonic acid	8,158	399,229	117	3.1		–	–

Inhibition or reduction in proline and arginine biosynthesis through Arginine and Proline Metabolism (map00330) and Arginine Biosynthesis (map00220) are supported by decreases in ornithine, citrulline, and proline. The lack of changes in abundances for urea indicate no measurable impact on the flux of the urea cycle – despite the decreases in ornithine and citrulline. The lack of observed arginine is suggestive of conversion of arginine to ornithine under the analytical conditions (Halket et al., 2005) or the limited presence of free arginine in the cell.

Inhibition or reduction in Peptidoglycan Biosynthesis (map00550) and/or peptide (protein) synthesis is suggested by decreases in alanine–alanine. Inhibition or reduction in β-alanine metabolism (map00410) is supported by decreases in β-alanine, which in turn is suggestive of reductions in arginine and uracil degradation. Differential changes in fatty acid metabolism (map01212) are suggested by the decreases in free isopentadecanoic acid (Reaction R02663) and increases in free stearic acid.

Inhibition or altered flux through glycolysis (map00010) is suggested through decreases in 3-phosphoglycerate. Activation or altered flux through components of the TCA cycle are suggested by increases in fumarate and malate. Inhibition or reduced flux of selected monosaccharides through Fructose and Mannose Metabolism (map00051) and Pentose and Glucuronate Interconversions (map00040) are, respectively, suggested by decreases in mannitol and arabinose.

Differential changes in Nucleotide Metabolism (map01232) are suggested by increases in 5'-CMP and 5′-MTA, along with decreases in 5'-AMP, pyrophosphate, thymidine, and uracil. Additionally, inhibition or reduction in Pyrimidine Metabolism (map00240) is suggested decreases by uracil and thymidine.

3.4. Impacts of Kleenol 30 on the extracellular metabolomes

Displayed in Figure 3 are biochemical maps that compare the extracellular metabolomes from *A. johnsonii* 2P08AA and *A. radioresistens* 50v1 (early stationary phase). Per strain, dried cultivation broth (cell free) yielded a total of 56 metabolites, which were processed and visualized as described above. Listed in Table 2 are the extracellular metabolomic changes in the 2P08AA and 50v1 strains after cultivation in the absence and presence 0.1% v/v K30. Pathway analyses were not conducted for extracellular metabolites.

When grouped by biochemical classes, cultivations of the 2P08AA strain in K30 yield differential impacts to extracellular sugar acids, monosaccharides, and organic acids (di- and monocarboxylic acids).

Yet, univariate tests show no changes after correction for multiple testing. Impacts to sugar acids ($p = 1.4\times10^{-5}$; $Q = 6.9\times10^{-5}$; ChemRich) are supported by substantial increases in extracellular gluconolactone (22-fold) and glycerate (34-fold). Impacts to di- and monocarboxylic acids, which were grouped as organic acids ($p = 3.0\times10^{-4}$; $Q = 7.6\times10^{-4}$; ChemRich), are supported by increases in oxalate and decreases in adipic acid (hexanedioic acid) and 3,4-dihydroxybenzoate (protocatechuate). Impacts to extracellular monosaccharides ($p = 7.6\times10^{-3}$; $Q = 1.3\times10^{-2}$; ChemRich) are supported by substantial increases in extracellular fructose (4.5-fold), galactose (22-fold), and mannose (57-fold) and decrease (2.5-fold) in extracellular ribose (pentose).

In contrast, cultivations of the 50v1 strain in K30 – after correction for multiple testing ($n = 56$) – yield significant changes in the extracellular galactonate, gluconate, gluconolactone, glycerate, mannose, ribose, tartrate, 4-hydroxybutyrate, and α-ketoglutarate. Likewise, grouping by biochemical classes are reveals significant changes in the extracellular metabolome.

Impacts to sugar acids ($p = 1.9\times10^{-8}$; $Q = 9.6\times10^{-8}$; ChemRich) are supported by substantial increases in extracellular galactonate (36-fold), gluconate (46-fold), gluconolactone (8.8-fold), glycerate (9.3-fold), and 2-methylglycerate (1.9-fold). Impacts to extracellular organic acids ($p = 7.8\times10^{-2}$; $Q = 0.16$; ChemRich) are suggested by the significant increases in tartrate and significant decreases in α-ketoglutatate, along with the potential decreases in citramalate and 4-hydroxybutyrate. Impacts to extracellular monosaccharides ($p = 9.6\times10^{-2}$; $Q = 0.16$; ChemRich) are suggested by significant increases in extracellular mannose (20-fold) and significant decreases in ribose (2.5-fold).

3.5. Impacts of Kleenol 30 on cultivation and the intracellular metabolome

3.5.1. Canonical correlation analyses

In Figure 4, we use canonical correlation analyses (CCA) to, respectively, compare metabolomes from *A. johnsonii* 2P08AA ($n = 3$) and *A. radioresistens* 50v1 ($n = 3$) to differing quantitative descriptors characterizing changes in the cultivation media and growth kinetics in the absence and presence of 0.1% v/v K30. Correlations for the intracellular (or whole cell) metabolomes from late log-phase cultures were assessed against growth rates at exponential phase, plate counts at late-log phase, maximum relative biomass at stationary phase, and total detergent concentrations in the media, which were assumed to be 0.025% w/w in cultures containing 0.1% v/v K30.

The CCA plots include the total array of detected metabolites (text), listed quantitative descriptors (vector lines), and transformed data after dimension reduction (glyphs). For the 2P08AA and 50v1 strains, stronger correlations along CCA Axis 1 (61.70, 69.46%) are observed when compared to CCA Axis 2 (24.72, 23.70%), respectively. Dimension reduction for the metabolomes from the 2P08AA and 50v1 strains (Figures 4A,B) respectively show clear separations between samples prepared in the absence and presence of 0.1% v/v K30. These trends suggest that the intracellular metabolomic compositions of both strains are impacted by K30 during cultivation. Described in the following sub-sections are comparisons to the quantitative descriptors. For selected metabolites, additional clarifications and/or fatty acid abbreviations are provided in parentheses.

3.5.2. Comparisons to survival

When considering changes in survival (Figure 4A), the vector describing plate counts for the 2P08AA strain (late log phase) overlaps with the reduced terms associated with 0% v/v K30 (filled red squares). This correlation suggests that survival trends for the 2P08AA strain (across 0 to 0.1% v/v K30) are associated with limited changes in the intracellular metabolome. This assessment is consistent with the associated univariate tests which indicate no changes in plate counts ($p > 0.05$) or metabolite abundances for the 2P08AA strain in 0.1% v/v K30 (FDR > 0.20).

From the CCA plot for the 2P08AA strain (Figure 4A), metabolites trending alongside the plate counts include trehalose, trehalose-6-phosphate, fructose-6-phosphate, and potentially glucose-6-phosphate. Univariate tests infer no changes in the abundances for these metabolites ($p > 0.05$ or FDR > 0.20). These trends suggest that the quantitative survival for the 2P08AA strain (in part) relates to lack of changes in central metabolism and compatible solute formation.

For the 50v1 strain (Figure 4B), the vector describing plate counts overlaps with the reduced terms associated with 0% v/v K30 (pink circles). This correlation suggests that survival trends for the 50v1 strain (across 0 to 0.1% v/v K30) are associated with limited changes in the intracellular metabolome. This assessment is contrary to the associated univariate tests that support ~50% reductions in survival ($p < 0.05$) and substantial changes in the metabolome ($p < 0.05$, FDR ≤ 0.20).

From the CCA plot for the 50v1 strain (Figure 4B), metabolites trending alongside the plate counts include 4-hydroxybenzoate, several amino acids (similar to those in Table 1), ribose-5-phosphate, N-acetylglucosamine, nicotinic acid, phenylacetic acid, bisphosphoglycercol, and potentially 5'-AMP and 5′-MTA. These trends suggest that survival of the 50v1 strain is related to changes in central metabolism, amino acid metabolism, nucleotide metabolism, and cell wall metabolism (e.g., metabolism of glycosoaminoglycans and peptidoglycans, which are based on N-acetylglucosamine).

Trends from the CCA plot for the 50v1 strain (Figure 4B) are additionally suggestive of changes in native benzene metabolism (e.g., phenylacetic acid and 4-hydroxybenzoate). However, univariate analyses yield no support ($p > 0.05$) for the *apparent* decreases in phenylacetic acid (~0.1-fold decreases) and 4-hydroxybenzoate (~0.9-fold decreases). Alternatively, described further in Section 3.5.3, phenylacetic acid and 4-hydroxybenzoate are potential biodegraded products of K30. Hence, trends for the 50v1 strain hint at a potential for biodegradation of K30 through benzene metabolism.

3.5.3. Comparisons to maximum relative biomass

When considering biomass, the vector describing the maximum relative biomass at stationary phase for the 2P08AA strain (Figure 4A) overlaps with the reduced terms associated with 0.1% v/v K30 (black triangles). This correlation suggests that trends in the maximum relative biomass for the 2P08AA strain (across 0 to 0.1% v/v K30) are associated with changes in the intracellular metabolome. This assessment is consistent with the associated univariate tests for the cultivation data that support increases in the maximum relative biomass ($p < 0.05$), yet counter to the associated univariate tests for the metabolomic data that indicate no change in the relative metabolite abundances *after* correction for multiple testing (FDR > 0.20).

From the CCA plot for the 2P08AA strain (Figure 4A), the metabolites trending alongside the maximum relative biomass include methionine, lignoceric acid (fatty acid; 23:0), oxoproline, and

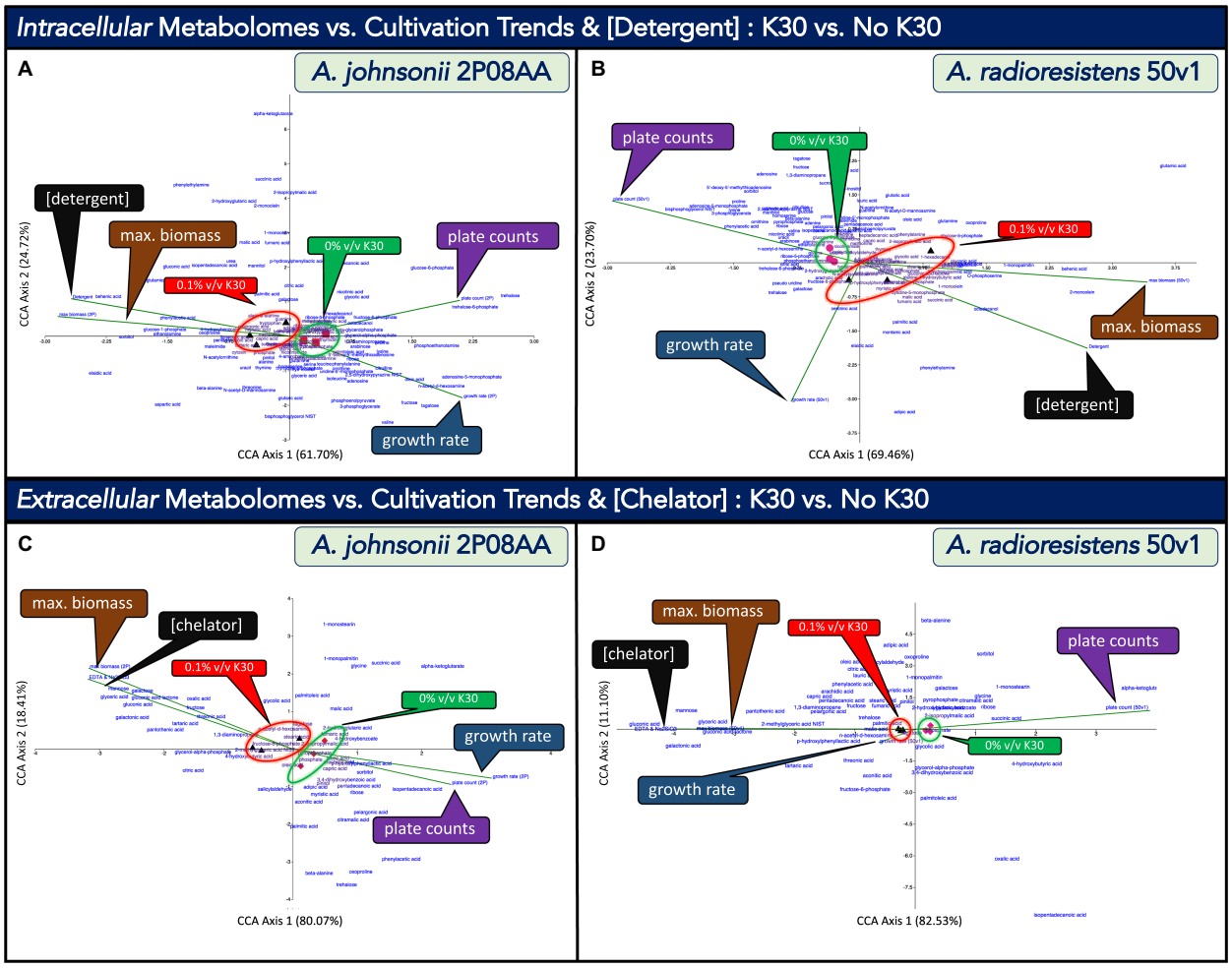

FIGURE 4
Canonical correspondence analyses (CCA) that compare the impacts of cultivation in 0.1% v/v Kleenol 30 (K30) on **(A)** the intracellular metabolome of *A. johnsonii* 2P08AA, **(B)** the extracellular metabolome of *A. johnsonii* 2P08AA, **(C)** the intracellular metabolome of *A. radioresistens* 50v1, and **(D)** the extracellular metabolome of *A. radioresistens* 50v1 against the quantitative descriptors of growth rates at exponential phase (blue callout boxes, green vectors), plate counts at late-log phase (purple callout boxes, green vectors), maximum relative biomass at stationary phase (brown callout boxes, green vectors), and either the total concentrations of detergents (0.025% w/w; assumed) or chelators (0.02% w/w; assumed) in the cultivation media (black callout boxes, green vectors); dimension reduction of the triplicate metabolomic measures associated with 0% v/v K30 (red squares, pink circles, and red and pink diamonds) and 0.1% v/v K30 (black triangles) are provided, reduced terms are highlighted by the green and red circles and callout boxes, and metabolites are arrayed as text.

glucose-1-phosphate. Univariate tests indicate no change in the relative abundances for these metabolites (FDR > 0.20). These combined trends suggest that increases in maximum relative biomass relate to minimal or no changes in glucose metabolism, amino acid metabolism, and unsaturated fatty acid abundances.

For the 50v1 strain (Figure 4B), the vector describing the maximum relative biomass overlaps with the reduced terms associated with 0.1% v/v K30 (black triangles). This correlation suggests that trends in the maximum relative biomass for the 50v1 strain (across 0 to 0.1% v/v K30) are associated with changes in the intracellular metabolome. This assessment is consistent with the associated univariate tests on the cultivation data ($p < 0.05$) and metabolomic data ($p < 0.05$, FDR ≤ 0.20), which yield support for increases in the maximum relative biomass and differential changes in metabolite abundances. In contrast to the 2P08AA strain, these trends for 50v1 strain suggest that increases in the maximum relative biomass are associated with several intracellular metabolomic changes.

From the CCA plot for the 50v1 strain (Figure 4B), metabolites trending alongside the increases in maximum relative biomass include lignoceric acid (fatty acid; 23:0), tryptophan, xanthine, stearic acid (fatty acid; 18:0), α-ketoglutarate, phosphate, 4-hydroxybutanoate (4-hydroxybutyric acid), 4-aminobutanoate (4-aminobutyric acid), O-phosphoserine, 1-monopalmitin (1-palmitoylglycerol; palmitoyl = 16:0), behenic acid (fatty acid; 22:0), and 2-monoolein (2-oleoylglycerol; oleoyl = $18{:}1^{\Delta 9}$). These trends suggest that increases in the maximum relative biomass for the 50v1 strain are related (*at the minimum*) to changes in butanoate metabolism (e.g., 4-hydroxybutanoate and 4-aminobutanoate), amino acid metabolism (e.g., tryptophan, α-ketoglutarate, and O-phosphoserine) and phosphate metabolism (phosphate and O-phosphoserine).

The trends for the 50v1 strain (Figure 4B) also suggest a relation to changes in free fatty acids and monoacylglycerols; where the associated metabolites from the CCA plot (and respective univariate analyses in parentheses) include lignoceric acid (~1.2-fold increases; $p > 0.05$),

stearic acid (~1.5-fold increases; $p > 0.05$), 1-monopalmitin (~2.2-fold increases; $p > 0.05$), behenic acid (~10-fold increases; $p > 0.05$), and 2-monoolein (~32-fold increases; $p > 0.05$). However, in comparison, ChemRich analyses yield no support for changes in the intracellular fatty acids.

Further, trends from the CCA plot for the 50v1 strain (Figure 4B) support a correlation between the maximum relative biomass and metabolism of polyhydroxyalkanoates (PHAs), which are intracellular polymers (e.g., poly-4-hydroxybutanoate and/or other co-polymers) used for carbon and energy storage (Khanna and Srivastava, 2005). Among the metabolites trending alongside the maximum relative biomass are α-ketoglutarate, glutamate, 4-aminobutanoate, and 4-hydroxybutanoate. These combined metabolites represent a stepwise pathway toward the synthesis of PHAs (KEGG map 00250 and map00650), where oxidized carbons are acquired through the TCA cycle (α-ketoglutarate) and sequentially shuttled through amino acid metabolism (glutamate) and butanoate metabolism (4-aminobutanoate) to yield a monomeric unit (4-hydroxybutanoate) commonly found in PHAs.

Together, these observations are relevant since the accumulation of PHAs can result in increases in relative optical densities (Slaninova et al., 2018), which is consistent with our growth curves and ensuing regression analyses that yield increases in the maximum relative biomass in the presence of 0.1% v/v K30. Hence, for the 50v1 strain, the increases in maximum relative biomass may relate to the increased synthesis of PHAs under the stresses imposed by K30.

3.5.4. Comparisons to growth rates

When considering growth rates (exponential phase), the vector for the 2P08AA strain (Figure 4A) overlaps with the reduced terms associated with 0% v/v K30 (red squares). This correlation suggests that growth rates trends for the 2P08AA strain (across 0 to 0.1% v/v K30) are associated with limited changes in the intracellular metabolome. This assessment is consistent with the associated univariate tests for growth rates that support moderate decreases of ~18% ($p < 0.05$) and the associated univariate tests for the metabolomes that imply no change in relative abundances (FDR > 0.20).

From the CCA plot of the 2P08AA strain, metabolites trending alongside the growth rates include palmitoleic acid (fatty acid; $16{:}1^{\Delta 9}$), 5′-MTA, ribose, several amino acids, oleic acid, N-acetylglucosamine, and 5'-AMP. These trends suggest that the decreases in growth rates are related to changes in amino acid metabolism, cell wall metabolism, and nucleotide metabolism. The trends also suggest relations to changes in free unsaturated fatty acid content through associations with palmitoleic acid (~0.7-fold decrease; $p > 0.05$) and oleic acid (~0.3-fold decrease; $p > 0.05$). However, ChemRich analyses yield no support for changes in unsaturated fatty acid metabolism.

For the 50v1 strain (Figure 4B), in contrast, the vector describing growth rates overlaps more closely with the reduced terms associated with 0.1% v/v K30 (black triangles). This correlation suggests that growth rate trends for the 50v1 strain (across 0 to 0.1% v/v K30) are associated with changes to the intracellular metabolome. In comparison, univariate tests on the cultivation data indicate no change in the growth rates ($p > 0.05$), while univariate tests on the metabolomic data support changes in the abundances for multiple metabolites ($p < 0.05$, FDR ≤ 0.20). These combined trends are suggestive of substantial post-exponential phase changes in the metabolomes, as growth rates for the 50v1 strain during exponential phase are unaltered by – and potentially not associated with – the multiple metabolomic changes observed during late-log phase.

3.5.5. Comparisons to detergent concentrations

When considering the K30 formulation (Figures 4A,B), the vectors describing detergent concentrations (~0–0.025% w/w) overlap with the reduced terms associated with 0.1% v/v K30 for both the 2P08AA and 50v1 strains (black triangles). These correlations suggest the metabolomes from both strains adjust in response to detergents in 0.1% v/v K30. We note the trends for detergent concentrations likely overlap with the maximum relative biomass term, which plots across the same respective quadrant.

For the 2P08AA strain, metabolites trending alongside the detergent concentrations include myristic acid (fatty acid; 14:0), pelargonic acid (fatty acid; 9:0), 4-hydroxybenzoate, phenylacetic acid, and behenic acid (fatty acid; 22:0). The trends for 4-hydroxybenzoate and phenylacetic acid lend support toward the potential for biodegradation of dodecyl benzene sulfonate and polyethylene glycol mono-nonylphenyl ether, the detergents from the K30 formulation. As described in Hashim et al. (1992), phenylacetic acid is a potential product of microbial degradation of dodecyl benzene sulfonate through oxidation (or metabolism) of the dodecyl group (to yield 4-sulfonylphenylacetic acid), followed by desulphonization (to yield phenylacetic acid). Similarly, we posit that biodegradation of polyethylene glycol mono-nonylphenyl ether could yield 4-hydroxybenzoate through scission of the polyethylene glycol units (to yield 4-nonylphenol), as described in Section 1 followed by oxidation or metabolism of the nonyl side group (to yield 4-hydroxybenzoate). In comparison, however, univariate tests yield no support for changes in the abundances for phenylacetic acid (~2.4-fold increases; $p = 0.39$) and 4-hydroxybenzoate (~1.5-fold increases; $p = 0.11$).

The trends for the 2P08AA strain are also suggestive of correlations between detergent concentrations and changes in free fatty acid content. Relevant metabolites from the CCA plot (and the associated univariate analyses in parentheses) include behenic acid (~15-fold increases; $p < 0.05$), myristic acid (~1.2-fold increases; $p > 0.05$), and pelargonic acid (~1.4-fold increases; $p > 0.05$). We note that behenic acid levels in fluvial biofilms increase after exposure to desiccation (Serra-Compte et al., 2018). We also speculate the increases in long chain saturated fatty acid content may promote aggregation with the detergents in the intracellular and/or membrane space, which could potentially serve as a survival mechanism and/or acquisition strategy during biodegradation. Analyses by ChemRich, however, yield no support for changes in fatty acid or lipid-related metabolites.

For the 50v1 strain (Figure 4B), metabolites that trend alongside detergent concentrations include tartrate, 1-monoolein (1-oleoylglycerol; oleoyl = $18{:}1^{\Delta 9}$), and octadecanol (fatty alcohol). These trends are suggestive of increases in an intracellular dicarboxylic acid (tartrate) and free lipid-related molecules (1-monoolein and octadecanol), which may, respectively, relate to metal retention in the cell and the aggregation of detergents in the intracellular or membrane space.

3.6. Impacts of Kleenol 30 on the cultivations and extracellular metabolomes

3.6.1. Canonical correlation analyses

In Figure 4, we use canonical correlation analyses (CCA) to, respectively, compare the extracellular metabolomes from *A. johnsonii* 2P08AA ($n = 3$) and *A. radioresistens* 50v1 ($n = 3$) from late log-phase cultures to the quantitative descriptors of growth rates at exponential phase, plate counts at late-log phase, maximum relative biomass at stationary phase, and total concentration of EDTA and sodium

metasilicate in the media, which was assumed to be 0.02% w/w in cultures containing 0.1% v/v K30.

The CCA plots in Figures 4C,D, which compare results from 0 and 0.1% v/v K30, include the total array of detected metabolites (text), listed quantitative descriptors (lines), and transformed data after dimension reduction (glyphs). For the 2P08AA and 50v1 strains, stronger correlations along CCA Axis 1 (67.18, 82.53%) are observed when compared to CCA Axis 2 (32.81, 11.10%), respectively. Dimension reduction for the metabolomes from the 2P08AA and 50v1 strains (Figures 4C,D) respectively show clear separations between samples prepared in the absence and presence of 0.1% v/v K30. These trends suggest that the extracellular metabolomic compositions of both strains are impacted by K30 during cultivation. Described in the following sub-sections are comparisons to the quantitative descriptors. For selected metabolites, additional explanations and/or fatty acid abbreviations are provided in parentheses.

3.6.2. Comparisons to survival and growth rates

When considering survival and cultivations, the vectors for plate counts and growth rates for the 2P08AA strain (Figure 4C) overlap with the reduced terms associated with 0% v/v K30 (red diamonds). These correlations suggest that survival and growth rate trends for the 2P08AA strain (across 0 to 0.1% v/v K30) are associated with minimal changes in the extracellular metabolome. These assessments are roughly consistent with the associated univariate analyses that indicate quantitative survivals, ~18% decreases in growth rate, and a lack of changes in the extracellular metabolome (after correction for multiple testing).

From the CCA plot, metabolites from the 2P08AA strain that trend alongside the plate counts *and* growth rates include 2-isopropylmalic acid, pyrophosphate, phosphate, arachidic acid (fatty acid; 20:0), lauric acid (fatty acid; 12:0), capric acid (fatty acid; 10:0), 4-hydroxyphenyllactic acid, sorbitol, and isopentadecanoic acid (13-methyl-14:0). These trends for the 2P08AA strain suggest that survival (which was not impacted) and growth rates (which minimally decreased) relate to a lack of change in the abundances of extracellular saturated fatty acids, phosphate, pyrophosphate, and α-hydroxy acids (2-isopropylmalic acid and 4-hydroxyphenyllactic acid). However, the potential *increases* in extracellular sorbitol (~5-fold increase, $p < 0.05$; Table 1) are suggestive of efflux of a compatible solute.

For the 50v1 strain (Figure 4D), in contrast, the vector describing plate counts overlaps with the reduced terms associated with 0% v/v K30 (pink diamonds), while the vector describing growth rates moderately overlaps with the reduced terms associated with 0.1% v/v K30 (black triangles). These opposing correlations suggest that survival trends (across 0 to 0.1% v/v K30) are associated with minimal changes in the extracellular metabolome, while growth rate trends (across 0 to 0.1% v/v K30) are associated with more notable changes in the extracellular metabolome.

Metabolites trending alongside the plate counts for the 50v1 strain include 2-isopropylmalic acid, 2-hydroxyglutarate, succinic acid, and α-ketoglutarate. These results suggest that survival for the 50v1 strain is related to changes in extracellular α-hydroxy acids (2-isopropylmalic acid, 2-hydroxyglutarate, and α-ketoglutarate) and a dicarboxylic acid (succinate); while univariate tests support ~9-fold decreases in extracellular α-ketoglutarate. Metabolites trending alongside the growth rates for the 50v1 strain include tagatose and N-acetylglucosamine, which suggests that changes in extracellular monosaccharides relate to maintaining stable growth rates.

3.6.3. Comparisons to maximum relative biomass and chelator concentrations

When considering changes in the maximum relative biomass (stationary phase) and chelator concentrations (EDTA and sodium metasilicate from the K30 formulation), similar trends are observed for the 2P08AA and 50v1 strains (Figures 4C,D). The vectors describing chelator concentrations for both strains overlap with the reduced terms associated with 0.1% v/v K30 (black triangles). These correlations suggest the extracellular metabolomes from both strains adjust in response to the change in chelator concentration across 0 to 0.1% v/v K30 (e.g., the metal sequestering agents of EDTA and sodium metasilicate).

From the CCA plot for the 2P08AA strain, metabolites trending alongside changes in the maximum relative biomass and/or chelator concentration include threonate, fructose, oxalate, galactonate, gluconate, gluconolactone, mannose, galactose, and glycerate. These trends suggest that chelator concentrations influence the abundances of extracellular monosaccharides and sugar acids. While these trends are consistent with univariate tests ($p < 0.05$), no support for changes in the abundances of the associated metabolites (Table 2) are obtained after correction for multiple testing (FDR ≤ 0.20).

For the 50v1 strain, metabolites trending alongside changes in the maximum relative biomass and/or chelator concentrations include N-acetylglucosamine, tartrate, 2-methylglycerate, gluconolactone, glycerate, mannose galactonate, and gluconate. These results suggest that the chelator concentrations influence the abundances of extracellular monosaccharides, modified monosaccharides, and sugar acids. These assessments generally are consistent with univariate analyses.

4. Discussion

4.1. Spacecraft-associated *Acinetobacter*

Molecular insights into the tolerance of spacecraft-associated *Acinetobacter* toward Kleenol 30, a NASA cleanroom floor detergent, were obtained through cultivation, kinetic, and metabolomic approaches. Comparisons were conducted using *A. johnsonii* 2P08AA and *A. radioresistens* 50v1, which were isolated at, respectively, unique locations within the spacecraft assembly facilities, which were subjected to differing cleaning regimes.

The strain *A. johnsonii* 2P08AA was isolated from the floor of the Mars Phoenix lander assembly facility, which was routinely cleansed with Kleenol 30. The strain *A. radioresistens* 50v1 was isolated from the surface of the pre-flight Mars Odyssey orbiter, which was likely cleaned with isopropyl alcohol (2-propanol, isopropanol, IPA) and never exposed to Kleenol 30.

Hence, comparisons across these differing sub-environments provide initial insights into the impacts of repeated cleansing, under the conditions of spacecraft assembly, toward biochemical and cultivation selection.

4.2. Survival of the spacecraft-associated *Acinetobacter* against Kleenol 30

Cultivations containing 0–2.0% v/v Kleenol 30 (K30) were conducted in a low-osmolarity minimal media (0.2x M9, 25 μM Fe) containing 150 mM ethanol, which served as the sole supplied carbon

source. Cultivation media containing 2.0% v/v K30 were bactericidal for the tested *Acinetobacter*, which suggests a biocide-type of activity for K30.

In contrast, in 1.0% v/v K30, appreciable cultivation tolerances were observed for the 2P08AA and 50v1 strains. Cultures containing 1.0% v/v K30 exhibited (1) ~20–30% survivals, (2) ~66 and 12% decreases in growth rates, and (3) eliminated lag phase times for the 2P08AA and 50v1 strains, respectively. These cultivation tolerances of <2% v/v K30 are significant since current NASA planetary protection practices utilize ~0.8-1.6% v/v K30 for floor cleansing. Our results, therefore, suggest that the spacecraft-associated *Acinetobacter* harbor a tolerance toward the current floor cleansing practices for NASA cleanrooms.

In 0.1% v/v K30, differential impacts were observed across the cultivation parameters. For the 2P08AA strain, cultures exhibited (1) no measurable changes in cell density at late-log phase (plate counts), (2) modest decreases in the growth rate (~18%), and (3) negligible times in the lag phase. These results indicate that K30 impacts the 2P08AA strain by accelerating growth out of the lag phase, slightly inhibiting growth during the exponential phase, and by yielding no changes cell density after cultivation to late-log phase.

For the 50v1 strain, cultures exhibited (1) ~50% survivals, (2) no changes in growth rate, and (3) ~70% decreases in the lag phase time. This is indicative of K30 impacting the 50v1 strain by mildly accelerating growth out of the lag phase, yielding no change in the growth rates during the exponential phase, and inhibiting cell density by ~50% when cultivated to late-log phase.

The differential cultivation trends observed in 0.1% v/v K30 are indicative of strain and growth-phase dependent responses to K30. In turn, these trends suggest that K30 reduces nutrient bioavailability in culture (e.g., alkaline earth and transition metals) and/or elicits specific biochemical responses (e.g., metabolism of K30 and/or enzymatic inhibition by K30) – which together manifest as acceleration out of the lag phase for both strains, slight inhibition in rates of cell division during the exponential phase for the 2P08AA strain, and moderate reductions in total cell density at late-log phase for the 50v1 strain.

4.3. Metabolomic profiling of the cultivation tolerances against Kleenol 30

To obtain metabolic insights into the tolerances toward Kleenol 30 (K30), we used cultures grown in 0.1% v/v K30 to obtain reliable biomasses at late-log phase for both strains (see comparison of 0.1 and 1.0% w/w K30 in Figures 1D). For *A. johnsonii* 2P08AA, cultivations with 0.1% v/v K30 exhibited (1) no significant and discreet changes in the abundances of intracellular metabolites, (2) several significant extracellular changes when considering broader classifications such as sugar acids, monosaccharides, organic acids (di- and monocarboxylic acids), and fatty acids, and (3) potential support for biodegradation and metabolism of both detergents in the K30 formulation.

The combined results for the 2P08AA strain suggest that the native and intracellular metabolic state of the 2P08AA strain readily accommodates cultivation in the presence of 0.1% v/v K30. The trends for the 2P08AA strain also suggest that survival is associated with adjustments in the extracellular metabolome and a potential for biodegradation of the Kleenol 30 detergents.

For *A. radioresistens* 50v1, cultivations in 0.1% v/v K30 exhibited (1) differential changes in the abundances of intracellular amino acids, compatible solutes, nucleotide-related metabolites, dicarboxylic acids, and saturated fatty acids, (2) substantial and differential changes in the abundances of extracellular sugar acids, monosaccharides, and organic acids, and (3) *no* clear statistical support for biodegradation and metabolism of the detergents from the K30 formulation (when excluding the potential for degradation *via* benzene metabolism).

These results for the 50v1 strain indicate that the intracellular and extracellular metabolomes of the 50v1 strain significantly adjust to accommodate cultivation in the presence of 0.1% v/v K30. These trends also suggest that survival is associated with intracellular changes to amino acid and peptide metabolism, nucleotide metabolism, central metabolism, fatty acid metabolism, and pyrimidine metabolism.

For the 50v1 strain, the changes in amino acid metabolism include decreases in lysine, proline, glycine, ornithine, homoserine, valine and others listed in Table 1. This is relevant since decreases in lysine and valine are observed during biofilm formation in *A. baumanni* 1,656–2 (Yeom et al., 2013), while decreases in amino acid metabolism are observed after treatments of *A. baumanni* AB5075 with mixed antibiotics (polymyxin B and rifampicin) (Zhao et al., 2021). In *E.coli* UTI189, decreases in intracellular lysine and valine are associated with biofilm formation (Lu et al., 2019). In *Bifodobacterium bifudum*, decreases in intracellular lysine, arginine, and proline are associated with biofilm formation (Sadiq et al., 2020). These observations suggest that the *Acinetobacter* undergo stress-like responses toward K30 that inhibit total cell mass (e.g., survival), which could include changes in early biofilm development.

Trends across nucleotide abundances and the cultivation terms are similarly suggestive of early biofilm-type development (Sarkar and Chakraborty, 2008; Castillo-Juarez et al., 2017) and/or quorum sensing related changes such as intracellular PHA synthesis (Kessler and Witholt, 2001; Xu et al., 2011). These trends include increases in the maximum relative biomass terms for the 2P08AA and 50v1 strains, decreases in 5′-MTA and 5'-AMP for the 50v1 strain, and substantial increases in extracellular monosaccharides (e.g., mannose, galactose, and fructose for the 2P08AA strain).

In comparison, biofilms of *E. coli* UTI189 show decreases in 5′-MTA and 5'-CMP, as well increases in metal-binding siderophores, when Fe^{3+} concentrations in culture decrease from 10 to 1 μM (Guo et al., 2021). Lowered 5′-MTA abundances are associated with biofilms of *Pseudomonas aeruginosa* PAO1 (Tielen et al., 2013). In *Pseudomonas fluorescens* PF08, exogenously added 5'-AMP inhibits biofilm formation (Wang et al., 2021). In *Streptococcus pyogenes*, the import of mannose induces lysozyme resistance *via* a quorum sensing pathway (Chang et al., 2015); while exogenously added galactose differentially inhibits and activates biofilm development in differing species of *Streptococcus* (Ryu et al., 2016).

4.4. Biochemical strategies against Kleenol 30

To obtain biochemical insights into the mechanisms of tolerance, the metabolomic trends were interpreted in context of the cultivation conditions. In this study, cultivations were conducted in low-osmolarity media (0.2x M9) supplemented with 25 μM Fe^{2+} ($Fe(NH_4)_2(SO_4)_2$), which slowly oxidized to Fe^{3+} under the aerobic cultivations in the capped glass tubes (per absorbance spectroscopy). However, in control experiments, cultures supplemented with $[Fe(EDTA)]^{1-}$ grew slower, when compared to $Fe(NH_4)_2(SO_4)_2$, while cultivations in acid-washed

glassware yielded no growth. Therefore, under the cultivation conditions, trace elements and species such as Zn^{2+}, Co^{2+}, Cu^{2+}, Mn^{2+}, BO_3^{3-} (borate; a B source), and MoO_4^{2-} (molybdate; a Mo source) were likely obtained from trace contaminants in the media and/or the glassware.

These details are relevant since K30 contains EDTA and sodium metasilicate, which are chelators that sequester transition and alkaline earth metals. Hence, in culture, chelation by EDTA would likely restrict the bioavailability of transition metals and inhibit growth – as observed in control studies. Limited bioavailabilities for Ca^{2+} and Mg^{2+} are also expected since sodium metasilicate (Na_2SiO_3) is a water softening agent that functions through ion exchange *via* chelation of Ca^{2+} or Mg^{2+} (and release of Na^+).

Under these considerations, therefore, our review of the extracellular metabolomes reveals changes in several biochemicals possessing metal-binding properties. Appraisal of the literature shows that sugar acids such as galactonate, gluconate, and gluconolactone form appreciably stable complexes with transition metals such as Fe^{3+}, Zn^{2+}, Co^{2+}, Cu^{2+}, and Mn^{2+} (Sawyer, 1964; Carper et al., 1989; Frutos et al., 1998; Gyurcsik and Nagy, 2000). For the alkaline earth metals of Ca^{2+} and Mg^{2+}, stable complexes are formed with sugar acids such as gluconolactone and glycerate (Taga et al., 1978; Meehan et al., 1979; Tajmir-Riahi, 1990), monosaccharides such as mannose (Angyal, 1973), and organic acids such as oxalate (Chutipongtanate et al., 2013; Izatulina et al., 2018) and tartrate (Hawthorne et al., 1982). In addition, borate and Ca^{2+} form stable complexes with gluconate, glycerate, and tartrate (van Duin et al., 1987); while molybdate yields stable complexes with mannose and fructose (Spence and Kiang, 1963; Sauvage et al., 1996).

Biochemically, therefore, these observations suggest that the 2P08AA strain targets trace Ca^{2+} and Mg^{2+} acquisition through potential increases in extracellular glycerate, gluconolactone, and oxalate, but not *via* gluconate and galactonate, which bind transition and alkaline earth metals but were not detected. In contrast, the 50v1 strain potentially targets both transition and alkaline earth metals given the increases ($p < 0.05$, FDR ≤ 0.20) in extracellular gluconate, galactonate, glycerate, gluconolactone, and tartrate. In fact, increases in glycerate export for the 50v1 strain are supported by the increases in extracellular glycerate and decreases in intracellular glycerate. Control of intracellular Ca^{2+} retention is also suggested by increases in extra- and intracellular tartrate. Multivariate tests support these total trends and suggest that chelator concentrations (from the K30 formulation) influence the abundances of extracellular metal-binding biochemicals.

Thus, our total results suggest that up-regulations (*per se*) in extracellular trace element acquisition strategies are common survival features to the spacecraft-associated *Acinetobacter*. Future studies using concentrated and clarified cultivation media may yield spectral support for the trace metal chelation. Additional common survival features may include regulation of the bulk osmolarity, as suggested by decreases in intracellular compatible solutes for the 50v1 strain (e.g., glycerate, 3-phosphoglycerate, and mannitol), statistical associations (CCA plot) between survival and changes in intracellular compatible solutes (e.g., trehalose) for the 2P08AA strain, and increase in an extracellular compatible solute for the 2P08AA strain (e.g., sorbitol).

When considering intracellular changes, differing responses to 0.1% v/v K30 are observed by the 2P08AA and 50v1 strains. While limited intracellular responses are observed for the 2P08AA strain, substantial intracellular changes are observed for the 50v1 strain. Multivariate tests for the 50v1 strain support a potential for the synthesis of light scattering PHAs during stationary phase in response to 0.1% v/v K30. Relatedly, univariate tests suggest decreases in the export of α-ketoglutarate and 4-hydroxybutanoate (e.g., decreases in extracellular abundances), while multivariate tests show correlations between intracellular PHA synthesis (e.g., α-ketoglutarate, 4-aminobutanoate, and 4-hydroxybutanoate) and increases in the *apparent* maximum relative biomass.

For the 2P08AA strain, multivariate analyses highlight a potential for partial metabolism of the detergents (from the Kleenol 30 formulation) – which would serve as an additional biochemical strategy toward survival. While these exact trends were not observed for the 50v1 strain, multivariate tests do support correlations between survival and changes in the degradation of aromatic compounds (benzene metabolism). In support, GC–MS studies in Mogul et al. (2018) provided evidence for scission of polyethylene glycol mono-nonylphenyl ether by the 50v1 strain. Future targeted cultivation studies are required to confirm the extent of biodegradation of the detergent by these strains.

When considering impacts of K30 on the lag phase, we observe a differential concentration dependence, where the time in lag phase is eliminated in the presence of 0.1 v/v K30 for the 2P08AA strain, and in 1.0% v/v K30 for the 50v1 strain. We venture that metabolism of the alkyl sides chains on the detergents (*via* ω-oxidation of the terminal carbon and subsequent cycles of β-oxidation) may serve as activators for acceleration out of the lag phase, and that degradation of the aromatic detergent cores (*via* benzene metabolism) may sustain the 50v1 strain during exponential phase, where growth rates show no inhibition in the presence of 0.1% v/v K30. If so, carbon and energy acquisition from the detergents could serve as an added biochemical strategy toward survival. Alternatively, the K30 detergents could potentially disperse any low abundance cellular aggregates during the lag phase, thereby yielding higher OD values and the apparent increases in biomass. Under this assumption, the observed concentration dependence across the strains would be suggestive of the cellular aggregates from both strains having differing stabilities.

5. Conclusion

In conclusion, our combined cultivation and metabolomic results lend supports toward the hypothesis that repetitive cleansing with Kleenol 30 presents as selective pressures toward members of the spacecraft microbiome – where the phenotypic outcomes likely include cultivation tolerances and measurable biochemical responses. Fittingly, our described results indicate that Kleenol 30 is more readily tolerated by the floor-associated *A. johnsonii* 2P08AA, when compared to the spacecraft surface-associated *A. radioresistens* 50v1. However, both strains display reasonable tolerances toward 1% v/v Kleenol 30, which is higher than the current formulation (~0.8-1.6% v/v) used in NASA planetary protection practices. These results indicate that the spacecraft-associated *Acinetobacter* may harbor tolerances toward the floor cleaning conditions.

Such tolerances are likely important considerations for lower bioburden planetary missions, such as orbiter missions to Europa (Planetary Protection Category III), life detection missions to Mars (Planetary Protection Category IVb) or Europa (Planetary Protection

Category IV), and investigations of Mars Special Regions (Planetary Protection Category IVc). In this context, our results suggest that higher floor cleanliness levels may be achieved with higher concentrations of Kleenol 30 (e.g., 2–3% v/v) or rotations with differing concentrations of Kleenol 30 (e.g., 1 and 3% v/v). Alternatively, rotation of differing floor cleansers could assist in achieving lower floor bioburdens (e.g., Kleenol 30 and a quaternary ammonium compound), with the caveat that the detergents and/or biocides retain compatibility with the spacecraft assembly procedures and spacecraft materials.

Data availability statement

Metabolomic data (Study ID ST002380, DatatrackID: 3552) are available through the Metabolomics Workbench (https://www.metabolomicsworkbench.org/) at the NIH Common Fund's National Metabolomics Data Repository (NMDR) and can be accessed directly via the project DOI: http://dx.doi.org/10.21228/M8XH73.

Author contributions

RM, DM, SL, and BR contributed to analysis of the data, assisted in drafting of the report, approved of submission of the manuscript. RM analyzed the metabolomic data, performed the statistical analyses, prepared the manuscript, and is the corresponding author. DM and BR conducted the survival assays and cultivation kinetics. SL prepared cultures for metabolomics analysis. All authors contributed to the article and approved the submitted version.

Funding

This work was supported by a grant (NNH18ZDA001N) from the Planetary Protection Research component of the National Aeronautics and Space Administration (NASA) Research Opportunities in Space and Earth Sciences program.

Acknowledgments

We acknowledge logistical support from the College of Science, Chemistry and Biochemistry Department, and Department of Biological Sciences at Cal Poly Pomona.

Conflict of interest

The authors declare that the research was conducted in the absence of any commercial or financial relationships that could be construed as a potential conflict of interest.

Publisher's note

All claims expressed in this article are solely those of the authors and do not necessarily represent those of their affiliated organizations, or those of the publisher, the editors and the reviewers. Any product that may be evaluated in this article, or claim that may be made by its manufacturer, is not guaranteed or endorsed by the publisher.

References

Agalloco, J. P., and Carleton, F. J. (2007). *Validation of Pharmaceutical Processes*. Boca Raton, Florida: CRC Press.

Angyal, S. (1973). "Complex formation between sugars and metal ions" in *Carbohydrate Chemistry–VI*. ed. W. M. Doane, Northern Regional Research Laboratory, Peoria, Illinois (Amsterdam, Netherlands: Elsevier), 131–146.

Barupal, D. K., and Fiehn, O. (2017). Chemical similarity enrichment analysis (ChemRICH) as alternative to biochemical pathway mapping for metabolomic datasets. *Sci. Rep.* 7:14567. doi: 10.1038/s41598-017-15231-w

Barupal, D. K., Haldiya, P. K., Wohlgemuth, G., Kind, T., Kothari, S. L., Pinkerton, K. E., et al. (2012). MetaMapp: mapping and visualizing metabolomic data by integrating information from biochemical pathways and chemical and mass spectral similarity. *BMC Bioinform.* 13, 1–15. doi: 10.1186/1471-2105-13-99

Barupal, D. K., Zhang, Y., Shen, T., Fan, S., Roberts, B. S., Fitzgerald, P., et al. (2019). A comprehensive plasma metabolomics dataset for a cohort of mouse knockouts within the international mouse phenotyping consortium. *Meta* 9:101. doi: 10.3390/metabo9050101

Begot, C., Desnier, I., Daudin, J. D., Labadie, J. C., and Lebert, A. (1996). Recommendations for calculating growth parameters by optical density measurements. *J. Microbiol. Methods* 25, 225–232. doi: 10.1016/0167-7012(95)00090-9

Benjamini, Y., and Hochberg, Y. (1995). Controlling the false discovery rate: a practical and powerful approach to multiple testing. *J. R. Stat. Soc. B* 57, 289–300. doi: 10.1111/j.2517-6161.1995.tb02031.x

Carper, W., Coffin, D., and Addis, J. (1989). Studies of magnesium and manganese interactions with gluconate and 1, 5-gluconolactone. *Spectrochim. Acta Part A* 45, 391–392. doi: 10.1016/0584-8539(89)80106-0

Castillo-Juarez, I., Lopez-Jacome, L. E., Soberón-Chávez, G., Tomás, M., Lee, J., Castañeda-Tamez, P., et al. (2017). Exploiting quorum sensing inhibition for the control of *Pseudomonas aeruginosa* and *Acinetobacter baumannii* biofilms. *Curr. Top. Med. Chem.* 17, 1915–1927. doi: 10.2174/1568026617666170105144104

Chang, J. C., Jimenez, J. C., and Federle, M. J. (2015). Induction of a quorum sensing pathway by environmental signals enhances group a streptococcal resistance to lysozyme. *Mol. Microbiol.* 97, 1097–1113. doi: 10.1111/mmi.13088

Checinska, A., Probst, A. J., Vaishampayan, P., White, J. R., Kumar, D., Stepanov, V. G., et al. (2015). Microbiomes of the dust particles collected from the international Space Station and spacecraft assembly facilities. *Microbiome* 3:50. doi: 10.1186/s40168-015-0116-3

Checinska Sielaff, A., Urbaniak, C., Mohan, G. B. M., Stepanov, V. G., Tran, Q., Wood, J. M., et al. (2019). Characterization of the total and viable bacterial and fungal communities associated with the international Space Station surfaces. *Microbiome* 7:50. doi: 10.1186/s40168-019-0666-x

Chutipongtanate, S., Sutthimethakorn, S., Chiangjong, W., and Thongboonkerd, V. (2013). Bacteria can promote calcium oxalate crystal growth and aggregation. *J. Biol. Inorg. Chem.* 18, 299–308. doi: 10.1007/s00775-012-0974-0

Danko, D. C., Sierra, M. A., Benardini, J. N., Guan, L., Wood, J. M., Singh, N., et al. (2021). A comprehensive metagenomics framework to characterize organisms relevant for planetary protection. *Microbiome* 9, 1–15. doi: 10.1186/s40168-021-01020-1

Daschner, F., Fahlberg, W. J., and Mallison, G. F. (1982). Floor disinfection in the United States. *Infect. Control Hosp. Epidemiol.* 3, 281–284. doi: 10.1017/S0195941700056289

Derecho, I., Mccoy, K. B., Vaishampayan, P., Venkateswaran, K., and Mogul, R. (2014). Characterization of hydrogen peroxide–resistant *Acinetobacter* species isolated during the Mars Phoenix spacecraft assembly. *Astrobiology* 14, 837–847. doi: 10.1089/ast.2014.1193

Eissa, M. E., Kamel, M., and Beshir, M. (2014). Study of antimicrobial power of amphoteric disinfectants of Tego series used in pharmaceutical industry. *Egypt. J. Biol. Sci. G* 6, 17–27. doi: 10.21608/eajbsg.2014.16626

Ellingson, K. D., Pogreba-Brown, K., Gerba, C. P., and Elliott, S. P. (2020). Impact of a novel antimicrobial surface coating on health care–associated infections and environmental bioburden at 2 urban hospitals. *Clin. Infect. Dis.* 71, 1807–1813. doi: 10.1093/cid/ciz1077

Empadinhas, N., and Da Costa, M. S. (2008). Osmoadaptation mechanisms in prokaryotes: distribution of compatible solutes. *Int. Microbiol.* 11, 151–161. PMID: 18843593

Farrow, J. M. 3rd, Wells, G., and Pesci, E. C. (2018). Desiccation tolerance in *Acinetobacter baumannii* is mediated by the two-component response regulator BfmR. *PLoS One* 13:e0205638. doi: 10.1371/journal.pone.0205638

Fernández-Cuenca, F., Tomás, M., Caballero-Moyano, F.-J., Bou, G., Martínez-Martínez, L., Vila, J., et al. (2015). Reduced susceptibility to biocides in *Acinetobacter baumannii*: association with resistance to antimicrobials, epidemiological behaviour, biological cost and effect on the expression of genes encoding porins and efflux pumps. *J. Antimicrob. Chemother.* 70, 3222–3229. doi: 10.1093/jac/dkv262

Fiehn, O., Garvey, W. T., Newman, J. W., Lok, K. H., Hoppel, C. L., and Adams, S. H. (2010). Plasma metabolomic profiles reflective of glucose homeostasis in non-diabetic and type 2 diabetic obese African-American women. *PLoS One* 5:e15234. doi: 10.1371/journal.pone.0015234

Fiehn, O., Wohlgemuth, G., and Scholz, M. (2005). "Setup and annotation of metabolomic experiments by integrating biological and mass spectrometric metadata" in *International Workshop on Data Integration in the Life Sciences*. ed. W. M. Doane, Northern Regional Research Laboratory, Peoria, Illinois (Berlin: Springer), 224–239.

Franceus, J., Pinel, D., and Desmet, T. (2017). Glucosylglycerate phosphorylase, an enzyme with novel specificity involved in compatible solute metabolism. *Appl. Environ. Microbiol.* 83:e01434. doi: 10.1128/AEM.01434-17

Frick, A., Mogul, R., Stabekis, P., Conley, C. A., and Ehrenfreund, P. (2014). Overview of current capabilities and research and technology developments for planetary protection. *Adv. Space Res.* 54, 221–240. doi: 10.1016/j.asr.2014.02.016

Frutos, A. A., Signorella, S., Sala, L. F., Escandar, G. M., Peregrin, J. M. S., and Moreno, V. (1998). Interaction of divalent metal ions with D-aldonic acids in the solid phase-II. Structural information fn1. *Polyhedron* 17, 3371–3378. doi: 10.1016/S0277-5387(98)00119-3

Guo, R., Luo, X., Liu, J., and Lu, H. (2021). Mass spectrometry based targeted metabolomics precisely characterized new functional metabolites that regulate biofilm formation in *Escherichia coli*. *Anal. Chim. Acta* 1145, 26–36. doi: 10.1016/j.aca.2020.12.021

Gyurcsik, B., and Nagy, L. (2000). Carbohydrates as ligands: coordination equilibria and structure of the metal complexes. *Coord. Chem. Rev.* 203, 81–149. doi: 10.1016/S0010-8545(99)00183-6

Haffenden, L. J., and Yaylayan, V. A. (2005). Mechanism of formation of redox-active hydroxylated benzenes and pyrazine in ^{13}C-labeled glycine/D-glucose model systems. *J. Agric. Food Chem* 53, 9742–9746. doi: 10.1021/jf051610r

Halket, J. M., Waterman, D., Przyborowska, A. M., Patel, R. K., Fraser, P. D., and Bramley, P. M. (2005). Chemical derivatization and mass spectral libraries in metabolic profiling by GC/MS and LC/MS/MS. *J. Exp. Biol.* 56, 219–243. doi: 10.1093/jxb/eri069

Hammer, Ø., Harper, D. A., and Ryan, P. D. (2001). PAST: paleontological statistics software package for education and data analysis. *Palaeontol. Electron.* 4:9.

Han, Z., Pappas, E., Simmons, A., Fox, J., Donskey, C. J., and Deshpande, A. (2021). Environmental cleaning and disinfection of hospital rooms: a nationwide survey. *Am. J. Infect. Cont.* 49, 34–39. doi: 10.1016/j.ajic.2020.08.008

Hashim, M., Kulandai, J., and Hassan, R. (1992). Biodegradability of branched alkylbenzene sulphonates. *J. Chem. Technol. Biotechnol.* 54, 207–214. doi: 10.1002/jctb.280540302

Hawthorne, F., Borys, I., and Ferguson, R. (1982). Structure of calcium tartrate tetrahydrate. *Acta Crystallogr. B* 38, 2461–2463. doi: 10.1107/S0567740882009042

Hendrickson, R., Urbaniak, C., Minich, J. J., Aronson, H. S., Martino, C., Stepanauskas, R., et al. (2021). Clean room microbiome complexity impacts planetary protection bioburden. *Microbiome* 9:238. doi: 10.1186/s40168-021-01159-x

Izatulina, A. R., Gurzhiy, V. V., Krzhizhanovskaya, M. G., Kuz'mina, M. A., Leoni, M., and Frank-Kamenetskaya, O. V. (2018). Hydrated calcium oxalates: crystal structures, thermal stability, and phase evolution. *Cryst. Growth Des.* 18, 5465–5478. doi: 10.1021/acs.cgd.8b00826

Kessler, B., and Witholt, B. (2001). Factors involved in the regulatory network of polyhydroxyalkanoate metabolism. *J. Biotechnol.* 86, 97–104. doi: 10.1016/S0168-1656(00)00404-1

Khanna, S., and Srivastava, A. K. (2005). Recent advances in microbial polyhydroxyalkanoates. *Process Biochem.* 40, 607–619. doi: 10.1016/j.procbio.2004.01.053

La Duc, M. T., Nicholson, W., Kern, R., and Venkateswaran, K. (2003). Microbial characterization of the Mars odyssey spacecraft and its encapsulation facility. *Environ. Microbiol.* 5, 977–985. doi: 10.1046/j.1462-2920.2003.00496.x

La Duc, M. T., Vaishampayan, P., Nilsson, H. R., Torok, T., and Venkateswaran, K. (2012). Pyrosequencing-derived bacterial, archaeal, and fungal diversity of spacecraft hardware destined for Mars. *Appl. Environ. Microbiol.* 78, 5912–5922. doi: 10.1128/AEM.01435-12

Lu, H., Que, Y., Wu, X., Guan, T., and Guo, H. (2019). Metabolomics deciphered metabolic reprogramming required for biofilm formation. *Sci. Rep.* 9:13160. doi: 10.1038/s41598-019-49603-1

Mahnert, A., Vaishampayan, P., Probst, A. J., Auerbach, A., Moissl-Eichinger, C., Venkateswaran, K., et al. (2015). Cleanroom maintenance significantly reduces abundance but not diversity of indoor microbiomes. *PLoS One* 10:e0134848. doi: 10.1371/journal.pone.0134848

McCoy, K., Derecho, I., Wong, T., Tran, H., Huynh, T., La Duc, M., et al. (2012). Insights into the extremotolerance of *Acinetobacter radioresistens* 50v1, a gram-negative bacterium isolated from the Mars odyssey spacecraft. *Astrobiology* 12, 854–862. doi: 10.1089/ast.2012.0835

Meehan, E., Einspahr, H., and Bugg, C. E. (1979). Calcium binding to hydroxycarboxylic acids: crystal structure of calcium di-dl-glycerate dihydrate. *Acta Crystallogr. B* 35, 828–832. doi: 10.1107/S0567740879004994

Meyer, B., and Cookson, B. (2010). Does microbial resistance or adaptation to biocides create a hazard in infection prevention and control? *J. Hosp. Infect.* 76, 200–205. doi: 10.1016/j.jhin.2010.05.020

Mogul, R., Barding, G. A. Jr., Lalla, S., Lee, S., Madrid, S., Baki, R., et al. (2018). Metabolism and biodegradation of spacecraft cleaning reagents by strains of spacecraft-associated *Acinetobacter*. *Astrobiology* 18, 1517–1527. doi: 10.1089/ast.2017.1814

Moissl-Eichinger, C., Auerbach, A. K., Probst, A. J., Mahnert, A., Tom, L., Piceno, Y., et al. (2015). Quo vadis? Microbial profiling revealed strong effects of cleanroom maintenance and routes of contamination in indoor environments. *Sci. Rep.* 5:9156. doi: 10.1038/srep09156

Mora, M., Mahnert, A., Koskinen, K., Pausan, M. R., Oberauner-Wappis, L., Krause, R., et al. (2016). Microorganisms in confined habitats: microbial monitoring and control of intensive care units, operating rooms, cleanrooms and the international Space Station. *Front. Microbiol.* 7:1573. doi: 10.3389/fmicb.2016.01573

Murtough, S., Hiom, S., Palmer, M., and Russell, A. (2001). Biocide rotation in the healthcare setting: is there a case for policy implementation? *J. Hosp. Infect.* 48, 1–6. doi: 10.1053/jhin.2001.0950

NASA. (2011). *Planetary Protection Provisions for Robotic Extraterrestrial Missions*. Washington, DC: National Aeronautics and Space Administration.

Peleg, A. Y., Seifert, H., and Paterson, D. L. (2008). *Acinetobacter baumannii*: emergence of a successful pathogen. *Clin. Microbiol. Rev.* 21, 538–582. doi: 10.1128/CMR.00058-07

Perry-Dow, K. A., De Man, T. J., Halpin, A. L., Shams, A. M., Rose, L. J., and Noble-Wang, J. A. (2022). The effect of disinfectants on the microbial community on environmental healthcare surfaces using next generation sequencing. *Am. J. Infect. Cont.* 50, 54–60. doi: 10.1016/j.ajic.2021.08.027

Pirog, T., Lutsai, D., and Muchnyk, F. (2021). Biotechnological potential of the *Acinetobacter* genus bacteria. *Mikrobiol. Zh.* 83, 92–109. doi: 10.15407/microbiolj83.03.092

Pompilio, A., Scribano, D., Sarshar, M., Di Bonaventura, G., Palamara, A. T., and Ambrosi, C. (2021). Gram-negative bacteria holding together in a biofilm: the *Acinetobacter baumannii* way. *Microorganisms* 9:1353. doi: 10.3390/microorganisms9071353

Rajamohan, G., Srinivasan, V., and Gebreyes, W. A. (2009). Biocide-tolerant multidrug-resistant *Acinetobacter baumannii* clinical strains are associated with higher biofilm formation. *J. Hosp. Infect.* 73, 287–289. doi: 10.1016/j.jhin.2009.07.015

Rummel, J. D. (1992). Planetary protection policy (U.S.A.). *Adv. Space Res.* 12, 129–131. doi: 10.1016/0273-1177(92)90166-U

Rutala, W. A., and Weber, D. J. (2019). Best practices for disinfection of noncritical environmental surfaces and equipment in health care facilities: a bundle approach. *Am. J. Infect. Cont.* 47, A96–A105. doi: 10.1016/j.ajic.2019.01.014

Rutala, W. A., and Weber, D. J.Healthcare Infection Control Practices Advisory Committee. (2008). *Guideline for Disinfection and Sterilization in Healthcare Facilities*. Atlanta, Georgia: Centers for Disease Control and Prevention.

Ryu, E.-J., Sim, J., Sim, J., Lee, J., and Choi, B.-K. (2016). D-galactose as an autoinducer 2 inhibitor to control the biofilm formation of periodontopathogens. *J. Microbiol.* 54, 632–637. doi: 10.1007/s12275-016-6345-8

Sadiq, F. A., Yan, B., Zhao, J., Zhang, H., and Chen, W. (2020). Untargeted metabolomics reveals metabolic state of *Bifidobacterium bifidum* in the biofilm and planktonic states. *LWT* 118:108772. doi: 10.1016/j.lwt.2019.108772

Sandle, T. (2012). *The CDC Handbook-a Guide to Cleaning and Disinfecting Clean Rooms*. England: Grosvenor House Publishing.

Sandle, T. (2015). *Pharmaceutical Microbiology: Essentials for Quality Assurance and Quality Control*. Sawston, United Kingdom: Woodhead Publishing.

Sarkar, S., and Chakraborty, R. (2008). Quorum sensing in metal tolerance of *Acinetobacter junii* BB1A is associated with biofilm production. *FEMS Microbiol. Lett.* 282, 160–165. doi: 10.1111/j.1574-6968.2008.01080.x

Sauvage, J.-P., Verchère, J.-F., and Chapelle, S. (1996). A multinuclear NMR spectroscopy study of the tungstate and molybdate complexes of d-fructose and l-sorbose. *Carbohydr. Res.* 286, 67–76. doi: 10.1016/0008-6215(96)00048-1

Sawyer, D. T. (1964). Metal-gluconate complexes. *Chem. Rev.* 64, 633–643. doi: 10.1021/cr60232a003

Serra-Compte, A., Corcoll, N., Huerta, B., Rodríguez-Mozaz, S., Sabater, S., Barceló, D., et al. (2018). Fluvial biofilms exposed to desiccation and pharmaceutical pollution: new insights using metabolomics. *Sci. Total Environ.* 618, 1382–1388. doi: 10.1016/j.scitotenv.2017.09.258

Shams, A. M., Rose, L. J., Edwards, J. R., Cali, S., Harris, A. D., Jacob, J. T., et al. (2016). Assessment of the overall and multidrug-resistant organism bioburden on environmental surfaces in healthcare facilities. *Infect. Control Hosp. Epidemiol.* 37, 1426–1432. doi: 10.1017/ice.2016.198

Slaninova, E., Sedlacek, P., Mravec, F., Mullerova, L., Samek, O., Koller, M., et al. (2018). Light scattering on PHA granules protects bacterial cells against the harmful effects of UV radiation. *App. Microbiol. Biotechnol.* 102, 1923–1931. doi: 10.1007/s00253-018-8760-8

Spence, J., and Kiang, S.-C. (1963). Complexes of sugars with molybdate. *J. Org. Chem.* 28, 244–245. doi: 10.1021/jo01036a522

Spry, J. A., Siegel, B., Race, M., Kminek, G., Pratt, L., and Coustenis, A. (2020). *Planetary Protection Requirements for Crewed Missions-an Update to the COSPAR Workshop Series: 2020*. International Conference on Environmental Systems.

Srinivasan, V. B., Venkataramaiah, M., Mondal, A., and Rajamohan, G. (2015). Functional characterization of AbeD, an RND-type membrane transporter in antimicrobial resistance in *Acinetobacter baumannii*. *PLoS One* 10:e0141314. doi: 10.1371/journal.pone.0141314

Sud, M., Fahy, E., Cotter, D., Azam, K., Vadivelu, I., Burant, C., et al. (2016). Metabolomics workbench: an international repository for metabolomics data and metadata, metabolite standards, protocols, tutorials and training, and analysis tools. *Nucleic Acids Res.* 44, D463–D470. doi: 10.1093/nar/gkv1042

Suleyman, G., Alangaden, G., and Bardossy, A. C. (2018). The role of environmental contamination in the transmission of nosocomial pathogens and healthcare-associated infections. *Cur. Infect. Dis. Rep.* 20, 1–11. doi: 10.1007/s11908-018-0620-2

Taga, T., Ohashi, M., and Osaki, K. (1978). Interactions of calcium ions with carbohydrates: crystal structure of calcium DL-Glycerate Dihydrate. *Bull. Chem. Soc. Japan* 51, 1697–1700.

Tajmir-Riahi, H. (1990). Carbohydrate complexes with alkaline earth metal ions. Interaction of D-glucono-1,5-lactone with the mg(II), ca(II), Sr(II), and Ba(II) cations in the crystalline solid and aqueous solution. *J. Inorg. Biochem.* 39, 33–41. doi: 10.1016/0162-0134(90)80013-N

Tam, H.-K., König, P., Himpich, S., Ngu, N. D., Abele, R., Müller, V., et al. (2022). Unidirectional mannitol synthesis of *Acinetobacter baumannii* MtlD is facilitated by the helix–loop–helix-mediated dimer formation. *Proc. Natl. Acad. Sci. U. S. A.* 119:e2107994119. doi: 10.1073/pnas.2107994119

Tembo, G. M., Chaggar, G. K., Li, X., Teska, P. J., and Oliver, H. F. (2022). Evaluation of automated floor cleaning, disinfection, and application methods against *Staphylococcus aureus*. *Am. J. Infect. Cont.* 19:S0196-6553(22)00535-1. doi: 10.1016/j.ajic.2022.07.011

Tielen, P., Rosin, N., Meyer, A.-K., Dohnt, K., Haddad, I., Jänsch, L., et al. (2013). Regulatory and metabolic networks for the adaptation of *Pseudomonas aeruginosa* biofilms to urinary tract-like conditions. *PLoS One* 8:e71845. doi: 10.1371/journal.pone.0071845

Trigg, S. A., Mcelhany, P., Maher, M., Perez, D., Busch, D. S., and Nichols, K. M. (2019). Uncovering mechanisms of global ocean change effects on the Dungeness crab (*Cancer magister*) through metabolomics analysis. *Sci. Rep.* 9, 1–12. doi: 10.1038/s41598-019-46947-6

Van Duin, M., Peters, J. A., Kieboom, A. P., and Van Bekkum, H. (1987). Synergic coordination of calcium in borate-polyhydroxycarboxylate systems. *Carbohydr. Res.* 162, 65–78. doi: 10.1016/0008-6215(87)80201-X

Wang, Y., Wang, Y., Chen, J., Koseki, S., Yang, Q., Yu, H., et al. (2021). Screening and preservation application of quorum sensing inhibitors of *Pseudomonas fluorescens* and *Shewanella baltica* in seafood products. *LWT* 149:111749. doi: 10.1016/j.lwt.2021.111749

White, G. F. (1993). Bacterial biodegradation of ethoxylated surfactants. *Pest. Sci.* 37, 159–166. doi: 10.1002/ps.2780370209

Wong, W. C., Zalesak, S., Yoets, A., Capriotti, J., Smith, M. J., and Castro, V. A. (2013). Effectiveness of HEPA filter vacuum in removing transient microbial contaminants on cargo bags destined for the international Space Station. *J. Occup. Environ. Hyg.* 10, D71–D75. doi: 10.1080/15459624.2013.784179

Xu, C., Li, M., Huang, Y., Zhang, Z., Bian, Z., and Song, S. (2011). Involvement of quorum-sensing in biosynthesis of polyhydroxyalkanoates in *Pseudomonas aeruginosa*. *Acta Microbiolog. Sin.* 51, 769–775. PMID: 21866701

Yeom, J., Shin, J.-H., Yang, J.-Y., Kim, J., and Hwang, G.-S. (2013). 1H NMR-based metabolite profiling of planktonic and biofilm cells in *Acinetobacter baumannii* 1656-2. *PLoS One* 8:e57730. doi: 10.1371/journal.pone.0057730

Zhao, J., Han, M.-L., Zhu, Y., Lin, Y.-W., Wang, Y.-W., Lu, J., et al. (2021). Comparative metabolomics reveals key pathways associated with the synergistic activity of polymyxin B and rifampicin combination against multidrug-resistant *Acinetobacter baumannii*. *Biochem. Pharmacol.* 184:114400. doi: 10.1016/j.bcp.2020.114400

frontiers | Frontiers in Microbiology

TYPE Original Research
PUBLISHED 18 April 2023
DOI 10.3389/fmicb.2023.1155726

OPEN ACCESS

EDITED BY
Camilla Urbaniak,
Planetary Protection Center of Excellence,
NASA Jet Propulsion Laboratory, United States

REVIEWED BY
Teresa Rinaldi,
Sapienza University of Rome, Italy
Marta Filipa Simões,
Macau University of Science and Technology, China

*CORRESPONDENCE
Jessica A. Lee
✉ jessica.a.lee@nasa.gov

SPECIALTY SECTION
This article was submitted to Extreme Microbiology, a section of the journal Frontiers in Microbiology

RECEIVED 31 January 2023
ACCEPTED 20 March 2023
PUBLISHED 18 April 2023

CITATION
Gesztesi J, Broddrick JT, Lannin T and Lee JA (2023) The chemical neighborhood of cells in a diffusion-limited system. *Front. Microbiol.* 14:1155726. doi: 10.3389/fmicb.2023.1155726

The chemical neighborhood of cells in a diffusion-limited system

Juliana Gesztesi[1,2], Jared T. Broddrick[3], Timothy Lannin[2] and Jessica A. Lee[3]*

[1]NASA Ames Research Center, Universities Space Research Association, Moffett Field, CA, United States, [2]College of Engineering, Northeastern University, Boston, MA, United States, [3]NASA Ames Research Center, Space Biosciences Research Branch, Moffett Field, CA, United States

Microorganisms follow us everywhere, and they will be essential to sustaining long-term human space exploration through applications such as vitamin synthesis, biomining, and more. Establishing a sustainable presence in space therefore requires that we better understand how stress due to the altered physical conditions of spaceflight affects our companion organisms. In microgravity environments such as orbital space stations, microorganisms likely experience the change in gravity primarily through changes in fluid mixing processes. Without sedimentation and density-driven convection, diffusion becomes the primary process governing the movement of growth substrates and wastes for microbial cells in suspension culture. Non-motile cells might therefore develop a substrate-deficient "zone of depletion" and experience stress due to starvation and/or waste build-up. This would in turn impact the concentration-dependent uptake rate of growth substrates and could be the cause of the altered growth rates previously observed in microorganisms in spaceflight and in ground-simulated microgravity. To better understand the extent of these concentration differences and their potential influence on substrate uptake rates, we used both an analytical solution and finite difference method to visualize concentration fields around individual cells. We modeled diffusion, using Fick's Second Law, and nutrient uptake, using Michaelis–Menten kinetics, and assessed how that distribution varies in systems with multiple cells and varied geometries. We determined the radius of the zone of depletion, within which cells had reduced the substrate concentration by 10%, to be 5.04mm for an individual *Escherichia coli* cell in the conditions we simulated. However, we saw a synergistic effect with multiple cells near each other: multiple cells in close proximity decreased the surrounding concentration by almost 95% from the initial substrate concentration. Our calculations provide researchers an inside look at suspension culture behavior in the diffusion-limited environment of microgravity at the scale of individual cells.

KEYWORDS

microgravity, diffusion modeling, Michaelis-Menten, glucose uptake, *E. coli*

Introduction

The expansion of space travel by both space agencies and private companies, as well as current plans to send astronauts back to the Moon for the first time in decades, have recently increased the relevance and traction of space microbiology. Humans carry 10–100 trillion cells of microorganisms on and within our bodies (Ursell et al., 2012). As humanity travels to space, we have no say in whether or not microbes accompany us: they will (Lopez et al., 2019). Moreover, microbes in space are of interest for their potential role in sustaining human life

during long-term missions. For example, microbes may play a role in the process of *In Situ* Resource Utilization (ISRU), as in biomining (Gumulya et al., 2022) or the conversion of methane waste into biomass (NASA Technology Transfer, n.d.). They will also likely be the first organisms employed in the *in situ* production of foods and pharmaceuticals, and in environmental life support systems (Berliner et al., 2021; Keller et al., 2021; Liu et al., 2021; McNulty et al., 2021).

Because microbes play a crucial role in our journey to space, numerous experiments have been carried out in spaceflight and in simulated microgravity experiments on Earth to characterize microbes' biological response to space conditions. A particularly puzzling feature of the space environment is the effect of microgravity on microbes, as there is no evidence that bacteria can detect the force of gravity directly, but they have been shown to respond to altered gravity conditions (Horneck et al., 2010; Bijlani et al., 2021; Wang et al., 2022). Numerous studies have reported differences in gene expression, antibiotic resistance, and virulence in spaceflight (Nickerson et al., 2003; Wilson et al., 2007; Aunins et al., 2018). At the scale of the microbial cell, the primary effects of microgravity may be due to alterations in the physical conditions that surround them, such as differences in mass transport (Todd, 1989; Klaus et al., 1997, 2004).

In liquid suspension culture, microbes experience a different physical environment in 1 g compared to microgravity. Within Earth's gravity, mixing can occur as a result of two forces. First, natural convection occurs when density is not homogenous throughout the entirety of the fluid, due to factors such as temperature or solute concentration, and the force of gravity brings denser fluid downward. Second, passive diffusion leads to mixing based on concentration gradients. When density-driven convection brings low- and high-concentration regions of fluid in close contact, mixing may be rapid. However, in a quiescent fluid in microgravity, density-driven convection ceases to occur and the mixing of nutrients in the culture becomes diffusion-limited. Thus, it is theorized that a non-motile cell creates a "zone of depletion" surrounding itself as it consumes growth substrates, if nutrient uptake occurs faster than the substrate can diffuse into the zone (Figure 1) (Todd, 1989; Klaus et al., 1997, 2004). Analyses showing different responses from motile cells (which can disrupt the quiescent medium and/or escape the depletion zone) and non-motile cells support this theory (Benoit and Klaus, 2007). Similarly, the changes in mass transport in microgravity would also lead to waste product accumulation surrounding the cell, which could similarly contribute to the changes in phenotype discussed earlier.

Rotating Wall Vessels (RWVs), devices typically used to simulate microgravity for ground-based microbiology experiments, are designed to mimic the quiescent environment of microgravity by balancing forces to keep cells within their zone of depletion (Hammond and Hammond, 2001; Klaus, 2001). RWVs are a form of clinostat rotating in a 2-dimensional plane, and many forms have been used in experiments, including both deep cylindrical (Allen et al., 2022) and shallow wide (Chao and Das, 2015) devices. (Other microgravity simulation devices, such as 3D clinostats and random positioning machines, involve more complex fluid dynamics and are not discussed here (Wuest et al., 2017). And while there are many spaceflight settings in which cells are in dry, surface-attached, or

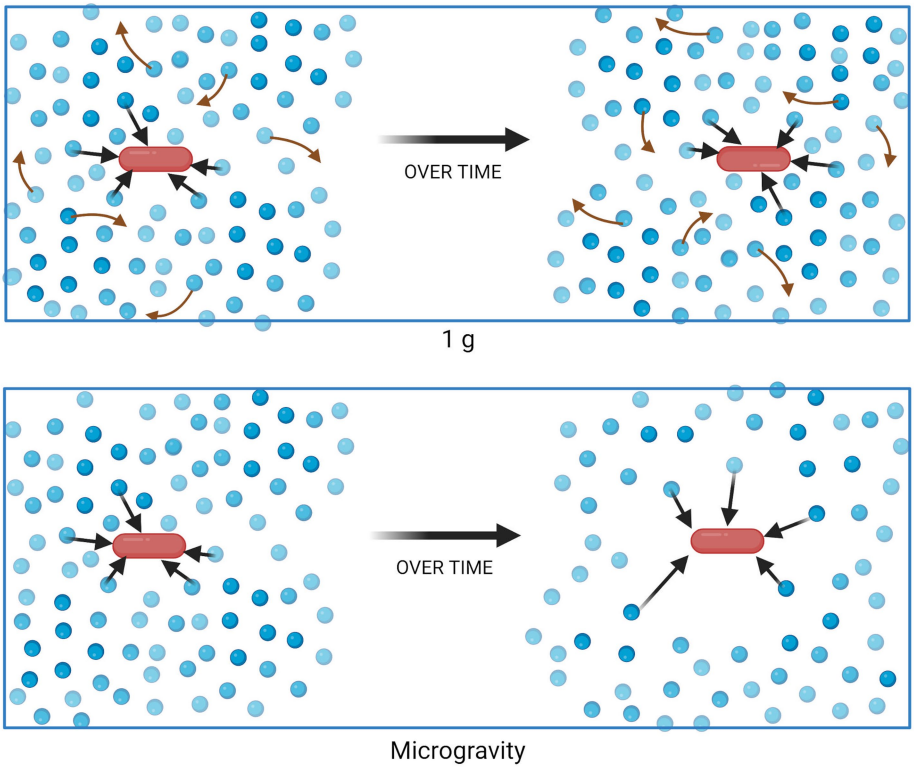

FIGURE 1
Nutrient uptake and distribution in a suspension culture in 1g (top) and microgravity (bottom). Blue circles represent molecules of a growth substrate, consumed (black arrows) by the red bacterial cell. Red arrows represent mixing of substrate due to density-driven convection, which does not occur in quiescent fluids in microgravity. Figure generated using BioRender.

mechanically mixed environments, the fluid environment is relevant to numerous applications, from fundamental biological experiments in CubeSat microfluidic culture devices (Bluck, 2007; Ricco et al., 2020), to bioreactors that omit stirring for ease of operation and reliability, such as those used for the BioNutrients project (Tabor, 2022), or those that employ perfusion technology to increase mass transport (Mozdzierz et al., 2015).

Unfortunately, it is difficult to test the depletion zone theory directly, since doing so would require measuring concentrations of nutrients directly surrounding an individual cell. Therefore, we explored computational modeling as a means to calculate the theoretical magnitude, extent, and temporal dynamics of this nutrient-deficient zone for single and multiple cells, and its potential effect on cells' nutrient uptake rates. Similar work has previously been carried out in the context of understanding nutrient uptake by marine plankton; however, these works have typically focused on individual cells (Lazier and Mann, 1989; Karp-Boss et al., 1996). We recognized that space applications may involve growing microbes in suspension culture to densities at which cells will be within a few micrometers of each other (for example, at a typical experimental population of 10^7 cells/mL, cells are on average only 46 µm apart), and therefore we sought to quantify how each cell's nutrient consumption might affect its neighbor. Understanding chemical gradients can provide insight into their potential importance as one of the mechanisms behind microbial behavior in spaceflight and enable more accurate simulations of microgravity in ground-based experiments.

Materials and methods

Application of Fick's second law

The first equation incorporated in this model is Fick's Second Law, which describes the diffusion of a solute in a fluid medium. This is given in Equation (1), where φ is the concentration of the solute, t is time, and D is the diffusivity of the solute in the given medium. The partial derivative of φ with respect to t (left-hand side) is related to D and the Laplacian (second spatial derivative) of φ (right-hand side).

$$\frac{\partial \varphi}{\partial t} = D\nabla^2\varphi. \tag{1}$$

Analytical solution: "One cell in infinite medium"

First, we tested an analytical solution derived from Fick's Second Law that describes diffusion from a continuous source in infinite media (Crank, 1979), shown in Equation (2). In our system, the source takes a negative value (therefore, acts a sink), and represents the uptake rate of nutrient by the cell. As in Equation (1), φ represents the concentration of solute at a given point (mmol); D is the diffusivity of a specific solute in a specific medium (cm^2/s); and t is the time since the source's start (sec). V_{max} denotes the value for this source (mmol/g/h, originally, but we converted to mmol/cell/s by multiplying by the average weight of an *Escherichia coli* cell and dividing by the number of seconds in an hour). r is the radial distance from the source (cm). We used parameters corresponding to non-motile *E. coli* cells growing in M9 glucose medium (see "Parameters" below) to calculate φ at each value of r from 0.018 to 2 cm in steps of 0.018 cm, for each value of t from 0 to 2 days in steps of 1 s.

$$\varphi = \varphi + \left(\frac{V_{\max}}{4\pi * D * t}\right) * erfc\left(\frac{r}{2\sqrt{D * t}}\right). \tag{2}$$

Finite difference method: "One or more cells per slice"

In order to be able to model multiple cells and to incorporate temporally dynamic feedback between uptake rates and concentrations, we used Finite Difference Method (FDM) to solve Fick's Second Law at each time step. FDM allows for the approximation of partial differential equations by utilizing boundary and initial conditions. Space and time are discretized into finite steps, and the solution at each discrete step is approximated using algebraic equations containing finite differences and values from nearby points. FDM is applied in Equation (3), which is an expansion of Equation (1) in 2D Cartesian coordinates (x, y).

$$\frac{\partial \varphi}{\partial t} = D\left(\frac{\partial^2 \varphi}{\partial x^2} + \frac{\partial^2 \varphi}{\partial y^2}\right). \tag{3}$$

The parameters φ, t, and D are as previously stated. The right hand of the equation is expanded to account for diffusion in each cartesian direction.

It should be noted that our FDM implementation models in pseudo-2D, where our system is essentially a repeating slice of 3-D space. Physically, we are showing a cross-section of a 3-D system with definite x, y bounds, but an indefinite z axis. We assume that the concentration gradient with respect to the z axis is zero: materials are equally likely to diffuse in either z direction. Therefore, we are solving for Fick's Second Law in two dimensions, x and y, shown in Equation (3). This is equivalent to what we might expect if we had a string of cells, one per slice, where the slice repeats in both z-directions indefinitely.

In our model, the microbial cell was treated as a point source on the slice that takes in a finite number of moles per second, with the point of uptake located at the center of the cell. The algebraic equation used for FDM is given in Equation (4), representing the forward-time central-space (FTCS) explicit scheme.

$$\varphi_{\text{new}i,j} = D * \delta t * \left(\frac{\left(\varphi_{i+1,j} - 2 * \varphi_{i,j} + \varphi_{i-1,j}\right)}{DX^2} + \frac{\left(\varphi_{i,j+1} - 2 * \varphi_{i,j} + \varphi_{i,j-1}\right)}{DY^2}\right) + \varphi_{i,j}. \tag{4}$$

Dx and Dy are the size of the discretized space in the x, y directions, respectively. We carried out calculations using 180 µm as δx and δy. The size of the domain is 2 cm by 2 cm. δt is the time step and is set at 10 milliseconds. Values for δx, δy, and δt and the size of the domain were determined using convergence studies (Supplementary material). We modeled an *E. coli* cell and estimated it to be 1 µm in diameter (El-Hajj and Newman, 2015), so for visualization purposes we ignore the values for concentration within

that space: for figures showing substrate concentrations, the value at the center of the cell (which was dictated by the concentration-dependent uptake rate) is displayed as an average of the four values surrounding it on the *x*, *y* plane, so that the plots do not show the discontinuity at the point of uptake.

Application of Michaelis–Menten uptake dynamics

The second major component of the model describes a cell's uptake rate of a nutrient. This rate is related to the surrounding concentration, as dictated by the classic Michaelis–Menten binding kinetics (Johnson and Goody, 2011) given in Equation (5). On a biological level, in the limit of large substrate (i.e., nutrient) concentration, all of the transport channels become occupied with substrate, so the limiting factor in uptake rate is the number of channels in the cell and the rate that they can transport, accounted for in the parameter V_{max} (in mmol/s). In the limit of small nutrient concentration, the uptake is limited by the receptor transport rate and the number of receptors, where these two factors are accounted for with parameters V_{max} and K_m (in mM), and the concentration of substrate at the cell surface (φ, in mM). Note that if substrate concentration, φ, is very high in comparison to the value of the Michaelis–Menten constant, K_m, the rational expression in parentheses approaches 1, and the rate, V, approaches its maximum value, V_{max}.

$$V = V_{\max}\left(\frac{\varphi}{K_m + \varphi}\right). \tag{5}$$

The FDM model used in our study accounts for the interdependence of these two equations by alternately solving for the diffusion of nutrient and determining the Michaelis–Menten uptake rate per each time step. The analytical solution in Equation (2) does not account for the relationship in Equation (5), but rather assumes that $V = V_{max}$ at all times.

MATLAB computations

The process for the FDM model proceeds as follows: first, time and space are discretized, variables are initialized, and the system orientation (number of cells and layout) is chosen. Then, the model calculates the initial setup of the system, where the concentration at each *x*, *y* location is equal to the initial value. Next, the uptake rate for each cell is determined by the Michaelis–Menten equation, where substrate concentration is defined as the average of the four values surrounding the uptake point (cell center); that uptake rate is allocated to the cell center location. Then, the model uses FDM to calculate the concentrations at each *x*, *y* location at the next time step, after the cell consumes its pre-allocated amount based on the Michaelis–Menten kinetics at initial conditions. A new uptake rate is determined by the Michaelis–Menten equation using the new surrounding concentration average, and that rate is the new value for the cell center. The process repeats for each time step, until the model reaches steady state. Steady state is defined as the point at which the change in the average concentration at the cell surface is less than 0.1 μM per timestep, which was decided by the use of convergence studies (Supplementary material).

All computations were carried out and figures generated in MATLAB version R2022a (Update 2), with no additional add-ons or toolboxes. The code is provided in Supplementary material.

Parameters

This model simulates a cell or multiple cells of non-motile *E. coli* growing in M9 minimal medium with 22 mM glucose (Cold Spring Harbor Protocols, 2010). This concentration was used for the initial values for the entirety of the space at the initial time step, and was the value fixed at the boundaries of the domain. Calculations were carried out in terms of absolute numbers of molecules rather than concentrations; the concentration 22 mM corresponds to 7.14×10^{-9} mmol per spatial segment as each has a discrete volume of 3.25×10^{-10} l. For ease of interpretation in reporting results, mmol were converted back again into mM by dividing by volume. Other parameters were as follows: D, the constant diffusivity of glucose in water, 600 $\mu m^2/s$ (Adam, 1946); V_{max}, the maximum uptake rate of glucose by the *E. coli* in suspension, 10 mmol/g/h (Harcombe et al., 2014); and K_m, the Michaelis–Menten constant of glucose uptake by *E. coli*, 1.75 μM (Natarajan and Srienc, 1999).

We were unable to find experimental data for the diffusivity of glucose in M9 minimal medium, so we used the diffusivity of glucose in water because the composition of M9 medium is greater than 99% (*w*/*v*) water (Cold Spring Harbor Protocols, 2010). The Stokes-Einstein equation describes the diffusivity of a particle in a solvent as a function of temperature (T), viscosity of the fluid (η), and particle radius (r), where k_B is the Boltzmann constant (Coglitore et al., 2017; Equation 6).

$$D = \frac{k_B * T}{6\pi * \eta * r}. \tag{6}$$

This relationship applies when the system has a low Reynolds number, as in the quiescent environment of microgravity; and when the molecules of the solvent are much smaller than that of the solute, as for the water-glucose system [water measures about 2.8 Å (D'Arrigo, 1978), while the diameter of a ring-form glucose molecule is about 8.6 Å (M., n.d.)]. Given the Stokes-Einstein equation, the only factor that would result in a difference in D between M9 and water would be viscosity, η; and we assume this to be negligible, given the low concentration of solutes in M9. In addition, the molecular weight of M9 solutes is sufficiently small that we do not expect them to impact diffusivity substantially, since as solute size and complexity decrease, the impact on diffusivity decreases as well (Chan et al., 2015).

Results

One cell in infinite medium

To examine the impact of nutrient uptake and diffusion on the fluid environment, we initially used a previously published analytical solution to model a single cell in suspension culture (Crank, 1979). We found

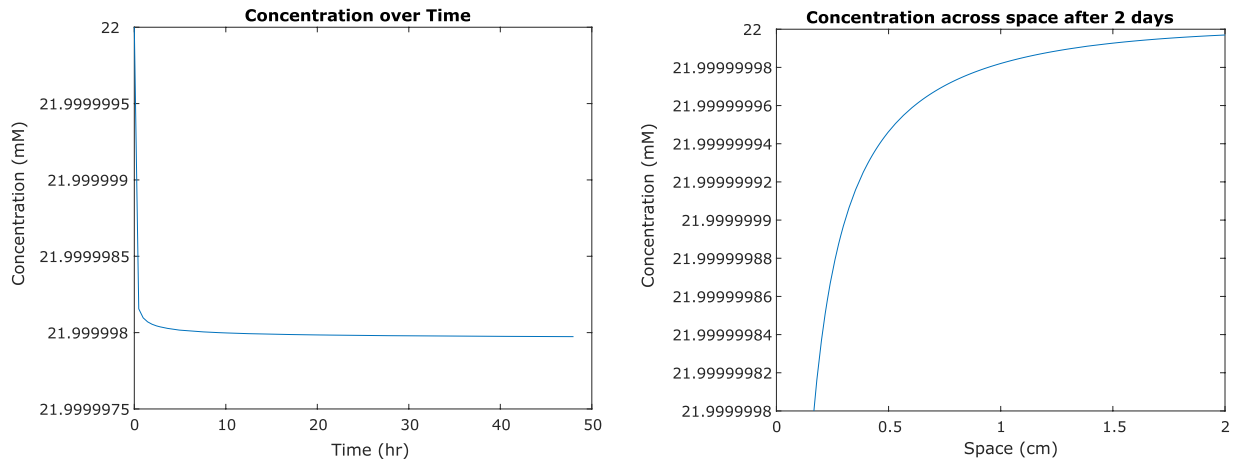

FIGURE 2
(Left) Concentration of glucose in medium at a distance of 0.2 mm from the center of a single *Escherichia coli* cell, as it changes over time. (Right) Concentration of glucose surrounding that cell at steady state, 2 days from initiation.

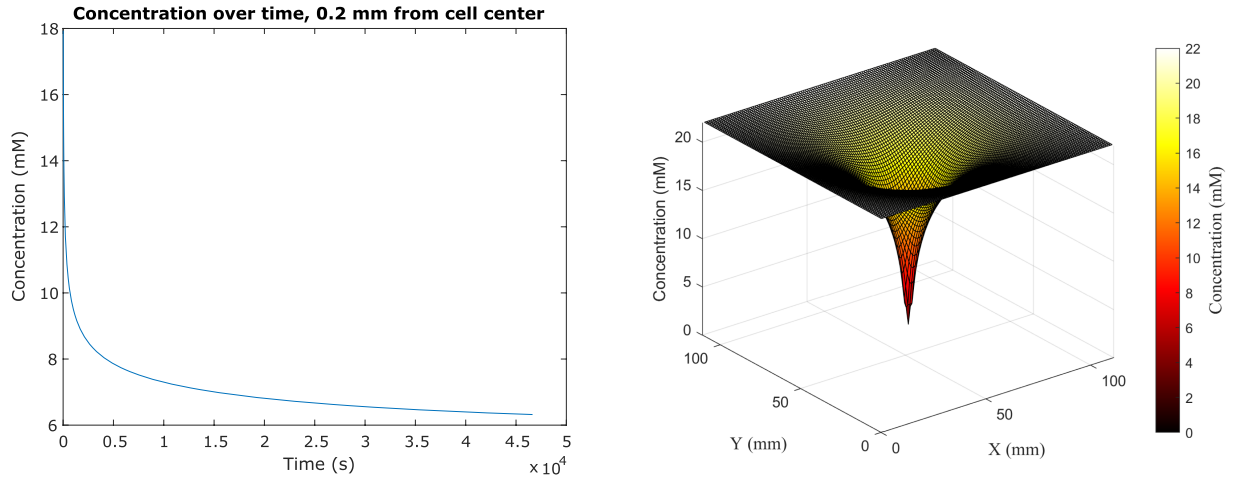

FIGURE 3
(Left) Average glucose concentration over time at a distance of 0.2 mm from the center of an *E. coli* cell in M9 medium. (Right) Surface plot showing glucose concentration across *x*, *y* space in the vicinity of the cell. Concentration is shown both on the *z*-axis and in the color gradient.

that glucose concentrations surrounding the cell decreased by less than 100 nM. The definition of steady state we developed for the FDM model was therefore not applicable, but we found that concentrations appeared to converge on a steady state after approximately 2 days of simulation time (Figure 2). As mentioned previously, these results do not account for concentration-dependent cell uptake rates.

One cell per slice

Because the analytical solution assumes a single cell in infinite medium with a constant glucose uptake rate, we had to use a different method to investigate scenarios more relevant to space biological applications. We therefore used the Finite Difference Method to track the change in glucose concentration surrounding the cell center dynamically, as it changed over time in feedback with changing cell uptake rates, until concentrations reached steady state (Figure 3). The system reached steady state at 46,440 s (or almost 13 h) of simulated time; at this time, the average concentration adjacent to the cell surface had decreased to 6.322 mM, which was a 71.3% decrease from the original 22 mM concentration in the medium. This surrounding concentration decreased the cell's glucose uptake rate by 0.0277%. The depletion zone (which we defined as more than a 10% decrease in surrounding concentration) extended to a radius of 5.04 mm around the cell.

Two cells per slice

We next examined how a cell can influence a neighbor's environment by modeling pairs of cells at varying distances from each other, testing this model with cells located 2, 4, or 6 spatial steps apart (360, 720, and 1,080 μm apart). For all scenarios, we examined the

TABLE 1 Results from FDM calculation of glucose concentrations surrounding two non-motile *Escherichia coli* cells in M9 medium in diffusion-limited microgravity suspension culture, at varying distances from each other.

	1,080μm apart	720μm apart	360μm apart
Average concentration 0.2 mm from cell center	4.024	3.537	4.408
Decrease from initial concentration	81.7%	83.9%	80.0%
Concentration at center between the cells (mM)	5.805	4.346	2.204
Size of depletion zone (radius, mm)	6.12	5.94	5.58
Steady state time point (s)	45,620	43,530	39,990
Decrease in uptake rate	0.0384%	0.0402%	0.0434%

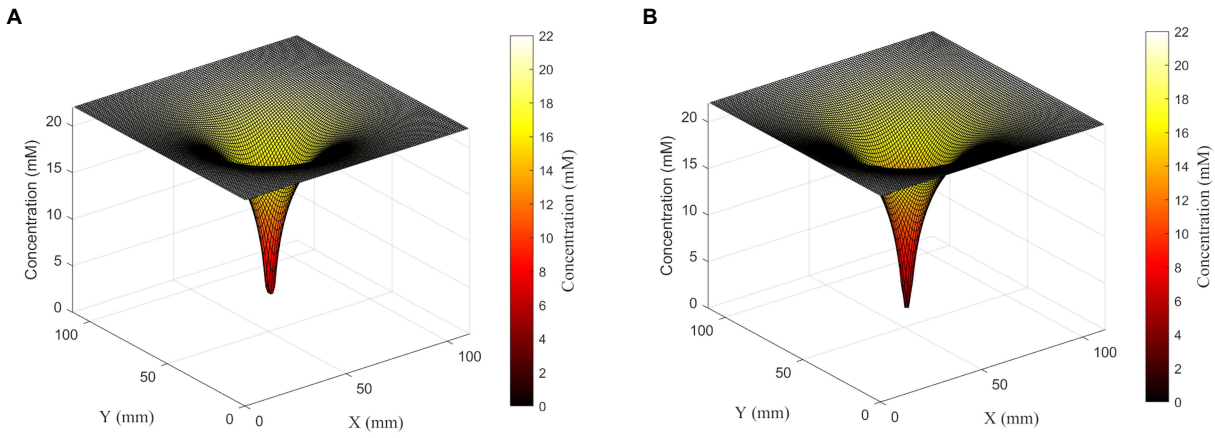

FIGURE 4
Surface plots showing glucose concentration field around a set of four cells in the linear configuration (left) or square configuration (right). Although cells are 360μm apart from each other, cells in both configurations form one deep concentration gradient. Glucose concentration is shown both on the *z*-axis and in the color gradient.

change in uptake rate over time (following Michaelis–Menten kinetics), and at steady state we assessed the concentration surrounding the cell, the concentration between the two cells, and the size of the depletion zone around a cell (Table 1; Figure 4).

We found that there is a synergistic effect in substrate uptake when two cells are close together: where an individual cell decreases its local glucose concentration to 6.322 mM before reaching steady state, two cells spaced 1,080 μm apart deplete it to 5.805 mM at the center between them (Table 1). And the effect of proximity increases with decreasing distance, up to the theoretical maximum of two adjacent cells (360 μm apart), which deplete their local glucose to 2.204 mM between them. However, the radius of each cell's 10% depletion zone decreases when it gets nearer to its neighbors, to a minimum of 5.58 mm.

Four cells per slice

To further explore the synergistic effects of multiple cells on local substrate concentrations, we performed a similar analysis on a four-cell system with different spatial distributions: four cells in a line with sequential separations of two spatial steps; and a square shape distribution where each cell is located at the square's vertex, and the square has a side length of 2 spatial steps. We found that the square distribution led to lower glucose concentrations between cells (Table 2; Figure 5).

Glucose uptake rates

In all of the systems described above, the changing concentrations changed glucose uptake rates very little. Even at the closest orientation of two cells we tested, the uptake rate decreased by less than 0.1% from the original uptake rate at 22 mM glucose; and the change in uptake rate was similar for the four-cell system. This agrees with expectations, given the very low K_m value for glucose uptake by *E. coli*. K_m describes the concentration of a substrate at which uptake is half of V_{max}; because K_m is low relative to experimentally relevant glucose concentrations, most concentrations we calculated fell in the plateau region of the Michaelis–Menten curve where uptake rate is close to V_{max} and changes little with changing concentration (Figure 5).

Discussion

Our results illustrate the degree to which cells in diffusion-limited environments such as microgravity can deplete growth substrates in their surrounding environment. The aim of this work was to generate quantitative information that would allow researchers to calculate the impact of these concentrations on cell behavior; and readers are welcome to implement the code we have developed (Supplementary material) to study similar processes in their organisms and media of interest.

TABLE 2 Results from finite difference method (FDM) calculation of glucose concentrations surrounding four non-motile *E. coli* cells in M9 medium in diffusion-limited microgravity suspension culture, in different spatial configurations.

	Linear distribution	Square distribution
Average concentration at system center (mM)	1.606	1.194
Decrease from initial concentration	92.7%	94.6%
Size of depletion zone (radius, mm)	4.86	5.94
Steady-state time point (s)	21,190	31,220
Decrease in uptake rate	0.0549%	0.0715%

Note that "average concentration 1 μm from cell center" is an average of all the points at that radial distance, though concentrations may be lower on one side of the cell than the other.

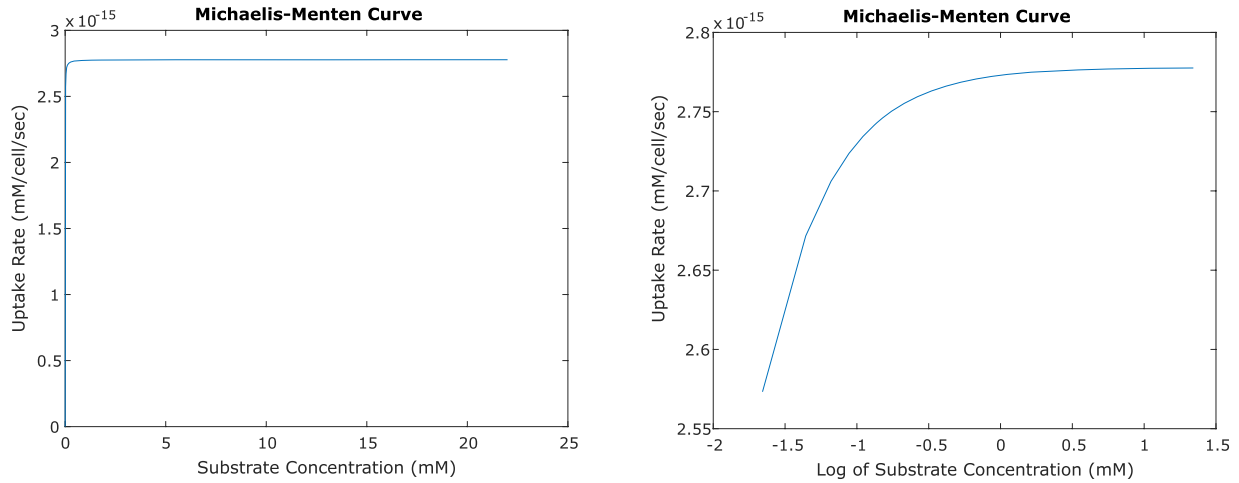

FIGURE 5
Relationship between uptake rate and substrate concentration for *E. coli* consuming glucose, based on Michaelis–Menten uptake dynamics, shown on a linear scale (left) and log-linear (right). At steady state, the activity of single cells and small numbers of cells result in surrounding concentrations that in turn result in uptake rates very close to V_{max}.

Microgravity is not the only context in which these concentration gradients are relevant. An individual microbial cell growing in any fluid environment on Earth is inevitably surrounded by a diffusive boundary layer, and the smaller the organism, the larger the role this layer plays in determining chemical flux to the cell. Others have previously calculated the contributions of sinking, swimming, and turbulence for increasing nutrient fluxes to planktonic cells in environments with gravity, relative to diffusion alone (Purcell, 1978; Lazier and Mann, 1989; Karp-Boss et al., 1996; Guasto et al., 2012). In addition, substrate diffusion is a key process regulating growth, physical structure, and phenotypic heterogeneity in microbial colonies growing on solid substrates such as laboratory agar culture plates, and in the microbial communities of naturally occurring biofilms (Harcombe et al., 2014; Nadell et al., 2016; Julou et al., 2020).

The values we calculated for glucose concentrations surrounding a single cell using FDM differed substantially from those calculated using the analytical solution. This is likely because of the difference in the way the spatial dimensions are treated: as described above, the analytical solution assumes diffusion in all directions, whereas our implementation of FDM assumes diffusion only in the *x*–*y* plane, as though our single cell and its surroundings were a slice that is repeated indefinitely in the *z* direction. While in the single-cell case this scenario may overestimate the effect of glucose consumption on concentrations, in environments crowded with cells it becomes a closer approximation of reality. And environments with multiple cells in close proximity are precisely those that we aimed to investigate with this implementation.

It important to acknowledge that we defined the depletion zone arbitrarily as more than a 10% decrease from initial substrate concentration, but defining the biological effects of that particular concentration decrease is outside the scope of this study. We did examine the effect of concentration on uptake rate and found very little change, due to the low K_m value for glucose by *E. coli*, 1.75 μM. This is notable especially given the fact that the FDM model likely overestimates the changes in glucose concentration. However, in scenarios different from those modeled here, such as other media and substrates, other cells, and other orientations, concentrations surrounding the cell might approach values that could influence uptake and/or growth rates. We used *E. coli* for this study because it is a well-studied model organism common in fundamental spaceflight research, but the influence of microgravity on bulk exchange is also of particular interest to microbial synthetic biology using diverse other chassis organisms (e.g., yeast, algae, *Streptomyces*, *Bacillus*). In the future such situations could be tested, as our model allows for parameters to be easily changed.

In the same vein, we have demonstrated the importance of interactions between neighboring cells. Even when cells are as far as 1,080 μm apart (from center to center of cell), the regions from which they consume glucose overlap enough to render their zones of depletion deeper (lower glucose concentrations) and wider (the radius of the 10% zone increases). The system of four cells told a similar story: groups of microbes located closely together have a synergistic effect that results in steeper concentration gradient than single cells standing alone in the medium. The difference we observed when increasing cell numbers from one to two to four, and from linear to square orientation, hinting at the results we might observe as a culture approaches high cell density and thousands of cells clustered with their zones overlapping, in the form of a three-dimensional colony. And the colony realm might in fact be very relevant to suspension culture in the space environment: when cells are non-motile and are not pushed away from each other by convection, cells in suspension culture in microgravity or in a RWV may spend most of their time not in isolation but rather as microcolonies.

Understanding the size and extent of the depletion zone has practical relevance to those seeking to understand the reasons for microbes to show altered phenotypes in microgravity, especially *via* experiments involving the simulation of microgravity on Earth. Rotating Wall Vessels (RWV) operate under the assumption that they provide a similar fluid environment to that of true microgravity by ensuring that cells travel in small circular paths that stay within their depletion zones (Hammond and Hammond, 2001; Klaus, 2001). Our results may be paired with calculations estimating the path traveled by microbial cells in RWVs (Allen et al., 2022) to aid in experimental design for future ground-based microgravity research.

Overall, our model provides important context for researchers attempting to understand what cells in suspension experience in microgravity and how these conditions affect them. Further research using the same methods to simulate other systems, possibly with an expansion to true 3D, would aid in improving our understanding of the big picture of the chemical environment surrounding a cell in microgravity. Our model could also be applied to an inverse problem, to calculate concentrations of waste products excreted by cells. Additionally, it could provide insight into communities that exchange growth nutrients, signaling compounds, or antibiotic toxins used in cell–cell competition—relationships that could be affected by these microgravity-induced concentration gradients. Pairing quantitative modeling tools with experimentation will allow us to probe more diverse questions and increase the value of spaceflight research.

Data availability statement

The original contributions presented in the study are included in the article and/or Supplementary material; further inquiries can be directed to the corresponding author.

Author contributions

JG and JL conceptualized the research question and wrote the manuscript. JG conceptualized and wrote the code for the project, and carried out the analysis and interpretation of results. JL provided the supervision. TL and JB gave advice on methodology and analysis, and reviewed and edited the manuscript. All authors contributed to the article and approved the submitted version.

Funding

This research was funded by the NASA Biological and Physical Sciences Division (BPS) through the Space Life Sciences Training Program (SLSTP), the NASA Ames Office of STEM Engagement, the NASA BPS Space Biology Program through grant opportunity NNH20ZDA001N-SB, and a MathWorks Teaching Fellowship.

Acknowledgments

The authors would like to acknowledge Maha Ulhaq, Daniel Palacios, and Rocky An for feedback on the project. We would also like to thank Sigrid Reinsch, Hami Ray, Iris Irby, and Brooke Shepard for coordination and support during the Space Life Sciences Training Program (SLSTP).

Conflict of interest

The authors declare that the research was conducted in the absence of any commercial or financial relationships that could be construed as a potential conflict of interest.

Publisher's note

Supplementary material

The Supplementary material for this article can be found online at: https://www.frontiersin.org/articles/10.3389/fmicb.2023.1155726/full#supplementary-material

References

Adam, N. K. (1946). Physical Chemistry of Cells and Tissues. *Nature* 158, 358–359. doi: 10.1038/158358a0

Allen, L. A., Kalani, A. H., Estante, F., Rosengren, A. J., Stodieck, L., Klaus, D., et al. (2022). Simulated micro-, lunar, and Martian gravities on earth—effects on *Escherichia coli* growth, phenotype, and sensitivity to antibiotics. *Life* 12:1399. doi: 10.3390/life12091399

Aunins, T. R., Erickson, K. E., Prasad, N., Levy, S. E., Jones, A., Shrestha, S., et al. (2018). Spaceflight modifies *Escherichia coli* gene expression in response to antibiotic exposure and reveals role of oxidative stress response. *Front. Microbiol.* 9:310. doi: 10.3389/fmicb.2018.00310

Benoit, M. R., and Klaus, D. M. (2007). Microgravity, bacteria, and the influence of motility. *Adv. Space Res.* 39, 1225–1232. doi: 10.1016/j.asr.2006.10.009

Berliner, A. J., Hilzinger, J. M., Abel, A. J., McNulty, M. J., Makrygiorgos, G., Averesch, N. J. H., et al. (2021). Towards a biomanufactory on Mars. *Front. Astron. Space Sci.* 8. doi: 10.3389/fspas.2021.711550

Bijlani, S., Stephens, E., Singh, N. K., Venkateswaran, K., and Wang, C. C. C. (2021). Advances in space microbiology. *IScience* 24:102395. doi: 10.1016/j.isci.2021.102395

Bluck, J. (2007). "NASA–GeneSat-1." Feature Articles, Other. Brian Dunbar. Available at: https://www.nasa.gov/centers/ames/missions/2007/genesat1.html (Accessed March 26, 2007).

Chan, T. C., Li, H. T., and Li, K. Y. (2015). Effects of shapes of solute molecules on diffusion: a study of dependences on solute size, solvent, and temperature. *J. Phys. Chem. B* 119, 15718–15728. doi: 10.1021/acs.jpcb.5b10550

Chao, T.-C., and Das, D. B. (2015). Numerical simulation of coupled cell motion and nutrient transport in NASA's rotating bioreactor. *Chem. Eng. J.* 259, 961–971. doi: 10.1016/j.cej.2014.08.077

Coglitore, D., Edwardson, S. P., Macko, P., Patterson, E. A., and Whelan, M. (2017). Transition from fractional to classical Stokes–Einstein behaviour in simple fluids. *R. Soc. Open Sci.* 4:170507. doi: 10.1098/rsos.170507

Cold Spring Harbor Protocols (2010). M9 Minimal Medium (Standard). *Cold Spring Harb. Protoc.* 2010:pdb.rec12295. doi: 10.1101/pdb.rec12295

Crank, J. (1979). *The Mathematics of Diffusion*. Oxford Science Publications. Clarendon Press.

D'Arrigo, J. S. (1978). Screening of membrane surface charges by divalent cations: an atomic representation. *Am. J. Phys.* 235, C109–C117. doi: 10.1152/ajpcell.1978.235.3.C109

El-Hajj, Z. W., and Newman, E. B. (2015). How much territory can a single *E. coli* cell control? *Front. Microbiol.* 6. doi: 10.3389/fmicb.2015.00309

Guasto, J. S., Rusconi, R., and Stocker, R. (2012). Fluid mechanics of planktonic microorganisms. *Annu. Rev. Fluid Mech.* 44, 373–400. doi: 10.1146/annurev-fluid-120710-101156

Gumulya, Y., Zea, L., and Kaksonen, A. H. (2022). In situ resource utilisation: the potential for space biomining. *Miner. Eng.* 176:107288. doi: 10.1016/j.mineng.2021.107288

Hammond, T. G., and Hammond, J. M. (2001). Optimized suspension culture: the rotating-wall vessel. *Am. J. Physiol-Renal Physiol.* 281, F12–F25. doi: 10.1152/ajprenal.2001.281.1.F12

Harcombe, W. R., Riehl, W. J., Dukovski, I., Granger, B. R., Betts, A., Lang, A. H., et al. (2014). Metabolic resource allocation in individual microbes determines ecosystem interactions and spatial dynamics. *Cell Rep.* 7, 1104–1115. doi: 10.1016/j.celrep.2014.03.070

Horneck, G., Klaus, D. M., and Mancinelli, R. L. (2010). Space Microbiology. *Microbiol. Mol. Biol. Rev.* 74, 121–156. doi: 10.1128/MMBR.00016-09

Johnson, K. A., and Goody, R. S. (2011). The original Michaelis constant: translation of the 1913 Michaelis-Menten paper. *Biochemistry* 50, 8264–8269. doi: 10.1021/bi201284u

Julou, T., Zweifel, L., Blank, D., Fiori, A., and van Nimwegen, E. (2020). Subpopulations of sensorless bacteria drive fitness in fluctuating environments. *PLoS Biol.* 18:e3000952. doi: 10.1371/journal.pbio.3000952

Karp-Boss, L., Boss, E., and Jumars, P. (1996). Nutrient fluxes to planktonic osmotrophs in the presence of fluid motion. *Oceanogr. Mar. Biol.* 34, 71–107.

Keller, R. J., Porter, W., Goli, K., Rosenthal, R., Butler, N., and Jones, J. A. (2021). Biologically-based and physiochemical life support and in situ resource utilization for exploration of the solar system—reviewing the current state and defining future development needs. *Life* 11:844. doi: 10.3390/life11080844

Klaus, D. M. (2001). Clinostats and bioreactors. *Gravit. Space Res.* 14, 55–64.

Klaus, D. M., Benoit, M. R., Nelson, E. S., and Hammond, T. G. (2004). Extracellular mass transport considerations for space flight research concerning suspended and adherent in vitro cell cultures. *J. Gravit. Physiol.* 11, 17–27.

Klaus, D., Simske, S., Todd, P., and Stodieck, L. (1997). Investigation of space flight effects on *Escherichia coli* and a proposed model of underlying physical mechanisms. *Microbiology* 143, 449–455. doi: 10.1099/00221287-143-2-449

Lazier, J. R. N., and Mann, K. H. (1989). Turbulence and the diffusive layers around small organisms. *Deep Sea Res. A. Oceanogr. Res. Papers* 36, 1721–1733. doi: 10.1016/0198-0149(89)90068-X

Liu, H., Yao, Z., Yuming, F., and Feng, J. (2021). Review of research into bioregenerative life support system(s) which can support humans living in space. *Life Sci. Space Res.* 31, 113–120. doi: 10.1016/j.lssr.2021.09.003

Lopez, J. V., Peixoto, R. S., and Rosado, A. S. (2019). Inevitable future: space colonization beyond earth with microbes first. *FEMS Microbiol. Ecol.* 95:fiz127. doi: 10.1093/femsec/fiz127

M., Uri. (n.d.). "Size of glucose ring molecule-BNID 110368." B10Numb3R5: The Database of Useful Biological Numbers. Available at: https://bionumbers.hms.harvard.edu/bionumber.aspx?id=110368 (Accessed March 10, 2023).

McNulty, M. J., Xiong, Y. M., Yates, K., Karuppanan, K., Hilzinger, J. M., Berliner, A. J., et al. (2021). Molecular pharming to support human life on the moon, Mars, and beyond. *Crit. Rev. Biotechnol.* 41, 849–864. doi: 10.1080/07388551.2021.1888070

Mozdzierz, N. J., Love, K. R., Lee, K. S., Lee, H. L. T., Shah, K. A., Ram, R. J., et al. (2015). A perfusion-capable microfluidic bioreactor for assessing microbial heterologous protein production. *Lab. Chip* 15, 2918–2922. doi: 10.1039/c5lc00443h

Nadell, C. D., Drescher, K., and Foster, K. R. (2016). Spatial structure, cooperation and competition in biofilms. *Nat. Rev. Microbiol.* 14, 589–600. doi: 10.1038/nrmicro.2016.84

NASA Technology Transfer. (n.d). "*In-situ* resource utilization (ISRU): methylotrophic microorganisms expressing soluble methane monooxygenase proteins|T2 portal." Available at: https://technology.nasa.gov/patent/TOP2-283 (Accessed July 8, 2022).

Natarajan, A., and Srienc, F. (1999). Dynamics of glucose uptake by single *Escherichia coli* cells. *Metab. Eng.* 1, 320–333. doi: 10.1006/mben.1999.0125

Nickerson, C. A., Mark Ott, C., Wilson, J. W., Ramamurthy, R., LeBlanc, C. L., Höner, K., et al. (2003). Low-shear modeled microgravity: a global environmental regulatory signal affecting bacterial gene expression, physiology, and pathogenesis. *J. Microbiol. Methods* 54, 1–11. doi: 10.1016/S0167-7012(03)00018-6

Purcell, E. M. (1978). The effect of fluid motions on the absorption of molecules by suspended particles. *J. Fluid Mech.* 84, 551–559. doi: 10.1017/S0022112078000324

Ricco, A. J., Maria, S. R. S., Hanel, R. P., and Bhattacharya, S. (2020). BioSentinel: A 6U Nanosatellite for Deep-Space Biological Science. *IEEE Aerospace and Electronic Systems Magazine* 35, 6–18. doi: 10.1109/MAES.2019.2953760

Tabor, A. (2022). "What is BioNutrients?" *NASA*. Available at: https://www.nasa.gov/ames/bionutrients/. (Accessed July 7, 2022).

Todd, P. (1989). Gravity-dependent phenomena at the scale of the single cell. *ASGSB Bull.* 2, 95–113.

Ursell, L. K., Metcalf, J. L., Parfrey, L. W., and Knight, R. (2012). Defining the human microbiome. *Nutr. Rev.* 70, S38–S44. doi: 10.1111/j.1753-4887.2012.00493.x

Wang, C., Xing, W., and Fan, L. (2022). A summary of previous investigations of the microgravity effects on bacterial virulence, infection and antibiotic resistance. *Acta Astronaut.* 196, 215–219. doi: 10.1016/j.actaastro.2022.04.029

Wilson, J. W., Ott, C. M., Bentrup, H. Z., Ramamurthy, R., Quick, L., Porwollik, S., et al. (2007). Space flight alters bacterial gene expression and virulence and reveals a role for global regulator Hfq. *Proc. Natl. Acad. Sci.* 104, 16299–16304. doi: 10.1073/pnas.0707155104

Wuest, S. L., Stern, P., Casartelli, E., and Egli, M. (2017). Fluid dynamics appearing during simulated microgravity using random positioning machines. *PLoS One* 12:e0170826. doi: 10.1371/journal.pone.0170826

frontiers | Frontiers in Microbiology

TYPE Original Research
PUBLISHED 17 May 2023
DOI 10.3389/fmicb.2023.1150224

OPEN ACCESS

EDITED BY
Donatella Tesei,
University of Natural Resources and Life Sciences Vienna, Austria

REVIEWED BY
Rajeshwar P. Sinha,
Banaras Hindu University, India
Madhan Tirumalai,
University of Houston, United States

*CORRESPONDENCE
Daniela Billi
✉ billi@uniroma2.it

RECEIVED 23 January 2023
ACCEPTED 21 April 2023
PUBLISHED 17 May 2023

CITATION
Fagliarone C, Mosca C, Di Stefano G, Leuko S, Moeller R, Rabbow E, Rettberg P and Billi D (2023) Enabling deep-space experimentations on cyanobacteria by monitoring cell division resumption in dried *Chroococcidiopsis* sp. 029 with accumulated DNA damage. *Front. Microbiol.* 14:1150224. doi: 10.3389/fmicb.2023.1150224

Enabling deep-space experimentations on cyanobacteria by monitoring cell division resumption in dried *Chroococcidiopsis* sp. 029 with accumulated DNA damage

Claudia Fagliarone[1], Claudia Mosca[1], Giorgia Di Stefano[1,2], Stefan Leuko[3], Ralf Moeller[3,4], Elke Rabbow[5], Petra Rettberg[5] and Daniela Billi[1]*

[1]Department of Biology, University of Rome Tor Vergata, Rome, Italy, [2]PhD Program in Cellular and Molecular Biology, Department of Biology, University of Rome Tor Vergata, Rome, Italy, [3]Aerospace Microbiology Research Group, Radiation Biology Department, Institute of Aerospace Medicine, German Aerospace Center (DLR), Cologne, Germany, [4]Department of Natural Sciences, University of Applied Sciences Bonn-Rhein-Sieg (BRSU), Rheinbach, Germany, [5]Astrobiology Research Group, Radiation Biology Department, Institute of Aerospace Medicine, German Aerospace Center (DLR), Cologne, Germany

Cyanobacteria are gaining considerable interest as a method of supporting the long-term presence of humans on the Moon and settlements on Mars due to their ability to produce oxygen and their potential as bio-factories for space biotechnology/synthetic biology and other applications. Since many unknowns remain in our knowledge to bridge the gap and move cyanobacterial bioprocesses from Earth to space, we investigated cell division resumption on the rehydration of dried *Chroococcidiopsis* sp. CCMEE 029 accumulated DNA damage while exposed to space vacuum, Mars-like conditions, and Fe-ion radiation. Upon rehydration, the monitoring of the *ftsZ* gene showed that cell division was arrested until DNA damage was repaired, which took 48 h under laboratory conditions. During the recovery, a progressive DNA repair lasting 48 h of rehydration was revealed by PCR-stop assay. This was followed by overexpression of the ftsZ gene, ranging from 7.5- to 9-fold compared to the non-hydrated samples. Knowing the time required for DNA repair and cell division resumption is mandatory for deep-space experiments that are designed to unravel the effects of reduced/microgravity on this process. It is also necessary to meet mission requirements for dried-sample implementation and real-time monitoring upon recovery. Future experiments as part of the lunar exploration mission Artemis and the lunar gateway station will undoubtedly help to move cyanobacterial bioprocesses beyond low Earth orbit. From an astrobiological perspective, these experiments will further our understanding of microbial responses to deep-space conditions.

KEYWORDS

outer space, DNA damage, cell division, Fe-ion radiation, desert cyanobacteria

Introduction

Long-term human presence on the Moon and future settlements on Mars will depend on the development of self-sufficient life support systems that will minimize dependence on resupply from Earth. Microorganisms offer great promise to support deep-space exploration: A so-called biomanufactory was proposed for human outposts on Mars, based on *in situ* resource utilization and biologically driven subunits for needed bioprocesses (Berliner et al., 2021). In such a scenario, cyanobacteria are gaining considerable interest due to their ability to produce oxygen and their potential as bio-factories for space biotechnology/synthetic biology applications (for a review see Mapstone et al., 2022). The "PowerCell" concept proposed cultivating cyanobacteria with raw materials available on the Moon and Mars to feed the bacteria used in biotechnology/synthetic biology (Rothschild, 2016). Recently, it was shown that the biomass produced by the desert cyanobacterium *Chroococcidiopsis* sp. 029 can be used as feedstock for bacteria (Billi et al., 2021).

Future lunar exploration mission Artemis and the lunar Gateway station (Crusan et al., 2019; Smith et al., 2020) will undoubtedly offer a unique opportunity to advance the use of cyanobacterial bioprocesses in space. Microorganisms on board the International Space Station (ISS) have exhibited global alterations in metabolic functions and gene expression, causing variations in biofilm formation, sporulation, and virulence (for a review see Milojevic and Weckwerth, 2020). Many unknowns remain in bridging the gaps in knowledge required to move cyanobacterial bioprocesses from Earth to space, and, for realistic microbial bioprocesses in space, a deeper understanding of the recovery process after traveling in space and subsequent reactivation is mandatory. In NASA's BioSentinel CubeSat, launched as a secondary payload on Artemis-1, dried cells of *Saccharomyces cerevisiae* are scheduled to be reactivated during an 18-month permanence in deep space, meaning that DNA damage repair will be monitored in deep space (Massaro Tieze et al., 2020; Santa Maria et al., 2020).

The investigations performed using ground-based simulations or facilities installed outside the ISS offer a baseline testbed for deep-space experiments by providing insights into microbial survivability after they have traveled through space and undergone subsequent reactivation. Post-flight analyses of the rehydration of the cyanobacterium *Chroococcidiopsis* sp. 029 exposed to space and Mars-like conditions during the BOSS (Biofilms Organisms Surfing Space) space mission showed: i) the upregulation of DNA repair genes in cells exposed to space vacuum (Mosca et al., 2021) and ii) the absence of increased genome variants in cells exposed to Mars-like conditions (Napoli et al., 2022). An upregulation of DNA repair genes was also reported during the rehydration of dried cells irradiated with Fe ions (Mosca et al., 2022) during the STARLIFE irradiation campaign (Moeller et al., 2017).

These results on the recovery of dried *Chroococcidiopsis* sp. 029 with accumulated DNA damage laid the foundation for its suitability for deep-space experimentation, which is necessary to unravel the effect of reduced/microgravity on the recovery process. However, even though the role of DNA repair genes was reported, it is fundamental to assess the timeframe needed for DNA repair and cell division resumption upon rehydration. This knowledge might be vital to meet mission requirements for dried-sample implementation and real-time monitoring upon recovery, in case of extensive pre-flight periods and unguaranteed sample return.

The link between DNA damage repair and cell division arrest is provided by the regulation of the *ftsZ* gene expression. In bacteria such as *Escherichia coli*, when RecA binds to single-stranded DNA, it stimulates the autocatalytic cleavage of LexA. This is then followed by the expression of the SOS repair genes, including the *sulA* gene that causes cell division delay through the inhibition of the FtsZ polymerization (Kreuzer, 2013). A comparative genome analysis suggested that the *E. coli*-like SOS model might not be valid for all cyanobacteria: The *lexA* gene, which regulates the SOS system, is unevenly distributed among the analyzed genomes, while the *sulA* gene, which stalls cell division until DNA reparation, is ubiquitous (Cassier-Chauvat et al., 2016). Thus far, it is unknown whether the *E. coli*-like SOS model is present in *Chroococcidiopsis* sp. 029, although it was reported that FtsZ is a critical component of its cell division machinery (Billi, 2009).

The present study aimed to determine the timeframe between DNA damage repair and cell division resumption upon the rehydration of dried *Chroococcidiopsis* sp. 029 that has undergone DNA damage. Lesions were accumulated during the exposure to space and Mars-like conditions during the BOSS space experiment and Fe-ion radiation during the STARLIFE project.

The presence of genome lesions and their repair upon rehydration was determined by using a PCR-stop assay by amplifying a 4-kbp genome fragment. Cell division resumption was determined by monitoring the expression of the cell division *ftsZ* gene by quantitative polymerase chain reaction (RT-qPCR) during 48 h of rehydration.

Materials and methods

Cyanobacterial strain and sample preparation

Chroococcidiopsis sp. 029 was isolated by Roseli Ocampo-Friedmann from cryptoendolithic growth in sandstone in the Negev Desert (Israel) and maintained at the University of Rome Tor Vergata, as part of the Culture Collection of Microorganisms from Extreme Environments established by E. Imre Friedmann. Cultures were grown under routine conditions at 25°C in BG-11 liquid medium (Rippka et al., 1979) under a photon flux density of 40 μmol/m^2/s provided by fluorescent cool-white bulbs. Dried samples for the BOSS space experiment of the EXPOSE-R2 space mission were prepared as previously reported (Billi et al., 2019). Biofilms were obtained by growing cyanobacterial cells on top of BG-11 agarized medium for about 2 months, following which they were allowed to air-dry for about 15 days under routine growth conditions and finally stored in the dark under laboratory conditions. Dried cells for the STARLIFE experiment were prepared as previously reported

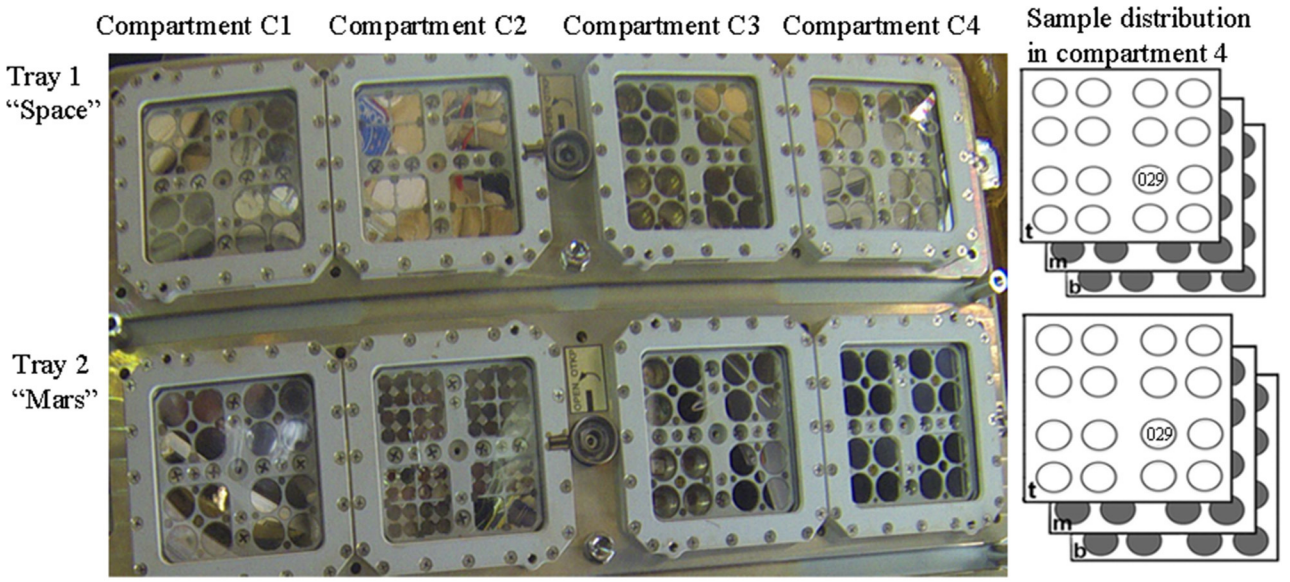

FIGURE 1
Sample distribution in the EXPOSE-R2 hardware. In compartment 4 of Tray 1 "Space" and Try 2 "Mars", samples were allocated in top-layer (t), middle (m), and bottom-layer carrier (b). Dried biofilms of *Chroococcidiopsis* sp. 029 used in this study were exposed in the position 11 middle-layer of the carrier. Photo credits: Roscosmos and ESA.

(Verseux et al., 2017). Briefly, cells from cultures in the early stationary phase were immobilized on Millipore filters, air-dried overnight in a sterile hood, and stored in the dark under laboratory conditions.

Exposure to space vacuum and Mars-like conditions in low Earth orbit

In the context of the BOSS space experiment, which aimed to investigate biofilm resistance under space and Mars-like conditions in LEO (Cottin and Rettberg, 2019), dried biofilms of *Chroococcidiopsis* sp. 029 were accommodated in the compartment C4 of the tray 1 "space" and of the tray 2 "Mars" of the EXPOSE-R2 hardware (Figure 1). In the present study, we analyzed samples from the middle-layer carrier that were exposed for 672 days to a space vacuum and 0.5 Gy of cosmic ionizing radiation and temperature values ranging from −20.9°C to 57.98°C (Dachev et al., 2017; Rabbow et al., 2017). After retrieval to Earth, 2.5-year-old samples (considering 900 days from launch to space and sample shipping to the laboratory) were stored for an additional 4.5 years in an air-dried state under laboratory conditions. Control biofilms were air-dried and stored in the dark at room temperature for 7 years.

Exposure to Fe-ion irradiation

Cells were first immobilized on Millipore filters and shipped to the Heavy Ion Medical Accelerator in Chiba (HIMAC, Gunma University Heavy Ion Medical Center, Japan) for irradiation, which was performed in June 2018 during the STARLIFE project, as previously reported (Mosca et al., 2022). After irradiation with 2 kGy of Fe ions, the air dried samples were stored in the dark at room temperature for 2 years.

Sample recovery

Aliquots of dried cells and dried-exposed cells (about 25 mm^2) were resuspended in 1 ml of BG-11 and allowed to recover under standard growth conditions as reported above.

DNA damage evaluation

Genomic DNA was extracted from dried samples and from samples at different time points of rehydration by modifying a method previously reported (Billi et al., 1998). Briefly, the lysis of *Chroococcidiopsis* cells was achieved by adding hot phenol and glass beads. Then the pooled aqueous phases were first extracted with phenol–chloroform–isoamyl alcohol and followed by chloroform–isoamyl alcohol as described (Mosca et al., 2019). The PCR-stop assay was performed by amplifying a 4-kbp genome fragment using 6 ng of genomic DNA in 12-μl reaction mixtures containing 0.5 μM each of primers Chroo-4 K-2-F (5′-GCTACTCGTTGCTTTGCGTC-3′) and Chroo-4 K-2-R (5′-TTCCCCATACTTTGCTTCCCA-3′) and 6 μl of High-Fidelity Master Mix (Thermo Fisher Scientific, Waltham, MA, USA) as described (Mosca et al., 2019). A no-template control was included. Each one of the 12-μl PCR reaction mixtures was loaded onto a 1.5% agarose gel containing 0.5 mg/ml of ethidium bromide,

subjected to electrophoresis for about 1 h at 90 V, and visualized with a trans-illuminator.

Gene expression upon recovery

At different time points of rehydration, total RNA was extracted as described (Fagliarone et al., 2020). Real-time reactions were performed in 12 µl, including 1 µg of cDNA template, 6 µl of iTaq^{TM} universal SYBR$^{®}$ Green Supermix (Bio-Rad Laboratories, Hercules, CA, USA), and 400 nM of forward primer chrftsZ-F (5′-GTTGACTTTGCCGATGTCCG-3′) and reverse primer chrftsZ-R (5′-CTTCTCTGGCACGGGACTTT-3′) that were designed based on a 473-bp fragment previously identified (Billi, 2009). PCR cycling conditions were as follows: a cycle of 95°C for 10 min, then 40 cycles of 95°C for 15 s, and 60°C for 1 min, followed by a ramp from 60 to 95°C for the melting curve stage. Quantification was performed using the Ct comparative method ($2^{-\Delta\Delta Ct}$ method) and using the 16S rRNA gene as the housekeeping gene (GenBank accession number AF279107) and employing the primers chr16S-F (5′-TACTACAATGCTACGGACAA-3′) and chr16S-R (5′-CCTGCAATCTGAACTGAG-3′). All cDNA quantities were normalized to 16S rRNA quantities, and fold changes of gene transcripts were compared to the values of non-rehydrated samples set as 1. Values >1 were considered upregulated, and values <1 were considered downregulated. Five rehydration time points (1, 6, 12, 24, and 48 h) were evaluated for dried cells exposed to Fe ions and 7 years of dried storage. Three rehydration time points (1, 6, and 48 h) were tested for dried biofilms exposed during the BOSS space mission, due to the limited availability of samples. In each PCR protocol, three replicates were performed, and no-template control was included.

Statistical analysis

Only one sample for each condition was allocated in the EXPOSE-R2 facility. Therefore, three replicates for biologically distinct samples (different cultures) exposed to air-drying under laboratory conditions and Fe-ion irradiation were used, as well as three replicates of a single sample exposed to space vacuum and Mars-like conditions. Data are shown with standard deviation, and significance was assessed by using Student's *t*-test.

Results

DNA damage accumulated in dried cells and its recovery upon rehydration

The presence of DNA damage was qualitatively determined by using a PCR-stop assay that evaluates the genome suitability as a template for PCR amplifications since lesions impede DNA polymerase progression (Kumar et al., 2004). When a 4-kbp genome fragment was amplified as a target, a reduction of the amplicon intensity was observed in dried biofilms exposed to Mars-like conditions (Figure 2, lane 4) compared to control liquid culture (Figure 2, lane 2) and dried control biofilms maintained in the dark at room temperature for 7 years (Figure 2, lane 3). No amplicons occurred in the PCR-stop assay performed with no genomic DNA (not shown). DNA damage in dried cells exposed to a space vacuum and to 2 kGy of Fe ions was previously reported (Mosca et al., 2021, 2022).

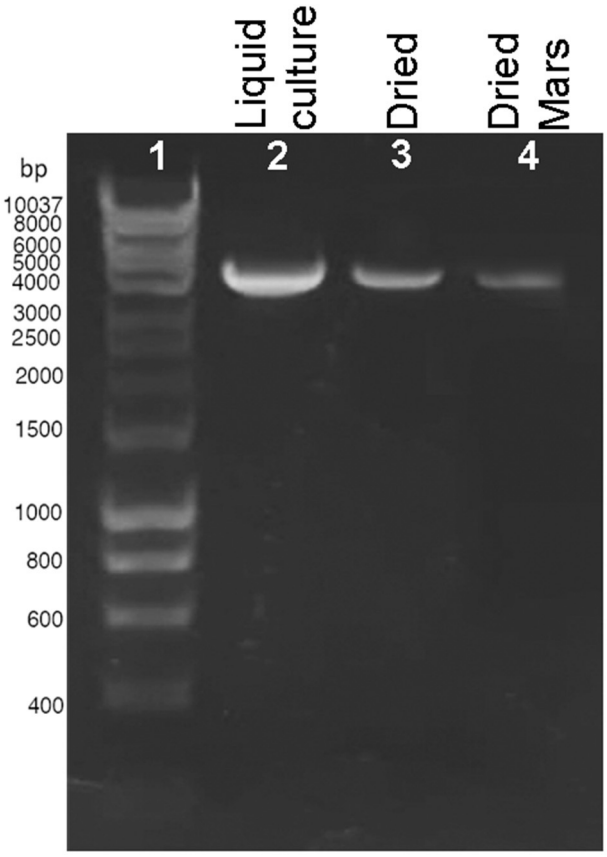

FIGURE 2
DNA damage accumulation in *Chroococcidiopsis* sp. 029 evaluated by PCR-stop assay with a 4-kbp amplification target. Control liquid culture (lane 2), dried biofilms maintained for 7 years in the dark, at room temperature (lane 3), and dried biofilms exposed to Mars-like conditions (lane 4). Lane 1: Hyperladder 1 kbp (Bioline Meridian Life Science, Memphis, TN, USA).

During 48 h of rehydration, the 4-kbp amplicon was gradually restored in both dried cells exposed to 2 kGy of Fe ions (Figure 3A) and dried biofilms maintained in the dark at room temperature for 7 years (Figure 3B). For both samples, the intensity of the amplicon band continued to increase after 6 h of rehydration (Figures 3A, B), and no amplicons were observed in the PCR-stop assay performed with no genomic DNA (not shown). Due to the limited sample availability of the dried samples employed in the BOSS space mission, the DNA recovery during rehydration was not evaluated.

ftsZ gene expression upon the rehydration of dried cells with damaged DNA

The cell division resumption was monitored during the 48 h of rehydration of dried cells with accumulated DNA damage, by determining the expression of the *ftsZ* gene (Figure 4). Dried

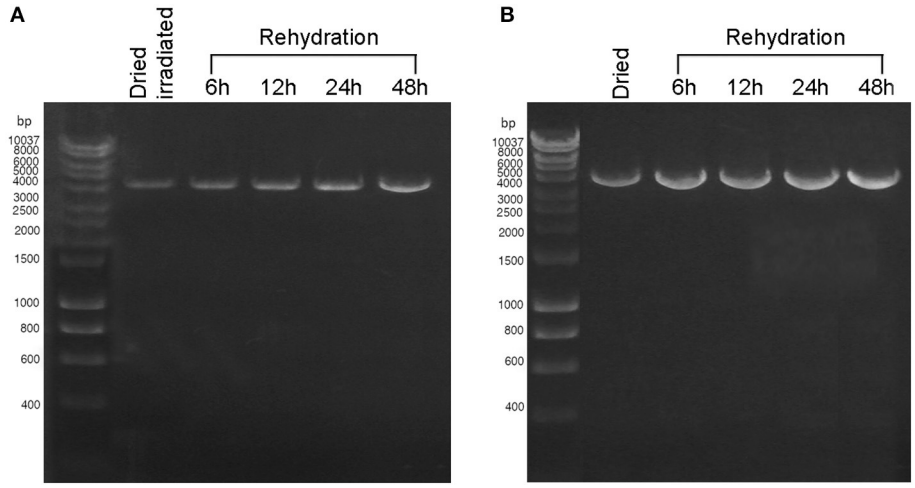

FIGURE 3
DNA damage restoration upon the rehydration of *Chroococcidiopsis* sp. 029 evaluated by PCR-stop assay with a 4-kbp amplification target. **(A)** Dried cells were exposed to 2 kGy of Fe ions (lane 2) and after 6, 12, 24, and 48-h recovery (lanes 3–6). **(B)** Dried cells were stored for 7 years in the dark at room temperature (lane 2) and after 6, 12, 24, and 48 h of recovery (lanes 3–6). Lane 1: Hyperladder 1 kbp (Bioline Meridian Life Science, Memphis, TN, USA).

biofilms exposed to a space vacuum did not show any upregulation of the *ftsZ* gene during 1 h and 6 h of rehydration, while this gene was 7.5-fold upregulated after 48 h of rehydration, compared to the non-rehydrated sample (Figure 4A). In comparison to the non-rehydrated sample, dried biofilms exposed to Mars-like conditions showed a 2.5-fold increase in the transcriptional level of the ftsZ gene after 6 h and a 9-fold increase after 48 h recovery (Figure 4B). During the rehydration of dried cells irradiated with 2 kGy of Fe ions, the *ftsZ* gene showed a 3-fold upregulation after 48 h of rehydration (Figure 4C). The *ftsZ* gene was not upregulated during 1, 6, 12, and 24 h of rehydration in biofilms that had been air-dried in the dark for 7 years at room temperature. However, the gene was 10.4-fold over-expressed after 48 h of rehydration compared to the non-rehydrated sample (Figure 4D).

Discussion

With the upcoming long-term space explorations, it is becoming increasingly important to broaden our understanding of microbial bioprocesses toward moving the same from Earth to space. Cyanobacteria are expected to play a key role in supporting long-term human presence on the Moon and future settlements on Mars (Mapstone et al., 2022). Thus, a deeper understanding of their recovery process after traveling in space and subsequent reactivation is very relevant.

Here, the timeframe required for DNA repair and cell division resumption under laboratory growth conditions was assessed during the rehydration of dried cells of the cyanobacterium *Chroococcidiopsis* sp. 029 that accumulated DNA damage during the BOSS space experiment (Mosca et al., 2021) and Fe-ion during the STARLIFE irradiation campaign (Mosca et al., 2022). Upon rehydration, the expression of the cell division gene *ftsZ* gene and the progression of the DNA damage restoration indicated that the cell division resumption required 48 h from the rehydration onset. Although the key role of FtsZ in the cell division machinery of *Chroococcidiopsis* sp. 029 was previously reported (Billi, 2009), the molecular mechanism involved in delaying cell division until DNA damage is repaired remains to be elucidated. However, a possible involvement of the *sulA* gene is anticipated since, in agreement with its ubiquity in cyanobacteria (Cassier-Chauvat et al., 2016), it is present in the genome of *Chroococcidiopsis* sp. 029 (Billi D. personal communication).

Due to the limited sample availability of the flight samples, the recovery of DNA damage was monitored by PCR-stop assay during the rehydration of air-dried cells and dried cells exposed to Fe-ion radiation, but not of dried cells exposed to Mars-like conditions and space vacuum. Although the PCR-stop assay did not determine the lesion type, the presence of DNA lesions in dried cells exposed to space vacuum and Fe-ion irradiation is known to be largely represented by single- and double-strand breaks and oxidative damage. Previous research has shown that genes of the homologous recombination RecF pathway and base excision are upregulated during the rehydration of dried cells exposed to space vacuum and Fe-ion irradiation (Mosca et al., 2021, 2022).

In the BOSS space mission, dried *Chroococcidiopsis* sp. 029 allocated in the middle-layer carrier of tray 1 "Space" was exposed to a space vacuum combined with 0.5 Gy of cosmic ionizing radiation (Dachev et al., 2017). Although this is a non-lethal dose for a cyanobacterium that can tolerate up to 12 kGy in the dried state (Verseux et al., 2017), it simulates the dose accumulated during a trip to Mars. Hence, it is anticipated that a 48-h recovery should be allowed in future space experiments aimed to investigate the effects of reduced gravity/microgravity on the DNA repair process upon the rehydration of dried cells that accumulated DNA damage.

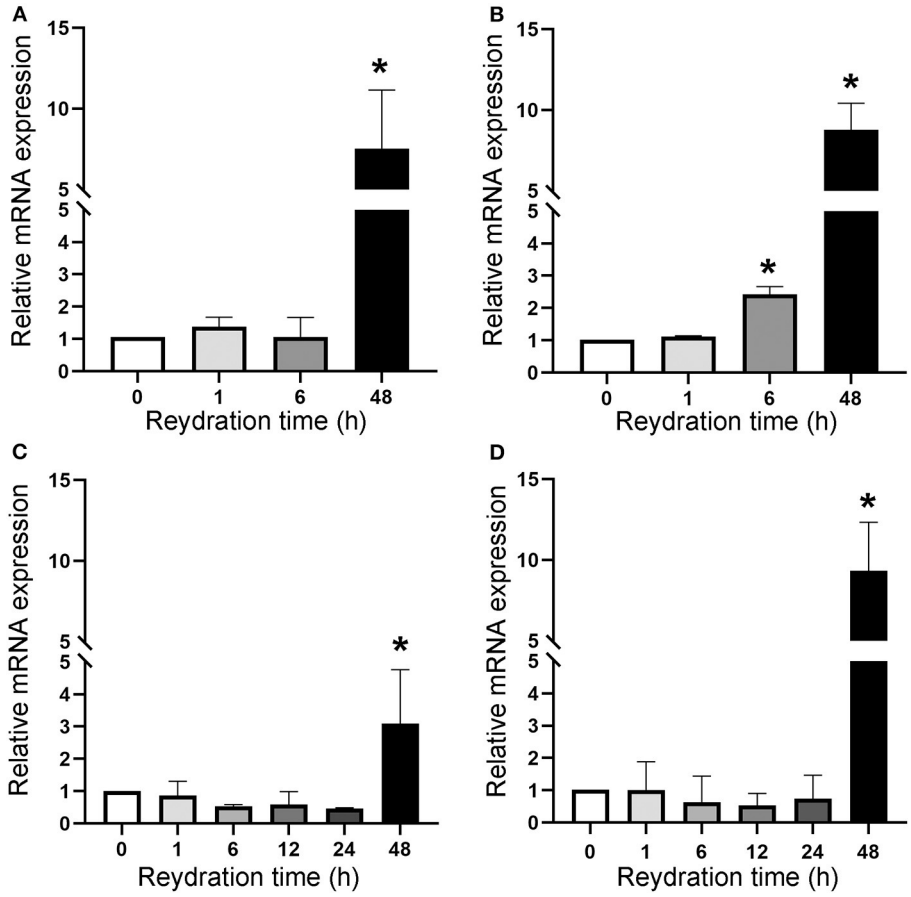

FIGURE 4
Expression of *ftsZ* gene upon the recovery of dried biofilms of *Chroococcidiopsis* sp. 029 exposed to space vacuum **(A),** Mars-like conditions **(B),** irradiation with Fe ions **(C)**, and in dried biofilms maintained for 7 years in the dark at room temperature **(D)**. Values from dried samples were considered control and set as 1. Data represent mean ± SD ($n = 3$), *$p < 0.05$.

In the BOSS space mission, dried *Chroococcidiopsis* sp. 029 allocated in the middle-layer carrier of tray 2 "Mars" experienced about 0.5 Gy of cosmic ionizing radiation in a Mars-like atmosphere (Rabbow et al., 2017). The exposure to 980 Pa of a gas mixture composed mainly of CO_2 might explain reduced DNA damage as suggested by a 2.5-fold expression of the *ftsZ* gene after 6 h of rehydration, whereas a 9-fold expression occurred after 48 h of rehydration. The absence of oxygen in the tray 2 "Mars" might have caused reduced DNA damage as previously reported (Schulte-Frohlinde et al., 1994). In the context of microbial-based technologies for space settlements on Mars, a scenario of accidental failures causing exposure to a combination of low-pressure and CO2 should be taken into account (Cockell, 2022). Thus, this result is relevant for biomanufactory on Mars.

The suitability of *Chroococcidiopsis* sp. 029 for deep-space investigations was further supported by DNA repair and cell division resumption of dried cells exposed to Fe ions, which are the more lethal components of the galactic cosmic radiation since they induce complex DNA damage (Horneck et al., 2010). The DNA repair and cell division resumption of dried biofilms stored for 7 years in air-dried state in the dark at room temperature further highlighted the suitability of this cyanobacterium for space missions that require extensive pre-flight periods.

In conclusion, the monitoring of the *ftsZ* gene expression determined the timeframe for DNA repair and cell division resumption. Data from this study have important implications for further studies on the effects of reduced gravity/microgravity on this process, as well as, for deep-space missions requiring the implementation of dried samples and real-time monitoring upon reactivation. Within the upcoming lunar exploration mission Artemis and lunar Gateway station, deep-space experiments will facilitate further understanding toward moving microbial bioprocesses beyond Earth. From an astrobiological perspective, such experimentation will further our understanding of microbial response to deep-space conditions.

Data availability statement

The original contributions presented in the study are included in the article, further inquiries can be directed to the corresponding author.

Author contributions

DB: supervision, conceptualization, and writing—review and editing. PR: conceived and coordinated the BOSS experiment.

RM: conceived and coordinated the STARLIFE experiment. ER and SL: contributed to sample exposure. CF, CM, and GDS: contributed to methodology, validation, and data analysis. All authors discussed the results and commented on the manuscript. All authors contributed to the article and approved the submitted version.

Funding

This research was supported by the Italian Space Agency (ASI, DC-VUM-2017-034, Grant No. 2019-3 U.0 Life in Space to DB). RM and SL were supported by the Grant DLR-FuE-Projekt ISS LIFE (Programm RF-FuW, Teilprogramm 475).

Conflict of interest

The authors declare that the research was conducted in the absence of any commercial or financial relationships that could be construed as a potential conflict of interest.

Publisher's note

References

Berliner, A. J., Hilzinger, J. M., Abel, A. J., McNulty, M. J., Makrygiorgos, G., Averesch, N. J. H., et al. (2021). Towards a biomanufactory on Mars. *Front. Astron. Space Sci.* 8. doi: 10.3389/fspas.2021.711550

Billi, D. (2009). Loss of topological relationships in a Pleurocapsalean cyanobacterium (*Chroococcidiopsis* sp.) with partially inactivated *ftsZ*. *Ann. Microbiol.* 59, 1–4. doi: 10.1007/BF03178322

Billi, D., Gallego Fernandez, B., Fagliarone, C., Chiavarini, S., and Rothschild, L. J. (2021). Exploiting a perchlorate-tolerant desert cyanobacterium to support bacterial growth for *in situ* resource utilization on Mars. *Int. J. Astrobiol.* 20, 29–35. doi: 10.1017/S1473550420000300

Billi, D., Grilli Caiola, M., Paolozzi, L., and Ghelardini, P. (1998). A method for DNA extraction from the desert cyanobacterium *Chroococcidiopsis* and its application to identification of *ftsZ*. *Appl. Environ. Microbiol.* 64, 4053–4056. doi: 10.1128/AEM.64.10.4053-4056.1998

Billi, D., Staibano, C., Verseux, C., Fagliarone, C., Mosca, C., Baqué, M., et al. (2019). Dried biofilms of desert strains of *Chroococcidiopsis* survived prolonged exposure to space and Mars-like conditions in low Earth orbit. *Astrobiology* 19, 1008–1017. doi: 10.1089/ast.2018.1900

Cassier-Chauvat, C., Veaudor, T., and Chauvat, F. (2016). Comparative genomics of DNA recombination and repair in cyanobacteria: biotechnological implications. *Front. Microbiol.* 7, 1809. doi: 10.3389/fmicb.2016.01809

Cockell, C. S. (2022). Bridging the gap between microbial limits and extremes in space: Space microbial biotechnology in the next 15years. *Microb. Biotechnol.* 15, 29–41. doi: 10.1111/1751-7915.13927

Cottin, H., and Rettberg, P. (2019). EXPOSE-R2 on the International Space Station (2014-2016): Results from the PSS and BOSS astrobiology experiments. *Astrobiology* 19, 975–978. doi: 10.1089/ast.2019.0625

Crusan, J., Bleacher, J., Caram, J., Craig, D., Goodliff, K., Herrmann, N., et al. (2019). *NASA's Gateway: An Update on Progress and Plans for Extending Human Presence to Cislunar Space*. Manhattan, NY: IEEE Aerospace Conference (IEEE). p. 1–19.

Dachev, T. P., Bankov, N. G., Tomov, B. T., Matviichuk, Y. N., Dimitrov, P. G., Häder, D.-P., et al. (2017). Overview of the ISS radiation environment observed during the ESA EXPOSE-R2 mission in 2014–2016. *Space Weather* 15, 1475–1489. doi: 10.1002/2016SW001580

Fagliarone, C., Napoli, A., Chiavarini, S., Baqué, M., de Vera, J.-P., and Billi, D. (2020). Biomarker preservation and survivability under and Mars-like UV flux of a desert cyanobacterium capable of trehalose and sucrose accumulation. *Front. Astron. Space Sci.* 7, 31. doi: 10.3389/fspas.2020.00031

Horneck, G., Klaus, D. M., and Mancinelli, R. L. (2010). Space microbiology. *Microbiol. Mol. Biol. Rev.* 74, 121–156. doi: 10.1128/MMBR.00016-09

Kreuzer, K. N. (2013). DNA damage responses in prokaryotes: Regulating gene expression, modulating growth patterns, and manipulating replication fork. *Cold Spring Harb. Perspect. Biol.* 5, a012674. doi: 10.1101/cshperspect.a012674

Kumar, A., Tyagi, M. B., and Jha, P. N. (2004). Evidences showing ultraviolet-B radiation-induced damage of DNA in cyanobacteria and its detection by PCR assay. *Biochem. Biophys. Res. Commun.* 318, 1025–1030. doi: 10.1016/j.bbrc.2004.04.129

Mapstone, L. J., Leite, M. N., Purton, S., Crawford, I. A., and Dartnell, L. (2022). Cyanobacteria and microalgae in supporting human habitation on Mars. *Biotechnol. Adv.* 59, 107946. doi: 10.1016/j.biotechadv.2022.107946

Massaro Tieze, S., Liddell, L. C., Santa Maria, S. R., and Bhattacharya, S. (2020). BioSentinel: a biological cubesat for deep space exploration. *Astrobiology Apr* 13. doi: 10.1089/ast.2019.2068

Milojevic, T., and Weckwerth, W. (2020). Molecular mechanisms of microbial survivability in outer space: a systems biology approach. *Front. Microbiol.* 11, 923. doi: 10.3389/fmicb.2020.00923

Moeller, R., Raguse, M., Leuko, S., Berger, T., Hellweg, C., Fujimori, A., et al. (2017). STARLIFE—An international campaign to study the role of galactic cosmic radiation in astrobiological model systems. *Astrobiology* 17, 101–109. doi: 10.1089/ast.2016.1571

Mosca, C., Fagliarone, C., Napoli, A., Rabbow, E., Rettberg, P., and Billi, D. (2021). Revival of anhydrobiotic cyanobacterium biofilms exposed to space vacuum and prolonged dryness: Implications for future missions beyond low Earth orbit. *Astrobiology* 21, 541–550. doi: 10.1089/ast.2020.2359

Mosca, C., Napoli, A., Fagliarone, C., Fujimori, A., Moeller, R., and Billi, D. (2022). Role of DNA repair pathways in the recovery of a dried, radioresistant cyanobacterium exposed to high-LET radiation: implications for the habitability of Mars. *Int J Astrobiol* 1–12. doi: 10.1017/S1473550422000131

Mosca, C., Rothschild, L. J., Napoli, A., Ferr,é, F., Pietrosanto, M., Fagliarone,. C., et al. (2019). Over-expression of UV-damage DNA repair genes and ribonucleic acid persistence contribute to the resilience of dried biofilms of the desert cyanobacetrium *Chroococcidiopsis* exposed to Mars-like UV flux and long-term desiccation. *Front. Microbiol.* 10, 2312. doi: 10.3389/fmicb.2019.02312

Napoli, A., Micheletti, D., Pindo, M., Larger, S., Cestaro, A., de Vera, J. P., et al. (2022). Absence of increased genomic variants in the cyanobacterium *Chroococcidiopsis* exposed to Mars-like conditions outside the space station. *Sci. Rep.* 12, 8437. doi: 10.1038/s41598-022-12631-5

Rabbow, E., Rettberg, P., Parpart, A., Panitz, C., Schulte, W., Molter, F., et al. (2017). EXPOSE-R2: the astrobiological ESA mission on board of the International Space Station. *Front. Microbiol.* 8, 1533. doi: 10.3389/fmicb.2017.01533

Rippka, R., Deruelles, J., Waterbury, J. B., Herdman, M., and Stanier, R. Y. (1979). Generic assignments, strain histories and properties of pure cultures of cyanobacteria. *J. Gen. Microbiol.* 111, l—61. doi: 10.1099/00221287-111-1-1

Rothschild, L. J. (2016). Synthetic biology meets bioprinting: enabling technologies for humans on Mars (and Earth). *Biochem. Soc. Trans.* 44, 1158–1164. doi: 10.1042/BST20160067

Santa Maria, S. R., Marina, D. B., Massaro Tieze, S., Liddell, L. C., and Bhattacharya, S. (2020). BioSentinel: long-term *Saccharomyces cerevisiae* preservation for a deep space biosensor mission. *Astrobiology*. doi: 10.1089/ast.2019.2073. [Epub ahead of print].

Schulte-Frohlinde, D., Ludwig, D. C., and Rettberg, P. (1994). Influence of thiols and oxygen on the survival of gamma-irradiated plasmid DNA and cells. *Adv. Space Res.* 14, 277–284. doi: 10.1016/0273-1177(94)90478-2

Smith, M., Craig, D., Herrmann, N., Mahoney, E., Krezel, J., McIntyre, N., et al. (2020). *The Artemis Program: An Overview of NASA's Activities to Return Humans to the Moon*. IEEE Aerospace Conference, Big Sky, MT.

Verseux, C., Baqué, M., Cifariello, R., Fagliarone, C., Raguse, M., Moeller, R., et al. (2017). Evaluation of the resistance of *Chroococcidiopsis* spp. to sparsely and densely ionizing irradiation. *Astrobiology* 17, 118–125. doi: 10.1089/ast.2015.1450

frontiers | Frontiers in Microbiology

TYPE Original Research
PUBLISHED 14 July 2023
DOI 10.3389/fmicb.2023.1134760

OPEN ACCESS

EDITED BY
Camilla Urbaniak,
NASA Jet Propulsion Laboratory,
United States

REVIEWED BY
Scott M. Perl,
NASA Jet Propulsion Laboratory (JPL),
United States
Ricardo Amils, Autonomous University of Madrid, Spain

*CORRESPONDENCE
Hugo Moors
✉ hugo.moors@sckcen.be

RECEIVED 30 December 2022
ACCEPTED 30 June 2023
PUBLISHED 14 July 2023

CITATION
Moors H, De Craen M, Smolders C, Provoost A and Leys N (2023) The waterbodies of the halo-volcanic Dallol complex: earth analogs to guide us, where to look for life in the universe.
Front. Microbiol. 14:1134760.
doi: 10.3389/fmicb.2023.1134760

The waterbodies of the halo-volcanic Dallol complex: earth analogs to guide us, where to look for life in the universe

Hugo Moors[1]*, Mieke De Craen[2,3], Carla Smolders[1], Ann Provoost[1] and Natalie Leys[1]

[1]Microbiology Unit, Belgian Nuclear Research Center (SCK CEN), Nuclear Medical Applications Institute (NMA), Mol, Belgium, [2]Research and Development Disposal, Belgian Nuclear Research Center (SCK CEN), Waste and Disposal (W&D), Mol, Belgium, [3]European Underground Research Infrastructure for Disposal of Nuclear Waste in Clay Environment, EIG EURIDICE, Mol, Belgium

Microbes are the Earth life forms that have the highest degree of adaptability to survive, live, or even proliferate in very hostile environments. It is even stated that microbes can cope with any extreme physico-chemical condition and are, therefore, omnipresent all over the Earth: on all the continents, inside its crust and in all its waterbodies. However, our study suggests that there exists areas and even water rich environments on Earth where no life is possible. To support the fact that water rich environments can be lifeless, we performed an extensive survey of 10 different hyper extreme waterbodies of the halo-volcanic Dallol complex (Danakil depression, Ethiopia, Horn of Africa). In our study, we combined physico-chemical analyses, mineralogical investigations, XRD and SEM–EDX analyses, ATP measurements, 16S rDNA microbial community determinations, and microbial culturing techniques. According to our findings, we suggest that the individual physico-chemical parameters, water activity, and kosmo-chaotropicity, are the two most important factors that determine whether an environment is lifeless or capable of hosting specific extreme lifeforms. Besides, waterbodies that contained saturated levels of sodium chloride but at the same time possessed extreme low pH values, appeared to be poly-extreme environments in which no life could be detected. However, we clearly discovered a low diversity microbial community in waterbodies that were fully saturated with sodium chloride and only mildly acidic. Our results can be beneficial to more precisely classify whole or certain areas of planetary bodies, including water rich environments, as either potentially habitable or factual uninhabitable environments.

KEYWORDS

Dallol, habitability, chaotropicity, water activity, salinity

1. Introduction

The question whether extraterrestrial life is or can be present, elsewhere in the universe, arose most likely at the same time when humans realized that besides Earth, other planetary bodies exist in space. The current technology allows space travel and with it, the possibility to investigate the surface and subsurface of other celestial bodies. Given the very high number of celestial bodies in our universe, it is essential to focus the search for extraterrestrial life to celestial bodies that are physico-chemical considered as habitable. Until now, telescopes like

Keppler and TESS discovered already 61 exoplanets that are located in a habitable zone (Arecibo, 2022). In this context, a habitable zone means the presence of sufficient atmospheric pressure and temperature at which liquid water can exist. However, whether a planet or a celestial object is or ever was habitable depends not only on the presence of liquid water, but also on its current or historical physico-chemical conditions.

The ongoing discovery on Earth of numerous extremophiles, microorganisms capable of surviving extreme harsh environmental conditions, make some scientist believe that there is no place on Earth where live cannot exist. However, no one will deny that nothing can survive inside a solid granite block or inside red hot lava spewed out by an active volcano. Demonstrating that even surface or subsurface waterbodies can be as lifeless as the inside of a rock is not easy and demands multiple lines of evidence before it can be stated in a scientific acceptable and convincing way (McKay, 2014).

It is always tempting to suggest the presence of life, when some biological related molecules, signals or indicators are detected. Yet, a call for very cautionary interpretation of presumed positive biological signals where one or more physico-chemical parameters clearly exceeds the current known limits of habitability (Grant, 2004; Hallsworth et al., 2007; McKay, 2014; Stevenson et al., 2015). One must always take into account that earth's atmosphere is far from sterile and explore all the numerous ways of unwanted external contaminations with living or dead microbes, biological debris, biological contaminations linked to the used methodology or materials that are prone to render false positive results (Kellogg and Griffin, 2006; Lee et al., 2012; Barberan et al., 2014; Maki et al., 2015; Amato et al., 2017; Weil et al., 2017; Behzad et al., 2018). Besides, certain physico-chemical conditions, like extreme high salinity, can be lethal for some living entities but can on the other hand enhance the fossilization process or preserve biology related structures and macromolecules, like proteins, nucleic acids or phospholipids for extended periods of time (Schreder-Gomes et al., 2022).

The halo-volcanic Dallol complex, located in the north east of the Danakil depression (Ethiopia), harbors dozens of the most extreme, hypersaline water bodies that exist on Earth (Gebresilassie et al., 2011; Perez and Chebude, 2017; Cavalazzi et al., 2019). Hypersaline waterbodies can only be present in regions having a salty geology. Evaporation is the main process for the formation of surface salt layers. But, the deep salty geology of the halo-volcanic Dallol complex is the result of ancient geological salt forming serpentinization reactions and hydrothermal activity as a consequence of the enormous subsurface heat generated by the locally ongoing continental rifting process and the close proximity of a magma reservoir (Schofield et al., 2014; Hovland et al., 2015; Warren, 2016; Pinto et al., 2017; Scribano et al., 2017; Hovland et al., 2018a,b; Cheng et al., 2019; Debure et al., 2019; Voisin et al., 2020). At the surface of the Danakil depression, thousands of years of intense solar radiation evaporated most of the remaining free surface water. The current subsurface volcanic activity still causes ascending aquifer flows of superheated water and on some locations even molten salts. The origin of the water of the ascending aquifers can be pure meteoric water, saline Red sea water or a mixture of both. Depending on the governing local physico-chemical conditions, encountered by the water flows during their rising flow path to the surface, the water can gain, salting in, or lose, salting out, substantial amounts of mineral substances of the passing salty host rock layers. When these hot saline mixtures reach the surface they give rise to a diversity of hydrothermal springs that feed basins of small waterbodies or in some cases even large lakes.

During our Danakil field expedition, in which we attempted to gain insight between extreme geology and the presence of life, 10 of these hyper saline waterbodies were extensively studied by *in situ* and *ex situ* geo-physico-chemical measurement methods, laboratory and microbiological analyses of collected samples, liquids as well as minerals and sediments collected from the shores.

2. Materials and methods

Different analytical methods were used to elucidate the environmental physico-chemical conditions that either allow or prevent microbiological life from being present. In view of accurate and representative geochemistry and geomicrobiology, special attention was given for the optimal preservation of liquid as well as solid samples. We performed *in situ* and *ex situ* physico-chemical water analyses. Mineralogy of the solid shore samples was analyzed by lithogeochemistry, whole rock analyses, and XRD and SEM–EDX investigations. The presence or absence, viability and activity of microbes, of liquid as well as solid samples, was analyzed by extra- and intracellular ATP measurements, DNA extractions of in the field obtained filtrates, residues of filtered liquid samples and dissolved solid mineral samples in our laboratories followed by 16S rDNA microbial community fingerprinting. To check microbial viability, cultivability and possible isolation, different microbial culturing techniques were attempted. Besides, SEM–EDX sample preparations were also optimized to allow the visualization of possibly present biological structures.

2.1. Geographic localization and *in situ* physico-chemical measurements

All liquid and solid samples were collected during our Danakil expedition carried out in January 2018. An excel list of all samples that were taken can be consulted in the Supplementary material. Localization of samples and *in situ* physico-chemical measurements were performed with a handheld multi-parameter measuring device, Hanna 9828, equipped with a build in GPS locator. A robust measuring probe, housing a series of rugged chemical field electrodes, was connected by means of a 5 m long watertight cable to the multi measuring device. The Hanna 9828 is capable of performing seven parallel physico-chemical measurements: Dissolved Oxygen (DO), pH, Oxidation Reduction Potential (ORP), Ionic Electrical Conductivity (IEC), Temperature (T), atmospheric pressure, and solution density. Functionality of the Hanna 9828 multi-meter was verified and thoroughly tested by measuring reference solutions, after multi point calibrations of the DO-, pH-, and IEC-measuring probes. The ORP, T, and pressure measuring probes were extensively tested in our home laboratories before the start of the expedition. Even the GPS function was tested at numerous places by comparing the displayed latitude and longitude coordinates with a multifunctional mobile Garmin Nuvi 500 GPS. During the field expedition, the pH and IEC were occasionally verified with NIST traceable reference solutions that were individually packed in small hermitically heat sealed Al-PE poaches (Hanna reference solutions). Figures 1A–C, shows a global

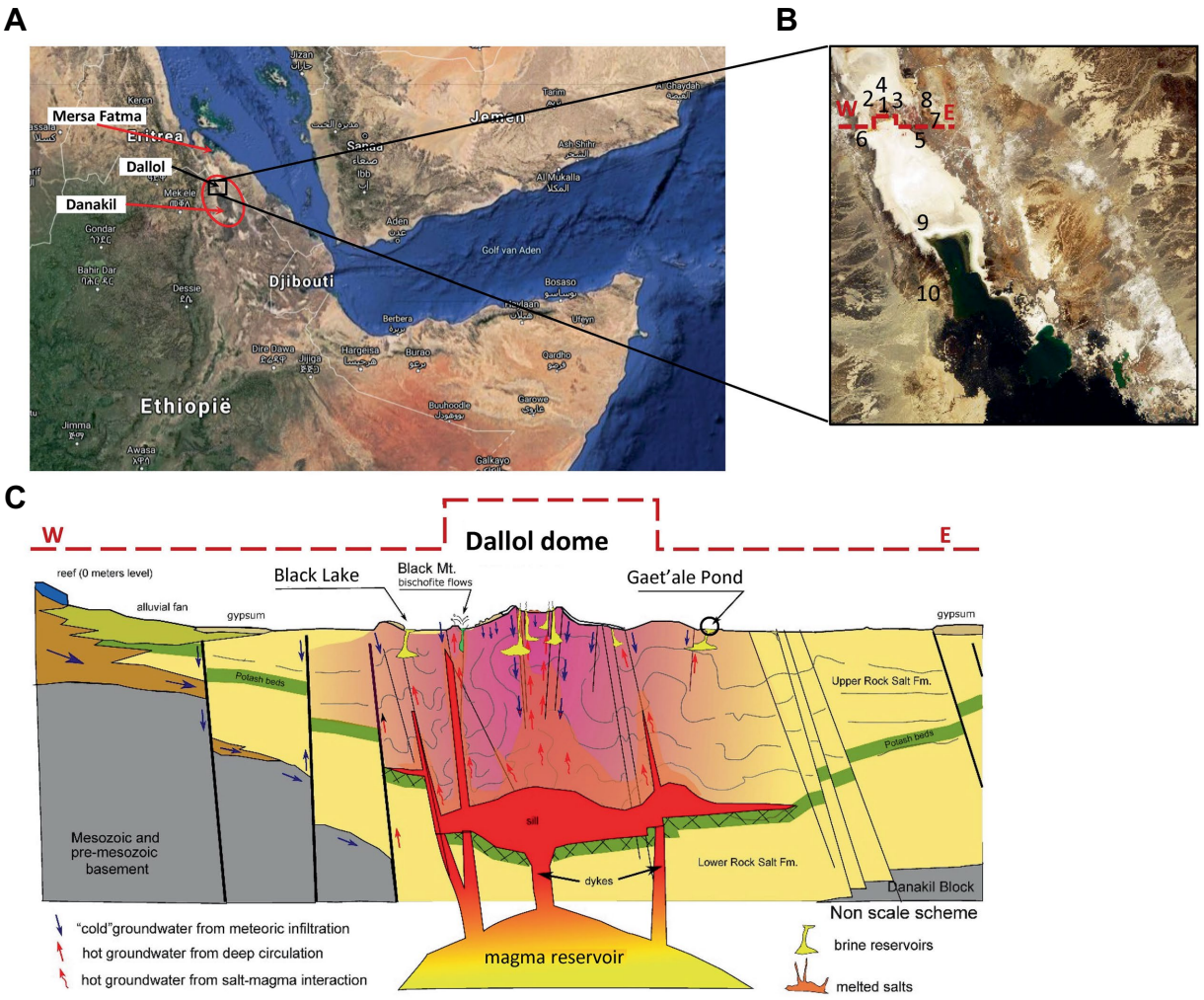

FIGURE 1
Overview of locations of the 10 sampled waterbodies of the halo-volcanic Dallol complex. Horn of Africa **(A)**, Zoom in on the locations of the 10 waterbodies, marked with numbers **(B)** and Transverse geological cross section, west to east, of the halo-volcanic Dalloll complex reproduced with permission and adapted from Lopez-Garcia et al. (2020) **(C)**.

map view, a zoom in view, showing the numbered locations, as they also appear in Tables 1–3, of the 10 hyper saline waterbodies that were sampled and a transverse geological cross section, adapted and reproduced with permissions, of the halo-volcanic Dallol complex of the sampling site (Lopez-Garcia et al., 2020).

2.2. Liquid sample handling

All liquid samples were collected in pre-cleaned and -sterilized 50 mL glass septum bottles, mounted and fixed on the top of a 6 m long telescopic carbon rod, submerged into the extreme brine solutions. Supplementary Figure S1 illustrates the collection of liquid samples. Filled septum bottles were removed from the brine and were immediately hermitically closed by a sterile, 13 mm tick butyl rubber septum. The septum was manually forced into the fill opening of sample bottle, thereby always avoiding the intake of any atmospheric gas. The result was a closed hermetic sealed septum bottle in which no gaseous headspace was present. All septum bottles closed with rubber septa were on the spot additionally sealed by forcibly crimping an aluminum closure ring on top of the glass bottle. This *in situ* liquid sampling procedure guaranteed that the liquid samples enclosed inside the vial remained geochemical– and microbial undisturbed throughout the whole period of on-site handling, custom clearances, long term airplane transportation, and controlled storage in our analytical laboratory.

2.3. Solid samples handling

All sediment, solid and mineral samples were taken by hand picking of samples, wearing umonium sterilized nitrile chirurgical gloves. Whenever needed, a geological hammer was used to break and isolate solid samples from the main geological host formation. After isolation, the solid samples were immediately stored into aluminum-poly ethylene coated sample bags. Upon each daily return to the base camp, all Al-PE packed solid samples bags were made vacuum and subsequently heat-sealed to obtain a fully isolated and gas tight packaging of solid samples as can be seen in Supplementary Figure S2.

TABLE 1 Overview of the GPS locations, general *in situ* and laboratorium physico-chemical determinations of brine densities, TDS, and water activity of the 10 waterbodies of the halo-volcanic Dallol complex.

Parameter	Central green pool (1)	Left green pool (2)	Right yellow pool (3)	White chimney environment (4)	Gaet'ale Pond (5)	Black lake (6)	Yellow mini pond (7)	Red micro pond (8)	Asale karst hole (9)	Karum Lake (10)
GPS Latitude (North)	14°14′10.8″	14°14′10.6″	14°14′10.8″	14°14′11.5″	14°12′48.1″	14°13′18.4″	14°13′40.4″	14°13′41.7″	14°06′57.6″	14°02′58.0″
GPS Longitude (East)	40°18′00.5″	40°18′00.2″	40°18′00.8″	40°17′59.5″	40°19′17.1″	40°17′10.6″	40°19′08.1″	40°19′06.3″	40°20′53.2″	40°22′32.2″
in situ measurements										
Temperature [°C]	46.1	34.0	35.5	>100	41.2	35.7	32.0	35.1	35.5	31.5
in situ pH	−0.5	−0.5	−0.4	−1.1	6.2	2.4	4.7	3.1	5.6	5.4
Conductivity [mS. cm^{-1} at 25°C]	> max.	> max.	> max.	> max.	> max.	> max.	> max.	> max.	> max.	> max.
E_H [mV vs. SHE]	556	569	595	466	336	396	296	434	382	392
Labo measurements										
$pH_{1/50\ diluted}$ [−]	0.7	0.8	0.9	0.7	3.4	2.8	3.7	3.5	4.4	4.5
Conductivity [mS. cm^{-1}]	422	418	404	424	598	521	395	494	373	375
E_H [mV vs. SHE]	620	619	630	627	460	478	396	426	407	416
Density [$Mg.m^{-3}$]	1.225	1.223	1.222	1.223	1.454	1.351	1.246	1.342	1.220	1.218
TDS measured [$g.l^{-1}$]	314	319	320	318	682	434	373	504	352	350
Water activity A_w [−]	0.725	0.728	0.731	0.729	0.234	0.324	0.684	0.463	0.734	0.735

10.3389/fmicb.2023.1134760

10.3389/fmicb.2023.1134760

TABLE 2 Summary of the measured major cat– and anions concentrations of the brine samples that were taken of the 10 different waterbodies of the halo-volcanic Dallol complex.

Parameter	Central green pool (1)	Left green pool (2)	Right yellow pool (3)	White chimney environment (4)	Gaet'ale Pond (5)	Black lake (6)	Yellow mini pond (7)	Red micro pond (8)	Asale karst hole (9)	Karum Lake (10)
Major cations, ICP-MS [mM]										
Na^+	3,893	3,846	4,153	3,746	58	88	2,091	245	3,519	4,149
Mg^{2+}	156	157	148	128	1,925	4,705	1,106	2,016	124	115
Ca^{2+}	85	84	79	80	4,048	207	1,267	2,685	434	424
K^+	195	197	168	157	40	46	260	322	90	88
$Fe^{2+/3+}$	273	280	226	221	1	27	10	4	0.3	0.3
Sr^{2+}	1	1	1	1	34	3	11	30	4	4
$[B(OH)_3]^0$	17	15	12	15	8	4	3	6	1	1
Major anions, IC [mM]										
Cl^-	5,834	5,665	5,857	5,602	12,168	10,077	6,767	10,704	5,211	5,887
F^-	18	16	14	17	<	<	4	11	<	<
Br^-	3	3	3	3	95	116	30	67	10	9
SO_4^{2-}	58	54	42	61	<	<	2	<	3	4
PO_4^{3-}	<	<	<	<	<	<	<	<	<	<
NO_3^-	<	<	<	<	<	<	<	<	<	<
NO_2^-	<	<	<	<	<	<	<	<	<	<
HCO_3^-	<	<	<	<	4	<	<	<	4	5
CO_3^{2-}	<	<	<	<	<	<	<	<	<	<
Charge balance [mEq]	−836	−690	−717	−966	49	−171	276	−739	−492	−579
Chao-kosmotropicity [kJ.kg^{-1}]	−19.7	−19.0	−24.8	−21.3	476.1	272.6	150.9	350.2	7.0	−1.3
TDS analyzed [g.l^{-1}]	336	326	337	333	651	494	380	564	294	332

This sample treatment effectively prevented any further exposure of the solid samples to the atmosphere thereby limiting unwanted mineral transitions, like oxidation, atmospheric gas interactions, or water uptake. The latter can lead to detrimental and unwanted mineral transformations. For instance, due to its deliquescence, i.e., excessive moisture uptake whereby the mineral dissolves in its own crystal water, the unstable mineral tachyhydrite ($CaMg_2Cl_6.12H_2O$) is known to transform into a Ca-rich mother liquor and the mineral bischofite ($MgCl_2.6H_2O$) when simply exposed to standard humid atmospheric conditions (Cheng et al., 2019). Our *in situ* isolation system of solid samples, by storing the solid samples into vacuum hermetic heatsealed Al-PE sample bags, assured an excellent mineral integrity and unaltered geochemistry during overseas transportation and long storage periods.

2.4. Brine solution density measurements

To determine the density of the liquid brine samples, a direct gravimetric analysis was applied. This density analysis is based on the accurate weight of a known volume of brine sample at a given temperature. Densities were determined at room temperature. An electrical powered and calibrated positive displacement pipet (Eppendorf AG, Germany) was used to transfer a volume of 1 cm^3 into a small glass petri dish. The corresponding weight of the brine sample was measured with an analytical scale, Sartorius BCE224-1S Entris® II (Sartorius, Germany). This procedure was performed on brine samples taken at various locations in each of the 10 investigated Dallol waterbodies. Every density analysis of each individual brine sample was performed in triplicate.

2.5. Determination of water activity of brine solutions

The measurement of the water activity (A_w) was performed with a resistive electrolytic hygrometer NovasinaTouch™ (Novasina AG, Suisse). The sensor of this water activity meter is a solidified gel electrolyte that is held between two very small glass rods by capillary

10.3389/fmicb.2023.1134760

TABLE 3 Overview of the mineralogy of the samples collected of the shores of the 10 waterbodies of the halo-volcanic Dallol complex.

Parameter	Central green pool (1)	Left green pool (2)	Right yellow pool (3)	White chimney environment (4)	Gaet'ale Pond (5)	Black lake (6)	Yellow mini pond (7)	Red micro pond (8)	Asale karst hole (9)	Karum Lake (10)
XRD-mineral analysis	NaCl, KCl, $CaSO_4.12H_2O$, and $Ca(Mn,Mg)(CO_3)_2$	NaCl, KCl, $CaSO_4.12H_2O$, and $Ca(Mn,Mg)(CO_3)_2$	NaCl, KCl, $CaSO_4.12H_2O$, and $Ca(Mn, Mg)(CO_3)_2$	NaCl, KCl, $CaSO_4.12H_2O$, $Ca(Mn,Mg)(CO_3)_2$, and $CaSO_4$	NaCl, KCl, $CaMg_2Cl_6.12H_2O$, and $MgCl_2$	$MgCl_2.6H_2O$, and $KMgCl_3.6H_2O$	NaCl, $CaMg_2Cl_6.12H_2O$	KCl, $KMgCl_3.6H_2O$	NaCl, KCl	NaCl, KCl
	Halite, sylvite, gypsum, and kutnohorite	Halite, sylvite, gypsum, and kutnohorite	Halite, sylvite, gypsum, and kutnohorite	Halite, sylvite, gypsum, kutnohorite, and anhydrite	Halite, sylvite, tachyhydrite, and chloromagnesite	Bischofite, carnalite	Halite, tachyhydrite like	Sylvite, carnalite	Halite, sylvite	Halite, sylvite

force. The electrical resistance of the gel electrolyte is measured. This electrical resistance is very sensitive to small changes of the relative air humidity inside a temperature controlled measuring chamber. The chronological evolution of relative air humidity was monitored over time until a steady signal was obtained. The final signal corresponds with the vapor–liquid equilibrium of the sample inside the measuring chamber. The NovasinaTouch™ apparatus converts the signal directly into the A_w value of the sample.

2.6. Gravimetric analysis of total dissolved salts

We also performed the standard indirect gravimetric analysis of the Total Dissolved Salts, TDS, of samples of the original brine solutions. This standard methodology to determine TDS of liquid samples consists of evaporating a sample to dryness by heating the sample in a ventilated oven to a temperature of about 110°C. However, due to the extreme high salt content of the Dallol brine samples it was impossible to obtain complete dryness. Most samples remained tick jelly like fluids, even after attempting to dry the samples for extended periods of time, at 110°C. We were forced to adapt the standard drying protocol by increasing the drying temperature to more than 240°C to ultimately obtain dry residues. Supplementary Figure S3 shows the outcome of our samples after applying the adapted drying protocol at 240°C. Supplementary Figure S3 also shows another major interference when determining TDS by a drying protocol. Reduced chemical species get oxidized introducing a clear oxygen bias on the weights recorded of dried samples. As an extra precaution, our dried samples were cooled down in a desiccator and immediately weighed to obtain stable and representative dry weights of the residues and consequently a more accurate result of the calculation of the measured TDS values.

2.7. Chemical analysis of brine solutions

All of the chemical analyses of the liquid samples were outsourced to Activation Laboratories Ltd. (Ancaster, Ontario, Canada). Activation Laboratories Ltd. has achieved the ultimate accreditation to international standards, with either ISO 17025 for specific registered tests or certification to ISO 9001:2008. ISO 17025 evaluates the quality system and specific analytical methodologies through proficiency testing and routine audits of the laboratory. The brine samples of the Dallol ponds were diluted with MilliQ water according to the guidelines of Activation Laboratories Ltd. These guidelines demand that brine samples had to be diluted until the salinity was lower than 0.05%. Such dilution is needed to allow accurate chemical analyses and to avoid the need for substantial measurement corrections that would be needed to be calculated if undiluted original brine samples would have been analyzed. It also allows to ignore the impact of substantial variations of brine densities on the chemical results. It is noteworthy to mention that the correct conversion of fluid densities in the chemical calculations, especially for high concentrated brine samples, are of the utmost importance when determining the analytical concentrations of the original samples.

To avoid chemical, biochemical, and microbiological biases during transport and analyses, all samples were treated according to

the sample treatment recommendations of Activation Laboratories Ltd. Additionally. Diluted samples were sterilized with a sterilization method that did not generate an extra bias for the specific applied analytical technique. Samples designated for Inductive Coupled Plasma—Optical Emission Spectrometry/Mass Spectrometry (ICP-OES/MS) were gravimetrically diluted with MilliQ water on a mass-to-mass ratio. The dilution range was predefined between 50- and 100-fold. After dilution, the samples were chemically stabilized for accurate analysis by acidification to a pH of about 2.0 with specific ICP-MS grade HNO_3. Heat sterilization, autoclaving for 20 min at 120°C, was performed in hermitic closed glass septum bottles. The use of hermitic closed glass septum vials guarantees the preservation of the chemistry of the samples. The bottles were only opened by Actlabs analytical technicians immediately before the actual analysis.

Samples designated for Ion Chromatography and alkalinity were gravimetrically diluted with MilliQ water on a mass-to-mass ratio. Technical triplicates were made with a predefined dilution range between 50- and 100-fold. To avoid possible analytical biases and to preserve the chemistry diluted IC samples were heat sterilized by autoclaving (20 min at 120°C) in hermetic closed glass septum vials. Because heat sterilization can generate biases for alkalinity analyses, diluted alkalinity samples were only filter sterilized by membranes with pore sizes of less than 0.22 µm. The filtered sample solutions were transported to Activation Laboratories Ltd. in traditional sterile blue screw capped 50 mL Falcon tubes.

2.8. Chaotropicity determination

Chaotropicity was calculated based on the methodology and data provided by Cray et al. (2013, 2015). As chloride was by far the most dominant and almost exclusive anion present in all the Dallol samples (cfr. Table 2), all the salts of the present cations were considered to be chloride salts with a corresponding molar salt concentration equal to the sum of all cation concentrations, taking into account the correct stoichiometry coefficients.

2.9. Mineralogy of shore samples, lithogeochemistry, and whole rock analyses

The main techniques used to study the mineralogy of all the solid shore samples were: scanning electron microscopy (SEM) associated with Energy Dispersive X-ray analysis (EDX; ProX table top SEM–EDX, Phenom, Netherlands) and with X-Ray Diffraction (XRD) technique. Different subsamples of collected solid samples of the shores of Gaet'ale Pond, Black Lake and Red micro Pond were dried overnight in a ventilated furnace at a temperature of 240°C and afterward, individually grinded with a pestle and a mortar to obtain the reduced grainsizes that are necessary for SEM–EDX and XRD analyses.

Additional lithographic and whole rock analysis data of the solid subsamples of Geat'ale Pond and Black Lake were obtained by lithogeochemical analyses. These specific geological analyses were all outsourced to Activation Laboratories Ltd. that has achieved the CAN-P-1579 mineral analysis accreditation. Activation Laboratories Ltd. are one of the very few commercial laboratories that has achieved this important analytical distinction. All mineral samples were dried overnight in a well ventilated furnace at a temperature of 240°C. After drying, each mineral sample was individually crushed in a laboratory ball mill to render grains of which 95% has a size that is lower than 75 µm. The following lithogeochemical/whole rock analyses were performed: Lithium metaborate/tetraborate fusion ICP of whole rock combined with trace element ICP/MS analysis, InfraRed (IR) Carbon and Sulfur analysis, Neutron Activation Analysis (INAA) to determine Chlorine content and Ion Specific Electrode analysis of the fluoride content.

2.10. Microbiological analyses

Microbial presence or absence was determined by measuring the concentration of Adenosine-5'-TriPhosphate, ATP. We used the highly sensitive total and intracellular BioThema ATP kits HS (Isogen Life Science B.V., Netherlands). These kits apply the standard addition method to exclude any bias due to the impact of the sample matrix (e.g., coloration, organic solutes, high salinities, …). To measure the intracellular ATP concentration, i.e., a true measure of present and intact living cells, 50 µL sample was incubated with an equal amount of ATP eliminating reagent, thus neutralizing the potential presence of extracellular ATP, originating from contamination or from dead cell debris. Next, 50 µL of a cell lysis solution was added, which acts in a double way. It inactivates the ATP eliminating reagent and lyse viable cells. The latter causes a release of intracellular ATP. Afterward, the total volume was mixed with 400 µL of ATP reagent HS (containing D-luciferin). The immediate light intensity was measured with a Lumitester C-100 (Kikkoman). Then, 10 µL of 100 nmol.L^{-1} ATP standard was added and the immediate light intensity was measured again. Both measurement allow the accurate calculation of the concentration of intracellular ATP. The first step, the ATP elimination step, is omitted to determine the total ATP concentration of a sample. Strong interfering sample matrices were diluted to obtain meaningful measurement results.

Scanning electron microscopy–Energy Dispersive X-ray investigations of solid minerals, field filtrates and debris on filtered brine samples were pretreated to allow SEM analysis of biological materials. First, the samples were dehydrated using an ascending series of ethanol concentrations. Second, the samples were dried by submersing in a Hexamethyldislizane solution followed by air drying. Finally, the samples were sputter-coated with a gold layer of 5 nm using a LUXOR^{Au} goldcoater (Luxor Tech, Belgium). This pretreatment ensures the preservation and thus the visualization of microbes or any biological structure that might be present in a sample during the SEM–EDX analyses.

DNA was extracted, with our in house developed DNA extraction method, from microbes retained and concentrated on filters after 0.22 µm filtration of brine samples of all 10 hypersaline Dallol waterbodies and from dissolved solid salt samples taken from most of the shores (Wouters et al., 2013). Extreme viscous brines were preliminary diluted to facilitate the filtration process. To control the DNA quality, PCR amplifications of the 16S rDNA with the universal 8F and 1492R primers were executed. All samples that rendered a positive 16S rDNA amplicon were analyzed by the company BaseClear (Netherlands) for a 16S rDNA microbial community sequencing. The FASQ-datafiles containing the DNA sequences were treated with our

new in house developed integrated bioinformatics pipeline, OCToPUS (Mysara et al., 2016b). This pipeline includes bioinformatics tools like: IPED for specifically denoising raw data of MiSeq (Mysara et al., 2016a), and CATCh for eliminating chimera sequences (Mysara et al., 2015). After passing the bioinformatics pipeline, we performed a literature survey of the biological background of the remaining consensus OTU reads and checked whether the most resembling species could be potentially and logically linked to the physico-chemical environment in which the it was discovered.

In parallel to the above techniques, attempts to cultivate microbes were carried out using six different halophile- and acidophile culture media (composition is given in Supplementary material): An own designed halophilic Dallol medium, called Simulated Asale medium (SAM), the reference halophilic *Salinibacter ruber* (DSMZ medium 936), and *Halobacterium* (DSMZ medium 97) media, an own adapted version of an acidophilic promoting *Sulfolobulus* medium (DSMZ medium 88), Seghal&Gibbons medium (DSMZ medium 1,336), typical medium used to isolate and enrich halophiles and, a own adapted version of the Postgate medium or DSMZ medium 63 to promote the growth of sulfate reducing microorganism (A63 medium). Culture attempts with the latter medium and medium 63 were performed in a glove box, under strict anaerobic conditions, i.e., 99% argon and 1% hydrogen. Potential growth was monitored by OD_{600} and by ATP measurements of all liquid cultures and by colony formation observation for culture attempts performed on agar plates. Inoculation of the media were done by pipetting, for liquid cultures, or spreading aliquots, for cultivations on solid agar, of liquid brine samples of all hypersaline Dallol waterbodies.

3. Results and discussion

3.1. Geography

Geographically, the 10 investigated hypersaline waterbodies of the halo-volcanic Dallol complex could be clustered in three clearly separated zones.

A first zone, the Dallol outcrop zone, harbored intense green or yellowish green colored waterbodies, either as stagnant brine pools or vividly fueled by water and steam spewing geysers (outflow temperatures were measured of up to 110°C). Figure 2 shows the waterbodies we investigated that were located in the outcrop zone. The water, coming out by these hot springs, contained huge amounts of reduced sulfur and iron species (cfr. Table 2). Both elements oxidizing very fast during the downward flows of the brines into the different basins. The top of most halite geyser mounds was white. An indication that the oxidation of sulfur or iron did not occur at the top of the mounds. Closer to the bottom of the halite mound, the color gradually changed to bright yellow, a color change most probably caused by the primary oxidation of sulfur species. Further down, at the lower base of the geysers, the color gradually changed to brown even evolving to intense dark brown. Most likely, a clear indication of the oxidation of ferrous compounds into ferric iron species. A recent study of Belilla et al. (2022) confirms our hypothesis on potential iron oxidation along the wall of halite geysers. Iron oxidation is exothermic thereby causing an additional increase of the temperature of the brine of the waterbody.

A second zone, the zone at the south-southeast base of the halo-volcanic Dallol complex, harbored larger and apparently much deeper hypersaline waterbodies. Figure 3 shows pictures of the four waterbodies we investigated of the south-southeast base zone of the halo-volcanic Dallol complex. The two most dominating waterbodies of this zone were the Gaet'ale Pond, also known as the Yellow Lake, and the Black lake. At the moment of sampling, the source that fueled the Gaet'ale Pond was inactive. Only a huge amount of volcanic carbon dioxide gas underneath the Gaet'ale basin, vigorously sparged the brine solution, forcing it to physico-chemically equilibrate with this acidic gas. Obviously, this will have an important impact on the pH of the brine and consequently promotes the acid mineral dissolution and precipitation processes (Darrah et al., 2013; DePaolo and Cole, 2013; Babel and Schreiber, 2014; Zhu et al., 2019). The brine of the Black Lake was mildly agitated by either a thermal generated advection flow or an ascending brine flow from underneath its basin. At the surface of the Black Lake, a constant slow surface movement coincided with the formation and disappearance of a thin white salt crust layer. Perhaps this tempered brine agitation was a remnant of a subsurface active bischofite flow in contact with the brine solution, causing this dynamic mineralization-dissolution process (Warren, 2015).

A third zone, the zone of the flat south plane further away from the halo-volcanic Dallol complex, harbors two of the main waterbodies we sampled, the Asale karst hole and the very large but shallow Karum Lake. Figure 4 shows pictures of the two waterbodies of the flat south plane zone. Both lakes have tight links with human activity. The Asale karst hole is likely artificially created by forcibly breaking its natural covering salt curst thereby opening and contacting this subsurface small water reservoir to normal atmospheric conditions. Karum Lake is most likely the result of the accumulation of surface water in the lowest region of the halo-volcanic Dallol complex. Karum lake is currently being used for industrial salt mining (Cavalazzi et al., 2019). Both waterbodies are completely dominated by sodium chloride (cfr. Table 2).

3.2. Physico-chemical analyses

Although the Hanna 9828 analytical field device should be capable of accurately measuring *in situ* seven physico-chemical parameters, it rarely succeeded to display any meaningful measurement. Most brine solutions of the Dallol waterbodies were too extreme to be measurable with a Hanna 9828 field device. Laboratory physico-chemical measurements of diluted brine samples were needed to obtain a better insight of the status of the physico-chemical conditions of the Dallol water bodies and to better correlate the physico-chemistry with the geographical observed zonification (cfr. Table 1). At the time of sampling only one water system, the white chimney/fumarole environment, had a temperature higher than 100°C. The *in situ* measured pH values of all the waterbodies of the outcrop zone were negative, while the *in situ* pH values of the base zone and the flat salt plane were only mildly acidic. As expected for volcanic active zones, *in situ* redox values indicated strong oxidizing solutions. All instrumental laboratory measurements of the diluted brine samples confirmed the extreme nature of the original brine solutions.

3.3. Brine chemistries

The concentrations of the major cat- and anions are given in Table 2. Figure 5 visualizes the extreme brine chemistries in a chemical

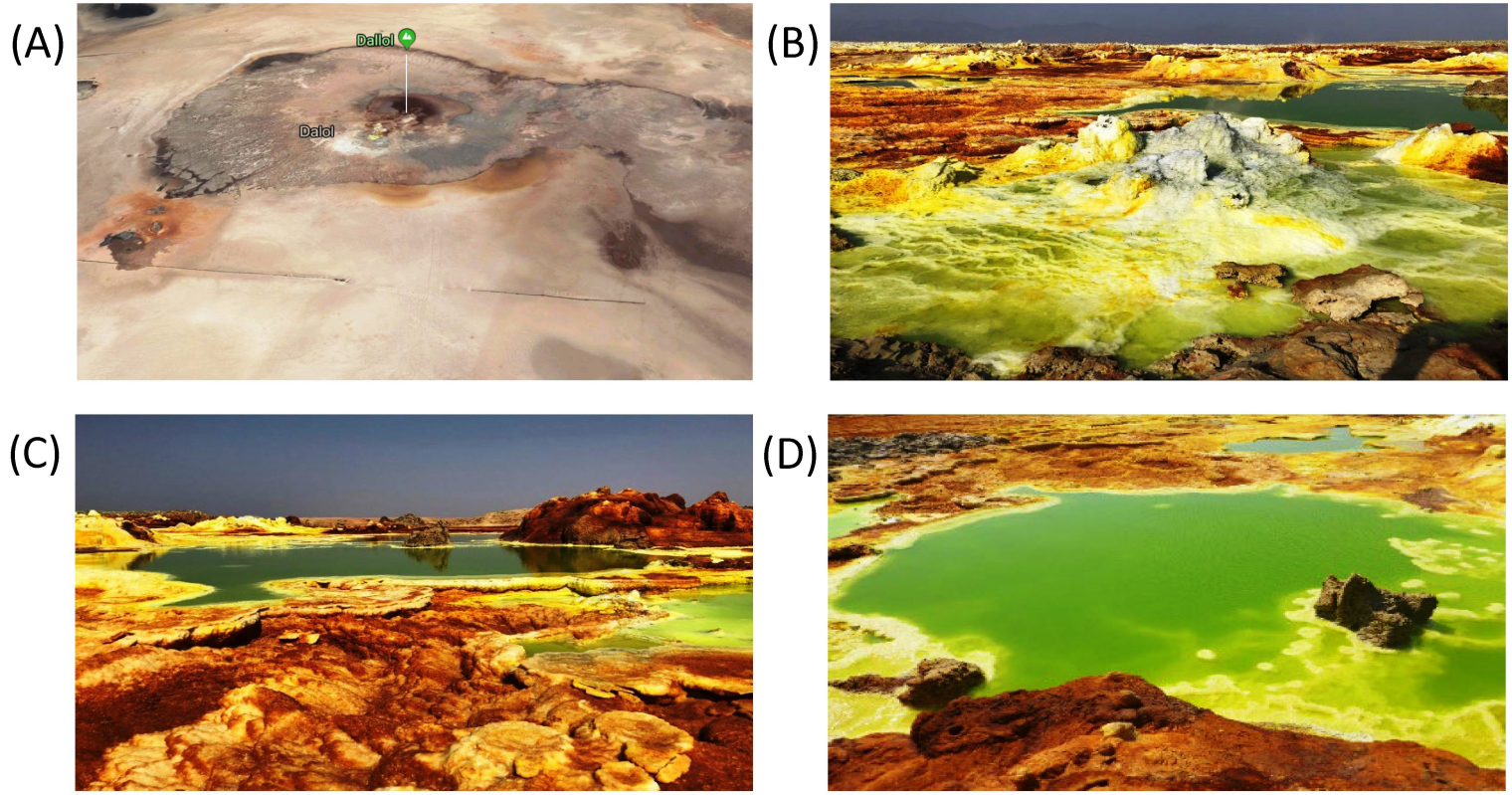

FIGURE 2
Typical waterbodies of the outcrop zone. Google earth satellite view of the Dallol outcrop zone **(A)**. Typical fumarole with waterbody **(B)**, Central green pool **(C)**, and Right yellow pool **(D)**, all located inside the krater of the halo-volcanic Dallol dome.

10.3389/fmicb.2023.1134760

10.3389/fmicb.2023.1134760

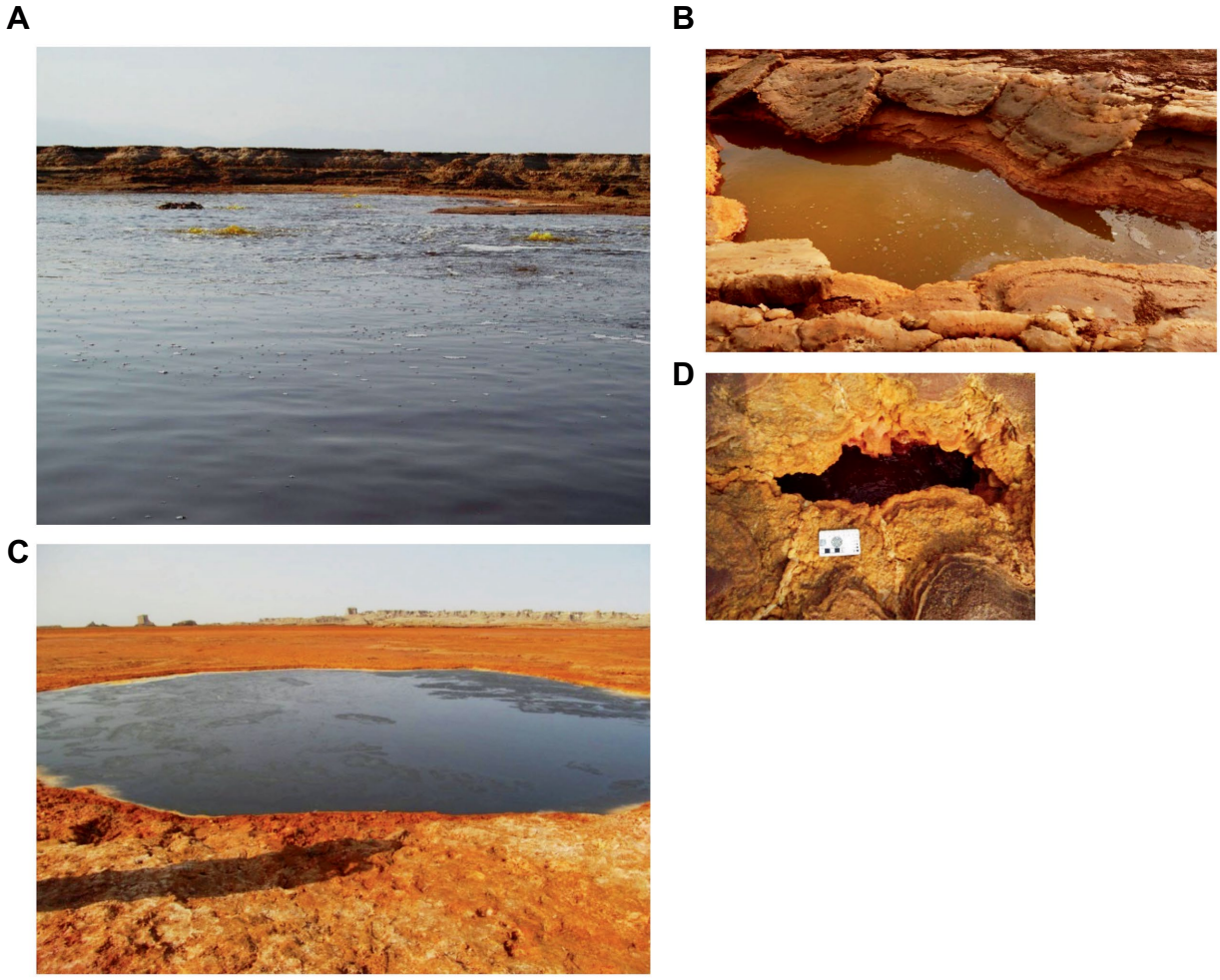

FIGURE 3
Waterbodies of the zone at the south south-east base of the Dallol dome, second zone. **(A)** Gaet'ale Pond. **(B)** Yellow mini pond, **(C)** Black Lake, and **(D)** Red micro pond.

FIGURE 4
Waterbodies of the zone of the flat south plane, third zone. **(A)** Big Karum Lake and **(B)** Asale Karst hole.

Piper diagram. The Piper diagram reveals clearly that chloride is the most dominant anion of all waterbodies. The major differences of the brine chemistries are related to the different cations, monovalent versus divalent. As a quality control factor, Table 2 also presents the ion charge balance of each brine. The calculated Chao-Kosmotropicity data and the analytical TDS values are presented in the last two rows. The major ion concentrations reveal three main types of solution chemistries, which coincide with the three observed geographic zones. The waterbodies of the outcrop zone are characterized with very hot and highly concentrated NaCl brines, rich in iron and sulfur. Oxidation processes in the outflowing superheated ferrous- and sulfidic rich source solutions give rise to some of the most acidic and colorful brines on our planet, as can be witnessed on Figure 2. The brines of the waterbodies of the south-southeast base of Dallol were clearly dominated by the divalent cations, Ca^{2+} and Mg^{2+}. The extreme high salinity, especially of the Gaet'ale Pond, gave rise to very high solution densities and viscosities, thereby giving its brine an pronounced oily look and feel. It is noteworthy to mention that these Dallol base brines also contain substantial Sr^{2+} concentrations. Like the waterbodies of outcrop zone, the two waterbodies of the flat south plane are dominated by sodium chloride. Asale karst hole and Karum

10.3389/fmicb.2023.1134760

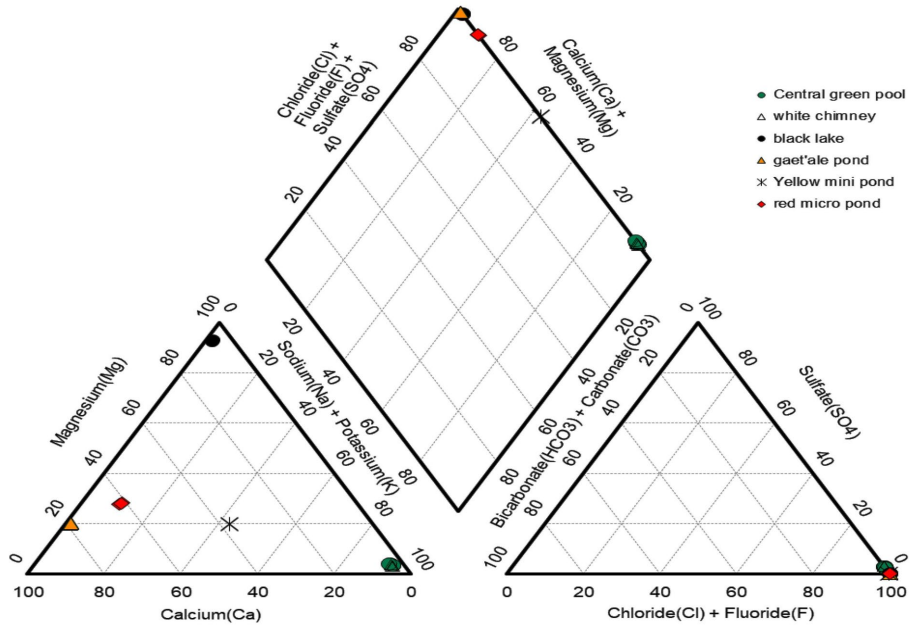

FIGURE 5
Piper diagram presenting the relative distribution of the major cat- and anions of six of the 10 waterbodies of the halo-volcanic Dallol complex.

lake are different as they contain a higher Ca^{2+} concentration (±430 mM) and a 1,000-fold less iron concentration (±0.3 mM). Besides, the pH was only mildly acidic pH (±5.5). These differences make the Asale karst hole and the Karum lake, the least chemical aggressive waterbodies.

Stable isotope data and principal component analysis (PCA) provided two additional strong indications that the brines of the Dallol waterbodies could indeed be clustered into three very different geochemical groups, spread over three different geographical zones. Stable isotope data obtained by Kotopoulou and collaborators are visualized in Figure 6. Their data clearly shows the different origins of the source waters of the waterbodies of the three separate geographic zones (Kotopoulou et al., 2019). Our PCA presented in Figure 7 indicates also that the Dallol waterbodies can indeed be divided into three different categories. The Yellow mini pond is the only waterbody that correlates somewhat less with the other waterbodies of the south-southeast base zone.

3.4. Mineralogical correlations

Our mineralogical determinations, presented in Table 3, shows that the minerals, found on the shores of the waterbodies in the three different zones, are in full agreement with the observed brine chemistries. Additional SEM pictures of the minerals of the waterbodies of the halo-volcanic Dallol complex are presented in Supplementary Figures S4–S6 of the Supplementary material. The outcrop zone was dominated by the minerals: halite (NaCl), sylvite (KCl), gypsum ($CaSO_4.2H_2O$), and kutnohorite [$Ca(Mn/Mg)(CO_3)_2$]. Around the extreme hot white chimney also some anhydrite ($CaSO_4$) was observed. The waterbodies of the south-southeast base zone were surrounded by the minerals: halite, sylivite, tachyhydrite ($CaMg_2Cl_6.12H_2O$), and chloromagnesite ($MgCl_2$). Carnalite ($KMgCl_3.6H_2O$) was observed near the Red micro pond and the shores of the Black Lake. The shores of the latter, however, were mostly dominated by bischofite ($MgCl_2.6H_2O$). The flat south plane zone contained only two types of minerals, halite and sylvite. The observed mineralogy in the vicinity of the Dallol waterbodies was, without any exception, in good agreement with the observed governing chemical parameters of the different brines.

3.5. Microbiology of Dallol

From the above data, it is clear that the halo-volcanic Dallol complex is a geological area that can be subdivided into three very different geochemical zones. Based on the physico-chemical data and the current existing literature on the limits of life, we expected that the waterbodies of two zones, the outcrop and the south-southeast base zone, would be lifeless (Hallsworth et al., 2007; Tosca et al., 2008; McKay, 2014; Stevenson et al., 2015). Only the flat south plane shows a physico-chemistry, i.e., temperature, pH water activity, chao-kosmotropicity, salinity, and ionic activity that might allow inhabitation by certain halophilic extremophiles. To verify our hypothesis of uninhabitable and inhabitable zones, we carried out a broad spectrum of non-culture and culture microbial techniques. All our measured internal and total ATP concentrations of liquid as well as solid samples were either below the limit of detection or just above. However, it is noteworthy to mention that the extreme chemistries of the brine samples hindered the ATP measurements. A 200-fold dilution had to be made before meaningful ATP measurements could be performed. Such high dilutions also had an impact on the limit of detection of the ATP measurements. We calculated a limit of detection of 1.4×10^{-14} Mol ATP for the diluted brine samples which was 3 orders of magnitude higher than expected.

Multiple attempts of DNA extraction have been undertaken. We were able to extract PCR grade of DNA from 10 samples out of

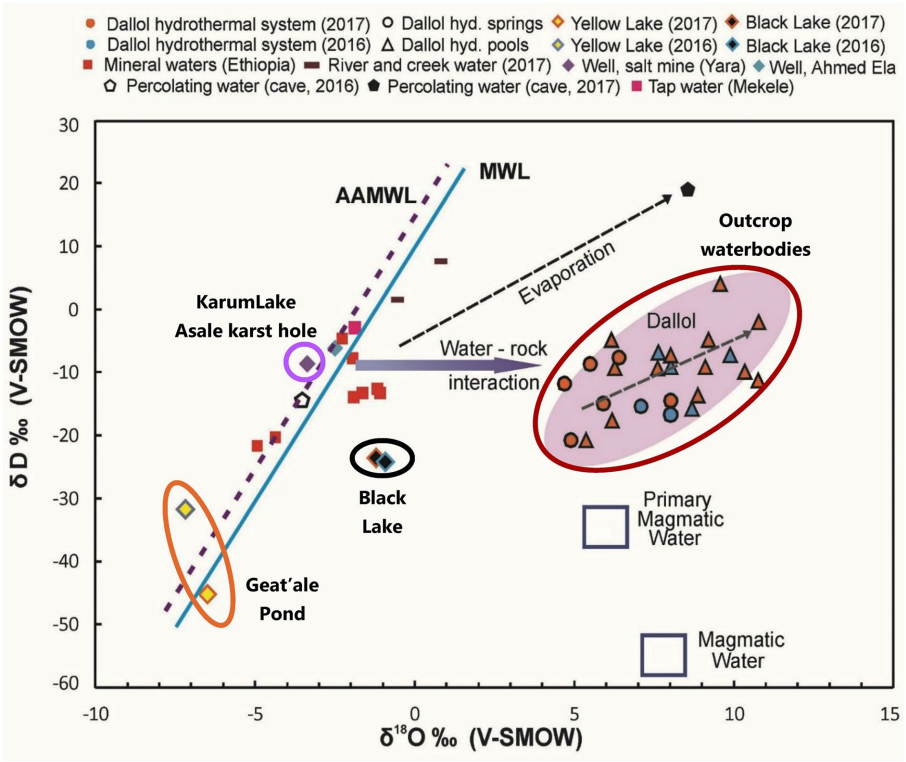

FIGURE 6
Stable isotopes analysis indicating the different and distinct origin of the waters of the halo-volcanic Dallol complex. With permission and adapted from Kotopoulou et al. (2019).

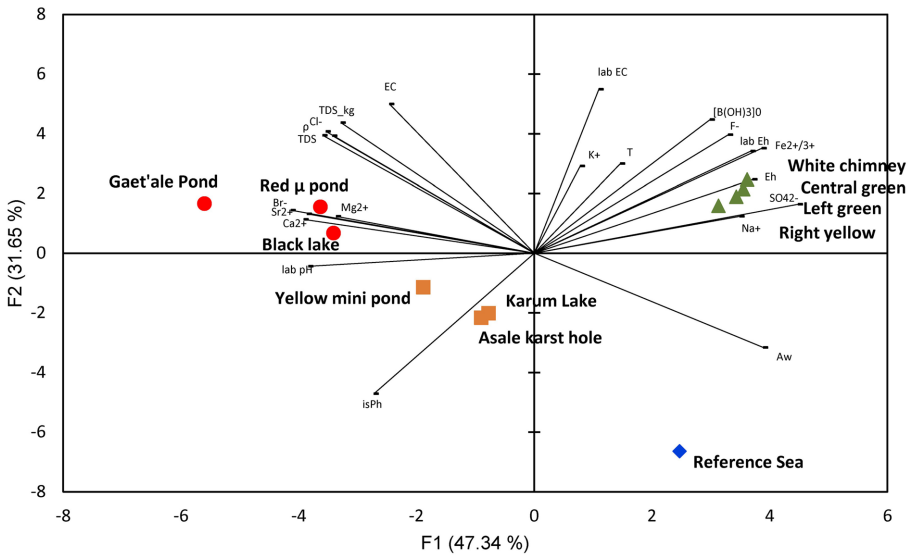

FIGURE 7
PCA analysis showing the clustering of the 10 waterbodies of the halo-volcanic Dallol complex into three groups based on 22 physico-chemical parameters.

the total of 25 original *in situ* taken liquid samples. Four DNA samples from brines of the waterbodies of the outcrop zone, three DNA samples from brines of the south-southeast base zone, and three DNA samples from the flat south plane zone. We outsourced the 16S rDNA microbial diversity analyses to the company BaseClear BV (Netherlands). As the used primers in the standard methodology of BaseClear preferentially bind bacterial DNA, the detection of possible present archaea was hampered. Even the results of the

second analysis, for which the company claimed to have used better archaea suited primers, was still largely dominated by bacterial 16S rDNA sequences. Our bioinformatics pipeline, OCToPUS, eliminated almost 80% of all the raw DNA reads based on its build in denoising- and chimera elimination algorithms. The remaining reads were clustered in 498 meaningful OTU's of high data quality. Details of the results of our analyses can be consulted in Supplementary material. Our biological literature survey revealed that most of the detected OTUs were likely the result of DNA contaminations typically found in substances of molecular biological kits, present on standard laboratory materials or introduced as aerosols during execution of laboratory procedures (Sheik et al., 2018; Weyrich et al., 2019). Many other OTUs were also likely the result of contaminations. But contaminations of DNA's that were introduced *in situ*, in the field, before sampling took place. This DNA was most probably introduced by occasionally passing eukaryotic animals like insects, bats or migrating birds, during activities of the local Afar population, as a consequence of the intensive tourist visits to the Dallol site, deposited by the annual floodings or simply as airborne microbial transmissions by clouds and dusts carried by winds and storms (Kellogg and Griffin, 2006; Barberan et al., 2014; Master, 2016; Amato et al., 2017; Gat et al., 2017; Weil et al., 2017; Behzad et al., 2018; Tignat-Perrier et al., 2019; Belilla et al., 2022). A full analysis of the results of the 16S rDNA analyses can be consulted in Supplementary material. Only a very limited amount of the detected OTUs, mostly belonging to archaea, could be designated as most likely indigenous species to the geosphere of the halo-volcanic Dallol complex. Table 4 lists the data and Supplementary Figure S7 shows a distribution of the OTU's detected in the brines of the Asale karst hole and Karum lake of which a number are known as true halophylic extremophyles. As can be noted on Supplementary Figure S7 and Table 4, five OTU's were detected simultaneously in both waterbodies of the South plane zone.

Almost all of the numerous cultivation attempts in liquid and on solid agar, using the original brine solutions as inoculum, rendered negative results. We only obtained positive signs of life, i.e., positive ATP results in the cultivation attempts with aliquots of brines of Asale karst hole and Karum lake, the south-southeast base zone, using liquid SAM and 936 medium. All attempts to transfer positive liquid SAM and 936 culture onto solid SAM and 936 medium plates, to obtain isolated colonies, failed. Therefore, we performed DNA extractions followed by 16S rDNA analysis of the positive liquid media. Among the many most likely laboratory contaminants, like bacillus species, also DNA sequences of *Limimonas* and canditatus *Nanosalina* were detected in the medium of the liquid cultures.

Although our SEM-analyses occasionally showed microbial like shapes, even of samples of the outcrop zone (Figure 8), the EDX element analyses of the microbial like shapes rarely confirmed the presence of biological related elements like carbon, nitrogen, or phosphorus. The microbial shapes had almost always the same composition as the attached mineral. Therefore, we assumed that these observations were the result of biomorphs, abiotic structures resembling biological shapes, or the result of a natural microbial fossilization process. As opposed to microbial degradation, microbial fossilization can occur under special circumstances. Typically in environments were rapid mineral precipitation is likely to happen. The hyper saline halo-volcanic Dallol complex is such an environment where the microbial fossilization process is likely to occur (Walter and Allwood, 2005).

TABLE 4 Overview of the most dominant (> 1% occurance) and possible indigenous microbial OTU's detected in the original brines of the Asale karst hole and the Karum lake.

OTU #	Group description	Asale karst hole (9)	Karum lake (10)
17	Salinibacter	47%	26%
31	Deltaproteobacteria_ unclassified	15%	17%
48	Bacteroidetes_unclassified	4%	13%
38	Bacteria_unclassified	14%	0%
91	Bacteria_unclassified	2%	10%
102	Saccharothrix	0%	4%
125	Methylobacterium	0%	2%
126	Bacteria_unclassified	0%	2%
143	Salinibacter	0%	2%
69	Candidatus_Nanosalina_ unclassified	2%	9%
61	Candidatus_Nanosalina_ unclassified	5%	0%
89	Candidatus_Nanosalina_ unclassified	5%	0%
127	Candidatus_Nanosalina_ unclassified	0%	2%
191	Candidatus_Nanosalina_ unclassified	0%	1%
Others		5%	13%

Five OTU's occurred in both waterbodies.

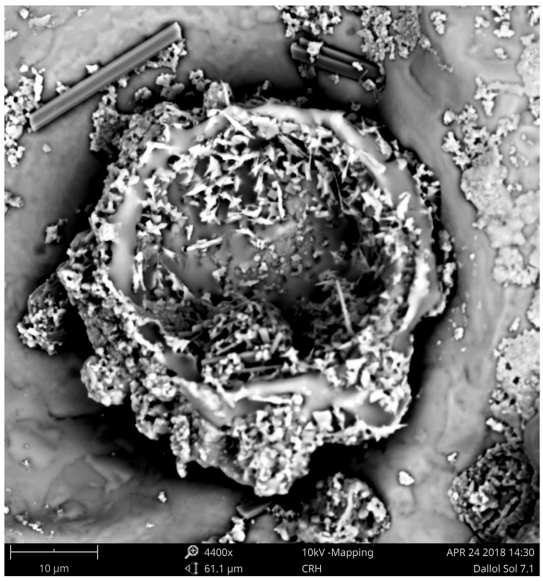

FIGURE 8
SEM pictures of a residue of the brine of the Central green pool (Outcrop zone) showing most likely the result of a microbial fossilization process or the shapes of abiotic biomorphs.

A 2019 study of Gómez suggested the existence of ultra-small microorganisms in the poly extreme waterbodies of the Dallol outcrop zone (Gomez et al., 2019). The conclusions were essentially based on the results of a combination of morphological and molecular analyses. Their results were not supported with chemical or biochemical analyses of metabolites that could indicate an active biology. In contrast of the 2019 study of Gómez, our microbiological survey did not detect the existence of an active archaeal life in the poly extreme waterbodies of the outcrop zone. Nor any positive isolation or cultivation result. Also, Belilla et al. (2019) published their work: Hyperdiverse archaea near life limits at the polyextreme geothermal Dallol area. Their extended multidisciplinary microbiological survey indicated the absence of any active microbiological life in the poly extreme waterbodies of the outcrop zone. Their observations and analyses are in agreement with our analyses. Although we succeeded to extract DNA from certain waterbodies of the outcrop zone, none of the OTU's made sense in the context of an extreme acid and saline environment. Quasi all OTU's could be directly related to human or animal microbiomes. We considered this as normal as during our sampling of the Dallol waterbodies, occasionally groups of dragonflies flew over the site, descended to consume the poisonous and deadly liquid of the waterbody, after which some disappeared and sank into the brine solution. We also discovered numerous dead flying eukaryotic animals in the close proximity on the shores of the waterbodies (cfr. Supplementary Figure S8).

4. Conclusion

All our measurements of the 10 investigated hyper saline lakes of the halo-volcanic Dallol complex, clearly indicated the exceptional extreme geological and physico-chemical nature of the region. Although the Dallol region was relatively small, it could still easily be divided into three smaller and very different subzones. This partitioning became also evident by the observed differences in geochemistry, mineralogy, and the different origins of the water of the brines. Our geological, physico-chemical, mineralogical, and microbiology analyses of samples of the halo-volcanic Dallol complex are in contrast with the 2019 Gómez study which suggests the presence of ultra-small microorganisms in the poly extreme waterbodies of the Dallol outcrop zone (Gomez et al., 2019). However, our results fully support the conclusions of Belilla et al. (2019). We also have to conclude that kosmo-chaotropicity and water activity are the two most important physico-chemical constraints for life. When it is proven that the kosmo-chaotropicity value of a geological zone exceeds 87.3 kJ.kg^{-1} or its A_w value is below 0.611, we should conclude that such zone is factual lifeless. Besides, the combination of extreme low pH and high salinity, even if this salinity is caused by the kosmotropic salt sodium chloride, is deleterious for any biological life form. However, our survey could identify several known halophilic archaea, *Halobaculum, Halobellus, Haloplanus, Natronarchaeum, Halomicroarcula, Halorientalis,* canditatus *Nanosalina*, and *Limimonas*, and one salt loving bacterial genus, *Salinibacter*, in the waterbodies that were fully saturated with sodium chloride but only mildly acidic. Although, no one can ever provide the prove of the total absence of life, our extended multidisciplinary survey strongly indicates that the halo-volcanic Dallol complex contains real lifeless geological zones, even zones in which waterbodies are present. In geological zones, so extreme that even chemical molecules have to fight to earn their essential crystal water, no biological life can exist. Our results and conclusions might be beneficial to more precisely consider areas of celestial objects as worthy or unworthy to be investigated in the frame of discovering extraterrestrial life.

Data availability statement

The datasets presented in this study can be found in online repositories. The names of the repository/repositories and accession number(s) can be found at: NCBI—PRJNA927119.

Author contributions

HM wrote the manuscript. MC contributed to the fieldwork. HM, CS, and AP performed the laboratory experimental works and sample preparations of samples that were outsourced. NL managed the microbiology research team of SCK CEN, made the fieldwork and laboratory analyses possible, and supported the whole project. All authors contributed to the article and approved the submitted version.

Funding

This work follows field work conducted in January 2018 at the Danakil Planetary Field Analog Site (TA1-5) of Europlanet 2020 RI, which has received funding from the Horizon 2020 research and innovation program of European Union under grant agreement No 654208.

Conflict of interest

The authors declare that the research was conducted in the absence of any commercial or financial relationships that could be construed as a potential conflict of interest.

Publisher's note

Supplementary material

The Supplementary material for this article can be found online at: https://www.frontiersin.org/articles/10.3389/fmicb.2023.1134760/full#supplementary-material

References

Amato, P., Joly, M., Besaury, L., Oudart, A., Taib, N., Mone, A. I., et al. (2017). Active microorganisms thrive among extremely diverse communities in cloud water. *PLoS One* 12:e0182869. doi: 10.1371/journal.pone.0182869

Arecibo, U.O.P.R.A. (2022). The habitable exoplanet catalog. Available at: https://phl.upr.edu/projects/habitable-exoplanets-catalog

Babel, M., and Schreiber, B. (2014). "Geochemistry of evaporites and evolution of seawater" in *Treatise on Geochemistry*. eds. D. Holland, Heinrich and K. Turekian Karl.

Barberan, A., Henley, J., Fierer, N., and Casamayor, E. O. (2014). Structure, inter-annual recurrence, and global-scale connectivity of airborne microbial communities. *Sci. Total Environ.* 487, 187–195. doi: 10.1016/j.scitotenv.2014.04.030

Behzad, H., Mineta, K., and Gojobori, T. (2018). Global ramifications of dust and sandstorm microbiota. *Genome Biol. Evol.* 10, 1970–1987. doi: 10.1093/gbe/evy134

Belilla, J., Iniesto, M., Moreira, D., Benzerara, K., Gerard, E., Lopez-Garcia, J. M., et al. (2022). Active microbial airborne dispersal and biomorphs as confounding factors for life detection in the cell-degrading brines of the Polyextreme Dallol geothermal field. *MBio* 13:e0030722. doi: 10.1128/mbio.00307-22

Belilla, J., Moreira, D., Jardillier, L., Reboul, G., Benzerara, K., Lopez-Garcia, J. M., et al. (2019). Hyperdiverse archaea near life limits at the polyextreme geothermal Dallol area. *Nat. Ecol. Evol.* 3:1552. doi: 10.1038/s41559-019-1005-0

Cavalazzi, B., Barbieri, R., Gomez, F., Capaccioni, B., Olsson-Francis, K., Pondrelli, M., et al. (2019). The Dallol geothermal area, northern Afar (Ethiopia)-an exceptional planetary field analog on earth. *Astrobiology* 19, 553–578. doi: 10.1089/ast.2018.1926

Cheng, H. D., Hai, Q. Y., Li, J., Song, J. G., and Ma, X. H. (2019). The sensitivity of temperature to Tachyhydrite formation: evidence from evaporation experiments of simulated brines based on compositions of fluid inclusions in halite. *Geofluids* 2019, 1–16. doi: 10.1155/2019/7808036

Cray, J. A., Russell, J. T., Timson, D. J., Singhal, R. S., and Hallsworth, J. E. (2013). A universal measure of chaotropicity and kosmotropicity. *Environ. Microbiol.* 15, 287–296. doi: 10.1111/1462-2920.12018

Cray, J. A., Stevenson, A., Ball, P., Bankar, S. B., Eleutherio, E. C., Ezeji, T. C., et al. (2015). Chaotropicity: a key factor in product tolerance of biofuel-producing microorganisms. *Curr. Opin. Biotechnol.* 33, 228–259. doi: 10.1016/j.copbio.2015.02.010

Darrah, T. H., Tedesco, D., Tassi, F., Vaselli, O., Cuoco, E., and Poreda, R. J. (2013). Gas chemistry of the Dallol region of the Danakil depression in the Afar region of the northern-most east African rift. *Chem. Geol.* 339, 16–29. doi: 10.1016/j.chemgeo.2012.10.036

Debure, M., Lassin, A., Marty, N. C., Claret, F., Virgone, A., Calassou, S., et al. (2019). Thermodynamic evidence of giant salt deposit formation by serpentinization: an alternative mechanism to solar evaporation. *Sci. Rep.* 9:11720. doi: 10.1038/s41598-019-48138-9

DePaolo, D. J., and Cole, D. R. (2013). Geochemistry of geologic carbon sequestration: an overview. *Geochem. Geol. Co2 Sequestr.* 77, 1–14. doi: 10.2138/rmg.2013.77.1

Gat, D., Mazar, Y., Cytryn, E., and Rudich, Y. (2017). Origin-dependent variations in the atmospheric microbiome Community in Eastern Mediterranean Dust Storms. *Environ. Sci. Technol.* 51, 6709–6718. doi: 10.1021/acs.est.7b00362

Gebresilassie, S., Tsegab, H., Kabeto, K., Gebreyohannes, T., Sewale, A., Amare, K., et al. (2011). Preliminary study on geology, mineral potential and characteristics of hot springs from Dallol area, Afar rift, northeastern Ethiopia: implications for natural resource exploration. *Mom. Ethiop. J. Sci.* 3, 17–30. doi: 10.4314/mejs.v3i2.67710

Gomez, F., Cavalazzi, B., Rodriguez, N., Amils, R., Ori, G. G., Olsson-Francis, K., et al. (2019). Ultra-small microorganisms in the polyextreme conditions of the Dallol volcano, northern Afar, Ethiopia. *Sci. Rep.* 9, 1–9. doi: 10.1038/s41598-019-44440-8

Grant, W. D. (2004). Life at low water activity. *Philos. Trans. Roy. Soc. London Ser. B. Biol. Sci.* 359, 1249–1267. doi: 10.1098/rstb.2004.1502

Hallsworth, J. E., Yakimov, M. M., Golyshin, P. N., Gillion, J. L., D'Auria, G., de Lima Alves, F., et al. (2007). Limits of life in MgCl2-containing environments: chaotropicity defines the window. *Environ. Microbiol.* 9, 801–813. doi: 10.1111/j.1462-2920.2006.01212.x

Hovland, M., Rueslåtten, H., and Johnsen, H. K. (2015). "Red Sea salt formations—a result of hydrothermal processes" in *The Red Sea: The Formation, Morphology, Oceanography and Environment of a Young Ocean Basin*. eds. N. M. A. Rasul and I. C. F. Stewart (Berlin: Springer Earth System Sciences), 187–203.

Hovland, M., Rueslatten, H., and Johnsen, H. K. (2018a). Large salt accumulations as a consequence of hydrothermal processes associated with 'Wilson cycles': a review part 1: towards a new understanding. *Mar. Pet. Geol.* 92, 987–1009. doi: 10.1016/j.marpetgeo.2017.12.029

Hovland, M., Rueslatten, H., and Johnsen, H. K. (2018b). Large salt accumulations as a consequence of hydrothermal processes associated with 'Wilson cycles': a review, part 2: application of a new salt forming model on selected cases. *Mar. Pet. Geol.* 92, 128–148. doi: 10.1016/j.marpetgeo.2018.02.015

Kellogg, C. A., and Griffin, D. W. (2006). Aerobiology and the global transport of desert dust. *Trends Ecol. Evol.* 21, 638–644. doi: 10.1016/j.tree.2006.07.004

Kotopoulou, E., Huertas, A. D., Garcia-Ruiz, J. M., Dominguez-Vera, J. M., Lopez-Garcia, J. M., Guerra-Tschuschke, I., et al. (2019). A Polyextreme hydrothermal system controlled by Iron: the case of Dallol at the Afar triangle. *Acs Earth Space Chem.* 3, 90–99. doi: 10.1021/acsearthspacechem.8b00141

Lee, C. K., Herbold, C. W., Polson, S. W., Wommack, K. E., Williamson, S. J., McDonald, I. R., et al. (2012). Groundtruthing next-gen sequencing for microbial ecology-biases and errors in community structure estimates from PCR amplicon pyrosequencing. *PLoS One* 7:e44224. doi: 10.1371/journal.pone.0044224

Lopez-Garcia, J. M., Moreira, D., Benzerara, K., Grunewald, O., and Lopez-Garcia, P. (2020). Origin and evolution of the halo-volcanic complex of Dallol: proto-volcanism in northern Afar (Ethiopia). *Front. Earth Sci.* 7:351. doi: 10.3389/feart.2019.00351

Maki, T., Hara, K., Kobayashi, F., Kurosaki, Y., Kakikawa, M., Matsuki, A., et al. (2015). Vertical distribution of airborne bacterial communities in an Asian-dust downwind area, Noto peninsula. *Atmos. Environ.* 119, 282–293. doi: 10.1016/j.atmosenv.2015.08.052

Master, S. (2016). Gaet'ale—a reactivated thermal spring and potential tourist hazard in the Asale salt flats, Danakil depression, Ethiopia. *J. Appl. Volcanol.* 5, 1–9. doi: 10.1186/s13617-015-0042-x

McKay, C. P. (2014). Requirements and limits for life in the context of exoplanets. *Proc. Natl. Acad. Sci. U. S. A.* 111, 12628–12633. doi: 10.1073/pnas.1304212111

Mysara, M., Leys, N., Raes, J., and Monsieurs, P. (2016a). IPED: a highly efficient denoising tool for Illumina MiSeq paired-end 16S rRNA gene amplicon sequencing data. *BMC Bioinformatics* 17:192. doi: 10.1186/s12859-016-1061-2

Mysara, M., Njima, M., Raes, J., Leys, N., and Monsieurs, P. (2016b). OCToPUS: From reads to operational taxonomic units: Comparative analysis of amplicon sequences processing pipelines. Available at: https://github.com/M-Mysara/OCToPUS

Mysara, M., Saeys, Y., Leys, N., Raes, J., and Monsieurs, P. (2015). CATCh, an ensemble classifier for chimera detection in 16S rRNA sequencing studies. *Appl. Environ. Microbiol.* 81, 1573–1584. doi: 10.1128/AEM.02896-14

Perez, E., and Chebude, Y. (2017). Chemical analysis of Gaet'ale, a hypersaline pond in Danakil depression (Ethiopia): new record for the Most saline water body on earth. *Aquat. Geochem.* 23, 109–117. doi: 10.1007/s10498-017-9312-z

Pinto, V. H. G., Manatschal, G., Karpoff, A. M., Ulrich, M., and Viana, A. R. (2017). Seawater storage and element transfer associated with mantle serpentinization in magma-poor rifted margins: a quantitative approach. *Earth Planet. Sci. Lett.* 459, 227–237. doi: 10.1016/j.epsl.2016.11.023

Schofield, N., Alsop, I., Warren, J., Underhill, J. R., Lehne, R., Beer, W., et al. (2014). Mobilizing salt: Magma-salt interactions. *Geology* 42, 599–602. doi: 10.1130/G35406.1

Schreder-Gomes, S. I., Benison, K. C., and Bernau, J. A. (2022). 830-million-year-old microorganisms in primary fluid inclusions in halite. *Geology*. doi: 10.1130/G49957.1

Scribano, V., Carbone, S., Manuella, F. C., Hovland, M., Rueslatten, H., and Johnsen, H. K. (2017). Origin of salt giants in abyssal serpentinite systems. *Int. J. Earth Sci.* 106, 2595–2608. doi: 10.1007/s00531-017-1448-y

Sheik, C. S., Reese, B. K., Twing, K. I., Sylvan, J. B., Grim, S. L., Schrenk, M. O., et al. (2018). Identification and removal of contaminant sequences from ribosomal gene databases: lessons from the census of deep life. *Front. Microbiol.* 9:840. doi: 10.3389/fmicb.2018.00840

Stevenson, A., Cray, J. A., Williams, J. P., Santos, R., Sahay, R., Neuenkirchen, N., et al. (2015). Is there a common water-activity limit for the three domains of life? *ISME J.* 9, 1333–1351. doi: 10.1038/ismej.2014.219

Tignat-Perrier, R., Dommergue, A., Thollot, A., Keuschnig, C., Magand, O., Vogel, T. M., et al. (2019). Global airborne microbial communities controlled by surrounding landscapes and wind conditions. *Sci. Rep.* 9:14441. doi: 10.1038/s41598-019-51073-4

Tosca, N. J., Knoll, A. H., and McLennan, S. M. (2008). Water activity and the challenge for life on early Mars. *Science* 320, 1204–1207. doi: 10.1126/science.1155432

Voisin, T., Erriguible, A., and Aymonier, C. (2020). A new solvent system: hydrothermal molten salt. *Sci. Adv.* 6, 18–31. doi: 10.1126/sciadv.aaz7770

Walter, M. R., and Allwood, A. C. (2005). "Biosediments and biofilms" in *Encyclopedia of Geology*. eds. R. C. Selley, L. R. M. Cocks and I. R. Plimer (Oxford: Elsevier), 279–294.

Warren, J. (2015). "Danakhil potash, Ethiopia: is the present geology the key?" Salty matters.

Warren, J. K. (2016). *Evaporites: A Geological Compendium* Switzerland: Springer International Publishing.

Weil, T., De Filippo, C., Albanese, D., Donati, C., Pindo, M., Pavarini, L., et al. (2017). Legal immigrants: invasion of alien microbial communities during winter occurring desert dust storms. *Microbiome* 5:32. doi: 10.1186/s40168-017-0249-7

Weyrich, L. S., Farrer, A. G., Eisenhofer, R., Arriola, L. A., Young, J., Selway, C. A., et al. (2019). Laboratory contamination over time during low-biomass sample analysis. *Mol. Ecol. Resour.* 19, 982–996. doi: 10.1111/1755-0998.13011

Wouters, K., Moors, H., Boven, P., and Leys, N. (2013). Evidence and characteristics of a diverse and metabolically active microbial community in deep subsurface clay borehole water. *FEMS Microbiol. Ecol.* 86, 458–473. doi: 10.1111/1574-6941.12171

Zhu, H. X., Xu, T. F., Tian, H. L., Feng, G. H., Yang, Z. J., and Zhou, B. (2019). Understanding of long-term CO2-brine-rock geochemical reactions using numerical modeling and natural analogue study. *Geofluids* 2019, 1–16. doi: 10.1155/2019/1426061

frontiers | Frontiers in Microbiology

TYPE Original Research
PUBLISHED 26 July 2023
DOI 10.3389/fmicb.2023.1176582

OPEN ACCESS

EDITED BY
Camilla Urbaniak,
NASA Jet Propulsion Laboratory, United States

REVIEWED BY
Kai Waldemar Finster,
Aarhus University, Denmark
Jesse Patrick Harrison,
CSC – IT Center for Science, Finland

*CORRESPONDENCE
Cristina Cid
✉ cidsc@inta.es;
✉ cidsc@cab.inta-csic.es

†These authors have contributed equally to this work

RECEIVED 28 February 2023
ACCEPTED 11 July 2023
PUBLISHED 26 July 2023

CITATION
Muñoz-Hisado V, Ruiz-Blas F, Sobrado JM, Garcia-Lopez E, Martinez-Alonso E, Alcázar A and Cid C (2023) Bacterial molecular machinery in the Martian cryosphere conditions.
Front. Microbiol. 14:1176582.
doi: 10.3389/fmicb.2023.1176582

Bacterial molecular machinery in the Martian cryosphere conditions

Víctor Muñoz-Hisado[1†], Fátima Ruiz-Blas[2†], Jesús Manuel Sobrado[1], Eva Garcia-Lopez[1], Emma Martinez-Alonso[3], Alberto Alcázar[3] and Cristina Cid[1*]

[1]Centro de Astrobiologia (CAB), CSIC-INTA, Madrid, Spain, [2]GFZ German Research Centre for Geosciences, Section Geomicrobiology, Telegrafenberg, Potsdam, Germany, [3]Hospital Ramón y Cajal, Instituto Ramón y Cajal de Investigación Sanitaria, Madrid, Spain

The exploration of Mars is one of the main objectives of space missions since the red planet is considered to be, or was in the past, potentially habitable. Although the surface of Mars is now dry and arid, abundant research suggests that water covered Mars billions of years ago. Recently, the existence of liquid water in subglacial lakes has been postulated below the South pole of Mars. Until now, experiments have been carried out on the survival of microorganisms in Martian surface conditions, but it remains unknown how their adaptation mechanisms would be in the Martian cryosphere. In this work, two bacterial species (*Bacillus subtilis* and *Curtobacterium flacumfaciens*) were subjected to a simulated Martian environment during 24 h using a planetary chamber. Afterward, the molecular machinery of both species was studied to investigate how they had been modified. Proteomes, the entire set of proteins expressed by each bacterium under Earth (named standard) conditions and Martian conditions, were compared using proteomic techniques. To establish this evaluation, both the expression levels of each protein, and the variation in their distribution within the different functional categories were considered. The results showed that these bacterial species followed a different strategy. The *Bacillus subtilis* resistance approach consisted of improving its stress response, membrane bioenergetics, degradation of biomolecules; and to a lesser extent, increasing its mobility and the formation of biofilms or resistance endospores. On the contrary, enduring strategy of *Curtobacterium flacumfaciens* comprised of strengthening the cell envelope, trying to protect cells from the extracellular environment. These results are especially important due to their implications for planetary protection, missions to Mars and sample return since contamination by microorganisms would invalidate the results of these investigations.

KEYWORDS

Mars, microorganisms, *Bacillus subtilis*, *Curtobacterium flacumfaciens*, stress response, planetary protection, proteomics, MALDI-TOF MS

1. Introduction

The exploration of Mars is one of the main objectives of space missions since the red planet is considered to be potentially habitable. Although possible life on Mars may be different from life on Earth, the main conditions of habitability could be common. Several minimum conditions of habitability have been defined: a solvent (water), a source of energy, a group of biologically essential elements (on Earth they are H, C, N, O, S, and P), and some physicochemical characteristics (temperature, pH, water activity, etc.) (Cockell et al., 2016). Mars is a cold and

dry planet, with temperatures ranging from −125°C to 20°C, with an atmosphere composed of 96% CO_2 (the rest is mainly N and Ar), an average atmospheric pressure of 7 mbar and UVB and UVC radiation levels about 200–315 nm (~361 kJ/m^2) (Garcia-Lopez and Cid, 2017; Cortesão et al., 2019). Several studies have determined that different microorganisms were resistant to the extreme environmental conditions such as radiation (Hansen et al., 2005, 2009), desiccation, temperature extremes and pressure (Baqué et al., 2013; Mastascusa et al., 2014), on the Martian surface. In addition, it should be taken into account that some elements present on the planet's surface, such as dust or rocks, could protect microorganisms from exposure to these extreme conditions, thus lengthening their lifespan (Cortesão et al., 2019). It has also been determined that some areas on Mars would facilitate the survival of these microorganisms due to their temperature or humidity features (Rummel et al., 2014; Rettberg et al., 2016), and the possibility of life transfer from one planet to another by means of rocks (Scalzi et al., 2012).

Furthermore, although the surface of Mars is now dry and arid, abundant research proposes that water covered Mars billions of years ago. Frozen water has been suggested to exist, not just at high latitudes at the Martian poles, but also at mid-latitudes (Bramson et al., 2015; Morgan et al., 2021). And recently, the detection of liquid water by several exploration instruments such as the Mars Advanced Radar for Subsurface and Ionosphere Sounding (MARSIS) have revived the debate about the origin and stability of liquid water under present-day Martian conditions (Lauro et al., 2021; Arnold et al., 2022). By analogy with what happens on Earth, glacier beds reach the pressure melting point, and subglacial lakes in Mars would be the result of the frictional heat produced by flowing ice concentrated at the base of the ice mass, which warms the ice-bedrock interface (Arnold et al., 2022).

The presence of microorganisms in the terrestrial cryosphere and in subglacial lakes (Rogers et al., 2013), broadens the spectrum of places where life could be possible on Mars. In this work, to check whether terrestrial microorganisms were capable of withstanding and living in the Martian cryosphere, i.e., subglacial lakes, two different species of bacteria (*Bacillus subtilis* and *Curtobacterium flaccumfaciens*) were exposed to Martian conditions in a simulation chamber. Subsequently, their molecular machinery was studied by proteomic techniques to investigate both the presence and absence of certain proteins and their expression levels. Hitherto, studies have been reported on the survival of *Bacillus subtilis* in Martian conditions as a spore (Cortesão et al., 2019), as well as its survival in soils analogous to those of Mars (Schuerger et al., 2017), focusing on the damage that would occur in DNA. The resistance of some bacteria and fungi subjected to Martian environmental conditions has also been published (Cortesão et al., 2021). However, how the cellular machinery of these cells changes and adapts has not yet been investigated. With this work, we try to increase knowledge about the possibilities of adaptation of these bacteria to the Martian environments.

The results of these experiments show that the survival of bacteria in Martian conditions is one of the greatest risks for planetary protection, that is, the practice that is responsible for protecting the other bodies of the solar system from contamination by terrestrial living organisms. Extremophile microorganisms could spread to other celestial bodies where environmental conditions were favorable.

These experiments are intended to answer several questions: (i) Are terrestrial bacteria capable of withstanding Martian cryosphere conditions? (ii) How does their molecular machinery adapt to changing environmental conditions such as temperature, pressure, and radiation? and (iii) Could a terrestrial microorganism colonize Mars?

2. Materials and methods

2.1. Sample collection

A summary of the overall experimental strategy is represented in Figure 1.

The stratospheric air samples were taken on August 24, 2020 at the Villaverde aerodrome, (Toledo, Spain), using a stratospheric balloon as part of the CAMELIA-MICRO project (PID2019-104205GB-C22) as described elsewhere (González-Toril et al., 2020). The Earth stratosphere has conditions somewhat similar to those of Mars in terms of temperature, pressure, and UV radiation, and therefore microorganisms capable of surviving in it could potentially grow on Mars (Wainwright et al., 2003; Griffin, 2004; Khodadad et al., 2017). Taking samples from the stratosphere and simulating Martian environments are difficult tasks to be carried out, but the development of stratospheric balloons (Smith and Sowa, 2020) and the construction of sampling chambers (Bryan et al., 2014; Della Corte et al., 2014) significantly facilitate this work. The air outside of the stratospheric balloon was collected using a sampling chamber incorporated into the balloon gondola. The sampling chamber was coupled to a vacuum pump that was activated when the balloon reached the desired height (between 35,613 m and 16,333 m for 1 h). Aerosols were collected on three Petri dishes with R2A culture medium (composition (g/L): 0.5 g of yeast extract/0.5 g of peptone/0.5 g of casamino acids/0.5 g of glucose/0.5 g of soluble starch/0.5 g of sodium pyruvate/0.5 g of KH_2PO_4/0.05 g of $MgSO_4{\cdot}7H_2O$) (Garcia-Descalzo et al., 2012) and incubated at 30°C. Thus, a small sample of the microorganisms present in this layer of the atmosphere could be obtained. Several bacterial colonies could be observed in Petri dishes, of which two were isolated and designated A and B. These bacteria were frozen with 40% glycerol and used for the following experiments. All procedures were performed using ethanol-sterilized tools and sterilized gloves in a UV-irradiated laminar flow hood. To control for laboratory contamination, 1 liter of MilliQ rinse water was subjected to identical analytical procedures.

2.2. DNA extraction and sequencing

Bacterial DNA was extracted and purified with a FastDNA SPIN Kit for Soil (MO BIO Laboratory, Inc.). DNA concentration was determined using a NanoDrop 2000p (Termofischer). Amplifications of DNA were performed using standard PCR methods as in Angulo-Preckler et al. (2020). Primers used to amplify the prokaryotic 16S rDNA were 27F (AGAGTTTGATCMTGGC) and 1492R (TACCTTGTTACGACGACTT) (Lane, 1991).

Abbreviations: 2D-DIGE, two-dimensional fluorescence difference gel electrophoresis; MALDI-TOF MS, matrix-assisted laser desorption/ionization-time of flight (MALDI-TOF) mass spectrometry (MS) Protein abbreviations are detailed in Supplementary Table S1.

10.3389/fmicb.2023.1176582

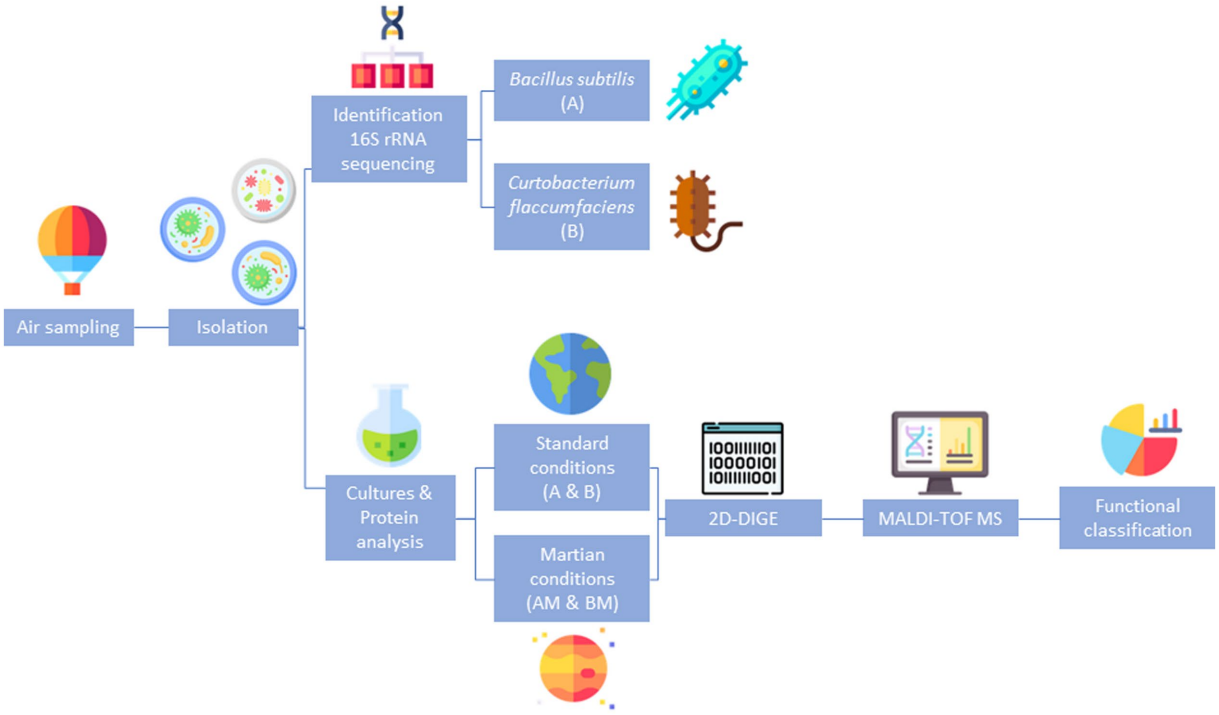

FIGURE 1
Summary of the overall experimental strategy. Schematic representation of the experimental design followed to identify differentially expressed proteins in the response of *Bacillus* and *Curtobacterium* to exposure to Martian conditions.

16S rDNA PCR amplicons were cloned using TOPO TA Cloning Kit (Invitrogen, Carlsbad, CA), and plasmid DNA was bidirectionally sequenced with a 48 capillary sequencer ABI 3730 XL (Applied Biosystems). Read-lengths of up to approximately 1,000 bp were achieved. Sequences were analyzed with UCHIME, to identify and remove chimeric reads, and classified to eliminate those that could be considered contaminants (Edgar et al., 2011).

Sequences were analyzed using BLAST at the NCBI database.[1] Representative sequences were aligned using the software of Clustal Omega (Sievers et al., 2020), the results were corrected manually and alignment uncertainties were omitted in the phylogenetic analysis. Their phylogenetic relationship was analyzed using the software MEGA 11 (Tamura et al., 2021) with parsimony, neighbor-joining, and maximum likelihood analyses. In all cases, general tree topology and clusters were stable, and reliability of the tree topologies was confirmed by bootstrap analysis using 1,000 replicate alignments. A consensus tree was generated. The isolated species were determined to be: A-*Bacillus subtilis* and B-*Curtobacterium flaccumfaciens*.

2.3. Bacterial growth experiments

The isolated A and B colonies were harvested from plates by gently scraping the colonies out using a cotton stick and cultured in glass flasks with 50 mL of TB culture medium (composition (g/L): yeast extract 24.0 g; tryptone 12.0 g; sodium pyruvate 4.0 g; K_2HPO_4 9.4 g; KH_2PO_4 2.2 g. Add 4 mL glycerol). The flasks were incubated at 30°C with continuous agitation at 120 rpm. The O.D. at 600 nm was checked until cultures reached the stationary growth phase. Growth curves are shown in Supplementary Figure S1. Four replicates of each culture were prepared.

2.4. Tolerance assays in MARTE chamber

To determine the effects of the Martian environment on bacteria, cultures grown in pressure, vacuum and temperature resistant glass flasks (SCHOTT-DURAN®) with 50 mL of TB culture medium were introduced in the MARTE chamber (Figure 2). The main differences between the conditions used in the chamber MARTE and the conditions reported on the planet Mars are summarized in Table 1. The chamber parameters were: Temperature: −15°C; Pressure: 8 mbar; CO_2 atmosphere: >95%; Radiation: Xenon lamp (Hamamatsu model 150w L11033 lamp (185–2000) nm: 666 W/m^2, UVA (320–395 nm): 1.46 W/m^2, UVB (265–322 nm): 0.33 W/m^2, UVC (225–280 nm): 0.25 W/m^2). Deuterium lamp (Hamamatsu model 140 W L10366 lamp (115–400) nm maximum 160 nm (95% emission) UVA + UVB + VIS (305–450 nm): 5.11 W/m^2). Time: Radiation 14 h, without radiation 8 h (nighttime), radiation 2 h (Sobrado et al., 2014; Sobrado, 2020). The light source is placed on top of the MARTE chamber. Several DN40CF flanges are placed on the body of the upper ring, pointing towards the sample to simulate the position of the sun with respect to Mars. During irradiation, cell suspensions were mixed continuously to

1 http://ncbi.nlm.nih.gov/BLAST

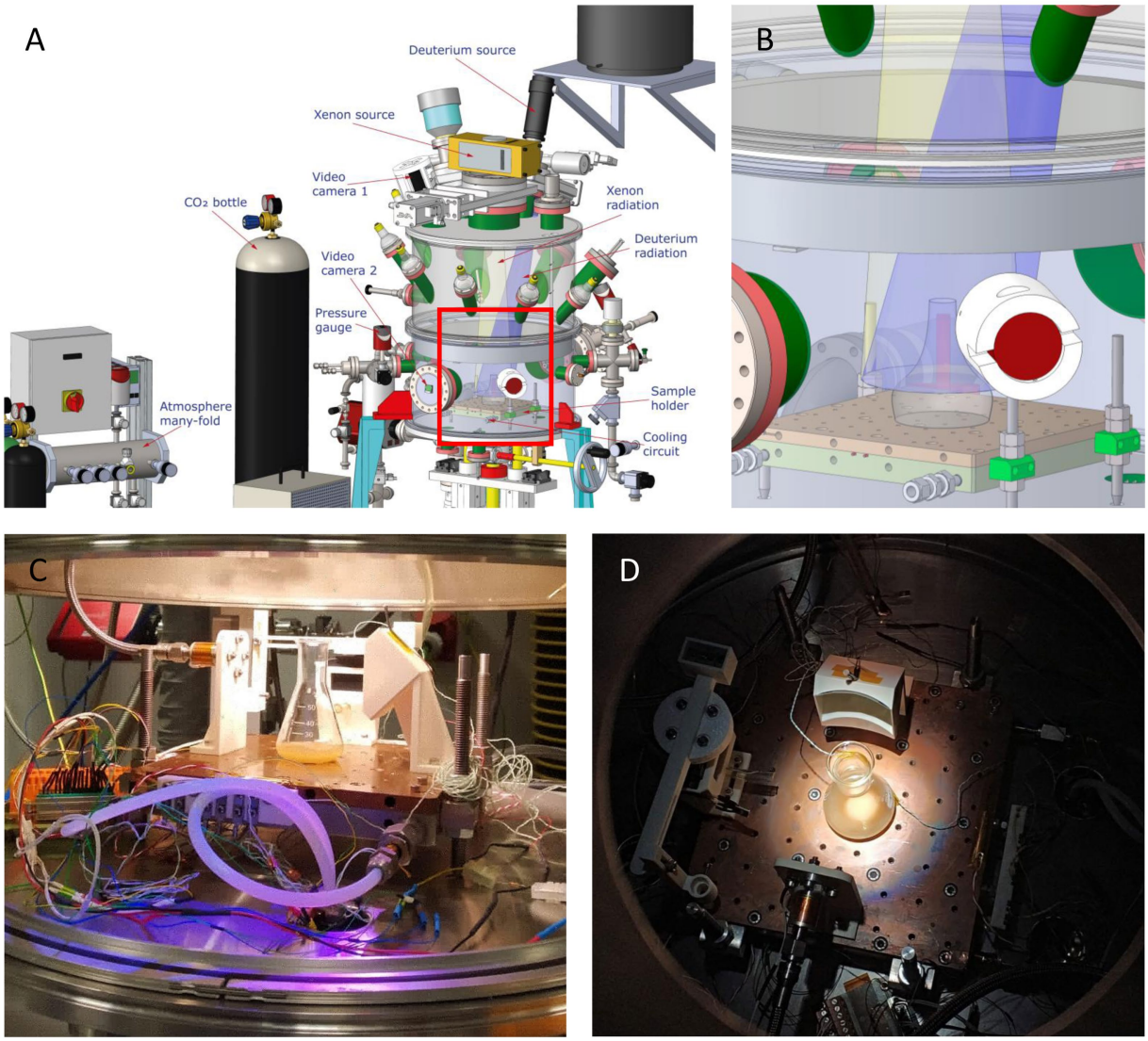

FIGURE 2
Tolerance Assays in MARTE chamber. **(A)** Schematic drawing of the MARTE chamber, indicating the positions of the deuterium and xenon sources and the direction of the radiation they emit. The position of the equipment that maintains the CO2 atmosphere, the pressure gauge, the inlet and outlet of the cooling circuit and the sample holder are also showed. **(B)** Detail of the inset in Figure 2A representing the sample holder where the bacterial culture is placed. **(C)** Image of the culture of sample A in the MARTE chamber taken with the video camera 2. **(D)** Image of the culture of sample B in the MARTE chamber taken with the video camera 1.

TABLE 1 Main differences between the conditions used in the chamber MARTE and the conditions reported on the planet Mars.

	MARTE chamber	Planet Mars	References
Temperature (°C)	−15	(10 in summer) −(−100 in winter at the poles)	Forget et al. (1995); Aerts et al. (2014)
Pressure (mbar)	8	7–20	Sobrado (2020)
Atmosphere	100% CO_2	95% CO_2; 2.7% N_2; 1.6% Ar; 0.13% H_20; 0.08% CO	Sobrado (2020)
Essential elements	C, H, N, O, P, S	C, H, N, O, P, S	McGlynn et al. (2012)
Solvent	TB culture medium	Brines	Martin-Torres et al. (2015)
Source of energy	Xenon lamp 666 W/m^2	Solar radiation 550 W/m^2	Cockell et al. (2016)

avoid shading effects. As the culture medium contains glycerol and salts it does not freeze and this prevents the cells from lysis. These new samples were named AM (sample A subjected to Martian conditions) and BM (sample B subjected to Martian conditions) (Figure 2). Four experiments (independent cultures) were prepared for each bacterial species.

2.5. Determination of microbial survival by standard plate counting

The survival of microorganisms was determined by standard plate counting as in Cortesão et al. (2021) (Supplementary Figure S2). Serial dilutions (1,10) were seeded on Petri dishes with R2A culture medium and incubated for 2 days at 30°C. Colony forming units (CFU) were counted, and the colony forming units per mL (CFU/mL) were calculated. The survival fraction was calculated as XM/X, in which XM is the CFU/mL of *B. subtilis* (AM) or *C. flacumfaciens* (BM) in Martian conditions and X is the CFU/mL of *Bacillus subtilis* (A) or *C. flacumfaciens* (B) in standard conditions. Four replicates of each culture were prepared. Statistical analyses were performed using GraphPad Prism version 7.0 (GraphPad Software, La Jolla California United States, www.graphpad.com).

2.6. Extraction of the soluble protein fraction

The preparation of cell extracts and protein determination was performed as described in Cid et al. (2010). The pellets of each flask were obtained by centrifugation for 20 min (10,000 × *g*; 4°C), washed and lysed in buffer A (20mMTris-HCl, pH 7.6; 140 mM potassium chloride; 2 mM benzamidine; 1 mM EDTA; 10 μg/mL pepstatin A, leupeptin, and antipain), using a French Press at 4°C. Cell debris was removed by centrifugation at 11,000 × *g* for 10 min to obtain a supernatant, and the protein extracts were processed using a 2D Clean-Up kit (GE Healthcare, Spain). The pellets were frozen and stored at −80°C. Protein concentration was quantified using the Qubit fluorometer (Invitrogen) previously calibrated according to the manufacturer's protocol. The samples were adjusted to a protein concentration of 5–10 mg/mL. All steps were carried out at 4°C.

2.7. 2D-DIGE

Proteins from bacterial cells were analyzed by 2D-DIGE experiments, to compare cultures to those cultures subjected to Martian conditions. Four biological replicates were obtained from each different culture. Samples (40 μg) from each experimental condition were made to 7 M urea/2 M thiourea, centrifuged, and labeled with Cy5 or Cy3 CyDye DIGE Fluor minimal dyes (Cytiva, United States); according to the Ettan DIGE protocol. A pooled standard of samples A + AM or B + BM was labeled with Cy2 (Supplementary Figure S3). After DTT addition, pairs of experimental and control samples were mixed and subjected to 2DE combining horizontal slab gel isoelectric focusing with SDS-PAGE as previously described (García-Descalzo et al., 2022).

Samples were applied to pH gradient strips for IEF. Carrier ampholyte urea IEF was performed using immobilized pH 4–7 gradient strips. After the first dimension, the IEF strips were equilibrated for the second dimension in two successive SDS equilibration buffer solutions containing Tris buffer 100 mM, urea 6 M, and glycerol 30% (w/v). The second dimension in SDS-PAGE was carried out on 12% acrylamide (2.6% crosslinking) gels (1.0 mm thick). Gels were stained with Coomassie Blue reagent for protein identification.

2.8. Protein identification

Protein gel images were processed and analyzed using the DeCyder Differential In-gel Analysis (DIA). The spots were co-detected, quantified, normalized, and matched between the four replicate experiments. Protein abundance changes between samples from each strain (A/AM ratio) or (B/BM ratio) were examined by ANOVA test. Spots present in at least three of four gels per group, with significant ANOVA test ($p \leq 0.01$), and an averaged ratio ± 2 were considered and selected for further MS analysis. Those spots selected were excised, digested with trypsin, and identified by matrix-assisted laser desorption/ionization time-of-flight mass spectrometry (MALDI-TOF MS). Combined peptide mass fingerprint and MS/MS ion search modes were applied against the NCBInr databases. The MASCOT (Matrix Science, London, United Kingdom) database search algorithm was used for protein identification [search parameters: enzyme: trypsin; fixed modifications: carbamidomethyl (C); variable modifications: oxidation (M); mass values: monoisotopic; protein mass: unrestricted; peptide mass tolerance: 80 ppm]. Protein scores higher than 66 were significant ($p < 0.05$) in the Mascot database search algorithm (Matrix science, UK) (Supplementary Table S1).

3. Results

3.1. Microbial survival to Martian conditions

The microbial survival after exposure of cultures to Martian conditions was represented in Supplementary Figure S2. Both bacterial species survived exposure to Martian conditions for 24 h. *Bacillus subtilis* was quite resistant to Martian conditions, although both cultures A and AM presented significant differences ($p < 0.0001$; $t = 337.1$ df = 6) in the number of CFU observed. The species *Curtobacterium flacumfaciens* was much less resistant than *Bacillus subtilis* and the differences in the number of CFU between B and BM were significant ($p < 0.0001$; $t = 29.84$ df = 6). Statistical differences were studied by student's t test. The average of four samples ($n = 4$) was reported in Supplementary Figures S2A,B.

3.2. Molecular machinery of *Bacillus subtilis* and *Curtobacterium flacumfaciens* under standard and Martian conditions

To assess whether these bacterial species were capable of adapting in the environmental conditions of the planet Mars, proteomes from cultures under standard conditions (samples A and B) and cultures submitted to the Martian environment simulation chamber (samples AM and BM) were compared (samples A vs. AM, and samples B vs. BM) (Figure 2). To establish this comparison, both the expression levels of each protein, and the variation in their distribution within the different functional categories were considered. The functional classification of proteins has been done following the nomenclature of protein-coding genes (Kunst et al., 1997).

It is noteworthy that, in both bacterial species, protein expression levels were lower in extracts obtained from cells subjected to Mars conditions than in extracts from standard cultures (Figure 3). Some proteins did not change their expression levels, for example, spots 8 and 17 of *Bacillus* and 3 and 4 of *Curtobacterium*. The greatest differences in expression levels were observed in spots 4 (GroEL) and 5 (Dihydrolipoyl dehydrogenase) of *Bacillus* and spots 16 (Peroxiredoxin) and 18 (Envelope stress response protein) of *Curtobacterium* (Supplementary Table S1).

3.3. Proteome-inferred microbial activity

An important general observation is that when comparing the proteomes, the *Bacillus* set of proteins contained a greater number of proteins and with more diverse functions than the *Curtobacterium* proteome (Supplementary Figure S3). This particularity demonstrates that *Bacillus* contains a large repertoire of molecules that exert different functions and gives this bacterium greater molecular versatility.

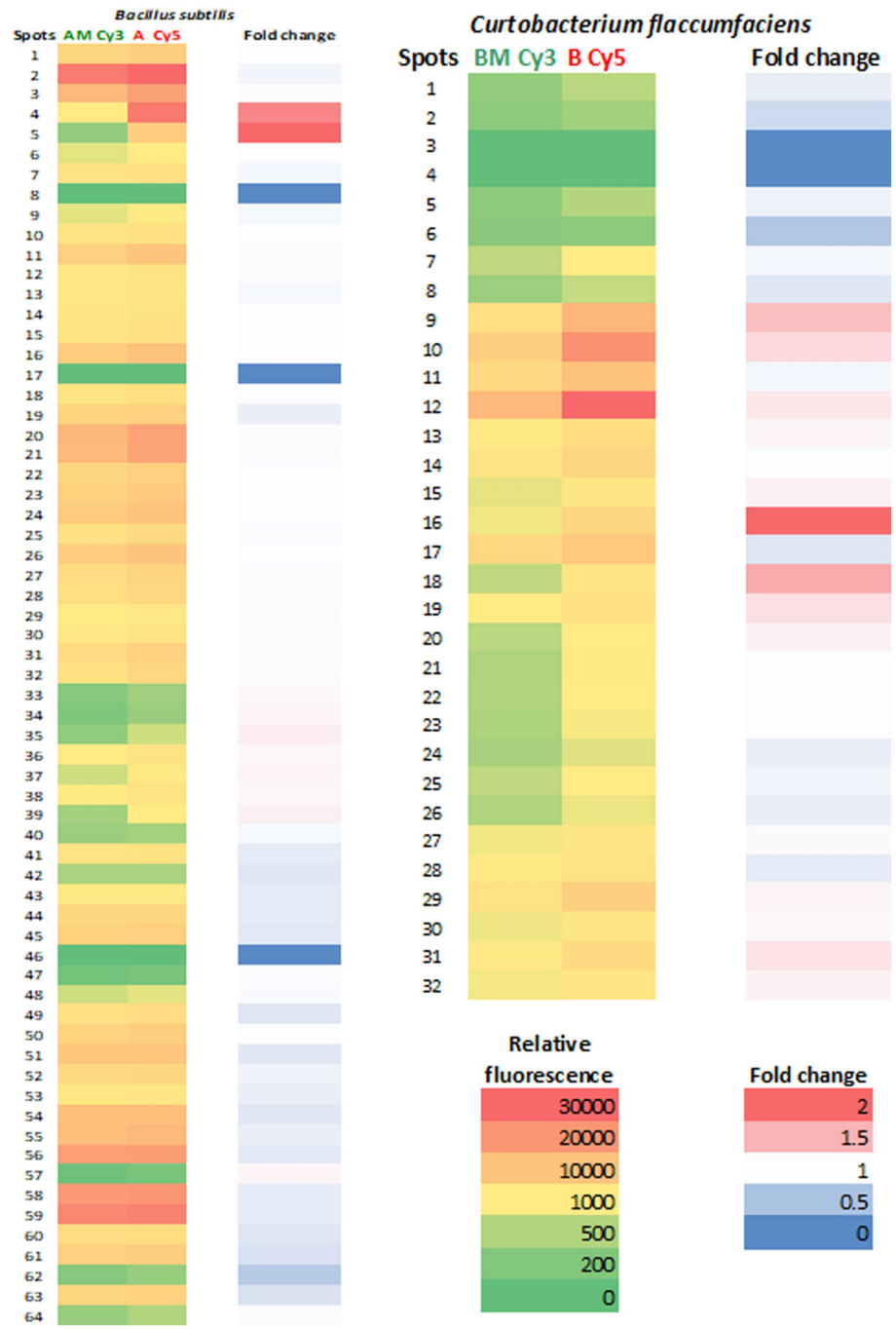

FIGURE 3
Fluorescence intensity of spots in 2D-DIGE gels. A heat map of ratios from 2D-DIGE experiments of the proteins over-expressed at standard conditions and Martian conditions. The relative fluorescence of each spot was represented in red/green color. The fold change (red/blue) is the value of standard/Martian ratio obtained in the 2D-DIGE experiments so that values closer to 2 indicate higher protein expression.

The identified proteins in these bacterial species could be classified within the next different functional categories (Figure 4; Supplementary Table S1).

3.3.1. Adaptation to atypical conditions

The proteins of this group are related to the stress response that can induce the death of the bacteria. Proteins of this category appeared in all proteomes, although they were the majority in the proteomes obtained from cultures under Martian conditions. The proteolytic subunit of the ATP-dependent endopeptidase Clp appeared in the proteomes of both bacteria (*Bacillus* and *Curtobacterium*). This peptidase degrades misfolded proteins, acting similarly to chymotrypsin (Zellmeier et al., 2006). In addition, general proteins secreted in response to stress, and proteins of the GrpE family were also identified under Martian conditions. These proteins participate together with DnaK in the response to hyperosmosis and heat shock; they are chaperones or Heat shock proteins that prevent the aggregation of proteins denatured by stress (García-Descalzo et al., 2014). In these bacteria, the presence of these proteins protects cells from the stress suffered by constant radiation and low temperatures.

This category also includes proteins responsible for eliminating or degrading certain molecules that can be harmful to the cell. The main enzyme in this group is superoxide dismutase, which catalyzes the degradation of superoxide to obtain oxygen and hydrogen peroxide. This enzyme is part of a universal antioxidant mechanism required for life-forms to survive the hyperoxic conditions of desiccation in Earth's atmosphere (Horne et al., 2022).

It was also noteworthy the presence of the enzyme thiol peroxidase in *Bacillus*, which is oxidized by hydrogen peroxide, reducing this molecule and preventing the oxidative stress in the cell. It is also related to the activation of certain genes (Ruiz-Blas et al., 2023). The presence of these proteins was very similar in both conditions, although, as in the previous cases, they were overexpressed in standard conditions (Figure 4).

3.3.2. Cell envelope

Proteins in this category are related to the formation of the peptidoglycan bacterial wall that protects the bacteria from external agents. Both microorganisms *Bacillus* and *Curtobacterium* are gram-positive bacteria which means that their peptidoglycan layer is very thick. A protein representative of this category in the *Bacillus* proteome was the enzyme D-alanine ligase, which joins two molecules of alanine through ATP hydrolysis. This reaction is fundamental in the biosynthesis of peptidoglycans, which are later used to form the cell wall (Yong-Fang et al., 2007).

3.3.3. Enzymes and prosthetic groups

The proteins contained in this category are related to the metabolism and synthesis of coenzymes and prosthetic groups. One of the proteins that appeared in *Bacillus* was the enzyme (R, R)-butanediol dehydrogenase, which utilizes NAD^+ and (R, R)-butane-2,3-diol as substrates, to obtain NADH, H^+, and (R)-acetoin as products (Höhn-Bentz and Radler, 1978). Several proteins of this group were also identified in *Curtobacterium*. For example, some enzymes with transferase activity such as PEP-utilizing enzyme (Anderson, 2005), and others such as methylenetetrahydrofolate reductase, metallo-hydrolase and L-lactate dehydrogenase (Chen et al., 2021).

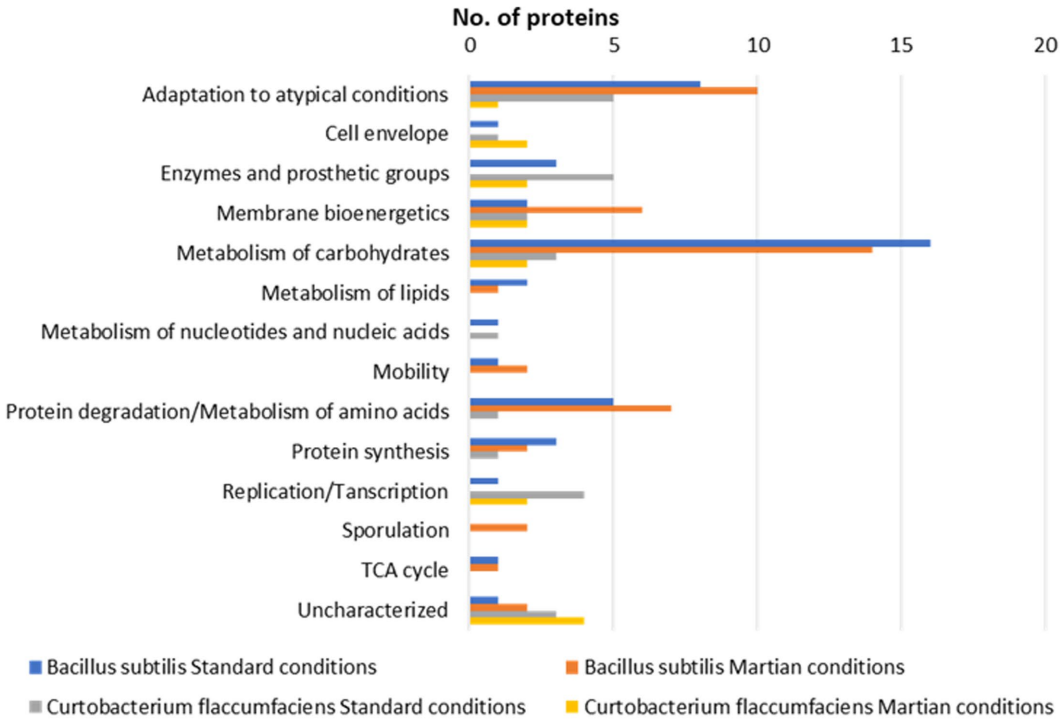

FIGURE 4
Functional classification. Representation of the number of proteins identified in 2D-DIGE gels from cultures of *Bacillus subtilis* and *Curtobacterium flacumfaciens* under standard and Martian conditions.

3.3.4. Membrane bioenergetics

This group of proteins is involved in the processes of the electron transport chain and ATP synthesis. Their function is the establishment of an electrochemical gradient that is used to synthesize ATP that will later be used in cellular processes as an energy source. The final acceptor of the electron transport chain under standard conditions is oxygen. But under Martian conditions, the atmosphere is mainly composed of CO_2, and it has been reported that *Bacillus subtilis* can survive in anaerobic conditions using nitrate as the final electron acceptor (Cruz Ramos et al., 2000). This fact could be demonstrated in these experiments by the presence of NADPH-dependent oxidoreductase enzymes, as NADPH is the preferred cofactor in anabolic conditions (Sellés Vidal et al., 2018). It could be concluded that in the simulation chamber for Martian conditions the bacteria were not carrying out the processes of cellular respiration, but fermentation. The observation of this group of proteinases in both bacteria implies that they are active and producing energy, either under aerobic or anaerobic conditions.

3.3.5. Metabolism of carbohydrates

The proteins included in this category are related to the breakdown of carbohydrates to obtain energy in the form of ATP. Therefore, the presence of these proteins indicates that the cell is functioning optimally since it is producing energy to carry out its basic functions. It can be observed that this is the majority group both under standard and Martian conditions, although the percentage of proteins is slightly lower in the latter situation. Within this group, the most numerous proteins are those involved in glycolysis, such as fructose-1,6-bisphosphate, present in both proteomes (Fujita and Freese, 1979). In the 2D-DIGE experiments, it was observed that the expression of these proteins was higher in the extracts of standard conditions in both proteomes.

3.3.6. Metabolism of lipids

The beta-oxidation of fatty acids is the metabolic pathway that breaks down complex fatty acids in the presence of oxygen to generate energy in the form of ATP. In addition, these reactions break down fatty acids to Acetyl-CoA, which is a substrate for some enzymes involved in the Krebs cycle.

One of the enzymes isolated in the proteome obtained from cultures under standard conditions that participates in this process was the enoyl-CoA hydratase, which transforms a double bond into a single one and a hydroxyl radical by adding a water molecule (Frandi et al., 2011).

Regarding the proteome obtained in Martian conditions, the phosphate acetyltransferase, which transforms acetate into acetyl-CoA, was detected and also appears in standard conditions. This reaction does not need to take place under aerobic conditions, and then acetyl-CoA can be used as a starting molecule in fermentation (Madigan et al., 2014).

This group is more present under standard conditions than under Martian conditions, and, again, the proteins that appear in both proteomes are more expressed in bacteria grown under standard conditions according to 2-DIGE electrophoresis.

3.3.7. Metabolism of nucleotides and nucleic acids

In this category, only one protein from *Bacillus*, the adenylate kinase, was isolated, both in the proteome from the culture under standard conditions, and in the proteome obtained from the culture under Martian conditions. This enzyme catalyzes the transfer of a phosphate group from ATP to AMP to obtain two equivalents of ADP. This reaction regulates cellular ATP homeostasis, thus making the cell produce energy to carry out all cellular processes (Davlieva and Shamoo, 2009).

In the *Curtobacterium* proteome, the ATP-binding cassette domain-containing protein was identified. This ubiquitous group of membrane proteins takes part in diverse biological functions. Their main role involves the unidirectional translocation of compounds across cellular membranes in an ATP-coupled process (Lewis et al., 2012).

3.3.8. Protein degradation/metabolism of amino acids

These proteins perform functions related to the degradation of proteins and amino acids to later synthesize new proteins. Amino acids are broken down because they are not needed or because the cell needs energy and cannot get it from the main pathways of carbohydrate metabolism.

This was the second largest group of proteins identified in both conditions, implying that proteins and amino acids are being broken down to synthesize other proteins that the cell needs or as an alternative method of obtaining energy. It can then be confirmed that under Martian conditions bacteria continue to carry out these processes in a similar way as they do under standard conditions since they are common to both proteomes (Figure 5). One of those proteins that appeared in both proteomes was alanine dehydrogenase. This enzyme catalyzes the reversible oxidative deamination of L-alanine to pyruvate. It is a key factor in the assimilation of L-alanine as an energy source through the tricarboxylic acid cycle during sporulation (Uhlenbusch et al., 1991; Borriss et al., 2018). In these cases, comparing the fluorescence intensity of the 2D-DIGE spots, it could be observed that the expression of these proteins was always higher under standard conditions (Figure 5). The investigation of radiation-induced damages of proteins has a long tradition in radiation biology, especially enzymes containing SH or SS groups (Durchschlag et al., 1996). This may be one of the fundamental causes of the decrease in fluorescence observed in protein gel spots obtained with cultures subjected to Martian conditions.

3.3.9. Protein synthesis

The presence of these molecules implies that bacteria are synthesizing proteins to carry out different cellular processes. Proteins such as the elongation factors G, Ts, and Tu were isolated in the proteomes of *Bacillus* and *Curtobacterium* under standard conditions (Doherty et al., 2006). Also in this category are the proteins that are involved in the synthesis of amino acids, since they are the basis for the formation of proteins, such as cysteine synthase, present in both *Bacillus* proteomes (Tanous et al., 2008).

This group was more present under standard conditions than under Martian conditions and, once again the proteins that appeared in both proteomes were more expressed in bacteria grown under standard conditions according to 2-DIGE electrophoresis.

3.3.10. Replication/transcription

These proteins are involved in processes related to the transmission of genetic information; therefore, their presence indicates that there is a reproduction of the bacterium if DNA replication is taking place, or that the transcription of DNA to RNA is taking place so that proteins

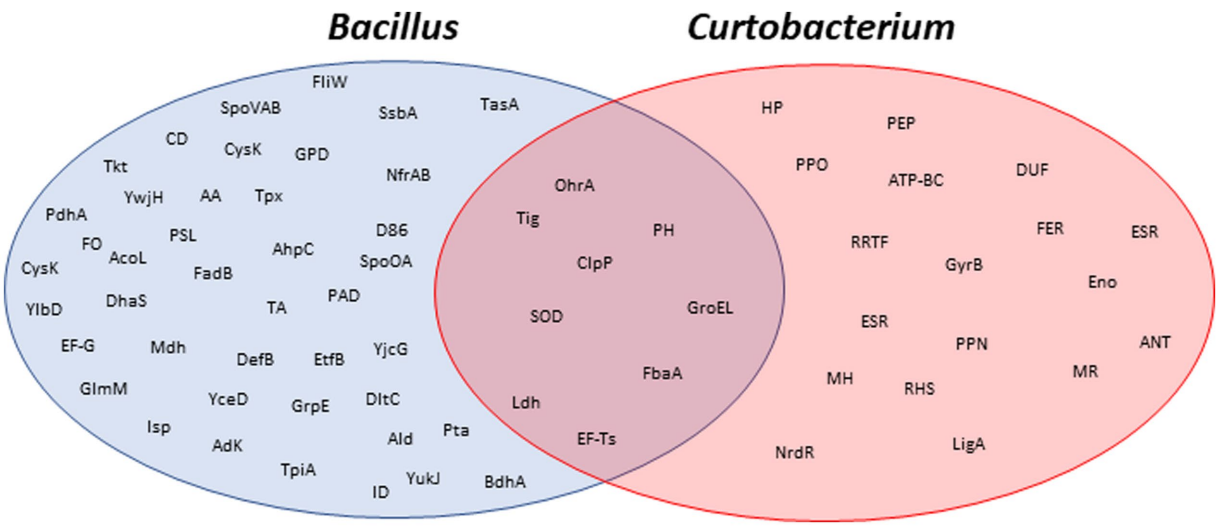

FIGURE 5
Venn diagrams of the identified proteins. Proteins identified by MALDI-TOF MS in 2D gels from *Bacillus subtilis* and *Curtobacterium flacumfaciens*. Protein abbreviations are detailed in Supplementary Table S1.

can be synthesized. Two proteins belonging to this group were isolated in *Bacillus* under Martian conditions. One of them was the response-regulating protein aspartate phosphatase A, which intervenes at the transcription level. This phosphatase inhibits the protein Spo0A which is responsible for spore formation (Howell et al., 2003). The other identified protein was the single-stranded DNA-binding protein B, which is necessary for the optimal *Bacillus subtilis* chromosome replication since it acts as an extra factor for the exchange of homologous DNA strands (Yadav et al., 2014).

No proteins from this group were identified in *Curtobacterium*, which may mean that genetic transmission is inhibited in this bacterium, or that the proteins of this group could not be detected.

3.3.11. TCA cycle

The proteins classified in this category are those that participate in the Krebs cycle or cycle of tricarboxylic acids. It is a metabolic pathway that cell use to obtain energy in the form of GTP under aerobic conditions from carbohydrates, lipids, and proteins. Finding these enzymes in the proteome of bacteria grown in the MARTE chamber was not expected, since the conditions were anaerobic. An enzyme that appeared in the proteome of bacteria grown under standard conditions was the $NADP^+$-dependent enzyme isocitrate dehydrogenase, which oxidizes and decarboxylates isocitrate in one of the stages of the Krebs cycle (Bartholomae et al., 2014). In addition, other types of enzymes that degrade carbohydrates, lipids, and proteins to molecules that serve as a substrate for enzymes involved in the Krebs cycle were identified in *Bacillus*. Once more, no proteins in this category were found in the *Curtobacterium* gels.

3.3.12. Mobility

Bacillus subtilis is a species capable of forming a flagellum that serves to move through the culture medium. In this case, only one protein related to this process has been detected, and it has been isolated in the proteome obtained from the culture under Martian conditions. The protein is flagellin, which is the subunit that polymerizes to give rise to filaments that form the bacterial flagellum. The hag gene is the one that encodes this protein in *Bacillus subtilis* and although in this case it only appears in extreme conditions, its expression does not have to be linked to this type of situation (Titz et al., 2006).

No proteins from this group were detected in *Curtobacterium*. Although *Curtobacterium* cells are small irregular rods with lateral flagella (Yong-Fang et al., 2007), their mobility is probably less agile than that of *Bacillus*.

3.3.13. Sporulation

Proteins belonging to this category have functions related to spore formation. The spores serve the bacteria to reduce their functions and their biological activity when the conditions for living are not optimal, remaining in a latent state in which they only conserve the genetic material, but do not carry out vital functions (Madigan et al., 2014). Proteins belonging to this group have only been detected in the proteome obtained from the culture in Martian conditions. As the conditions to which the bacteria were subjected were very extreme, some of them may have transformed into spores to preserve the genetic material and resist these conditions. Despite this, it is a minority group within the proteome, since it only accounts for 5% of the proteins obtained in total. The proteins obtained favor sporulation, such as those of the YlaJ family or the spoVABEA sporulation proteins (Johnson et al., 2017). This group also includes the proteins involved in biofilm formation, such as the protein that synthesizes the main components of the biofilm matrix. They form fibers that bind cells together and create a protective layer on the surface of the culture that protects the rest of bacteria. Both for the formation of this film and the spores, bacteria usually harmonize thanks to the mechanism of "quorum sensing", an extracellular communication process in which cells excrete substances known as auto-inductors that serve surrounding cells as a chemical signal to induce collective gene expression. This molecular communication has generated a keen interest in the scientific community over recent years (Kalamara et al., 2018; Ryan-Payseur and Freitag, 2018; Mukherjee and Bassler, 2019; Špacapan et al., 2020).

Curtobacterium flacumfaciens is a non-spore-forming microorganism (Khanal et al., 2023). Therefore, no proteins of this category were found in the proteome of this bacterium.

3.3.14. Uncharacterized

This category includes both indeterminate proteins, such as hypothetical proteins, as well as proteins that, although their position in the genome is known and characterized, do not have a specific function, such as those of the Yukj or YlbD families (Ijaq et al., 2015).

4. Discussion

In recent years it has been determined that vegetative cells of bacteria (*Deinococcus radiodurans*, *Escherichia coli*), and endospores of several species of *Bacillus* and budding yeast (*Saccharomyces cerevisiae*) are capable of surviving in a simulator of Martian conditions (Horne et al., 2022). This study complements this discovery since it not only reproduces the test of subjecting the bacterial culture to conditions of radiation, temperature, and atmosphere similar to those of the planet Mars, but also studies how the cellular machinery of microorganisms that could populate the Martian cryosphere changes. Our study has been restricted to the first 24 h because after the first hours of exposure, resistance elements such as spores begin to develop, and the cellular machinery would be different from that of vegetative cells. Sporulation occurs after different stress signals, which requires previous bacterial growth. The time needed to obtain resistant spores has been reported between 15 h (at 40°C) and 40 h (at 27°C), depending on the temperature (Gauvry et al., 2019). In addition, it is known that the structure, composition and properties of the spores are determined by the environmental conditions in which spores are formed (Bressuire-Isoard et al., 2018).

This research compares the proteomes obtained from the culture grown under standard conditions and the culture grown under Martian conditions considering both the protein expression levels and the variation in their distribution within the different functional categories. The experiments reported here were carried out with a model bacterial species, *Bacillus subtilis*, whose molecular machinery is well known. In addition, these experiments were carried out with another more unknown bacterium, such as *Curtobacterium*. This bacterial species had never been subjected to this type of research before.

From the results obtained, it can be concluded that both *Bacillus subtilis* and *Curtobacterium flacumfaciens* would be capable of surviving on Martian cryosphere conditions with a moderate level of stress for at least the time that our test lasted (24 h). This observation opened new questions. What strategy did each of the two species follow to cope with the Martian cryosphere conditions?

From the results obtained, it can be concluded that both species share common mechanisms of resistance (Figure 5). For example, the two bacteria synthesized a battery of proteins for their adaptation to atypical conditions. Among them, it is worth noting those that have an antioxidant function such as superoxide dismutase. Under Martian conditions, the proteins that allow metabolism to be maintained under anaerobic conditions are remarkable.

4.1. *Bacillus* under Martian conditions

The study of the isolated proteins determined that this species continued carrying out the bacterial processes that it presented in standard conditions after entering the Martian conditions simulator, although some proteins expressed as a defense mechanism also appeared. *Bacillus subtilis* submitted to Martian conditions increased the number of proteins belonging to the categories of Adaptation to atypical conditions, Membrane bioenergetics, and Protein degradation (Figure 4). The presence of proteins related to Motility and Sporulation were also significant which means that cells tended to move, or develop resistance forms such as spores.

4.2. *Curtobacterium* under Martian conditions

However, the bacterial species *Curtobacterium flacumfaciens* developed different strategies from those of *Bacillus*. The number of proteins in the cell envelope increased, trying to protect cells from the extracellular environment. It was also noteworthy the large number of unknown proteins detected (Figure 4). Despite being well known as a plant pathogen, the molecular machinery of *Curtobacterium* is largely unknown compared to that of *Bacillus*. It is necessary to investigate its genome and proteome to conclude the resistance strategies of this microorganism.

5. Conclusion

- The analyzed bacterial species (*Bacillus subtilis* and *Curtobacterium flacumfaciens*) withstood the environmental conditions of Martian cryosphere, i.e., subglacial lakes.
- The *Bacillus* proteome contained a larger number of proteins with more diverse functions than the *Curtobacterium* proteome.
- Proteins from bacteria under standard conditions were overexpressed relative to proteins from cells under Martian conditions. Their protein synthesis systems must be impaired in Martian conditions.
- Both species share common resistance mechanisms such as protein synthesis for the adaptation to atypical conditions, or fermentative metabolism under anaerobic conditions.
- The resistance strategy of *Bacillus* consists of increasing its stress response, membrane bioenergetics, biomolecule degradation, increasing its mobility and finally the formation of resistance biofilms or spores.
- In contrast, the *Curtobacterium* approach consists of strengthening the cell envelope, trying to protect the cells from the extracellular environment.
- These findings are relevant due to their application in planetary protection. They warn about the possible risk of contamination by microorganisms in the missions that are being carried out for the exploration of planets such as Mars. All these missions should ensure that scientific investigations related to the origin, evolution, and distribution of life are not compromised.

Data availability statement

The mass spectrometry proteomics data are deposited to the ProteomeXchange Consortium via the PRIDE repository with the dataset identifiers PXD027245 (samples A and AM) and PXD027249 (samples B and BM).

Author contributions

CC conceived and planned the experiments and managed the acquisition of funds. FR-B, VM-H, and EG-L performed the bacterial cultures, genomics experiments and proteomics gels. JS built the chamber MARTE and controlled it during the experiments. EM-A and AA carried out MALDI-TOF experiments. CC and FR-B wrote, revised and edited the manuscript. All authors contributed to the article and approved the submitted version.

Funding

This research has been funded by the Spanish State Research Agency (AEI) project nos. PID2019-104205GB-C22, PID2020-114047GB-100, and MDM-2017-0737 CAB (CSIC-INTA), Unidad de Excelencia María de Maeztu. EG-L is recipient of a Fellowship (PTA2016-12325-I). This work is part of the CSIC Interdisciplinary Thematic Platform (PTI) Polar zone Observatory (PTI-POLARCSIC) activities.

Acknowledgments

Bacterial isolates of Bacillus and Curtobacterium were generously provided by Elena González-Toril. We are indebted to INTA staff for sampling microbial aerosols using atmospheric balloons. We thank Paula Alcazar for reading this manuscript and for her helpful suggestions and revisions.

Conflict of interest

The authors declare that the research was conducted in the absence of any commercial or financial relationships that could be construed as a potential conflict of interest.

Publisher's note

Supplementary material

The Supplementary material for this article can be found online at: https://www.frontiersin.org/articles/10.3389/fmicb.2023.1176582/full#supplementary-material

References

Aerts, J. W., Röling, W. F., Elsaesser, A., and Ehrenfreund, P. (2014). Biota and biomolecules in extreme environments on earth: implications for life detection on Mars. *Life* 4, 535–565. doi: 10.3390/life4040535

Anderson, K. S. (2005). Detection of novel enzyme intermediates in PEP-utilizing enzymes. *Arch. Biochem. Biophys.* 433, 47–58. doi: 10.1016/j.abb.2004.10.016

Angulo-Preckler, C., García-López, E., Figuerola, B., Avila, C., and Cid, C. (2020). Natural chemical control of marine associated microbial communities by sessile Antarctic invertebrates. *Aquat. Microb. Ecol.* 85, 197–210. doi: 10.3354/ame01948

Arnold, N. S., Butcher, F. E. G., Conway, S. J., Gallagher, C., and Balme, M. R. (2022). Surface topographic impact of subglacial water beneath the south polar ice cap of Mars. *Nat. Astron.* 6, 1256–1262. doi: 10.1038/s41550-022-01782-0

Baqué, M., de Vera, J. P., Rettberg, P., and Billi, D. (2013). The BOSS and BIOMEX space experiments on the EXPOSE-R2 mission: endurance of the desert cyanobacterium *Chroococcidiopsis* under simulated space vacuum, Martian atmosphere, UVC radiation and temperature extremes. *Acta. Astronaut.* 91, 180–186. doi: 10.1016/j.actaastro.2013.05.015

Bartholomae, M., Meyer, F. M., Commichau, F. M., Burkovski, A., Hillen, W., and Seidel, G. (2014). Complex formation between malate dehydrogenase and isocitrate dehydrogenase from *Bacillus subtilis* is regulated by tricarboxylic acid cycle metabolites. *FEBS J.* 281, 1132–1143. doi: 10.1111/febs.12679

Borriss, R., Danchin, A., Harwood, C. R., Médigue, C., Rocha, E. P. C., Sekowska, A., et al. (2018). *Bacillus subtilis*, the model gram-positive bacterium: 20 years of annotation refinement. *Microb. Biotechnol.* 11, 3–17. doi: 10.1111/1751-7915.13043

Bramson, A. M., Byrne, S., Putzig, N. E., Sutton, S., Plaut, J. J., Brothers, T. C., et al. (2015). Widespread excess ice in Arcadia Planitia, Mars. *Geophys. Res. Lett.* 42, 6566–6574. doi: 10.1002/2015GL064844

Bressuire-Isoard, C., Broussolle, V., and Carlin, F. (2018). Sporulation environment influences spore properties in *Bacillus*: evidence and insights on underlying molecular and physiological mechanisms. *FEMS Microbiol. Rev.* 42, 614–626. doi: 10.1093/femsre/fuy021

Bryan, N. C., Stewart, M., Granger, D., Guzik, T. G., and Christner, B. C. (2014). A method for sampling microbial aerosols using high altitude balloons. *J. Microbiol. Methods* 107, 161–168. doi: 10.1016/j.mimet.2014.10.007

Chen, G., Khojasteh, M., Taheri-Dehkordi, A., Taghavi, S. M., Rahimi, T., and Osdaghi, E. (2021). Complete genome sequencing provides novel insight into the virulence repertories and phylogenetic position of dry beans pathogen *Curtobacterium flaccumfaciens* pv. *Flacumfaciens*. *Phytopathology* 111, 268–280. doi: 10.1094/PHYTO-06-20-0243-R

Cid, C., Garcia-Descalzo, L., Casado-Lafuente, V., Amils, R., and Aguilera, A. (2010). Proteomic analysis of the response of an acidophilic strain of *Chlamydomonas* sp. (Chlorophyta) to natural metal-rich water. *Proteomics* 10, 2026–2036. doi: 10.1002/pmic.200900592

Cockell, C. S., Bush, T., Bryce, C., Direito, S., Fox-Powell, M., Harrison, J. P., et al. (2016). Habitability: a review. *Astrobiology* 16, 89–117. doi: 10.1089/ast.2015.1295

Cortesão, M., Fuchs, F. M., Commichau, F. M., Eichenberger, P., Schuerger, A. C., Nicholson, W. L., et al. (2019). *Bacillus subtilis* spore resistance to simulated Mars surface conditions. *Front. Microbiol.* 10:333. doi: 10.3389/fmicb.2019.00333

Cortesão, M., Siems, K., Koch, S., Beblo-Vranesevic, K., Rabbow, E., Berger, T., et al. (2021). MARSBOx: fungal and bacterial endurance from a balloon-flown analog Mission in the stratosphere. *Front. Microbiol.* 12:601713. doi: 10.3389/fmicb.2021.601713

Cruz Ramos, H., Hoffmann, T., Marino, M., Nedjari, H., Presecan-Siedel, E., Dreesen, O., et al. (2000). Fermentative metabolism of *Bacillus subtilis*: physiology and regulation of gene expression. *J. Bacteriol.* 182, 3072–3080. doi: 10.1128/JB.182.11.3072-3080.2000

Davlieva, M., and Shamoo, Y. (2009). Structure and biochemical characterization of an adenylate kinase originating from the psychrophilic organism *Marinibacillus marinus*. *Acta. Crystallogr. Sect. F Struct. Biol. Cryst. Commun.* 65, 751–756. doi: 10.1107/S1744309109024348

Della Corte, V., Rietmeijer, F. J. M., Rotundi, A., and Ferrari, M. (2014). Introducing a new stratospheric dust-collecting system with potential use for upper atmospheric microbiology investigations. *Astrobiology* 14, 694–705. doi: 10.1089/ast.2014.1167

Doherty, G. P., Meredith, D. H., and Lewis, P. J. (2006). Subcellular partitioning of transcription factors in *Bacillus subtilis*. *J. Bacteriol.* 188, 4101–4110. doi: 10.1128/JB.01934-05

Durchschlag, H., Fochler, C., Feser, B., Hausmann, S., Seroneit, T., Swientek, M., et al. (1996). Effects of X- and UV-irradiation on proteins. *Radiat. Phys. Chem.* 47, 501–505. doi: 10.1016/0969-806X(95)00138-N

Edgar, R. C., Haas, B. J., Clemente, J. C., Quince, C., and Knigh, R. (2011). UCHIME improves sensitivity and speed of chimera detection. *Bioinformatics* 27, 2194–2200. doi: 10.1093/bioinformatics/btr381

Forget, F., Hansen, G. B., and Pollack, J. B. (1995). Low brightness temperatures of Martian polar caps: CO2 clouds or low surface emissivity? *J. Geophys. Res.* 100, 21219–21234. doi: 10.1029/95JE02378

Frandi, A., Zucca, P., Marvasi, M., Mastromei, G., Sanjust, E., and Perito, B. (2011). *Bacillus subtilis* fadB (ysiB) gene encodes an enoyl-CoA hydratase. *Ann. Microbiol.* 61, 371–374. doi: 10.1007/s13213-010-0121-5

Fujita, Y., and Freese, E. (1979). Purification and properties of fructose-1,6-bisphosphatase of *Bacillus subtilis*. *J. Biol. Chem.* 254, 5340–5349. doi: 10.1016/S0021-9258(18)50601-3

García-Descalzo, L., García-López, E., Alcázar, A., Baquero, F., and Cid, C. (2014). Proteomic analysis of the adaptation to warming in the Antarctic bacteria *Shewanella frigidimarina*. *Biochim. Biophys. Acta.* 1844, 2229–2240. doi: 10.1016/j.bbapap.2014.08.006

García-Descalzo, L., García-López, E., and Cid, C. (2022). Comparative proteomic analysis of psychrophilic vs. mesophilic bacterial species reveals different strategies to achieve temperature adaptation. *Front. Microbiol.* 13:841359. doi: 10.3389/fmicb.2022.841359

Garcia-Descalzo, L., García-López, A., Moreno, A. M., Alcazar, A., Baquero, F., and Cid, C. (2012). Mass spectrometry for direct identification of biosignatures and microorganisms in earth analogs of Mars. *Planet Space Sci.* 72, 138–145. doi: 10.1016/j.pss.2012.08.009

Garcia-Lopez, E., and Cid, C. (2017). Glaciers and ice sheets as analog environments of potentially habitable icy worlds. *Front. Microbiol.* 8:1407. doi: 10.3389/fmicb.2017.01407

Gauvry, E., Mathot, A. G., Couvert, O., Leguérinel, I., Jules, M., and Coroller, L. (2019). Differentiation of vegetative cells into spores: a kinetic model applied to *Bacillus subtilis*. *Appl. Environ. Microbiol.* 85, e00322–e00319. doi: 10.1128/AEM.00322-19

González-Toril, E., Osuna, S., Viúdez-Moreiras, D., Navarro-Cid, I., Toro, S. D. D., Sor, S., et al. (2020). Impacts of Saharan dust intrusions on bacterial communities of the low troposphere. *Sci. Rep.* 10:6837. doi: 10.1038/s41598-020-63797-9

Griffin, D. (2004). Terrestrial microorganisms at an altitude of 20,000 m in Earth's atmosphere. *Aerobiologia* 20, 135–140. doi: 10.1023/B:AERO.0000032948.84077.12

Hansen, A. A., Jensen, L. L., Kristoffersen, T., Mikkelsen, K., Merrison, J., Finster, K. W., et al. (2009). Effects of long-term simulated Martian conditions on a freeze-dried and homogenized bacterial permafrost community. *Astrobiology* 9, 229–240. doi: 10.1089/ast.2008.0244.

Hansen, A. A., Merrison, J., Nørnberg, P., Lomstein, B. A., and Finster, K. (2005). Activity and stability of a complex bacterial soil community under simulated Martian conditions. *Int. J. Astrobiol.* 4, 135–144. doi: 10.1017/S1473550405002557

Höhn-Bentz, H., and Radler, F. (1978). Bacterial 2,3-butanediol dehydrogenases. *Arch. Microbiol.* 116, 197–203. doi: 10.1007/BF00406037

Horne, W. H., Volpe, R. P., Korza, G., DePratti, S., Conze, I. H., Shuryak, I., et al. (2022). Effects of desiccation and freezing on microbial ionizing radiation survivability: considerations for Mars sample return. *Astrobiology* 22, 1337–1350. doi: 10.1089/ast.2022.0065

Howell, A., Dubrac, S., Andersen, K. K., Noone, D., Fert, J., Msadek, T., et al. (2003). Genes controlled by the essential YycG/YycF two-component system of *Bacillus subtilis* revealed through a novel hybrid regulator approach. *Mol. Microbiol.* 49, 1639–1655. doi: 10.1046/j.1365-2958.2003.03661.x

Ijaq, J., Chandrasekharan, M., Poddar, R., Bethi, N., and Sundararajan, V. S. (2015). Annotation and curation of uncharacterized proteins-challenges. *Front. Genet.* 6:119. doi: 10.3389/fgene.2015.00119

Johnson, C. L., and Moir, A. (2017). Proteins YlaJ and YhcN contribute to the efficiency of spore germination in Bacillus subtilis. *FEMS Microbiol. Lett.* 364. doi: 10.1093/femsle/fnx047

Kalamara, M., Spacapan, M., Mandic-Mulec, I., and Stanley-Wall, N. R. (2018). Social behaviours by *Bacillus subtilis*: quorum sensing, kin discrimination and beyond. *Mol. Microbiol.* 110, 863–878. doi: 10.1111/mmi.14127

Khanal, M., Bhatta, B. P., Timilsina, S., Ghimire, S., Cochran, K., and Malla, S. (2023). *Curtobacterium allii* sp. nov., the actinobacterial pathogen causing onion bulb rot. *Antonie Van Leeuwenhoek* 116, 83–96. doi: 10.1007/s10482-022-01775-z

Khodadad, C. L., Wong, G. M., James, L. M., Thakrar, P. J., Lane, M. A., Catechis, J. A., et al. (2017). Stratosphere conditions inactivate bacterial endospores from a Mars spacecraft assembly facility. *Astrobiology* 17, 337–350. doi: 10.1089/ast.2016.1549

Kunst, F., Ogasawara, N., Moszer, I., Albertini, A. M., Alloni, G., Azevedo, V., et al. (1997). The complete genome sequence of the gram-positive bacterium *Bacillus subtilis*. *Nature* 390, 249–256. doi: 10.1038/36786

Lane, D. J. (1991). "16S/23S rRNA sequencing" in *Nucleic acid techniques in bacterial systematic*. eds. E. Stackebrandt and M. Goodfellow (New York, NY: Wiley), 115–175.

Lauro, S. E., Pettinelli, E., Caprarelli, G., Guallini, L., Rossi, A. P., Mattei, E., et al. (2021). Multiple subglacial water bodies below the south pole of Mars unveiled by new MARSIS data. *Nat. Astron.* 5, 63–70. doi: 10.1038/s41550-020-1200-6

Lewis, V. G., Ween, M. P., and McDevitt, C. A. (2012). The role of ATP-binding cassette transporters in bacterial pathogenicity. *Protoplasma* 249, 919–942. doi: 10.1007/s00709-011-0360-8

Madigan, M. T., Martinko, J. M., Bender, K. S., Buckley, D. H., and Stahl, D. A. (2014). *Brock biology of microorganisms. 14th* Edn Pearson Education.

Martin-Torres, J., Zorzano, M. P., Valentin-Serrano, P., Harri, A. M., Genzer, M., Kemppainen, O., et al. (2015). Transient liquid water and water activity at Gale crater on Mars. *Nat. Geosci.* 8, 357–361. doi: 10.1038/ngeo2412

Mastascusa, V., Romano, I., Di Donato, P., Poli, A., Della Corte, V., Rotundi, A., et al. (2014). Extremophiles survival to simulated space conditions: an astrobiology model study. *Astrobiology* 44, 231–237. doi: 10.1007/s11084-014-9397-y

McGlynn, I. O., Fedo, C. M., and McSween, H. Y. (2012). Soil mineralogy at the Mars exploration rover landing sites: an assessment of the competing roles of physical sorting and chemical weathering. *J. Geophys. Res.* 117: E01006. doi: 10.1029/2011JE003861

Morgan, G. A., Putzig, N. E., Perry, M. R., Sizemore, H. G., Bramson, A. M., Petersen, E. I., et al. (2021). Availability of subsurface water-ice resources in the northern mid-latitudes of Mars. *Nat. Astron.* 5, 230–236. doi: 10.1038/s41550-020-01290-z

Mukherjee, S., and Bassler, B. L. (2019). Bacterial quorum sensing in complex and dynamically changing environments. *Nat. Rev. Microbiol.* 17, 371–382. doi: 10.1038/s41579-019-0186-5

Rettberg, P., Anesio, A. M., Baker, V. R., Baross, J. A., Cady, S. L., Detsis, E., et al. (2016). Planetary protection and Mars special regions-a suggestion for updating the definition. *Astrobiology* 16, 119–125. doi: 10.1089/ast.2016.1472

Rogers, S. O., Shtarkman, Y. M., Koçer, Z. A., Edgar, R., Veerapaneni, R., and D'Elia, T. (2013). Ecology of subglacial lake vostok (Antarctica), based on metagenomic/metatranscriptomic analyses of accretion ice. *Biology* 2, 629–650. doi: 10.3390/biology2020629

Ruiz-Blas, F., Muñoz-Hisado, V., Garcia-Lopez, E., Moreno, A., Bartolomé, M., Leunda, M., et al. (2023). The hidden microbial ecosystem in the perennial ice from a Pyrenean ice cave. *Front. Microbiol.* 14:1110091. doi: 10.3389/fmicb.2023.1110091

Rummel, J. D., Beaty, D. W., Jones, M. A., Bakermans, C., Barlow, N. G., Boston, P. J., et al. (2014). A new analysis of Mars "special regions": findings of the second MEPAG special regions science analysis group (SR-SAG2). *Astrobiology* 14, 887–968. doi: 10.1089/ast.2014.1227

Ryan-Payseur, B. K., and Freitag, N. E. (2018). *Bacillus subtilis* biofilms: a matter of individual choice. *MBio* 9, e02339–e02318. doi: 10.1128/mBio.02339-18

Scalzi, G., Selbmann, L., Zucconi, L., Rabbow, E., Horneck, G., Albertano, P., et al. (2012). LIFE experiment: isolation of Cryptoendolithic organisms from Antarctic colonized sandstone exposed to space and simulated Mars conditions on the international Space Station. *Orig. Life Evol. Biosph.* 42, 253–262. doi: 10.1007/s11084-012-9282-5

Schuerger, A. C., Ming, D. W., and Golden, D. C. (2017). Biotoxicity of Mars soils: 2. Survival of *Bacillus subtilis* and *Enterococcus faecalis* in aqueous extracts derived from six Mars analog soils. *Icarus* 290, 215–223. doi: 10.1016/j.icarus.2017.02.023

Sellés Vidal, L., Kelly, C. L., Mordaka, P. M., and Heap, J. T. (2018). Review of NAD(P)H-dependent oxidoreductases: properties, engineering and application. *Biochim. Biophys. Acta. Proteins Proteom.* 1866, 327–347. doi: 10.1016/j.bbapap.2017.11.005

Sievers, F., Barton, G. J., and Higgins, D. G. (2020). Multiple Sequence Alignment. *Bioinformatics* 14, 309–323. doi: 10.1002/prot.340140216

Smith, D. J., and Sowa, M. B. (2020). Ballooning for biologists: Mission essentials for flying life science experiments to near space on NASA large scientific balloons. *Gravit. Space Res.* 5, 52–73.

Sobrado, J. M. (2020). Mimicking the Martian hydrological cycle: a set-up for introduce liquid water in vacuum. *Sensors* 20:6150. doi: 10.3390/s20216150

Sobrado, J. M., Martín-Soler, J., and Martín-Gago, J. A. (2014). Mimicking Mars: a vacuum simulation chamber for testing environmental instrumentation for Mars exploration. *Rev. Sci. Instrum.* 85:035111. doi: 10.1063/1.4868592

Špacapan, M., Danevčič, T., Štefanic, P., Porter, M., Stanley-Wall, N. R., and Mandic-Mulec, I. (2020). The ComX quorum sensing peptide of *Bacillus subtilis* affects biofilm formation negatively and sporulation positively. *Microorganisms* 8:1131. doi: 10.3390/microorganisms8081131

Tamura, G., Stecher, G., and Kumar, S. (2021). MEGA11: molecular evolutionary genetics analysis version 11. *Mol. Biol. Evol.* 38, 3022–3027. doi: 10.1093/molbev/msab120

Tanous, C., Soutourina, O., Raynal, B., Hullo, M., Mervelet, P., Gilles, A., et al. (2008). The CymR regulator in complex with the enzyme CysK controls cysteine metabolism in *Bacillus subtilis*. *J. Biol. Chem.* 283, 35551–35560. doi: 10.1074/jbc.M805951200

Titz, B., Rajagopala, S. V., Ester, C., Häuser, R., Uetz, P. (2006). Novel conserved assembly factor of the bacterial flagellum. *J. Bacteriol.* 188, 7700–7706. doi: 10.1128/JB.00820-06

Uhlenbusch, I., Sahm, H., and Sprenger, G. A. (1991). Expression of an L-alanine dehydrogenase gene in *Zymomonas mobilis* and excretion of L-alanine. *Appl. Environ. Microbiol.* 57, 1360–1366. doi: 10.1128/aem.57.5.1360-1366.1991

Wainwright, M., Wickramasinghe, N. C., Narlikar, J. V., and Rajaratnam, P. (2003). Microorganisms cultured from stratospheric air samples obtained at 41 km. *FEMS Microbiol. Lett.* 218, 161–165. doi: 10.1111/j.1574-6968.2003.tb11513.x

Yadav, T., Carrasco, B., Serrano, E., and Alonso, J. C. (2014). Roles of *Bacillus subtilis* DprA and SsbA in RecA-mediated genetic recombination. *J. Biol. Chem.* 289, 27640–27652. doi: 10.1074/jbc.M114.577924

Yong-Fang, C., Yan-Ni, Y., Xiao-Mei, Z., and Jian-Hua, G. (2007). *Curtobacterium flaccumfaciens* pv. *Beticola*. A new Pathovar of pathogens in sugar beet. *Plant Dis.* 91, 677–684. doi: 10.1094/PDIS-91-6-0677

Zellmeier, S., Schumann, W., and Wiegert, T. (2006). Involvement of Clp protease activity in modulating the *Bacillus subtilis* σw stress response. *Mol. Microbiol.* 61, 1569–1582. doi: 10.1111/j.1365-2958.2006.05323.x

frontiers | Frontiers in Microbiology

TYPE Original Research
PUBLISHED 13 December 2023
DOI 10.3389/fmicb.2023.1253436

OPEN ACCESS

EDITED BY
Rob Van Houdt,
Belgian Nuclear Research Center (SCK CEN), Belgium

REVIEWED BY
Teresa Rinaldi,
Sapienza University of Rome, Italy
Robert J. C. McLean,
Texas State University, United States
Gerald McDonnell,
Johnson & Johnson, United States

*CORRESPONDENCE
Shunta Kimura
✉ kimura.shunta@jaxa.jp
Shino Suzuki
✉ suzuki.shino2@jaxa.jp

RECEIVED 05 July 2023
ACCEPTED 28 November 2023
PUBLISHED 13 December 2023

CITATION
Kimura S, Ishikawa S, Hayashi N, Fujita K, Inatomi Y and Suzuki S (2023) Bacterial and fungal bioburden reduction on material surfaces using various sterilization techniques suitable for spacecraft decontamination. *Front. Microbiol.* 14:1253436. doi: 10.3389/fmicb.2023.1253436

Bacterial and fungal bioburden reduction on material surfaces using various sterilization techniques suitable for spacecraft decontamination

Shunta Kimura[1,2,3]*, Shu Ishikawa[4], Nobuya Hayashi[5], Kazuhisa Fujita[1,6], Yuko Inatomi[1,2,3] and Shino Suzuki[1,2,3,7]*

[1]Institute of Space and Astronautical Science, Japan Aerospace Exploration Agency, Sagamihara, Japan, [2]Space Exploration Innovation Hub Center, Japan Aerospace Exploration Agency, Sagamihara, Japan, [3]Graduate Institute for Advanced Studies, SOKENDAI, Sagamihara, Japan, [4]Engineering Division, Kajima Corporation, Tokyo, Japan, [5]Interdisciplinary Graduate School of Engineering Sciences, Kyushu University, Fukuoka, Japan, [6]Safety and Mission Assurance Department, Japan Aerospace Exploration Agency, Tsukuba, Japan, [7]Geobiology and Astrobiology Laboratory, RIKEN Cluster for Pioneering Research, Wako, Saitama, Japan

Planetary protection is a guiding principle aiming to prevent microbial contamination of the solar system by spacecraft (forward contamination) and extraterrestrial contamination of the Earth (backward contamination). Bioburden reduction on spacecraft, including cruise and landing systems, is required to prevent microbial contamination from Earth during space exploration missions. Several sterilization methods are available; however, selecting appropriate methods is essential to eliminate a broad spectrum of microorganisms without damaging spacecraft components during manufacturing and assembly. Here, we compared the effects of different bioburden reduction techniques, including dry heat, UV light, isopropyl alcohol (IPA), hydrogen peroxide (H_2O_2), vaporized hydrogen peroxide (VHP), and oxygen and argon plasma on microorganisms with different resistance capacities. These microorganisms included *Bacillus atrophaeus* spores and *Aspergillus niger* spores, *Deinococcus radiodurans*, and *Brevundimonas diminuta*, all important microorganisms for considering planetary protection. *Bacillus atrophaeus* spores showed the highest resistance to dry heat but could be reliably sterilized (i.e., under detection limit) through extended time or increased temperature. *Aspergillus niger* spores and *D. radiodurans* were highly resistant to UV light. Seventy percent of IPA and 7.5% of H_2O_2 treatments effectively sterilized *D. radiodurans* and *B. diminuta* but showed no immediate bactericidal effect against *B. atrophaeus* spores. IPA immediately sterilized *A. niger* spores, but H_2O_2 did not. During VHP treatment under reduced pressure, viable *B. atrophaeus* spores and *A. niger* spores were quickly reduced by approximately two log orders. Oxygen plasma sterilized *D. radiodurans* but did not eliminate *B. atrophaeus* spores. In contrast, argon plasma sterilized *B. atrophaeus* but not *D. radiodurans*. Therefore, dry heat could be used for heat-resistant component bioburden reduction, and VHP or plasma for non-heat-resistant components in bulk bioburden reduction. Furthermore, IPA, H_2O_2, or UV could be used for additional surface bioburden reduction during assembly and testing. The systemic comparison of sterilization efficiencies under identical experimental conditions in this study provides basic criteria for determining which sterilization techniques should be selected during bioburden reduction for forward planetary protection.

KEYWORDS

sterilization, bioburden reduction, planetary protection, forward contamination, spacecraft, microbial contamination

1 Introduction

Space exploration missions are promoted to comply with the Planetary Protection Policy and Requirements established by the Committee on Space Research (COSPAR) to ensure that future scientific investigations related to the chemical evolution of the solar-system bodies and the origin and distribution of life are not compromised (DeVincenzi et al., 1998; Nicholson et al., 2009; Kminek et al., 2019; COSPAR, 2021; Coustenis et al., 2023). The microbial contamination (bioburden) of flight systems, including landers or rovers, must be below the acceptable limit, especially for missions to Mars, Europa, Enceladus, and other solar-system bodies where the existence of extant life cannot be excluded (National Research Council, 2006; Grotzinger et al., 2012; European Cooperation for Space Standardization, 2019; Kminek et al., 2019; Rettberg et al., 2019; NASA, 2021, 2022).

Several sterilization methods are available for bioburden reduction, each with different mechanisms of effect, advantages, and disadvantages. Thus, a comparative study on sterilization methods against different microorganisms is essential to selecting appropriate techniques for bioburden reduction. Dry heat has been the standard method for sterilizing spacecraft since the Viking lander (Barengoltz and Stabekis, 1983; Grotzinger et al., 2012; European Cooperation for Space Standardization, 2013a; Shirey et al., 2017). However, this method is not applicable to non-heat-resistant materials such as electronics (European Cooperation for Space Standardization, 2013a): Dry heat also negatively affects metals, such as accelerated aging and possible softening (European Cooperation for Space Standardization, 2008a). UV irradiation is also widely used as a disinfection method. However, UV light can cause component surface degradation and cannot reach shaded areas. Alcohol disinfection is commonly used for bioburden reduction during spacecraft assembly, such as for the Mars Science Laboratory or Mars 2020 (Grotzinger et al., 2012; Farley et al., 2020); however, alcohol wets the object and only disinfects the surfaces. Isopropyl alcohol (IPA) is considered to be preferable over ethanol because some bacteria may use ethanol as a carbon source (Mogul et al., 2018). Treatment with aqueous solution and vapor of hydrogen peroxide (H_2O_2) is a non-residual method because it degrades into water and oxygen (Rohatgi et al., 2002; Kempf et al., 2005; Chung et al., 2006, 2008; European Cooperation for Space Standardization, 2013b; Rummel and Pugel, 2019). However, this method requires a high chemical concentration and may alter the material, including surface oxidation, strength loss, or volume change (European Cooperation for Space Standardization, 2008a). Plasma sterilization has the advantages of no residual chemicals and minimal adverse effects on components (Moisan et al., 2001, 2002; Hayashi et al., 2018; Choudhury et al., 2023); however, quantitative knowledge is still limited, and plasma sterilization has not been tested for spacecraft bioburden reduction.

We selected four microorganisms that are considered to be important in planetary protection based on previous studies (Patel et al., 2017; Craven et al., 2021; NASA, 2022): *Bacillus atrophaeus* is a gram-positive and spore forming bacterium, and its endogenous spores are commonly used for testing the resistance to dry heat, ethylene oxide, steam, and radiation (Setlow, 2006; Craven et al., 2021; NASA, 2022). In planetary protection, bioburden reduction aims to minimize the presence of entire microorganisms on spacecraft, with a specific focus on reducing the number of microbial spores that can survive a wet heat shock at 80°C for 15 min. This focus is considered crucial because spores have the capability to endure extremely harsh conditions for long periods (e.g., over 10,000 years), and in fact, for the mission of potentially habitable planet, the number of spores per spacecraft is documented in the Planetary Protection Policy (European Cooperation for Space Standardization, 2008b; Benardini et al., 2014a,b; Planetary Protection Independent Review Board, 2019). *Deinococcus radiodurans* is a gram-positive, non-spore forming bacterium known for their ability to survive exposure to strong radiation and desiccation in space (Anderson, 1956; Makarova et al., 2001; Cox and Battista, 2005; Kawaguchi et al., 2020). A gram-negative bacterium, *Brevundimonus diminuta* is a standard organism for validating the quality of sterilizing-grade membrane filters because its small cell size and monodispersed with a narrow size distribution (Sandle, 2013; Ryan and Pembroke, 2018; Roy, 2019). *Aspergillus niger* is a filamentous fungus whose spores are highly pigmented, resistant to UV-C radiation, and easily dispersed in the air (Schuster et al., 2002; Cortesão et al., 2020).

In addition to their different physiological properties, the four microorganisms have actually been detected in spacecraft related cleanrooms or labs. While a wide variety of microorganisms have been detected in spacecraft assembly and other related facilities by various methods, including incubation, DNA-based detection, and MALDI-TOF mass spectrometry, *Bacillus* spp. are often reported as the predominant species (Puleo et al., 1977; Venkateswaran et al., 2001; La Duc et al., 2004; Moissl-Eichinger et al., 2015; Koskinen et al., 2017; Hendrickson et al., 2021; Wood et al., 2021; Schubert et al., 2023). Of the bacteria detected on the six Mars spacecrafts, approximately 30% of those belonged to the genus *Bacillus*, 1–2% to the genus *Brevundimonas,* and 1–2% to the genus *Deinococcus* (Schwendner et al., 2020). Kminek et al. reported that the genera *Bacillus* and *Brevundimonas* accounted for 9 and 4% of the microorganisms in the cleanroom, respectively (Kminek et al., 2019). The genus *Deinococcus* was also often detected, and reported that they were in all NASA's cleanrooms at the Jet Propulsion Laboratory, Kennedy Space Center, and Johnson Space Center (Moissl et al., 2007; Wood et al., 2021). Cultivable fungi were also detected in the cleanroom in spacecraft assembly facility of NASA (Hendrickson

Abbreviations: ATCC, American type culture collection; COSPAR, Committee on Space Research; CT value, Concentration-time value; IPA, Isopropyl alcohol; NBRC, NITE Biological Resource Center; NITE, National Institute of Technology and Evaluation; UV light, Ultraviolet light; VHP, Vaporized hydrogen peroxide.

et al., 2017). Regberg et al. (2018) reported that between 83 and 97% of the microorganisms were fungi in the meteorite lab cleanrooms at NASA.

To select suitable sterilization techniques for bioburden reduction for forward planetary protection, we compared the effects of dry heat, UV light, IPA, H_2O_2, VHP, and oxygen and argon plasma on four different microorganisms in this study. A colony counting method, gold standard for sterilization tests, was used to evaluate living organisms after microbial reduction treatment (European Cooperation for Space Standardization, 2008b; Patel et al., 2017; Chen et al., 2023). *Bacillus atrophaeus* and *A. niger* were used in the spore state as represented the bacterial and fungal spores. *Deinococcus radiodurans* and *B. diminuta*, which do not form spores, were used as dried vegetative cells. Based on comprehensive and systematic information, we proposed the optimal bioburden reduction process of spacecraft.

2 Materials and methods

2.1 Microbial strains and culture conditions

A list of the microorganisms used in this study is shown in Supplementary Table S1. *Bacillus atrophaeus* NBRC 13721, *D. radiodurans* NBRC 15346, and *B. diminuta* NBRC 14213 were purchased from NITE Biological Resource Center (NBRC; Chiba, Japan). *Aspergillus niger* ATCC 16888 was purchased from Microbiologics (St. Cloud, MN, United States). *Deinococcus radiodurans* and *B. diminuta* were cultivated in NBRC No. 702 liquid medium [10 g Hipolypepton (390-02116, Fujifilm Wako, Japan), 2 g yeast extract, and 1 g $MgSO_4{\cdot}7H_2O$ per liter; pH 7.0] at 30°C, with shaking at 120 rpm (WB-205QMC, WakenBtech, Japan). *Bacillus atrophaeus* spores were harvested from the agar plates after 10 days of incubation at 37°C for spore formation [8 g nutrient broth, 4 g yeast extract, 0.0157 g $MnCl_2{\cdot}4H_2O$, and 15 g agar/L] by gently scraping with sterilized saline solution (0.9% NaCl) using a cell spreader. The spores were washed thrice with saline solution, incubated at 80°C for 15 min, washed twice with ethanol, and rewashed with saline solution. *Aspergillus niger* spores were harvested after 10 days of incubation at 25°C from NBRC No. 5 agar plates [20 g malt extract, 20 g glucose, 1 g peptone, and 20 g agar/L; pH 6.0] by gently stroking with a droplet of 0.05% TritonX-100 solution using a Pasteur pipette. The spores were suspended in a sterilized saline solution (0.9% NaCl). Spore formation was determined using phase contrast microscopy (IX73, Olympus, Japan) and the spore content was approximately 90%.

2.2 Preparing inoculated coupons for bioburden reduction experiments

The vegetative cell suspensions (10 or 50 µL) of mid-log phase cultures with an optical density of 0.4 (CO7500, Funakoshi, Japan) of *D. radiodurans* and *B. diminuta* and the 10 µL of *B. atrophaeus* spore solutions and 50 µL of *A. niger* spore solutions were dropped onto glass slides and aluminum plates with holes (φ18 mm and a depth of 2.8 mm) and air-dried for over 1 h in biological safety cabinets (AC2-4 N7, Esco, Singapore). The glass slide coupons were used for bioburden reduction experiments using dry heat, UV, vaporized hydrogen peroxide (VHP), and oxygen and argon plasma (Figure 1). The aluminum plate coupons were used for the bioburden reduction experiments using 70% IPA and 7.5% H_2O_2. Approximately 6–7 log orders of bacterial cells (including spores) and 4–5 log orders of fungal spores per 1 cm in diameter were dried on each plate. Coupons used as controls were prepared at the same time as the samples, stored in desiccators at a relative humidity of ≤30% and a temperature of 22.8°C, and incubated for the same time as the samples. Drying, microbial reduction treatment, collection, and evaluation of live cells were performed within 30 days for the plasma sterilization test and 7 days for the other tests. After drying, survival during inoculated coupons storage was examined by placing them in the desiccators. The thicknesses of surface-attached microbial cells or spores were measured by calculating the average height over 100 µm horizontally ($n \geq 8$) using a laser microscope (VK-X 100, Keyence, Japan).

2.3 Dry heat treatment

Dry heat treatment was performed in a dry oven (MOV-212S, Sanyo, Japan). The treatment time was measured from when the samples were placed in the preheated oven (100, 112, 120, 140, 160, and 180°C) until removal. Inoculated coupons were covered in aluminum foil throughout the treatment. After the treatment, inoculated coupons were removed from the oven and cooled at 22.8°C. The surface temperatures on the inoculated coupons were measured using a data logger (GL240, Graph Tech, Japan).

2.4 UV irradiation

UV irradiation was performed using a UV lamp with a 253.7 nm wavelength (GL 15, Toshiba, Japan) mounted on a clean bench (MCV-131BNS, Sanyo, Japan). The UV intensity was measured using a data logger (YK-37UVSD, Mothertool, Japan), and the UV dose was adjusted to 1.26 J/cm^2/h. The relative humidity was <60%. Throughout the treatment, inoculated coupons were not exposed to intense light sources other than the UV lamp to prevent the photoactivation of the cellular DNA repair systems mediated by photolyase.

2.5 Isopropyl alcohol or H_2O_2 treatment

Alcohol and H_2O_2 treatment were performed by adding 250 µL of 70% IPA (2-propanol; 32435-2B, Kanto Chemical, Japan) and 7.5% H_2O_2 (20779-65, Nacalai Tesque, Japan) to the samples, respectively. The concentrations followed the methods of the Mars Organic Molecule Analyzer for bioburden-controlled clean rooms (Lalime and Berlin, 2016). After the treatments, each sample was diluted with sterilized saline solution (0.9% NaCl) to >200-fold for IPA and > 20,000-fold for H_2O_2 to avoid cell death by residual IPA or H_2O_2. We have confirmed that microbicidal activities did not continue under each diluted condition.

2.6 Vaporized hydrogen peroxide treatment

Vaporized hydrogen peroxide treatments were performed using a vacuum chamber (diameter: 210 mm; length: 495 mm; volume: 17.1 L). The chamber was evacuated, and 35% of liquid H_2O_2 was

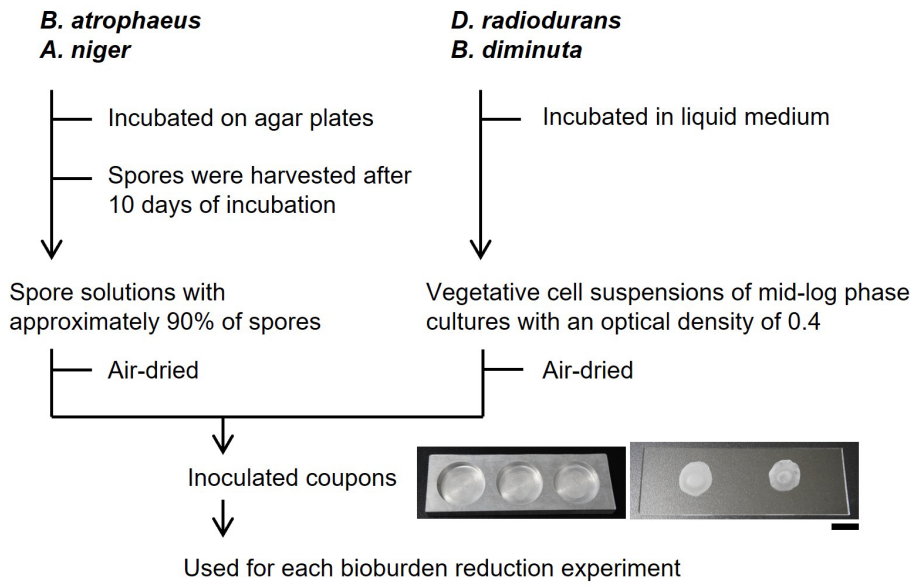

FIGURE 1
Schematics of bioburden reduction experiments. The scale bar shows 1 cm.

supplied from the top of the reactor through continuous evacuation using a vacuum pump and was gasified under a pressure of 400 ± 20 Pa. The temperature inside the vacuum chamber was maintained at 22.8°C. Hence, the relative humidity and concentration of VHP in the treatment were calculated as <11.6% RH and 1.07 ± 0.06 mg/L, respectively. The total moles of mixed gas comprising H_2O and H_2O_2 derived from 35% H_2O_2 (by weight) were calculated as 2.44 mmol using the ideal gas law as the pressure in the evacuated chamber was 50 Pa without 35% H_2O_2. Subsequently, the moles of VHP molecules in the chamber were determined as 0.54 mmol (18.4 mg) according to Dalton's law. The concentration-time (CT) values of VHP treatment were calculated as the product of VHP concentration and exposure time.

2.7 Plasma treatment

Plasma treatments were performed using a capacitively coupled radio-frequency discharge reactor (Hayashi et al., 2006, 2018). The discharge electrode was a serpentine folding-shaped stainless-steel wire (diameter: 4 mm; total length: 1,800 mm) placed approximately 20 mm beneath the upper wall of the reactor. Pure oxygen or argon gas was supplied from the top of the reactor with a pressure of 60 Pa. A radio-frequency voltage of 13.56 MHz was applied to the discharge electrode. The discharge power was maintained at 80 W. The temperature inside the vacuum chamber was maintained at <65°C. The samples were placed 90 mm below the top of the discharge electrode.

2.8 Colony count

After each microbicidal treatment, the microbial cells attached to inoculated coupons were collected by pipetting in triplicate using a total of 100 μL NBRC No. 702 medium. After dilution with NBRC No. 702 media, *B. atrophaeus*, *B. diminuta*, and *D. radiodurans* cells were inoculated on NBRC No. 802 agar plates [pH 7.0, composition: 10 g hipolypepton (390-02116, Fujifilm Wako, Japan), 2 g yeast extract, and 1 g $MgSO_4 \cdot 7H_2O$, and 15 g agar/L]. *Aspergillus niger* spores were inoculated on potato dextrose agar plates (Solabia, France). The agar plates were incubated at 30°C for bacteria and 25°C for fungi in an incubator (IC602, Yamato, Japan): 24–48 h for *B. atrophaeus* cells and 72–96 h for the other microorganisms. The resultant colonies were counted (Scan 300, Interscience, France) to calculate the survival rate. All experiments were performed simultaneously on two dry microbial pellets, and the values were averaged. All experiments were repeated at least once for confirmation of repeatability. Cells collection was confirmed by colony counting and the repeatability was approximately 80%.

2.9 Thermal cell death kinetic models

During dry or moist heat treatment, the thermal death of microbial cells generally follows the first-order of kinetics (Pflug et al., 2001) as described by Equation (1)

$$-\frac{dN}{dt} = k_T N \tag{1}$$

where N and t are the viable cell number and time (min or h), respectively, and k_T is the death rate constant (min^{-1} or h^{-1}) at a constant heating temperature T (°C). When taking the integral of both sides of Equation (1), Equation (2) is obtained using N_0 as the initial viable cell number.

$$\log\frac{N}{N_0} = \left(-\frac{k_T}{\ln 10}\right)t \tag{2}$$

The D-value (D_T, min or h) is the time required to reduce a microbial population by 10-fold at heating temperature T and is calculated from the slope of the line obtained from the logarithmic plot of survival rate, log (N/N_0) against t. Therefore, Equation (3) can be described by Stoforos (2015) as:

$$D_T = \frac{\ln 10}{k_T} \tag{3}$$

The z-value (°C) is defined as the change in temperature that will increase the D-value by a factor of 10 and is also calculated from the slope of the line obtained from the plot of log D_T against T.

2.10 F-value

The F-value (min or h) is the heating time equivalent at any heating temperature T for a specified z-value and reference temperature T_R (Moldenhauer, 2013). Generally, the F-value is obtained through Equation (4),

$$F_{T_R} = \int L_T \mathrm{d}t = \int \frac{k_T}{k_{T_R}} \mathrm{d}t = \int 10^{(T-T_R)/z} \mathrm{d}t \tag{4}$$

where L_T is the lethal rate defined as the constant death rate at temperature T divided by that of reference temperature T_R. When T is a constant value, Equation (5) is obtained.

$$F_{T_R} = 10^{(T-T_R)/z} t = 10^{(T-T_R)/z} F_T \tag{5}$$

During heating and cooling periods, thermal processes were performed under time-varying temperatures $T(t)$, and the F-value is obtained by Equation (6), where F_P is the F-value of the process, which also approximates Equation (7).

$$F_P = \int L_{T(t)} \mathrm{d}t = \int \frac{k_{T(t)}}{k_{T_R}} \mathrm{d}t = \int 10^{(T(t)-T_R)/z} \mathrm{d}t \tag{6}$$

$$F_P \cong \sum_{n=1}^{n} L_{\bar{T}(\Delta t_n)} \Delta t_n = \sum_{n=1}^{n} 10^{(\bar{T}(\Delta t_n)-T_R)/z} \Delta t_n \tag{7}$$

In Equation (7), $\bar{T}(\Delta t_n)$ is the average temperature of the process at the time interval Δt_n. Additionally, using Equation (5), the F_P-values between two thermal processes with different processing temperatures T_1 and T_2 can be described as Equation (8).

$$F_{P,T1} = 10^{(T2-T1)/z} F_{P,T2} \tag{8}$$

Generally, when the F-value of the dry heat sterilization is calculated, a z-value of 20°C is used as that temperature is indicated as the z-value of the bacterial spores (Gould, 2004).

2.11 Determining the accuracy of the processing time length in each dry heat treatment using the F_P-value

The F_P-value of each dry heat treatment was obtained using Equation (7). The total processing time, t, was first divided into n pieces of segments, each with an interval of 20 s. Subsequently, L-values at the average temperature of each time segment were calculated and added (Supplementary Table S2; Supplementary Figures S1, S2). In this calculation, the processing temperature of each dry heat treatment was considered as each reference temperature T_R, and a z-value of 20°C was used. When the processing time value, t, was markedly shorter than the obtained F_P, survival rate data at that time were not used to estimate the D-values.

3 Results

3.1 Properties of simulated bioburden attached to test coupon surfaces

No substantial changes in the colony-forming units of dried *B. atrophaeus* and *D. radiodurans* cells were observed after a storage period of over 30 days (Supplementary Figure S3). The change in dried *A. niger* after 30 days of storage was less than one log reduction. In contrast, dried *B. diminuta* cells showed a one log reduction after 7 days of storage and an approximately three log reduction after 1 month. Supplementary Table S3 shows the thickness of dried cells (approximately 1 cm in diameter) on the glass slide used in the bioburden reduction tests. The dried *D. radiodurans* and *B. diminuta* cells tended to become thicker than those of *B. atrophaeus* and *A. niger*. The cells thicknesses of *B. atrophaeus* and *A. niger* locally exceeded 10 μm due to clumped cells.

3.2 Dry heat treatment

While each dry heat treatment was set at 100, 112, 120, 140, 160, and 180°C, the actual temperatures were 100.8 ± 0.2, 113.4 ± 0.2, 122.0 ± 0.3, 141.9 ± 0.5, 161.3 ± 0.6, and 181.8 ± 0.4°C, respectively. The results for dry heat treatment set at 100-, 112-, and 120°C for *B. atrophaeus* are shown in Figure 2A. The reduction curves obtained from these temperatures were linear for two or three log orders. Subsequent microbial reduction showed tailing. The D-values for 100-, 112-, and 120°C-heat treatments were calculated as 604, 163, and 65.8 min, respectively. The dry heat treatment of *B. atrophaeus* exposed to 140-, 160-, and 180°C are shown in Figure 2B. Over six log orders of spores could be inactivated at 140°C for 5 h, 160°C for 45 min, and 180°C for 6 min. However, the D-values could not be determined for these treatments because the survival rate values dropped before the temperature of the inoculated coupons reached a steady state (Supplementary Table S2; Supplementary Figures S1, S2). *Deinococcus radiodurans*, *B. diminuta*, and *A. niger* dry heat treatment results are shown in Figure 2C. The three microorganisms were sterilized (i.e., under detection limit) more rapidly than *B. atrophaeus* (Table 1). All strains tested in this study were sterilized using a dry heat set at 120°C and above.

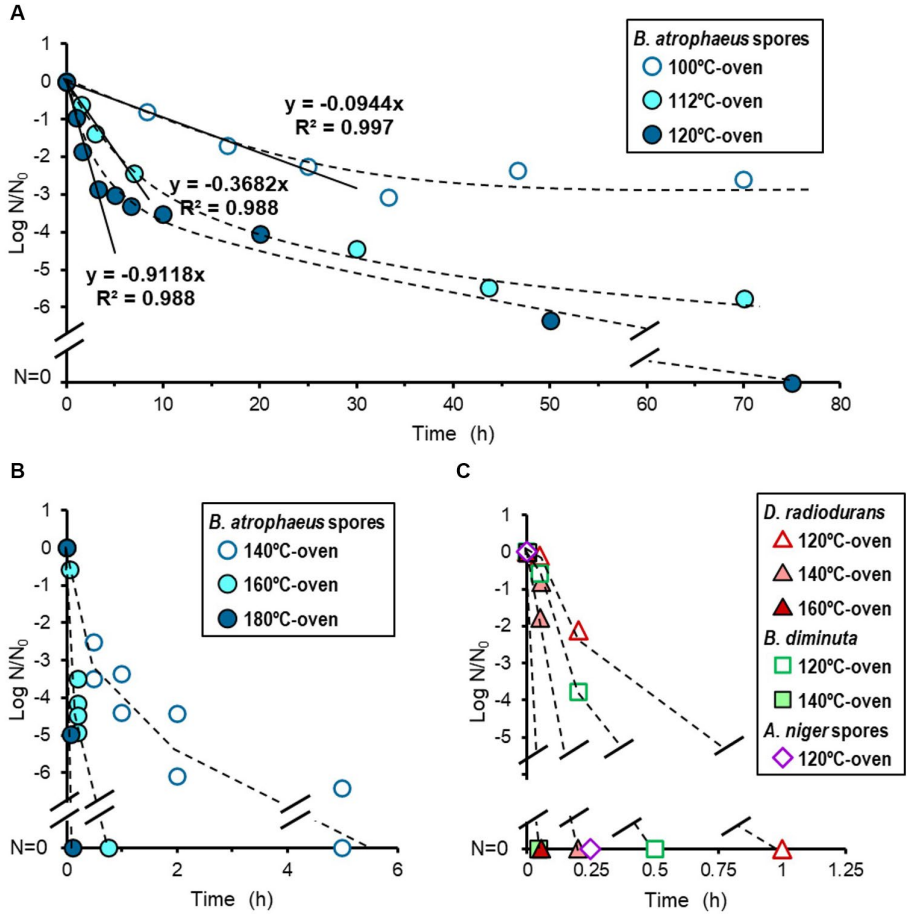

FIGURE 2
Microbial reduction after dry heat treatment. Reduction curves of *Bacillus atrophaeus* spores heated using a 100-, 112-, and 120°C-oven **(A)** and a 140-, 160-, and 180°C-oven **(B)**. Reduction curves of *Deinococcus radiodurans*, *Brevundimonas diminuta*, and *Aspergillus niger* spores **(C)**.

3.3 UV irradiation

The reduction curve of UV treatment is shown in Figure 3. The irradiation intensity measured by the UV lamp at 32.7 cm was 0.35 ± 0.1 mW/cm^2, equal to 1 J/cm^2 for 47.62 min of irradiation. An approximately five log reduction was observed in *B. atrophaeus* and *B. diminuta* after a UV irradiation of 2.5 J/cm^2 (2 h irradiation). In contrast, UV light irradiation resistance was observed for *D. radiodurans* and *A. niger*. For both strains, a tailing of the survival curve was observed after the 1.5–2 log reduction in viable cells at a UV dose of 1.26 J/cm^2 (1 h irradiation). *Deinococcus radiodurans* required a UV dose of 37.8 J/cm^2 (irradiate for 30 h) for sterilization, whereas *A. niger* remained at a 2–3 log reduction in viable cells after the same treatment. These results suggested that the UV sterilization was effective for *B. diminuta* and *B. atrophaeus* but relatively ineffective for *D. radiodurans* and *A. niger* (Table 1), differing from the dry heat treatment results.

3.4 Treatment with alcohol and H_2O_2

The reduction curve after alcohol treatment is shown in Figure 4A. Seventy percent IPA solution was dropped onto the dried cells, and no suspension or wiping treatment was performed. *Brevundimonas diminuta*, *D. radiodurans*, and *A. niger* were sterilized quickly within a few minutes. However, no *B. atrophaeus* sporicidal activity was observed even when IPA infiltration was continued for 120 min.

The reduction value of viable cells after H_2O_2 treatment is shown in Figure 4B. H_2O_2 treatment was performed similarly to the IPA treatment. *Brevundimonas diminuta* and *D. radiodurans* were also sterilized quickly. In contrast, *B. atrophaeus* and *A. niger* microbicidal activities were scarcely observed after 10 min of treatment. Continuous H_2O_2 treatments inactivated more than four log orders of *A. niger* spores after 30 min and over six log orders of *B. atrophaeus* spores in almost all tests after 60 min (data not shown).

3.5 VHP treatment

Vaporized hydrogen peroxide treatment was performed under low pressure (400 ± 20 Pa) at 22.8°C with a relative humidity of ≤11.6%. VHP was continuously supplied and exhausted at 0.93 ± 0.06 mg/L/min throughout the treatment (Supplementary Figure S4). The VHP concentration was maintained at 1.07 ± 0.06 mg/L in the chamber. The CT value of the treatment increased by 64.2 mg·min/L every hour.

TABLE 1 Treatment time required to sterilize the surficial bioburden using dry heat, UV irradiation, and treatment with antimicrobial agents, including vaporized hydrogen peroxide (VHP) and oxygen- and argon plasma.

Treatment		Microorganism			
		Bacillus atrophaeus NBRC13721 (spores)	*Deinococcus radiodurans* NBRC15346	*Brevundimonas diminuta* NBRC14213	*Aspergillus niger* ATCC16888 (spores)
Dry heat[†]	Treated in an oven maintained at 120°C	75 h (7.3)*	<1 h (5.8)	<0.5 h (5.7)	<0.5 h (4.2)
	Treated in an oven maintained at 140°C	*ca.* 6 h (7.7)	<0.5 h (5.9)	<0.5 h (6.4)	Not tested
UV irradiation	Exposure to UV light (253.7 nm) at a dose of 1.26 J/cm²/h	*ca.* 4 h (7.2)	30 h (5.9)	*ca.* 4 h (5.6)	Not achieved at 30 h (3.2–3.6)
Antimicrobial agents	70% isopropyl alcohol (IPA), treatment for 10 min	Not achieved at 10 min (<1.0)	<5 min (6.5)	<5 min (6.4)	<5 min (4.5)
	7.5% hydrogen peroxide, treated for 10 min	Not achieved at 10 min (<1.0)[§]	<5 min (>4.6)	<5 min (>4.3)	Not achieved at 10 min (<1.0)[§]
Vaporized hydrogen peroxide (VHP)[‡]	CT values of the treatment were increased by 64.2 mg•min/L per hour (400 Pa, 22.8°C, <11.6%RH)	Not achieved at 9 h (2.0–2.9)	<0.5 h (6.4)	<0.5 h (6.4)	Not achieved at 9 h (3.8)
Plasma	Oxygen-plasma	Not achieved at 8 h (4.1–4.8)	*ca.* 8 h (6.3)	Tested, but data are insufficient	<2 h (4.3)
	Argon-plasma	2–4 h (7.2)	Not achieved at 8 h (1.4–1.6)	Tested, but data are insufficient	4 h (4.4)

*Numbers in parentheses indicates log reduction values of bioburden. [†]Processing temperature at the coupon surfaces were 122.0 ± 0.3 and 141.9 ± 0.5°C in a 120- and 140°C-oven, respectively. [‡]VHP was supplied and discharged continuously at 0.932 mg/L/min via vacuuming. [§]When the samples were treated for over 60 and 30 min, 6 log and 4 log reductions were observed in *Bacillus atrophaeus* and *Aspergillus niger* spores, respectively.

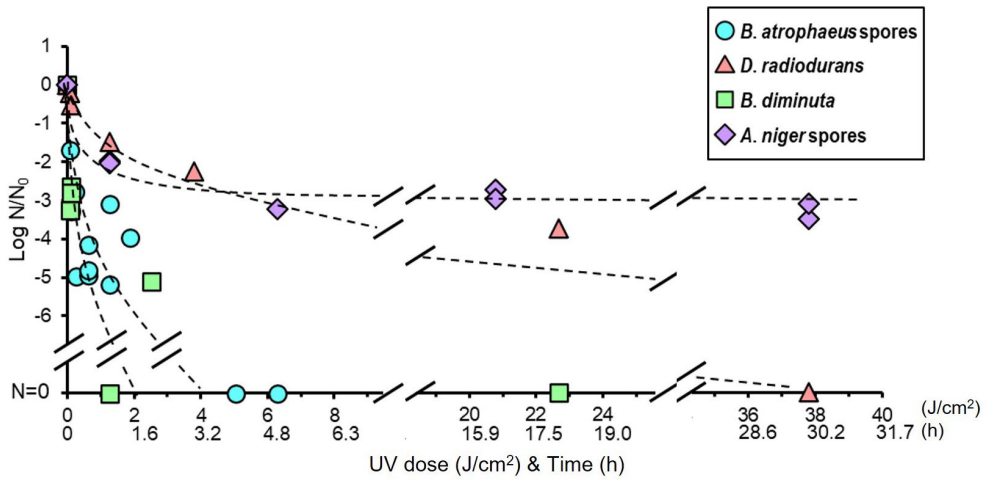

FIGURE 3
Microbial reduction after UV light irradiation of dry *Bacillus atrophaeus* spores, *Deinococcus radiodurans*, *Brevundimonas diminuta*, and *Aspergillus niger* spores.

The VHP treatment results are shown in Figure 5. *Brevundimonas diminuta* and *D. radiodurans* were immediately sterilized; however, *A. niger* and *B. atrophaeus* were inactivated by one to two log orders after 10 min of exposure, corresponding to the CT value of 10.7 mg•min/L, and further effect was not observed. No substantial reduction was observed in vacuum-only treatment for all microorganisms in this study.

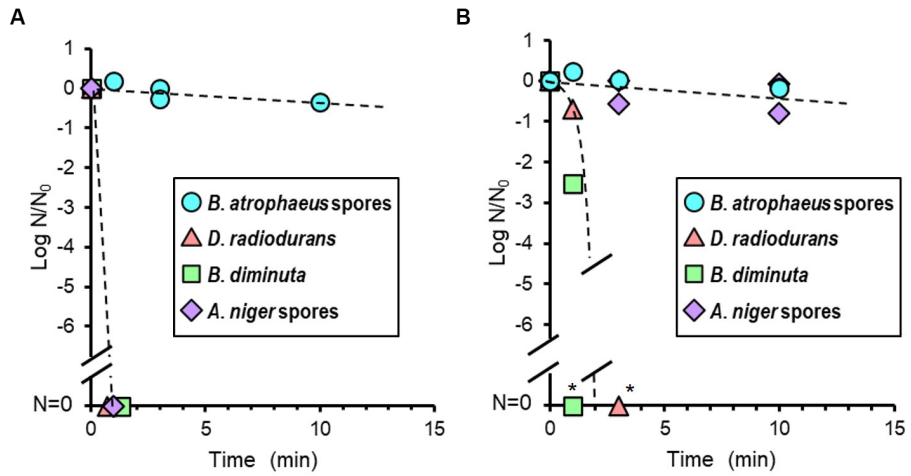

FIGURE 4
Microbial reduction after 70% of isopropyl alcohol (IPA; **A**) and 7.5% hydrogen peroxide (H_2O_2) treatments **(B)** of dry *Bacillus atrophaeus* spores, *Deinococcus radiodurans*, *Brevundimonas diminuta*, and *Aspergillus niger* spores. *Due to the dilution associated with processing steps, the dynamic range is <5 log order.

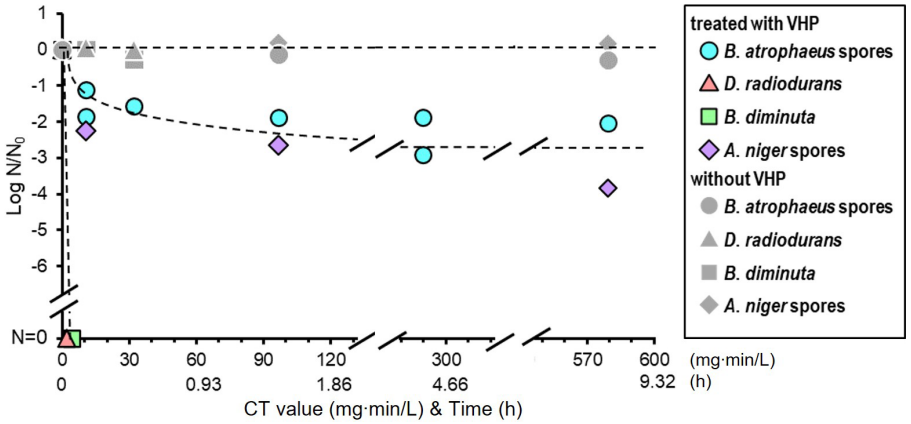

FIGURE 5
Microbial reduction after vaporized hydrogen peroxide (VHP) treatments of dry *Bacillus atrophaeus* spores, *Deinococcus radiodurans*, *Brevundimonas diminuta*, and *Aspergillus niger* spores.

3.6 Oxygen- and argon plasma treatment

Temperatures in the vacuum chamber during oxygen- and argon plasma treatment were increased during the first 20 min and reached constant values of 64 and 59°C, respectively. The reduction curves of test strains after oxygen plasma treatment are shown in Figure 6A. *Aspergillus niger* was sterilized after 1.3 h of treatment. *Deinococcus radiodurans* showed a reduction curve with a shoulder and was sterilized after 8 h. *Bacillus atrophaeus* showed a reduction curve with a tailing, and approximately two and four log orders of reduction in survival spores were observed at 1.3 and 8 h, respectively. The reduction curve after argon plasma treatment is shown in Figure 6B. Approximately 1.5 log orders of *D. radiodurans* cells were killed after 8 h of treatment; however, sterilization was incomplete under these conditions. In contrast, *B. atrophaeus* and *A. niger* were sufficiently sterilized within 4 h. Plasma treatment can reduce *B. atrophaeus* spores by three or more log order; however, the survival of *D. radiodurans* must be investigated. *Brevundimonas diminuta* sterilization using oxygen- and argon plasma treatment has been confirmed with at least two log reductions (data not shown); however, sufficient initial cell numbers were not prepared because *B. diminuta* died during dry storage (Supplementary Figure S3).

4 Discussion

4.1 Relationships of sensitivity between microbial samples and bioburden reduction techniques

A spacecraft is composed of several essential components, including an engine, power subsystem, steering system,

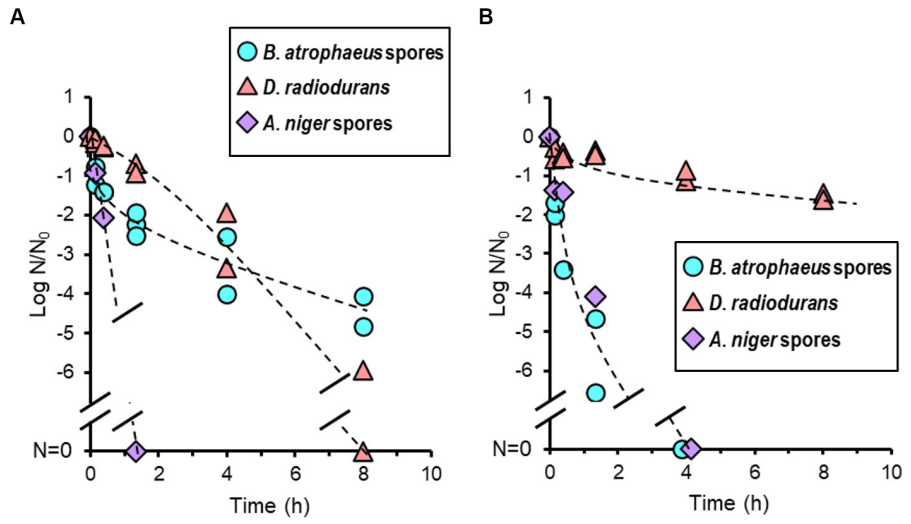

FIGURE 6
Microbial reduction after oxygen **(A)** and argon plasma treatments **(B)** of dry *Bacillus atrophaeus* spores, *Deinococcus radiodurans*, and *Aspergillus niger* spores.

communications system, and scientific instruments. Typically, it operates in space for several years. Consequently, planetary protection engineers must carefully choose suitable sterilization methods to ensure to reduce microbial cells without causing any damage to the spacecraft components. This study is valuable for this purpose, as it meticulously compares representative sterilization methods and provides sterilization efficiencies in *D*- or *z*-values wherever feasible.

Bacillus atrophaeus had the highest resistance to dry heat, 70% IPA, 7.5% H_2O_2, and VHP compared to the other strains (Table 1). In contrast, *B. atrophaeus* did not show resistance to UV light irradiation and argon plasma. *Deinococcus radiodurans* showed higher resistance to UV light and argon plasma than *B. atrophaeus* but did not show resistance to other treatments, except for oxygen plasma treatment. *Aspergillus niger* was resistant to UV light, similar to *D. radiodurans*, and also showed resistance to 7.5% H_2O_2 and VHP, like *B. atrophaeus*. *Brevundimonas diminuta* did not show resistance to any bioburden reduction method used in this study. *Brevundimonas diminuta* are sterilized when treated under conditions that would inactivate *B. atrophaeus*, *D. radiodurans*, and *A. niger*.

4.2 Microbicidal mechanisms and properties of sterilization methods

Logarithmic microbial cell death is theoretically observed when cellular damage from the sterilization treatment is homogeneous within the microbial cell population, which is often seen when cells are in a liquid solution. Inoculated coupons used in this study had a mass of air-dried vegetative or spored cells attached to the surface of the material; thus, the cellular damage in the microbial population tended to be heterogeneous since the damage caused by sterilization can differ depending on the location of the cells.

Heat sterilization, either dry or wet, is known to be effective. Air-dried *D. radiodurans* and *B. diminuta* cells and *B. subtilis* spores are reported to be easily killed, presumably by protein denaturation and DNA damage (Setlow, 2006). The tailing portion of the reduction curve of *B. atrophaeus* treated with dry heat were observed (Figure 2A) It is possible that there is variation in heat sensitivity within the inoculated *B. atrophaeus* population, resulting in a decrease in more sensitive cells during the earlier stages of the bioburden reduction process. Compared to the dry heat treatment conducted by Kempf et al. (2008) and Schubert and Beaudet (2011) who used an oil bath or stainless-steel vessel cylinders, our dry heat treatment (oven heating) was closer situation to the dry heat chamber of spacecraft component for bioburden reduction. However, in this study, the velocity during the heat-up or cool-down processes was slower than that described by Kempf et al. (2008) and Schubert and Beaudet (2011). The coupon temperature (processing temperature) took approximately 20 min to reach a steady-state temperature condition at any oven temperature during dry heat treatment (Supplementary Figures S1, S2). The accuracy of the processing time was confirmed using the F_P-value (Supplementary Table S2). The *D*-values were calculated when the heating time during the non-steady state (heating and cooling) could be ignored compared to the total processing time of dry heat treatments. The reduction curve for *B. atrophaeus* ATCC9372 (synonym for NBRC13721) spores obtained in this study agrees with that reported by Kempf et al. (2008) and Schubert and Beaudet (2011), with an estimated *z*-value of 22.0°C, similar to the *z*-value of general bacterial spores during dry heating (Supplementary Figure S5).

UV light is known to cause DNA damage, leading to microbial inactivation (Horneck et al., 1984, 2006, 2010; Horneck, 1993). *Deinococcus radiodurans* and *A. niger* are reported to have strong radioresistance due to their superior DNA repair mechanism (Cox and Battista, 2005; Cortesão et al., 2020). Our results also showed that the UV light resistance was higher in these species than the other microorganisms (Figure 3). The inoculated *A. niger* coupons used in our bioburden reduction experiments were approximately 4 µm thick (Supplementary Table S3) and > 10 µm thick locally. The tailing off in the reduction curve of the UV treatment may be caused by the fact that only the cells at the outermost layer of the multi-layered structure

were killed by the UV light and the UV light could not reach cells located within the inner position of the layer (Kawaguchi et al., 2020; Cortesão et al., 2021; Schuerger and Headrick, 2023). The *B. atrophaeus* and *A. niger* were suspended in the saline solution and *D. radiodurans* and *B. diminuta* were suspended in media before dropped on the coupon, so the ingredients of the incubation medium might shield against UV treatment in the test of *D. radiodurans* and *B. diminuta* and the UV radiation to sample coupon without media can be more effective.

Treatment with three different chemical agents, IPA, H_2O_2, and VHP, also exhibited varying sterilization profiles among the four microorganisms. Alcohol is thought to be a nonspecific antimicrobial agent because of the diverse toxicity mechanisms (Ali et al., 2001) and treatment with H_2O_2, which is mediated by the hydroxyl radical (•OH) generated by the Fenton reaction with intracellular iron, also presumably kill any types of microorganisms (Repine et al., 1981; Clifford and Repine, 1982). However, only slight reduction was observed when *B. atrophaeus* were treated with 70% IPA for 120 min or 7.5% H_2O_2 for 10 min and when *A. niger* was treated with 7.5% H_2O_2 for 10 min (Figure 4). VHP treatment is more effective to the spores of *B. atrophaeus* and *A. niger* but they could not be completely sterilized with VHP as well in this study (Figure 5). All these indicated that chemical treatment may not be quite effective to the fungal and bacterial spores due to the lower envelope permeabilities of spored cells although the mechanism of action of VHP may differ from that of liquid H_2O_2 (Linley et al., 2012). Meanwhile, *D. radiodurans* and *B. diminuta* were quickly sterilized using VHP (Figure 5), as with IPA and liquid H_2O_2.

The mechanism of oxygen-plasma sterilization is considered an etching effect of the cell surface by oxygen plasma and cell membrane disruption by hydroxyl radicals and atomic oxygen. The heat generated as a side effect may also have bioburden reduction effects. The mechanism of argon plasma bioburden reduction is also an etching of the cell surface and the UV light emitted from de-excitation particles in the plasma (Moisan et al., 2001, 2002). Interestingly, oxygen and argon plasma showed different sterilization spectra from any other sterilization techniques used in this study (Figure 6). Oxygen and argon plasma inactivated *A. niger*. Argon plasma sterilized *B. atrophaeus*, whereas *D. radiodurans* was not sterilized, differing from the oxygen plasma results but similar to its response to UV light. However, although *A. niger* was UV light-resistant, it was quickly sterilized; therefore, other mechanisms could contribute to *D. radiodurans* being resistant.

4.3 Bioburden reduction strategies for spacecraft

Decontamination processes of spacecraft components can be divided into initial bioburden reduction prior to delivery to assembly facilities and additional bioburden reduction during assembly and testing (Chen et al., 2023). Encapsulated, enclosed, or mated bioburdens are challenging to reduce through additional bioburden reduction (Kminek et al., 2019); however, if they are sufficiently sterilized, re-contamination risk is small. In contrast, the exposed surfaces on the spacecraft components could be easily re-contaminated but re-disinfection is also easy with additional treatment.

For the initial overall bioburden reduction of spacecraft components before assembly, the dry heat method must be suitable if the material is heat resistant. Dry heat has the capability to inactivate various microbial species, as shown in Figure 2, and it reproduces results consistently and can penetrate both surface and deep layers within the components. Using Equation (8), the processing times of dry heat for various processing temperatures obtained in this study can be converted to the dry heat treatment processing times for an optimal reference temperature using F_p-values. Reduction curves were estimated for dry heat treatments at 111.7 and 125.0°C as typically described in the COSPAR guidelines (Supplementary Figure S6; European Cooperation for Space Standardization, 2013a; Kminek et al., 2019; NASA, 2022). Tailings in the curves and data variability were observed after four logs order of reduction. Less than four log spores of initial bioburden would be desirable for accurate bioburden reduction using dry heat.

Techniques other than dry heat should be carefully used for non-heat-resistant components in initial and additional bioburden reduction. IPA sterilized *D. radiodurans*, *B. diminuta*, and *A. niger* immediately, whereas H_2O_2 (solution and vapor) sterilized *D. radiodurans* and *B. diminuta* immediately. Although IPA treatment is a convenient technique, it was ineffective concerning *B. atrophaeus* (Figure 4A), and H_2O_2 was not effective immediately for *B. atrophaeus* and *A. niger* (Figure 4B). Chemical treatments must be more effective when applied with wiping than when used alone for bioburden reduction. UV light is a valuable technique for surface sterilization as *B. atrophaeus* can be sterilized relatively easily (Figure 3). In contrast, when UV light is used to reduce the bioburden, being aware of microorganisms that show higher resistance than *B. atrophaeus*, such as *D. radiodurans* and *A. niger*, is essential. VHP treatment did not sterilize *B. atrophaeus* or *A. niger*, but it achieved two log orders of bioburden reduction in 10 min, even at room temperature (Figure 5). If used with a cleaning process in advance, VHP could be an effective sterilization technique. Plasma treatment produces UV light and heat as secondary factors in addition to the respective sterilization factors (Moisan et al., 2002). Although quantifying each effect is challenging, the bioburden reduction of several microbial species could be achieved (Figure 6), and continuously introducing different types of gases may be helpful for the sterilization. Plasma sterilization can be effective because it can be performed at relatively low temperatures, does not use chemicals, and has no residual properties. In addition to the low-pressure plasma tested in this study, portable atmospheric-pressure plasma may be effective in additional bioburden reduction.

For fitting to the individual systems or situations, the required time for the sterilization can be reduced by optimizing the conditions, such as increasing the voltage for UV light and plasma treatments, increasing the number of lamps and adjusting the distance to the light source for UV treatment, changing the pressure and agent concentration for VHP, changing the agent concentration for H_2O_2, and the temperature and humidity for all bioburden reduction techniques, or using a combination of each sterilization technique. For example, VHP batch treatment could sterilize *Geobacillus stearothermophilus* spores to approximately five log orders when treated with heat (Chung et al., 2006), unlike this study that performed treatments at room temperature. Furthermore, less exposure to an aerosolized hypochlorous solution is required to obtain similar sporicidal activity levels at 100%RH than at 70%RH (Ishikawa et al., 2019). Considering that the effectiveness of sterilization treatments

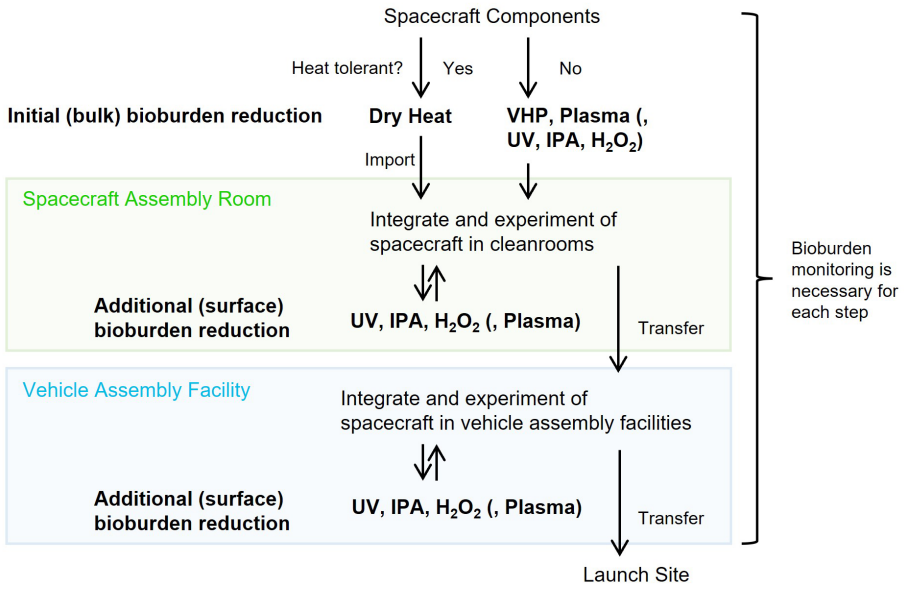

FIGURE 7
Conceivable bioburden reduction alternatives to integrate into spacecraft.

varies among different microorganism species, bioburden reduction methods should be evaluated using the most tolerant microorganisms for each technique as model organisms. For instance, *A. niger* should be employed to assess the UV treatment, and *D. radiodurans* should be used for argon plasma treatments. Furthermore, it should be noted that solid surface bioburden may result in less uniform microbial reduction. Hence, sterilization methods should be designed under conditions where the initial bioburden is sufficiently low. For this purpose, it could be valuable to reduce contamination through pre-cleaning before the bioburden reduction process.

The anticipated process of the spacecraft components from the introduction into the facility to assembly and launch is shown in Figure 7. Dry heat treatment is appropriate for initial bioburden reduction if the components are heat-resistant. UV light, VHP, and plasma treatment are options for non-heat-resistant components. IPA is the primary method for additional surficial bioburden reduction in assembly cleanrooms. However, H_2O_2, UV light, or portable plasma treatment could be alternatives if IPA is insufficient to reduce the bioburden. These sterilization techniques, combined with storing components in a high-efficiency particulate air-filtered space and reducing the bioburden in liquids using autoclaves and filter filtration, would provide a system for launching a sterile spacecraft. Bioburden monitoring at each of these stages is essential. Bioburden reduction confirmation through incubation is the standard method; however, this technique is time-consuming, and detection is limited to microorganisms that form colonies on solid media. Therefore, using a rapid, culture-independent detection method is preferred.

This study quantitatively compared the effectiveness of bioburden reduction techniques on typical resistant microorganisms that can attach to spacecraft (Table 1). The results of this study are useful for selecting the appropriate sterilization methods for planetary protection, and this study will also help planetary protection engineers to choose the most tolerant model organism when they assess each bioburden reduction method. However, other more resistant microorganisms may be present in the natural system. Future studies should expand our knowledge of bioburden reduction methods to improve the techniques, including using different detection methods, expanding the range of microorganisms and developing new sterilization methods. These efforts should aim to reduce the risk of contaminating other planets.

5 Conclusion

Systemically comparing the various sterilization techniques under the same experimental conditions revealed the different sensitivities among microorganisms. *Bacillus atrophaeus* showed the highest resistance to dry heat, alcohol, 7.5% H_2O_2, and VHP. *Deinococcus radiodurans* and *A. niger* were more resistant to UV than *B. atrophaeus*, and *D. radiodurans* showed the highest resistance to argon plasma treatment. Notably, IPA, widely used for bioburden reduction in planetary protection, had no inactivation effect on *B. atrophaeus* spores. These experimental results provide an accurate estimation of the effectiveness of the sterilization techniques during spacecraft assembly. The method used for bioburden reduction depends on the compatibility of the spacecraft components to withstand the particular technique. Evaluating the damage caused to the spacecraft components by sterilization and selecting and using components that can withstand the entire sterilization process would be effective for future space exploration missions compatible with planetary protection policies and requirements.

Data availability statement

The raw data supporting the conclusions of this article will be made available by the authors, without undue reservation.

Author contributions

SK: Conceptualization, Data curation, Funding acquisition, Investigation, Methodology, Validation, Writing – original draft, Writing – review & editing, Formal analysis, Project administration, Resources. SI: Formal analysis, Methodology, Validation, Writing – original draft, Writing – review & editing. NH: Data curation, Methodology, Writing – review & editing. KF: Investigation, Writing – review & editing. YI: Funding acquisition, Investigation, Writing – review & editing, Project administration, Resources. SS: Conceptualization, Funding acquisition, Investigation, Methodology, Supervision, Validation, Writing – original draft, Writing – review & editing, Project administration, Resources.

Funding

The author(s) declare financial support was received for the research, authorship, and/or publication of this article. This research was supported by the Space Exploration Innovation Hub Center (TansaX) and Front-loading on Technology for Space and Astronautical Science of the Japan Aerospace Exploration Agency (JAXA). This research was partly funded by the Astrobiology Center (ABC) Program of the National Institutes of Natural Sciences (NINS) nos. AB041015 and AB0514, JST ACT-X no. JPMJAX2015 to SK, and JSPS KAKENHI no. 20H04620 to SS.

Acknowledgments

The authors greatly appreciate Yoshinobu Matsumura (Department of Life Science and Biotechnology, Kansai University) for the valuable discussions, Chiharu Tanaka (Center for Fungal Consultation, incorporated nonprofit organization, Japan) for providing information on the experimental spore methods, Tetsuya Matsunaga (ISAS, JAXA) for helping with the observation using a 3D laser scanning microscope, and Shoko Mamiya and Chieko Kawanokuchi (TansaX, JAXA) for the technical assistance. We would like to thank Editage (www.editage.com) for English language editing.

Conflict of interest

SI was employed by Kajima Corporation.

The remaining authors declare that the research was conducted in the absence of any commercial or financial relationships that could be construed as a potential conflict of interest.

Publisher's note

Supplementary material

The Supplementary material for this article can be found online at: https://www.frontiersin.org/articles/10.3389/fmicb.2023.1253436/full#supplementary-material

References

Ali, Y., Dolan, M. J., Fendler, E. J., and Larson, E. L. (2001). "Alcohols" in *Disinfection, Sterilization and Preservation*. ed. S. S. Block. *5th* ed (Philadelphia, USA: Lippincott Williams & Wilkins), 229–253.

Anderson, A. W. (1956). Studies on a radio-resistant micrococcus. I. Isolation, morphology, cultural characteristics, and resistance to gamma radiation. *Food Technol.* 10, 575–578.

Barengoltz, J., and Stabekis, P. D. (1983). U.S. planetary protection program: implementation highlights. *Adv. Space Res.* 3, 5–12. doi: 10.1016/0273-1177(83)90166-7

Benardini, J. N. III, La Duc, M. T., Ballou, D., and Koukol, R. (2014b). Implementing planetary protection on the atlas V fairing and ground systems used to launch the Mars science laboratory. *Astrobiology* 14, 33–41. doi: 10.1089/ast.2013.1011

Benardini, J. N. III, La Duc, M. T., Beaudet, R. A., and Koukol, R. (2014a). Implementing planetary protection measures on the Mars science laboratory. *Astrobiology* 14, 27–32. doi: 10.1089/ast.2013.0989

Chen, F., Ly, C., Mikellides, I., Bernard, D., and Cooper, M. (2023). Mars 2020 Mission biological return sample contamination control approach and verification. *Astrobiology* 23, 862–879. doi: 10.1089/ast.2022.0048

Choudhury, B., Revazishvili, T., Lozada, M., Roy, S., Mastro, E. N., Portugal, S., et al. (2023). Distributed compact plasma reactor decontamination for planetary protection in space missions. *Sci. Rep.* 13:1928. doi: 10.1038/s41598-023-29049-2

Chung, S., Barengoltz, J., Kern, R., Koukol, R., and Cash, H. (2006). *The Validation of Vapor Phase Hydrogen Peroxide Microbial Reduction for Planetary Protection and a Proposed Vacuum Process Specification*. Pasadena, California: JPL Publication, 06.

Chung, S., Kern, R., Koukol, R., Barengoltz, J., and Cash, H. (2008). Vapor hydrogen peroxide as alternative to dry heat microbial reduction. *Adv. Space Res.* 42, 1150–1160. doi: 10.1016/j.asr.2008.01.005

Clifford, D. P., and Repine, J. E. (1982). Hydrogen peroxide mediated killing of bacteria. *Mol. Cell. Biochem.* 49, 143–149. doi: 10.1007/BF00231175

Cortesão, M., De Haas, A., Unterbusch, R., Fujimori, A., Schütze, T., Meyer, V., et al. (2020). *Aspergillus Niger* spores are highly resistant to space radiation. *Front. Microbiol.* 11:560. doi: 10.3389/fmicb.2020.00560

Cortesão, M., Siems, K., Koch, S., Beblo-Vranesevic, K., Rabbow, E., Berger, T., et al. (2021). MARSBOx: fungal and bacterial endurance from a balloon-flown analog mission in the stratosphere. *Front. Microbiol.* 12:601713. doi: 10.3389/fmicb.2021.601713

COSPAR (2021). COSPAR policy on planetary protection. Available at: https://cosparhq.cnes.fr/assets/uploads/2021/07/PPPolicy_2021_3-June.pdf (Accessed July 5, 2023).

Coustenis, A., Hedman, N., Doran, P. T., Al Shehhi, O., Ammannito, E., Fujimoto, M., et al. (2023). Planetary protection: an international concern and responsibility. *Front. Astron. Space Sci.* 10:156. doi: 10.3389/fspas.2023.1172546

Cox, M. M., and Battista, J. R. (2005). *Deinococcus radiodurans*: the consummate survivor. *Nat. Rev. Microbiol.* 3, 882–892. doi: 10.1038/nrmicro1264

Craven, E., Winters, M., Smith, A. L., Lalime, E., Mancinelli, R., Shirey, B., et al. (2021). Biological safety in the context of backward planetary protection and Mars sample return: conclusions from the sterilization working group. *Int. J. Astrobiol.* 20, 1–28. doi: 10.1017/S1473550420000397

DeVincenzi, D. L., Race, M. S., and Klein, H. P. (1998). Planetary protection, sample return missions and Mars exploration: history, status, and future needs. *J. Geophys. Res. Planets* 103, 28577–28585. doi: 10.1029/98JE01600

European Cooperation for Space Standardization (2008a). Materials and hardware compatibility tests for sterilization processes. ECSS-Q-ST-70-53C.

European Cooperation for Space Standardization (2008b). Microbial examination of flight hardware and cleanrooms. ECSS-Q-ST-70-55C.

European Cooperation for Space Standardization (2013a). Space product assurance: Dry heat bioburden reduction for flight hardware, ECSS-Q-ST-70-57C.

European Cooperation for Space Standardization (2013b). Space product assurance: Vapour phase bioburden reduction for flight hardware, ECSS-Q-ST-70-56C.

European Cooperation for Space Standardization (2019). Space sustainability: Planetary protection, ECSS-U-ST-20C.

Farley, K. A., Williford, K. H., Stack, K. M., Bhartia, R., Chen, A., de la Torre, M., et al. (2020). Mars 2020 mission overview. *Space Sci.* 216, 1–41. doi: 10.1007/s11214-020-00762-y

Gould, G. W. (2004). "Heat sterilization" in *Russell, Hugo and Ayliffe's Principles and Practice of Disinfection, Preservation and Sterilization*. eds. A. P. Fraise, P. A. Lambert and J.-Y. Maillaed. *4th* ed (Oxford, UK: Blackwell Publishing Ltd), 361–383.

Grotzinger, J. P., Crisp, J., Vasavada, A. R., Anderson, R. C., Baker, C. J., Barry, R., et al. (2012). Mars science laboratory mission and science investigation. *Space Sci.* 170, 5–56. doi: 10.1007/s11214-012-9892-2

Hayashi, N., Goto, M., Itarashiki, T., Yonesu, A., and Sakudo, A. (2018). Current plasma sterilization and disinfection studies. *J. Photopolym. Sci. Technol.* 31, 389–398. doi: 10.2494/photopolymer.31.389

Hayashi, N., Guan, W., Tsutsui, S., Tomari, T., and Hanada, Y. (2006). Sterilization of medical equipment using radicals produced by oxygen/water vapor RF plasma. *JJAP.* 45, 8358–8363. doi: 10.1143/JJAP.45.8358

Hendrickson, R., Lundgren, P., Mohan, G. B. M., Urbaniak, C., Benardini, J., and Venkateswaran, K. (2017). "Comprehensive measurement of microbial burden in nutrient-deprived cleanrooms" in *47th International Conference on Environmental Systems. ICES-2017-177*.

Hendrickson, R., Urbaniak, C., Minich, J. J., Aronson, H. S., Martino, C., Stepanauskas, R., et al. (2021). Clean room microbiome complexity impacts planetary protection bioburden. *Microbiome* 9, 238–217. doi: 10.1186/s40168-021-01159-x

Horneck, G. (1993). Responses of *Bacillus subtilis* spores to space environment: results from experiments in space. *Orig. Life Evol. Biosph.* 23, 37–52. doi: 10.1007/BF01581989

Horneck, G., Bücker, H., Reitz, G., Requardt, H., Dose, K., Martens, K. D., et al. (1984). Microorganisms in the space environment. *Science* 225, 226–228. doi: 10.1126/science.225.4658.226

Horneck, G., Klaus, D. M., and Mancinelli, R. L. (2010). Space microbiology. *MMBR* 74, 121–156. doi: 10.1128/MMBR.00016-09

Horneck, G., Rettberg, P., Facius, R., and Scherer, K. (2006). "Quantification of biological effectiveness of UV radiation" in *Environmental UV Radiation: Impact on Ecosystems and Human Health and Predictive Models: Proceedings of the NATO Advanced Study Institute on Environmental UV Radiation: Impact on Ecosystems and Human Health and Predictive Models*. Pisa, Italy June 2001. Springer Netherlands, 51–69.

Ishikawa, S., Ueno, S., Mitsui, M., Matsumura, Y., and Hatsuoka, T. (2019). Construction of its evaluation system in originally designed test chamber system and sporicidal activity of aerosolized hypochlorite solution to *Bacillus subtilis* spores. *Biocontrol Sci.* 24, 57–65. doi: 10.4265/bio.24.57

Kawaguchi, Y., Shibuya, M., Kinoshita, I., Yatabe, J., Narumi, I., Shibata, H., et al. (2020). DNA damage and survival time course of deinococcal cell pellets during 3 years of exposure to outer space. *Front. Microbiol.* 11:2050. doi: 10.3389/fmicb.2020.02050

Kempf, M. J., Chen, F., Kern, R., and Venkateswaran, K. (2005). Recurrent isolation of hydrogen peroxide-resistant spores of *Bacillus pumilus* from a spacecraft assembly facility. *Astrobiology* 5, 391–405. doi: 10.1089/ast.2005.5.391

Kempf, M. J., Schubert, W. W., and Beaudet, R. A. (2008). Determination of lethality rate constants and D-values for *Bacillus atrophaeus* (ATCC 9372) spores exposed to dry heat from 115°C to 170°C. *Astrobiology* 8, 1169–1182. doi: 10.1089/ast.2007.0208

Kminek, G., Fellous, J. L., Rettberg, P., Moissl-Eichinger, C., Sephton, M. A., Royle, S. H., et al. (2019). *The International Planetary Protection Handbook. An Online-Only Supplement to Space Research Today*, vol. 205. Available at: https://www.sciencedirect.com/journal/space-research-today.

Koskinen, K., Rettberg, P., Pukall, R., Auerbach, A., Wink, L., Barczyk, S., et al. (2017). Microbial biodiversity assessment of the European Space Agency's ExoMars 2016 mission. *Microbiome* 5, 143–116. doi: 10.1186/s40168-017-0358-3

La Duc, M. T., Kern, R., and Venkateswaran, K. (2004). Microbial monitoring of spacecraft and associated environments. *Microb. Ecol.* 47, 150–158. doi: 10.1007/s00248-003-1012-0

Lalime, E. N., and Berlin, D. (2016). Establishing and monitoring an aseptic workspace for building the MOMA mass spectrometer. *Syst. Contaminat. Predict. Control Perform.* 2016, 149–159. doi: 10.1117/12.2238226

Linley, E., Denyer, S. P., McDonnell, G., Simons, C., and Maillard, J. Y. (2012). Use of hydrogen peroxide as a biocide: new consideration of its mechanisms of biocidal action. *J. Antimicrob. Chemother.* 67, 1589–1596. doi: 10.1093/jac/dks129

Makarova, K. S., Aravind, L., Wolf, Y. I., Tatusov, R. L., Minton, K. W., Koonin, E. V. J., et al. (2001). Genome of the extremely radiation-resistant bacterium *Deinococcus radiodurans* viewed from the perspective of comparative genomics. *MMBR* 65, 44–79. doi: 10.1128/mmbr.65.1.44-79.2001

Mogul, R., Barding, G. A. Jr., Lalla, S., Lee, S., Madrid, S., Baki, R., et al. (2018). Metabolism and biodegradation of spacecraft cleaning reagents by strains of spacecraft-associated *Acinetobacter*. *Astrobiology* 18, 1517–1527. doi: 10.1089/ast.2017.1814

Moisan, M., Barbeau, J., Crevier, M. C., Pelletier, J., Philip, N., and Saoudi, B. (2002). Plasma sterilization. Methods and mechanisms. *Pure Appl. Chem.* 74, 349–358. doi: 10.1351/pac200274030349

Moisan, M., Barbeau, J., Moreau, S., Pelletier, J., Tabrizian, M., and L'H, Y. (2001). Low-temperature sterilization using gas plasmas: a review of the experiments and an analysis of the inactivation mechanisms. *Int. J. Pharm.* 226, 1–21. doi: 10.1016/S0378-5173(01)00752-9

Moissl, C., Osman, S., La Duc, M. T., Dekas, A., Brodie, E., DeSantis, T., et al. (2007). Molecular bacterial community analysis of clean rooms where spacecraft are assembled. *FEMS Microbiol. Ecol.* 61, 509–521. doi: 10.1111/j.1574-6941.2007.00360.x

Moissl-Eichinger, C., Auerbach, A. K., Probst, A. J., Mahnert, A., Tom, L., Piceno, Y., et al. (2015). Quo vadis? Microbial profiling revealed strong effects of cleanroom maintenance and routes of contamination in indoor environments. *Sci. Rep.* 5:9156. doi: 10.1038/srep09156

Moldenhauer, J. (2013). "Validation of moist and dry heat sterilization" in *Sterile Product Development: Formulation, Process, Quality and Regulatory Considerations*. eds. P. Kolhe, M. Shah and N. Rathore (Berlin/Heidelberg, Germany: Springer Science+Business Media), 535–574.

NASA (2021). Planetary protection provisions for robotic extraterrestrial missions. NPR 8715.24.

NASA (2022). Implementing planetary protection requirements for space flight. NASA-STD-8719.27.

National Research Council (2006). *Preventing the Forward Contamination of Mars*. Washington, DC: The National Academies Press

Nicholson, W. L., Schuerger, A. C., and Race, M. S. (2009). Migrating microbes and planetary protection. *Trends Microbiol.* 17, 389–392. doi: 10.1016/j.tim.2009.07.001

Patel, M., Gow, J., Paton, S., and Truscott, P. (2017). SterLim: Sterilisation limits for sample return planetary protection measures. ESA contract no. 4000112742/14/NL/HB.

Pflug, I. J., Holcomb, R. G., and Gómez, M. M. (2001). "Principles of the thermal destruction of microorganisms" in *Disinfection, Sterilization and Preservation*. ed. S. S. Block. *5th* ed (Philadelphia, USA: Lippincott Williams & Wilkins), 79–129.

Planetary Protection Independent Review Board (2019). NASA planetary protection independent review board (PPIRB).

Puleo, J. R., Fields, N. D., Bergstrom, S. L., Oxborrow, G. S., Stabekis, P. D., and Koukol, R. (1977). Microbiological profiles of the Viking spacecraft. *Appl. Environ. Microbiol.* 33, 379–384. doi: 10.1128/aem.33.2.379-384.1977

Regberg, A. B., Burton, A. S., Castro, C. L., Stahl, S. E., Wallace, S. L., and McCubbin, F. M. (2018). "Microbial ecology of the Johnson Space Center meteorite curation lab and associated infrastructure" in *49th Annual Lunar and Planetary Science Conference (No. 2083, p. 2056)*.

Repine, J. E., Fox, R. B., and Berger, E. M. (1981). Hydrogen peroxide kills *Staphylococcus aureus* by reacting with staphylococcal iron to form hydroxyl radical. *J. Biol. Chem.* 256, 7094–7096. doi: 10.1016/S0021-9258(19)68927-1

Rettberg, P., Antunes, A., Brucato, J., Cabezas, P., Collins, G., Haddaji, A., et al. (2019). Biological contamination prevention for outer solar system moons of astrobiological interest: what do we need to know? *Astrobiology* 19, 951–974. doi: 10.1089/ast.2018.1996

Rohatgi, N., Schubert, W., Koukol, R., Foster, T. L., and Stabekis, P. D. (2002). Certification of vapor phase hydrogen peroxide sterilization process for spacecraft application. SAE Technical Paper 2002-01-2471.

Roy, S. (2019). An insight into membrane filter validation. *ASMI* 2, 29–31. doi: 10.31080/ASMI.2019.02.0425

Rummel, J. D., and Pugel, D. B. (2019). Planetary protection technologies for planetary science instruments, spacecraft, and missions: report of the NASA planetary protection technology definition team (PPTDT). *Life Sci. Space Res.* 23, 60–68. doi: 10.1016/j.lssr.2019.06.003

Ryan, M. P., and Pembroke, J. T. (2018). *Brevundimonas* spp: emerging global opportunistic pathogens. *Virulence* 9, 480–493. doi: 10.1080/21505594.2017.1419116

Sandle, T. (2013). "Sterilisation by filtration" in *Sterility, Sterilisation and Sterility Assurance for Pharmaceuticals Technology, Validation and Current Regulations* (Woodhead Publishing Series in Biomedicine), 143–155.

Schubert, W. W., and Beaudet, R. A. (2011). Determination of lethality rate constants and D-values for heat-resistant Bacillus spores ATCC 29669 exposed to dry heat from 125°C to 200°C. *Astrobiology* 11, 213–223. doi: 10.1089/ast.2010.0502

Schubert, W. W., Seto, E. P., Hinzer, A. A., and Guan, L. (2023). Identification and archive of Mars 2020 spacecraft microbial isolates. *Astrobiology* 23, 835–845. doi: 10.1089/ast.2022.0052

Schuerger, A. C., and Headrick, E. L. (2023). Microbial protocols for spacecraft: 3. Spore monolayer preparation methods for ultraviolet irradiation exposures. *Astrobiology* 23, 908–920. doi: 10.1089/ast.2022.0072

Schuster, E., Dunn-Coleman, N., Frisvad, J., and van Dijck, P. (2002). On the safety of *Aspergillus niger*: a review. *Appl. Microbiol. Biotechnol.* 59, 426–435. doi: 10.1007/s00253-002-1032-6

Schwendner, P., Jobson, M. E., and Schuerger, A. C. (2020). Addition of anaerobic electron acceptors to solid media did not enhance growth of 125 spacecraft bacteria under simulated low-pressure Martian conditions. *Sci. Rep.* 10, 18290–18211. doi: 10.1038/s41598-020-75222-2

Setlow, P. (2006). Spores of *Bacillus subtilis*: their resistance to and killing by radiation, heat and chemicals. *J. Appl. Microbiol.* 101, 514–525. doi: 10.1111/j.1365-2672.2005.02736.x

Shirey, T. B., Schubert, W., and Benardini, J. (2017). "An overview of surface heat microbial reduction as a viable microbial reduction modality for spacecraft surfaces" in *47th International Conference on Environmental Systems*, ICES-2017-201.

Stoforos, N. G. (2015). "Thermal processing" in *Handbook of Food Processing: Food Preservation*. eds. T. Varzakas and C. Tzia (Florida, USA: CRC Press), 27–56.

Venkateswaran, K., Satomi, M., Chung, S., Kern, R., Koukol, R., Basic, C., et al. (2001). Molecular microbial diversity of a spacecraft assembly facility. *Syst. Appl. Microbiol.* 24, 311–320. doi: 10.1078/0723-2020-00018

Wood, J. M., Singh, N. K., Guan, L., Seuylemezian, A., Benardini, J. N., and Venkateswaran, K. (2021). Performance of multiple metagenomics pipelines in understanding microbial diversity of a low-biomass spacecraft assembly facility. *Front. Microbiol.* 12:685254. doi: 10.3389/fmicb.2021.685254

Frontiers in Microbiology

Explores the habitable world and the potential of microbial life

The largest and most cited microbiology journal which advances our understanding of the role microbes play in addressing global challenges such as healthcare, food security, and climate change.

Discover the latest Research Topics

See more →

Frontiers

Avenue du Tribunal-Fédéral 34
1005 Lausanne, Switzerland
frontiersin.org

Contact us

+41 (0)21 510 17 00
frontiersin.org/about/contact